CARDIOVASCULAR MECHANOBIOLOGY, 2nd Edition

EDITED BY: Markus Hecker and Dirk J. Duncker
PUBLISHED IN: Frontiers in Physiology

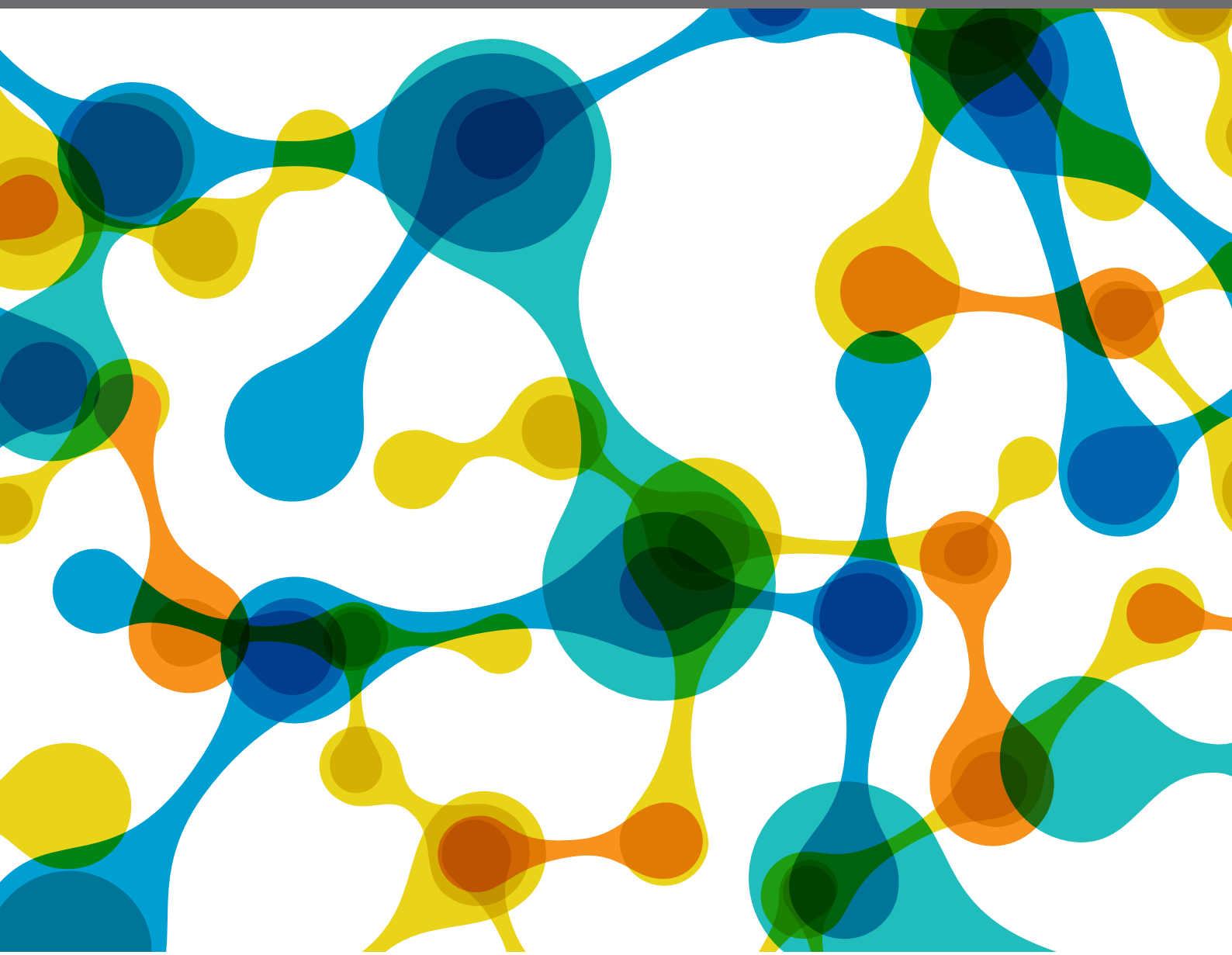

frontiers Research Topics

ISSN 1664-8714
ISBN 978-2-8325-3050-4
DOI 10.3389/978-2-8325-3050-4

About Frontiers

Frontiers is more than just an open-access publisher of scholarly articles: it is a pioneering approach to the world of academia, radically improving the way scholarly research is managed. The grand vision of Frontiers is a world where all people have an equal opportunity to seek, share and generate knowledge. Frontiers provides immediate and permanent online open access to all its publications, but this alone is not enough to realize our grand goals.

Frontiers Journal Series

The Frontiers Journal Series is a multi-tier and interdisciplinary set of open-access, online journals, promising a paradigm shift from the current review, selection and dissemination processes in academic publishing. All Frontiers journals are driven by researchers for researchers; therefore, they constitute a service to the scholarly community. At the same time, the Frontiers Journal Series operates on a revolutionary invention, the tiered publishing system, initially addressing specific communities of scholars, and gradually climbing up to broader public understanding, thus serving the interests of the lay society, too.

Dedication to Quality

Each Frontiers article is a landmark of the highest quality, thanks to genuinely collaborative interactions between authors and review editors, who include some of the world's best academicians. Research must be certified by peers before entering a stream of knowledge that may eventually reach the public - and shape society; therefore, Frontiers only applies the most rigorous and unbiased reviews.
Frontiers revolutionizes research publishing by freely delivering the most outstanding research, evaluated with no bias from both the academic and social point of view. By applying the most advanced information technologies, Frontiers is catapulting scholarly publishing into a new generation.

What are Frontiers Research Topics?

Frontiers Research Topics are very popular trademarks of the Frontiers Journals Series: they are collections of at least ten articles, all centered on a particular subject. With their unique mix of varied contributions from Original Research to Review Articles, Frontiers Research Topics unify the most influential researchers, the latest key findings and historical advances in a hot research area! Find out more on how to host your own Frontiers Research Topic or contribute to one as an author by contacting the Frontiers Editorial Office: frontiersin.org/about/contact

CARDIOVASCULAR MECHANOBIOLOGY, 2nd Edition

Topic Editors:
Markus Hecker, Heidelberg University, Germany
Dirk J. Duncker, Erasmus University Medical Center, Netherlands

Publisher's note: In this 2nd edition, the following article has been updated:

Emig R, Zgierski-Johnston CM, Beyersdorf F, Rylski B, Ravens U, Weber W, Kohl P, Hörner M and Peyronnet R (2020) Human Atrial Fibroblast Adaptation to Heterogeneities in Substrate Stiffness. Front. Physiol. 10:1526. doi: 10.3389/fphys.2019.01526

Citation: Hecker, M., Duncker, D. J., eds. (2023). Cardiovascular Mechanobiology, 2nd Edition. Lausanne: Frontiers Media SA. doi: 10.3389/978-2-8325-3050-4

Table of Contents

frontiers in Physiology

EDITORIAL
published: 20 January 2022
doi: 10.3389/fphys.2021.833941

Editorial: Cardiovascular Mechanobiology

Markus Hecker[1]* *and Dirk J. Duncker*[2]*

[1] Department of Cardiovascular Physiology, Heidelberg University, Heidelberg, Germany, [2] Department of Cardiology, Erasmus University Medical Center, Thoraxcenter, Rotterdam, Netherlands

Keywords: mechanobiology, cardiac, vascular, wall tension, wall shear stress, cardiovascular disease

Editorial on the Research Topic

Cardiovascular Mechanobiology

Biomechanical forces play a major role in organ development, shape, and function. When exceeding the physiological range, however, they can become detrimental for organ structure and function. This is probably best exemplified by the cardiovascular system, with both the heart and blood vessels being continuously exposed to the biomechanical forces exerted by the pressure and flow of blood, which produce not only acute changes in cardiovascular function but also result in structural changes in the cardiovascular system.

The field of cardiovascular mechanobiology is a fascinating and clinically highly relevant Research Topic, with many research groups contributing to the advancement of our understanding of the acute and chronic adaptations and maladaptations produced by biomechanical forces. These insights continue to generate novel targets for therapy of a variety of cardiovascular diseases. Several aspects of cardiovascular mechanobiology are presented in this very timely Frontiers Research Topic "*Cardiovascular Mechanobiology,*" containing a total of 10 articles, with a balanced mix of 5 review and 5 original articles.

In the first review article, Jackson discusses the mechanobiology of myogenic tone in peripheral resistance arteries and arterioles, presenting the current understanding of the multiple mechanisms that have been implicated in myogenic tone, including the roles played by G-protein coupled receptors, ion channels, and protein kinases in vascular smooth muscle cells. The article highlights the areas where our knowledge and understanding of myogenic tone has remained incomplete and that warrant further research.

In the second review paper, Sporkova et al. review the mechanisms underlying the mechanobiological cues mediating the inward remodelling of small arteries and arterioles in response to chronic stretch produced by, for example, hypertension. Particular focus is on the role that LIM domain containing proteins play in mechanosensing and transduction in vascular smooth muscle and endothelial cells, translating extra- and intracellular mechanobiological cues into changes in gene expression in these cells that drive vascular remodelling.

Brandt et al. review the mechanobiological aspects of microvascular function and structure in health and disease with a particular focus on the coronary microcirculation. An in-depth review is provided on the factors involved in coronary microvascular functional and structural alterations in obstructive and non-obstructive coronary artery disease and the molecular mechanisms involved, providing novel potential targets for the treatment of ischemic heart disease.

The mechanobiology of endothelial-to-mesenchymal transition and its role in cardiovascular disease is reviewed by Islam et al. highlighting the emerging role of shear stress, cyclic strain, matrix stiffness, and composition in endothelial-to-mesenchymal transition, which is a hot topic particularly in maladaptive cardiac remodelling due to pressure overload but also in response to myocardial infarction. The authors also identify areas requiring further investigation.

Edited and reviewed by:
Gerald A. Meininger,
University of Missouri, United States

***Correspondence:**
Markus Hecker
hecker@physiologie.uni-heidelberg.de
Dirk J. Duncker
d.duncker@erasmusmc.nl

Specialty section:
This article was submitted to Vascular Physiology, a section of the journal Frontiers in Physiology

Received: *12 December 2021*
Accepted: *30 December 2021*
Published: *20 January 2022*

Citation:
Hecker M and Duncker DJ (2022) Editorial: Cardiovascular Mechanobiology. Front. Physiol. 12:833941. doi: 10.3389/fphys.2021.833941

Finally, Lityagina and Dobreva review novel insight into the epigenetic aspects of cardiovascular mechanobiology. Specifically, they describe how mechanical forces are transduced to chromatin through the tensed actomyosin cytoskeleton, the linker of nucleoskeleton and cytoskeleton (LINC) complex and the nuclear lamina, and the importance of these mechanisms in cardiovascular disease.

In the original research articles various aspects of the mechanobiology of vascular smooth muscle cells, endothelial cells, as well as cardiomyocytes were investigated. Using inducible pluripotent stem cell (iPSC)-derived cardiomyocytes, Körner et al. tested the hypothesis that the environmental stiffness influences structural and functional properties of iPSC-derived cardiomyocytes. The authors observed that soft surfaces with stiffnesses in the physiological range improve the expression pattern and interaction of cardiac proteins relevant for excitation-contraction coupling. Moreover, soft substrates influenced contractile properties and improved intercellular coupling in iPSC-derived cardiomyocytes, indicating that mechanical stiffness of the cell environment drives iPSC-derived cardiomyocytes toward further maturation by inducing adaptive responses.

In the next article, Akinbote et al. investigated vessel-stroma crosstalk in normal conditions and in the presence of fibrosis, using human iPSC-derived endothelial cells co-cultured in the absence and presence of primary human cardiac and lung fibroblasts in a microfluidic device to generate cardiac and pulmonary-like microvasculature that can be perfused at near physiological flow rates. Their study not only demonstrates the strong impact of stromal-endothelial cell interactions on vessel formation and extravascular matrix regulation, but their human 3D *in vitro* set-up could be very useful in future studies examining anti-fibrotic therapies on patient-specific iPSCs.

Wall shear stress has been proposed to influence intracranial aneurysmal growth and rupture. Consequently, Morel et al. investigated the effects of low and supra-high aneurysmal wall shear stress on porcine arterial endothelial cells. The authors observed that differential regulation of gene expression observed under various wall shear stress conditions translates into a different organisation of the endothelial cell architecture, suggesting that this adaptation of endothelial cells to different aneurysmal wall shear stress conditions may affect vascular remodelling in intracranial aneurysms.

Myocardin related transcription factors (MRTFs), including myocardin itself, MRTF-A, and MRTF-B are co-factors of serum response factor (SRF) that activate the smooth muscle cell gene program and play a key role in smooth muscle cell differentiation and mechanobiology. Liu, Bankell et al. investigated the role of alterations in MRTF signalling in vascular inflammation, and observed a cell type specific (vascular smooth muscle but not endothelial cells) suppression of inflammatory mediators. In a second study, Liu, Rippe et al. studied the regulation of muscarinic receptors by MRTFs and observed that muscarinic receptor M3 expression was driven by MRTFs in a cell specific manner, i.e., by MRTF-B/SRF in endothelial cells and by myocardin/SRF in vascular smooth muscle cells.

These highly diverse review and original research articles, covering a wide range of studies, illustrate the broad biological implications of mechanosensing and mechanotransduction in the cardiovascular system. We wish you an interesting and enjoyable journey through this Frontiers Research Topic!

AUTHOR CONTRIBUTIONS

All authors contributed equally to the writing of this article and organisation of the Research Topic.

Conflict of Interest: The authors declare that the research was conducted in the absence of any commercial or financial relationships that could be construed as a potential conflict of interest.

frontiers in Physiology

ORIGINAL RESEARCH
published: 10 January 2020
doi: 10.3389/fphys.2019.01526

Human Atrial Fibroblast Adaptation to Heterogeneities in Substrate Stiffness

*Ramona Emig[1,2,3], Callum M. Zgierski-Johnston[1,2], Friedhelm Beyersdorf[2,4], Bartosz Rylski[2,4], Ursula Ravens[1,2], Wilfried Weber[3,5], Peter Kohl[1,2,5], Maximilian Hörner[3,5] and Rémi Peyronnet[1,2]**

[1]Institute for Experimental Cardiovascular Medicine, University Heart Center Freiburg - Bad Krozingen, Medical Center-University of Freiburg, Freiburg, Germany, [2]Faculty of Medicine, University of Freiburg, Freiburg, Germany, [3]Faculty of Biology, University of Freiburg, Freiburg, Germany, [4]Department of Cardiovascular Surgery, University Heart Center Freiburg, University of Freiburg, Freiburg, Germany, [5]Signalling Research Centres BIOSS and CIBSS, University of Freiburg, Freiburg, Germany

OPEN ACCESS

Edited by:
Boris Martinac, Victor Chang Cardiac Research Institute, Australia

Reviewed by:
Neil Turner, University of Leeds, United Kingdom
Andrew Raymond Battle, Queensland University of Technology, Australia

***Correspondence:**
Rémi Peyronnet
remi.peyronnet@universitaets-herzzentrum.de

Specialty section:
This article was submitted to Membrane Physiology and Membrane Biophysics, a section of the journal Frontiers in Physiology

Received: *22 May 2019*
Accepted: *04 December 2019*
Published: *10 January 2020*

Citation:
Emig R, Zgierski-Johnston CM, Beyersdorf F, Rylski B, Ravens U, Weber W, Kohl P, Hörner M and Peyronnet R (2020) Human Atrial Fibroblast Adaptation to Heterogeneities in Substrate Stiffness. Front. Physiol. 10:1526. doi: 10.3389/fphys.2019.01526

Fibrosis is associated with aging and many cardiac pathologies. It is characterized both by myofibroblast differentiation and by excessive accumulation of extracellular matrix proteins. Fibrosis-related tissue remodeling results in significant changes in tissue structure and function, including passive mechanical properties. This research area has gained significant momentum with the recent development of new tools and approaches to better characterize and understand the ability of cells to sense and respond to their biophysical environment. We use a novel hydrogel, termed CyPhyGel, to provide an advanced *in vitro* model of remodeling-related changes in tissue stiffness. Based on light-controlled dimerization of a Cyanobacterial Phytochrome, it enables contactless and reversible tuning of hydrogel mechanical properties with high spatial and temporal resolution. Human primary atrial fibroblasts were cultured on CyPhyGels. After 4 days of culturing on stiff (~4.6 kPa) or soft (~2.7 kPa) CyPhyGels, we analyzed fibroblast cell area and stiffness. Cells grown on the softer substrate were smaller and softer, compared to cells grown on the stiffer substrate. This difference was absent when both soft and stiff growth substrates were combined in a single CyPhyGel, with the resulting cell areas being similar to those on homogeneously stiff gels and cell stiffnesses being similar to those on homogeneously soft substrates. Using CyPhyGels to mimic tissue stiffness heterogeneities *in vitro*, our results confirm the ability of cardiac fibroblasts to adapt to their mechanical environment, and suggest the presence of a paracrine mechanism that tunes fibroblast structural and functional properties associated with mechanically induced phenotype conversion toward myofibroblasts. In the context of regionally increased tissue stiffness, such as upon scarring or in diffuse fibrosis, such a mechanism could help to prevent abrupt changes in cell properties at the border zone between normal and diseased tissue. The light-tunable mechanical properties of CyPhyGels and their suitability for studying human primary cardiac cells make them an attractive model system for cardiac mechanobiology research. Further investigations will explore the interactions between biophysical and soluble factors

in the response of cardiac fibroblasts to spatially and temporally heterogeneous mechanical cues.

Keywords: fibrosis, mechanosensing, hydrogel, light-tunable, nanoindentation

INTRODUCTION

Cardiac tissue damage due to causes such as aging, mechanical overload, or injury is associated with the development of fibrosis. Fibrosis is characterized both by myofibroblast differentiation and excessive accumulation of extracellular matrix (ECM) proteins (Herum et al., 2017). This remodeling is driven mainly by fibroblasts (Manabe et al., 2002; Travers et al., 2016), changes in tissue structure, and mechanics with consequences ranging from impaired cardiac output to increased arrhythmia vulnerability (Nguyen and Qu, 2014). Ultimately, presence and extent of fibrosis are a leading risk factor for sudden cardiac death (Disertori et al., 2016). Thus far, there are no effective therapeutic approaches toward reversing cardiac fibrosis mainly due to insufficient knowledge about the underlying basic mechanisms.

Possible therapeutic approaches must consider changes in tissue mechanics, which act both as a cause and a consequence of remodeling. Fibroblast sensing of their mechanical environment has been shown to play a role in fibrotic remodeling (Hinz, 2013; van Putten et al., 2016). In recent years, several *in vitro* models have been developed to study fibroblast mechanosensing. A major class of these models utilizes synthetic substrates that include hydrogels and silicones. These allow investigators to prescribe the mechanical environment of cultured cells (Rosales and Kristi, 2016; Li et al., 2018). Alternatively, naturally occurring substrates like decellularized tissue (Ott et al., 2008) or living cardiac tissue slices (Perbellini et al., 2018) have been used to provide cells with near-physiological growth substrates, but these are more complex and less reproducible models. Substrates that more closely mimic *in vivo* conditions are essential as, while the overall stiffness of fibrotic tissue is raised when ECM production overcomes degradation (Levental et al., 2010), the stiffness distribution is highly heterogeneous. Areas with more or less ECM constitute different mechanical microdomains. In diffuse fibrosis, for example, in atrial fibrillation, islands of stiff ECM are distributed within softer tissue (Tanaka et al., 2007). Given that the mechanical effects on single cells are dominated by their microenvironment, *in vitro* models should replicate these stiffness heterogeneities, ideally in a controllable manner.

A model allowing the introduction of spatial gradients in the mechanical properties has been used to show that the stiffness-guided migration of fibroblasts, a process called durotaxis, depends on the type of matrix proteins (Hartman et al., 2017). Further, hydrogels with micropatterned stiff and soft areas were used to show adaptation of cell spreading over a wide range of stiffnesses (Sunyer et al., 2012) and to study the role of matrix organization for mesenchymal stem cell differentiation (Yang et al., 2016). However, these models do not allow one to dynamically and reversibly modify passive mechanical properties of the growth substrate in time or space. A novel hydrogel system (which we termed here CyPhyGel), based on the Cyanobacterial Phytochrome Cph1, may address this limitation by allowing light-controlled, reversible changes in hydrogel stiffness (Hörner et al., 2019b). To do so, cell-compatible red light is used to switch Cph1 between its monomeric (740 nm) or dimeric (660 nm) forms, thereby reducing or increasing the number of crosslinks in the growth substrate in a contact-free manner, respectively. The stiffness of CyPhyGels can be changed between 1.5 and 5.5 kPa (Effective Young's modulus). Changes in stiffness occur within seconds of illumination, are gradable, stable in the absence of light, and reversible (Hörner et al., 2019b). In this study, we use CyPhyGels to investigate human cardiac fibroblast adaptation to heterogeneities in the stiffness of their mechanical environment beyond durotaxis.

MATERIALS AND METHODS

Production of Cph1-Based Hydrogels (CyPhyGels)

CyPhyGels were produced as described previously (Hörner et al., 2019b) with the following modifications. In short, the photoreceptor Cph1* [Cph1-Y263F (amino acids 1–514) fused to a tandem arginine-glycine-aspartic acid motif, a hexahistidine tag and C-terminal cysteine] was recombinantly produced by high-cell-density fermentation in *E. coli* BL21 STAR (DE3) and purified *via* immobilized metal ion affinity chromatography (Hörner et al., 2019a). Purified Cph1* was concentrated to ~200 mg/mL by ultrafiltration (PES membrane, 10 kDa molecular weight cutoff). The elution buffer from purification was exchanged with reaction buffer (phosphate buffered saline [PBS], containing, in mM 137 NaCl, 2.7 KCl, 10 Na_2HPO_4, 1.8 KH_2PO_4, 2 mM ethylenediaminetetraacetic acid, pH 8) using a desalting column (5 kDa molecular weight cut-off). After concentrating the protein as before to ~100 mg/mL, it was reduced with tris(2-carboxyethyl)phosphine (TCEP) at a molar Cph1*:TCEP ratio of 1:0.7 for 1 h at room temperature. Without removing the reducing agent, the protein was covalently coupled to 8-arm polyethylene-glycol vinyl-sulfone (PEG-VS, 40 kDa, NOF Europe GmbH, Germany) in reaction buffer supplemented with 100 mM triethanolamine at a final concentration of 70 mg/mL Cph1* and a molar VS:Cph1* ratio of 2:1.

Immediately after addition of PEG-VS, 30 µL of the reaction mix were spread on 22 mm × 22 mm square glass coverslips, resulting in CyPhyGels with a thickness between 50 and 90 µm (data not shown). The reaction mixes were incubated in a humidified atmosphere to allow gelation at room temperature for at least 16 h under continuous illumination with 660 nm (1 mW/cm^2). Afterward, CyPhyGels on coverslips were transferred into PBS (pH 7.4) and stored in the dark at room temperature. Their mechanical properties after different illumination protocols

(see "Stiffness Tuning of CyPhyGels") were tested by nanoindentation (see "Nanoindentation of CyPhyGels and Fibroblasts"). CyPhyGels were used no earlier than 1 week after preparation, as their stiffness increased over several days following gelation (**Supplementary Figure S1**).

Stiffness Tuning of CyPhyGels

Light emitting diodes (LED) with peak wavelengths of 660 nm to stiffen CyPhyGels, and 740 nm to soften CyPhyGels (LZ4-40R208 and LZ4-40R308, respectively; LED Engin, USA) were coupled to bandpass filters restricting specimen illumination to ± 6.5 nm around the target wavelength (FF01–660/13 and FF01–740/13, respectively; Semrock, USA). CyPhyGels were illuminated at 1 mW/cm^2 for a minimum of 5 min.

To obtain heterogeneous CyPhyGels, characterized by containing one stiff and one soft half, we implemented a sequential illumination protocol (**Figure 1A**). After initial stiffening of the whole CyPhyGel by illumination with 660 nm, a photomask (**Figure 1A**, bottom right) was carefully positioned over half of the gel by means of a micromanipulator. Using a telecentric lens, the exposed part of the CyPhyGel was then illuminated at 740 nm to tune it to its softest state (**Figure 1A**).

Broad-bandwidth "white" light (e.g. room lighting or microscope light) resulted in stiffening of CyPhyGels in less than 10 min (**Supplementary Figure S2**). Therefore, CyPhyGels tuned to the desired stiffness were kept in dark conditions or handled under green light. For nanoindentation, the microscope light was filtered with a 490 ± 5 nm band pass filter (D490/10X, Semrock, USA), which prevented gross changes in CyPhyGel stiffness over a period of up to 1 h (**Supplementary Figure S2**).

Culture of Primary Human Atrial Fibroblasts

Primary human fibroblasts were obtained from right atrial appendage tissue of patients in sinus rhythm undergoing open heart surgery at the University Heart Center Freiburg-Bad Krozingen. Patients gave informed consent on the use of the tissue (with approval by the Ethics Commission of the University of Freiburg, reference: 393/16: 214/18). Upon excision by the surgeon, the tissue was placed in room temperature cardioplegic solution (containing, in mM 120 NaCl, 25 KCl, 10 HEPES, 10 glucose, 1 $MgCl_2$; pH 7.4, 300 mOsm) and immediately transported to the laboratory. After removing the epicardial layer, the tissue was cut into pieces of 1–2 mm^3. Tissue fragments were placed in culture plates (3.5 cm diameter, 3–4 pieces per well) with abraded surfaces, containing 2 mL Dulbecco's Modified Eagle Medium supplemented with 10% fetal bovine serum and 1% penicillin/streptomycin (all Sigma-Aldrich, Germany). Medium was refreshed every 3–4 days. Due to their proliferative and migratory potential, fibroblasts are the major cell type growing out of the tissue chunk (Poulet et al., 2016). Immunocytochemical analysis could not detect the presence of endothelial (tested by CD31) or smooth muscle cells (tested

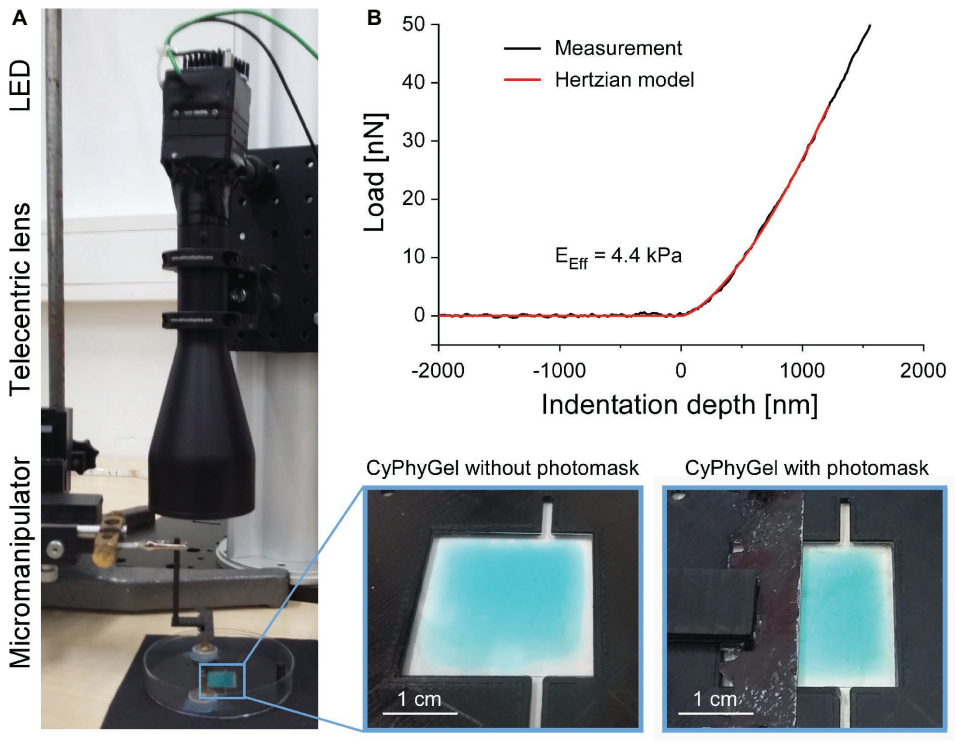

FIGURE 1 | Generation and mechanical testing of heterogeneous CyPhyGels. **(A)** Illumination system for generation of mechanically heterogeneous CyPhyGels. After initial stiffening of a whole CyPhyGel by exposure to 660 nm illumination (final intensity: 1 mW/cm^2, 5 min), a telecentric lens is positioned in front of a second LED, which is used for 740 nm illumination (final intensity: 1 mW/cm^2, 5 min) of the partially covered CyPhyGel. **(B)** Representative load-indentation curve resulting from nanoindentation (black) and the fitted Hertzian model for contact mechanics (red) used to calculate the Effective Young's modulus, E_{Eff}.

by desmin) in the outgrowth cultures (data not shown). The original outgrowing fibroblasts were referred to as "Passage 0." Once 80–90% confluency was reached, cells were detached with Trypsin-EDTA (Sigma-Aldrich, Germany) and re-cultured (Passage 1) at a density of 6,500 cells/cm^2. This procedure was repeated up to six times (generating Passages 2–6).

For experiments shown in this manuscript, fibroblasts from three patients at Passages 4 and 5 were seeded at low density (2,000 cells/cm^2) on previously tuned CyPhyGels. Cell culture work was conducted using green light to limit changes in CyPhyGel stiffness from environmental light exposure. After seeding, culture dishes were covered by aluminum foil during the whole culture period (4 days, no medium change).

Nanoindentation of CyPhyGels and Fibroblasts

The Effective Young's modulus, E_{Eff}, was assessed using the Chiaro nanoindenter system (Optics11, Amsterdam, Netherlands). A spherical tip, attached to a calibrated cantilever, is used to indent the sample while a laser beam is shone onto the reflective cantilever surface. Reflected laser light is analyzed interferometrically to measure phase shifts, which correlate with cantilever bending. From this, the force required for sample indentation is calculated. E_{Eff} was derived using the Hertzian model for contact mechanics (Hertz, 1881; Chen, 2014) under the assumption of a Poisson's ratio of 0.5 for incompressible materials, which is commonly used for mechanical testing of cells and tissue (**Figure 1B**; Guz et al., 2014). Throughout this manuscript, E_{Eff} is referred to as stiffness. Sample indentations of 2–4 µm were performed at a displacement speed of 5 µm/s. Data analysis used the Optics11 DataViewer (V2.0.27).

For CyPhyGel characterization, cantilevers with spring constants of 0.45–0.5 N/m and tips of 20–23 µm radii were used. For cell assessment, cantilevers with spring constants of 0.01–0.02 N/m and tips with 3–3.5 µm radii were used. The stiffness of single cells was determined by performing surface-normal indentations at two to three different positions that were not overlapping with the nucleus. For every indentation, the Hertzian model was used to fit the force-displacement curve from initial cell surface contact up to 1 µm indentation, to avoid mechanical interference from the underlying growth substrate. Cell stiffness was assessed 4 days after seeding on CyPhyGels.

Cell Fixation, Staining, Confocal Imaging, and Image Analysis

For confocal imaging, fibroblasts were cultured on CyPhyGels of different stiffness for 4 days, fixed using 4% paraformaldehyde (Roth, Germany) in PBS for 15 min. Glycoproteins at the cell membrane were stained with AlexaFluor555-conjugated wheat germ agglutinin (WGA, 1 µg/mL, Invitrogen, Germany) in 3% bovine serum albumin in PBS for 1 h, followed by three 10-min washing steps in PBS. Thereafter, cells were permeabilized using 0.5% Triton-X100 (Sigma-Aldrich, Germany) in PBS for 15 min and blocked using 3% bovine serum albumin in PBS for 1 h. Primary antibody against alpha smooth muscle actin (αSMA; ab7817, Abcam, Germany) was applied 1:50 in 1% bovine serum albumin in PBS overnight. After three washing steps in PBS, AlexaFluor488-coupled secondary anti-mouse was applied 1:500 in PBS for 1 h. Nuclear counterstaining was performed using Hoechst-33342 (20 µM, ThermoFisher, Germany) for 2–3 min in PBS. All staining was performed at room temperature.

Imaging was performed on a Leica TCS SP8 X confocal microscope using a 20× multi-immersion objective (HC PL APO 20x/0.75 IMM) with water as immersion medium. For imaging, the CyPhyGels were mounted upside-down in a PBS-filled microscopy dish (µ-Dish 35 mm, ibidi, Germany). Cell area was determined using ImageJ after manually tracing cell borders based on WGA signal.

Statistics

If not stated otherwise, data are presented as single data points and mean ± SEM. Data points were considered outliers when they differed by more than three standard deviations from the mean. After removing outliers, statistical significance of two groups with more than 20 data points was determined by Student's *t*-test for unpaired data with equal variances. Two groups with less than 20 data points were compared using the non-parametric Mann-Whitney test. More than two groups were analyzed by Two-way ANOVA followed by *post-hoc* comparison of the mean values using the Tukey test. All statistical analyses were performed in OriginPro 2019.

RESULTS

Tuning Mechanical Properties of CyPhyGels by Light

CyPhyGels, uniformly exposed to illumination at 660 nm had an E_{Eff} of 4.59 ± 0.11 kPa, while after illumination with 740 nm, E_{Eff} was 2.72 ± 0.06 kPa (**Figures 2A,B**). Similar maximal and minimal E_{Eff} were found for the two differentially tuned halves of heterogeneous CyPhyGels. For spatial characterization of the stiffness gradient, heterogeneous CyPhyGels were mapped, in 50 µm steps, along a line perpendicular to the boundary between their stiff and soft halves. E_{Eff} changed from 4.48 ± 0.58 to 2.12 ± 0.30 kPa (**Figure 2C**). Using a higher resolution step size (5 µm) near the boundary, we found that the transition between stiff and soft areas occurs within a 100–150 µm wide band (**Figure 2D**). The width of the border zone was constant over at least 1 mm (**Supplementary Figure S3**).

To assess whether heterogeneity in CyPhyGel stiffness was sustained over time, stiffness was measured 6 days after sequential illumination, which corresponds to the duration of an experiment. The two areas with different stiffness were still clearly distinguishable (**Figure 2E**). The slight increase in stiffness in the soft area over 6 days is due to exposure to external light during CyPhyGel handling and cell culture procedures (**Supplementary Figure S2**).

Cell Area Analysis

One adaptation of fibroblasts to matrix stiffness is the extent of cell spreading, quantified by cell area (Herum et al., 2017). We cultured human primary atrial fibroblasts on CyPhyGels

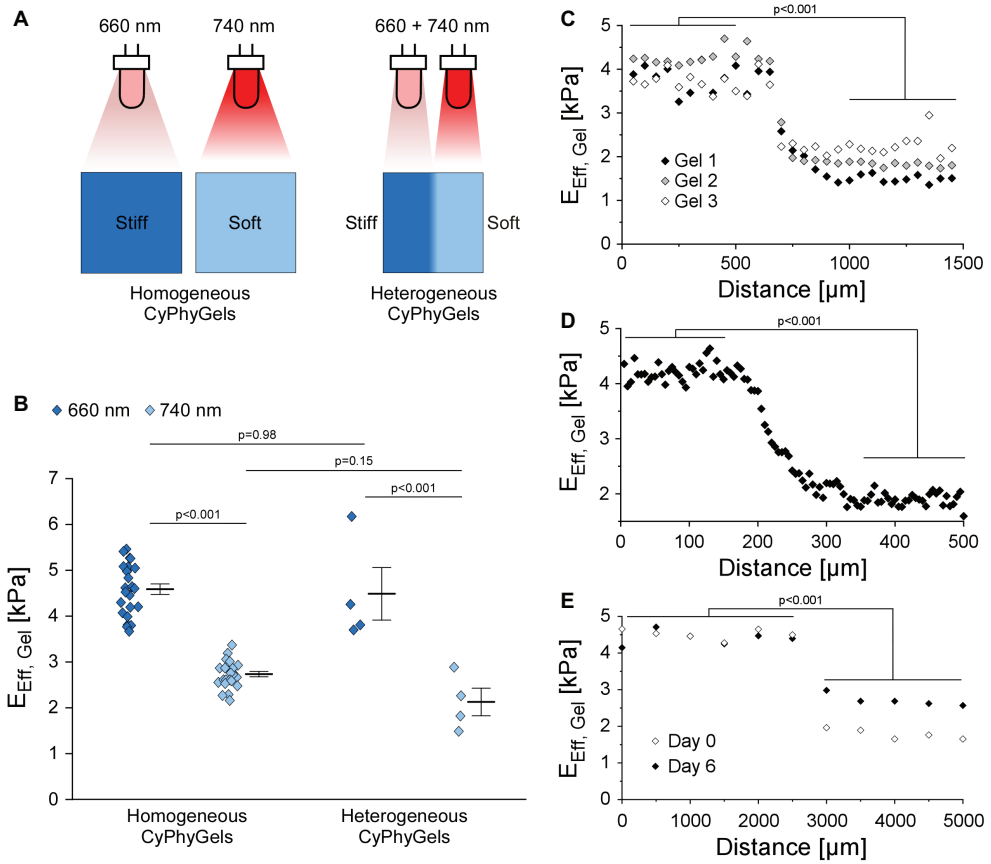

FIGURE 2 | Mechanical properties of CyPhyGels. **(A)** Schematic representation of CyPhyGel configurations used in this experiment. **(B)** E_{Eff} of CyPhyGels, exposed to homogeneous illumination with either 660 or 740 nm (n = 24) or sequentially illuminated and thus mechanically heterogeneous (n = 4), was determined by nanoindentation. **(C)** E_{Eff} along an axis perpendicular to the border between stiff and soft halves of three representative heterogeneous CyPhyGels, illustrating the step-change in gel stiffness (50 µm distance between consecutive measurement points, n = 3). **(D)** Higher resolution assessment of the transition area in Gel 3 from panel C (5 µm distance between measurement points). **(E)** E_{Eff} of Gel 3 from panel C immediately after illumination (Day 0) and 6 days later, corresponding to the duration of an experiment.

that were tuned to homogeneously stiff, homogeneously soft, or heterogeneous states. While fibroblasts on the stiff CyPhyGels had an average cell area of 6,351 ± 349 µm^2, the area of fibroblasts on the soft CyPhyGels was 4,398 ± 293 µm^2 (**Figure 3B**).

There was no significant difference in cell area occupied by fibroblasts grown on the stiff *versus* the soft half of heterogeneous CyPhyGels (6,563 ± 494 µm^2 on the stiff half; 6,451 ± 440 µm^2 on the soft half, **Figure 3B**). Further, we cultured fibroblasts on CyPhyGels of the same stiffness and area as the two halves of heterogeneous CyPhyGels. These were illuminated homogeneously and one stiff and one soft CyPhyGel were placed next to each other with a separation of 1 mm (**Figure 3A**, hereafter referred to as separated CyPhyGels). In this setting, the area of cells on the stiff CyPhyGel was higher than those on a soft CyPhyGel (6,306 ± 446 µm^2 compared to 4,149 ± 251 µm^2, **Figure 3B**). Representative images of plasma membrane-stained fibroblasts in all conditions are shown in **Figure 3C**.

Cell Stiffness Analysis

Human primary atrial fibroblasts, cultured on stiff CyPhyGels, were stiffer (1.09 ± 0.15 kPa) than those grown on soft CyPhyGels (0.50 ± 0.06 kPa, **Figure 4A**). Fibroblasts, cultured on heterogeneous CyPhyGels, showed no significant difference in cell stiffness between stiff (0.49 ± 0.05 kPa) and soft areas (0.46 ± 0.05 kPa, **Figure 4A**). When cultured on separated CyPhyGels, fibroblast stiffness was not different from that on heterogeneous CyPhyGels with 0.47 ± 0.06 kPa on the stiff and 0.45 ± 0.07 kPa on the soft CyPhyGel (**Figure 4A**). The higher cell stiffness on homogeneously stiff CyPhyGels was not a result of higher αSMA expression levels (**Supplementary Figure S4**).

To assess any possible contribution of the mechanical properties of the CyPhyGel on cell stiffness measurements, we acutely reversed CyPhyGel stiffness. Switching CyPhyGels from stiff to soft state and *vice versa* takes less than 1 min (**Supplementary Figure S5**). Cells, grown on a homogeneously stiff CyPhyGel, were assessed before and after switching the CyPhyGel to its soft state, and *vice versa*. Cell stiffness before and after switching did not differ significantly, neither for cells initially cultured on stiff (0.99 ± 0.30 kPa before *versus* 1.17 ± 0.46 kPa after acute stiffness reversal) or soft CyPhyGels (0.74 ± 0.16 kPa before *versus* 0.73 ± 0.18 kPa after stiffness reversal, **Figure 4B**).

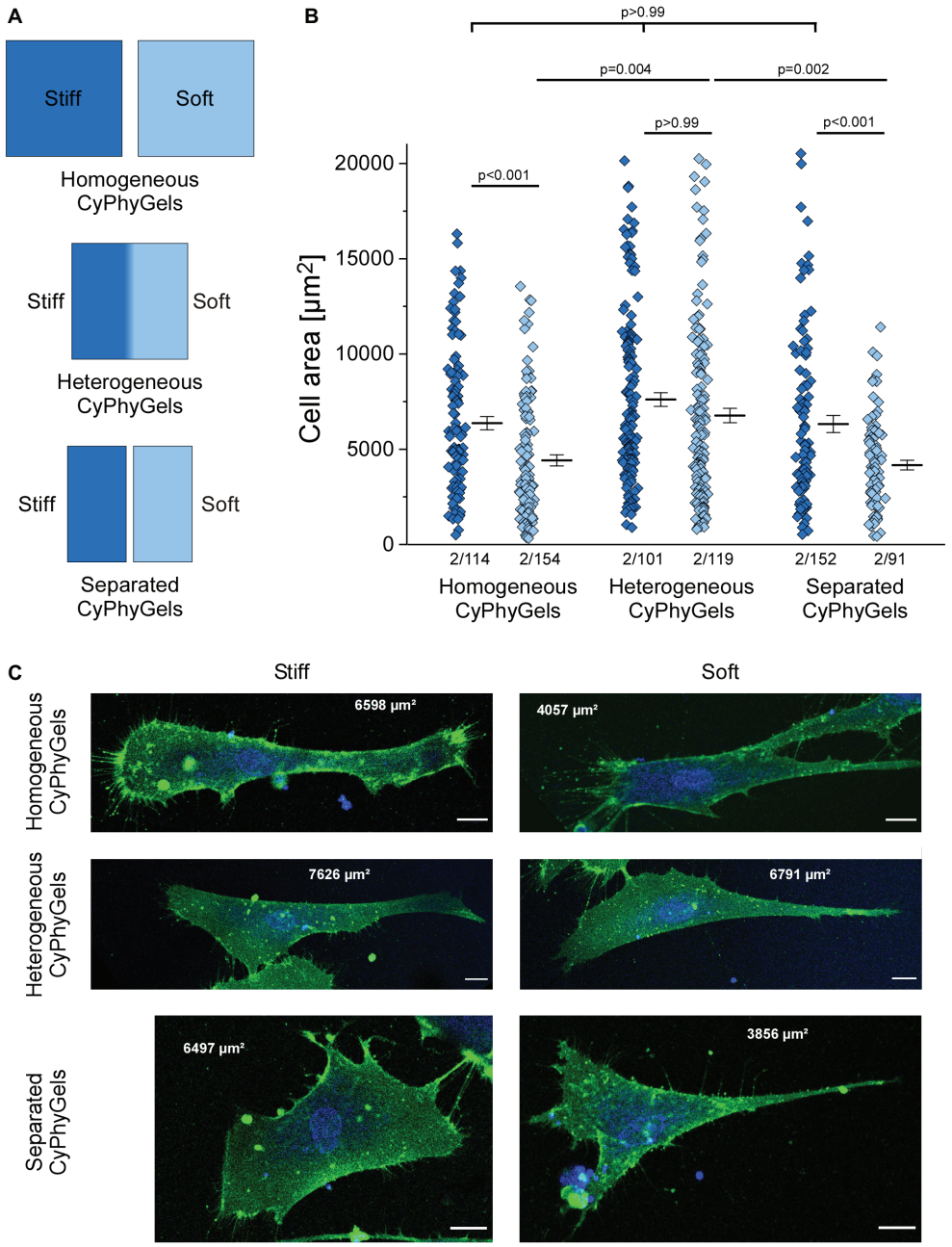

FIGURE 3 | Area of human primary atrial fibroblasts after 4 days of culture on CyPhyGels in different configurations. **(A)** Schematic presentation of CyPhyGels used for the experiments in **Figures 3, 4**. **(B)** Fibroblasts grown on homogeneously soft CyPhyGels spread less than those grown on homogeneously stiff CyPhyGels. The same applies to separated CyPhyGels, while no difference was found among fibroblasts grown on heterogeneous CyPhyGels (Number of patients/number of cells). **(C)** Representative images of fibroblasts on different CyPhyGels. Green = cell membrane. Blue = nuclear counterstain. Scale bars = 20 µm (Number of patients/number of cells).

DISCUSSION

Cardiac fibrosis is a multifactorial process accompanying most cardiac malfunctions, and it increases with age. It is characterized by extensive accumulation of ECM proteins, as well as differentiation of fibroblasts into myofibroblasts, both adding to changes in tissue mechanics. Many studies in the past have addressed the questions of how cells sense and respond to the mechanics of their environment. These studies are usually based on model systems in which cells are cultured on substrates with homogeneous mechanical properties.

In this study, we used a novel hydrogel system, which allows one to dynamically change substrate stiffness by illumination with either 660 nm or 740 nm light. We show that CyPhyGel stiffness (E_{Eff}) can be changed between ~4.6 and ~2.7 kPa, in line with previous results by Hörner et al. (2019b). We confirm

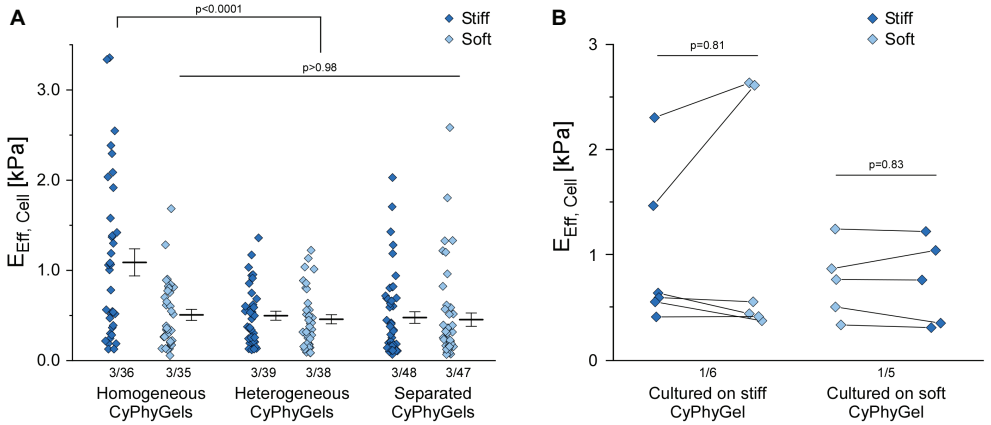

FIGURE 4 | Stiffness of human primary atrial fibroblasts grown on CyPhyGels. **(A)** Fibroblasts grown on homogeneously stiff CyPhyGels are stiffer than those grown on soft CyPhyGels. When cultured on heterogeneous or separated CyPhyGels, fibroblast stiffness is not different from that of fibroblasts on homogeneously soft CyPhyGels. **(B)** E_{Eff} of 11 cells was determined before and after an acute change of CyPhyGel stiffness. No systematic difference in recorded cell stiffness was found (Number of patients/number of cells).

the utility of CyPhyGels in experimental conditions involving the cell culture of human primary atrial fibroblasts.

The light-induced stiffness difference is biologically relevant, as we found human primary atrial fibroblasts adapt to the higher substrate stiffness with increased cell area and stiffness. For healthy cardiac tissue, elastic moduli from 5 to 20 kPa have been described, while under pathologic conditions, the elastic modulus of the tissue changes dynamically. During the inflammatory phase following myocardial infarction, tissue stiffness in the infarct area is decreased due to collagen degradation and death of cardiomyocytes. This is followed by massive collagen deposition over weeks leading to an increase in tissue stiffness to more than 55 kPa, depending on species, form of fibrosis, and duration of tissue remodeling (Holmes et al., 2005; Berry et al., 2006; Gluck et al., 2017; Farré et al., 2018). In contrast, the elastic modulus of *in vitro* mouse fibroblast spheroids was determined to be in the range of 0.5–3.5 kPa (Jorgenson et al., 2017). Thus, there are significant differences between the relevant stiffness ranges for *in vivo* and *in vitro* systems, and the here presented CyPhyGels have a relevant dynamic range.

In this study, fibroblasts were also cultured on CyPhyGels with heterogeneous stiffness. The stiffnesses of the two sides of heterogeneous CyPhyGels were the same as for homogeneously illuminated CyPhyGels. The boundary between stiff and soft halves was well defined, confined to ~150 µm, i.e., on a par with the size of one or two cultured fibroblasts.

While fibroblasts on homogeneous CyPhyGels adapt to their culture substrate with higher cell area and stiffness than those on the stiff CyPhyGel, such adaptation was not present on heterogeneous CyPhyGels. In terms of cell area, the fibroblasts on heterogeneous CyPhyGels are as large as fibroblasts on homogeneously stiff CyPhyGels, while cell stiffness resembles that of fibroblasts on homogeneously soft CyPhyGels. To figure out whether this effect was mediated by direct cell–cell contact or *via* secreted mediators, we performed the same experiments with a physical separation of 1 mm between the stiff and the soft CyPhyGel. In this setting, fibroblasts were not able to directly contact each other, while secretory mediators were transmitted *via* the culture medium. Surprisingly, we found an adaptation of cell area to matrix stiffness on separated CyPhyGels, while cell stiffness was still the same as on homogeneously soft CyPhyGels. Our results suggest that the adaptation of cell spreading and cell stiffness in response to matrix stiffness are regulated by distinct mechanisms, where cell spreading can be modulated by cell-cell contact, while cell stiffness can be modulated by paracrine mediators. Several secreted factors, including transforming growth factor β, angiotensin and interleukins, have been described to play a role in cardiac fibrosis by upregulating collagen production or driving myofibroblast differentiation (Wang et al., 2016; Zhang et al., 2016; Khalil et al., 2017; Schafer et al., 2017; Kuragano et al., 2018). On the other hand, anti-fibrotic effects have been described for conditioned medium from bone marrow-derived stem cells and cardiac progenitor cells and may involve secreted growth factors and/or microRNAs (Kishore et al., 2013; Fang et al., 2016). Further experiments will be necessary to identify the mechanisms responsible for the effects observed in this study.

The higher cell area and stiffness observed on stiffer substrates can be interpreted as indicative of differentiation toward a myofibroblastic phenotype. However, we did not find a higher proportion of fibroblasts expressing the myofibroblast indicator αSMA on stiff CyPhyGels. This might be explained by a potential pre-activation of fibroblasts during their culture time on plastic and the low range of stiffnesses that is covered by CyPhyGels. Current literature on mechanical control of fibroblast phenoconversion usually utilizes larger stiffness differences (Sunyer et al., 2012; Herum et al., 2017), which might trigger increased αSMA expression more efficiently. Also, there are some discrepancies regarding the regulation of αSMA expression response to matrix stiffness. While usually αSMA is thought to be upregulated with higher matrix stiffness, the opposite was also shown for human

valve interstitial fibroblasts (Mabry et al., 2015). This, in line with our results, indicates that the regulation of fibrotic events in response to matrix stiffness is highly complex and involves many factors. Distinct phenotypic properties seem to be regulated by different stimuli. Future work will assess, for example, how culturing on plastic may affect mechanosensing in fibroblasts. All in all, more studies will be required to integrate the results described here with previous knowledge on fibrotic mechanisms gathered from mechanically invariable substrates.

CyPhyGels, by enabling spatial and temporal alterations in the stiffness of the growth substrate, will aid the design and implementation of improved experimental models for studying the basic mechanisms underlying fibrosis. We show that fibroblasts can be grown on CyPhyGels of different stiffness, and that they sense and respond to the stiffness changes that can be imparted by CyPhyGels. Further studies will assess the speed at which cells respond to stiffness changes, explore whether fibrosis can be reversed by altering substrate stiffness, and whether mechanical memory plays a role in fibrosis.

CONCLUSION

We present a novel *in vitro* model suitable for the study of dynamic biological responses to local and temporal changes in matrix stiffness. This model will be used to shed light on mechanisms of communication between cells in differing mechanical microenvironments, for example to mimic fibrotic or scarred myocardium. Our results indicate that cardiac fibroblast adaptations to mechanical properties of the growth matrix may be able to be tuned *via* paracrine factors as well as direct cell-cell contact.

DATA AVAILABILITY STATEMENT

The datasets generated for this study are available on request to the corresponding author.

ETHICS STATEMENT

The studies involving human participants were reviewed and approved by Ethics Commission of the University of Freiburg, Freiburg, Germany (reference: 393/16: 214/18). The patients/participants provided their written informed consent to participate in this study.

AUTHOR CONTRIBUTIONS

PK, RP, CZ-J, UR, and RE contributed to the conception and design of the study. MH and WW developed the CyPhyGels and supported its experimental application. FB and BR provided access to surgical tissue samples. RE performed and analyzed the experiments. RE, CZ-J, and RP drafted the manuscript. All authors contributed to manuscript revision, read and approved the submitted version.

FUNDING

This research was supported by the European Research Council (Advanced Grant CardioNECT, Project ID: #323099, PK), a research grant from the Ministry of Science, Research and Arts Baden-Württemberg (MWK-BW Sonderlinie Medizin, #3091311631) and the German Research Foundation (DFG) under the Excellence Strategy (CIBSS-EXC-2189-Project ID 390939984).

ACKNOWLEDGMENTS

The authors thank the Department for Cardiovascular Surgery of the University Heart Centre Freiburg - Bad Krozingen, and the CardioVascular BioBank Freiburg for providing access to human atrial tissue. Special thanks for technical support go to Kristina Kollmar, Cinthia Buchmann, Pia Iaconianni, and Gabriele Lechner.

Imaging data was obtained at the microscopy facility SCI-MED (Super-Resolution Confocal/Multiphoton Imaging for Multiparametric Experimental Designs, Institute for Experimental Cardiovascular Medicine, Freiburg). The authors would like to thank head of SCI-MED Dr Josef Madl for expert supporting in image acquisition and analysis.

SUPPLEMENTARY MATERIAL

The Supplementary Material for this article can be found online at: https://www.frontiersin.org/articles/10.3389/fphys.2019.01526/full#supplementary-material

SUPPLEMENTARY FIGURE S1 | After preparation, CyPhyGels were stored in PBS at room temperature in darkness. Their stiffness in response to 660 or 740 nm illumination was determined over 40 days after preparation. After 1 week, CyPhyGel stiffness is reversibly tunable between ~3 and ~5 kPa for at least 40 days ($n = 3$).

SUPPLEMENTARY FIGURE S2 | E_{Eff} of CyPhyGels exposed to different light regimes. When exposed to green background light only, soft-tuned CyPhyGels stayed soft for at least 1 h. Exposure to white light (e.g. microscope or room light, >10 mW/cm^2) resulted in complete stiffening of the CyPhyGel within 10 min. Filtering the microscope light using a 490 ± 5 nm band pass filter (final light intensity ~0.05 mW/cm^2), minimized the stiffening for at least 1 h. All experiments were performed under green background light.

SUPPLEMENTARY FIGURE S3 | 2D mapping of E_{Eff} of a heterogeneous CyPhyGel in a squared area of 1 mm × 1 mm, including the border zone, measured with a step size of 50 μm. The left part of the mapped area is stiffer than the right part. The border zone is well delineated and about 100–150 μm wide.

SUPPLEMENTARY FIGURE S4 | αSMA expression in human primary atrial fibroblasts cultured on different CyPhyGels. **(A)** Fibroblasts were fixed in 4% paraformaldehyde and immunostained for αSMA after 4 days in culture on CyPhyGels in different configurations. Red = αSMA. Blue = nuclear counterstain. Scale bars = 150 μm. **(B)** αSMA-positive cells of two patients were determined as percentage of total cells after applying the same intensity threshold to all images.

SUPPLEMENTARY FIGURE S5 | Kinetics of CyPhyGel stiffness switch in response to changed illumination. At 50 s, the illumination was switched from 660 to 740 nm or *vice versa*. As controls, CyPhyGels were constantly illuminated with either of the two respective wavelengths. All illuminations were performed at 1 mW/cm^2.

REFERENCES

Berry, M. F., Engler, A. J., Joseph Woo, Y., Pirolli, T. J., Bish, L. T., Jayasankar, V., et al. (2006). Mesenchymal stem cell injection after myocardial infarction improves myocardial compliance. *Am. J. Phys. Heart Circ. Phys.* 290, H2196–H2203. doi: 10.1152/ajpheart.01017.2005

Chen, J. (2014). Nanobiomechanics of living cells: a review. *Interface Focus* 4:20130055. doi: 10.1098/rsfs.2013.0055

Disertori, M., Rigoni, M., Pace, N., Casolo, G., Masè, M., Gonzini, L., et al. (2016). Myocardial fibrosis assessment by LGE is a powerful predictor of ventricular tachyarrhythmias in ischemic and nonischemic LV dysfunction: a meta-analysis. *JACC Cardiovasc. Imaging* 9, 1046–1055. doi: 10.1016/J.JCMG.2016.01.033

Fang, F., Huang, R.-L., Zheng, Y., Liu, M., and Huo, R. (2016). Bone marrow derived mesenchymal stem cells inhibit the proliferative and profibrotic phenotype of hypertrophic scar fibroblasts and keloid fibroblasts through paracrine signaling. *J. Dermatol. Sci.* 83, 95–105. doi: 10.1016/J.JDERMSCI.2016.03.003

Farré, N., Jorba, I., Torres, M., Falcones, B., Martí-Almor, J., Farré, R., et al. (2018). Passive stiffness of left ventricular myocardial tissue is reduced by ovariectomy in a post-menopause mouse model. *Front. Physiol.* 9:1545. doi: 10.3389/fphys.2018.01545

Gluck, J. M., Herren, A. W., Yechikov, S., Kao, H. K. J., Khan, A., Phinney, B. S., et al. (2017). Biochemical and biomechanical properties of the pacemaking sinoatrial node extracellular matrix are distinct from contractile left ventricular matrix. *PLoS One* 12:e0185125. doi: 10.1371/journal.pone.0185125

Guz, N., Dokukin, M., Kalaparthi, V., and Sokolov, I. (2014). If cell mechanics can be described by elastic modulus: study of different models and probes used in indentation experiments. *Biophys. J.* 107, 564–575. doi: 10.1016/J.BPJ.2014.06.033

Hartman, C. D., Isenberg, B. C., Chua, S. G., and Wong, J. Y. (2017). Extracellular matrix type modulates cell migration on mechanical gradients. *Exp. Cell Res.* 359, 361–366. doi: 10.1016/J.YEXCR.2017.08.018

Hertz, H. (1881). Uber Die Beruhrung Fester Elastischer Korper (on the contact of elastic solids). *J. Reine Angew. Math.* 92, 156–171.

Herum, K. M., Choppe, J., Kumar, A., Engler, A. J., and McCulloch, A. D. (2017). Mechanical regulation of cardiac fibroblast profibrotic phenotypes. *Mol. Biol. Cell* 28, 1871–1882. doi: 10.1091/mbc.E17-01-0014

Hinz, B. (2013). Matrix mechanics and regulation of the fibroblast phenotype. *Periodontol.* 63, 14–28. doi: 10.1111/prd.12030

Holmes, J. W., Borg, T. K., and Covell, J. W. (2005). Structure and mechanics of healing myocardial infarcts. *Annu. Rev. Biomed. Eng.* 7, 223–253. doi: 10.1146/annurev.bioeng.7.060804.100453

Hörner, M., Gerhardt, K., Salavei, P., Hoess, P., Härrer, D., Kaiser, J., et al. (2019a). Production of phytochromes by high-cell-density *E. coli* fermentation. *ACS Synth. Biol.* 8, 2442–2450. doi: 10.1021/acssynbio.9b00267

Hörner, M., Raute, K., Hummel, B., Madl, J., Creusen, G., Thomas, O. S., et al. (2019b). Phytochrome-based extracellular matrix with reversibly tunable mechanical properties. *Adv. Mater.* 31:1806727. doi: 10.1002/adma.201806727

Jorgenson, A. J., Choi, K. M., Sicard, D., Smith, K. M. J., Hiemer, S. E., Varelas, X., et al. (2017). TAZ activation drives fibroblast spheroid growth, expression of profibrotic paracrine signals, and context-dependent ECM gene expression. *Am. J. Phys. Cell Phys.* 312, C277–C285. doi: 10.1152/ajpcell.00205.2016

Khalil, H., Kanisicak, O., Prasad, V., Correll, R. N., Fu, X., Schips, T., et al. (2017). Fibroblast-specific TGF-B–Smad2/3 signaling underlies cardiac fibrosis. *J. Clin. Invest.* 127, 3770–3783. doi: 10.1172/JCI94753

Kishore, R., Verma, S. K., Mackie, A. R., Vaughan, E. E., Abramova, T. V., Aiko, I., et al. (2013). Bone marrow progenitor cell therapy-mediated paracrine regulation of cardiac MiRNA-155 modulates fibrotic response in diabetic hearts. *PLoS One* 8:e60161. doi: 10.1371/journal.pone.0060161

Kuragano, M., Uyeda, T. Q. P., Kamijo, K., Murakami, Y., and Takahashi, M. (2018). Different contributions of nonmuscle myosin IIA and IIB to the organization of stress fiber subtypes in fibroblasts. *Mol. Biol. Cell* 29, 911–922. doi: 10.1091/mbc.E17-04-0215

Levental, I., Levental, K. R., Klein, E. A., Assoian, R., Miller, R. T., Wells, R. G., et al. (2010). A simple indentation device for measuring micrometer-scale tissue stiffness. *J. Phys. Condens. Matter* 22:194120. doi: 10.1088/0953-8984/22/19/194120

Li, X., Sun, Q., Li, Q., Kawazoe, N., and Chen, G. (2018). Functional hydrogels with Tunable structures and properties for tissue engineering applications. *Front. Chem.* 6:499. doi: 10.3389/fchem.2018.00499

Mabry, K. M., Lawrence, R. L., and Anseth, K. S. (2015). Dynamic stiffening of poly(ethylene glycol)-based hydrogels to direct valvular interstitial cell phenotype in a three-dimensional environment. *Biomaterials* 49, 47–56. doi: 10.1016/J.BIOMATERIALS.2015.01.047

Manabe, I., Shindo, T., and Nagai, R. (2002). Gene expression in fibroblasts and fibrosis: involvement in cardiac hypertrophy. *Circ. Res.* 91, 1103–1113. Available at: http://www.ncbi.nlm.nih.gov/pubmed/12480810

Nguyen, T. P., and Qu, Z. (2014). Cardiac fibrosis and arrhythmogenesis: the road to repair is paved with perils. *J. Mol. Cell. Cardiol.* 70, 83–91. doi: 10.1016/J.YJMCC.2013.10.018

Ott, H. C., Matthiesen, T. S., Goh, S.-K., Black, L. D., Kren, S. M., Netoff, T. I., et al. (2008). Perfusion-decellularized matrix: using nature's platform to engineer a bioartificial heart. *Nat. Med.* 14, 213–221. doi: 10.1038/nm1684

Perbellini, F., Watson, S. A., Scigliano, M., Alayoubi, S., Tkach, S., Bardi, I., et al. (2018). Investigation of cardiac fibroblasts using myocardial slices. *Cardiovasc. Res.* 114, 77–89. doi: 10.1093/cvr/cvx152

Poulet, C., Unzel, S. K., Uttner, E. B., Lindner, D., Westermann, D., and Ravens, U. (2016). Altered physiological functions and ion currents in atrial fibroblasts from patients with chronic atrial fibrillation. *Physiol. Rep.* 4, pii: e12681. doi: 10.14814/phy2.12681

Rosales, A. M., and Kristi, S. A. (2016). The design of reversible hydrogels to capture extracellular matrix dynamics. *Nat. Rev. Mater.* 1, 15012. doi: 10.1038/natrevmats.2015.12

Schafer, S., Viswanathan, S., Widjaja, A. A., Lim, W.-W., Moreno-Moral, A., DeLaughter, D. M., et al. (2017). IL-11 is a crucial determinant of cardiovascular fibrosis. *Nature* 552, 110–115. doi: 10.1038/nature24676

Sunyer, R., Jin, A. J., Nossal, R., and Sackett, D. L. (2012). Fabrication of hydrogels with steep stiffness gradients for studying cell mechanical response. *PLoS One* 7:e46107. doi: 10.1371/journal.pone.0046107

Tanaka, K., Zlochiver, S., Vikstrom, K. L., Yamazaki, M., Moreno, J., Klos, M., et al. (2007). Spatial distribution of fibrosis governs fibrillation wave dynamics in the posterior left atrium during heart failure. *Circ. Res.* 101, 839–847. doi: 10.1161/CIRCRESAHA.107.153858

Travers, J. G., Kamal, F. A., Robbins, J., Yutzey, K. E., and Blaxall, B. C. (2016). Cardiac fibrosis: the fibroblast awakens. *Circ. Res.* 118, 1021–1040. doi: 10.1161/CIRCRESAHA.115.306565

van Putten, S., Shafieyan, Y., and Hinz, B. (2016). Mechanical control of cardiac myofibroblasts. *J. Mol. Cell. Cardiol.* 93, 133–142. doi: 10.1016/j.yjmcc.2015.11.025

Wang, J.-H., Zhao, L., Pan, X., Chen, N.-N., Chen, J., Gong, Q.-L., et al. (2016). Hypoxia-stimulated cardiac fibroblast production of IL-6 promotes myocardial fibrosis via the TGF-B1 signaling pathway. *Lab. Investig.* 96, 839–852. doi: 10.1038/labinvest.2016.65

Yang, C., DelRio, F. W., Ma, H., Killaars, A. R., Basta, L. P., Kyburz, K. A., et al. (2016). Spatially patterned matrix elasticity directs stem cell fate. *Proc. Natl. Acad. Sci.* 113, E4439–E4445. doi: 10.1073/pnas.1609731113

Zhang, F., Dang, Y., Li, Y., Hao, Q., Li, R., and Qi, X. (2016). Cardiac contractility modulation attenuate myocardial fibrosis by inhibiting TGF-B1/Smad3 signaling pathway in a rabbit model of chronic heart failure. *Cell. Physiol. Biochem.* 39, 294–302. doi: 10.1159/000445624

Conflict of Interest: The authors declare that the research was conducted in the absence of any commercial or financial relationships that could be construed as a potential conflict of interest.

frontiers in Physiology

REVIEW
published: 22 July 2021
doi: 10.3389/fphys.2021.699517

Myogenic Tone in Peripheral Resistance Arteries and Arterioles: The Pressure Is On!

*William F. Jackson**

Department of Pharmacology and Toxicology, College of Osteopathic Medicine, Michigan State University, East Lansing, MI, United States

Resistance arteries and downstream arterioles in the peripheral microcirculation contribute substantially to peripheral vascular resistance, control of blood pressure, the distribution of blood flow to and within tissues, capillary pressure, and microvascular fluid exchange. A hall-mark feature of these vessels is myogenic tone. This pressure-induced, steady-state level of vascular smooth muscle activity maintains arteriolar and resistance artery internal diameter at 50–80% of their maximum passive diameter providing these vessels with the ability to dilate, reducing vascular resistance, and increasing blood flow, or constrict to produce the opposite effect. Despite the central importance of resistance artery and arteriolar myogenic tone in cardiovascular physiology and pathophysiology, our understanding of signaling pathways underlying this key microvascular property remains incomplete. This brief review will present our current understanding of the multiple mechanisms that appear to underlie myogenic tone, including the roles played by G-protein-coupled receptors, a variety of ion channels, and several kinases that have been linked to pressure-induced, steady-state activity of vascular smooth muscle cells (VSMCs) in the wall of resistance arteries and arterioles. Emphasis will be placed on the portions of the signaling pathways underlying myogenic tone for which there is lack of consensus in the literature and areas where our understanding is clearly incomplete.

Keywords: myogenic tone, arterioles, resistance arteries, ion channels, G-proteins, mechanotransduction

OPEN ACCESS

Edited by:
Markus Hecker,
Heidelberg University, Germany

Reviewed by:
Gerald A. Meininger,
University of Missouri, United States
Cor de Wit,
University of Lübeck, Germany
Timothy W. Secomb,
University of Arizona, United States
Christian Aalkjaer,
Aarhus University, Denmark

***Correspondence:**
William F. Jackson
jacks783@msu.edu

Specialty section:
This article was submitted to Vascular Physiology, a section of the journal Frontiers in Physiology

Received: *23 April 2021*
Accepted: *21 June 2021*
Published: *22 July 2021*

Citation:
Jackson WF (2021) Myogenic Tone in Peripheral Resistance Arteries and Arterioles: The Pressure Is On! Front. Physiol. 12:699517. doi: 10.3389/fphys.2021.699517

INTRODUCTION

Myogenic tone is a hall-mark feature of resistance arteries and their downstream arterioles. This pressure-induced contractile activity of vascular smooth muscle contributes substantially to all functions of the resistance vasculature, including maintenance of peripheral vascular resistance, control of blood pressure, distribution of blood flow to and within tissues, and regulation of capillary pressure and microvascular fluid exchange. However, our understanding of the molecular mechanisms responsible for myogenic tone remains incomplete. This review will outline the multiple mechanisms that appear to underlie this key microvascular process, including important roles for G-protein-coupled receptors, multiple ion channels, and several protein kinases emphasizing the portions of the signaling pathways for which there is a lack of consensus.

SETTING THE STAGE

What Are Resistance Arteries and Arterioles?

Resistance arteries are arterial vessels that feed blood flow to the microcirculation and contribute to peripheral vascular resistance (Zweifach and Lipowsky, 1984; Segal, 2000). These small arteries have internal, maximal diameters ranging from 500 to 100 μm and have two or more layers of vascular smooth muscle in their walls. Arterioles are downstream from resistance arteries, usually have internal, maximal diameters less than 100 μm, and importantly, have only a single layer of vascular smooth muscle wrapped circumferentially around the endothelial cell tube that forms the lumen of these microvessels. Another distinguishing characteristic of arterioles is that they are usually embedded within the parenchyma to which they supply blood flow. Arterioles form a branching network of vessels that ultimately provide blood flow to the capillary bed, with 3–5 levels of branching, dependent on the tissue/organ being perfused. The last arterial microvessels with vascular smooth muscle cells (VSMCs) in their walls are termed terminal arterioles which then branch into 1–20 capillaries. As with resistance arteries, arterioles contribute substantially to determination and control of vascular resistance and blood pressure (Renkin, 1984; Zweifach and Lipowsky, 1984; Pries and Secomb, 2011).

In skeletal muscle, for example, resistance arteries contribute about 30–40% of total skeletal muscle vascular resistance (Segal and Duling, 1986; Segal, 2000), with downstream arterioles contributing 50% and capillary and venules contributing the remainder of the hydraulic resistance (Fronek and Zweifach, 1975). Thus, for example, during skeletal muscle contraction, when blood flow can increase 100-fold (Saltin et al., 1998; Mortensen and Saltin, 2014), coordinated vasodilation of arterioles in the microcirculation and upstream resistance arteries is essential for attainment of these massive increases in blood flow (Segal and Duling, 1986; Segal, 2000).

What Are the Myogenic Response and Myogenic Tone?

A step-wise increase in the blood pressure within a resistance artery or arteriole leads to a rapid, pressure-induced increase in vessel diameter as shown in **Figure 1A**. If the pressure is maintained, the smooth muscle in the wall of the vessel will respond, contracting and returning the internal diameter of the vessel to or below its initial diameter (**Figure 1A**). This is the classic myogenic response (Johnson, 1980; Davis and Hill, 1999; Hill et al., 2001; Davis et al., 2011) that was originally described by Bayliss over a century ago (Bayliss, 1902). The steady-state level of contractile activity of the vascular smooth muscle in a pressurized blood vessel is myogenic tone (**Figure 1B**). It should be noted that myogenic tone not only encompasses the steady-state activity of the smooth muscle contractile machinery (actin-myosin cross bridge cycling), but also remodeling of the actin cytoskeleton (Gunst and Zhang, 2008) and alterations in interactions of smooth muscle cells with the extracellular matrix that accompanies maintained vasoconstriction (Martinez-Lemus et al., 2004) or vasodilation (Clifford et al., 2018). An important point is that the time scale for these latter events (remodeling of the actin cytoskeleton and interactions and remodeling of the extracellular matrix) may occur on much longer time scales than simple Ca^{2+}-dependent cross-bridge cycling during maintained levels of myogenic tone.

These two processes, the myogenic response and myogenic tone (**Figure 1**), participate in the blood flow autoregulation in organs, such as the brain (Tuma, 2011), heart (Laughlin et al., 1996; Zhang et al., 2011), kidney (Navar et al., 2011), eye (Riva and Schmetterer, 2011), intestine (Granger et al., 2011), and skeletal muscle (Shepherd, 1983), buffering organ blood flow and capillary pressure in the face of changes in blood pressure (Johnson, 1980; Davis et al., 2011). The myogenic response and myogenic tone also appear to contribute to blood pressure regulation by amplifying vasoconstrictor-induced vasoconstriction (Meininger and Trzeciakowski, 1988, 1990). Myogenic tone offers a resting level of smooth muscle contractile activity such that resistance arteries and arterioles can both dilate and constrict around their resting diameters, maintaining cardiovascular homeostasis (Renkin, 1984; Davis et al., 2011).

Steps Involved in the Myogenic Response Leading to Myogenic Tone

Two questions need to be answered to understand the mechanisms responsible for the myogenic response and myogenic tone: (1) How are changes in luminal pressure sensed by smooth muscle cells in the wall of resistance arteries and arterioles? and (2) How are changes in luminal pressure transduced into vascular smooth muscle contraction and maintained tone in these vessels?

HOW IS PRESSURE SENSED IN RESISTANCE ARTERIES AND ARTERIOLES?

In a resistance artery or arteriole, increased luminal pressure results in a radial force that increases tangential wall stress (tension) as described by the Law of Laplace: tangential wall stress = Pr/Δ, where P is the pressure in the lumen of the vessel, r is the lumen radius, and Δ is the thickness of the vessel wall. The increased wall stress passively dilates the vessel and "stretches" (induces strain in) the smooth muscle cells in the vessel wall. The passive dilation will continue until either, the passive wall tension (due to collagen, elastin, cytoskeletal elements, etc.) matches the pressure-induced tangential wall stress, or the VSMCs actively contract and generate enough active wall stress to overcome the pressure-driven tangential wall stress.

It has been argued that wall strain (change in length) is unlikely to be the main variable sensed in the myogenic response because, for example, arterioles, often constrict to diameters below their starting point with step increases in pressure (Johnson, 1980; Carlson and Secomb, 2005). However, cytoskeletal remodeling appears to occur coincident and in parallel with, smooth muscle contraction and relaxation such

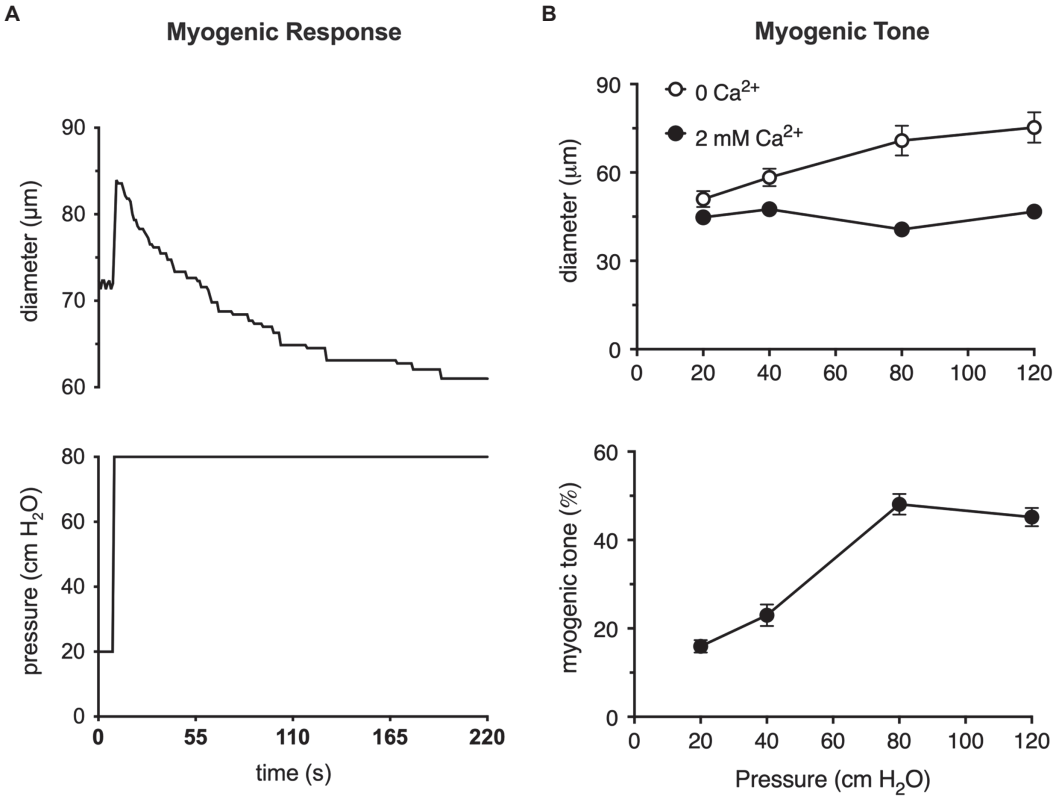

FIGURE 1 | The myogenic response and myogenic tone in arterioles. **(A)** Myogenic response in a cannulated hamster cremaster arteriole, *ex vivo*, prepared as described (Westcott and Jackson, 2011). Shown in the upper panel is a digitized diameter record of the response of a second-order cremaster arteriole to a step-increase in luminal pressure from 20 to 80 cm H_2O as depicted in the lower panel. At the onset of the pressure step, arteriolar diameter increases due to passive distention of the vessel. As the smooth muscle responds and begins to contract, diameter recovers to a new steady-state diameter that is slightly less than the diameter at 20 cm H_2O. This behavior is the myogenic response. **(B)** Myogenic tone in cannulated hamster cremaster arterioles. Top panel shows the steady-state diameters of arterioles at different pressures in the absence of extracellular Ca^{2+} (passive) and presence of 2 mM Ca^{2+} (active). Bottom panel shows the % myogenic tone at the given pressures computed from the data in the top panel as myogenic tone = (passive diameter–active diameter)/passive diameter × 100%. At pressures greater than 20 cm H_2O, arterioles develop significant myogenic tone (i.e., steady-state pressure-induced constriction). Data in **(A)** are replotted from Jackson (2012), with permission. Data in **(B)** are replotted from Westcott and Jackson, (2011) and Jackson, (2012), with permission.

that cell "length" is not a constant (Gunst and Zhang, 2008). Thus, whether it is stress or strain that is sensed in the vessel wall remains to be clarified (Hill and Meininger, 1994; Davis and Hill, 1999; Hill et al., 2001; Davis et al., 2011). Nonetheless, several mechanisms have been proposed to act as sensors during the myogenic response leading up to steady-state myogenic tone including: several G-protein coupled receptors (Brayden et al., 2013; Schleifenbaum et al., 2014; Storch et al., 2015; Kauffenstein et al., 2016; Mederos et al., 2016; Hong et al., 2017; Pires et al., 2017; Chennupati et al., 2019), several cation channels (Welsh et al., 2002; Jernigan and Drummond, 2005; Gannon et al., 2008; VanLandingham et al., 2009; Nemeth et al., 2020), integrins (Davis et al., 2001; Martinez-Lemus et al., 2005; Colinas et al., 2015), matrix metalloproteinases (MMPs), and epidermal growth factor receptors (EGFR; Lucchesi et al., 2004; Amin et al., 2011); and membrane-bound tumor necrosis factor α (mTNFα), TNFα receptor (TNFR), and downstream sphingosine-1-phosphate (S1P) signaling (Kroetsch et al., 2017; **Figure 2**). What remains unclear is what determines which of these putative mechanosensitive elements are expressed in a particular blood vessel and how this expression is controlled under different physiological and pathological conditions. It is also not clear whether the different potential mechanosensitive elements represent independent "sensors" or whether some are linked together. For example, while there is evidence that TRPC6 channels are mechanosensitive and could serve as independent sensors of pressure-induced stress/strain in vascular smooth muscle (Spassova et al., 2006), it is also quite clear that these channels lie downstream from mechanosensitive G-protein coupled receptors, like the angiotensin II type 1 receptors (AT1R) that appear to mediate myogenic reactivity in rodent cerebral resistance arteries (Gonzales et al., 2014). Another example is the potential link between G-protein coupled receptors, such as the AT1R and the EGFR. There is considerable evidence for transactivation of the EGFR and its downstream targets upon activation of AT1R by angiotensin II (Forrester et al., 2016). Thus, it seems likely that mechanical activation of AT1R would do the same and may reconcile studies identifying EGFR as a key component of myogenic signaling in coronary artery vascular smooth muscle

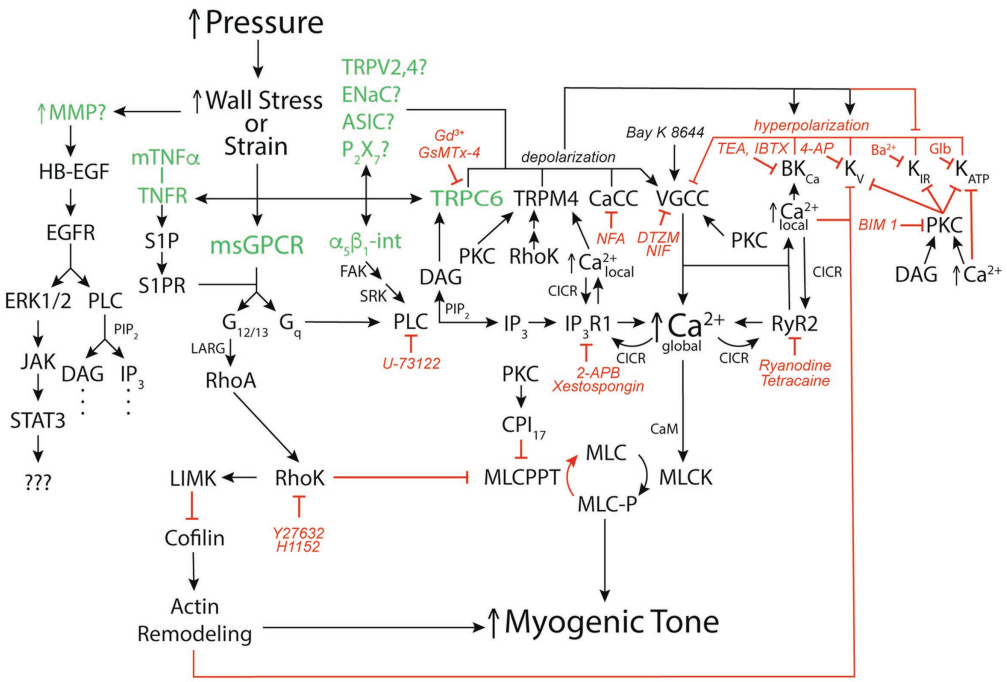

FIGURE 2 | Signaling pathways for pressure-induced myogenic tone. Schematic diagram of reported signaling pathways involved in myogenic tone in resistance arteries and arterioles. Green font color depicts putative mechanosensors in pressure-induced myogenic tone. Black arrows show stimulation, increases or activation of signaling molecules, ion channels, or enzymes that participate in myogenic tone. Red capped lines indicate inhibition, decreases or deactivation of signaling molecules, ion channels, or enzymes involved in myogenic tone. Also shown are pharmacological agents that we have used to interrogate the ion channels and signaling pathways in arteriolar myogenic tone. MMP, matrix metalloproteinase; HB-EGF, heparin-bound epidermal growth factor; EGFR, epidermal growth factor receptor; ERK1/2, extracellular-signal-related kinases 1 or 2; JAK, janus kinase; STAT3, signal transducer and activator of transcription 3; mTNFα, membrane-bound tumor necrosis factor α; TNFR, TNFα Receptor; S1P, sphingosine-1-phosphate; S1PR, S1P receptor; $\alpha_5\beta_1$-int, $\alpha_5\beta_1$ integrin: FAK, focal adhesion kinase; SRK, Src-related kinases; CaCC, Ca^{2+}-activated Cl^- channel; TRPV2,4, transient receptor potential vanilloid-family 2 or 4 channels; ENaC, epithelial Na^+ channel; ASIC, acid sensing ion channel; P_2X_7, P_2X_7 purinergic receptor; VGCC, voltage-gated Ca^{2+} channel; BK_{Ca}, large-conductance Ca^{2+}-activated K^+ channel; K_V, voltage-gated K^+ channel; K_{IR}, inwardly-rectifying K^+ channel; K_{ATP}, ATP-sensitive K^+ channel; msGPCR, mechanosensitive G-protein-coupled receptor; DAG, diacylglycerol; PKC, protein kinase C; NFA, niflumic acid; DTZM, diltiazem; NIF, nifedipine; TEA, tetraethylammonium; IBTX, iberiotoxin; 4-AP, 4-aminopyridine; GLIB, glibenclamide; BIM I, bisindolylmaleimide I; PLC, phospholipase C; PIP_2, phosphatidylinositol bisphosphate; IP_3, inositol, 1,4,5 trisphosphate; IP_3R1, IP_3 receptor 1; RyR, ryanodine receptor; CICR, Ca^{2+}-induced-Ca^{2+} release; LARG, guanine nucleotide exchange factor LARG; RhoA, small G-protein Rho; 2-APB, 2-Aminoethoxydiphenyl borate; RhoK. Rho kinase; LIMK, LIM kinase; CPI_{17}, C-kinase potentiated protein phosphatase-1 Inhibitor; MLCPPT, myosin light-chain phosphatase; MCL, myosin light-chain; MLCK, myosin light-chain kinase; See text for more details and references.

(Lucchesi et al., 2004; Amin et al., 2011) with studies identifying AT1R as the key mechanosensor in myogenic tone (Mederos y Schnitzler et al., 2008; Yasuda et al., 2008; Storch et al., 2012; Gonzales et al., 2014; Mederos et al., 2016; Hong et al., 2017; Pires et al., 2017). However, it is not clear how signaling downstream from the EGFR involving extracellular signal-related kinases 1 and 2 (ERK1/2), janus kinase (JAK), and signal transducer and activator of transcription 3 (STAT3; Amin et al., 2011) fits into the overall scheme of myogenic tone. Similarly, while a role for mTNFα, its receptor and downstream S1P have been proposed to mediate myogenic tone (Peter et al., 2008; Lidington et al., 2009; Yang et al., 2012; Hui et al., 2015; Yagi et al., 2015; Sauve et al., 2016; Kroetsch et al., 2017), it is not clear how this mechanism "fits" with the bulk of data supporting membrane depolarization and activation of voltage-gated Ca^{2+} channels (VGCCs) as the fundamental basis for myogenic tone. Certainly, activation of PLCγ is a potential downstream signal in the S1P-pathway feeding into the same signaling pathway that has been proposed for AT1R, for example Gonzales et al. (2014). In addition, S1P signaling reportedly can lie downstream from the AT1R (Wilson et al., 2015). Unfortunately, few investigators have tried to perform critical tests of alternative hypotheses for all the proposed mechanisms underlying myogenic tone to try and sort out which mechanisms are functional in a particular blood vessel. In addition, most investigators tend to focus on single or at most a few blood vessels such that the generality of proposed mechanisms remains unclear and will require additional research. Investigators are encouraged to explore multiple mechanisms in arteries/arterioles from different vascular beds so that patterns can be better assessed.

Finally, it is not yet known exactly how membrane proteins are activated by increases in membrane stress or strain. Based on studies in other systems, membrane-bound proteins may be activated or altered by forces transmitted *via* connections with the extracellular matrix and/or the cytoskeleton, by changes in membrane curvature and/or by membrane thinning-induced protein conformational changes (Leiphart et al., 2019).

How Are Changes in Luminal Pressure Transduced Into Myogenic Tone?

Regardless of the precipitating mechanisms, *in vitro*, pressure myography studies have repeatedly shown that pressure-induced myogenic tone involves vascular smooth muscle membrane depolarization, activation of VGCCs, and an increase in intracellular Ca^{2+} (Harder, 1984; Knot and Nelson, 1998; Kotecha and Hill, 2005; **Figure 2**). As will be discussed in a subsequent section, there also may be activation of the small G-protein RhoA and the Rho kinase pathway which induces Ca^{2+} sensitization (Lagaud et al., 2002; Moreno-Dominguez et al., 2013) and Rho-kinase (Moreno-Dominguez et al., 2013) or protein kinase C (PKC)-dependent remodeling of the actin cytoskeleton (Moreno-Dominguez et al., 2013; Hong et al., 2016) that also can contribute to myogenic tone (**Figure 2**).

Which Ion Channels Contribute to Pressure-Induced Membrane Depolarization?

A number of ion channels have been proposed to contribute to pressure-induced depolarization of VSMCs (Harder, 1984; Knot and Nelson, 1998; Kotecha and Hill, 2005) including: members of the transient receptor potential (TRP)-family of cation channels, such as TRPC6 (Welsh et al., 2002; Gonzales et al., 2014), TRPM4 (Earley et al., 2004; Gonzales et al., 2014), TRPV2 (McGahon et al., 2016), and TRPV4 (Soni et al., 2017); members of the degenerin family of channels including the epithelial Na^+ channel (ENaC) family (Jernigan and Drummond, 2005, 2006; VanLandingham et al., 2009; Drummond and Stec, 2015), the acid-sensitive ion channel (ASIC) family of channels (Gannon et al., 2015), and purinergic P_2X_7 Purinergic Receptor (P_2X_7) channels (Kauffenstein et al., 2016; **Figure 2**). In addition, Ca^{2+}-activated Cl^- channels (CaCC; ANO1/TMEM16A) may be activated by Ca^{2+} influx through TRPC6 channels (Bulley et al., 2012; Wang et al., 2016) and also contribute to pressure-induced depolarization of VSMCs (**Figure 2**). Finally, the activity of several K^+ channels may be inhibited by either the membrane depolarization [inwardly-rectifying K^+ channel (K_{IR}) channels], increases in intracellular Ca^{2+} [voltage-gated K^+ channel (K_V) and ATP-sensitive K^+ channel (K_{ATP}) channels], or increased activity of kinases such as protein kinase C (K_V and K_{ATP} channels) and Rho kinase (K_V channels) and indirectly contribute to pressure-induced depolarization (Tykocki et al., 2017; **Figure 2**). As for other aspects of myogenic tone, there appears to be vascular bed- and, perhaps, species-dependent differences in the ion channels that participate in pressure-induced depolarization making generalizations difficult. Our understanding of the mechanisms responsible for this heterogeneity is lacking.

What Activates the Ion Channels Responsible for Pressure-Induced Depolarization?

The answer to this question remains incomplete. In cerebral resistance arteries, TRPC6 and TRPM4 appear to be activated indirectly (Gonzales et al., 2014), likely downstream from pressure-induced activation of AT1R and phospholipase Cγ (PLCγ; Gonzales et al., 2014) with diacylglycerol (DAG) from hydrolysis of membrane phosphatidyl-inositol-bis-phosphate (PIP_2) activating TRPC6 and Ca^{2+} from Ca^{2+}- and IP_3-induced release of Ca^{2+} through IP_3 receptor (IP_3R) activating TRPM4 (Gonzales et al., 2014; **Figure 2**). In cerebral penetrating arterioles, Rho kinase may be involved in the activation of TRPM4 by setting its Ca^{2+} sensitivity (Li and Brayden, 2017; **Figure 2**). However, not all blood vessels appear to require PLC for pressure-induced myogenic tone. For example, we have shown that myogenic tone and global Ca^{2+} levels in hamster cheek pouch arterioles are unaffected by inhibition of PLC and IP_3R, and yet are inhibited by nanomolar concentrations of Gd^{3+} and micromolar concentrations of GsMTX-4, established inhibitors of mechanosensitive ion channels (Jackson and Boerman, 2017). Thus, it is possible that, in cheek pouch arterioles, pressure-induced mechanical activation of TRPC6, for example, directly contributes to membrane depolarization and myogenic tone (**Figure 2**).

Which Ion Channels Contribute to the Negative-Feedback Regulation of Myogenic Tone?

Membrane depolarization in cells that express VGCCs is inherently a positive feedback process that would lead to depolarization approaching the Nernst equilibrium potential for Ca^{2+} (approximately +60 mV) and maximal vasoconstriction if it were not for negative feedback mechanisms that limit membrane depolarization and the activity of VGCCs. In VSMCs, this negative feedback is provided by large-conductance Ca^{2+}-activated K^+ (BK_{Ca}) channels and several voltage-gated K^+ (K_V) channel family members including K_V1.5, 2.1, and 7.X channels (Tykocki et al., 2017; **Figure 2**). The membrane depolarization induced by TRPC6, TRPM4, etc. activates both BK_{Ca} and K_V channels, limiting membrane depolarization (Tykocki et al., 2017; **Figure 2**). The BK_{Ca} channels are also activated by increased Ca^{2+} (Tykocki et al., 2017). In resistance arteries, the source of Ca^{2+} responsible for activation of BK_{Ca} channels is Ca^{2+} sparks released through ryanodine receptors (RyR; Nelson et al., 1995; Westcott and Jackson, 2011; Westcott et al., 2012), whereas in downstream arterioles, BK_{Ca} channels appear to be activated by Ca^{2+} entry through VGCCs and other membrane channels (Guia et al., 1999; Westcott and Jackson, 2011; Westcott et al., 2012; Suzuki et al., 2013; **Figure 2**).

Which Ion Channels Contribute to Pressure-Induced Increases in Global Intracellular Ca^{2+}?

L-type VGCCs composed of CaV1.2 α-pore-forming subunits contribute substantially to pressure-induced myogenic tone that is observed in pressurized resistance arteries and arterioles studied *ex vivo* (Tykocki et al., 2017; **Figure 2**). L-type CaV1.2 VGCCs appear essential for the initiation of the myogenic response because block of these channels prevents the development of myogenic tone (Knot and Nelson, 1998; Kotecha and Hill, 2005). In rat middle cerebral arteries, the

voltage dependence of intracellular Ca^{2+} and myogenic tone is the same as that for currents through L-type VGCCs, and both depolarization-induced increases in intracellular Ca^{2+} and myogenic tone are prevented or completely reversed by L-type VGCC blockers (Knot and Nelson, 1998). In first-order rat cremaster muscle arterioles, the relationship between membrane potential and tone is steeper than observed in cerebral arteries, and a significant portion of pressure-induced tone remains after block of L-type VGCCs (Kotecha and Hill, 2005). Block of L-type VGCCs also only inhibits a portion of Ca^{2+}-dependent myogenic tone in second-order hamster cremaster (86%) and cheek pouch (54%) arterioles (Jackson and Boerman, 2017). These data suggest that Ca^{2+} entry through additional ion channels, such as T-type VGCCs (CaV3.X) or mechano-sensitive cation channels such as TRPC6, for example, also contribute to elevated $[Ca^{2+}]_{in}$ and activation of contraction, particularly in the microcirculation (Tykocki et al., 2017). While it has been shown that smooth muscle-specific knockout of CaV1.2 abolishes myogenic reactivity in murine tibialis arteries (Moosmang et al., 2003), these data are difficult to interpret because CaV1.2 appears essential for the initiation of the myogenic response and hence, myogenic tone (Knot and Nelson, 1998; Kotecha and Hill, 2005).

The role played by SMC CaV1.2 channels in myogenic tone in arterioles, *in situ*, is not as clear. While there are a number of *in situ* studies supporting a role for CaV1.2 channels in various vascular beds (see Tykocki et al., 2017 for refs.), several intravital microscopy studies of arterioles in rat (Hill and Meininger, 1994), hamster (Jackson, 2012) and mouse (Pemberton et al., 1996; Ngo et al., 2013) cremaster muscles, and hamster cheek pouch (Boric et al., 1990; Welsh et al., 1998) have shown that topical application of L-type channel blockers has little effect on resting myogenic tone. Importantly, the efficacy the Ca^{2+} channel blockers was verified because they abolished vasomotion (Hill and Meininger, 1994; Welsh et al., 1998; Jackson, 2012; Ngo et al., 2013) and prevented O_2-induced vasoconstriction (Welsh et al., 1998; Jackson, 2012). The resting tone in these studies appeared to be voltage-dependent because K_{ATP} channel agonists such as pinacidil (Jackson, 1993; Hill and Meininger, 1994) and cromakalim (Jackson, 1993) cause near maximal dilation of arterioles in these preparations. These data suggest that some other voltage-dependent channel, such as T-type CaV3.X channels for example, can determine resting tone in these microvascular beds under the conditions studied, that is simply not recapitulated in the *ex vivo* study of isolated resistance arteries and arterioles where CaV1.2 channels appear essential.

In some resistance arteries and arterioles, Ca^{2+} influx through VGCCs also appears to be amplified by Ca^{2+} release from intracellular stores (**Figure 2**). In cremaster arterioles, for example, Ca^{2+} influx through L-type VGCCs activates Ca^{2+} release through IP_3Rs in the form of Ca^{2+} waves that contribute to myogenic tone (Westcott and Jackson, 2011; Westcott et al., 2012; Jackson and Boerman, 2018). In resistance arteries upstream from cremaster arterioles, Ca^{2+} waves also contribute to myogenic tone, but appear to involve both IP_3R and RyR (Westcott and Jackson, 2011; Westcott et al., 2012).

How Is the Pressure-Dependent Ca^{2+} Signal Translated Into Tone?

The global increase in intracellular Ca^{2+} that results from activation of membrane mechanoreceptive processes, depolarization, activation of VGCCs, and amplification by Ca^{2+} release from intracellular stores is translated into smooth muscle contraction mainly through binding of Ca^{2+} to the Ca^{2+}-binding protein, calmodulin (CaM), and Ca^{2+}-CaM-dependent activation of myosin light-chain kinase (MLCK). This results in phosphorylation of the 20 kD myosin light-chains which is the primary trigger for contraction and force production in vascular smooth muscle (Zou et al., 1995; Cole and Welsh, 2011; **Figure 2**). Myosin light-chain phosphorylation then allows interaction of filamentous actin with myosin, the formation of actin-myosin cross-bridges, cross-bridge cycling, and smooth muscle contraction or force generation (increased myogenic tone; Zou et al., 1995; Cole and Welsh, 2011; **Figure 2**). This process continues while Ca^{2+} remains elevated and cross-bridge cycling occurs. A reduction in intracellular Ca^{2+} or dephosphorylation of the myosin light-chains by myosin light-chain phosphatase (MLCPPT) turns off this process and allows smooth muscle relaxation (decreased myogenic tone; Zou et al., 1995; Cole and Welsh, 2011). The ratio of activity of MLCK/MLCPPT determines the Ca^{2+} sensitivity of the system (Cole and Welsh, 2011). Guanine nucleotide exchange factors (GEFs), such as LARG, couple G-proteins, such as $G_{12/13}$ to activation of the small GTPase, RhoA which subsequently activates Rho Kinase (Chennupati et al., 2019; **Figure 2**). Active Rho Kinase has several targets that modulate myogenic tone including: phosphorylation and inhibition of MLCPPT and an increase in Ca^{2+} sensitivity (Cole and Welsh, 2011); activation of LIM kinase (LIMK) and subsequent inhibition of cofilin and actin-cytoskeleton remodeling (Loirand et al., 2006; Moreno-Dominguez et al., 2013); inhibition of K_V channels (Luykenaar et al., 2009); activation of TRPM4 channels (Li and Brayden, 2017); and activation of VGCCs (Guan et al., 2019; **Figure 2**). All of these Rho Kinase-related effects promote increased myogenic tone. Myogenic tone can also be increased/sustained through G-protein-dependent activation of PKC that not only modulates ion channels, but also the Ca^{2+} sensitivity of the contractile machinery through phosphorylation of the protein CPI_{17} which inhibits MLCPPT (Cole and Welsh, 2011). As noted previously, PKC also can lead to actin cytoskeleton remodeling that contributes to myogenic tone (Moreno-Dominguez et al., 2013; Hong et al., 2016; **Figure 2**).

WHAT IS RESPONSIBLE FOR THE APPARENT HETEROGENEITY IN MECHANISMS UNDERLYING MYOGENIC TONE?

As outlined in previous sections, there are likely multiple mechanisms that resistance arteries and arterioles use to produce and modulate myogenic tone depending on their location in the body and the physiology/pathophysiology of the system. What determines the primary mechanisms that are functional

in a resistance artery or arteriole under a given set of physiological or pathophysiological conditions remains to be established. In experimental diabetes and subarachnoid hemorrhage, for example, it has been shown that there is apparent upregulation of the role played by mTNFα and S1P-signaling in myogenic tone of skeletal muscle (Sauve et al., 2016) and cerebral (Yagi et al., 2015) resistance arteries. However, the mechanisms responsible for this upregulation remain to be established. Another example is the differences that we have found in the mechanisms of myogenic tone in hamster cremaster vs. cheek pouch second-order arterioles (Jackson and Boerman, 2017). In cremaster arterioles, PLC and IP_3R substantially contribute to Ca^{2+} signals (Ca^{2+} waves) and pressure-induced myogenic tone, whereas cheek pouch arterioles generate a similar level of tone that is independent of PLC and IP_3R signaling (Jackson and Boerman, 2017). The mechanisms responsible for this regional heterogeneity are not known. Nonetheless, these differences in mechanisms likely mean that vascular smooth muscle in resistance arteries and arterioles has a "toolbox" of mechanisms that are potentially available to support the vital process of the myogenic response and myogenic tone in health and disease. Regional heterogeneity in mechanisms of myogenic tone may also provide new drug targets to treat vascular disease in an organ or tissue specific manner. For this to become a reality, much more research will be required to: (1) identify all of the potential signaling pathways that can contribute to myogenic tone in a selection of resistance arteries and arterioles from different vascular beds around the body using high density transcriptomic and proteomic approaches, understanding that many ion channels and receptors are normally expressed at very low levels in VSMCs, despite having major contributions to vessel function; (2) gain a better understanding of the regulation of message and protein expression for all these components using sophisticated pathway and informatic analysis of the "signals" detected in the transcriptomic and proteomic screens; and (3) perform appropriate functional *in situ* and *ex vivo* studies measuring diameter (as a readout of smooth muscle contraction at given levels of pressure), membrane potential, both local and global Ca^{2+} signals as well as careful biochemical assessment of pathway activity (protein phosphorylation, etc., see Moreno-Dominguez et al., 2013; for example) using conditional, cell-specific knockout, knockdown and knockin strategies as well as careful pharmacology to evaluate the role of the various signaling pathways that can contribute to myogenic tone in both resistance arteries and arterioles from around the body. This is a daunting task, but one that appears essential to move this field forward.

AUTHOR CONTRIBUTIONS

WJ conceived, wrote, and edited this manuscript and is solely responsible for its content. The content is solely the responsibility of the author and does not necessarily represent the official views of the National Institutes of Health.

FUNDING

This work was supported by National Heart, Lung, and Blood Institute grants HL-137694 and PO1-HL-070687.

REFERENCES

Amin, A. H., Abd Elmageed, Z. Y., Partyka, M., and Matrougui, K. (2011). Mechanisms of myogenic tone of coronary arteriole: role of down stream signaling of the EGFR tyrosine kinase. *Microvasc. Res.* 81, 135–142. doi: 10.1016/j.mvr.2010.11.001

Bayliss, W. M. (1902). On the local reactions of the arterial wall to changes of internal pressure. *J. Physiol.* 28, 220–231. doi: 10.1113/jphysiol.1902.sp000911

Boric, M. P., Donoso, V., Fournier, A., St Pierre, S., and Huidobro-Toro, J. P. (1990). Endothelin reduces microvascular blood flow by acting on arterioles and venules of the hamster cheek pouch. *Eur. J. Pharmacol.* 190, 123–133. doi: 10.1016/0014-2999(90)94119-i

Brayden, J. E., Li, Y., and Tavares, M. J. (2013). Purinergic receptors regulate myogenic tone in cerebral parenchymal arterioles. *J. Cereb. Blood Flow Metab.* 33, 293–299. doi: 10.1038/jcbfm.2012.169

Bulley, S., Neeb, Z. P., Burris, S. K., Bannister, J. P., Thomas-Gatewood, C. M., Jangsangthong, W., et al. (2012). TMEM16A/ANO1 channels contribute to the myogenic response in cerebral arteries. *Circ. Res.* 111, 1027–1036. doi: 10.1161/CIRCRESAHA.112.277145

Carlson, B. E., and Secomb, T. W. (2005). A theoretical model for the myogenic response based on the length-tension characteristics of vascular smooth muscle. *Microcirculation* 12, 327–338. doi: 10.1080/10739680590934745

Chennupati, R., Wirth, A., Favre, J., Li, R., Bonnavion, R., Jin, Y. J., et al. (2019). Myogenic vasoconstriction requires G12/G13 and LARG to maintain local and systemic vascular resistance. *eLife* 8:e49374. doi: 10.7554/eLife.49374

Clifford, P. S., Ferguson, B. S., Jasperse, J. L., and Hill, M. A. (2018). Arteriolar vasodilation involves actin depolymerization. *Am. J. Physiol. Heart Circ. Physiol.* 315, H423–H428. doi: 10.1152/ajpheart.00723.2017

Cole, W. C., and Welsh, D. G. (2011). Role of myosin light chain kinase and myosin light chain phosphatase in the resistance arterial myogenic response to intravascular pressure. *Arch. Biochem. Biophys.* 510, 160–173. doi: 10.1016/j.abb.2011.02.024

Colinas, O., Moreno-Dominguez, A., Zhu, H. L., Walsh, E. J., Perez-Garcia, M. T., Walsh, M. P., et al. (2015). alpha5-integrin-mediated cellular signaling contributes to the myogenic response of cerebral resistance arteries. *Biochem. Pharmacol.* 97, 281–291. doi: 10.1016/j.bcp.2015.08.088

Davis, M. J., and Hill, M. A. (1999). Signaling mechanisms underlying the vascular myogenic response. *Physiol. Rev.* 79, 387–423. doi: 10.1152/physrev.1999.79.2.387

Davis, M. J., Hill, M. A., and Kuo, L. (2011). "Local regulation of microvascular perfusion," in *Comprehensive Physiology*. ed. R. L. Terjung (Hoboken, NJ: John Wiley & Sons, Inc.), 161–284.

Davis, M. J., Wu, X., Nurkiewicz, T. R., Kawasaki, J., Davis, G. E., Hill, M. A., et al. (2001). Integrins and mechanotransduction of the vascular myogenic response. *Am. J. Physiol. Heart Circ. Physiol.* 280, H1427–H1433. doi: 10.1152/ajpheart.2001.280.4.H1427

Drummond, H. A., and Stec, D. E. (2015). betaENaC acts as a mechanosensor in renal vascular smooth muscle cells that contributes to renal myogenic blood flow regulation, protection from renal injury and hypertension. *J. Nephrol. Res.* 1, 1–9. doi: 10.17554/j.issn.2410-0579.2015.01.12

Earley, S., Waldron, B. J., and Brayden, J. E. (2004). Critical role for transient receptor potential channel TRPM4 in myogenic constriction of cerebral arteries. *Circ. Res.* 95, 922–929. doi: 10.1161/01.RES.0000147311.54833.03

Forrester, S. J., Kawai, T., O'Brien, S., Thomas, W., Harris, R. C., and Eguchi, S. (2016). Epidermal growth factor receptor transactivation: mechanisms, pathophysiology, and potential therapies in the cardiovascular system. *Annu. Rev. Pharmacol. Toxicol.* 56, 627–653. doi: 10.1146/annurev-pharmtox-070115-095427

Fronek, K., and Zweifach, B. W. (1975). Microvascular pressure distribution in skeletal muscle and the effect of vasodilation. *Am. J. Phys.* 228, 791–796.

Gannon, K. P., McKey, S. E., Stec, D. E., and Drummond, H. A. (2015). Altered myogenic vasoconstriction and regulation of whole kidney blood

flow in the ASIC2 knockout mouse. *Am. J. Physiol. Ren. Physiol.* 308, F339–F348. doi: 10.1152/ajprenal.00572.2014

Gannon, K. P., Vanlandingham, L. G., Jernigan, N. L., Grifoni, S. C., Hamilton, G., and Drummond, H. A. (2008). Impaired pressure-induced constriction in mouse middle cerebral arteries of ASIC2 knockout mice. *Am. J. Physiol. Heart Circ. Physiol.* 294, H1793–H1803. doi: 10.1152/ajpheart.01380.2007

Gonzales, A. L., Yang, Y., Sullivan, M. N., Sanders, L., Dabertrand, F., Hill-Eubanks, D. C., et al. (2014). A PLCgamma1-dependent, force-sensitive signaling network in the myogenic constriction of cerebral arteries. *Sci. Signal.* 7:ra49. doi: 10.1126/scisignal.2004732

Granger, D. N., Kvietys, P. R., Korthuis, R. J., and Premen, A. J. (2011). "Microcirculation of the intestinal mucosa," in *Comprehensive Physiology*. ed. R. L. Terjung (Hoboken, NJ: John Wiley & Sons, Inc.), 1405–1474.

Guan, Z., Baty, J. J., Zhang, S., Remedies, C. E., and Inscho, E. W. (2019). Rho kinase inhibitors reduce voltage-dependent Ca^{2+} channel signaling in aortic and renal microvascular smooth muscle cells. *Am. J. Physiol. Ren. Physiol.* 317, F1132–F1141. doi: 10.1152/ajprenal.00212.2018

Guia, A., Wan, X., Courtemanche, M., and Leblanc, N. (1999). Local Ca^{2+} entry through L-type Ca^{2+} channels activates Ca^{2+}−dependent K^+ channels in rabbit coronary myocytes. *Circ. Res.* 84, 1032–1042. doi: 10.1161/01.RES.84.9.1032

Gunst, S. J., and Zhang, W. (2008). Actin cytoskeletal dynamics in smooth muscle: a new paradigm for the regulation of smooth muscle contraction. *Am. J. Phys. Cell Physiol.* 295, C576–C587. doi: 10.1152/ajpcell.00253.2008

Harder, D. R. (1984). Pressure-dependent membrane depolarization in cat middle cerebral artery. *Circ. Res.* 55, 197–202. doi: 10.1161/01.RES.55.2.197

Hill, M. A., and Meininger, G. A. (1994). Calcium entry and myogenic phenomena in skeletal muscle arterioles. *Am. J. Phys.* 267, H1085–H1092. doi: 10.1152/ajpheart.1994.267.3.H1085

Hill, M. A., Zou, H., Potocnik, S. J., Meininger, G. A., and Davis, M. J. (2001). Invited review: arteriolar smooth muscle mechanotransduction: Ca^{2+} signaling pathways underlying myogenic reactivity. *J. Appl. Physiol.* 91, 973–983. doi: 10.1152/jappl.2001.91.2.973

Hong, K., Li, M., Nourian, Z., Meininger, G. A., and Hill, M. A. (2017). Angiotensin II type 1 receptor mechanoactivation involves RGS5 (regulator of G protein signaling 5) in skeletal muscle arteries: impaired trafficking of RGS5 in hypertension. *Hypertension* 70, 1264–1272. doi: 10.1161/HYPERTENSIONAHA.117.09757

Hong, K., Zhao, G., Hong, Z., Sun, Z., Yang, Y., Clifford, P. S., et al. (2016). Mechanical activation of angiotensin II type 1 receptors causes actin remodelling and myogenic responsiveness in skeletal muscle arterioles. *J. Physiol.* 594, 7027–7047. doi: 10.1113/JP272834

Hui, S., Levy, A. S., Slack, D. L., Burnstein, M. J., Errett, L., Bonneau, D., et al. (2015). Sphingosine-1-phosphate signaling regulates myogenic responsiveness in human resistance arteries. *PLoS One* 10:e0138142. doi: 10.1371/journal.pone.0138142

Jackson, W. F. (1993). Arteriolar tone is determined by activity of ATP-sensitive potassium channels. *Am. J. Phys.* 265, H1797–H1803.

Jackson, W. F. (2012). "Microcirculation," in *Muscle*. eds. J. A. Olson and E. N. Hill (Boston/Waltham, MA: Academic Press), 1197–1206.

Jackson, W. F., and Boerman, E. M. (2017). Regional heterogeneity in the mechanisms of myogenic tone in hamster arterioles. *Am. J. Physiol. Heart Circ. Physiol.* 313, H667–H675. doi: 10.1152/ajpheart.00183.2017

Jackson, W. F., and Boerman, E. M. (2018). Voltage-gated Ca^{2+} channel activity modulates smooth muscle cell calcium waves in hamster cremaster arterioles. *Am. J. Physiol. Heart Circ. Physiol.* 315, H871–H878. doi: 10.1152/ajpheart.00292.2018

Jernigan, N. L., and Drummond, H. A. (2005). Vascular ENaC proteins are required for renal myogenic constriction. *Am. J. Physiol. Ren. Physiol.* 289, F891–F901. doi: 10.1152/ajprenal.00019.2005

Jernigan, N. L., and Drummond, H. A. (2006). Myogenic vasoconstriction in mouse renal interlobar arteries: role of endogenous beta and gammaENaC. *Am. J. Physiol. Ren. Physiol.* 291, F1184–F1191. doi: 10.1152/ajprenal.00177.2006

Johnson, P. C. (1980). "The myogenic response," in *Handbood of Physiology: Section 2, The Cardiovascular System, Volume II, Vascular Smooth Muscle*. eds. D. F. Bohr A. P. Somlyo and H. V. Sparks (Bethesda, MD: American Physiological Society), 409–442.

Kauffenstein, G., Tamareille, S., Prunier, F., Roy, C., Ayer, A., Toutain, B., et al. (2016). Central role of P2Y6 UDP receptor in arteriolar myogenic tone. *Arterioscler. Thromb. Vasc. Biol.* 36, 1598–1606. doi: 10.1161/ATVBAHA.116.307739

Knot, H. J., and Nelson, M. T. (1998). Regulation of arterial diameter and wall Ca^{2+} in cerebral arteries of rat by membrane potential and intravascular pressure. *J. Physiol.* 508, 199–209. doi: 10.1111/j.1469-7793.1998.199br.x

Kotecha, N., and Hill, M. A. (2005). Myogenic contraction in rat skeletal muscle arterioles: smooth muscle membrane potential and Ca^{2+} signaling. *Am. J. Physiol. Heart Circ. Physiol.* 289, H1326–H1334. doi: 10.1152/ajpheart.00323.2005

Kroetsch, J. T., Levy, A. S., Zhang, H., Aschar-Sobbi, R., Lidington, D., Offermanns, S., et al. (2017). Constitutive smooth muscle tumour necrosis factor regulates microvascular myogenic responsiveness and systemic blood pressure. *Nat. Commun.* 8:14805. doi: 10.1038/ncomms14805

Lagaud, G., Gaudreault, N., Moore, E. D., Van Breemen, C., and Laher, I. (2002). Pressure-dependent myogenic constriction of cerebral arteries occurs independently of voltage-dependent activation. *Am. J. Physiol. Heart Circ. Physiol.* 283, H2187–H2195. doi: 10.1152/ajpheart.00554.2002

Laughlin, M. H., Korthuis, R. J., Duncker, D. J., and Bache, R. J. (1996). *Control of Blood Flow to Cardiac and Skeletal Muscle During Exercise*. New York: Published for the American Physiological Society by Oxford University Press.

Leiphart, R. J., Chen, D., Peredo, A. P., Loneker, A. E., and Janmey, P. A. (2019). Mechanosensing at cellular interfaces. *Langmuir* 35, 7509–7519. doi: 10.1021/acs.langmuir.8b02841

Li, Y., and Brayden, J. E. (2017). Rho kinase activity governs arteriolar myogenic depolarization. *J. Cereb. Blood Flow Metab.* 37, 140–152. doi: 10.1177/0271678X15621069

Lidington, D., Peter, B. F., Meissner, A., Kroetsch, J. T., Pitson, S. M., Pohl, U., et al. (2009). The phosphorylation motif at serine 225 governs the localization and function of sphingosine kinase 1 in resistance arteries. *Arterioscler. Thromb. Vasc. Biol.* 29, 1916–1922. doi: 10.1161/ATVBAHA.109.194803

Loirand, G., Guerin, P., and Pacaud, P. (2006). Rho kinases in cardiovascular physiology and pathophysiology. *Circ. Res.* 98, 322–334. doi: 10.1161/01.RES.0000201960.04223.3c

Lucchesi, P. A., Sabri, A., Belmadani, S., and Matrougui, K. (2004). Involvement of metalloproteinases 2/9 in epidermal growth factor receptor transactivation in pressure-induced myogenic tone in mouse mesenteric resistance arteries. *Circulation* 110, 3587–3593. doi: 10.1161/01.CIR.0000148780.36121.47

Luykenaar, K. D., El-Rahman, R. A., Walsh, M. P., and Welsh, D. G. (2009). Rho-kinase-mediated suppression of KDR current in cerebral arteries requires an intact actin cytoskeleton. *Am. J. Physiol. Heart Circ. Physiol.* 296, H917–H926. doi: 10.1152/ajpheart.01206.2008

Martinez-Lemus, L. A., Crow, T., Davis, M. J., and Meininger, G. A. (2005). alphavbeta3- and alpha5beta1-integrin blockade inhibits myogenic constriction of skeletal muscle resistance arterioles. *Am. J. Physiol. Heart Circ. Physiol.* 289, H322–H329. doi: 10.1152/ajpheart.00923.2003

Martinez-Lemus, L. A., Hill, M. A., Bolz, S. S., Pohl, U., and Meininger, G. A. (2004). Acute mechanoadaptation of vascular smooth muscle cells in response to continuous arteriolar vasoconstriction: implications for functional remodeling. *FASEB J.* 18, 708–710. doi: 10.1096/fj.03-0634fje

McGahon, M. K., Fernandez, J. A., Dash, D. P., McKee, J., Simpson, D. A., Zholos, A. V., et al. (2016). TRPV2 channels contribute to stretch-activated cation currents and myogenic constriction in retinal arterioles. *Invest. Ophthalmol. Vis. Sci.* 57, 5637–5647. doi: 10.1167/iovs.16-20279

Mederos, Y. S. M., Storch, U., and Gudermann, T. (2016). Mechanosensitive Gq/11 protein-coupled receptors mediate myogenic vasoconstriction. *Microcirculation* 23, 621–625. doi: 10.1111/micc.12293

Mederos y Schnitzler, M., Storch, U., Meibers, S., Nurwakagari, P., Breit, A., Essin, K., et al. (2008). Gq-coupled receptors as mechanosensors mediating myogenic vasoconstriction. *EMBO J.* 27, 3092–3103. doi: 10.1038/emboj.2008.233

Meininger, G. A., and Trzeciakowski, J. P. (1988). Vasoconstriction is amplified by autoregulation during vasoconstrictor-induced hypertension. *Am. J. Phys.* 254, H709–H718. doi: 10.1152/ajpheart.1988.254.4.H709

Meininger, G. A., and Trzeciakowski, J. P. (1990). Combined effects of autoregulation and vasoconstrictors on hindquarters vascular resistance. *Am. J. Phys.* 258, H1032–H1041. doi: 10.1152/ajpheart.1990.258.4.H1032

Moosmang, S., Schulla, V., Welling, A., Feil, R., Feil, S., Wegener, J. W., et al. (2003). Dominant role of smooth muscle L-type calcium channel Cav1.2 for blood pressure regulation. *EMBO J.* 22, 6027–6034. doi: 10.1093/emboj/cdg583

Moreno-Dominguez, A., Colinas, O., El-Yazbi, A., Walsh, E. J., Hill, M. A., Walsh, M. P., et al. (2013). Ca^{2+} sensitization due to myosin light chain phosphatase inhibition and cytoskeletal reorganization in the myogenic response of skeletal muscle resistance arteries. *J. Physiol.* 591, 1235–1250. doi: 10.1113/jphysiol.2012.243576

Mortensen, S. P., and Saltin, B. (2014). Regulation of the skeletal muscle blood flow in humans. *Exp. Physiol.* 99, 1552–1558. doi: 10.1113/expphysiol.2014.081620

Navar, L. G., Arendshorst, W. J., Pallone, T. L., Inscho, E. W., Imig, J. D., and Bell, P. D. (2011). "The renal microcirculation," in *Comprehensive Physiology*. ed. R. L. Terjung (Hoboken, NJ: John Wiley & Sons, Inc.), 550–683.

Nelson, M. T., Cheng, H., Rubart, M., Santana, L. F., Bonev, A. D., Knot, H. J., et al. (1995). Relaxation of arterial smooth muscle by calcium sparks. *Science* 270, 633–637. doi: 10.1126/science.270.5236.633

Nemeth, Z., Hildebrandt, E., Ryan, M. J., Granger, J. P., and Drummond, H. A. (2020). Pressure-induced constriction of the middle cerebral artery is abolished in TrpC6 knockout mice. *Am. J. Physiol. Heart Circ. Physiol.* 319, H42–H50. doi: 10.1152/ajpheart.00126.2020

Ngo, A. T., Riemann, M., Holstein-Rathlou, N. H., Torp-Pedersen, C., and Jensen, L. J. (2013). Significance of K(ATP) channels, L-type Ca^{2+} channels and CYP450-4A enzymes in oxygen sensing in mouse cremaster muscle arterioles in vivo. *BMC Physiol.* 13:8. doi: 10.1186/1472-6793-13-8

Pemberton, M., Anderson, G. L., and Barker, J. H. (1996). Characterization of microvascular vasoconstriction following ischemia/reperfusion in skeletal muscle using videomicroscopy. *Microsurgery* 17, 9–16. doi: 10.1002/(SICI)1098-2752(1996)17:1<9::AID-MICR2>3.0.CO;2-K

Peter, B. F., Lidington, D., Harada, A., Bolz, H. J., Vogel, L., Heximer, S., et al. (2008). Role of sphingosine-1-phosphate phosphohydrolase 1 in the regulation of resistance artery tone. *Circ. Res.* 103, 315–324. doi: 10.1161/CIRCRESAHA.108.173575

Pries, A. R., and Secomb, T. W. (2011). "Blood flow in microvascular networks," in *Comprehensive Physiology*. ed. R. L. Terjung (Hoboken, NJ: John Wiley & Sons, Inc.), 3–36.

Pires, P. W., Ko, E. A., Pritchard, H. A. T., Rudokas, M., Yamasaki, E., and Earley, S. (2017). The angiotensin II receptor type 1b is the primary sensor of intraluminal pressure in cerebral artery smooth muscle cells. *J. Physiol.* 595, 4735–4753. doi: 10.1113/JP274310

Renkin, E. M. (1984). "Control of microcirculation and blood-tissue exchange," in *Handbook of Physiology: Section 2, The Cardiovascular System, Vol. IV, Microcirculation, part 2*. eds. E. M. Renkin and C. C. Michel (Bethesda, MD: American Physiological Society), 627–687.

Riva, C. E., and Schmetterer, L. (2011). "Microcirculation of the ocular fundus," in *Comprehensive Physiology*. ed. R. L. Terjung (Hoboken, NJ: John Wiley & Sons, Inc.), 735–765.

Saltin, B., Radegran, G., Koskolou, M. D., and Roach, R. C. (1998). Skeletal muscle blood flow in humans and its regulation during exercise. *Acta Physiol. Scand.* 162, 421–436. doi: 10.1046/j.1365-201X.1998.0293e.x

Sauve, M., Hui, S. K., Dinh, D. D., Foltz, W. D., Momen, A., Nedospasov, S. A., et al. (2016). Tumor necrosis factor/sphingosine-1-phosphate signaling augments resistance artery myogenic tone in diabetes. *Diabetes* 65, 1916–1928. doi: 10.2337/db15-1450

Schleifenbaum, J., Kassmann, M., Szijarto, I. A., Hercule, H. C., Tano, J. Y., Weinert, S., et al. (2014). Stretch-activation of angiotensin II type 1a receptors contributes to the myogenic response of mouse mesenteric and renal arteries. *Circ. Res.* 115, 263–272. doi: 10.1161/CIRCRESAHA.115.302882

Segal, S. S. (2000). Integration of blood flow control to skeletal muscle: key role of feed arteries. *Acta Physiol. Scand.* 168, 511–518. doi: 10.1046/j.1365-201x.2000.00703.x

Segal, S. S., and Duling, B. R. (1986). Communication between feed arteries and microvessels in hamster striated-muscle—segmental vascular-responses are functionally coordinated. *Circ. Res.* 59, 283–290. doi: 10.1161/01.RES.59.3.283

Shepherd, J. T. (1983). "Circulation to skeletal muscle," in *Handbook of Physiology, Section 2, The Cardiovascular System, Volume III*. eds. E. M. Renkin and C. C. Michel (Bethesda, MD: American Physiological Society), 319–370.

Soni, H., Peixoto-Neves, D., Matthews, A. T., and Adebiyi, A. (2017). TRPV4 channels contribute to renal myogenic autoregulation in neonatal pigs. *Am. J. Physiol. Ren. Physiol.* 313, F1136–F1148. doi: 10.1152/ajprenal.00300.2017

Spassova, M. A., Hewavitharana, T., Xu, W., Soboloff, J., and Gill, D. L. (2006). A common mechanism underlies stretch activation and receptor activation of TRPC6 channels. *Proc. Natl. Acad. Sci. U. S. A.* 103, 16586–16591. doi: 10.1073/pnas.0606894103

Storch, U., Blodow, S., Gudermann, T., and Mederos, Y. S. M. (2015). Cysteinyl leukotriene 1 receptors as novel mechanosensors mediating myogenic tone together with angiotensin II type 1 receptors-brief report. *Arterioscler. Thromb. Vasc. Biol.* 35, 121–126. doi: 10.1161/ATVBAHA.114.304844

Storch, U., Mederos y Schnitzler, M., and Gudermann, T. (2012). G protein-mediated stretch reception. *Am. J. Physiol. Heart Circ. Physiol.* 302, H1241–H1249. doi: 10.1152/ajpheart.00818.2011

Suzuki, Y., Yamamura, H., Ohya, S., and Imaizumi, Y. (2013). Caveolin-1 facilitates the direct coupling between large conductance Ca^{2+}–activated K^+ (BKCa) and Cav1.2 Ca^{2+} channels and their clustering to regulate membrane excitability in vascular myocytes. *J. Biol. Chem.* 288, 36750–36761. doi: 10.1074/jbc.M113.511485

Tuma, R. F. (2011). "The cerebral microcirculation," in *Comprehensive Physiology*. ed. R. L. Terjung (Hoboken, NJ: John Wiley & Sons, Inc.), 485–520.

Tykocki, N. R., Boerman, E. M., and Jackson, W. F. (2017). Smooth muscle ion channels and regulation of vascular tone in resistance arteries and arterioles. *Compr. Physiol.* 7, 485–581. doi: 10.1002/cphy.c160011

VanLandingham, L. G., Gannon, K. P., and Drummond, H. A. (2009). Pressure-induced constriction is inhibited in a mouse model of reduced betaENaC. *Am. J. Phys. Regul. Integr. Comp. Phys.* 297, R723–R728. doi: 10.1152/ajpregu.00212.2009

Wang, Q., Leo, M. D., Narayanan, D., Kuruvilla, K. P., and Jaggar, J. H. (2016). Local coupling of TRPC6 to ANO1/TMEM16A channels in smooth muscle cells amplifies vasoconstriction in cerebral arteries. *Am. J. Phys. Cell Physiol.* 310, C1001–C1009. doi: 10.1152/ajpcell.00092.2016

Welsh, D. G., Jackson, W. F., and Segal, S. S. (1998). Oxygen induces electromechanical coupling in arteriolar smooth muscle cells: a role for L-type Ca^{2+} channels. *Am. J. Phys.* 274, H2018–H2024. doi: 10.1152/ajpheart.1998.274.6.H2018

Welsh, D. G., Morielli, A. D., Nelson, M. T., and Brayden, J. E. (2002). Transient receptor potential channels regulate myogenic tone of resistance arteries. *Circ. Res.* 90, 248–250. doi: 10.1161/hh0302.105662

Westcott, E. B., Goodwin, E. L., Segal, S. S., and Jackson, W. F. (2012). Function and expression of ryanodine receptors and inositol 1,4,5-trisphosphate receptors in smooth muscle cells of murine feed arteries and arterioles. *J. Physiol.* 590, 1849–1869. doi: 10.1113/jphysiol.2011.222083

Westcott, E. B., and Jackson, W. F. (2011). Heterogeneous function of ryanodine receptors, but not IP3 receptors, in hamster cremaster muscle feed arteries and arterioles. *Am. J. Physiol. Heart Circ. Physiol.* 300, H1616–H1630. doi: 10.1152/ajpheart.00728.2010

Wilson, P. C., Fitzgibbon, W. R., Garrett, S. M., Jaffa, A. A., Luttrell, L. M., Brands, M. W., et al. (2015). Inhibition of sphingosine kinase 1 ameliorates angiotensin II-induced hypertension and inhibits transmembrane calcium entry via store-operated calcium channel. *Mol. Endocrinol.* 29, 896–908. doi: 10.1210/me.2014-1388

Yagi, K., Lidington, D., Wan, H., Fares, J. C., Meissner, A., Sumiyoshi, M., et al. (2015). Therapeutically targeting tumor necrosis factor-alpha/sphingosine-1-phosphate signaling corrects myogenic reactivity in subarachnoid hemorrhage. *Stroke* 46, 2260–2270. doi: 10.1161/STROKEAHA.114.006365

Yang, J., Noyan-Ashraf, M. H., Meissner, A., Voigtlaender-Bolz, J., Kroetsch, J. T., Foltz, W., et al. (2012). Proximal cerebral arteries develop myogenic responsiveness in heart failure via tumor necrosis factor-alpha-dependent activation of sphingosine-1-phosphate signaling. *Circulation* 126, 196–206. doi: 10.1161/CIRCULATIONAHA.111.039644

Yasuda, N., Miura, S., Akazawa, H., Tanaka, T., Qin, Y., Kiya, Y., et al. (2008). Conformational switch of angiotensin II type 1 receptor underlying mechanical stress-induced activation. *EMBO Rep.* 9, 179–186. doi: 10.1038/sj.embor.7401157

Zhang, C., Rogers, P. A., Merkus, D., Muller-Delp, J. M., Tiefenbacher, C. P., Potter, B., et al. (2011). "Regulation of coronary microvascular resistance in health and disease," in *Comprehensive Physiology*. ed. R. L. Terjung (Hoboken, NJ: John Wiley & Sons, Inc.), 521–549.

Zou, H., Ratz, P. H., and Hill, M. A. (1995). Role of myosin phosphorylation and $[Ca^{2+}]i$ in myogenic reactivity and arteriolar tone. *Am. J. Phys.* 269, H1590–H1596. doi: 10.1152/ajpheart.1995.269.5.H1590

Zweifach, B. W., and Lipowsky, H. H. (1984). "Pressure-flow relations in blood and lymph micocirculation," in *Handbook of Physiology, Section 2: The Cardiovascular System, Vol. IV, Microcirculation. Part 1*. eds. E. M. Renkin and C. C. Michel (Bethesda, MD: American Physiological Society), 251–305.

Conflict of Interest: The author declares that the research was conducted in the absence of any commercial or financial relationships that could be construed as a potential conflict of interest.

frontiers in Physiology

MINI REVIEW
published: 02 August 2021
doi: 10.3389/fphys.2021.710809

The LINC Between Mechanical Forces and Chromatin

*Olga Lityagina[1] and Gergana Dobreva[1,2]**

[1] Medical Faculty Mannheim, Heidelberg University, Mannheim, Germany, [2] German Centre for Cardiovascular Research (DZHK), Partner Site Heidelberg/Mannheim, Mannheim, Germany

The heart continually senses and responds to mechanical stimuli that balance cardiac structure and activity. Tensile forces, compressive forces, and shear stress are sensed by the different cardiac cell types and converted into signals instructing proper heart morphogenesis, postnatal growth, and function. Defects in mechanotransduction, the ability of cells to convert mechanical stimuli into biochemical signals, are implicated in cardiovascular disease development and progression. In this review, we summarize the current knowledge on how mechanical forces are transduced to chromatin through the tensed actomyosin cytoskeleton, the linker of nucleoskeleton and cytoskeleton (LINC) complex and the nuclear lamina. We also discuss the functional significance of the LINC complex in cardiovascular disease.

Keywords: LINC complex, nuclear lamins, mechanotransduction, epigenetics, cardiovascular disease, cardiomyocyte, endothelial cell

OPEN ACCESS

Edited by:
Dirk J. Duncker, Erasmus University Medical Center, Netherlands

Reviewed by:
Leighton Izu, University of California, Davis, United States
Thomas M. Vondriska, University of California, Los Angeles, United States

***Correspondence:**
Gergana Dobreva
gergana.dobreva@medma.uni-heidelberg.de

Specialty section:
This article was submitted to Striated Muscle Physiology, a section of the journal Frontiers in Physiology

Received: *19 May 2021*
Accepted: *14 July 2021*
Published: *02 August 2021*

Citation:
Lityagina O and Dobreva G (2021) The LINC Between Mechanical Forces and Chromatin. Front. Physiol. 12:710809. doi: 10.3389/fphys.2021.710809

INTRODUCTION

Mechanical forces play a key role in the development, maturation and function of the heart. During heart formation, contractions of cardiomyocytes (CMs) cause blood to flow over the cardiac endothelial lining, which leads to generation of mechanical cues such as shear stress and cyclic strain that further aid and guide cardiac morphogenesis (Granados-Riveron and Brook, 2012). After birth, these forces instruct and maintain the healthy heart functional state (Andrés-Delgado and Mercader, 2016). The type and magnitude of mechanical forces, such as shear stress, cyclic stretch, and alterations in the extracellular matrix (ECM) stiffness, have to be faithfully recognized from the different cardiac cell types to allow their adaptation to the dynamic changes of their surrounding by modifying gene expression. The inability of cells to correctly translate mechanical cues into biochemical signals, caused by mutations or deregulation of proteins that disturb mechanosensing and mechanotransduction, can contribute to the development and progression of cardiovascular diseases (Jaalouk and Lammerding, 2009).

The role of cytosolic signaling pathways and mechanosensitive transcription factors in mediating cellular responses to mechanical forces has been long recognized and extensively studied. Mechanosensitive ion channels and transmembrane receptors, as well as cytoskeleton and sarcomeric proteins have been shown to activate signaling cascades [e.g., through Rho GTPases, MAPKs, phospholipase C, calcium/calcineurin, focal adhesion kinase (FAK), Src, integrin-linked kinase (ILK) etc.], which converge into the nucleus to induce transcriptional programming that dictates cell behavior and function (Hahn and Schwartz, 2009; Jaalouk and Lammerding, 2009; Wang et al., 2009). For example, active Rho-GTPase signaling and actomyosin-mediated contractility result in the translocation of mechanosensitive transcription factors MRTFA (MKL1) and YAP/TAZ from the cytoplasm to the nucleus, where they initiate specific transcriptional

programs (Dupont et al., 2011; Dorn et al., 2018). While nucleocytoplasmic shuttling of transcriptional regulators to mediate responses elicited by mechanical stimuli has been extensively studied, more recent work has suggested a role for the nucleus in direct propagation of mechanical stress via the linker of nucleoskeleton and cytoskeleton (LINC) complex, a process referred to as nuclear mechanotransduction (Wang et al., 2009; Kirby and Lammerding, 2018). The LINC complex consists of KASH-domain spectrin repeat proteins (Nesprins), located in the outer nuclear membrane and SUN (Sad1 and UNC84)-domain transmembrane proteins, located in the inner nuclear membrane (**Figure 1A**). Nesprins bind to cytoskeletal elements such as microtubuli, intermediate filaments and actin in the cytoplasm and to the SUN proteins in the perinuclear space (Isermann and Lammerding, 2013). In CMs, nesprins can connect directly to the Z-disk or indirectly through other proteins (Stroud et al., 2014; **Figure 1B**). Inside the nucleus, SUN proteins bind to lamin A, which, in turn, anchors chromatin to the nuclear lamina. The nuclear lamina consists of A-type (lamin A and C) and B-type lamins (lamin B1 and B2), which form distinct meshworks (Shimi et al., 2008). While lamins B1 and B2 are localized at the periphery and associate mainly with transcriptionally silent chromatin (Reddy et al., 2008; Wen et al., 2009), lamins A and C are found at the nuclear periphery as well as in the nuclear interior and associate with both hetero- and transcriptionally active euchromatin (Gesson et al., 2016). However, three-dimensional structured illumination microscopy analysis of lamin meshworks in HeLa cells showed that the loss of A-type lamins results in alterations in B-type meshworks and *vice versa* (Shimi et al., 2008), suggesting that their activity might be interconnected and that mechanosensitive mechanisms could affect both lamin A and lamin B lamina-associated chromatin domains (LADs). A few other proteins, including Emerin, Luma (TMEM43) and LAP2α have been shown to interact with the LINC complex components (Stroud, 2018). In this review, we summarize the current knowledge on the mechanisms of a direct mechanical force propagation to chromatin through the tensed actomyosin cytoskeleton, the LINC complex and the nuclear lamina and their malfunction in cardiovascular diseases.

FORCE TRANSMISSION TO THE NUCLEUS

The connection between the ECM and the cell cytoskeleton is established through dynamic, integrin-containing multi-protein complexes that simultaneously bind to ECM proteins and anchor actin filaments, the focal adhesions (**Figures 1**, **2**). In response to tensile stress, as modeled by culturing mouse embryonic fibroblasts (MEF) on large and elongated micropatterns, cells establish strong connections to the substrate (mature focal adhesions) at the two opposite poles along the long axis of the cell, which leads to the formation of actin stress fibers along the cell's long axis in the apical plane (Alisafaei et al., 2019). Actin stress fibers are contractile cytoskeletal structures, composed mainly from actin and non-muscle myosin II (actomyosin). Stress fibers then propagate tensile forces from the mature focal adhesions to the nucleus (Alisafaei et al., 2019; **Figures 1**, **2**). Local shear stress, as modeled through the movement of a magnetic bead attached to the cell membrane of Chinese hamster ovary (CHO) cells is also propagated to the nucleus in an actomyosin-dependent fashion via focal adhesions (Tajik et al., 2016). However, forces that are applied on the cell membrane, but bypass the focal adhesions, can also be transmitted via actin, albeit less effectively compared to the force propagation from focal adhesions (Tajik et al., 2016). Interestingly, prolonged stretching of MEFs induces thickening of discrete actin stress fibers coupled to dense accumulation of lamin A/C in the apical side of the nucleus and the formation of lamin A/C dents along the individual actin fibers (Kim et al., 2017). These indentation sites are characterized by a local enrichment of LINC complexes, which connect the stress fibers to the nuclear lamina, as shown in endothelial cells (Versaevel et al., 2015). Isolated nuclei alone are also able to respond to tension force applied directly via Nesprin-1 (Guilluy et al., 2014), demonstrating that the LINC complex is crucial for the force transmission into the nucleus.

INFLUENCE OF MECHANICAL FORCES ON NUCLEAR MORPHOLOGY, CHROMATIN ORGANIZATION, AND GENE TRANSCRIPTION

Recent studies using different models have greatly expanded our understanding of the effects of mechanical forces on nuclear morphology and chromatin organization and the role of the actomyosin meshworks in force transmission (**Figures 1**, **2**). For example, tensile forces arising from culturing fibroblasts on fibronectin-coated micropatterns to mimic the *in vivo* microenvironment have been shown to trigger an actomyosin-dependent alterations in nuclear morphology, lamin A/C levels and shuttling of epigenetic factors (Alisafaei et al., 2019). In a similar way, 1 h cyclic stretch (1 Hz, 8% uniaxial cyclic stretch within the physiological range) alters the nucleus shape, which becomes flattened (approx. 35% reduction in nuclear height) and slightly elongated in the direction of stretch (Kim et al., 2017). Interestingly, tensile force-induced nuclear flattening stretches the nuclear pores, which decreases the mechanical restriction of nuclear pores-mediated molecular transport and results in accumulation of the mechanosensitive transcription factor YAP in the nucleus (Elosegui-Artola et al., 2017; **Figure 2**), providing an interconnection between the cytosolic pathways-mediated response of cells to mechanical forces and direct force transmission to the nucleus through the actomyosin cytoskeleton and the LINC complex. Further, stretch of the nuclear envelope in response to tensile stress results in increased lamin A/C levels (Swift et al., 2013; Alisafaei et al., 2019) and decreased mobility through inhibition of lamin A/C Ser22 phosphorylation, which regulates lamin A/C turnover and physical properties, as shown in mesenchymal stem cells (Buxboim et al., 2014). In addition, as a result of compressive forces on nuclei the nuclear lamina acquires structurally polarized state, in which epitopes at the N- and C-terminus of lamins A/C at the basal

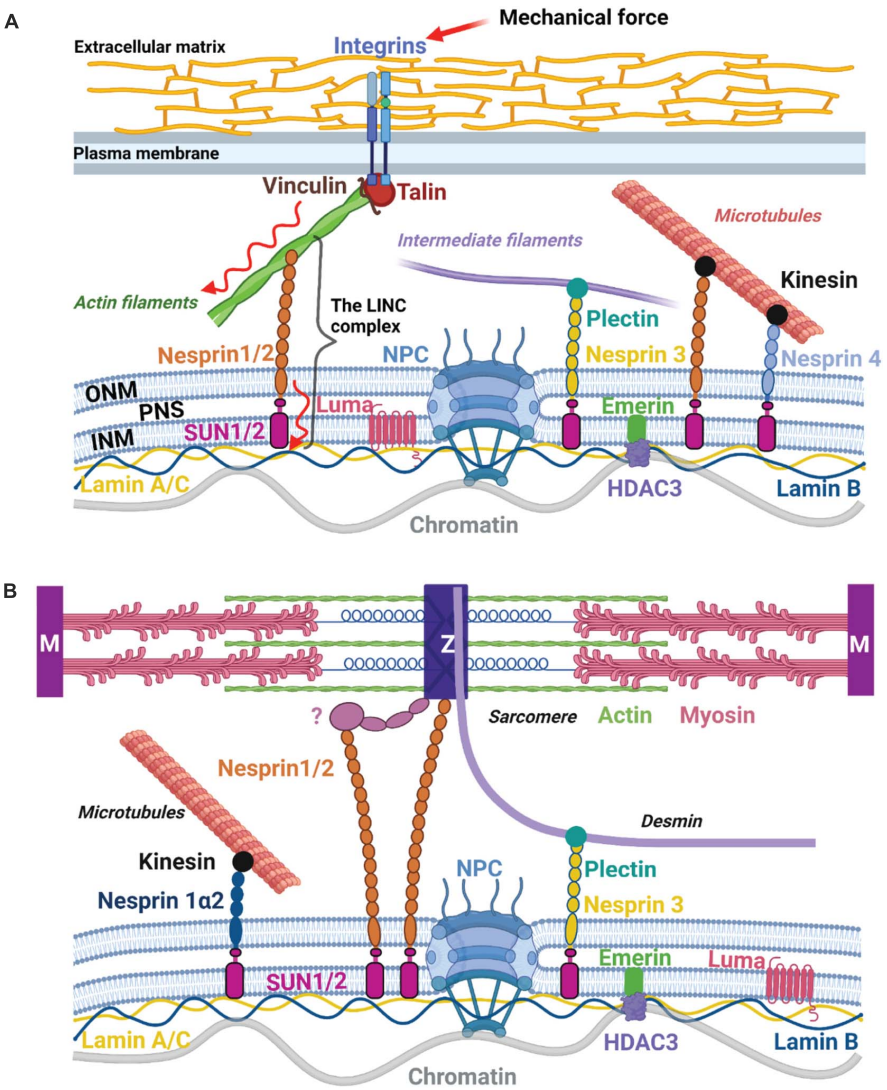

FIGURE 1 | The LINC complex and nuclear mechanotransduction. **(A)** Composition of the LINC complex and nuclear mechanotransduction. The LINC complex consists of KASH-domain containing proteins (Nesprins) located in the outer nuclear membrane (ONM) and SUN-domain proteins located in the inner nuclear membrane (INM). Nesprins bind to different cytoskeletal components in the cytoplasm and to the SUN-domain proteins in the perinuclear space (PNS). On the other side, SUN proteins interact with the nuclear lamins and other inner nuclear membrane-associated proteins such as Emerin and Luma (TMEM43). The nuclear lamina, in turn, anchors chromatin to the nuclear periphery. LINC complex composition varies in different cell types. Mechanical forces (increase in ECM matrix stiffness, shear stress, and stretch) sensed by the mechanosensitive cell-surface receptors and transduced via the cytoskeleton and the LINC complex to the nuclear lamina may directly influence chromatin architecture and gene expression. **(B)** The CM LINC complex. In CMs Nesprins-1/2 connect to the Z-disk (Z) – directly or indirectly through other proteins indicated with a question mark, while Nesprin-3 binds to Desmin through Plectin. Figures were created with BioRender.com and are not to scale.

nuclear envelope become inaccessible (Ihalainen et al., 2015). Recent studies have demonstrated that lamins anchor LADs at the nuclear periphery and are responsible for maintaining proper interactions among topologically associated chromatin domains (TADs), as well as for the maintaining of active and inactive chromatin and transcriptional states (Zheng et al., 2018). Importantly, loss of chromatin tethering to the nuclear lamina following HDAC3 deletion causes release of CM-specific gene regions from the nuclear periphery, leading to precocious CM differentiation and heart disease pathogenesis (Poleshko et al., 2017). Ablation of CTCF, an architectural protein enriched at LAD and TAD boundaries that binds DNA and facilitates chromatin looping, in cardiomyocytes results in cardiomyopathy (Rosa-Garrido et al., 2017). Thus, mechanical forces-induced conformational changes in the nuclear lamina might have a profound effect on chromatin organization, chromatin dynamics and gene expression in cardiovascular cells.

Several studies suggested that both chromatin organization and nuclear lamins have an impact on nuclear stiffening and might work synergistically to maintain nuclear rigidity

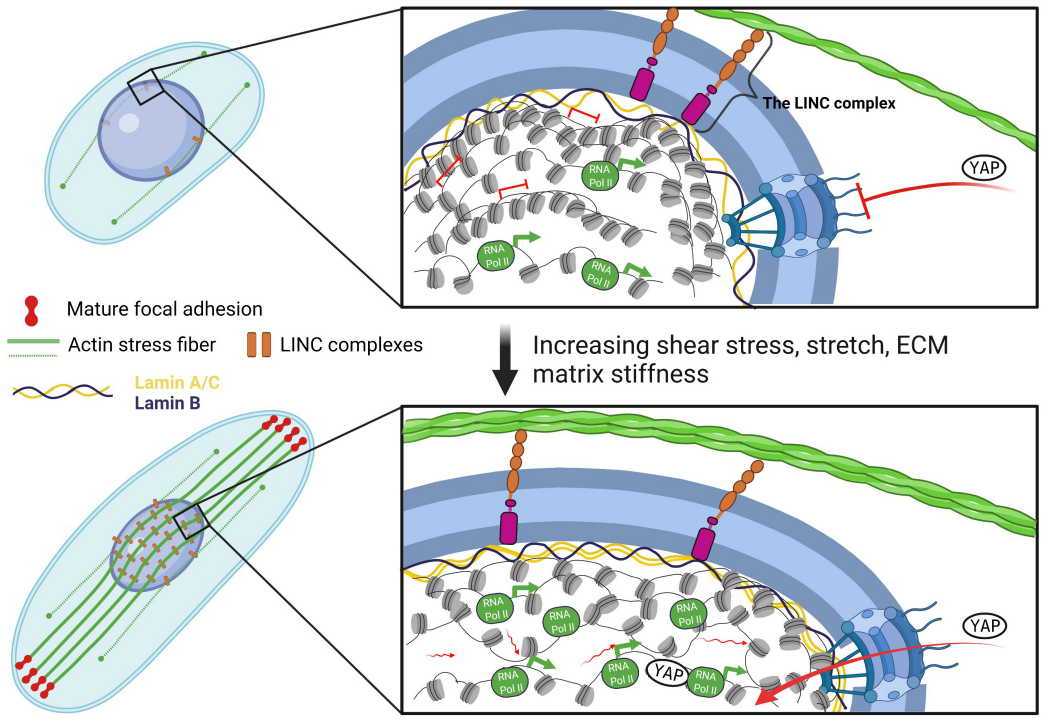

FIGURE 2 | Direct mechanical force transmission to chromatin through the LINC complex. Increasing mechanical forces lead to the formation of apical actin stress fibers, which propagate these cues to the nucleus via the LINC complex and cause its flattening and elongation. Nuclear deformation results in quantitative and conformational changes in the nuclear lamina, leading to alterations in chromatin fluidity and architecture coupled to changes in RNA Pol II occupancy and gene transcription. Additionally, nuclear pores are stretched as a consequence of nuclear elongation, which enables YAP translocation through decreased mechanical restriction of nuclear pore-mediated molecular transport. Tension-induced epigenetic and transcriptional response feeds back to the cytoskeleton and the extracellular matrix to balance outside and inside forces.

in response to mechanical stress. Indeed, chromatin decondensation decreases while lamin A overexpression increases the anisotropic nuclear deformations caused by constant force application on fibroblast nuclei using a pyramidal atomic force microscope (AFM) tip (Haase et al., 2016). A more recent study using isolated nuclei from HeLa cells demonstrated that in nuclei stretched at a physiologically relevant speed of 50 nm/s, lamin A/C levels modulate the nuclear stiffness primarily in response to more than 3 μm of stretch, whereas euchromatin/heterochromatin levels mainly control nuclear stiffening at less than 3 μm stretch (Stephens et al., 2017). Moreover, disruption of the LINC complex abrogates the difference between heterochromatin and euchromatin elasticities/stiffnesses at the peak nuclear deformation induced by CM contraction (Ghosh et al., 2021), suggesting that an intact LINC complex is also necessary for maintaining chromatin stiffness. Chromatin decondensation further results in an increased movement of chromatin, while inhibition of myosin II and decoupling the nucleus from the cytoskeleton decreases chromatin mobility in HUVEC cells (Spagnol and Noel Dahl, 2014), further supporting the notion that the intact actomyosin apparatus and the LINC complex are critical factors for the mechanical signal transmission to chromatin. Accordingly, an increase in euchromatin formation and/or heterochromatin depletion leads to decreased nuclear rigidity (softer nuclei) and formation of nuclear blebs in fibroblasts (Furusawa et al., 2015; Stephens et al., 2018). In turn, nuclear blebbing can be counteracted through extracellular multivalent cation transduction, which simulates the transient calcium (Ca^{2+}) influx associated with activation of mechanosensitive channels and increases heterochromatin formation (Stephens et al., 2019). Intriguingly, a recent study utilizing skin epidermis stem/progenitor cells reported Ca^{2+}-dependent rapid nuclear response preventing DNA damage upon nuclear deformation evoked by cyclic stretch, followed by a long-term adaptation mechanisms modulating chromatin organization (Nava et al., 2020). In the rapid cell response to mechanical stress, Ca^{2+} released from the endoplasmic reticulum (ER) reduces lamina-associated heterochromatin, thereby diminishing nuclear membrane tension and increasing chromatin fluidity to prevent DNA breaks. Subsequently, nuclear strain is hampered by cell-cell contacts-mediated cytoskeleton reorganization and cell and nuclear reorientation along the long axis, allowing chromatin adaptation for long-term mechanoprotection. On the other hand, Ca^{2+} release from the ER is dependent on lamin A levels and nuclear stiffness (Nava et al., 2020), suggesting that cytosolic and nuclear mechanotransduction pathways are tightly intertwined through both positive and negative feedbacks. Consistently, acute modulation of contractility and ECM elasticity of embryonic hearts resulted in rapid and reversible changes in lamin A

levels, DNA damage as well as cell cycle and loss of function experiments revealed a key role of lamin A in safeguarding against DNA-damage and cell cycle arrest of cardiomyocytes subjected to mechanical stress (Cho et al., 2019).

As discussed above, myriad studies have demonstrated the critical role of the LINC complex and lamin A in nuclear and chromatin reorganization as well as preventing DNA damage upon biophysical forces. On the other hand, chromatin structure regulates gene transcription by determining the accessibility of the transcriptional machinery to DNA, implying that changes in chromatin organization in response to mechanical stimuli could have a direct impact on gene transcription. Indeed, forces applied on the CHO cell surface via integrin-bound Arg-Gly-Asp-coated magnetic beads stretch chromatin and instantly upregulate gene transcription (Tajik et al., 2016). Specifically, using GFP tagged bacterial-chromosome dihydrofolate reductase (DHFR) transgene, Tajik et al. (2016) demonstrated that mechanical forces propagated to chromatin via the actomyosin and the LINC complex induce chromatin stretching coupled to transcriptional upregulation of DHFR. Further study from the same group revealed that the direction of force application and the stress amplitude also influence the extent of chromatin fluidity and gene expression (Wei et al., 2020). Although these conclusions were based on the transcriptional changes of the artificial DHFR transgene, a recent study suggested that the endogenous genes *EGR1* and *CAV1* respond similarly to directional mechanical stimulation (Sun et al., 2020). Moreover, force-induced gene upregulation depends on the levels and the spatial location of H3K9me3 histone mark, i.e., force-induced demethylation of H3K9me3 in the nuclear interior, but not near the nuclear periphery, leads to Pol II recruitment to promoters of mechanoresponsive genes to rapidly upregulate their transcription (Sun et al., 2020). Similarly, short-term stretch (30 min) of epidermal progenitor cells resulted in decrease of H3K9me3 (Nava et al., 2020), while long-term stretch resulted in decrease in global transcription due to increased H3K27me3-occupancy resulting in silencing of epidermal differentiation genes (Le et al., 2016; Nava et al., 2020), suggesting different modes of epigenetic response to short- and long-term stretch. In the heart, increased mechanical stress induced through TAC surgery, also leads to chromatin reorganization and higher transcriptional activity through increased recruitment of RNA polymerase II in CMs *in vivo,* which is dependent on the spatial location of genes in the nucleus (Karbassi et al., 2019). While duration and magnitude of mechanical stress application proportionally upregulates gene transcription (Tajik et al., 2016; Wei et al., 2020) and could play an important role in cell adaptation, too long lasting stress could induce non-reversible adaptations, which, in turn, might lead to disease development or contribute to disease progression.

THE LINC COMPLEX IN CARDIOVASCULAR DISEASE

Consistent with the important biological functions of the LINC complex in mechanical stress response, mutations in different components of the LINC complex and its interaction partners (Nesprin-1 and Nesprin-2, lamin A, Emerin, and TMEM43) are associated with diseases of the heart and striated muscles that experience high levels of mechanical stress, including dilated cardiomyopathy (DCM), arrhythmogenic cardiomyopathy (ACM), and Emery-Dreifuss muscular dystrophy (EDMD) (Stroud et al., 2014). One of the most frequently mutated genes associated with familial DCM is Lamin A/C (*LMNA*) (Hershberger et al., 2013). Cheedipudi et al. (2019) found redistribution of LADs in hearts of DCM patients carrying pathogenic *LMNA*-mutations, which correlated with CpG methylation and gene expression changes. In addition, abnormal binding of lamin A or LAP2α-lamin A/C complexes to euchromatin and dysregulation of the WNT/β-catenin and TGFβ-BMP pathways might also contribute to the disease phenotype (Zhang et al., 2021). Further evidence that *LMNA* mutations disrupt lamina-chromatin interactions and influence gene expression comes from *in vitro* experiments using human induced pluripotent stem cells (hiPSCs)-derived CMs. HiPSCs-CMs harboring DCM-associated T10I and R541C *LMNA* mutations exhibit specific alterations in the peripheral chromatin, resulting in an increased and aberrant expression of non-myocyte lineage genes (Shah et al., 2021). Taken together, these studies support a key role of lamin A/C in chromatin organization for proper cardiac function.

Dilated cardiomyopathy development and progression is often associated with altered Ca^{2+} handling in cardiac myocytes. Indeed, *Lmna* H222P mutation results in an abnormal increase of sarcolipin, an inhibitor of the sarco/endoplasmic reticulum (SR) Ca^{2+} ATPase (SERCA) in mouse ventricular CMs, leading to altered calcium handling already in the early stage of DCM, before changes in left ventricular function have occurred (Morales Rodriguez et al., 2020). Further, age-dependent biochemical remodeling of the ryanodine receptor 2 (RYR2) in the heart that lead to "leaky" RYRs and a subsequent increase of the SR Ca^{2+} leak has been shown to play a role in cardiomyopathy caused by *LMNA* H222P mutation (Dridi et al., 2021). A recent study showed that iPSC-CMs harboring K117fs *LMNA* mutation, which ultimately causes *LMNA* haploinsufficiency, display aberrant calcium homeostasis that leads to arrhythmias (Lee et al., 2019). Mechanistically, Lee et al. (2019) demonstrated that abnormal epigenetic activation of *PDGFRB*, caused by the K117fs *LMNA* mutation, resulted in an increased CAMK2D and RYR2 phosphorylation and arrhythmias. To what extend changes in Ca^{2+} levels resulting from RYR2 phosphorylation induces further changes in chromatin structure in *LMNA* mutant CMs still needs to be elucidated. Intriguingly, epigenetic silencing of *SCN5A* caused by a different *LMNA* mutation, K219T, leads to decreased expression of $Na_v1.5$ channel, altered action potential, reduced peak sodium current and diminished conduction velocity in iPSC-CMs (Salvarani et al., 2019), further highlighting the role of lamin A in epigenetic regulation of ion homeostasis in CMs. However, more studies are required to elucidate the common and distinct mechanisms caused by different

pathogenic *LMNA* mutations on CM ion handling and triggered arrhythmias.

Since CMs represent the main functional unit of the heart, most studies investigating the development and progression of cardiac diseases associated with *LMNA* mutations have been focusing on this cell type. However, within the heart, CMs, endothelial cells (ECs) and fibroblasts (FBs) all sense and respond to mechanical stimuli and communicate, thereby affecting each other's behavior and functionality (Tirziu et al., 2010; Granados-Riveron and Brook, 2012; Tian and Morrisey, 2012; Saucerman et al., 2019). Up to now, only few studies examined the EC contribution to cardiac laminopathies (Osmanagic-Myers et al., 2018; Sayed et al., 2020). Sayed et al. (2020) showed that *LMNA* K117fs mutation causes epigenetic silencing of Krüppel-like factor 2 (KLF2) in hiPSCs–derived ECs, which in turn leads to impaired KLF2-mediated EC response to shear stress and EC dysfunction. Impaired shear stress response has also been noted in endothelium-specific progeria mouse model (Osmanagic-Myers et al., 2018). Endothelial specific progerin expression affected the levels and structural organization of actin as well as nuclear envelope proteins involved in shear stress force transmission, namely SUN1/2 and Emerin. Although cardiac FBs play an important role in ECM homeostasis, the distribution of mechanical forces through the cardiac tissue, but also in adverse cardiac remodeling after myocardial infarction, the role of lamin A loss in fibroblasts in cardiac disease development is not known. Thus, understanding the fibroblast contribution and the heterocellular crosstalk in cardiac laminopathies will be instrumental for the discovery and design and novel therapeutic strategies for this life-threatening disease.

Alterations in other members of the LINC complex also play an instrumental role in cardiac disease pathogenesis. For example, SUN2-null mice display cardiac hypertrophy with concomitant increase in AKT/MAPK signaling, similar to mice lacking A-type lamins, but do not develop fibrosis or upregulate pathological hypertrophy markers, in contrast to lamin A/C-null mice (Stewart et al., 2019). Haploinsufficiency of *TMEM43* gene specifically in CMs leads to a late-onset cardiomyopathy accompanied by myocardial fibrosis (Rouhi et al., 2020). Nesprins play an important role in the protection of CMs against mechanical stress-induced pathophysiological changes. Depletion of Nesprin-3 or its binding partner desmin leads to a nucleus collapse, loss of genome organization, DNA damage and broad transcriptional changes that may contribute to the pathophysiological changes observed in desmin-related cardiomyopathies (Heffler et al., 2020), highlighting an important role of the desmin cytoskeleton in nuclear stability and genome organization. Dual ablation of both Nesprin 1 and 2 in CMs results in early onset cardiomyopathy with mutant CMs exhibiting altered nuclear positioning and shape as well as chromatin architecture (Banerjee et al., 2014). Moreover, several studies conducted in *Drosophila* have suggested that the LINC complex members are crucial for nuclear positioning-guided sarcomere formation (Auld and Folker, 2016; Wang et al., 2018). Muscle specific depletion of either the KASH domain–containing protein klarsicht (klar) or the SUN domain–containing protein klaroid (koi) blocked the recruitment of the Z-line protein ZASP to the nucleus during the early stages of sarcomere assembly, resulting in sarcomere formation defects (Auld and Folker, 2016). However, further investigations need to be conducted to address whether nuclear positioning precedes sarcomere formation in the mammalian heart. Nesprins might also be important in regulating ECs function upon mechanical forces-induced pathophysiological changes. In human umbilical vein ECs, knockdown of either Nesprin-1 or Nesprin-2 leads to an increase in EC spreading and stress fiber levels and decreases EC migration (King et al., 2014). Moreover, knockdown of Nesprin-3 attenuated the directional migration of human aortic ECs in response to shear stress (Morgan et al., 2011). Thus, understanding the role of the different components of the LINC complex in cardiac endothelial cells will be critical to understanding the mechanosensitive mechanisms in EC controlling cardiac function.

Taken together, these data demonstrate the importance of the LINC complex and its interaction partners for proper cardiovascular function and highlights the role of the LINC complex as a regulatory hub translating mechanical signals into chromatin changes.

CONCLUDING REMARKS AND PERSPECTIVES

The response of cells to mechanical cues is a complex multilevel process that allows cells to adapt to the changes in their microenvironment. Recent studies have brought into the spotlight the direct mechanical force propagation to chromatin and the molecular players involved in this process, such as the actomyosin, the LINC complex and the nuclear lamins. Tension-induced epigenetic and transcriptional programming in the distinct cardiovascular cell types feeds back to the cytoskeleton and the extracellular matrix to balance the outside and inside forces. Thus, dissecting the players at the interface of mechanical forces and epigenetics and understanding the heterocellular crosstalk in the heart evoked by biophysical stimuli will bring key insights into the mechanosensitive mechanisms underlying cardiovascular function and dysfunction, and pinpoint novel therapeutic targets for cardiovascular diseases, the leading cause of death globally.

AUTHOR CONTRIBUTIONS

Both authors listed have made a substantial, direct and intellectual contribution to the work, and approved it for publication.

FUNDING

GD was supported by the SFB 1366, the TRR81, the SFB 873 funded by the DFG as well as the DZHK, funded by BMBF.

REFERENCES

Alisafaei, F., Jokhun, D. S., Shivashankar, G. V., and Shenoy, V. B. (2019). Regulation of nuclear architecture, mechanics, and nucleocytoplasmic shuttling of epigenetic factors by cell geometric constraints. *Proc. Natl. Acad. Sci. U. S. A.* 116, 13200–13209. doi: 10.1073/pnas.1902035116

Andrés-Delgado, L., and Mercader, N. (2016). Interplay between cardiac function and heart development. *Biochim. Biophys. Acta* 1863, 1707–1716. doi: 10.1016/j.bbamcr.2016.03.004

Auld, A. L., and Folker, E. S. (2016). Nucleus-dependent sarcomere assembly is mediated by the LINC complex. *Mol. Biol. Cell* 27, 2351–2359. doi: 10.1091/mbc.e16-01-0021

Banerjee, I., Zhang, J., Moore-Morris, T., Pfeiffer, E., Buchholz, K. S., Liu, A., et al. (2014). Targeted ablation of Nesprin 1 and Nesprin 2 from murine myocardium results in cardiomyopathy, altered nuclear morphology and inhibition of the biomechanical gene response. *PLoS Genet.* 10:e1004114. doi: 10.1371/journal.pgen.1004114

Buxboim, A., Swift, J., Irianto, J., Spinler, K. R., Dingal, P. C. D. P., Athirasala, A., et al. (2014). Matrix elasticity regulates lamin-A,C phosphorylation and turnover with feedback to actomyosin. *Curr. Biol.* 24, 1909–1917. doi: 10.1016/j.cub.2014.07.001

Cheedipudi, S. M., Matkovich, S. J., Coarfa, C., Hu, X., Robertson, M. J., Sweet, M., et al. (2019). Genomic reorganization of lamin-associated domains in cardiac myocytes is associated with differential gene expression and DNA methylation in human dilated cardiomyopathy. *Circ. Res.* 124, 1198–1213. doi: 10.1161/circresaha.118.314177

Cho, S., Vashisth, M., Abbas, A., Majkut, S., Vogel, K., Xia, Y., et al. (2019). Mechanosensing by the lamina protects against nuclear rupture, DNA damage, and cell-cycle arrest. *Dev. Cell* 49, 920–935.e5.

Dorn, T., Kornherr, J., Parrotta, E. I., Zawada, D., Ayetey, H., Santamaria, G., et al. (2018). Interplay of cell–cell contacts and RhoA/MRTF-A signaling regulates cardiomyocyte identity. *EMBO J.* 37:e98133.

Dridi, H., Wu, W., Reiken, S. R., Ofer, R. M., Liu, Y., Yuan, Q., et al. (2021). Ryanodine receptor remodeling in cardiomyopathy and muscular dystrophy caused by lamin A/C gene mutation. *Hum. Mol. Genet.* 29, 3919–3934. doi: 10.1093/hmg/ddaa278

Dupont, S., Morsut, L., Aragona, M., Enzo, E., Giulitti, S., Cordenonsi, M., et al. (2011). Role of YAP/TAZ in mechanotransduction. *Nature* 474, 179–183.

Elosegui-Artola, A., Andreu, I., Beedle, A. E. M., Lezamiz, A., Uroz, M., Kosmalska, A. J., et al. (2017). Force triggers YAP nuclear entry by regulating transport across nuclear pores. *Cell* 171, 1397–1410.e14.

Furusawa, T., Rochman, M., Taher, L., Dimitriadis, E. K., Nagashima, K., Anderson, S., et al. (2015). Chromatin decompaction by the nucleosomal binding protein HMGN5 impairs nuclear sturdiness. *Nat. Commun.* 6:6138.

Gesson, K., Rescheneder, P., Skoruppa, M. P., von Haeseler, A., Dechat, T., and Foisner, R. (2016). A-type lamins bind both hetero- and euchromatin, the latter being regulated by lamina-associated polypeptide 2 alpha. *Genome Res.* 26, 462–473. doi: 10.1101/gr.196220.115

Ghosh, S., Cuevas, V. C., Seelbinder, B., and Neu, C. P. (2021). Image-based elastography of heterochromatin and euchromatin domains in the deforming cell nucleus. *Small* 17:e2006109.

Granados-Riveron, J. T., and Brook, J. D. (2012). The impact of mechanical forces in heart morphogenesis. *Circ. Cardiovasc. Genet.* 5, 132–142. doi: 10.1161/circgenetics.111.961086

Guilluy, C., Osborne, L. D., Landeghem, L. V., Sharek, L., Superfine, R., Garcia-Mata, R., et al. (2014). Isolated nuclei adapt to force and reveal a mechanotransduction pathway in the nucleus. *Nat. Cell Biol.* 16, 376–381. doi: 10.1038/ncb2927

Haase, K., Macadangdang, J. K. L., Edrington, C. H., Cuerrier, C. M., Hadjiantoniou, S., Harden, J. L., et al. (2016). Extracellular forces cause the nucleus to deform in a highly controlled anisotropic manner. *Sci. Rep.* 6:21300.

Hahn, C., and Schwartz, M. A. (2009). Mechanotransduction in vascular physiology and atherogenesis. *Nat. Rev. Mol. Cell Biol.* 10, 53–62. doi: 10.1038/nrm2596

Heffler, J., Shah, P. P., Robison, P., Phyo, S., Veliz, K., Uchida, K., et al. (2020). A balance between intermediate filaments and microtubules maintains nuclear architecture in the cardiomyocyte. *Circ. Res.* 126, e10–e26.

Hershberger, R. E., Hedges, D. J., and Morales, A. (2013). Dilated cardiomyopathy: the complexity of a diverse genetic architecture. *Nat. Rev. Cardiol.* 10, 531–547. doi: 10.1038/nrcardio.2013.105

Ihalainen, T. O., Aires, L., Herzog, F. A., Schwartlander, R., Moeller, J., and Vogel, V. (2015). Differential basal-to-apical accessibility of lamin A/C epitopes in the nuclear lamina regulated by changes in cytoskeletal tension. *Nat. Mater.* 14, 1252–1261. doi: 10.1038/nmat4389

Isermann, P., and Lammerding, J. (2013). Nuclear mechanics and mechanotransduction in health and disease. *Curr. Biol.* 23, R1113–R1121.

Jaalouk, D. E., and Lammerding, J. (2009). Mechanotransduction gone awry. *Nat. Rev. Mol. Cell Biol.* 10, 63–73. doi: 10.1038/nrm2597

Karbassi, E., Rosa-Garrido, M., Chapski, D. J., Wu, Y., Ren, S., Wang, Y., et al. (2019). Direct visualization of cardiac transcription factories reveals regulatory principles of nuclear architecture during pathological remodeling. *J. Mol. Cell. Cardiol.* 128, 198–211. doi: 10.1016/j.yjmcc.2019.02.003

Kim, J.-K., Louhghalam, A., Lee, G., Schafer, B. W., Wirtz, D., Kim, D. H., et al. (2017). Nuclear lamin A/C harnesses the perinuclear apical actin cables to protect nuclear morphology. *Nat. Commun.* 8:2123.

King, S. J., Nowak, K., Suryavanshi, N., Holt, I., Shanahan, C. M., and Ridley, A. J. (2014). Nesprin-1 and nesprin-2 regulate endothelial cell shape and migration. *Cytoskeleton* 71, 423–434. doi: 10.1002/cm.21182

Kirby, T. J., and Lammerding, J. (2018). Emerging views of the nucleus as a cellular mechanosensor. *Nat. Cell Biol.* 20, 373–381. doi: 10.1038/s41556-018-0038-y

Le, H. Q., Ghatak, S., Yeung, C. Y. C., Tellkamp, C., Günschmann, C., Dieterich, C., et al. (2016). Mechanical regulation of transcription controls Polycomb-mediated gene silencing during lineage commitment. *Nat. Cell. Biol.* 18, 864–875. doi: 10.1038/ncb3387

Lee, J., Termglinchan, V., Diecke, S., Itzhaki, I., Lam, C. K., Garg, P., et al. (2019). Activation of PDGF pathway links LMNA mutation to dilated cardiomyopathy. *Nature* 572, 335–340. doi: 10.1038/s41586-019-1406-x

Morales Rodriguez, B., Domínguez-Rodríguez, A., Benitah, J. P., Lefebvre, F., Marais, T., Mougenot, N., et al. (2020). Activation of sarcolipin expression and altered calcium cycling in LMNA cardiomyopathy. *Biochem. Biophys. Rep.* 22:100767. doi: 10.1016/j.bbrep.2020.100767

Morgan, J. T., Pfeiffer, E. R., Thirkill, T. L., Kumar, P., Peng, G., Fridolfsson, H. N., et al. (2011). Nesprin-3 regulates endothelial cell morphology, perinuclear cytoskeletal architecture, and flow-induced polarization. *Mol. Biol. Cell* 22, 4324–4334. doi: 10.1091/mbc.e11-04-0287

Nava, M. M., Miroshnikova, Y. A., Biggs, L. C., Whitefield, D. B., Metge, F., Boucas, J., et al. (2020). Heterochromatin-driven nuclear softening protects the genome against mechanical stress-induced damage. *Cell* 181, 800–817.e22.

Osmanagic-Myers, S., Kiss, A., Manakanatas, C., Hamza, O., Sedlmayer, F., Szabo, P. L., et al. (2018). Endothelial progerin expression causes cardiovascular pathology through an impaired mechanoresponse. *J. Clin. Investig.* 129, 531–545. doi: 10.1172/jci121297

Poleshko, A., Shah, P. P., Gupta, M., Babu, A., Morley, M. P., Manderfield, L. J., et al. (2017). Genome-nuclear lamina interactions regulate cardiac stem cell lineage restriction. *Cell* 171, 573–587.e14.

Reddy, K. L., Zullo, J. M., Bertolino, E., and Singh, H. (2008). Transcriptional repression mediated by repositioning of genes to the nuclear lamina. *Nature* 452, 243–247. doi: 10.1038/nature06727

Rosa-Garrido, M., Chapski, D. J., Schmitt, A. D., Kimball, T. H., Karbassi, E., Monte, E., et al. (2017). High-resolution mapping of chromatin conformation in cardiac myocytes reveals structural remodeling of the epigenome in heart failure. *Circulation* 136, 1613–1625. doi: 10.1161/circulationaha.117.029430

Rouhi, L., Cheedipudi, S. M., Chen, S. N., Fan, S., Lombardi, R., Chen, X., et al. (2020). Haploinsufficiency of Tmem43 in cardiac myocytes activates the DNA damage response pathway leading to a late-onset senescence-associated pro-fibrotic cardiomyopathy. *Cardiovasc. Res.* doi: 10.1093/cvr/cvaa300 [Epub ahead of print].

Salvarani, N., Crasto, S., Miragoli, M., Bertero, A., Paulis, M., Kunderfranco, P., et al. (2019). The K219T-Lamin mutation induces conduction defects through epigenetic inhibition of SCN5A in human cardiac laminopathy. *Nat. Commun.* 10:2267.

Saucerman, J. J., Tan, P. M., Buchholz, K. S., McCulloch, A. D., and Omens, J. H. (2019). Mechanical regulation of gene expression in cardiac myocytes and fibroblasts. *Nat. Rev. Cardiol.* 16, 361–378. doi: 10.1038/s41569-019-0155-8

Sayed, N., Liu, C., Ameen, M., Himmati, F., Zhang, J. Z., Khanamiri, S., et al. (2020). Clinical trial in a dish using iPSCs shows lovastatin improves endothelial dysfunction and cellular cross-talk in LMNA cardiomyopathy. *Sci. Transl. Med.* 12:eaax9276. doi: 10.1126/scitranslmed.aax9276

Shah, P. P., Lv, W., Rhoades, J. H., Poleshko, A., Abbey, D., Caporizzo, M. A., et al. (2021). Pathogenic LMNA variants disrupt cardiac lamina-chromatin interactions and de-repress alternative fate genes. *Cell Stem Cell* 28, 938–954.e9.

Shimi, T., Pfleghaar, K., Kojima, S., Pack, C. G., Solovei, I., Goldman, A. E., et al. (2008). The A- and B-type nuclear lamin networks: microdomains involved in chromatin organization and transcription. *Genes Dev.* 22, 3409–3421. doi: 10.1101/gad.1735208

Spagnol, S. T., and Noel Dahl, K. (2014). Active cytoskeletal force and chromatin condensation independently modulate intranuclear network fluctuations. *Integr. Biol.* 6, 523–531. doi: 10.1039/c3ib40226f

Stephens, A. D., Banigan, E. J., Adam, S. A., Goldman, R. D., and Marko, J. F. (2017). Chromatin and lamin A determine two different mechanical response regimes of the cell nucleus. *Mol. Biol. Cell* 28, 1984–1996. doi: 10.1091/mbc.e16-09-0653

Stephens, A. D., Liu, P. Z., Banigan, E. J., Almassalha, L. M., Backman, V., Adam, S. A., et al. (2018). Chromatin histone modifications and rigidity affect nuclear morphology independent of lamins. *Mol. Biol. Cell* 29, 220–233. doi: 10.1091/mbc.e17-06-0410

Stephens, A. D., Liu, P. Z., Kandula, V., Chen, H., Almassalha, L. M., Herman, C., et al. (2019). Physicochemical mechanotransduction alters nuclear shape and mechanics via heterochromatin formation. *Mol. Biol. Cell* 30, 2320–2330. doi: 10.1091/mbc.e19-05-0286

Stewart, R. M., Rodriguez, E. C., and King, M. C. (2019). Ablation of SUN2-containing LINC complexes drives cardiac hypertrophy without interstitial fibrosis. *Mol. Biol. Cell* 30, 1664–1675. doi: 10.1091/mbc.e18-07-0438

Stroud, M. J. (2018). Linker of nucleoskeleton and cytoskeleton complex proteins in cardiomyopathy. *Biophys. Rev.* 10, 1033–1051. doi: 10.1007/s12551-018-0431-6

Stroud, M. J., Banerjee, I., Veevers, J., and Chen, J. (2014). Linker of nucleoskeleton and cytoskeleton complex proteins in cardiac structure, function, and disease. *Circ. Res.* 114, 538–548. doi: 10.1161/circresaha.114.301236

Sun, J., Chen, J., Mohagheghian, E., and Wang, N. (2020). Force-induced gene up-regulation does not follow the weak power law but depends on H3K9 demethylation. *Sci. Adv.* 6:eaay9095. doi: 10.1126/sciadv.aay9095

Swift, J., Ivanovska, I. L., Buxboim, A., Harada, T., Dingal, P. C. D. P., Pinter, J., et al. (2013). Nuclear Lamin-A scales with tissue stiffness and enhances matrix-directed differentiation. *Science* 341:1240104. doi: 10.1126/science.1240104

Tajik, A., Zhang, Y., Wei, F., Sun, J., Jia, Q., Zhou, W., et al. (2016). Transcription upregulation via force-induced direct stretching of chromatin. *Nat. Mater.* 15, 1287–1296. doi: 10.1038/nmat4729

Tian, Y., and Morrisey, E. E. (2012). Importance of myocyte-nonmyocyte interactions in cardiac development and disease. *Circ. Res.* 110, 1023–1034. doi: 10.1161/circresaha.111.243899

Tirziu, D., Giordano, F. J., and Simons, M. (2010). Cell communications in the heart. *Circulation* 122, 928–937. doi: 10.1161/circulationaha.108.847731

Versaevel, M., Braquenier, J. B., Riaz, M., Grevesse, T., Lantoine, J., and Gabriele, S. (2015). Super-resolution microscopy reveals LINC complex recruitment at nuclear indentation sites. *Sci. Rep.* 4:7362.

Wang, N., Tytell, J. D., and Ingber, D. E. (2009). Mechanotransduction at a distance: mechanically coupling the extracellular matrix with the nucleus. *Nat. Rev. Mol. Cell Biol.* 10, 75–82. doi: 10.1038/nrm2594

Wang, S., Stoops, E., Cp, U., Markus, B., Reuveny, A., Ordan, E., et al. (2018). Mechanotransduction via the LINC complex regulates DNA replication in myonuclei. *J. Cell Biol.* 217, 2005–2018. doi: 10.1083/jcb.201708137

Wei, F., Xu, X., Zhang, C., Liao, Y., Ji, B., and Wang, N. (2020). Stress fiber anisotropy contributes to force-mode dependent chromatin stretching and gene upregulation in living cells. *Nat. Commun.* 11:4902.

Wen, B., Wu, H., Shinkai, Y., Irizarry, R. A., and Feinberg, A. P. (2009). Large histone H3 lysine 9 dimethylated chromatin blocks distinguish differentiated from embryonic stem cells. *Nat. Genet.* 41, 246–250. doi: 10.1038/ng.297

Zhang, X., Shao, X., Zhang, R., Zhu, R., and Feng, R. (2021). Integrated analysis reveals the alterations that LMNA interacts with euchromatin in LMNA mutation-associated dilated cardiomyopathy. *Clin. Epigenetics* 13:3.

Zheng, X., Hu, J., Yue, S., Kristiani, L., Kim, M., Sauria, M., et al. (2018). Lamins organize the global three-dimensional genome from the nuclear periphery. *Mol. Cell* 71, 802–815.e7.

Conflict of Interest: The authors declare that the research was conducted in the absence of any commercial or financial relationships that could be construed as a potential conflict of interest.

Publisher's Note: All claims expressed in this article are solely those of the authors and do not necessarily represent those of their affiliated organizations, or those of the publisher, the editors and the reviewers. Any product that may be evaluated in this article, or claim that may be made by its manufacturer, is not guaranteed or endorsed by the publisher.

frontiers in Physiology

ORIGINAL RESEARCH
published: 19 August 2021
doi: 10.3389/fphys.2021.710619

Substrate Stiffness Influences Structural and Functional Remodeling in Induced Pluripotent Stem Cell-Derived Cardiomyocytes

*Arlene Körner[1,2], Matias Mosqueira[1], Markus Hecker[1,2] and Nina D. Ullrich[1,2]**

[1]Division of Cardiovascular Physiology, Institute of Physiology and Pathophysiology, Heidelberg University, Heidelberg, Germany, [2]German Center for Cardiovascular Research (DZHK), Partner Site Heidelberg-Mannheim, Heidelberg, Germany

Novel treatment strategies for cardiac tissue regeneration are heading for the use of engineered cardiac tissue made from induced pluripotent stem cell-derived cardiomyocytes (iPSC-CMs). Despite the proven cardiogenic phenotype of these cells, a significant lack of structural and functional properties of mature myocytes prevents safe integration into the diseased heart. To date, maturation processes of cardiomyocytes remain largely unknown but may comprise biophysical cues from the immediate cell environment. Mechanosensing is one critical ability of cells to react to environmental changes. Accordingly, the surrounding substrate stiffness, comprised of extracellular matrix (ECM), cells, and growth surface, critically influences the myocyte's physiology, as known from deleterious remodeling processes in fibrotic hearts. Conversely, the mechanical properties during culture of iPSC-CMs may impact on their structural and functional maturation. Here, we tested the hypothesis that the environmental stiffness influences structural and functional properties of iPSC-CMs and investigated the effect of different substrate stiffnesses on cell contractility, excitation-contraction (EC) coupling, and intercellular coupling. Culture surfaces with defined stiffnesses ranging from rigid glass with 25 GPa to PDMS of physiological softness were coated with ECM proteins and seeded with murine iPSC-CMs. Using confocal imaging, cardiac protein expression was assessed. Ca^{2+} handling and contractile properties were analyzed on different substrate stiffnesses. Intercellular coupling *via* gap junctions was investigated by fluorescence recovery after photobleaching (FRAP). Our data revealed greater organization of L-type Ca^{2+} channels and ryanodine receptors and increased EC-coupling gain, demonstrating structural and functional maturation in cells grown on soft surfaces. In addition, increased shortening and altered contraction dynamics revealed increased myofilament Ca^{2+} sensitivity in phase-plane loops. Moreover, connexin 43 expression was significantly increased in iPSC-CMs grown on soft surfaces leading to improved intercellular coupling. Taken together, our results demonstrate that soft surfaces with stiffnesses in the physiological range improve the expression pattern and interaction of cardiac proteins relevant for EC-coupling. In parallel, soft substrates influence contractile properties and improve intercellular coupling in iPSC-CMs. We conclude that the mechanical stiffness of the cell environment plays an important role in driving iPSC-CMs toward further maturation by inducing adaptive responses.

OPEN ACCESS

Edited by:
Claudia Penna, University of Turin, Italy

Reviewed by:
Elisa Di Pasquale, National Research Council, Italy
Guiling Zhao, University of Maryland, Baltimore, United States

***Correspondence:**
Nina D. Ullrich
nina.ullrich@physiologie.uni-heidelberg.de

Specialty section:
This article was submitted to Vascular Physiology, a section of the journal Frontiers in Physiology

Received: *16 May 2021*
Accepted: *26 July 2021*
Published: *19 August 2021*

Citation:
Körner A, Mosqueira M, Hecker M and Ullrich ND (2021) Substrate Stiffness Influences Structural and Functional Remodeling in Induced Pluripotent Stem Cell-Derived Cardiomyocytes. Front. Physiol. 12:710619. doi: 10.3389/fphys.2021.710619

Keywords: induced pluripotent stem cell-derived cardiomyocytes, excitation-contraction coupling, contraction, gap junctions, stiffness

INTRODUCTION

Cardiovascular medicine is presently facing a new challenge with rapidly rising numbers of patients suffering from heart disease, the leading cause of death worldwide (Virani et al., 2020). Because of the limited regenerative potential of the adult heart, dying cardiomyocytes are replaced by non-contractile connective tissue thereby inducing detrimental structural remodeling (Jiang et al., 2018). More precisely, massive fibroblast proliferation and collagen deposition lead to the formation of a firm scar (Pfeffer and Braunwald, 1990). Remodeling of extracellular matrix (ECM) finally results in fibrosis involving increased stiffness of the cardiac environment (30–55 kPa instead of 10–15 kPa of healthy cardiac tissue) and leading to impaired contractility (Gaetani et al., 2020). Since therapeutic options for heart failure patients are limited, research in cardiac regenerative medicine is heading toward the generation of engineered human myocardium (EHM) made of induced pluripotent stem cell-derived cardiomyocytes (iPSC-CMs; Fujita and Zimmermann, 2018). Over the last years, reliable differentiation protocols have been established and successful production of iPSC-CMs with an adequately high yield for clinical applications has turned an initial research tool into a realistic option for myocardial repair (Burridge et al., 2012). The electrophysiological profile and contractile activity of iPSC-CMs confirm true cardiogenic features and fuel hope for the development of novel and promising treatment strategies (Silbernagel et al., 2020). Indeed, remuscularization by iPSC-CMs grafts and improvement of cardiac function after myocardial infarction have already been demonstrated in various animal models (Chong et al., 2014; Gao et al., 2018; Pecha et al., 2019).

Nevertheless, iPSC-CMs still present an immature and variable phenotype with functional features similar to cardiomyocytes of early developmental stages (Yang et al., 2014). In contrast to the elongated anisotropic shape and precise microarchitecture of adult cardiomyocytes, iPSC-CMs show an irregular and unspecific geometry resulting in a diffuse intracellular distribution of myofibrils with variable degrees of sarcomere organization (Gherghiceanu et al., 2011; Silbernagel et al., 2020). Another ultrastructural deficiency in iPSC-CMs is given by the lack of transverse (t)-tubules (Yang et al., 2014). In the adult heart, these highly specialized sarcolemmal structures come in close vicinity to the end-cisterns of the sarcoplasmic reticulum (SR) spaced by a 15 to 20 nm wide dyadic cleft. This special arrangement allows for close interaction of the sarcolemmal L-type Ca^{2+} channels (LTCCs) and the ryanodine receptors (RyR2s), the Ca^{2+} release channels of the SR. Both channels are fundamental to the mechanism of excitation-contraction (EC) coupling and control cytosolic Ca^{2+} entry by Ca^{2+}-induced Ca^{2+} release (CICR), which links electrical excitation to contractile activity and force production by the myocyte in a highly spatiotemporally synchronized way (Bers, 2002; Kane et al., 2015). Although CICR has been demonstrated in iPSC-CMs (Itzhaki et al., 2011), these cells show immature Ca^{2+} handling and desynchronized Ca^{2+} transients (Lieu et al., 2009). The spontaneous contractile activity of iPSC-CMs is another hallmark of immaturity, which is probably caused by spontaneous Ca^{2+} release from the SR triggering depolarizing membrane current *via* the sodium-calcium-exchanger (NCX; Zahanich et al., 2011; Kane et al., 2015; Karbassi et al., 2020).

The consequence of missing t-tubules and thus poor coupling of LTCCs and RyR2s is inefficient Ca^{2+} handling, which may lead to enhanced activity of the so-called orphaned RyR2s (Lee et al., 2011; Rao et al., 2013). Moreover, in addition to inefficient EC-coupling, we have recently described weaknesses in intercellular coupling between iPSC-CMs. As iPSC-CMs do not develop a precise structural orientation, intercalated disks are not well-defined with the consequence of a diffuse distribution of gap junctions and their main subunit connexin-43 (Cx43). Since the expression pattern of Cx43 is not localized at specific end poles of the cell as known from adult cardiomyocytes, electrical signal propagation is not directed but diffuse and heterogeneous across the cell layer. In addition, reduced clustering of Cx43 results in significantly slower conduction velocity compared to native cardiomyocytes (Kucera et al., 2015; Marcu et al., 2015; Jiang et al., 2018; Sottas et al., 2018; Karbassi et al., 2020).

In light of future therapeutic applications, immature Ca^{2+} handling and reduced intercellular coupling in iPSC-CMs present high-risk factors for the development of arrhythmogenic modifications after implantation (Shiba et al., 2012; Chong et al., 2014). To improve the electrophysiological properties of iPSC-CMs, different approaches have been tested to enhance functional maturation in iPSC-CMs at the level of EC-coupling. They include natural time-dependent maturation processes during long-term culture, the addition of hormones, such as triiodothyronine (Kamakura et al., 2013; Lundy et al., 2013; Yang et al., 2014), or enhanced expression of Cx43 (Sottas et al., 2018). Moreover, co-cultures with non-cardiomyocytes were shown to promote maturity features (Kroll et al., 2017; Yoshida et al., 2018), which may also explain the successful transplantation experiments of iPSC-CMs into adult hearts providing a more natural cell environment compared to culture conditions (Kadota et al., 2017). Another important aspect of the cardiac environment influencing maturation is the composition of the ECM (Young et al., 2014). The combination of iPSC-CM growth together with non-cardiomyocytes in a specifically composed ECM led to the development of 3D-engineered human myocardium, which improved cardiac properties after implantation in animal models (Tiburcy et al., 2017; Weinberger et al., 2017; Ronaldson-Bouchard et al., 2018; Yeung et al., 2019).

Furthermore, the stiffness of the surrounding material is another critical parameter of the natural cardiac environment, and its influence on the functional improvement and maturation of EC-coupling in iPSC-CMs has not been elucidated yet.

Tissue stiffness changes significantly during cardiac development from the fetal to the adult heart, and conversely, structural remodeling in the diseased heart, such as inflammation and fibrotic lesions, leads to further changes in cardiac tissue stiffness. Altered protein expression, including the expression of different isoforms of integrin receptors, may control the sensing and interaction of the cell with its environment and trigger outside-in signaling pathways, which induce long-term remodeling processes influencing structural and functional properties of the cardiomyocytes (Ward and Iskratsch, 2020). Extrapolated to the development of iPSC-CMs, the stiffness of the growth surface and immediate environment may have a strong impact on further maturation processes in these young cardiomyocytes.

In this study, we tested the hypothesis that substrate stiffness of the cell environment influences the structural and functional maturation of iPSC-CMs. Cells were grown on different culture surfaces with defined stiffnesses ranging from rigid glass (25 GPa) to the silicone-based organic polymer polydimethylsiloxane (PDMS) of different softness (28 kPa, 15 kPa, and 1.5 kPa). We focused on intracellular Ca^{2+} handling and analyzed EC-coupling properties with a special focus on the expression and function of the LTCC and RyR2. Moreover, we investigated Cx43 expression in iPSC-CMs grown on soft surfaces and evaluated intercellular communication in cell monolayers. We demonstrate that iPSC-CMs grown on surfaces of physiological stiffness exhibit more mature structural and functional properties at the level of Ca^{2+} handling and intercellular coupling compared to cells grown on rigid surfaces. Thus, specific control of the environmental properties increases the potential of iPSC-CMs to develop into mature cardiomyocytes that can be used for cardiac engineering and cell replacement therapies for diseased hearts.

MATERIALS AND METHODS

Cell Models

Murine iPSC-CMs were received from Ncardia (Cologne, Germany) and kept in liquid nitrogen until use. Culture dishes were coated with a mixture of laminin and fibronectin in PBS (1:1:100) overnight at 37°C to enable attachment of iPSC-CMs. After defrosting, cells were seeded in Cor.AT® medium (Ncardia, Cologne, Germany) at a density of 2×10^4 cells per dish for Ca^{2+} measurements and on glass coverslips in 24-well plates (Sarstedt, Nümbrecht, Germany) for immunostainings, and at 10^4 cells per dish onto glass-bottom dishes (35 mm, MatTek, Ashland, MA, United States) and PDMS-coated dishes (35 mm, Ibidi GmbH, Gräfelfing, Germany) for electrophysiological experiments and live-cell imaging analysis.

To avoid the growth of undifferentiated cells and non-cardiomyocytes, the cardiomyocyte-specific α-myosin heavy chain (α-MHC) promoter was chosen to control pac gene expression for puromycin resistance. Puromycin (1 μg/ml) was added for the selection of cardiac-specific cells for the first 48 h in culture. Afterward, cells were kept in culture in puromycin-free Cor.At® medium. Cells were maintained in culture at 37°C and 5% CO_2 and used within 4 weeks.

Live-Cell Imaging and Cellular Electrophysiology

For all live-cell imaging experiments, the standard bath solution was cardiac Tyrode's solution containing (in mm): NaCl 140, KCl 5.4, $CaCl_2$ 1.8, $MgCl_2$ 1.1, HEPES 5, glucose 10, pH 7.4.

Measurement of Ca^{2+} Transients and Myocyte Contractility

Ca^{2+} transients of iPSC-CMs were recorded using the ratiometric Ca^{2+}-sensitive fluorescent indicator fura-2 AM (Thermo Fisher Scientific, Dreieich, Germany). Cells were loaded with 1.5 μm fura-2 AM diluted in Tyrode's solution and incubated for 20 min, followed by 10 min of de-esterification. iPSC-CMs were constantly perfused with prewarmed Tyrode's solution containing Probenecid (100 μm) to avoid sequestration or secretion of fura-2. Using the IonOptix system (IonOptix, Dublin, Ireland), Ca^{2+} transients were recorded in parallel with edge detection to measure contractions. Data were collected by using the IonWizard software developed by IonOptix. Cells were exposed to light emitted by a xenon lamp passing through rapidly switching filters of 340 nm and 360 nm to determine the ratio of bound and unbound Ca^{2+} ions in the cells. Fluorescence emission light was collected at 510 nm. Data are presented as fura-2 ratio (F_{340}/F_{360}).

For functional evaluation of spontaneous activity, only rhythmically beating iPSC-CMs were used. Five representative Ca^{2+} transients and contractions at steady state were analyzed per cell using OriginPro® software (OriginLab Corporation, Northampton, MA, United States). Assessed parameters comprised peak Ca^{2+} transients and shortening amplitudes, time-to-peak (TTP), full duration at half maximum (FDHM), decay, and frequency of spontaneous activity. Decay of contractions was fitted with a Boltzmann function, whereas decay of Ca^{2+} transients was calculated by an exponential decay function. Diastolic Ca^{2+} levels of paced iPSC-CMs were only evaluated if cells responded to the frequency of electrical stimulation at 1 Hz and 2 Hz (10 V) by a field stimulator (Myopacer, IonOptix, Dublin, Ireland).

Electrophysiology With Simultaneous Ca^{2+} Imaging

For investigation of the EC-coupling mechanism, Ca^{2+} currents (I_{CaL}) were measured in iPSC-CMs *via* the patch-clamp technique with simultaneous recording of Ca^{2+} signals by confocal line-scan imaging. Experiments were performed using a HEKA EPC-10 patch-clamp amplifier (HEKA Elektronik GmbH, Reutlingen, Germany) connected to an Olympus IX81 laser scanning confocal microscope (Olympus Fluoview FV1000, Olympus, Hamburg, Germany). For patch-clamp recordings, borosilicate glass pipettes were pulled to obtain tip resistances of 2–9 MΩ and filled with an internal solution containing 8 mm NaCl, 120 mm CsAsp, 20 mm TEA-Cl, 5.9 mm $MgCl_2$, 20 mm HEPES, 5 mm K_2-ATP, and 50 μm of the Ca^{2+}-sensitive fluorescent indicator K_5-fluo-3 (Thermo Fisher Scientific, Dreieich, Germany). For I_{CaL} measurements, iPSC-CMs were constantly perfused with warm Tyrode's solution (37°C) containing 5 mm CsCl.

For analysis of the EC-coupling gain, a two-step protocol was applied (adapted from Ullrich et al., 2012). After inactivation of voltage-dependent Na^+ channels by a 500 ms ramp ranging from the holding potential of −80 mv to −40 mv, the first test step was set to −25 mv for 400 ms, followed by a second 400 ms test step from −40 mv to +10 mv to record maximal I_{CaL} and Ca^{2+} release amplitudes.

For line-scan imaging, the excitation wavelength was set at 473 nm and fluorescence emission was collected between 490 nm and 545 nm. Line-scan images were recorded at 2 µs/pixel, 2 ms/line, and 4,000 lines/image. ImageJ/Fiji software was used for image analysis. The fluorescence intensity of line-scan images was plotted over time. The background was subtracted, and line profiles were normalized to baseline. Data are displayed as F/F_0.

For analysis of the EC-coupling gain, the ratio of the peak Ca^{2+} transient amplitude at −25 mv and corresponding peak I_{CaL} amplitude was calculated. Cells with T-type Ca^{2+} current at −25 mv (high amplitude and fast inactivation) and/or cells with low fluo-3 loading ($F/F_0 < 1.2$) were excluded from analysis. As a control, the ratio of the maximal Ca^{2+} transient and current amplitudes at +10 mv was calculated. I_{CaL} at +10 mv was used for the measurement of maximal current amplitude and inactivation kinetics. Fitting I_{CaL} with a biexponential function in OriginPro allowed the comparison of tau_1 (τ_1) as an indicator of Ca^{2+}-dependent inactivation.

For examination of fractional release and NCX activity in iPSC-CMs, patched cells were stimulated to steady-state activity at a frequency of 1 Hz, followed by application of the RyR2 agonist caffeine (10 mm in Tyrode's solution, Sigma-Aldrich) for total depletion of the SR. In parallel with the measurement of SR Ca^{2+} content, caffeine-elicited NCX currents were recorded.

Fluorescence Recovery After Photobleaching

For functional evaluation of gap junctions, fluorescence recovery after photobleaching (FRAP) was measured using the gap junction-permeant dye calcein (0.5 µm calcein-AM, Thermo Fisher Scientific, Dreieich, Germany). Photobleaching and imaging were done on the Olympus FluoView LSCM using a 60x water immersion objective (1.2 NA). iPSC-CMs were loaded with 0.5 µm calcein-AM in Tyrode's solution for 20 min. After 10 min of de-esterification in Tyrode's solution, calcein-diffusion dynamics between iPSC-CMs were assessed as an indicator of functional Cx43 expression and gap junction formation. One cell in a cluster was bleached with a laser power of 50% at 10 µs/pixel for 5 s, and fluorescence recovery was recorded in 52 images taken every 10 s with a laser power of 0.5–1.5% at 2 µs/pixel. Importantly, the target cell had to be fully surrounded by neighboring cells (in 2D), thus representing one building block in a conductive and connected cell layer. Further analysis was done in ImageJ to plot the time course of fluorescence recovery of the bleached cell. After subtraction of background and bleaching point, the graph was normalized to the initial value of fluorescence intensity (before bleaching). The final traces were fitted in OriginPro software with a biexponential function to investigate the fast time constant 1 ($\tau 1$) as an indicator of diffusion rate.

Immunocytochemistry and Image Analysis

For immunostainings, cells were washed with PBS, fixed with 4% paraformaldehyde (Thermo Fisher Scientific, Dreieich, Germany) for 20 min, and washed three times with PBS for 10 min. Different time points were chosen to examine the influence of growth duration on the expression pattern and spatial organization of different Ca^{2+} handling proteins. Cells grown on PDMS-coated dishes were fixed at days 10, 20, and 25 after seeding, cells on glass coverslips after 9, 13, and 20 days. To block unspecific binding sites, cells were incubated with bovine serum albumin dissolved in PBS (10 mg/ml, Sigma-Aldrich, Germany) for 0.5 h at room temperature. For permeabilization of iPSC-CMs, the blocking solution contained 0.1% Triton X-100. Cells were incubated with primary antibodies against Cx43 (mouse, monoclonal, 1:500, MAB3067, MerckMillipore, Darmstadt, Germany), SERCA (mouse, monoclonal, 1:200, ab2861, MerckMillipore, Darmstadt, Germany), NCX1 (mouse, monoclonal, 1:200, MA3-926, Thermo Fisher Scientific, Waltham, MA, United States) or RyR2 (mouse, monoclonal, 1:200, ab2861, AbCam, Cambridge, MA, United States), and $Ca_v1.2$ (rabbit, polyclonal, 1:200, AB10515, MerckMillipore, Darmstadt, Germany) at room temperature for 90 min. After three times washing with PBS for 10 min, cells were incubated with appropriate secondary antibodies conjugated to Alexa Fluor dyes (1:500, Thermo Fisher Scientific) with different excitation-emission spectra for 1 h. After three times washing with PBS for 10 min, samples were incubated for 1 h in Phalloidin-TRITC (1:2000, P1951-1MG, Sigma-Aldrich, Missouri, United States) for actin staining. After final washing steps in PBS, cells were mounted with fluoroshield containing DAPI for nuclei staining (Sigma-Aldrich, Germany).

Samples were imaged with a Leica TCS SP8 LSCM (Leica Microsystems CMS GmbH, Mannheim, Germany) using the acquisition software LAS-X (Vers. 3.5.0.18371, Leica Microsystems CMS GmbH, Mannheim, Germany) for high-resolution images. 20x oil immersion objective was selected to record an overview of Cx43 stainings, and 63x oil immersion objective was used for detailed imaging of SERCA, NCX1, RyR2, and $Ca_v1.2$ expression. Laser excitation at 405 nm, 488 nm, 552 nm, and 638 nm was used in sequential scans. Emission spectra were chosen *via* tunable filters, and emission detection was achieved by photomultiplier tubes (PMT) and hybrid detectors (HyD). Image processing and Cx43 sarcolemmal expression analysis were done using ImageJ/Fiji as described in (Sottas et al., 2018). Due to the strong light absorbance of PDMS-coated surfaces, weak specific fluorescence signals were denoised using the ImageJ plugin PureDenoise developed by Florian Luisier (EPFL, Switzerland).

Data Analysis and Statistics

For statistical data analysis and graph design, OriginPro® software (OriginLab Corporation, Northampton, MA, United States) was used. Images were processed in ImageJ. Data are presented as mean ± standard error of the mean (SEM) with n equaling the number of individually analyzed cells. Experiments were repeated in five rounds with iPSC-CMs

defrosted from five individual vials at different time points (5 vials à 1 Mio cells, acquired from Ncardia). Depending on the data set, statistical significance was determined by Student's *t*-tests or one-way ANOVA followed by multiple comparison tests, indicated by * for $p < 0.05$.

RESULTS

Impact of Different Growth Surface Stiffnesses on iPSC-CMs Contractility

For live-imaging and functional analysis, cells are usually seeded on rigid glass surfaces, which present an unphysiologically high stiffness of 25 GPa. In order to investigate the impact of different physiological substrate stiffnesses on the maturation potential of iPSC-CMs, cells were seeded at high density on glass and for comparison on PDMS culture surfaces with stiffnesses of 28 kPa, 15 kPa, and 1.5 kPa, respectively, corresponding to the environment of neonatal and adult cardiomyocytes. All surfaces were coated with laminin and fibronectin for cell adhesion. Different growth materials did not have any impact on cell adhesion or cell survival during the culture time of up to 4 weeks (data not shown). But a simple examination of cell contractile behavior revealed that compared to glass, the contractile activity of iPSC-CMs appeared stronger and temporally better synchronized across the cell monolayer (**Supplementary Video S1–S4**) indicating increased contractility and intercellular connectivity. To quantify these observations, we investigated EC-coupling and intercellular communication in these cells.

Effects of Different Substrate Stiffnesses on Ca^{2+} Handling and Contractility in iPSC-CMs

To evaluate Ca^{2+} handling and contractile activity in iPSC-CMs, spontaneous Ca^{2+} transients and contraction dynamics were measured in cells seeded on PDMS-coated or glass-bottom dishes. Cells were loaded with the fluorescent Ca^{2+}-sensitive dye fura-2 AM (1.5 µm) to record Ca^{2+} transients, and cell shortening was optically measured *via* edge detection. Due to their immaturity, iPSC-CMs showed high variability in their spontaneous activity pattern. For evaluation of comparable cells, we categorized iPSC-CMs into three different groups of rhythmic, arrhythmic, and oscillating cells (**Figure 1A**). In order to avoid high variability in the experiments, only rhythmically beating cells were included for further analysis. **Figure 1A** demonstrates that the ratio of rhythmically beating cells, as assessed from Ca^{2+} transients' measurements, was higher on glass and on 1.5 kPa-PDMS compared to 28 kPa-PDMS and 15 kPa-PDMS. In contrast to iPSC-CMs seeded on glass, oscillating spontaneous activity was only observed in cells grown on PDMS-coated dishes. According to the distribution of spontaneous activity patterns, rhythmic iPSC-CMs revealed higher spontaneous beating frequencies when grown on glass or 1.5 kPa-PDMS compared to 28 kPa-PDMS and 15 kPa-PDMS (**Figure 1B**). In **Figure 1C**, representative recordings of Ca^{2+} transients illustrate the response to different pacing frequencies, as well as the frequency-dependent changes of diastolic Ca^{2+} levels at 1 and 2 Hz. As shown in **Supplementary Table S1**, the statistical evaluation revealed similar diastolic Ca^{2+} levels in iPSC-CMs during spontaneous beating activity on all tested growth surfaces. Pacing at 1 and 2 Hz slightly enhanced cytosolic basal Ca^{2+} levels on all tested growth surfaces, indicating immature Ca^{2+} handling processes especially at higher stimulation frequencies. Diastolic Ca^{2+} levels revealed no significant differences except for iPSC-CMs on 28 kPa-PDMS compared to glass during pacing at 2 Hz.

Characterization of CICR in iPSC-CMs Grown on Substrates With Different Stiffnesses

To investigate CICR in more detail, we measured membrane Ca^{2+} currents (I_{CaL}) using the whole-cell patch-clamp technique and recorded simultaneously intracellular Ca^{2+} transients by confocal imaging in the line-scan mode. As demonstrated in **Figure 2A**, for electrical stimulation *via* patch-clamp, a two-step protocol was applied to measure I_{CaL} at negative potentials and at maximal current activation. In parallel, changes in cytosolic Ca^{2+} levels were recorded by confocal imaging of fluo-3 included in the patch pipette solution. Starting first from a holding potential of −80 mv, a 500 ms voltage-ramp to −40 mv was applied to activate and immediately inactivate the fast voltage-dependent Na^+ current. After 800 ms at −40 mv, the first test step was applied. E_m was set to −25 mv to activate I_{CaL} and CICR at low amplitude. The second test step to +10 mv fully activated I_{CaL} and served as control measurement for I_{CaL} and CICR. Changes in fluorescence intensity were plotted over time to generate line profiles from the line-scan image, as depicted in **Figure 2Aa**. Analysis of peak I_{CaL} and Ca^{2+} transients at +10 mv showed similar amplitudes in iPSC-CMs grown on substrates with different stiffnesses (**Figure 2B**). Data are summarized in **Supplementary Table S2**. The EC-coupling gain was calculated from the ratio of the peak Ca^{2+} transient amplitude and peak I_{CaL} at −25 mv and at +10 mv. The data showed an increased EC-coupling gain on soft surfaces (**Figure 2Ab**), which is also reflected by the increase in variability of the individual gain values at −25 mv compared to +10 mv (coefficient of variation C_{var}: 0.49 for glass, 0.61 for 28 kPa-PDMS, 0.9 for 15 kPa-PDMS, and 1.12 for 1.5 kPa-PDMS). The EC-coupling gain at −25 mv was significantly increased in comparison with +10 mv when stiffness was 15 kPa ($p = 0.0445$) or 1.5 kPa ($p = 0.0453$; **Supplementary Table S2**).

In order to investigate SR Ca^{2+} load, the SR Ca^{2+} content was assessed by caffeine-mediated Ca^{2+} release (10 mM) in iPSC-CMs grown on surfaces with different stiffness. **Figure 2Ca** illustrates the experimental protocol: After steady-state stimulation at 1 Hz in patch-clamped cells, caffeine was applied. NCX currents and Ca^{2+} transients were recorded simultaneously. Peak amplitudes of steady-state Ca^{2+} transients and caffeine-induced Ca^{2+} transients are summarized in **Figures 2Cb,2Cc**, respectively, and **Supplementary Table S3** demonstrating a similar SR Ca^{2+} load (**Figure 2Cc**) and fractional release

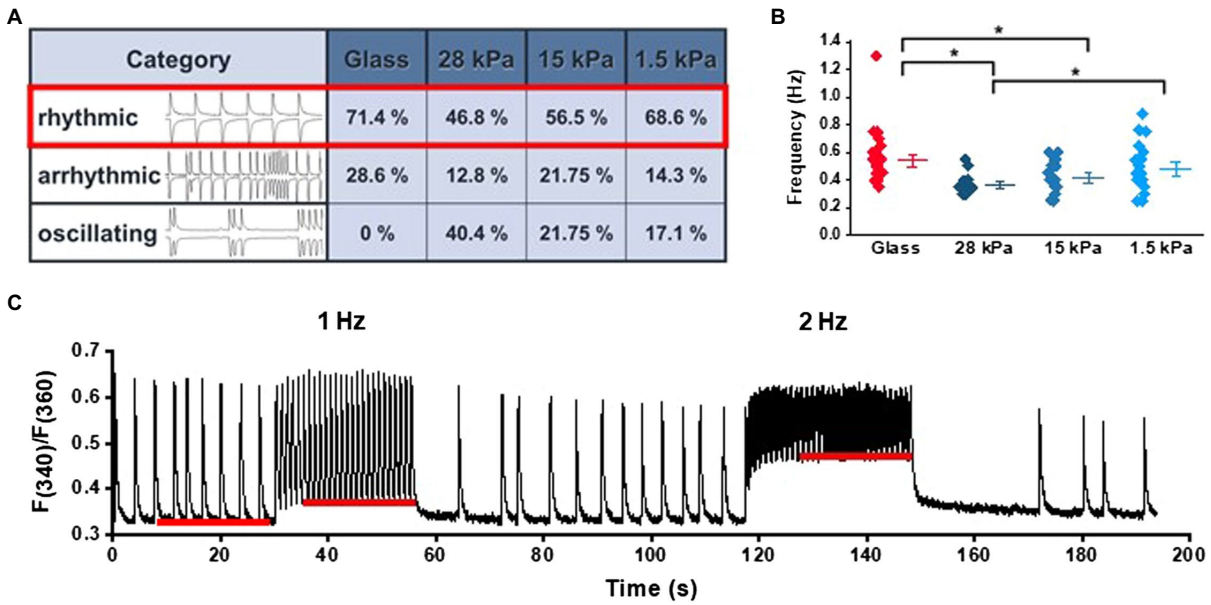

FIGURE 1 | Ca^{2+} signaling in iPSC-CMs grown on substrates with different stiffnesses during spontaneous activity and electrical pacing. **(A)** Categorization of different phenotypes of spontaneous activity ranging from rhythmic, arrhythmic to oscillating activity patterns in cells grown on surfaces with different stiffnesses ($n = 42$ on glass, $n = 47$ on 28 kPa-PDMS, $n = 44$ on 15 kPa-PDMS, and $n = 35$ on 1.5 kPa-PDMS). **(B)** Quantification of the spontaneous beating frequency of rhythmic cells (glass: $n = 30$; 28 kPa-PDMS: $n = 21$; 15 kPa-PDMS: $n = 25$; and 1.5 kPa-PDMS: $n = 24$). **(C)** Sample trace of Ca^{2+} transients recorded during spontaneous activity and during episodes of electrical pacing at 1 Hz or 2 Hz. The red lines illustrate frequency-dependent changes of diastolic Ca^{2+} levels.

(**Figure 2D**) at the different conditions. NCX currents were measured during Ca^{2+} release evoked by prolonged caffeine application. By integration of inward currents, total charge movement across the sarcolemma was measured indicative of global NCX activity. Statistical analysis revealed similar NCX activity in iPSC-CMs grown on substrates with different stiffnesses (**Figure 2E**; **Supplementary Table S3**).

Structural Remodeling of $Ca_v1.2$ and RyR2 Expression in iPSC-CMs Grown on Soft Surfaces

We further investigated different Ca^{2+} handling proteins on a structural level. As recently published by our group, functional maturation, such as improved cytosolic Ca^{2+} handling, during EC-coupling can be triggered by structural remodeling in iPSC-CMs (Silbernagel et al., 2020). Here, we considered subcellular structural reorganization as a possible cause for the apparent changes in the EC-coupling gain in iPSC-CMs grown on soft surfaces. To examine the expression pattern of proteins relevant for CICR, the LTCC α-subunit $Ca_v1.2$, RyR2, SERCA, and NCX were stained in immunocytochemical assays in iPSC-CMs grown on substrates of different stiffnesses for 20 days (**Figure 3**). In total, 12 dishes of 4 different stiffnesses from 3 different time points were stained and imaged. Interestingly, while the expression pattern of $Ca_v1.2$ exhibited a dotted pattern in cells grown on glass, a pronounced striation pattern of $Ca_v1.2$ expression formed on all soft growth surfaces after 20 days in culture (**Figure 3A**). Structural remodeling of the investigated Ca^{2+} channels and Ca^{2+} handling proteins may happen early during culture on soft PDMS-coated culture surfaces, as already on day 10, cells showed the same expression pattern of the investigated proteins as on day 20. Moreover, the images demonstrate a high organization level of RyR2 expression, again in a striated manner, in cells grown on soft surfaces indicating a well-developed SR network. On the contrary, in iPSC-CMs grown on glass, RyR2 staining revealed only a punctate expression pattern, pointing toward a rather immature distribution of RyR2 and SR organization within these cells. Overview images of $Ca_v1.2$ and RyR2 expression are shown in **Supplementary Figure S1**. Merging the expression pattern of $Ca_v1.2$ and RyR2 revealed an alternating parallel alignment of both Ca^{2+} channels in iPSC-CMs grown on soft surfaces suggesting close localization to each other. As shown in **Figure 3A** on the right side, line profiles of LTCC and RyR2 expression confirmed the high degree of parallel alignment as indicated by the alternating intensity peaks of fluorescence derived from the ion channels' expression pattern. Notably, this structural proximity is essential for efficient functional coupling of LTCC and RyR2 during CICR, which may lead to improvement of the EC-coupling mechanism – indicative of a beginning functional maturation. Furthermore, the expression pattern of SERCA was investigated in iPSC-CMs grown on substrates with different stiffnesses for 20–25 days. Images are summarized in **Figure 3B** and demonstrate a dense network (in green) reaching toward the cell periphery lining the actin filaments of the myofibrils as well as strong perinuclear expression. Detailed images are shown in **Supplementary Figure S2**. This expression pattern of SERCA demonstrates a well-organized subcellular arrangement

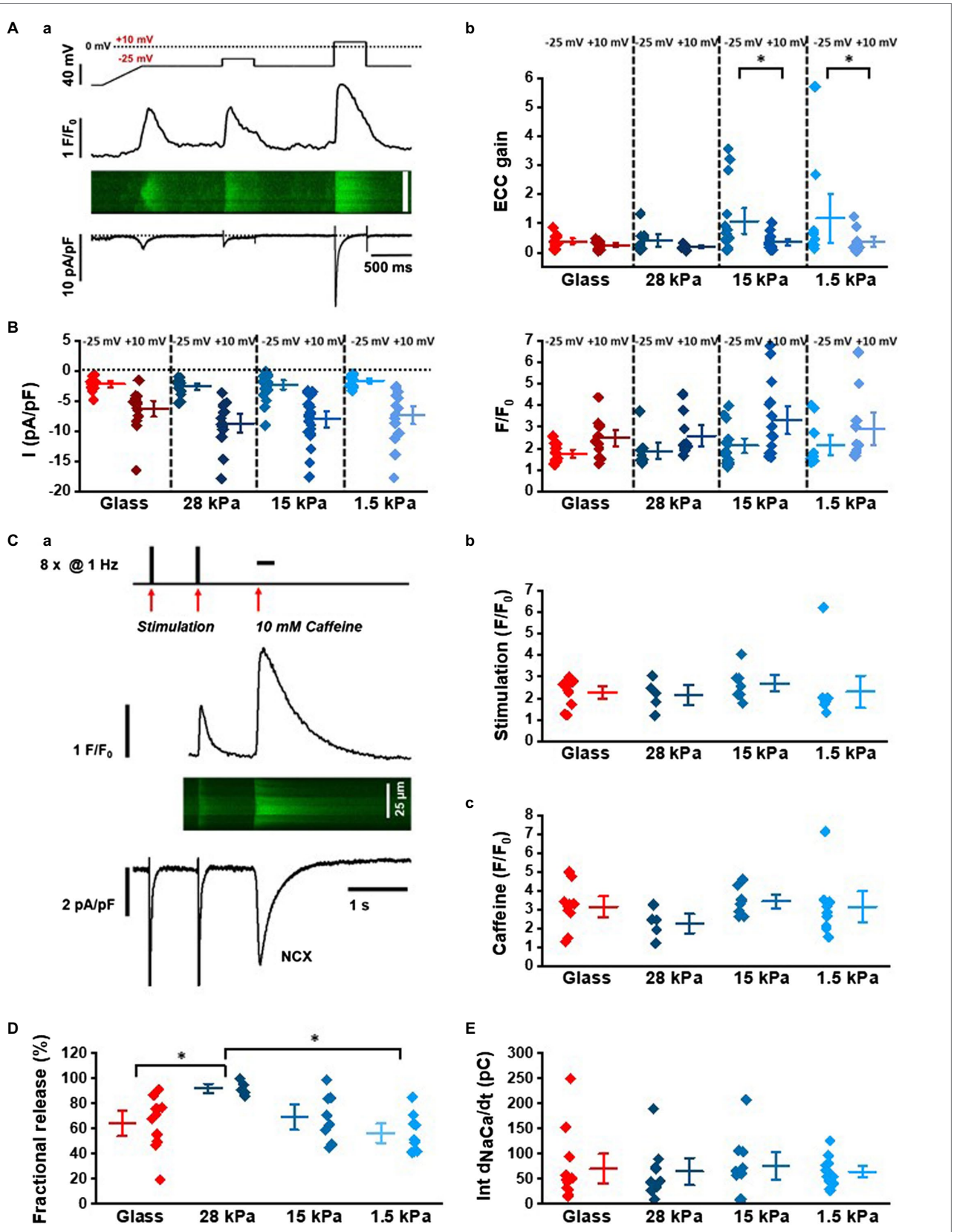
A
a
0 mV
+10 mV
-25 mV
40 mV
1 F/F0
10 pA/pF
500 ms
b
-25 mV +10 mV
ECC gain
Glass
28 kPa
15 kPa
1.5 kPa
B
I (pA/pF)
F/F0
C
a
8 x @ 1 Hz
Stimulation
10 mM Caffeine
1 F/F0
25 µm
2 pA/pF
1 s
NCX
b
Stimulation (F/F0)
c
Caffeine (F/F0)
D
Fractional release (%)
E
Int dNaCa/dt (pC)

(Continued)

FIGURE 2 | Characterization of Ca^{2+}-induced Ca^{2+} release in patch-clamped iPSC-CMs grown on surfaces with different matrix stiffnesses. **(Aa)** Stimulation protocol and representative recordings of I_{CaL}, Ca^{2+} transients in the line-scan mode and line profile of the line-scan. **(Ab)** Analysis of EC-coupling gain at −25 mv and + 10 mv calculated from peak I_{CaL} and Ca^{2+} transient amplitudes. These data sets were statistically compared by two-way ANOVA with Holm-Sidak's *post-hoc* pairwise multiple comparisons *vs.* control. **(B)** Peak I_{CaL} (left) and Ca^{2+} transient amplitudes (right) at −25 mv and +10 mv in cells seeded on different stiffnesses. **(C)** Assessment of NCX activity and fractional SR release with caffeine: **(Ca)** Representative line-scan image, line profile of Ca^{2+} transients, and membrane current evoked by 1 Hz-steady-state activation and caffeine-induced Ca^{2+} release (10 mM caffeine). **(Cb)** Ca^{2+} transient amplitudes during steady-state activation (n = 9–15 experiments). **(Cc)** Peak amplitudes of caffeine-induced Ca^{2+} transients (n = 5–10 experiments). **(D)** Fractional release calculated from the ratio of peak Ca^{2+} transient amplitudes during electrical pacing and caffeine-induced Ca^{2+} release. **(E)** Integrated NCX membrane currents measured during caffeine exposition in iPSC-CMs grown on substrates with different stiffnesses.

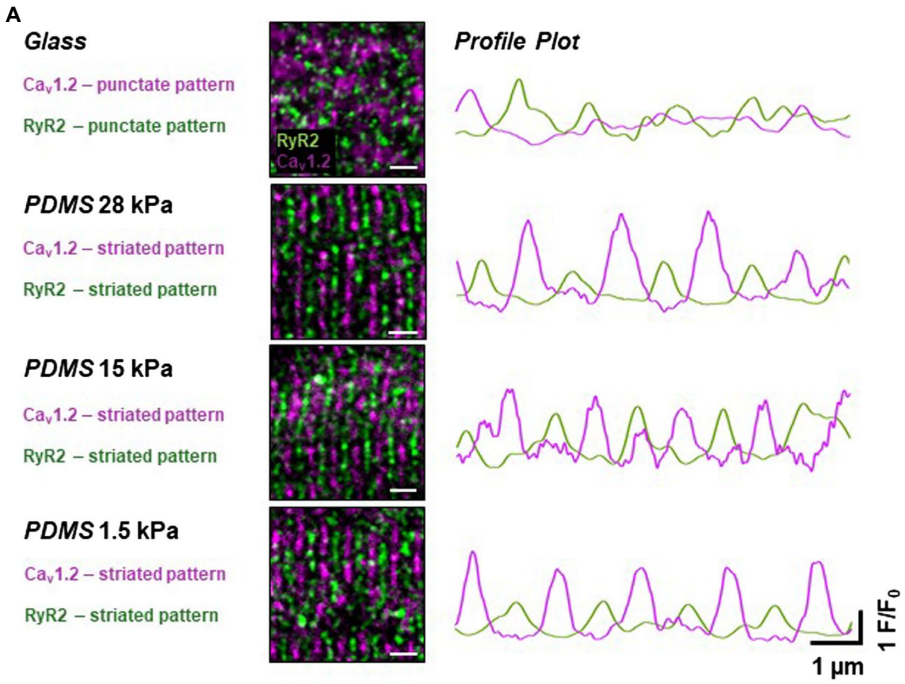

FIGURE 3 | Expression pattern of Ca^{2+} handling proteins in iPSC-CMs grown on different soft surfaces. **(A)** Immunostainings of L-type Ca^{2+} channel $Ca_v1.2$ (purple) and RyR2 [green, scale bar (SB) = 2 µm] and intensity profiles drawn from regions of interest along the vertical axis indicating parallel alignment of both ion channel expression patterns relative to each other by alternating peaks in iPSC-CMs plated on soft surfaces compared to glass. **(B)** Expression pattern of SERCA (green), actin (red), and nucleus (blue) revealing similar distribution of the SR network in iPSC-CMs grown on all tested surfaces (SB = 10 µm). **(C)** Representative image of NCX stainings (green) together with actin (red) and nucleus (blue) showing a dotted distribution all over the sarcolemma (SB = 10 µm).

of the SR. However, no significant difference of SERCA expression depending on the substrate stiffnesses was observed in iPSC-CMs grown on different surfaces. **Figure 3C** and **Supplementary Figure S3** show a representative picture of the sarcolemmal distribution of NCX in iPSC-CMs examined by immunocytochemistry. In total, 12 dishes of 4 different stiffnesses from 3 different time points were stained and imaged. The expression pattern of NCX revealed a dotted distribution over the entire sarcolemma of iPSC-CMs, which was similar in cells grown on different surfaces. Occasionally, small areas reveal stretches of more continuous NCX signals (**Supplementary Figure S3**).

Influence of Environmental Stiffness on Ca^{2+} Transients and Contractions

In order to further investigate cytosolic Ca^{2+} handling and Ca^{2+}-induced contraction properties in iPSC-CMs on growth surfaces with different stiffnesses, Ca^{2+} transients and cell shortening were measured and analyzed simultaneously. Representative Ca^{2+} and contraction traces of rhythmically beating iPSC-CMs are depicted in **Figure 4A**. While Ca^{2+} transients exhibited similar characteristics on different surfaces (peak amplitude, TTP, FDHM, and decay time), relative shortening amplitude was significantly larger in iPSC-CMs grown on 1.5 kPa-PDMS compared to higher stiffnesses of glass, 28 kPa-PDMS or 15 kPa-PDMS, indicating significantly enhanced contractility (**Figure 4B**). All data from these experiments are summarized in **Supplementary Table S4**. Moreover, TTP of contractions was significantly slower in cells grown on 1.5 kPa-PDMS surfaces than on 28 kPa-PDMS and glass and on 15 kPa-PDMS compared to glass (**Figure 4B**). Additionally, analysis of contractions revealed significantly and increasingly longer durations (expressed as FDHM) in iPSC-CMs plated on soft surfaces than on glass (**Figure 4C**) suggesting slower relaxation on soft surfaces as reflected by

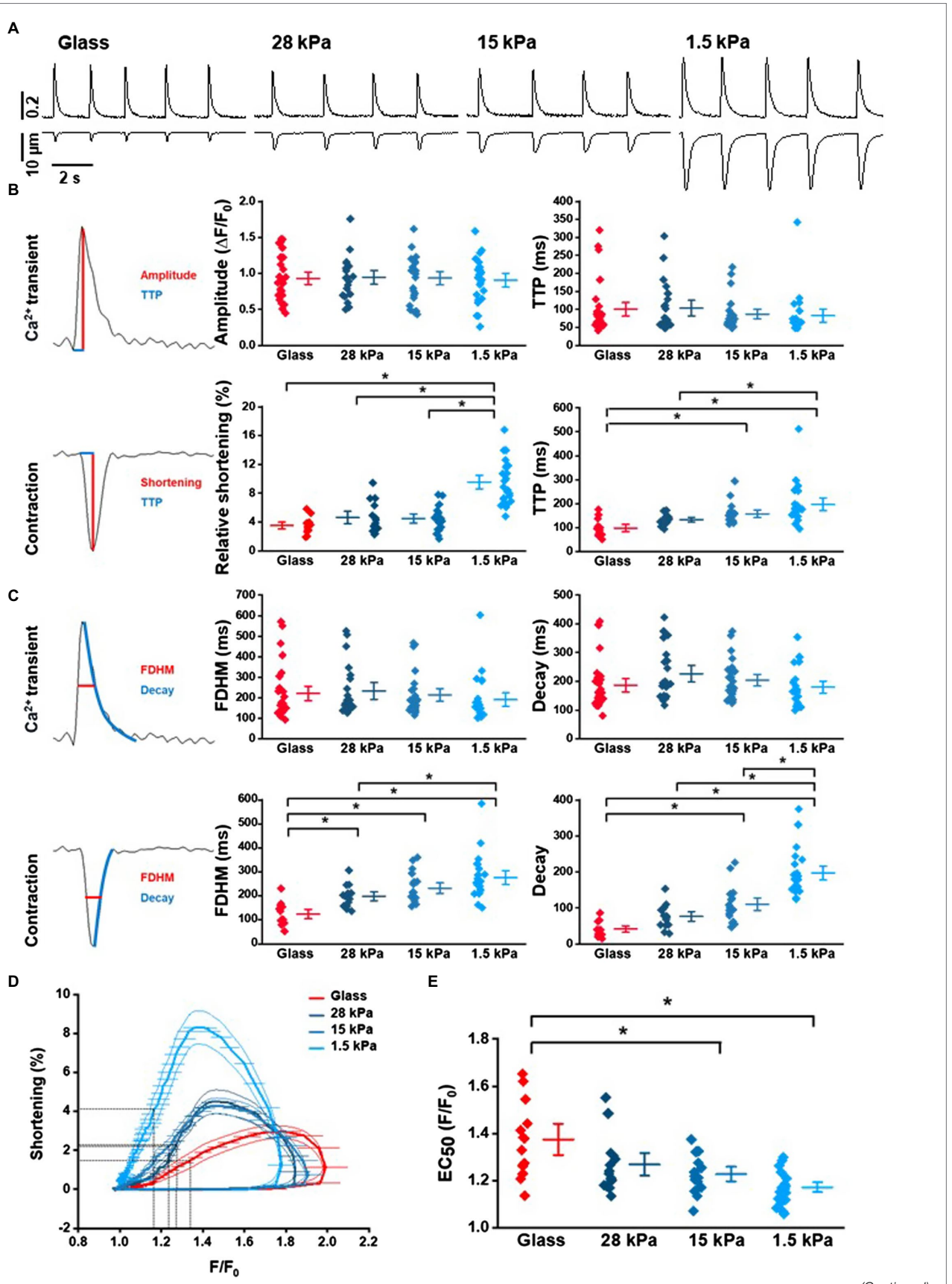
A
Glass
28 kPa
15 kPa
1.5 kPa
0.2
10 µm
2 s
B
Ca2+ transient
Amplitude
TTP
Amplitude (ΔF/F0)
TTP (ms)
Contraction
Shortening
TTP
Relative shortening (%)
TTP (ms)
C
Ca2+ transient
FDHM
Decay
FDHM (ms)
Decay (ms)
Contraction
FDHM
Decay
FDHM (ms)
Decay
Glass
28 kPa
15 kPa
1.5 kPa
D
Shortening (%)
F/F0
Glass
28 kPa
15 kPa
1.5 kPa
E
EC50 (F/F0)
Glass
28 kPa
15 kPa
1.5 kPa

(Continued)

FIGURE 4 | Ca^{2+} transient and contraction analysis in iPSC-CMs depending on of growth surface. **(A)** Representative traces of spontaneous Ca^{2+} transients and cell shortening of iPSC-CMs grown on glass or PDMS with 28 kPa, 15 kPa, or 1.5 kPa. **(B)** Analysis of peak amplitudes and time-to-peak (TTP) of Ca^{2+} transients and relative cell shortening in rhythmically beating cells ($n = 13–23$ measurements). Statistical evaluation revealed significantly larger shortening amplitudes in cells grown on 1.5 kPa compared to any other surface stiffness, and slower TTP of contractions on 1.5 kPa compared to 28 kPa or glass and on 15 kPa compared to glass (one-way ANOVA, $p < 0.05$). **(C)** Analysis of FDHM and decay kinetics of Ca^{2+} transients and contractions on glass compared to soft surfaces. **(D)** Analysis of Ca^{2+} sensitivity in Ca^{2+} loops revealing increased myofilament Ca^{2+} sensitivity in iPSC-CMs grown on 1.5 kPa and 15 kPa compared to glass. Data are taken from the traces of Ca^{2+} transients (x-axis) and cell shortening (y-axis). **(E)** Statistical analysis of the EC_{50} values during the relaxation phase from **(D)**. Statistically significant differences are indicated by * for $p < 0.05$.

significantly slower decay times in cells on 1.5 kPa-PDMS compared to 15 kPa-PDMS, 28 kPa-PDMS, and glass. To investigate whether growth surface stiffness influences Ca^{2+} removal properties after release, Ca^{2+} transient decay dynamics were analyzed. SERCA function was assessed by fitting the decay of Ca^{2+} transients with a monoexponential function to obtain the time constant of Ca^{2+} removal (**Figure 4C**). While Ca^{2+} removal dynamics were not different, cell relaxation expressed as the decay of shortening was significantly prolonged on soft surfaces.

To investigate the underlying cause of the altered contractile dynamics of iPSC-CMs on soft substrates, cell shortening and relaxation were plotted as a function of the intracellular Ca^{2+} concentration. The resulting phase-plane diagrams are depicted in **Figure 4D**. Presented Ca^{2+}-contraction loops revealed a leftward shift of the relaxation phase in iPSC-CMs grown on soft surfaces indicating an increase in the Ca^{2+} sensitivity of the myofilaments. Statistical analysis of the Ca^{2+} concentration at half-maximal relaxation (EC_{50}) on substrates with different stiffnesses revealed significantly higher myofilament Ca^{2+} sensitivity in iPSC-CMs seeded on 1.5 kPa-PDMS and 15 kPa-PDMS compared to glass (**Figure 4E**). All data from these experiments are summarized in **Supplementary Table S4**.

Influence of Different Substrate Stiffnesses on Cx43 Expression Pattern

In the next set of experiments, we focused on the second major observation of improved and synchronous beating activity in iPSC-CMs grown on soft surfaces compared to glass. To investigate the expression pattern of Cx43 in iPSC-CMs, we performed immunostainings with cells grown on substrates with different stiffnesses for 10–13 days. In total, 12 dishes of 4 different stiffnesses were processed at 3 different time points. **Figure 5A** shows representative images of the typical localization of Cx43 (in green) at cell borders and in perinuclear areas in iPSC-CMs plated on glass, 28 kPa-PDMS, 15 kPa-PDMS, and 1.5 kPa-PDMS. To quantify only the Cx43 expression that is relevant to form gap junctions for intercellular coupling, we calculated the proportion of the Cx43-occupied area of the cell membrane to the cell's entire circumference, as illustrated in **Figure 5B**. Statistical evaluation revealed a significantly higher ratio of Cx43 expression at the cell membrane in iPSC-CMs grown on soft surfaces comprising 28 kPa-PDMS, 15 kPa-PDMS, and 1.5 kPa-PDMS compared to glass (**Figure 5C**). To support this quantification, we further examined intercellular coupling in iPSC-CMs grown on substrates with different stiffnesses at the functional level.

Enhanced Intercellular Coupling on Soft Surfaces

For functional evaluation of gap junctions, we analyzed FRAP using the gap junction permeant fluorescent dye calcein-AM (0.5 mM). After removal of the acetoxy-methylester group of calcein by cytosolic esterases, the dye was no longer able to diffuse across the lipid bilayer. Consequently, gap junctions presented the only possibility for calcein to leave intact cells. Calcein was bleached in one cell of a cell group, and fluorescence recovery of calcein diffusing in from neighboring cells was measured over time revealing the diffusion dynamics between iPSC-CMs (**Figure 6A**). Representative images of treated iPSC-CMs grown on glass and 28 kPa-PDMS before, during, and after bleaching are depicted in **Figure 6B**. In contrast to cell bleaching on the glass surface, which showed only 14% of fluorescent recovery at 20 s and 32% at 80 s after bleaching, fluorescence recovery of a bleached cell grown on 28 kPa-PDMS amounted to 29% and 44% within the same time frame. For analysis of fluorescence recovery, fluorescence intensity was plotted over time and fitted with a biexponential function to calculate the diffusion rate constants (**Figure 6Ca**). **Figure 6Cb** summarizes the first time constant ($\tau 1$) of the recovery time course revealing a steeper slope within the first 100 s of FRAP in iPSC-CMs grown on all soft surfaces compared to glass. Statistical evaluation of $\tau 1$ confirmed significantly faster diffusion rates in cells seeded on 28 kPa-PDMS, 15 kPa-PDMS, and 1.5 kPa-PDMS compared to glass. In addition, the variability of $\tau 1$, assessed by $C_{var.,}$ is significantly reduced in cells grown on soft surfaces compared to glass (C_{var}: Glass: 0.92, 28 kPa-PDMS: 0.63, 15 kPa-PDMS: 0.73, and 1.5 kPa-PDMS: 0.54). These results demonstrate significantly enhanced diffusion dynamics of calcein and therefore an increased presence of functional gap junctions, which allowed faster FRAP in iPSC-CMs grown on soft surfaces.

DISCUSSION

For the development of an adult heart with its unique electrophysiological and contractile properties, numerous specific growth conditions are required. Electrical stimulation by pacemaker cells, humoral regulation, and the balance between extrinsic and intrinsic mechanical load are just some of the essential factors that influence structural and functional maturation of cardiomyocytes during the early stages of development (Zhu et al., 2014). In this context, another important environmental cue is mediated by the

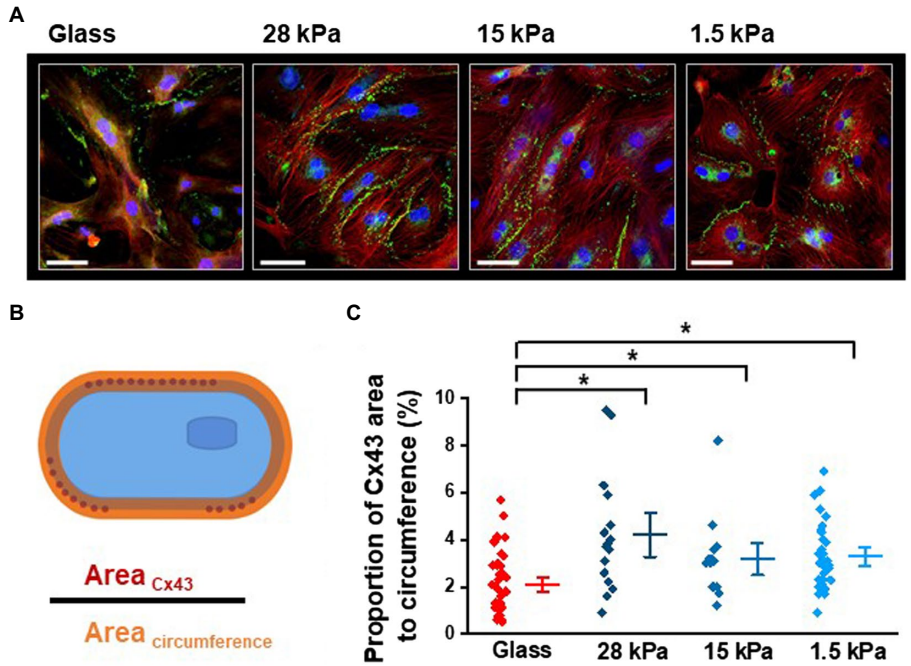

FIGURE 5 | Influence of different growth surface stiffnesses on Cx43 expression in iPSC-CMs. **(A)** Representative images showing Cx43 expression in green and nuclear signal in blue. Cx43 is characteristically located at the cell borders in iPSC-CMs, but is also expressed in the perinuclear regions (SB = 50 µm). **(B)** Illustration of the quantitative analysis of Cx43-occupied area of the cell membrane in relation to the area of the entire sarcolemma. **(C)** Statistical evaluation of the proportion of Cx43-occupied area to the circumference revealing enhanced sarcolemmal expression of Cx43 in iPSC-CMs grown on soft surfaces compared to glass. Glass: $n = 40$; 28 kPa-PDMS: $n = 16$; 15 kPa-PDMS: $n = 14$; and 1.5 kPa-PDMS: $n = 21$.

composition of the ECM defining the stiffness surrounding each cell and therefore the passive resistance that cardiomyocytes must pull against during contraction. Modification of this environmental stiffness during cardiac development may have a significant impact on the transition of early to adult cardiomyocytes (Ward and Iskratsch, 2020). Moreover, pathophysiological ventricular remodeling upon cardiac fibrosis and heart disease suggests activation of different signaling pathways in response to ECM restructuring (Sit et al., 2019). This process is also called mechano-chemotransduction (MCT; Chen-Izu and Izu, 2017). Although not fully understood yet, some molecular players and signaling pathways have already been identified in adult and developing cardiomyocytes (Gaetani et al., 2020; Izu et al., 2020; Ward and Iskratsch, 2020).

Considering cardiomyocytes derived from pluripotent stem cells, investigations of MCT may reveal new targets for improving their functional properties to enhance their potential to be used for cardiac cell therapy. In other words, a detailed analysis of the influence of specific environmental cues on elementary features of iPSC-CMs may help to mature these cells *in vitro*. The goal of this study was therefore to examine the impact of the environmental stiffness on cardiomyocyte function at the level of EC-coupling and intercellular communication in iPSC-CMs and to find out whether an environment with physiological stiffness may provide a new possibility to enhance mature properties of iPSC-CMs.

Enhanced Contractility in iPSC-CMs Grown on Soft Surfaces

EC-coupling, the fundamental mechanism linking electrical excitation to contractile activity and force production, is strictly controlled by CICR. On a structural level, efficient EC-coupling requires close interaction of LTCCs and RyR2s, which is usually provided by the regular formation of dyads, where t-tubular and SR membranes come close together and enable spatiotemporally synchronized CICR. Deviations from the optimized microarchitecture of adult cardiomyocytes are seen in immature prenatal and iPSC-CMs or in diseased cardiomyocytes, where such a missing membrane organization leads to an enhanced appearance of so-called orphaned RyR2s (Lee et al., 2011; Rao et al., 2013). Examination of the EC-coupling gain not only helps to identify weaknesses in this mechanism but also allows to detect improvements in Ca^{2+} handling in response to a specific treatment. iPSC-CMs plated on soft surfaces of 15 or 1.5 kPa-PDMS showed greater Ca^{2+} release upon triggering influx current at −25 mv, indicative of better coupling between LTCCs and RyR2s. Considering possible explanations for this enhanced EC-coupling gain, changes in the expression pattern of LTCCs and RyR2s, i.e., a switch from punctuate to regular striation pattern, may explain this finding very well and indicate structural remodeling toward maturation. In this new arrangement, the number of non-coupled RyR2s is reduced, while the increased colocalization of LTCCs and RyR2s favors higher EC-coupling efficiency in iPSC-CMs.

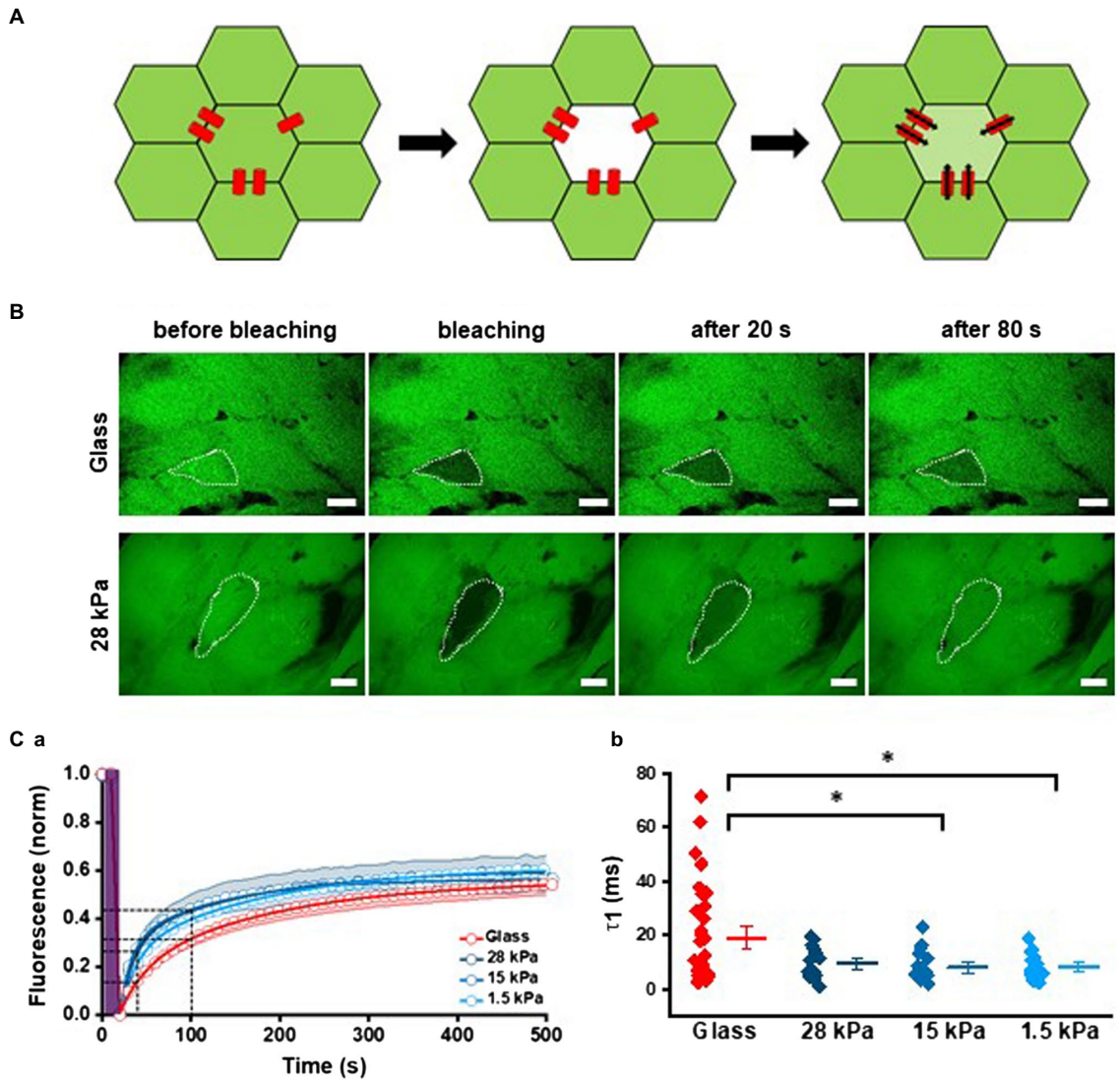

FIGURE 6 | Enhanced intercellular coupling on soft surfaces. **(A)** Schematic illustration of FRAP experiments. *Left:* the cell layer is stained with calcein (shown in green). *Middle:* one cell within a cell cluster is bleached by high laser power (5 s). *Right:* after bleaching recovery of fluorescence by calcein diffusion through gap junctions from neighbored cells is monitored over time. **(B)** Representative FRAP experiments with iPSC-CMs grown on glass and 28 kPa. The target cell is marked by a white dotted line. The first image corresponds to $t = 0$ s before bleaching, and the second image was taken at $t = 20$ s immediately after bleaching. At $t = 40$ s and 100 s, the third and fourth images were taken. **(Ca)** Average time courses of FRAP for each stiffness were plotted and fitted with a biexponential function. FRAP was significantly faster in iPSC-CMs grown on all PDMS-coated surfaces compared to glass. **(Cb)** Statistical evaluation of tau1 (τ1). For cells grown on glass $n = 35$; for 28 kPa-PDMS $n = 15$; for 15 kPa-PDMS $n = 17$; and for 1.5 kPa-PDMS $n = 18$.

Another possibility for the enhanced EC-coupling gain might be an increase in the Ca^{2+} sensitivity of RyR2s due to posttranslational modifications. In addition to reactive oxygen and nitrogen species, Ca^{2+}-dependent RyR2 activation is physiologically regulated by phosphorylation *via* protein kinase A (PKA) and Ca^{2+}/calmodulin-dependent kinase II (CaMKII; Niggli et al., 2013). Interestingly, increased RyR2 sensitivity mediated by the neuronal isoform of the nitric oxide synthase (nNOS) and CaMKII was shown to be induced by multiaxial mechanical stress during cardiomyocyte contraction (Jian et al., 2014; Mosqueira et al., 2021). As cellular afterload response results in modulation of RyR2 activity in adult cardiomyocytes, substrates with different stiffnesses may influence signaling pathways leading to altered Ca^{2+} sensitivity of RyR2s in iPSC-CMs as well. Moreover, NCX stainings revealed small stretches of sarcolemmal invaginations from the surface into the cell body. It is only by speculation that one can assume here the beginning of t-tubular-like structures, but this cannot be excluded. Enhanced t-tubular structures in remodeled iPSC-CMs may even better explain the increase in the EC-coupling gain. Further experiments will be needed to investigate the initiation of t-tubules by environmental cues. Therefore, our findings suggest that cardiac-like environmental stiffness induces enhanced EC-coupling gain at the level of CICR by activation of intracellular signaling

cascades inducing structural remodeling of LTCC and RyR2 and modifying RyR2 function.

Moreover, a deeper investigation of EC-coupling revealed altered contraction dynamics with increased shortening in iPSC-CMs plated on substrates with softer stiffnesses, overall leading to larger contractions. As one good reason for impaired contractility on rigid surfaces, we first assumed that high stiffness may prevent adherent iPSC-CMs from contracting to their full extent. In contrast, on flexible surfaces, the contractile cells may pull against the soft material, leading to higher contraction amplitudes and longer contraction duration. However, there was no linear relationship between stiffness and change in contractility across the large range of tested surface stiffnesses indicating additional mechanisms responsible for functional changes apart from passive inhibition. Supporting this evidence, van Deel et al. distinguished between passive inhibitory effects and active changes induced by environmental stiffness by acutely detaching adult cardiomyocytes from their growth surface just before contractility was measured. They demonstrated that the functional adaptations of the cardiomyocytes were independent of the direct passive effect of matrix rigidity on cell function (van Deel et al., 2017). This study supports our idea that changes in environmental stiffness induce intrinsic cellular effects that alter contractile dynamics in iPSC-CMs. Although the exact underlying mechanism remains to be determined, changes in Ca^{2+} handling or modifications of myofilament proteins were discussed.

Considering active matrix-induced alterations, we wanted to find out whether MCT may influence signaling pathways leading to improved EC-coupling with increased contractility. As a possible explanation for enhanced contractile dynamics in iPSC-CMs grown on soft surfaces, differences in Ca^{2+} handling may be considered, since an increase in the EC-coupling gain means that at the same electrical stimulus (*via* I_{CaL}), more Ca^{2+} is being released from the SR and therefore available for myofilament activation. In addition, the contractile response to different surfaces in adult cardiomyocytes may also depend on adaptions in myofilaments, an idea that also seems to apply to iPSC-CMs (Galie et al., 2013). Our data support previous evidence, where decreased sarcomere and myofibril activity due to intracellular over-tension were shown in iPSC-CMs grown on 35 kPa hydrogels leading to 90% less mechanical output compared to iPSC-CMs seeded on softer surfaces of 10 kPa or 6 kPa hydrogels (Ribeiro et al., 2015). Nevertheless, myofilament buckling during relaxation in iPSC-CMs plated on 6 kPa indicated the need for some intracellular tension to maintain correct myofibril alignment (Ribeiro et al., 2015). These results correspond to preferred ranges of matrix elasticity for optimal contractile work in embryonic and neonatal cardiomyocytes (Engler et al., 2008; Bhana et al., 2010). Therefore, an intermediate stiffness comparable to native myocardium may optimally maturate myofilament organization and function. Moreover, a more robust expression of cardiac troponin I (cTnI) was found in neonatal and iPSC-CMs seeded on soft surfaces (Bhana et al., 2010; Ribeiro et al., 2015; Herron et al., 2016). Thus, changes in myofilament Ca^{2+} sensitivity present a reasonable cause for altered contraction dynamics in iPSC-CMs seeded on substrates with lower stiffness. In the phase-plane diagram, cell shortening and relaxation were plotted as a function of the intracellular Ca^{2+} concentration during a twitch. Our data revealed a pronounced leftward shift of the relaxation phase in iPSC-CMs grown on soft surfaces indicating higher myofilament Ca^{2+} sensitivity. In principle, changes in myofilament Ca^{2+} sensitivity are evoked by modified on- and off-rates of myofilament activation, which are mainly, but not exclusively caused by altered association and dissociation rates of Ca^{2+} to cardiac troponin C (cTnC; Chung et al., 2016). Considering matrix-induced changes in gene expression and long-term structural adaptations, enhanced myofibril organization may contribute to increased myofilament Ca^{2+} sensitivity in iPSC-CMs grown on soft surfaces (Young et al., 2014).

Taken together, investigation of EC-coupling and contraction demonstrated a significant influence of growth surface properties on structural maturation at the level of CICR and myofilament activation. Therefore, providing an environment with natural stiffness improves the contractile potential of iPSC-CMs toward more mature and physiological function.

Increased Intercellular Coupling in iPSC-CMs Grown on Soft Surfaces Due to Improved Cx43 Expression

For functional integration of engineered myocardium in diseased adult hearts, adequate propagation of excitation across the cardiac tissue and graft is essential for coordinated impulse propagation. Slow and irregular electrical signal transmission in embryonic (ESC-) and iPSC-CMs caused by weak intercellular coupling poses a high risk for the development of a conduction barrier and arising arrhythmias (Shiba et al., 2012; Kucera et al., 2015; Sottas et al., 2018). In our experimental approach, we tested the hypothesis that growth surfaces with different stiffnesses affect cell-cell communication in iPSC-CMs by influencing the expression pattern of Cx43. Our evaluation of Cx43 immunostainings showed an increased expression of Cx43 at the sarcolemma indicating enhanced gap junction formation, which was functionally confirmed by FRAP analysis: iPSC-CMs grown on soft surfaces revealed faster diffusion rates. Assuming substrate stiffness as the triggering factor, several steps in the Cx43 lifecycle can be considered as possible target points: Critical to intercellular communication are transcription factors influencing gene expression, endoplasmic reticulum and Golgi assembly and transport, forward trafficking to the sarcolemma, organization within the gap junction plaque, and retrograde transport for degradation (Zhang and Shaw, 2014). Most of these processes are regulated by posttranslational modifications, and as Cx43 has a high turnover rate, especially the process of trafficking may also play an important role during remodeling. Recently, Herron et al. suggested enhanced α5β1-integrin receptor activation as a possible reason for increased intercellular coupling in iPSC-CMs grown on soft surfaces (Herron et al., 2016). Indeed, integrins are considered the main receptors associated with sensing mechanical signals and changes in load (Ward and Iskratsch, 2020). In the developing heart, for example, repression of

integrin α5 during early stages results in reduced cardiomyocyte differentiation and impaired contractility (Neiman et al., 2019). Therefore, further investigations of integrin receptor expression depending on the environmental stiffness may reveal novel approaches to promote maturation in iPSC-CMs.

In conclusion, here we showed non-linear cellular responses to substrates with different stiffnesses at a macroscale level in iPSC-CMs indicating the existence of MCT. We demonstrated that soft growth surfaces trigger structural maturation at the level of CICR and promote Ca^{2+} handling properties leading to enhanced EC-coupling gain and contractility in iPSC-CMs. Moreover, this study provides the first experimental evidence of an increased presence of functional gap junctions, which lead to better intercellular coupling with stronger synchronization of the electro-mechanical activity in iPSC-CMs grown on soft surfaces. By exhibiting relevant targets of MCT in iPSC-CMs, our results may trigger further investigation of mechanical signaling pathways leading not only to new maturation strategies of iPSC-CMs, but also to the identification of new targets for the treatment of cardiac diseases with changed ECM stiffness.

DATA AVAILABILITY STATEMENT

The original contributions presented in the study are included in the article/**Supplementary Material**, further inquiries can be directed to the corresponding author.

AUTHOR CONTRIBUTIONS

NU conceived the study. AK and NU designed the experiments, conducted the experiments, analyzed and interpreted the data, generated the figures and wrote the manuscript. MM and MH critically reviewed and edited the manuscript. All authors have reviewed the data and approved the final manuscript.

FUNDING

This work was supported by the German Research Council (DFG, UL 466/2-1 to NU). AK was supported by the Otto Hess fellowship.

ACKNOWLEDGMENTS

We thank Manuela Höfer and Jinmeng Sun for their excellent technical and experimental support and the team of Joachim Kirsch for helpful discussions.

SUPPLEMENTARY MATERIAL

The Supplementary Material for this article can be found online at: https://www.frontiersin.org/articles/10.3389/fphys.2021.710619/full#supplementary-material

REFERENCES

Bers, D. M. (2002). Cardiac excitation–contraction coupling. *Nature* 415, 198–205. doi: 10.1038/415198a

Bhana, B., Iyer, R. K., Chen, W. L. K., Zhao, R., Sider, K. L., Likhitpanichkul, M., et al. (2010). Influence of substrate stiffness on the phenotype of heart cells. *Biotechnol. Bioeng.* 105, 1148–1160. doi: 10.1002/bit.22647

Burridge, P. W., Keller, G., Gold, J. D., and Wu, J. C. (2012). Production of de novo cardiomyocytes: human pluripotent stem cell differentiation and direct reprogramming. *Cell Stem Cell* 10, 16–28. doi: 10.1016/j.stem.2011.12.013

Chen-Izu, Y., and Izu, L. T. (2017). Mechano-chemo-transduction in cardiac myocytes. *J. Physiol.* 595, 3949–3958. doi: 10.1113/JP273101

Chong, J. J. H., Yang, X., Don, C. W., Minami, E., Liu, Y. W., Weyers, J. J., et al. (2014). Human embryonic-stem-cell-derived cardiomyocytes regenerate non-human primate hearts. *Nature* 510, 273–277. doi: 10.1038/nature13233

Chung, J. H., Biesiadecki, B. J., Ziolo, M. T., Davis, J. P., and Janssen, P. M. L. (2016). Myofilament calcium sensitivity: role in regulation of *in vivo* cardiac contraction and relaxation. *Front. Physiol.* 7, 1–9. doi: 10.3389/fphys.2016.00562

Engler, A. J., Carag-Krieger, C., Johnson, C. P., Raab, M., Tang, H. Y., Speicher, D. W., et al. (2008). Embryonic cardiomyocytes beat best on a matrix with heart-like elasticity: scar-like rigidity inhibits beating. *J. Cell Sci.* 121, 3794–3802. doi: 10.1242/jcs.029678

Fujita, B., and Zimmermann, W. H. (2018). Myocardial tissue engineering strategies for heart repair: current state of the art. *Interact. Cardiovasc. Thorac. Surg.* 27, 916–920. doi: 10.1093/icvts/ivy208

Gaetani, R., Zizzi, E. A., Deriu, M. A., morbiducci, U., Pesce, M., and Messina, E. (2020). When stiffness matters: Mechanosensing in heart development and disease. *Front. Cell Dev. Biol.* 8, 1–16. doi: 10.3389/fcell.2020.00334

Galie, P. A., Khalid, N., Carnahan, K. E., Westfall, M. V., and Stegemann, J. P. (2013). Substrate stiffness affects sarcomere and costamere structure and electrophysiological function of isolated adult cardiomyocytes. *Cardiovasc. Pathol.* 22, 219–227. doi: 10.1016/j.carpath.2012.10.003

Gao, L., Gregorich, Z. R., Zhu, W., Mattapally, S., Oduk, Y., Lou, X., et al. (2018). Large cardiac muscle patches engineered from human induced-pluripotent stem cell-derived cardiac cells improve recovery from myocardial infarction in swine. *Circulation* 137, 1712–1730. doi: 10.1161/CIRCULATIONAHA.117.030785

Gherghiceanu, M., Barad, L., Novak, A., Reiter, I., Itskovitz-Eldor, J., Binah, O., et al. (2011). Cardiomyocytes derived from human embryonic and induced pluripotent stem cells: comparative ultrastructure. *J. Cell. Mol. Med.* 15, 2539–2551. doi: 10.1111/j.1582-4934.2011.01417.x

Herron, T. J., Da Rocha, A. M., Campbell, K. F., Ponce-Balbuena, D., Willis, B. C., Guerrero-Serna, G., et al. (2016). Extracellular matrix-mediated maturation of human pluripotent stem cell-derived cardiac monolayer structure and electrophysiological function. *Circ. Arrhythm. Electrophysiol.* 9, 1–12. doi: 10.1161/CIRCEP.113.003638

Itzhaki, I., Rapoport, S., Huber, I., Mizrahi, I., Zwi-Dantsis, L., Arbel, G., et al. (2011). Calcium handling in human induced pluripotent stem cell derived cardiomyocytes. *PLoS One* 6:e18037. doi: 10.1371/journal.pone.0018037

Izu, L. T., Kohl, P., Boyden, P. A., Miura, M., Banyasz, T., Chiamvimonvat, N., et al. (2020). Mechano-electric and mechano-chemo-transduction in cardiomyocytes. *J. Physiol.* 598, 1285–1305. doi: 10.1113/JP276494

Jian, Z., Han, H., Zhang, T., Puglisi, J., Izu, L. T., Shaw, J. A., et al. (2014). Mechanochemotransduction During Cardiomyocyte contraction is mediated by localized nitric oxide signaling. *Sci. Signal.* 7:ra27. doi: 10.1126/scisignal.2005046

Jiang, Y., Park, P., Hong, S. M., and Ban, K. (2018). Maturation of cardiomyocytes derived from human pluripotent stem cells: Current strategies and limitations. *Mol. Cell* 41, 613–621. doi: 10.14348/molcells.2018.0143

Kadota, S., Pabon, L., Reinecke, H., and Murry, C. E. (2017). *In vivo* maturation of human induced pluripotent stem cell-derived Cardiomyocytes in neonatal and adult rat hearts. *Stem Cell Rep.* 8, 278–289. doi: 10.1016/j.stemcr.2016.10.009

Kamakura, T., Makiyama, T., Sasaki, K., Yoshida, Y., Wuriyanghai, Y., Chen, J., et al. (2013). Ultrastructural maturation of human-induced pluripotent stem cell-derived cardiomyocytes in a long-term culture. *Circ. J.* 77, 1307–1314. doi: 10.1253/circj.CJ-12-0987

Kane, C., Couch, L., and Terracciano, C. M. N. (2015). Excitation-contraction coupling of human induced pluripotent stem cell-derived cardiomyocytes. *Front. Cell Dev. Biol.* 3, 1–8. doi: 10.3389/fcell.2015.00059

Karbassi, E., Fenix, A., Marchiano, S., Muraoka, N., Yang, X., and Murry, C. E. (2020). Implications for regenerative medicine. *Nat. Rev. Cardiol.* 17, 341–359. doi: 10.1038/s41569-019-0331-x

Kroll, K., Chabria, M., Wang, K., Häusermann, F., Schuler, F., and Polonchuk, L. (2017). Electro-mechanical conditioning of human iPSC-derived cardiomyocytes for translational research. *Prog. Biophys. Mol. Biol.* 130, 212–222. doi: 10.1016/j.pbiomolbio.2017.07.003

Kucera, J. P., Prudat, Y., Marcu, I. C., Azzarito, M., and Ullrich, N. D. (2015). Slow conduction in mixed cultured strands of primary ventricular cells and stem cell-derived cardiomyocytes. *Front. Cell Dev. Biol.* 3, 1–13. doi: 10.3389/fcell.2015.00058

Lee, Y. K., Ng, K. M., Lai, W. H., Chan, Y. C., Lau, Y. M., Lian, Q., et al. (2011). Calcium homeostasis in human induced pluripotent stem cell-derived Cardiomyocytes. *Stem Cell Rev. Rep.* 7, 976–986. doi: 10.1007/s12015-011-9273-3

Lieu, D. K., Liu, J., Siu, C. W., McNerney, G. P., Tse, H. F., Abu-Khalil, A., et al. (2009). Absence of transverse tubules contributes to non-uniform Ca^{2+} wavefronts in mouse and human embryonic stem cell-derived cardiomyocytes. *Stem Cells Dev.* 18, 1493–1500. doi: 10.1089/scd.2009.0052

Lundy, S. D., Zhu, W. Z., Regnier, M., and Laflamme, M. A. (2013). Structural and functional maturation of cardiomyocytes derived from human pluripotent stem cells. *Stem Cells Dev.* 22, 1991–2002. doi: 10.1089/scd.2012.0490

Marcu, I. C., Illaste, A., Heuking, P., Jaconi, M. E., and Ullrich, N. D. (2015). Functional characterization and comparison of intercellular communication in stem cell-derived Cardiomyocytes. *Stem Cells* 33, 2208–2218. doi: 10.1002/stem.2009

Mosqueira, M., Konietzny, R., Andresen, C., Wang, C., Fink, H. A., and R., (2021). Cardiomyocyte depolarization triggers NOS-dependent NO transient after calcium release, reducing the subsequent calcium transient. *Basic Res. Cardiol.* 116:18. doi: 10.1007/s00395-021-00860-0

Neiman, G., Scarafía, M. A., La Greca, A., Santín Velazque, N. L., Garate, X., Waisman, A., et al. (2019). Integrin alpha-5 subunit is critical for the early stages of human pluripotent stem cell cardiac differentiation. *Sci. Rep.* 9, 1–10. doi: 10.1038/s41598-019-54352-2

Niggli, E., Ullrich, N. D., Gutierrez, D., Kyrychenko, S., Poláková, E., and Shirokova, N. (2013). Biochimica et Biophysica Acta posttranslational modi fi cations of cardiac ryanodine receptors: Ca(2+) signaling and EC-coupling. *Biochim. Biophys. Acta* 1833, 866–875. doi: 10.1016/j.bbamcr.2012.08.016

Pecha, S., Yorgan, K., Röhl, M., Geertz, B., Hansen, A., Weinberger, F., et al. (2019). Human iPS cell-derived engineered heart tissue does not affect ventricular arrhythmias in a Guinea pig cryo-injury model. *Sci. Rep.* 9, 1–12. doi: 10.1038/s41598-019-46409-z

Pfeffer, M. A., and Braunwald, E. (1990). Ventricular remodeling after myocardial infarction: experimental observations and clinical implications. *Circulation* 81, 1161–1172. doi: 10.1161/01.CIR.81.4.1161

Rao, C., Prodromakis, T., Kolker, L., Chaudhry, U. A. R., Trantidou, T., Sridhar, A., et al. (2013). The effect of microgrooved culture substrates on calcium cycling of cardiac myocytes derived from human induced pluripotent stem cells. *Biomaterials* 34, 2399–2411. doi: 10.1016/j.biomaterials.2012.11.055

Ribeiro, A. J. S., Ang, Y. S., Fu, J. D., Rivas, R. N., Mohamed, T. M. A., Higgs, G. C., et al. (2015). Contractility of single cardiomyocytes differentiated from pluripotent stem cells depends on physiological shape and substrate stiffness. *Proc. Natl. Acad. Sci. U. S. A.* 112, 12705–12710. doi: 10.1073/pnas.1508073112

Ronaldson-Bouchard, K., Ma, S. P., Yeager, K., Chen, T., Song, L. J., Sirabella, D., et al. (2018). Advanced maturation of human cardiac tissue grown from pluripotent stem cells. *Nature* 556, 239–243. doi: 10.1038/s41586-018-0016-3

Shiba, Y., Fernandes, S., Zhu, W.-Z., Filice, D., Muskheli, V., Kim, J., et al. (2012). Human ES-cell-derived cardiomyocytes electrically couple and suppress arrhythmias in injured hearts. *Nature* 489, 322–325. doi: 10.1038/nature11317

Silbernagel, N., Körner, A., Balitzki, J., Jaggy, M., Bertels, S., Richter, B., et al. (2020). Shaping the heart: structural and functional maturation of iPSC-cardiomyocytes in 3D-micro-scaffolds. *Biomaterials* 227:119551. doi: 10.1016/j.biomaterials.2019.119551

Sit, B., Gutmann, D., and Iskratsch, T. (2019). Costameres, dense plaques and podosomes: the cell matrix adhesions in cardiovascular mechanosensing. *J. Muscle Res. Cell Motil.* 40, 197–209. doi: 10.1007/s10974-019-09529-7

Sottas, V., Wahl, C. M., Trache, M. C., Bartolf-Kopp, M., Cambridge, S., Hecker, M., et al. (2018). Improving electrical properties of iPSC-cardiomyocytes by enhancing Cx43 expression. *J. Mol. Cell. Cardiol.* 120, 31–41. doi: 10.1016/j.yjmcc.2018.05.010

Tiburcy, M., Hudson, J. E., Balfanz, P., Schlick, S., Meyer, T., Liao, M. L. C., et al. (2017). Defined engineered human myocardium with advanced maturation for applications in heart failure modeling and repair. *Circulation* 135, 1832–1847. doi: 10.1161/CIRCULATIONAHA.116.024145

Ullrich, N. D., Valdivia, H. H., and Niggli, E. (2012). PKA phosphorylation of cardiac ryanodine receptor modulates SR luminal Ca^{2+} sensitivity. *J. Mol. Cell. Cardiol.* 53, 33–42. doi: 10.1016/j.yjmcc.2012.03.015

van Deel, E. D., Najafi, A., Fontoura, D., Valent, E., Goebel, M., Kardux, K., et al. (2017). *In vitro* model to study the effects of matrix stiffening on Ca2+ handling and myofilament function in isolated adult rat cardiomyocytes. *J. Physiol.* 595, 4597–4610. doi: 10.1113/JP274460

Virani, S. S., Alonso, A., Benjamin, E. J., Bittencourt, M. S., Callaway, C. W., Carson, A. P., et al. (2020). Heart disease and stroke statistics—2020 update: a report from the American Heart Association. *Circulation* 141, e139–e596. doi: 10.1161/CIR.0000000000000757

Ward, M., and Iskratsch, T. (2020). Mix and (mis-)match – The mechanosensing machinery in the changing environment of the developing, healthy adult and diseased heart. *Biochim. Biophys. Acta, Mol. Cell Res.* 1867:118436. doi: 10.1016/j.bbamcr.2019.01.017

Weinberger, F., Mannhardt, I., and Eschenhagen, T. (2017). Engineering cardiac muscle tissue: a maturating field of research. *Circ. Res.* 120, 1487–1500. doi: 10.1161/CIRCRESAHA.117.310738

Yang, X., Pabon, L., and Murry, C. E. (2014). Engineering adolescence: maturation of human pluripotent stem cell-derived cardiomyocytes. *Circ. Res.* 114, 511–523. doi: 10.1161/CIRCRESAHA.114.300558

Yeung, E., Fukunishi, T., Bai, Y., Bedja, D., Pitaktong, I., Mattson, G., et al. (2019). Cardiac regeneration using human-induced pluripotent stem cell-derived biomaterial-free 3D-bioprinted cardiac patch *in vivo*. *J. Tissue Eng. Regen. Med.* 13, 2031–2039. doi: 10.1002/term.2954

Yoshida, S., Miyagawa, S., Fukushima, S., Kawamura, T., Kashiyama, N., Ohashi, F., et al. (2018). Maturation of human induced pluripotent stem cell-derived Cardiomyocytes by soluble factors from human mesenchymal stem cells. *Mol. Ther.* 26, 2681–2695. doi: 10.1016/j.ymthe.2018.08.012

Young, J. L., Kretchmer, K., Ondeck, M. G., Zambon, A. C., and Engler, A. J. (2014). Mechanosensitive kinases regulate stiffness-induced cardiomyocyte maturation. *Sci. Rep.* 4, 1–11. doi: 10.1038/srep06425

Zahanich, I., Sirenko, S. G., Maltseva, L. A., Tarasova, Y. S., Spurgeon, H. A., Boheler, K. R., et al. (2011). Rhythmic beating of stem cell-derived cardiac cells requires dynamic coupling of electrophysiology and ca cycling. *J. Mol. Cell. Cardiol.* 50, 66–76. doi: 10.1016/j.yjmcc.2010.09.018

Zhang, S. S., and Shaw, R. M. (2014). Trafficking highways to the intercalated disc: new insights unlocking the specificity of connexin 43 localization. *Cell Commun. Adhes.* 21, 43–54. doi: 10.3109/15419061.2013.876014

Zhu, R., Blazeski, A., Poon, E., Costa, K. D., Tung, L., and Boheler, K. R. (2014). Physical developmental cues for the maturation of human pluripotent stem cell-derived cardiomyocytes. *Stem Cell Res Ther* 5, 1–11. doi: 10.1186/scrt507

Conflict of Interest: The authors declare that the research was conducted in the absence of any commercial or financial relationships that could be construed as a potential conflict of interest.

Publisher's Note: All claims expressed in this article are solely those of the authors and do not necessarily represent those of their affiliated organizations, or those of the publisher, the editors and the reviewers. Any product that may be evaluated in this article, or claim that may be made by its manufacturer, is not guaranteed or endorsed by the publisher.

frontiers in Physiology

ORIGINAL RESEARCH
published: 03 September 2021
doi: 10.3389/fphys.2021.710968

Regulation of the Muscarinic M_3 Receptor by Myocardin-Related Transcription Factors

Li Liu[1,2], Catarina Rippe[1], Ola Hansson[3,4], Dmytro Kryvokhyzha[3], Steven Fisher[5], Mari Ekman[1†] and Karl Swärd[1*†]*

[1]Department of Experimental Medical Science, Lund, Sweden, [2]Department of Urology, Qingyuan People's Hospital, The Sixth Affiliated Hospital of Guangzhou Medical University, Qingyuan, China, [3]Department of Clinical Sciences, Lund University Diabetes Centre, Malmö, Sweden, [4]Institute for Molecular Medicine Finland (FIMM), Helsinki University, Helsinki, Finland, [5]Department of Medicine (Cardiology) and Physiology and Biophysics, University of Maryland-Baltimore, Baltimore, MD, United States

OPEN ACCESS

Edited by:
Markus Hecker, Heidelberg University, Germany

Reviewed by:
Andreas H Wagner, Heidelberg University, Germany
Adán Dagnino-Acosta, University of Colima, Mexico

***Correspondence:**
Karl Swärd
karl.sward@med.lu.se
Mari Ekman
mari.ekman@med.lu.se

†These authors have contributed equally to this work and share the senior authorship

Specialty section:
This article was submitted to Vascular Physiology, a section of the journal Frontiers in Physiology

Received: *17 May 2021*
Accepted: *26 July 2021*
Published: *03 September 2021*

Citation:
Liu L, Rippe C, Hansson O, Kryvokhyzha D, Fisher S, Ekman M and Swärd K (2021) Regulation of the Muscarinic M_3 Receptor by Myocardin-Related Transcription Factors. Front. Physiol. 12:710968. doi: 10.3389/fphys.2021.710968

Myocardin-related transcription factors (MRTFs: myocardin/*MYOCD*, MRTF-A/*MRTFA*, and MRTF-B/*MRTFB*) are co-factors of serum response factor (SRF) that activate the smooth muscle cell (SMC) gene program and that play roles in cardiovascular development and mechanobiology. Gain and loss of function experiments have defined the SMC gene program under control of MRTFs, yet full understanding of their impact is lacking. In the present study, we tested the hypothesis that the muscarinic M_3 receptor (*CHRM3*) is regulated by MRTFs together with SRF. Forced expression of MYOCD (8d) in human coronary artery (SMC) followed by RNA-sequencing showed increased levels of M_2, M_3, and M_5 receptors (*CHRM2*: 2-fold, *CHRM3*: 16-fold, and *CHRM5*: 2-fold). The effect of MYOCD on M_3 was confirmed by RT-qPCR using both coronary artery and urinary bladder SMCs, and correlation analyses using human transcriptomic datasets suggested that M_3 may also be regulated by MRTF-B. Head-to-head comparisons of MYOCD, MRTF-A and MRTF-B, argued that while all MRTFs are effective, MRTF-B is the most powerful transactivator of *CHRM3*, causing a 600-fold increase at 120 h. Accordingly, MRTF-B conferred responsiveness to the muscarinic agonist carbachol in Ca^{2+} imaging experiments. M_3 was suppressed on treatment with the MRTF-SRF inhibitor CCG-1423 using SMCs transduced with either MRTF-A or MRTF-B and using intact mouse esophagus in culture (by 92 ± 2%). Moreover, silencing of SRF with a short hairpin reduced *CHRM3* (by >60%) in parallel with α-actin (*ACTA2*). Tamoxifen inducible knockout of Srf in smooth muscle reduced *Srf* (by 54 ± 4%) and *Chrm3* (by 41 ± 6%) in the urinary bladder at 10 days, but *Srf* was much less reduced or unchanged in aorta, ileum, colon, trachea, and esophagus. Longer induction (21d) further accentuated the reduction of *Chrm3* in the bladder and ileum, but no change was seen in the aorta. Single cell RNA-sequencing revealed that *Mrtfb* dominates in ECs, while *Myocd* dominates in SMCs, raising the possibility that *Chrm3* may be driven by Mrtfb-Srf in the endothelium and by Myocd-Srf in SMCs. These findings define a novel transcriptional control mechanism for muscarinic M_3 receptors in human cells, and in mice, that could be targeted for therapy.

Keywords: cholinergic neurotransmission, pharmacology, acetylcholine, signaling, vasodilatation

INTRODUCTION

G protein-coupled receptors (GPCRs) represent the largest group of proteins targeted by clinical drugs, with well over 100 being affected by FDA-approved substances (Sriram and Insel, 2018). Among these are the muscarinic M_2 (*CHRM2*) and M_3 (*CHRM3*) receptors (Wess et al., 2007). Muscarinic receptors are expressed in the brain, on target organs of the parasympathetic nervous system, including pacemaking cells in the heart, smooth muscle cells (SMCs), glandular cells, and on endothelial cells (Caulfield, 1993; Wess et al., 2007). Agonists and antagonists of M_2 and M_3 are used in clinical conditions ranging from airway obstruction (chronic obstructive pulmonary disease) to bladder overactivity and glaucoma (Ritter et al., 2020). Anticholinesterases, which indirectly affect muscarinic receptors by inhibiting breakdown of acetylcholine, may additionally be of some utility in Alzheimer's disease (Ritter et al., 2020).

M_2 and M_3 receptors are often co-expressed, and their physiological functions have been defined in mice using knockout strategies (Wess et al., 2007). M_3 deficient mice, for example, have reduced body weights and impaired salivation, dilated pupils under bright light, and urinary retention caused by reduction of muscarinic contractility in the bladder (Matsui et al., 2000; Yamada et al., 2001). Moreover, both cholinergic vasodilatation (Gericke et al., 2011) and vasoconstriction (Gericke et al., 2014) are largely abolished. Dual knockout of M_2 and M_3 causes further impairment of gastrointestinal (Matsui et al., 2002) and airway (Struckmann et al., 2003) contractility compared to the isolated knockout of M_3, but viability remains unaffected. In addition, knockout studies have defined roles of muscarinic receptors in neuronal activity and plasticity in the brain (Thomsen et al., 2018). In contrast to the wealth of knowledge generated on physiological functions of muscarinic receptor subtypes, there is a paucity of information regarding the transcriptional control of these receptors. This is a void of knowledge that needs to be filled because transcriptional control mechanisms could be suited for therapy.

Myocardin-related transcription factors (MRTFs: myocardin/*MYOCD*, MRTF-A/*MRTFA*, and MRTF-B/*MRTFB*) act together with the serum response factor (SRF) to drive a broad mesodermal gene program (Miano, 2003, 2015; Olson and Nordheim, 2010; Sward et al., 2016). MRTFs play important roles beyond development in tissues, such as the heart (Parlakian et al., 2005; Mokalled et al., 2015), smooth muscle (Huang et al., 2015), and endothelial cells (Weinl et al., 2013, 2015). A defining property of MRTFs is that they respond to mechanical signals, such as biomechanical force (Chan et al., 2010), stretch (Zhao et al., 2007; Cui et al., 2015), and matrix stiffness (Jain et al., 2013; Foster et al., 2017; Hadden et al., 2017), and the underlying mechanism likely involves actin dynamics (Zhao et al., 2007; Finch-Edmondson and Sudol, 2016). Numerous recent studies have cataloged genes that are activated by overexpression of wild type and constitutively active MRTFs using RNA-sequencing (Zhao et al., 2016; Kim et al., 2017; Hu et al., 2019), but GPCRs and ion channels are often underrepresented in such dataset (Miano et al., 2007), and many of these datasets have limited sample sizes. Polymerase chain reaction (PCR)-based studies with larger sample sizes have demonstrated that MRTFs may play a role for GPCR expression (Krawczyk et al., 2018).

In recent work, we characterized conditional and smooth muscle-specific knockouts of YAP and TAZ, which are coactivators of TEA domain transcription factors (TEADs), and uncovered a lethal colonic phenotype (Daoud et al., 2020). Like MRTFs, YAP and TAZ are mechano-activated (Hadden et al., 2017), and highly expressed in smooth muscle. YAP may act together with MRTFs, especially MRTF-B, and this synergy is governed by a direct physical interaction (Kim et al., 2017). Among transcripts that were reduced in the colon and urinary bladder of YAP/TAZ knockout mice were *Chrm2* and *Chrm3*. Other transcripts that were concordantly reduced were established target genes of MRTF-SRF signaling. Indeed, we found that knockout of YAP and TAZ also caused a parallel reduction of *Srf*. Together, these findings raise the possibility that *Chrm2* and *Chrm3* (M_2 and M_3) may be regulated by MRTF-SRF. The current study was initiated to address this hypothesis (depicted graphically in **Figure 1A**) and to fill the current gap of knowledge regarding transcriptional regulation of clinically relevant GPCRs.

MATERIALS AND METHODS

Bulk RNA-Sequencing

RNA was prepared (miRNeasy, Qiagen) from human coronary artery SMCs transduced with either Ad-CMV-null or Ad-CMV-MYOCD virus (200 MOI, see below). RNA integrity was assessed using TapeStation (Agilent). Next, libraries were prepared using the TruSeq® Stranded Total RNA Library Prep. For demultiplexing index, adapters were added (TruSeq RNA Single Indexes Set A,12 Indexes). Sequencing was performed using NextSeq 500/550 High Output Kit v2.5 on an Illumina NextSeq 500 instrument (75 bp, paired end). Reads were mapped with STAR (Dobin et al., 2013) in 2-pass mode and counted with featureCounts (Liao et al., 2014). Normalization and differential gene expression analysis were performed using DESeq2 (Love et al., 2014). Qualities of sequences, alignments, and read counting were assessed with fastQC (De Sena Brandine and Smith, 2019), qualimap (Okonechnikov et al., 2016), and multiQC (Ewels et al., 2016). All the code, including a conda environment, Snakemake file, and R markdown notebooks, are available at https://github.com/LUDC-bioinformatics/SMC_MYOCD

Cell Culture and Adenoviral Overexpression and Silencing

Human coronary artery SMCs were from Thermo Scientific/Gibco (C0175C) and cultured in medium 231 (M231500) with growth supplement (SMGS: S00725) and 50 U/50 µg/ml PEST (Biochrom, A2212). Human bladder smooth muscle cells (HBSMCs) were isolated from detrusor strips as described (Zhu et al., 2017). HBSMCs were cultured in DMEM/Ham's F-12

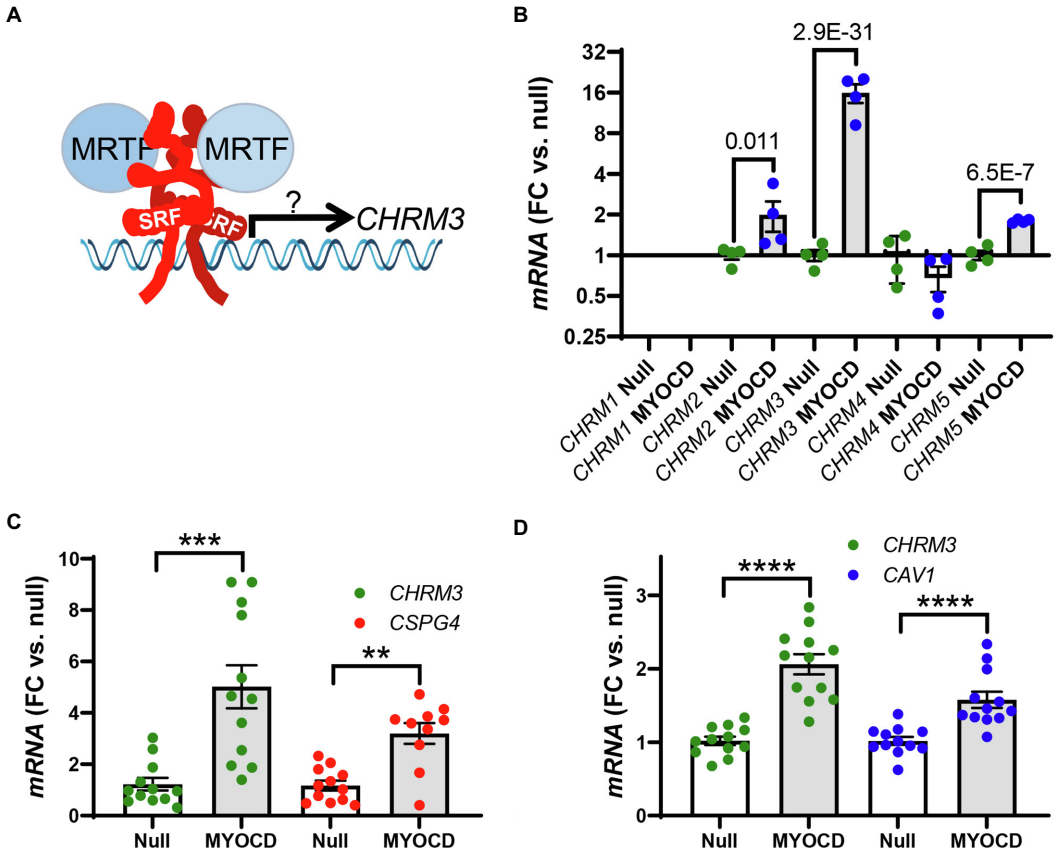

FIGURE 1 | The transcriptional coactivator myocardin (MYOCD) regulates expression of the M_3 muscarinic receptor (*CHRM3*). Panel **A** shows a schematic representation of the hypothesis that we set out to test in the present work, namely, that myocardin-related transcription factors (MRTFs) control expression of the M_3 muscarinic receptor for acetylcholine (*CHRM3*). Panel **B** shows data from an RNA-sequencing experiment were MYOCD was overexpressed in cultured human coronary artery smooth muscle cells (hCASMCs) for 8 days (n = 4 null and 4 MYOCD). Ad-CMV-MYOCD was used for overexpression, and Ad-CMV-null virus at the same multiplicity of infection was used as control. The full dataset of differentially expressed genes is given in the **Supplementary Material**. Brackets in panel **B** show adjusted P-values for the indicated comparisons of M_2 (*CHRM2*), M_3 (*CHRM3*), and M_5 (*CHRM5*) receptor transcripts between conditions. Panels **C** and **D** show confirmation using RT-qPCR ($n = 12$ throughout) that overexpression of myocardin (96 h) upregulates the M_3 receptor transcript. Experiments were run using human coronary artery SMCs in **C** and using human bladder SMCs in **D**. *CSPG4* and *CAV1* were used as positive control targets in **C**, **D**. Bar graphs in this and the following figures show means ± SEM, but individual data points are also given. *****p<0.0001, ***p<0.001* and ***p<0.01.*

medium with glutamine (Biochrom; FG4815), 10% fetal bovine serum (FBS; Biochrom; S0115), and 50 U/50 µg/ml PEST (Biochrom; A2212). Human coronary artery endothelial cells were obtained from Lonza (CC-2585) and cultured in EGM-2 MV Microvascular Endothelial Cell Growth Medium-2 BulletKit (CC-3202), which contains EBM-2 Basal Medium (CC-3156) and EGM-2 MV Microvascular Endothelial Cell Growth Medium SingleQuotsTM supplements (CC-4147). All primary cells were used in passages 3–8 and they were maintained in a standard cell culture incubator (37°C, 95% air, and 5% CO_2).

Adenoviral vectors for overexpression and silencing were obtained from Vector Biolabs (Ad-h-MYOCD, ADV-216227; Ad-h-MKL1/eGFP, ADV-215499; Ad-h-MKL2, ADV-215500; Ad-CMV-Null, #1300; AD-h-YAP1, ADV-227945; Ad-h-shSRF, shADV-224,323; and Ad-GFP-U6-shRNA, #1122) and used at the indicated titers (multiplicities of infection, MOI). Here, Ad-CMV-Null, #1300 and Ad-GFP-U6-shRNA, #1122 were used as negative controls. Most transduced cells were harvested at 96 h unless specified. For instance, in **Figure 1B**, the cells were collected on the eigth day after transduction, and in **Figure 2**, the transduction time was 120 h.

Cell Treatment

In **Figure 2H**, human coronary artery SMCs were transduced with MRTF-A virus or MRTF-B virus (200 MOI) in 1% Smooth Muscle Differentiation Supplement (SMDS, Life Technologies, S-008-5) M231 medium for 96 h. Subsequently, the medium was exchanged for fresh 1% SMDS medium, and 10 µM CCG-1423 (Tocris Bioscience, #5233) or the corresponding volume of DMSO (Sigma-Aldrich, #D5879) added directly the medium. Cells were then harvested after an additional 72 h.

To depolymerize actin in human coronary artery endothelial cells, Latrunculin B (Lat B, 100 nM, Calbiochem, #428020) or DMSO (Sigma-Aldrich, #D5879) was added at 96 h after transducing with MRTF-B virus, and cells were harvested after

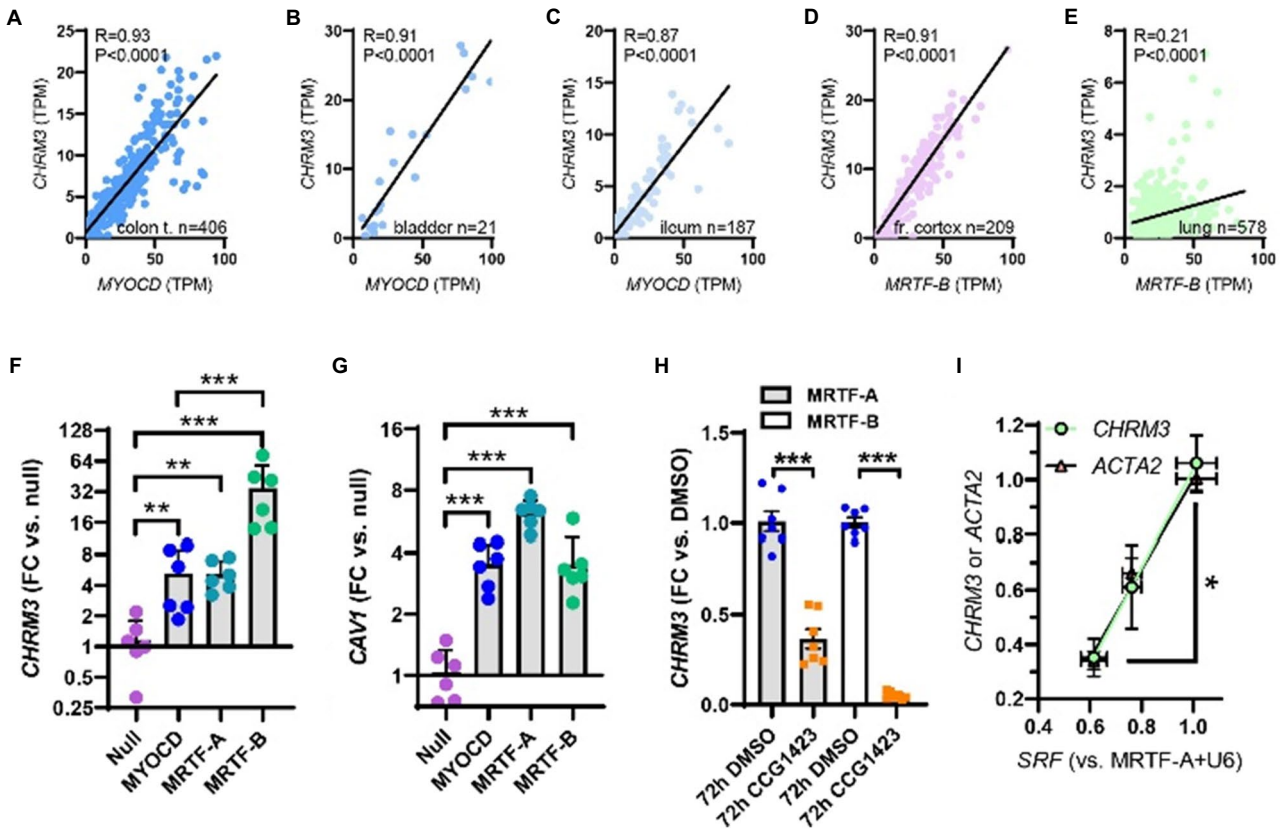

FIGURE 2 | Myocardin (MYOCD) correlates with the M_3 muscarinic receptor (*CHRM3*) across human tissues and SRF is critical for *CHRM3* regulation by MRTFs. **(A)** through **(C)** show correlations at the mRNA level of MYOCD vs. M_3 (*CHRM3*) in the human gastrointestinal tract and urinary bladder. In brain **(D)** and lung **(E)**, *MRTFB*, rather than *MYOCD*, correlated with M_3. This prompted us to examine if all MRTFs (MYOCD, MRTF-A, and MRTF-B) regulate M_3 at the mRNA level. Viral overexpression in human coronary artery SMCs showed that MRTF-B was a more effective transactivator of *CHRM3* than MYOCD (**F**, $n=6$), despite having the same effect as MYOCD on another target (*CAV1*, **G**). **(H)** Shows reduction of *CHRM3* after treatment for 72 h with the MRTF-SRF inhibitor CCG-1423 (10 μM, $n=6$). Cells were transduced with either MRTF-A (gray bars) or MRTF-B (white bars). **(I)** Shows that knockdown of serum response factor (SRF, 0, 30, and 100 MOI of Ad-shSRF) reduces *CHRM3* (green/black circles) in parallel with *ACTA2* (pink/black triangles, $n=4$, per condition). MRTF-A was overexpressed throughout in **(I)**. ***$p<0.001$, **$p<0.01$, and *$p<0.05$.

additional 24 h. Before adding the LatB, cells were also transferred to low-serum medium (2.5% FBS) for a 24 h period.

To inhibit the YAP-TEAD interaction, 2μM verteporfin (Sigma-Aldrich, SML0534-5MG) or the corresponding volume of DMSO (Sigma-Aldrich, #D5879) was added to the medium after transduction with MRTF-B virus for 72 h (human coronary artery SMCs). Cells were harvested for RNA extraction after an additional 24 h.

RT-qPCR

At the end of the culture period, cells were washed (PBS, P4417, Sigma-Aldrich), lysed (Qiazol, Qiagen, #79306), and RNA was isolated using the Qiagen miRNeasy mini kit (Qiagen, #217004) in a QIAcube workstation. The NanoDrop 2000c (Thermo Scientific) instrument was used to determine RNA purity and concentration. For quantification of specific transcripts, we used the StepOnePlus thermal cycler (Applied Biosystems), the QuantiFast SYBR Green RT-PCR kit (Qiagen, 204,156), and QuantiTect Primer assays (Qiagen) for *CHRM3* (QT00200354), *CHRM2* (QT00092134), *CSPG4* (QT00120407), *CAV1* (QT00012607), *SRF* (QT00084063), *ACTA2* (QT000088102), *18S* (QT00199367), *Chrm2* (QT00290297), *Chrm3* (QT00312774), *Srf* (QT00126378), and *18 s* (QT02448075). The exact primer sequences are considered proprietary by Qiagen. As a house-keeping reference gene, we used *18S*, and the fold changes (null or vehicle) were calculated using the Pfaffl method. The relative transcript levels are represented by official gene symbol in italics in all graphs and the units are fold changes (FC) versus control.

Correlation Analyses Using the GTExPortal.org

R-scripts and methods for downloading, and TMM normalizing, RNA-sequencing data from the GTExPortal.org have been described elsewhere (Krawczyk et al., 2015; Sward et al., 2019). For the current analyses, data were downloaded in the summer of 2020. Correlations between *MYOCD* and *CHRM3* were

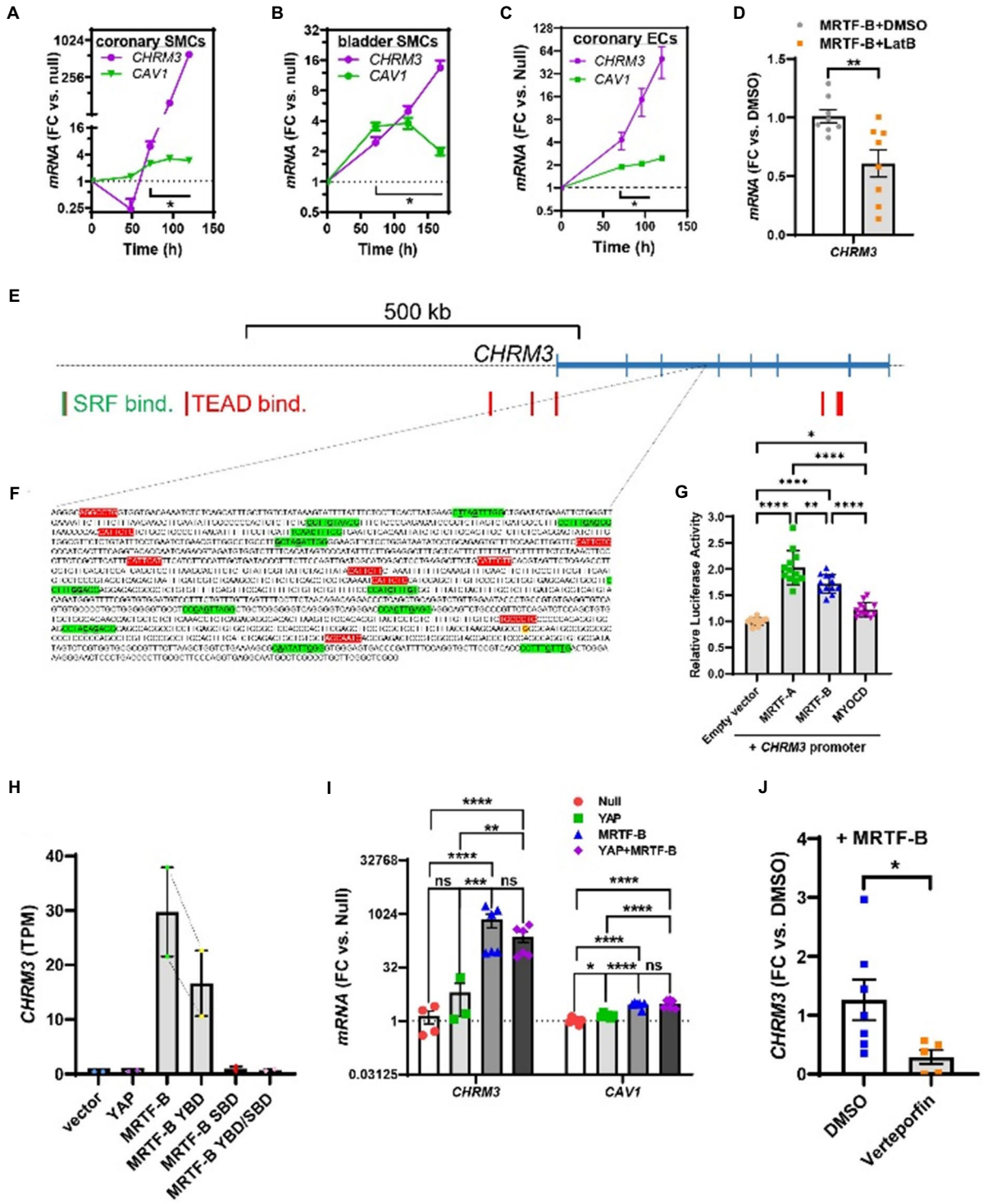

FIGURE 3 | Time-course data, promoter reporter assays, and MRTF-B-YAP cooperation. MRTF-B was overexpressed in different cell types (200 MOI), and cells were harvested at different times. RNA was subsequently isolated, and *CHRM3* was measured by RT-qPCR. **(A)** Shows time-dependent upregulation of *CHRM3* in human coronary artery SMCs. Significant increases were seen at times exceeding 48 h, and a 597-fold increase was seen at 120 h ($p = 0.0004$, $n = 3$). Because there was no indication that the increase of *CHRM3* reached a plateau at longer transduction times, we designed an experiment using even longer incubations in human bladder SMCs **(B)**. Again, there was no tendency of a plateau. Moreover, the maximal increase was somewhat smaller than in coronary artery SMCs. Similar results were obtained in human coronary artery endothelial cells [**(C)**, 200 MOI]. **(D)** Shows that *CHRM3* was reduced by Latrunculin B (100 nM, gray bar) in MRTF-B-transduced ECs. Inspection of the *CHRM3* gene locus on chromosome 1 **(E)** revealed SRF binding (green vertical bars) and TEAD binding (red vertical bars) to many sequences 5' of, and over, the longest transcript (blue). Direct examination of a commercial promoter reporter sequence (NM_000740, transcript variant 2,

(Continued)

FIGURE 3 | hg38; chr1+: 239627686–239,629,364; TSS = 239,629,073) did not reveal any true CArGs, but 11 motifs with 2 deviations from the classical CArG sequence [CC(A/T)$_6$GG, green highlights, deviations underlined, **(F)**] were present, along with 9 TEAD motifs [red highlights, **(F)**]. The transcription start site for the promoter is highlighted in yellow with red lettering. This "CArG-deficient" promoter responded to MRTFs in a luciferase reporter assay **(G)** run using HEK 293 cells. **(H)** Shows *CHRM3* mRNA expression in MCF10 cells transfected with YAP, MRTF-B, and two MRTF-B mutants; the YBD mutant does not bind YAP, and the SBD mutant does not bind SRF. **(I)** Shows the effects of YAP and MRTF-B transduction, alone and in combination, on *CHRM3* in human coronary artery SMCs. Ct values for *CHRM3* were sometimes too high for reliable detection (null and YAP). This is the reason why the sample size is less than $n = 6$ for *CHRM3* in the null and YAP groups, even if six experiments were run for the panel. **(J)** Shows the effect of the YAP-TEAD inhibitor verteporfin in MRTF-B-transduced coronary artery SMCs. Two samples were lost in the verteporfin group again due to lack of amplification. ****p<0.0001, ***p<0.001, **p<0.01, and *p<0.05.

examined in transverse colon ($n = 406$), urinary bladder ($n = 21$), and terminal ileum ($n = 187$) using the Spearman method in GraphPad Prism. Correlations between *MRTFB* and *CHRM3* were examined in the frontal cortex ($n = 209$), tibial artery ($n = 663$), aorta ($n = 432$), and lung ($n = 578$), respectively. Individual TPM (transcripts per million) values along with R- and P-values are given in the graphs or running text.

Organ Culture and Treatment With CCG-1423

Six wild-type C57Bl/6 female mice, weighing 20–25 g from ongoing breeding efforts, were euthanized by cervical dislocation. The abdomen was opened, and the urinary bladder was taken out and put in 2 ml Eppendorf tubes prefilled with ice cold and sterile HEPES-buffered Krebs solution (135.5 mm NaCl, 5.9 mm KCl, 1.2 mm MgCl2, 2.5 mm CaCl2, 11.6 mm glucose, 11.6 mm HEPES, pH 7.4, and 0.5% PEST). A part of the stomach/ventricle was also excised, and the trachea and esophagus were removed together and put in prefilled tubes as above. The tissues were transported to the laboratory where the trachea and esophagus were dissected free from surrounding connective tissue, and the mucosa was removed from the urinary bladder and the ventricle under a dissection microscope. All tissues were cut into two equal pieces in the craniosacral direction. One piece was cultured with vehicle (DMSO) and the other with the MRTF-SRF inhibitor CCG-1423 (10 μM) in DMEM Ham's F12 medium with 50 U/ml penicillin, 50 μg/ml streptomycin, 2% dialyzed FCS, and 10 nM insulin. Following organ culture for 96 h, the tissues were frozen in liquid nitrogen. RNA was isolated using the RNeasy Minikit® from Qiagen and mRNA levels were determined by RT-qPCR (StepOne®).

Wire Myography

The organ culture procedure was almost identical to that described above but using endothelial cell culture medium instead of DMEM/HAM F12. Caudal artery segments were cultured on myograph wires allowing for immediate mounting in a Mulvany myograph (610 M; Danish Myo Technology) as described (Dahan et al., 2014) following culture. After stretching to a basal tension of 5 mN in the absence of Ca^{2+}, and equilibration in normal Ca^{2+}-containing HEPES buffer, arteries were depolarized using K^+-high solution (60 mM). Following washing 0.3 μM cirazoline was added, and after 8 min, carbachol (10–8 to 10–5 M) was added in a cumulative manner. Average force (in mN) over the stimulation period was used for analysis.

Protein Isolation and Western Blotting

After 120 h of transduction with virus, cells were washed in ice cold PBS (Thermo Fisher Scientific, # 20012027) twice. They were harvested by scraping following addition of lysis buffer (70 μl 60 mM Tris-HCl, 2% SDS, 10% glycerol, pH 6.8). To prepare the reduced and unreduced samples in parallel, the lysates were adjusted to 1 μg/μl with or without mercaptoethanol (5%) after determining the protein concentration (BIO-RAD DC protein assay kit, #500–0112). Lysates to which mercaptoethanol was added were also heated to 95°C for 5 min. All the samples were stored at −80 °C. 25 μg of protein was loaded per lane on AnyKd gels (BIO-RAD, #161–0395) along with PrecisionPlus Kaleidoscope markers (BIO-RAD, #161–0395). Gels were run at 200 V until the front ran off using the Tris/Glycine/SDS buffer system (BIO-RAD, #161–0732). The Trans-Blot Turbo transfer system and 0.2 μM nitrocellulose (BIO-RAD, #170–4159) were used for transfer. Following blocking for 2 h in Casein block (BIO-RAD, #161–0782), membranes were incubated with CHRM3 primary antibody (Abcam, ab126168, 1:200) in sealed plastic bags. Bags were tumbled in the cold room (4°C) for 4 days. Membranes were subsequently washed in Tris-buffered saline (BIO-RAD, 170–6435) with 0.1% Tween (BIO-RAD, 161–0781) three times (10 min each), incubated with anti-rabbit HRP (horseradish peroxidase)-conjugated secondary antibodies (1:10000, Cell Signaling Technology, #7074S) for 2 h, and washed again. The West Femto substrate (Thermo Fisher Scientific, #34096) and the Odyssey Fc Imager (LI-COR Biosciences) were used for detection. After initial detection, membranes were stripped in Stripping buffer (Thermo Scientific, 46430) for 30 min, at 60°C, washed as above and blocked again for 2 h in Casein block. Thereafter, membranes were incubated with HSP90 primary antibody (BD Biosciences, 610418, 1:1000) in the cold room (4°C) for 2 days. After three washes as above, membranes were incubated with anti-mouse HRP (horseradish peroxidase)-conjugated secondary antibodies (1:10000, Cell Signaling Technology, #7076S) for 2 h and washed again. Bands were normalized to HSP90 in the same lane.

Inducible and SMC-Specific Knockout of Srf

B6.129S6-Srftm1Rmn/J mice were obtained from the Jackson laboratory (stock number #006658). These mice have loxP sites flanking promoter and exon 1 sequences of the Srf gene (Ramanan et al., 2005). The Srf-floxed mutant mice ($Srf^{fl/fl}$) were bred with hemizygous Myh11-Cre/ERT2 mice (Wirth et al., 2008), allowing for knockout of Srf in smooth muscle upon treatment with tamoxifen (Daoud et al., 2021). Cre

expression was induced by intraperitoneal injection of tamoxifen (1 mg/mouse/day) in ethanol/sunflower oil (1:10) for 5 consecutive days. Floxed but Cre-negative mice treated with tamoxifen were used as controls in the first round. In the second round, we also included a group of floxed Cre-positive mice receiving vehicle as controls. Mice were killed by cervical dislocation and organs were excised and transferred to ice cold HEPES-buffered Krebs solution (135.5 mmol/L NaCl, 5.9 mmol/L KCl, 1.2 mmol/L $MgCl_2$, 11.6 mmol/L HEPES, 11.5 mmol/L glucose, and 143.8 mmol/L Cl^-, pH 7.35 at 37°C) with no Ca^{2+}. After transportation to the laboratory, organs (urinary bladder, colon, ileum, trachea, esophagus, caudal artery, aorta, and kidney) were cleaned under dissection microscopes, quickly blotted on filter paper to remove excess solution, and frozen in liquid N_2. After storage at −80 °C, RNA was isolated as described. Mouse primers for *Chrm3*, *Chrm2*, *Srf*, and *18 s* were obtained from Qiagen. Primer sequences are considered proprietary information. Five wild-type and five knockout mice were used for the experiments with 10d induction, but two samples were lost to workup (one aorta and one bladder). Therefore, the n-value for these is only four. For 21d induction, we used 5 vehicle controls (VC), 5 tamoxifen controls (TC), and 12 tamoxifen knockouts (TKO), and no samples were lost to workup. There was no difference between the VC and TC groups in expression of *Srf* or *Chrm3* in ileum or aorta, but there was a borderline significant difference in the bladder (TC<VC). All differences in TKO bladder were highly significant versus both VC and TC and irrespective of data pooling (ANOVA-Tukey). We therefore pooled 21d control data (VC+TC) throughout for simplicity.

Promoter Reporter Assay

The promoter reporter plasmid for *CHRM3* contained a dual-luciferase vector backbone and was from GeneCopoeia (HPRM30679). HEK293 cells were seeded in 24 well plates and transfection was conducted in antibiotic-free DMEM media with 10% fetal bovine serum (Thermo Fisher, #23320–002). The *CHRM3* plasmid was transfected together with either p3xFLAG-MKL1 plasmid (Addgene, #11978), p3xFLAG MKL2 plasmid (Addgene, #27175), or MYOCD plasmid (Origene, #SC327690,) using Lipofectamine 2000 (Thermo Fisher Scientific, #11668030). After 72 h, the medium was collected, and the Secrete-Pair Dual Luminescence Assay Kit was used as recommended in the manufacturer's protocol (GeneCopoeia, #LFO32). Signal was measured in a GloMax 20/20 Luminometer (Promega, #E5311) and the ratio of Gaussian luciferase and alkaline phosphatase (a proxy for transfected cell number) was taken as a measure of promotor activity.

Single Cell RNA-Sequencing Data

To explore the possibility that different MRTFs dominate in different arterial cell types, we accessed a single cell RNA-seq dataset (He et al., 2018; Vanlandewijck et al., 2018) and extracted read count averages for different cell types. To plot the data, all read count averages for specific transcripts were normalized to the cell type with highest read count average of that transcript.

Ca^{2+} Measurements

Cells grown on the glass-bottom dishes were transduced with MRTF-B or null virus for 120 h and washed with HEPES-buffered Krebs solution (in mM: NaCl 135.5, KCl 5.9, $MgCl_2$ 1.2, glucose 11.6, HEPES 11.6, and $CaCl_2$ 2.5, pH 7.4) twice. Thereafter, cells were incubated with the intracellular calcium indicator Fluo-4, AM (5 μM, Thermo Fisher Scientific, F14201) or X-Rhod-1, AM (1 μM, Thermo Fisher Scientific, #X14210) and Pluronic F-127 (0.02% (w/v), Molecular Probes, #P-1572) in Krebs buffer at room temperature for 1 h. Cells were again washed with buffer twice for 10 min. Real-time Ca^{2+} imaging was done using a confocal microscope (LSM 5 PASCAL, Carl Zeiss, Germany). After 200 s of data acquisition as a baseline, 3 μM carbachol was mixed into the buffer, and fluorescence was recorded for another 200 s. Thereafter, 1 mM ATP was mixed into the buffer and acquisition was stopped after an additional 200 s. The ZEISS ZEN microscope software was used to measure the fluorescence intensities in regions of interest (ROI). ROIs were positioned over the 20 cells with the largest relative response in all fields of view and the average intensity over these ROIs was used for statistical testing. F_0 represents the mean of fluorescence intensity over the first 200 s, and F_1 represents the fluorescence intensity at any given time. Ca^{2+} changes were expressed as F_1/F_0 (%) and are plotted with 95% confidence intervals.

Statistics

Statistical testing was done using log2-transformed expression data. For comparisons between two groups, we used the Mann-Whitney U test for unpaired data. In some panels, such as the time-course figures in **Figures 3A-C**, the controls used for statistical testing are not plotted in the graphs in the interest of clarity. Moreover, in **Figures 3A-C**, the sample size was too small for Mann-Whitney testing, and we therefore used student t-test. For multiple comparisons, one-way ANOVAs followed by Tukey's post-hoc test was used. The residual distributions (QQ plots) of the log2-transformed RT-qPCR data in the ANOVAs were linear with a slope of 1, supporting a normal distribution. Two-way ANOVAs were used in the Ca^{2+} imaging experiments.

RESULTS

RNA-Sequencing Shows That *CHRM3* Is Regulated by Myocardin

We first generated an RNA-sequencing dataset for identification of transcripts regulated by myocardin. Myocardin was overexpressed using an adenoviral vector (Ad-CMV-MYOCD) in cultured human coronary artery SMCs. With 36–49 million pair end reads per sample and four samples per group, this dataset provides good transcriptome coverage for several downstream applications. Among the differentially expressed transcripts (the differential expression analysis is provided in the supplementary data), we noted that the muscarinic M_2 receptor (*CHRM2*), the M_3 receptor (*CHRM3*), and the M_5

receptor (*CHRM5*) were increased 8 days after overexpression of myocardin compared to null adenovirus (**Figure 1B**, brackets give adjusted P-values). For independent confirmation, we assayed *CHRM3* alongside a positive control (*CSPG4* or *CAV1;* Krawczyk et al., 2015; Rippe et al., 2021) using RT-qPCR at four days of transduction with Ad-CMV-MYOCD or Ad-CMV-null viruses. *CHRM5* was not examined further due to uncertainty regarding its biological function, and *CHRM2* was not detectable with the primer assay used, but the increase of *CHRM3* was readily confirmed (**Figure 1C**). We also measured *CHRM3* in cultured human bladder SMCs and again observed an increase following transduction of myocardin (**Figure 1D**). We concluded that overexpression of myocardin increases the transcript level of the muscarinic M_3 receptor in different human SMCs.

All MRTFs Increase *CHRM3*

We have previously reported that myocardin correlates with some of its target genes at the mRNA level (Krawczyk et al., 2015; Sward et al., 2019). To examine if this was the case for *CHRM3*, we used human RNA-seq data downloaded from the GTExPortal.org (Consortium, 2013). Correlations were examined in different organs using the Spearman method. *MYOCD* correlated tightly with *CHRM3* in the transverse colon (**Figure 2A**), the urinary bladder (**Figure 2B**), and the ileum (**Figure 2C**). *MYOCD* also correlated with *CHRM3* in the coronary artery ($R = 0.46$, $p < 0.0001$, not shown), but not in the other two arteries represented in the database (aorta and tibial artery, not shown). Similarly, *MYOCD* did not correlate with *CHRM3* in the brain (frontal cortex, not shown). We therefore instead tested if *MRTFA* and *MRTFB* correlate with *CHRM3*, and we observed a strong positive correlation for *MRTFB* in the brain (**Figure 2D**). This was also seen in the lung, where *MRTFB* correlated with *CHRM3* (**Figure 2E**), in the tibial artery (*MRTFB* vs. *CHRM3*: $R = 0.32$, $p < 0.0001$, not shown), and the aorta (*MRTFB* vs. *CHRM3*: $R = 0.28$, $p < 0.0001$, not shown). These analyses suggested that MRTF-B may increase *CHRM3* like *MYOCD* and therefore prompted us to experimentally determine if all MRTF family members increase *CHRM3* expression. Indeed, in side-by-side adenoviral transductions, all MRTFs increased *CHRM3* (**Figure 2F**), and the effect of MRTF-B was larger (34-fold) than the effects of MYOCD (5-fold) and MRTF-A (5-fold) at the same virus titers. This difference between MRTFs is likely real, because MRTF-B did not increase *CAV1* more effectively than MYOCD in the same samples (**Figure 2G**). All MRTFs thus have the capacity to regulate transcription of the muscarinic M_3 receptor in human SMCs, but MRTF-B appears most effective in this regard.

The MRTF-SRF Inhibitor CCG-1423 Reduces *CHRM3* in MRTF-Transduced Cells

From a therapeutic point of view, it is important to examine if substances that have been developed to inhibit MRTF-SRF signaling (Bell et al., 2013; Lundquist et al., 2014) also affect expression of the muscarinic M_3 receptor. One of these substances is CCG-1423, and it inhibits serum response element-driven gene activation with an IC_{50} value of 1–5 μM via interference with MRTF-SRF-dependent transcriptional activation (Evelyn et al., 2007). Indeed, CCG-1423 (10 μM) reduced *CHRM3* at 72 h of treatment in MRTF-transduced SMCs (**Figure 2H**). The effect appeared greater in cells transduced with MRTF-B than in cells transduced with MRTF-A, which may reflect the larger effect of MRTF-B on *CHRM3*. No effect was seen without MRTF transduction (not shown), or at earlier times (not shown), findings that we attribute to low basal M_3 levels in cultured SMCs.

Short Hairpin Silencing of SRF Reduces *CHRM3* Expression

To examine the SRF-dependence of the MRTF effect on *CHRM3*, we next used a short hairpin construct (Ad-shSRF, two virus titers) to knock down SRF in cells transduced with MRTF-A. The levels of *SRF*, *ACTA2*, and *CHRM3* were determined by RT-qPCR in silenced and control cells (U6). We found that *CHRM3* was reduced upon SRF silencing (**Figure 2I**, green), paralleling the established target gene *ACTA2* (**Figure 2I**, black/pink triangles). The MRTF-A effect on *CHRM3* thus requires SRF.

Time-Course Studies

To better estimate the full effect-size of MRTF-B, we next performed time-course studies where we harvested human coronary artery SMCs at various times after coactivator transduction. The effect on *CHRM3* was compared with the effect on *CAV1* (Krawczyk et al., 2015). After an initial small drop, *CHRM3* started to increase at 72 h after MRTF-B transduction (**Figure 3A**), and it continued to increase beyond 96 h without any sign of saturation. At 120 h, *CHRM3* was increased 597-fold ($p = 0.0004$), and this effect dwarfed the effect on *CAV1* in the same samples. Of note, 72 h was required for increases of both *CAV1* and *CHRM3* to become significant. We next designed a similar experiment for bladder SMCs, but with even longer incubations to hopefully capture the full range of regulation. Again, *CHRM3* increased well beyond 100 h while *CAV1* did not (**Figure 3B**) and there was no sign of saturation. We also tested the effect of MRTF-B in human coronary artery endothelial cells (ECs) but failed to saturate the effect (**Figure 3C**). While significant, the effect on *CHRM3* in both ECs and bladder SMCs appeared somewhat smaller than in coronary SMCs (compare **Figures 3A–C**). However, Ct values for *CHRM3* in coronary artery SMCs were high to start with (Ct rank order for *CHRM3*: bladder SMCs<coronary SMCs<ECs), suggesting a low basal level of expression compared to bladder SMCs. In keeping with the sensitivity of MRTFs to actin dynamics, we found that depolymerization of actin (Latrunculin B: LatB, 24 h) in MRTF-B transduced ECs reduced *CHRM3* (**Figure 3D**).

Promoter Reporter Data and Dependence on YAP-TEAD

Human chromatin immunoprecipitation sequencing data (Encode3, UCSC genome browser) did not reveal SRF binding in the immediate vicinity of *CHRM3* on chromosome 1, even if SRF binding was noted >500 kb upstream of the gene

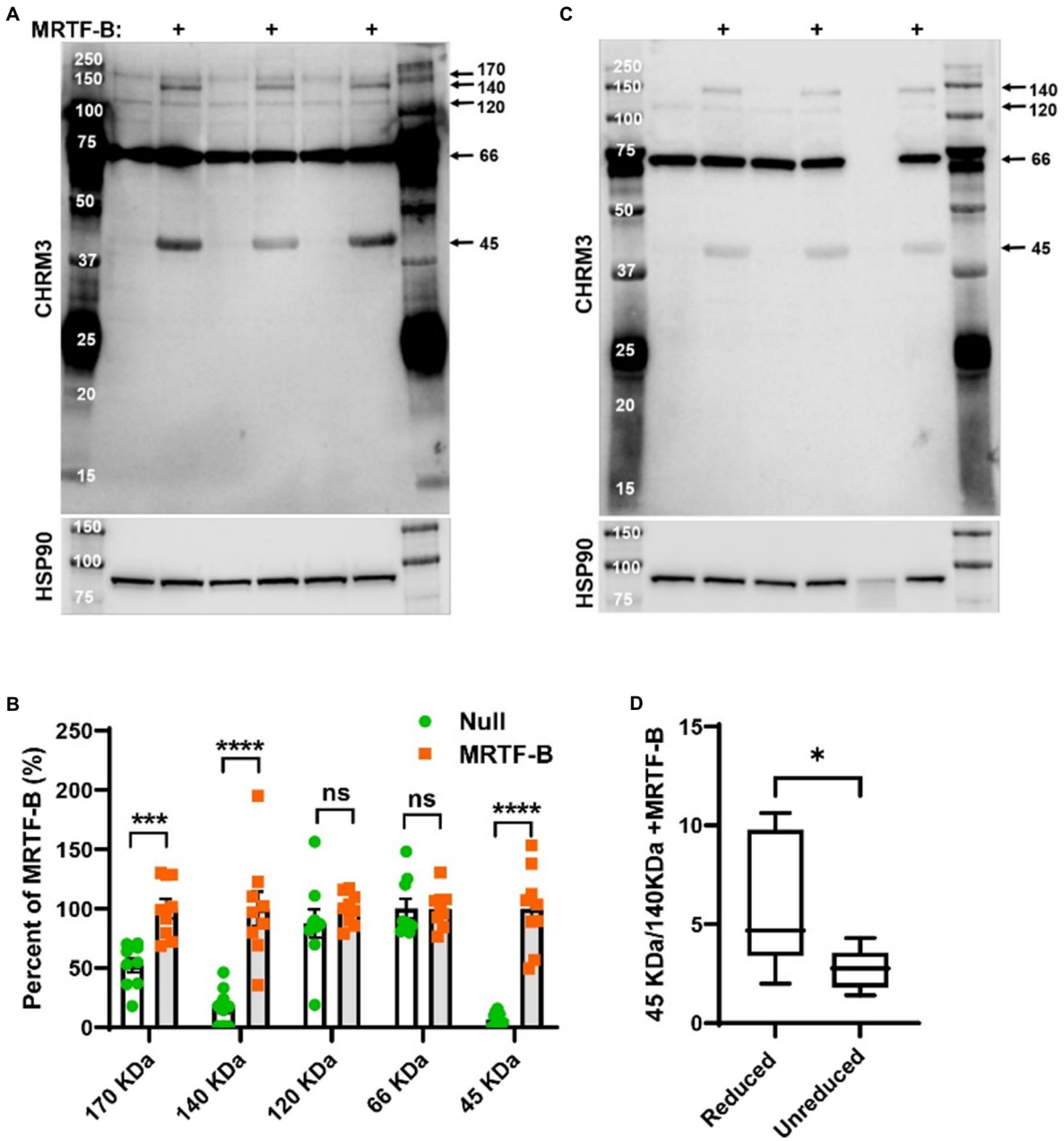

FIGURE 4 | MRTF-B increases CHRM3 immunoreactive bands in human coronary artery smooth muscle cells. Protein lysates from human coronary artery SMCs treated with null virus and with MRTF-B virus for 120 h, respectively, were used for Western blotting using an antibody raised against a human CHRM3 in **(A)**. After developing the blot, it was stripped and incubated with HSP90 antibody (shown below) to assess equal protein loading. At least five bands were detected with the CHRM3 antibody, and three bands at ≈170, ≈140, and ≈45 kDa changed significantly with MRTF-B as shown in the compiled analysis in **(B)**. Quantification in panel **(B)** was done using the blots in **(A)**. Proteins from the same original lysates were also prepared in non-reducing conditions, to examine if the relationship between bands changed **(C)**. The volume was insufficient for one of the null samples in this experiment (lane 6). Non-reducing conditions favored the 140 kDa band at the expense of the 45 kDa band **(D)**, suggesting multimerization. ****$p<0.0001$, ***$p<0.001$, and *$p<0.05$.

(**Figure 3E**, green vertical bar, far left). Binding of TEA domain transcription factors (TEADs), known to be important for YAP/TAZ and a subset of MRTF-controlled genes (Kim et al., 2017), was seen over and near the *CHRM3* locus (**Figure 3E**, red vertical bars). We also inspected CArG box predictions in the mouse that are conserved in man and found 1 CArG box ≈18.5 kb upstream of *Chrm3* (on chromosome 13, not shown), and an additional 10 conserved CArG boxes evenly distributed across the *Chrm3* locus (not shown). Finally, manual inspection of a commercial promoter reporter sequence revealed lack of perfect CArGs motifs, but 12 motifs with two deviations each from the canonical CArG sequence (**Figure 3F**, green highlights, deviations underlined). This promoter also contained nine TEAD motifs (so called MCAT motifs, red highlights in

Figure 3F), six of which are predicted to be functional based on identical motifs in other promoters. Co-transfection of this reporter with MRTFs caused 2-fold activation (HEK 293 cells, **Figure 3G**), albeit not with the natural rank order of efficacy. Taken together, these analyses suggest that there are many conserved CArGs (11) that could contribute to regulation distributed over the *CHRM3* locus and that a *CHRM3* promoter that lacks true CArGs is activated by MRTFs.

Previous work demonstrated that both MRTF-A and MRTF-B may bind YAP-TEAD to activate a reporter with 8 TEAD-binding motifs and no SRF-binding motifs (Kim et al., 2017). The same study also demonstrated MRTF-B shows a preference for binding to YAP-TEAD, whereas MRTF-A shows a preference for binding to SRF. The stronger effect of MRTF-B compared to MRTF-A and MYOCD on *CHRM3* may therefore depend on dual activation of YAP-TEAD and SRF-dependent transcription. To approach this possibility, we interrogated an RNA-sequencing dataset with two replicates, where MRTF-B was overexpressed alongside YAP-binding deficient (YBD) and SRF-binding deficient (SBD) mutants of MRTF-B, as well as a double mutant (YBD/SBD). In this dataset (Kim et al., 2017), *CHRM3* was increased by MRTF-B compared to empty vector as shown in **Figure 3H**. The effect of the YBD mutant was 45% smaller than control MRTF-B, and the SBD mutant was without effect (**Figure 3H**). This independently supports a key role of SRF, but also bolsters the idea that MRTF-B may depend on YAP-TEAD. For such target genes, remarkable synergy was reported on combined overexpression of MRTF-B and YAP compared to overexpression of MRTF-B or YAP alone (Kim et al., 2017). Therefore, we next examined the possibility that YAP and MRTF-B act in synergy. This was done by overexpressing these coactivators alone and together. However, overexpression of YAP alone had no significant effect, and it did not boost the effect of MRTF-B (**Figure 3I**). Overexpressed YAP had a transcriptional impact, because it increased *CAV1* in the same cells, albeit not as effectively as MRTF-B (**Figure 3I**).

To further probe if YAP-TEAD signaling plays a role for *CHRM3* expression, we used an inhibitor. Verteporfin was identified in a screen for inhibitors of the YAP-TEAD interaction (Liu-Chittenden et al., 2012), and it has been used in numerous reports to study the functional role of this transcriptional complex. Here, cells were transduced with MRTF-B for 3 days, and 2 μM verteporfin or vehicle was added for an additional 24 h. Verteporfin reduced the *CHRM3* transcript compared to vehicle (**Figure 3J**). The size of this effect is underestimated by the data in **Figure 3J**, because two samples were lost in the verteporfin group on account of insufficient amplification. Taken together, these findings further suggest that YAP-TEAD signaling is necessary but not sufficient for *CHRM3* expression and that YAP-TEAD and MRTF-SRF likely act cooperatively to drive *CHRM3* expression.

Detection of the CHRM3 Protein in MRTF-B Transduced Cells by Western Blotting

Previous work on a modified and tagged version of rat *Chrm3* revealed that M_3 monomers migrate at 45 kDa, dimers at 90 kDa, and multimers at >120 kDa, along with a proteolytically processed dimer at 75 kDa (Zeng and Wess, 1999). Using an antibody raised against a peptide from human CHRM3, we observed three bands at ≈45, ≈140, and ≈170 kDa that increased in MRTF-B transduced cells, with the most prominent changes occurring at ≈45 kDa, and at ≈140 kDa (**Figures 4A,B**). The antibody also detected bands at 66 and 120 kDa, but the latter did not change in MRTF-B transduced cells (**Figures 4A,B**), and the 66 kDa band, which was the strongest, was also seen in the lanes with molecular weight markers (**Figure 4A**). Because disulfide bridge-dependent multimerization (Zeng and Wess, 1999) was found to be responsible for Chrm3 bands at higher molecular weights, we next prepared the same protein lysates without reducing agent and boiling (**Figure 4C**). Insufficient lysate was available for one of the samples (**Figure 4C**, lane 6). Careful quantification showed that the 45 kDa band declined at the expense of an increase of the 140 kDa band in non-reducing conditions compared to reducing conditions (**Figures 4C,D**). The 45 kDa and 140 kDa bands are therefore interdependent species. Taken together, these findings support MRTF-B-driven increases of protein bands, likely monomers and trimers, that interact with an antibody against human CHRM3.

CCG-1423 Reduces *Chrm3* in Organ Cultured Esophagus

Our loss of function experiments so far depended on prior overexpression of MRTFs in cell culture. To bypass the need for MRTF overexpression, we isolated organs from C57Bl/6 mice and maintained them in organ culture for 96 h with and without CCG-1423 (10 μM). Organs were harvested and frozen at the end of the culture period, and RNA was extracted. Three out of four of the organs (trachea, stomach, and bladder) did not cope well with organ culture with CCG-1423 for 96 h, showing sizeable reductions of the house-keeping genes examined (*18 s*, *Gapdh*), but in the esophagus, *Chrm3* was reduced with CCG-1423 (**Figure 5A**), and the decline of *18 s* was small. *Chrm2* levels remained unchanged, but variability was considerable. This supported the view that *Chrm3* may be controlled by MRTFs in mouse cells *in situ*.

We also measured force in wire myographs after organ culture with CCG-1423. Both force development in response to the α1-adrenergic agonist cirazoline (Cir, 0.3 μM), and relaxation in response to the muscarinic agonist carbachol (Cch, 10^{-8} to 10^{-5} M), were maintained after 96 h using the mouse caudal artery (endothelial cell culture medium; **Figure 5B**, red tracing), but inclusion of CCG-1423 during culture essentially eliminated force (**Figure 5B**, black tracing, $n = 6$, $p < 0.001$). Attempts to knock down *Srf* in organ culture, using the short hairpin used in human cells above, were also not successful (not shown). This called for a more robust and specific method to manipulate MRTF-SRF signaling in intact organs.

Inducible and Smooth Muscle-Specific Deletion of Srf *in vivo*

To examine regulation of *Chrm3* by MRTF-SRF signaling *in vivo*, we generated smooth muscle-specific and inducible knockouts (KOs) of Srf (Park et al., 2015). Any changes in

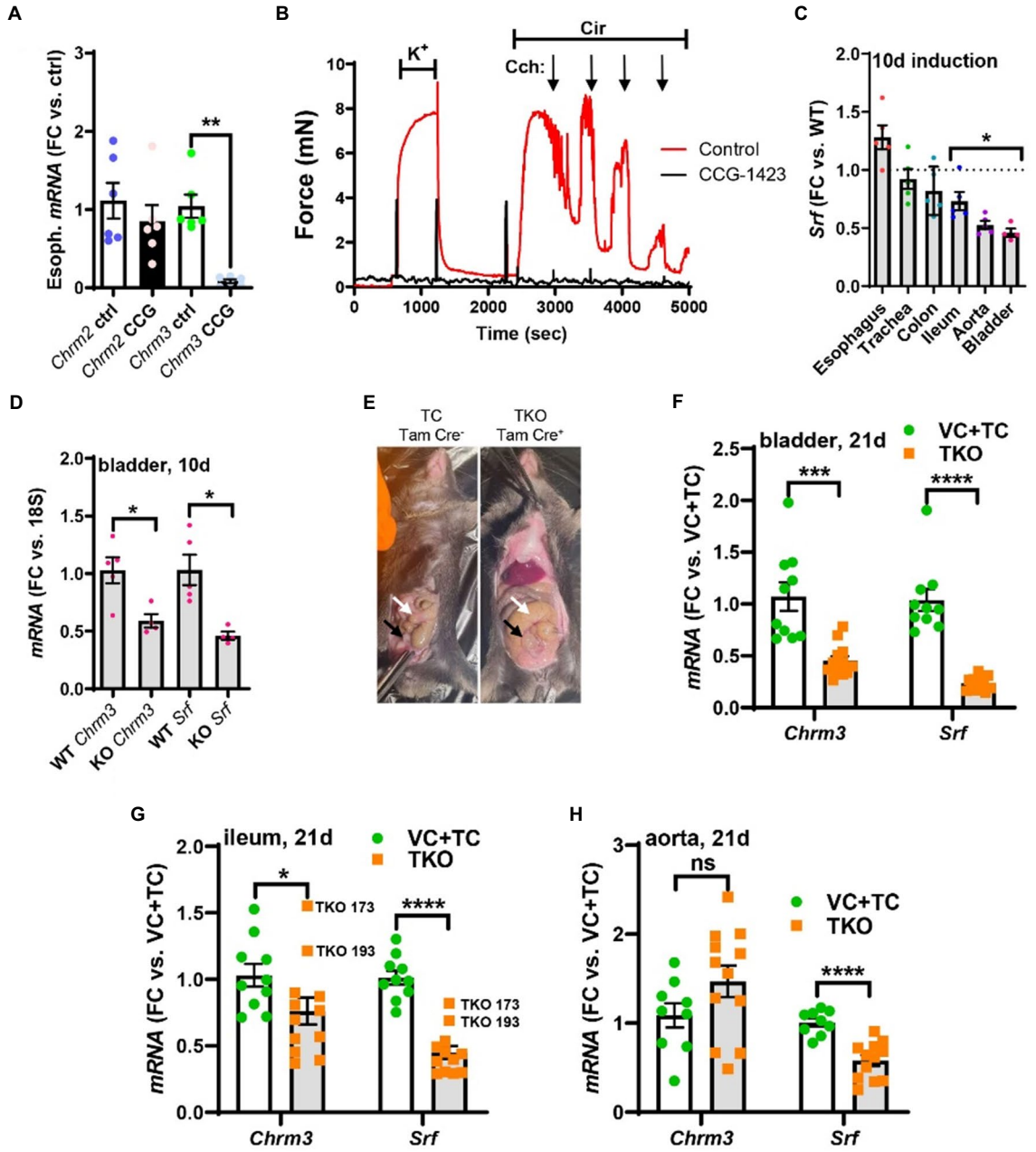

FIGURE 5 | Pharmacological inhibition of MRTF-SRF signaling in organ culture, and knockout of Srf *in vivo*, reduces M_3 receptor expression. To examine if MRTF-SRF signaling regulates muscarinic M_3 receptor expression *in situ*, we first isolated organs from wild-type C57Bl/6 mice. Organs were split in half and maintained for 96 h in organ culture with vehicle (DMSO) or CCG-1423 (10 μM). A clear reduction of *Chrm3* relative to the house-keeping gene *18 s* was seen in the esophagus **(A)**, but in the remainder of the organs, the house-keeping genes examined declined (not shown). We also found that organ culture of the mouse caudal artery in the presence of CCG-1423 eliminated force development on stimulation with the α1-adrenergic agonist cirazoline **(B)**, suggesting that this experimental paradigm is unsuitable for studying effects on endothelium-dependent dilatation. Mice with SMC-specific knockout of Srf were next obtained by injecting $Srf^{fl/fl}$ mice harboring the Myh11-Cre/ERT2 transgene with tamoxifen for 5 consecutive days (knockout: KO). Cre-negative $Srf^{fl/fl}$ mice injected with tamoxifen were used as controls (wild-type: WT). Organs were harvested and frozen 10 days after the first injection and transcript levels were determined by RT-qPCR. At this time, body weights were unchanged, but Srf depletion was seen in some organs **(C)**. **(D)** Shows that *Chrm3* was reduced in parallel with *Srf* in the bladder, but this was not seen elsewhere (not shown). We therefore next used mice at 21 days post tamoxifen. Two control groups were included in this second experiment along with the tamoxifen-treated knockouts (TKO): vehicle-treated Cre-positive mice (VC) and tamoxifen-treated Cre-negative mice (TC). At 21 days, mobility on provocation was reduced, the intestines had started to swell [**(E)**, white arrows], and the urinary bladders were often enlarged [**(E)**, black arrows]. Both *Chrm3* and *Srf* were reduced in the bladder **(F)** and ileum **(G)**. For the ileum, the two knockouts with the most modest *Srf* depletion (TKO 173 and TKO 193) are highlighted. No change of *Chrm3* was seen in the aorta **(H)**, despite significant *Srf* depletion. These findings show that MRTF-SRF signaling is critical for *Chrm3* expression in gastrointestinal and urogenital organs *in vivo*. ***$p<0.001$, **$p<0.01$, and *$p<0.05$.

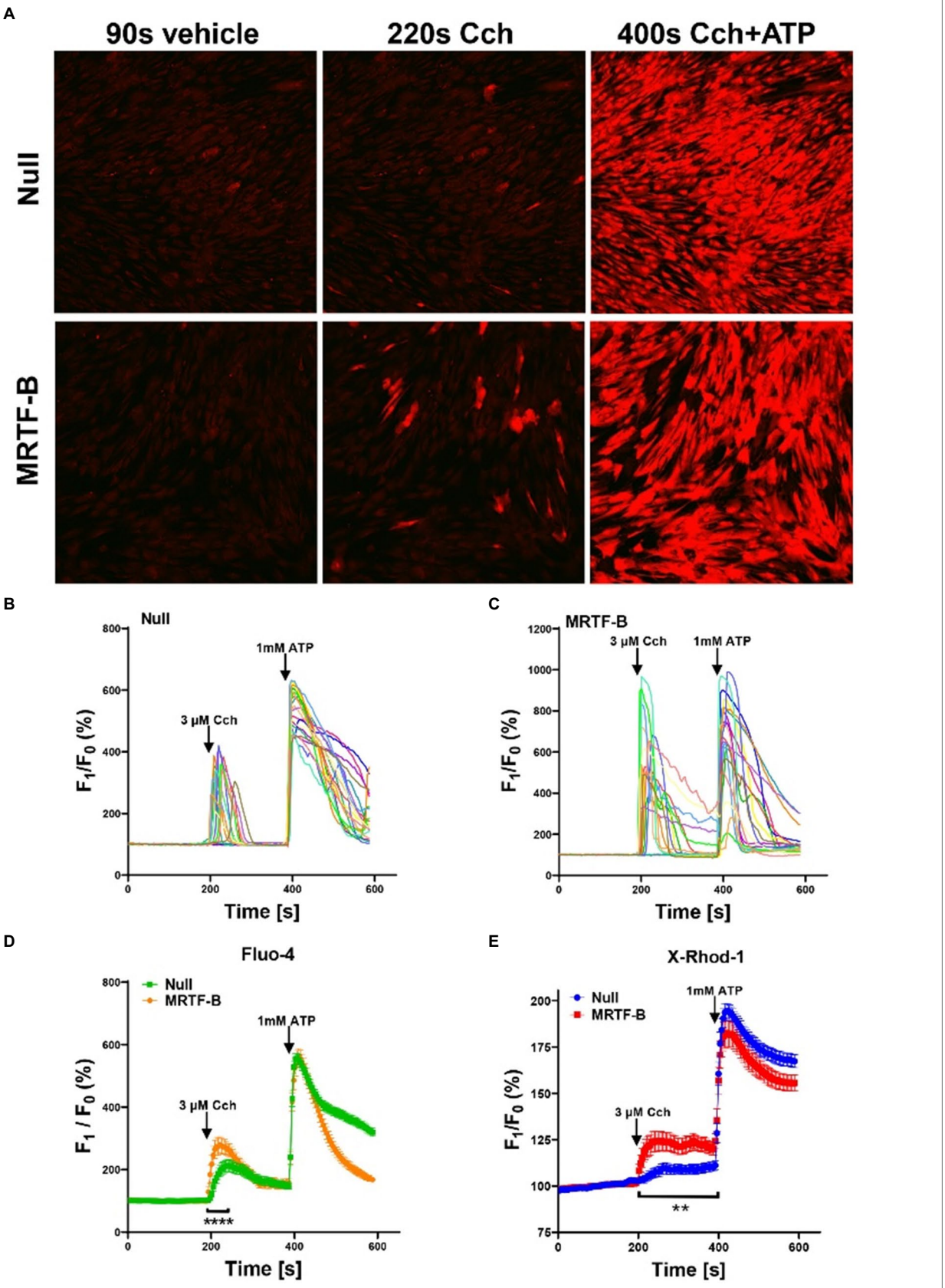
A
90s vehicle
220s Cch
400s Cch+ATP
Null
MRTF-B
B
Null
1mM ATP
3 μM Cch
F1/F0 (%)
Time [s]
C
MRTF-B
3 μM Cch
1mM ATP
F1/F0 (%)
Time [s]
D
Fluo-4
Null
MRTF-B
1mM ATP
3 μM Cch
****
F1 / F0 (%)
Time [s]
E
X-Rhod-1
Null
MRTF-B
1mM ATP
3 μM Cch
**
F1/F0 (%)
Time [s]

(Continued)

FIGURE 6 | Ca^{2+} imaging of MRTF-B-transduced human coronary artery SMCs. To examine if MRTF-B transduction increases responsiveness to the muscarinic agonist carbachol, cells were treated as indicated for 5 days in culture. They were subsequently washed and loaded with Fluo-4 and imaged using confocal microscopy. Only a fraction of the cells responded to carbachol [**(A)**, middle], but the responses were larger in MRTF-B-transduced cells. **(B,C)** Show the 20 cells responding best to carbachol in the experiment in **(A)**. **(D)** Shows compiled data from three independent experiments with Fluo-4. The Ca^{2+} signal between 200 and 250 s was significantly increased by prior MRTF-B transduction. **(E)** Shows intracellular Ca^{2+} in human coronary artery SMCs after transduction of MRTF-B or null virus, respectively ($N = 6$), but measured Ca^{2+} using X-Rhod-1. Error bars in **(D,E)** represent 95% confidence intervals. ****$p<0.0001$ and **$p<0.01$.

whole tissue lysates in this model should reflect changes in smooth muscle. To generate KOs, we treated homozygous Srf-floxed mice harboring a tamoxifen-regulated and smooth muscle-specific (*Myh11* promoter driven) Cre transgene with tamoxifen. Cre-negative floxed mice treated with tamoxifen were used as controls (WT). Srf knockout in SMCs results in intestinal pseudo-obstruction starting 21 days after the first injection (Park et al., 2015) due to reduced cholinergic SMC contraction and impaired gastrointestinal motility (Angstenberger et al., 2007; Mericskay et al., 2007; Park et al., 2015). Here, organs were initially isolated for RT-qPCR on day 10 after the first of five injections. We picked this time based on our previous observation that knockout of YAP and TAZ, using the same Cre-deleter mouse and injection protocol, causes a ≈75% reduction in colon at 10 days (Daoud et al., 2021). No evidence of animal discomfort, such as ruffled fur, reduced mobility, or kyphosis, was observed here at 10 days, and body weights remained unchanged (not shown). 10 days therefore represent the pre-symptomatic stage. Various organs were isolated, and *Srf* levels were determined by RT-qPCR. *Srf* was depleted by 54 ± 4% in the urinary bladder, 47 ± 3% in the aorta, and 26 ± 8% in the ileum (**Figure 5C**), but no significant reductions were seen in the remainder of the organs examined. *Chrm3*, but not *Chrm2* (not shown), levels were reduced in the urinary bladder from KO compared to WT mice (**Figure 5D**). Reduction of *Chrm3* was not significant elsewhere (not shown), but *Chrm3* reduction correlated with *Srf* depletion across all organs ($p = 0.044$, $R = 0.44$, Pearson, not shown).

In view of the rather limited changes at 10 days, we next tried a longer induction time (21 days). This time we used two control groups. One group of mice were Cre-postive and treated with vehicle (VC: vehicle control). Another group of mice were Cre-negative, and they received tamoxifen (TC: tamoxifen control). The third group included mice that were Cre-positive and that were treated with tamoxifen (TKO: tamoxifen treated knockouts). The two control groups were not different and were therefore pooled in the final analysis. At 21d, mobility on provocation was reduced in several knockout animals, and intestinal swelling was apparent in most of them (**Figure 5E**). The mice appeared healthy in most other regards. 21d therefore represents the early clinical phase. Reductions of *Srf* and *Chrm3* in the urinary bladder were augmented at 21d compared to 10d (compare **Figures 5F,D**). *Chrm3* was now also reduced in the ileum (**Figure 5G**) but not in the aorta (**Figure 5H**). Interestingly, two ileum samples (TKO 173 and TKO 193) with poor *Srf* depletion also had poor *Chrm3* depletion (**Figure 5G**). Taken together, these findings show that *Chrm3* in the bladder is reduced already in the pre-symptomatic phase and that the early clinical phase coincides with depletion of intestinal *Chrm3* in SMC-specific Srf knockouts. Maintained *Chrm3* expression in the aorta may be due either to a threshold effect, because Srf was less forcefully reduced, or to preferential expression in non-SMCs, such as endothelial cells. We favor the latter explanation for reasons given below.

MRTF-B Increases the Responsiveness to the Muscarinic Agonist Carbachol in SMCs

To support the concept that MRTF-SRF signaling regulates cholinergic responsiveness, human coronary artery SMCs that had been transduced with MRTF-B, were loaded with the fluorescent indicator Fluo-4, and stimulated with the muscarinic agonist carbachol (3 μM) and ATP (1 mM). Many cells were unresponsive to carbachol (**Figure 6A**, middle), both in the control group, and after MRTF-B transduction. This may relate to a low transduction efficiency (30–50% of all cells) and the short transduction time. However, MRTF-B transduced cells responded more forcefully to carbachol (**Figures 6B,C**), and data from three independent experiments showed that the peak response (200–250 s) to carbachol was significantly increased in the MRTF-B group compared to the control group (**Figure 6D**).

With the intention of measuring Ca^{2+} only in transduced cells, we also used X-Rhod-1 for Ca^{2+} measurements. X-Rhod-1 reports both cytosolic and mitochondrial Ca^{2+}, but it fluoresces at a wavelength compatible with the tagged MYOCD that was available to us. After pilot experiments, we did not follow through with the MYOCD experiments, but overexpression of untagged MRTF-B again enhanced the Ca^{2+} response to carbachol, while the Ca^{2+} response to ATP was similar (**Figure 6E**). In our loading conditions, only a minority of the cells (≈8%) showed a mitochondrial staining pattern, and in most cells, staining appeared to be diffusely cytoplasmic (not shown). Taken together, use of two different fluorescent Ca^{2+} indicators therefore support the view that MRTF-B promotes cholinergic responsiveness in cultured human SMCs.

MRTF-B Is the Dominating MRTF in ECs

To better understand MRTF expression in different vascular cell types, we next examined a single cell RNA-sequencing dataset for cerebrovascular cells (Vanlandewijck et al., 2018). *Myocd* was enriched in arteriolar and arterial SMCs as expected (**Figures 7A,B**, pink). *Mrtfa* was highest in fibroblasts, but

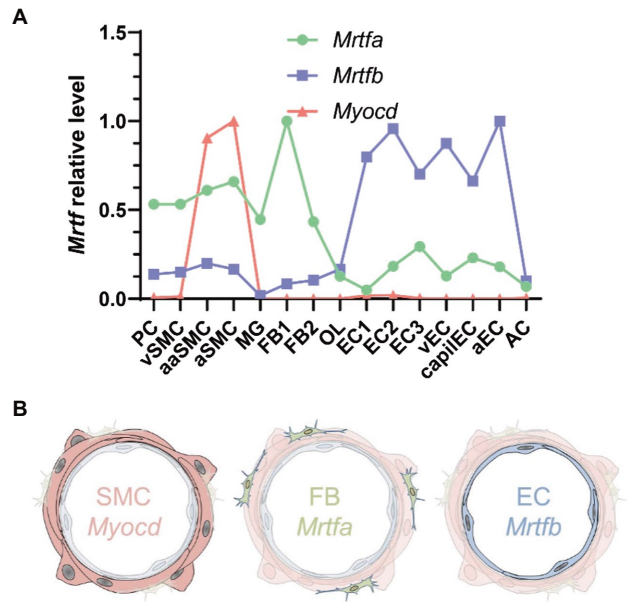

FIGURE 7 | MRTF distribution across the vascular wall. **(A)** Shows cell-averaged mRNA expression data for the indicated transcripts in different cerebrovascular cell types. PC, pericytes; SMC, smooth muscle cells; MG, microglia; OL, oligodendrocytes; FB, fibroblasts; EC, endothelial cells; AC, astrocytes; v, venous; cap, capillary; a, arterial; aa, arteriolar; and 1, 2, and 3, subtype. **(B)** Shows a schematic representation of Myocd in SMCs, Mrtfa in FBs, and Mrtfb in ECs.

sizeable expression was also seen in pericytes and SMCs (**Figures 7A,B**, green). *Mrtfb* was enriched in endothelial cells (ECs, **Figures 7A,B**, blue). This provided a possible explanation for the lack of effect of SMC-specific Srf knockout on *Chrm3* in lysates of the whole aorta.

DISCUSSION

The research effort described here aimed to test the hypothesis that the muscarinic M_3 receptor (*CHRM3*) is regulated by MRTF-SRF signaling using a combination of gain and loss of function approaches *in vitro* and *in vivo*. We demonstrate that the muscarinic M_3 receptor transcript (*CHRM3*) is increased after overexpression of MRTFs, well known for their ability to respond to mechanical forces and actin dynamics (Olson and Nordheim, 2010). *CHRM3* was moreover reduced by SRF depletion in cultured SMCs and in the intact urinary bladder and ileum. Our findings suggest that M_3 in endothelial cells is regulated by MRTF-B-SRF, while in SMCs, the combined influence of all MRTFs (*MYOCD>MRTFA>MRTB*) may be relevant. We demonstrate that MRTF-B is a more effective transactivator of M_3 than MYOCD when both are overexpressed in the same cell type in parallel. This difference may allow for tissue-specific targeting of receptor expression should more selective substances to inhibit MRTF-SRF signaling be developed. This would be important since current drugs, such as the muscarinic antagonists, have serious side effects (e.g., dryness of mouth) that limit their clinical utility.

Our experiments show that the effect of MRTFs on *CHRM3* is difficult to saturate. This differs from the effect on *CAV1* which readily saturates. We are uncertain of the reason for this, but we note that multiple rather poor CArG-like sequences and numerus TEAD motifs are present in one of the promoters (and indeed across the entire gene locus). We also find that this promoter is activated in a luciferase reporter assay. One possibility, therefore, is that binding between MRTFs and the promoter involves (1) multiple weak SRF interactions, that are difficult to detect by ChIP-seq, in addition to (2) direct binding to YAP-TEAD (Kim et al., 2017), such that many productive complexes form at high concentration of MRTFs. If true, this would imply that cells need to proceed relatively far toward the SMC fate for M_3 to be expressed at a meaningful level and that both YAP-TEAD and MRTF-SRF signaling are needed. Such a model fits available pharmacological and knockout data [this study, (Daoud et al., 2021)] and could perhaps explain differences in M_3 expression between different types of SMCs (i.e., gastrointestinal vs. vascular). However, differences in the MRTF-B/MYOCD ratio are an equally plausible explanation for differences in M_3 expression between cell types.

It is now four decades ago that endothelium- and nitric oxide-dependent dilatation of arteries by acetylcholine was discovered (Furchgott and Zawadzki, 1980; Palmer et al., 1987). It remained unclear for many years what the physiological role of this phenomenon is, but meticulous work conducted over the last decade has established autocrine cholinergic signaling in endothelial cells as critical for flow-mediated dilatation (Wilson et al., 2016). Moreover, it is only recently that the transcriptional control mechanisms responsible for endothelium-dependent dilatation have started to be uncovered. Several groups, including ours, have demonstrated that soluble guanylyl cyclase, the major nitric oxide receptor in the vascular media, is regulated by NOTCH signaling (Chang et al., 2011; Rippe et al., 2017). It has also been demonstrated that Srf in SMCs is important for nitric oxide-dependent dilatation (Galmiche et al., 2013), but the precise mechanism of that effect remains to be identified. One possibility is that it occurs via *Kcnmb1*, an important subunit of the large conductance Ca^{2+}-activated potassium channel, which is regulated by Myocd-Srf (Long et al., 2009). This ion channel plays a key role in nitric oxide-dependent dilatation (Leo et al., 2014). However, additional effectors cannot be ruled out (Galmiche et al., 2013). By implicating MRTF-B-SRF in control of muscarinic M_3 receptors in endothelial cells, our current findings add another layer of regulation to this complex mode of communication between cell types in the vascular wall.

Our experiments on Srf-deficient mouse tissues show reduction of M_3 receptor transcripts in the urinary bladder and ileum *in vivo* at 21 days. It is interesting to note that the early clinical phase of this model coincides with intestinal depletion of *Chrm3*. No change of *Chrm3* was seen in the aorta, and we suspect that maintained *Chrm3* expression in the aorta is due to preserved MRTF-B-SRF signaling in the endothelium. An endothelial-specific Srf knockout will be needed to address this hypothesis, or, alternatively, dual knockout of MRTF-A and MRTF-B in the endothelium. Similarly, myocardin knockout

in SMCs would be required to prove a role for myocardin in *Chrm3* expression in this cell type. Thus, specific deletion of MRTF alleles in different vascular cell types would have further strengthened our conclusions, but this was considered beyond the scope of the present work. SMC-specific and inducible Srf knockout, as was done here, eventually result in death from intestinal pseudo-obstruction, associated with reduced gastrointestinal transit *in vivo* and reduced cholinergic activation of colon and bladder preparations *in vitro* (Angstenberger et al., 2007; Mericskay et al., 2007; Park et al., 2015). Given that colonic motility and cholinergic contractility are similarly reduced in M_3-deficient mice (Kondo et al., 2011), it seems plausible that depletion of M_3 receptors represents one molecular mechanism for reduced contraction in Srf knockouts. Indeed, mutations in *CHRM3* in humans cause "prune belly syndrome" with combined intestinal and bladder distension (Weber et al., 2011).

Bioinformatics analyses demonstrate correlations between *MYOCD* and *CHRM3* in human gastrointestinal and urogenital organs. This reinforces the view that MYOCD-SRF is an important, perhaps major, transcriptional control mechanism for *CHRM3* in these organs, but it does not rule out other control mechanisms. One such mechanism likely involves YAP-TEAD as suggested by our previous studies on inducible YAP/TAZ knockout mice (Daoud et al., 2021), and by pharmacological data herein. In the brain and lung, and in some arteries, *MYOCD* did not correlate with *CHRM3*. Instead, we observed correlations with *MRTFB*. In arteries, we believe that these correlations are driven primarily by the regulation of *CHRM3* by MRTF-B in endothelial cells because we found that MRTF-B increased the level of *CHRM3* in this cell type in culture. We did not examine if MRTF-B regulates *CHRM3* in neurons. However, it has been demonstrated that Mrtf-a and Mrtf-b together play essential roles for brain development (Mokalled et al., 2010). Perhaps, these MRTFs remain important for neuronal gene expression in adult life, contributing to the correlations observed in brain.

The activities of MRTF-A and MRTF-B depend on dynamics of the actin cytoskeleton (Olson and Nordheim, 2010). This implies that intracellular effectors of actin filament formation, such as Rho-associated kinase, may influence M_3 expression. We found that Latrunculin B, which depolymerizes actin, reduces M_3 in cells transduced with MRTF-B. Prior work demonstrated that Rho-associated kinase, which polymerizes actin, reduces eNOS expression (Ming et al., 2002). There may thus be a balancing influence of increased actin filament formation on M_3 (predicted to increase) and eNOS (predicted to fall), which could leave cholinergic dilatation unchanged, but this remains to be examined. Given the reported activation of MRTF-A by substrate stiffness (Jain et al., 2013; Foster et al., 2017), it may be considered that M_3 levels increase in, e.g., fibrotic disease. Matrix stiffness could perhaps also contribute to the paradoxical vasoconstriction of arteries in response to acetylcholine that is seen in certain pathological conditions (Ludmer et al., 1986), but it could also be that endothelial damage simply uncovers direct activation of SMCs via muscarinic M_3 receptors.

We chose to focus the current work on *CHRM3* in view of its fundamental biological and medical importance (Wess et al., 2007; Gericke et al., 2011, 2014) but our initial RNA-sequencing analysis suggested upregulation of the muscarinic M_2 and M_5 receptors by MYOCD. A common upstream regulator of M_2 and M_3 could explain why these receptors are often co-expressed, but we were unable confirm the effect on M_2 using RT-qPCR. We are uncertain of the explanation for this. One possibility is that the effect of MYOCD on *CHRM2* is smaller than is the effect on *CHRM3*, as suggested by the RNA-sequencing, but technical issues with the human *CHRM2* primer cannot be ruled out. The mouse primer for *Chrm2* appeared to work well in cultured mouse organs and using Srf-deficient tissues, but no reduction was apparent in either case, even if *Chrm3* was reduced. Regulation of M_2 and M_5 therefore needs to be investigated further.

To summarize, the current work has identified the muscarinic M_3 receptor, *CHRM3*, as a target of MRTFs and serum response factor in human SMCs *in vitro* and in the mouse urinary bladder and ileum *in vivo*. Among the MRTFs, MRTF-B appears to be the strongest transactivator of *CHRM3*, consistent with the high expression of MRTF-B in endothelial cells and in keeping with a dominance of endothelium-dependent dilatation over direct SMC-dependent cholinergic vasoconstriction.

DATA AVAILABILITY STATEMENT

The raw bulk RNA-Seq data is submitted to the Sequence Read Archive with the BioProject PRJNA731342 (https://www.ncbi.nlm.nih.gov/bioproject/PRJNA731342).

ETHICS STATEMENT

The animal study was reviewed and approved by the Malmö – Lunds djurförsöksetiska nämnd.

AUTHOR CONTRIBUTIONS

LL, CR, OH, DK, SF, ME, and KS participated in the study design. LL, CR, ME, and KS collected the data. KS generated the funding and wrote the manuscript. All authors were involved in manuscript revisions. All authors read and approved the submitted version.

FUNDING

This work was supported by grants from the Swedish Research Council VR, (2020–00908, to KS, 2009–1039 and 2018–02635 to OH), the Heart-Lung Foundation (20200222), to KS, the Swedish Foundation for Strategic Research (IRC15-0067), to OH, NIH (R01 HL142971-A1), to SF, and VA MERIT award (BX004443) to SF.

ACKNOWLEDGMENTS

We are thankful to Malin Svensson at the LUDC sequencing facility, Liqun He for sharing MRTF read counts from the

single cell RNA-seq dataset on brain vessels, Bengt Uvelius for human bladder biopsies retrieved in prior studies to generate the SMCs used here, and Katarzyna Kawka for genotyping, tamoxifen injections, and technical support in general.

SUPPLEMENTARY MATERIAL

The Supplementary Material for this article can be found online at https://www.frontiersin.org/articles/10.3389/fphys.2021.710968/full#supplementary-material

REFERENCES

Angstenberger, M., Wegener, J. W., Pichler, B. J., Judenhofer, M. S., Feil, S., Alberti, S., et al. (2007). Severe intestinal obstruction on induced smooth muscle-specific ablation of the transcription factor SRF in adult mice. *Gastroenterology* 133, 1948–1959. doi: 10.1053/j.gastro.2007.08.078

Bell, J. L., Haak, A. J., Wade, S. M., Kirchhoff, P. D., Neubig, R. R., and Larsen, S. D. (2013). Optimization of novel nipecotic bis(amide) inhibitors of the Rho/MKL1/SRF transcriptional pathway as potential anti-metastasis agents. *Bioorg. Med. Chem. Lett.* 23, 3826–3832. doi: 10.1016/j.bmcl.2013.04.080

Caulfield, M. P. (1993). Muscarinic receptors--characterization, coupling and function. *Pharmacol. Ther.* 58, 319–379. doi: 10.1016/0163-7258(93)90027-B

Chan, M. W., Chaudary, F., Lee, W., Copeland, J. W., and Mcculloch, C. A. (2010). Force-induced myofibroblast differentiation through collagen receptors is dependent on mammalian diaphanous (mDia). *J. Biol. Chem.* 285, 9273–9281. doi: 10.1074/jbc.M109.075218

Chang, A. C., Fu, Y., Garside, V. C., Niessen, K., Chang, L., Fuller, M., et al. (2011). Notch initiates the endothelial-to-mesenchymal transition in the atrioventricular canal through autocrine activation of soluble guanylyl cyclase. *Dev. Cell* 21, 288–300. doi: 10.1016/j.devcel.2011.06.022

Consortium, G.T. (2013). The Genotype-Tissue Expression (GTEx) project. *Nat. Genet.* 45, 580–585. doi: 10.1038/ng.2653

Cui, Y., Hameed, F. M., Yang, B., Lee, K., Pan, C. Q., Park, S., et al. (2015). Cyclic stretching of soft substrates induces spreading and growth. *Nat. Commun.* 6:6333. doi: 10.1038/ncomms7333

Dahan, D., Ekman, M., Larsson-Callerfelt, A. K., Turczynska, K., Boettger, T., Braun, T., et al. (2014). Induction of angiotensin-converting enzyme after miR-143/145 deletion is critical for impaired smooth muscle contractility. *Am. J. Physiol. Cell Physiol.* 307, C1093–C1101. doi: 10.1152/ajpcell.00250.2014

Daoud, F., Holmberg, J., Alajbegovic, A., Grossi, M., Rippe, C., Sward, K., et al. (2020). Inducible Deletion of YAP and TAZ in Adult Mouse Smooth Muscle Causes Rapid and Lethal Colonic Pseudo-Obstruction. *Cell Mol Gastroenterol Hepatol* 11, 623–637. doi: 10.1016/j.jcmgh.2020.09.014

Daoud, F., Holmberg, J., Alajbegovic, A., Grossi, M., Rippe, C., Sward, K., et al. (2021). Inducible deletion of YAP and TAZ in adult mouse smooth muscle causes rapid and lethal colonic pseudo-obstruction. *Cell. Mol. Gastroenterol. Hepatol.* 11, 623–637. doi: 10.1016/j.jcmgh.2020.09.014

De Sena Brandine, G., and Smith, A. D. (2019). Falco: high-speed FastQC emulation for quality control of sequencing data. *F1000Res* 8:1874. doi: 10.12688/f1000research.21142.1

Dobin, A., Davis, C. A., Schlesinger, F., Drenkow, J., Zaleski, C., Jha, S., et al. (2013). STAR: ultrafast universal RNA-seq aligner. *Bioinformatics* 29, 15–21. doi: 10.1093/bioinformatics/bts635

Evelyn, C. R., Wade, S. M., Wang, Q., Wu, M., Iniguez-Lluhi, J. A., Merajver, S. D., et al. (2007). CCG-1423: a small-molecule inhibitor of RhoA transcriptional signaling. *Mol. Cancer Ther.* 6, 2249–2260. doi: 10.1158/1535-7163.MCT-06-0782

Ewels, P., Magnusson, M., Lundin, S., and Kaller, M. (2016). MultiQC: summarize analysis results for multiple tools and samples in a single report. *Bioinformatics* 32, 3047–3048. doi: 10.1093/bioinformatics/btw354

Finch-Edmondson, M., and Sudol, M. (2016). Framework to function: mechanosensitive regulators of gene transcription. *Cell. Mol. Biol. Lett.* 21:28. doi: 10.1186/s11658-016-0028-7

Foster, C. T., Gualdrini, F., and Treisman, R. (2017). Mutual dependence of the MRTF-SRF and YAP-TEAD pathways in cancer-associated fibroblasts is indirect and mediated by cytoskeletal dynamics. *Genes Dev.* 31, 2361–2375. doi: 10.1101/gad.304501.117

Furchgott, R. F., and Zawadzki, J. V. (1980). The obligatory role of endothelial cells in the relaxation of arterial smooth muscle by acetylcholine. *Nature* 288, 373–376. doi: 10.1038/288373a0

Galmiche, G., Labat, C., Mericskay, M., Aissa, K. A., Blanc, J., Retailleau, K., et al. (2013). Inactivation of serum response factor contributes to decrease vascular muscular tone and arterial stiffness in mice. *Circ. Res.* 112, 1035–1045. doi: 10.1161/CIRCRESAHA.113.301076

Gericke, A., Sniatecki, J. J., Mayer, V. G., Goloborodko, E., Patzak, A., Wess, J., et al. (2011). Role of M1, M3, and M5 muscarinic acetylcholine receptors in cholinergic dilation of small arteries studied with gene-targeted mice. *Am. J. Physiol. Heart Circ. Physiol.* 300, H1602–H1608. doi: 10.1152/ajpheart.00982.2010

Gericke, A., Steege, A., Manicam, C., Bohmer, T., Wess, J., and Pfeiffer, N. (2014). Role of the M3 muscarinic acetylcholine receptor subtype in murine ophthalmic arteries after endothelial removal. *Invest. Ophthalmol. Vis. Sci.* 55, 625–631. doi: 10.1167/iovs.13-13549

Hadden, W. J., Young, J. L., Holle, A. W., Mcfetridge, M. L., Kim, D. Y., Wijesinghe, P., et al. (2017). Stem cell migration and mechanotransduction on linear stiffness gradient hydrogels. *Proc. Natl. Acad. Sci.* 114, 5647–5652. doi: 10.1073/pnas.1618239114

He, L., Vanlandewijck, M., Mae, M. A., Andrae, J., Ando, K., Del Gaudio, F., et al. (2018). Single-cell RNA sequencing of mouse brain and lung vascular and vessel-associated cell types. *Sci Data* 5:180160. doi: 10.1038/sdata.2018.160

Hu, X., Liu, Z. Z., Chen, X., Schulz, V. P., Kumar, A., Hartman, A. A., et al. (2019). MKL1-actin pathway restricts chromatin accessibility and prevents mature pluripotency activation. *Nat. Commun.* 10:1695. doi: 10.1038/s41467-019-09636-6

Huang, J., Wang, T., Wright, A. C., Yang, J., Zhou, S., Li, L., et al. (2015). Myocardin is required for maintenance of vascular and visceral smooth muscle homeostasis during postnatal development. *Proc. Natl. Acad. Sci.* 112, 4447–4452. doi: 10.1073/pnas.1420363112

Jain, N., Iyer, K. V., Kumar, A., and Shivashankar, G. V. (2013). Cell geometric constraints induce modular gene-expression patterns via redistribution of HDAC3 regulated by actomyosin contractility. *Proc. Natl. Acad. Sci.* 110, 11349–11354. doi: 10.1073/pnas.1300801110

Kim, T., Hwang, D., Lee, D., Kim, J. H., Kim, S. Y., and Lim, D. S. (2017). MRTF potentiates TEAD-YAP transcriptional activity causing metastasis. *EMBO J.* 36, 520–535. doi: 10.15252/embj.201695137

Kondo, T., Nakajima, M., Teraoka, H., Unno, T., Komori, S., Yamada, M., et al. (2011). Muscarinic receptor subtypes involved in regulation of colonic motility in mice: functional studies using muscarinic receptor-deficient mice. *Eur. J. Pharmacol.* 670, 236–243. doi: 10.1016/j.ejphar.2011.08.034

Krawczyk, K. K., Skovsted, G. F., Perisic, L., Dreier, R., Berg, J. O., Hedin, U., et al. (2018). Expression of endothelin type B receptors (EDNRB) on smooth muscle cells is controlled by MKL2, ternary complex factors, and actin dynamics. *Am. J. Physiol. Cell Physiol.* 315, C873–C884. doi: 10.1152/ajpcell.00170.2018

Krawczyk, K. K., Yao Mattisson, I., Ekman, M., Oskolkov, N., Grantinge, R., Kotowska, D., et al. (2015). Myocardin family members drive formation of caveolae. *PLoS One* 10:e0133931. doi: 10.1371/journal.pone.0133931

Leo, M. D., Bannister, J. P., Narayanan, D., Nair, A., Grubbs, J. E., Gabrick, K. S., et al. (2014). Dynamic regulation of beta1 subunit trafficking controls vascular contractility. *Proc. Natl. Acad. Sci.* 111, 2361–2366. doi: 10.1073/pnas.1317527111

Liao, Y., Smyth, G. K., and Shi, W. (2014). featureCounts: an efficient general purpose program for assigning sequence reads to genomic features. *Bioinformatics* 30, 923–930. doi: 10.1093/bioinformatics/btt656

Liu-Chittenden, Y., Huang, B., Shim, J. S., Chen, Q., Lee, S. J., Anders, R. A., et al. (2012). Genetic and pharmacological disruption of the TEAD-YAP complex suppresses the oncogenic activity of YAP. *Genes Dev.* 26, 1300–1305. doi: 10.1101/gad.192856.112

Long, X., Tharp, D. L., Georger, M. A., Slivano, O. J., Lee, M. Y., Wamhoff, B. R., et al. (2009). The smooth muscle cell-restricted KCNMB1 ion channel subunit is a direct transcriptional target of serum response factor and myocardin. *J. Biol. Chem.* 284, 33671–33682. doi: 10.1074/jbc.M109.050419

Love, M. I., Huber, W., and Anders, S. (2014). Moderated estimation of fold change and dispersion for RNA-seq data with DESeq2. *Genome Biol.* 15:550. doi: 10.1186/s13059-014-0550-8

Ludmer, P. L., Selwyn, A. P., Shook, T. L., Wayne, R. R., Mudge, G. H., Alexander, R. W., et al. (1986). Paradoxical vasoconstriction induced by acetylcholine in atherosclerotic coronary arteries. *N. Engl. J. Med.* 315, 1046–1051. doi: 10.1056/NEJM198610233151702

Lundquist, M. R., Storaska, A. J., Liu, T. C., Larsen, S. D., Evans, T., Neubig, R. R., et al. (2014). Redox modification of nuclear actin by MICAL-2 regulates SRF signaling. *Cell* 156, 563–576. doi: 10.1016/j.cell.2013.12.035

Matsui, M., Motomura, D., Fujikawa, T., Jiang, J., Takahashi, S., Manabe, T., et al. (2002). Mice lacking M2 and M3 muscarinic acetylcholine receptors are devoid of cholinergic smooth muscle contractions but still viable. *J. Neurosci.* 22, 10627–10632. doi: 10.1523/JNEUROSCI.22-24-10627.2002

Matsui, M., Motomura, D., Karasawa, H., Fujikawa, T., Jiang, J., Komiya, Y., et al. (2000). Multiple functional defects in peripheral autonomic organs in mice lacking muscarinic acetylcholine receptor gene for the M3 subtype. *Proc. Natl. Acad. Sci.* 97, 9579–9584. doi: 10.1073/pnas.97.17.9579

Mericskay, M., Blanc, J., Tritsch, E., Moriez, R., Aubert, P., Neunlist, M., et al. (2007). Inducible mouse model of chronic intestinal pseudo-obstruction by smooth muscle-specific inactivation of the SRF gene. *Gastroenterology* 133, 1960–1970. doi: 10.1053/j.gastro.2007.09.010

Miano, J. M. (2003). Serum response factor: toggling between disparate programs of gene expression. *J. Mol. Cell. Cardiol.* 35, 577–593. doi: 10.1016/S0022-2828(03)00110-X

Miano, J. M. (2015). Myocardin in biology and disease. *J. Biomed. Res.* 29, 3–19. doi: 10.7555/JBR.29.20140151

Miano, J. M., Long, X., and Fujiwara, K. (2007). Serum response factor: master regulator of the actin cytoskeleton and contractile apparatus. *Am. J. Physiol. Cell Physiol.* 292, C70–C81. doi: 10.1152/ajpcell.00386.2006

Ming, X. F., Viswambharan, H., Barandier, C., Ruffieux, J., Kaibuchi, K., Rusconi, S., et al. (2002). Rho GTPase/Rho kinase negatively regulates endothelial nitric oxide synthase phosphorylation through the inhibition of protein kinase B/Akt in human endothelial cells. *Mol. Cell. Biol.* 22, 8467–8477. doi: 10.1128/MCB.22.24.8467-8477.2002

Mokalled, M. H., Carroll, K. J., Cenik, B. K., Chen, B., Liu, N., Olson, E. N., et al. (2015). Myocardin-related transcription factors are required for cardiac development and function. *Dev. Biol.* 406, 109–116. doi: 10.1016/j.ydbio.2015.09.006

Mokalled, M. H., Johnson, A., Kim, Y., Oh, J., and Olson, E. N. (2010). Myocardin-related transcription factors regulate the Cdk5/Pctaire1 kinase cascade to control neurite outgrowth, neuronal migration and brain development. *Development* 137, 2365–2374. doi: 10.1242/dev.047605

Okonechnikov, K., Conesa, A., and Garcia-Alcalde, F. (2016). Qualimap 2: advanced multi-sample quality control for high-throughput sequencing data. *Bioinformatics* 32, 292–294. doi: 10.1093/bioinformatics/btv566

Olson, E. N., and Nordheim, A. (2010). Linking actin dynamics and gene transcription to drive cellular motile functions. *Nat. Rev. Mol. Cell Biol.* 11, 353–365. doi: 10.1038/nrm2890

Palmer, R. M., Ferrige, A. G., and Moncada, S. (1987). Nitric oxide release accounts for the biological activity of endothelium-derived relaxing factor. *Nature* 327, 524–526. doi: 10.1038/327524a0

Park, C., Lee, M. Y., Slivano, O. J., Park, P. J., Ha, S., Berent, R. M., et al. (2015). Loss of serum response factor induces microRNA-mediated apoptosis in intestinal smooth muscle cells. *Cell Death Dis.* 6:e2011. doi: 10.1038/cddis.2015.353

Parlakian, A., Charvet, C., Escoubet, B., Mericskay, M., Molkentin, J. D., Gary-Bobo, G., et al. (2005). Temporally controlled onset of dilated cardiomyopathy through disruption of the SRF gene in adult heart. *Circulation* 112, 2930–2939. doi: 10.1161/CIRCULATIONAHA.105.533778

Ramanan, N., Shen, Y., Sarsfield, S., Lemberger, T., Schutz, G., Linden, D. J., et al. (2005). SRF mediates activity-induced gene expression and synaptic plasticity but not neuronal viability. *Nat. Neurosci.* 8, 759–767. doi: 10.1038/nn1462

Rippe, C., Moren, B., Liu, L., Stenkula, K. G., Mustaniemi, J., Wennstrom, M., et al. (2021). NG2/CSPG4, CD146/MCAM and VAP1/AOC3 are regulated by myocardin-related transcription factors in smooth muscle cells. *Sci. Rep.* 11:5955. doi: 10.1038/s41598-021-85335-x

Rippe, C., Zhu, B., Krawczyk, K. K., Bavel, E. V., Albinsson, S., Sjolund, J., et al. (2017). Hypertension reduces soluble guanylyl cyclase expression in the mouse aorta via the Notch signaling pathway. *Sci. Rep.* 7:1334. doi: 10.1038/s41598-017-01392-1

Ritter, J., Flower, R. J., Henderson, G., Loke, Y. K., Macewan, D. J., Rang, H. P., et al. (2020). *Rang and Dale's Pharmacology.* Churchill, livingston.

Sriram, K., and Insel, P. A. (2018). G Protein-Coupled receptors as targets for approved drugs: how many targets and how many drugs? *Mol. Pharmacol.* 93, 251–258. doi: 10.1124/mol.117.111062

Struckmann, N., Schwering, S., Wiegand, S., Gschnell, A., Yamada, M., Kummer, W., et al. (2003). Role of muscarinic receptor subtypes in the constriction of peripheral airways: studies on receptor-deficient mice. *Mol. Pharmacol.* 64, 1444–1451. doi: 10.1124/mol.64.6.1444

Sward, K., Krawczyk, K. K., Moren, B., Zhu, B., Matic, L., Holmberg, J., et al. (2019). Identification of the intermediate filament protein synemin/SYNM as a target of myocardin family coactivators. *Am. J. Physiol. Cell Physiol.* 317, C1128–C1142. doi: 10.1152/ajpcell.00047.2019

Sward, K., Stenkula, K. G., Rippe, C., Alajbegovic, A., Gomez, M. F., and Albinsson, S. (2016). Emerging roles of the myocardin family of proteins in lipid and glucose metabolism. *J. Physiol.* 594, 4741–4752. doi: 10.1113/JP271913

Thomsen, M., Sorensen, G., and Dencker, D. (2018). Physiological roles of CNS muscarinic receptors gained from knockout mice. *Neuropharmacology* 136, 411–420. doi: 10.1016/j.neuropharm.2017.09.011

Vanlandewijck, M., He, L., Mae, M. A., Andrae, J., Ando, K., Del Gaudio, F., et al. (2018). A molecular atlas of cell types and zonation in the brain vasculature. *Nature* 554, 475–480. doi: 10.1038/nature25739

Weber, S., Thiele, H., Mir, S., Toliat, M. R., Sozeri, B., Reutter, H., et al. (2011). Muscarinic acetylcholine receptor M3 mutation causes urinary bladder disease and a prune-belly-like syndrome. *Am. J. Hum. Genet.* 89, 668–674. doi: 10.1016/j.ajhg.2011.10.007

Weinl, C., Castaneda Vega, S., Riehle, H., Stritt, C., Calaminus, C., Wolburg, H., et al. (2015). Endothelial depletion of murine SRF/MRTF provokes intracerebral hemorrhagic stroke. *Proc. Natl. Acad. Sci.* 112, 9914–9919. doi: 10.1073/pnas.1509047112

Weinl, C., Riehle, H., Park, D., Stritt, C., Beck, S., Huber, G., et al. (2013). Endothelial SRF/MRTF ablation causes vascular disease phenotypes in murine retinae. *J. Clin. Invest.* 123, 2193–2206. doi: 10.1172/JCI64201

Wess, J., Eglen, R. M., and Gautam, D. (2007). Muscarinic acetylcholine receptors: mutant mice provide new insights for drug development. *Nat. Rev. Drug Discov.* 6, 721–733. doi: 10.1038/nrd2379

Wilson, C., Lee, M. D., and Mccarron, J. G. (2016). Acetylcholine released by endothelial cells facilitates flow-mediated dilatation. *J. Physiol.* 594, 7267–7307. doi: 10.1113/JP272927

Wirth, A., Benyo, Z., Lukasova, M., Leutgeb, B., Wettschureck, N., Gorbey, S., et al. (2008). G12-G13-LARG-mediated signaling in vascular smooth muscle is required for salt-induced hypertension. *Nat. Med.* 14, 64–68. doi: 10.1038/nm1666

Yamada, M., Miyakawa, T., Duttaroy, A., Yamanaka, A., Moriguchi, T., Makita, R., et al. (2001). Mice lacking the M3 muscarinic acetylcholine receptor are hypophagic and lean. *Nature* 410, 207–212. doi: 10.1038/35065604

Zeng, F. Y., and Wess, J. (1999). Identification and molecular characterization of m3 muscarinic receptor dimers. *J. Biol. Chem.* 274, 19487–19497. doi: 10.1074/jbc.274.27.19487

Zhao, X. H., Laschinger, C., Arora, P., Szaszi, K., Kapus, A., and Mcculloch, C. A. (2007). Force activates smooth muscle alpha-actin promoter activity through the Rho signaling pathway. *J. Cell Sci.* 120, 1801–1809. doi: 10.1242/jcs.001586

Zhao, J., Zhang, W., Lin, M., Wu, W., Jiang, P., Tou, E., et al. (2016). MYOSLID is a novel serum response factor-dependent long noncoding RNA that amplifies the vascular smooth muscle differentiation program. *Arterioscler. Thromb. Vasc. Biol.* 36, 2088–2099. doi: 10.1161/ATVBAHA.116.307879

Zhu, B., Rippe, C., Thi Hien, T., Zeng, J., Albinsson, S., Stenkula, K. G., et al. (2017). Similar regulatory mechanisms of caveolins and cavins by myocardin

family coactivators in arterial and bladder smooth muscle. *PLoS One* 12:e0176759. doi: 10.1371/journal.pone.0189462

Conflict of Interest: The authors declare that the research was conducted in the absence of any commercial or financial relationships that could be construed as a potential conflict of interest.

Publisher's Note: All claims expressed in this article are solely those of the authors and do not necessarily represent those of their affiliated organizations, or those of the publisher, the editors and the reviewers. Any product that may be evaluated in this article, or claim that may be made by its manufacturer, is not guaranteed or endorsed by the publisher.

frontiers in Physiology

ERRATUM
published: 08 October 2021
doi: 10.3389/fphys.2021.782588

Erratum: Regulation of the Muscarinic M_3 Receptor by Myocardin-Related Transcription Factors

*Frontiers Production Office**

Frontiers Media SA, Lausanne, Switzerland

Keywords: cholinergic neurotransmission, pharmacology, acetylcholine, signaling, vasodilatation

OPEN ACCESS

Approved by:
Frontiers Editorial Office, Frontiers Media SA, Switzerland

***Correspondence:**
Frontiers Production Office
production.office@frontiersin.org

Specialty section:
This article was submitted to Vascular Physiology, a section of the journal Frontiers in Physiology

Received: *24 September 2021*
Accepted: *24 September 2021*
Published: *08 October 2021*

Citation:
Frontiers Production Office (2021) Erratum: Regulation of the Muscarinic M_3 Receptor by Myocardin-Related Transcription Factors. Front. Physiol. 12:782588. doi: 10.3389/fphys.2021.782588

An Erratum on

Regulation of the Muscarinic M_3 Receptor by Myocardin-Related Transcription Factors
by Liu, L., Rippe, C., Hansson, O., Kryvokhyzha, D., Fisher, S., Ekman, M., and Swärd, K. (2021). Front. Physiol. 12:710968. doi: 10.3389/fphys.2021.710968

Due to a production error, **Figures 2–7** were erroneously mismatched to their figure legends. The correct figures and their legends appear below.

The publisher apologizes for this mistake. The original article has been updated.

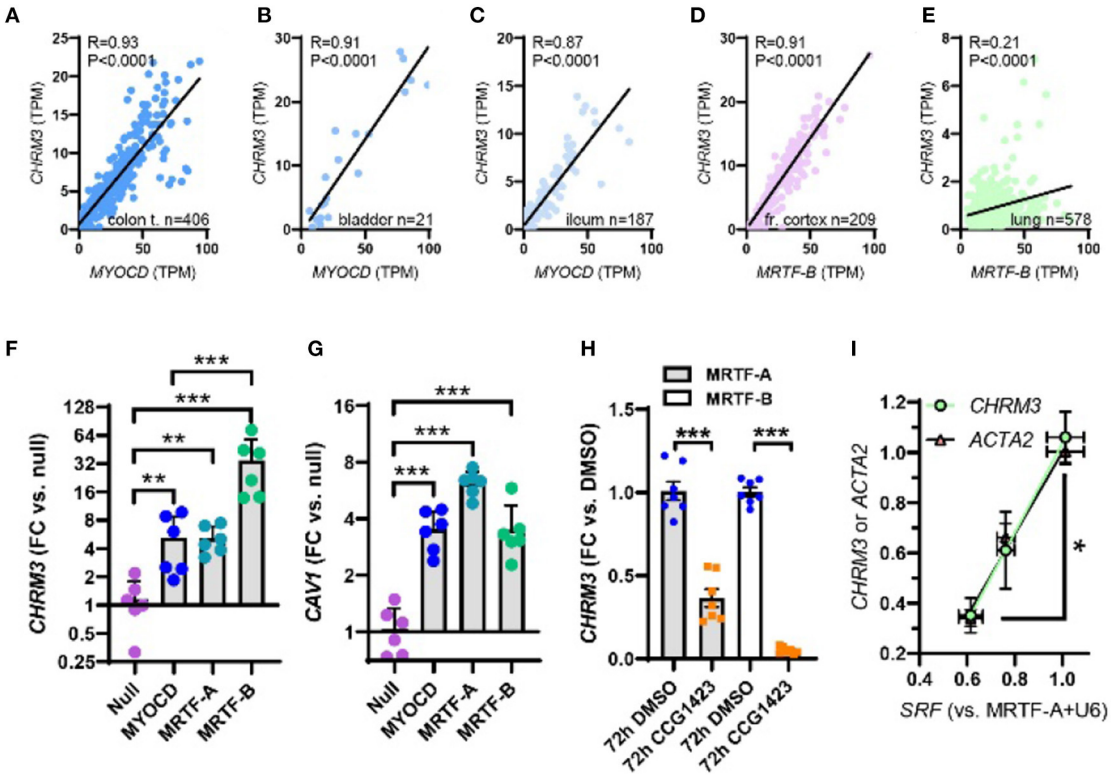

FIGURE 2 | Myocardin (MYOCD) correlates with the M3 muscarinic receptor (*CHRM3*) across human tissues and SRF is critical for *CHRM3* regulation by MRTFs. **(A)** through **(C)** show correlations at the mRNA level of MYOCD vs. M3 (*CHRM3*) in the human gastrointestinal tract and urinary bladder. In brain **(D)** and lung **(E)**, *MRTFB*, rather than *MYOCD*, correlated with M3. This prompted us to examine if all MRTFs (MYOCD, MRTF-A, and MRTF-B) regulate M3 at the mRNA level. Viral overexpression in human coronary artery SMCs showed that MRTF-B was a more effective transactivator of *CHRM3* than MYOCD [**(F)**, $n = 6$], despite having the same effect as MYOCD on another target [*CAV1*, **(G)**]. **(H)** Shows reduction of *CHRM3* after treatment for 72 h with the MRTF-SRF inhibitor CCG-1423 (10 μM, $n = 6$). Cells were transduced with either MRTF-A (gray bars) or MRTF-B (white bars). **(I)** Shows that knockdown of serum response factor (SRF, 0, 30, and 100 MOI of Ad-shSRF) reduces *CHRM3* (green/black circles) in parallel with *ACTA2* (pink/black triangles, $n = 4$, per condition). MRTF-A was overexpressed throughout in **(I)**. $^{***}p < 0.001$, $^{**}p < 0.01$, and $^{*}p < 0.05$.

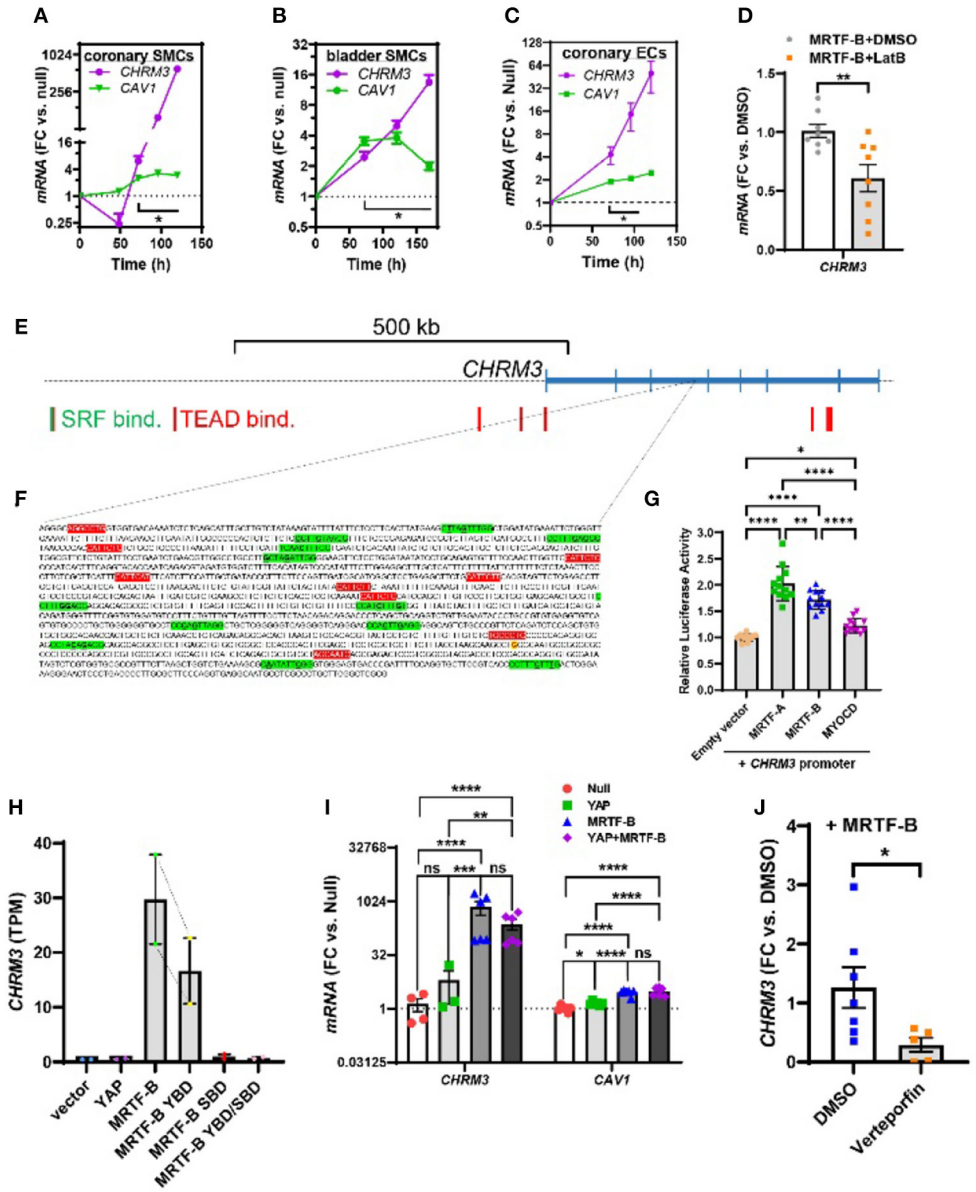

FIGURE 3 | Time-course data, promoter reporter assays, and MRTF-B-YAP cooperation. MRTF-B was overexpressed in different cell types (200 MOI), and cells were harvested at different times. RNA was subsequently isolated, and *CHRM3* was measured by RT-qPCR. **(A)** Shows time-dependent upregulation of *CHRM3* in human coronary artery SMCs. Significant increases were seen at times exceeding 48 h, and a 597-fold increase was seen at 120 h ($p = 0.0004$, $n = 3$). Because there was no indication that the increase of *CHRM3* reached a plateau at longer transduction times, we designed an experiment using even longer incubations in human bladder SMCs **(B)**. Again, there was no tendency of a plateau. Moreover, the maximal increase was somewhat smaller than in coronary artery SMCs. Similar results were obtained in human coronary artery endothelial cells [**(C)**, 200 MOI]. **(D)** Shows that *CHRM3* was reduced by Latrunculin B (100 nM, gray bar) in MRTF-B-transduced ECs. Inspection of the *CHRM3* gene locus on chromosome 1 **(E)** revealed SRF binding (green vertical bars) and TEAD binding (red vertical bars) to many 5' sequences of, and over, the longest transcript (blue). Direct examination of a commercial promoter reporter sequence (NM_000740, transcript variant 2, hg38; chr1+: 239,627,686–239,629,364; TSS = 239,629,073) did not reveal any true CArGs, but 11 motifs with 2 deviations from the classical CArG sequence [CC(A/T)6GG, green highlights, deviations underlined, **(F)**] were present, along with 9 TEAD motifs [red highlights, **(F)**]. The transcription start site for the promoter is highlighted in yellow with red lettering. This "CArG-deficient" promoter responded to MRTFs in a luciferase reporter assay **(G)** run using HEK 293 cells. **(H)** Shows *CHRM3* mRNA expression in MCF10 cells transfected with YAP, MRTF-B, and two MRTF-B mutants; the YBD mutant does not bind YAP, and the SBD mutant does not bind SRF. **(I)** Shows the effects of YAP and MRTF-B transduction, alone and in combination, on *CHRM3* in human coronary artery SMCs. Ct values for *CHRM3* were sometimes too high for reliable detection (null and YAP). This is the reason why the sample size is less than $n = 6$ for *CHRM3* in the null and YAP groups, even if six experiments were run for the panel. **(J)** Shows the effect of the YAP-TEAD inhibitor verteporfin in MRTF-B-transduced coronary artery SMCs. Two samples were lost in the verteporfin group again due to lack of amplification. ****$p < 0.0001$, ***$p < 0.001$, **$p < 0.01$, and *$p < 0.05$.

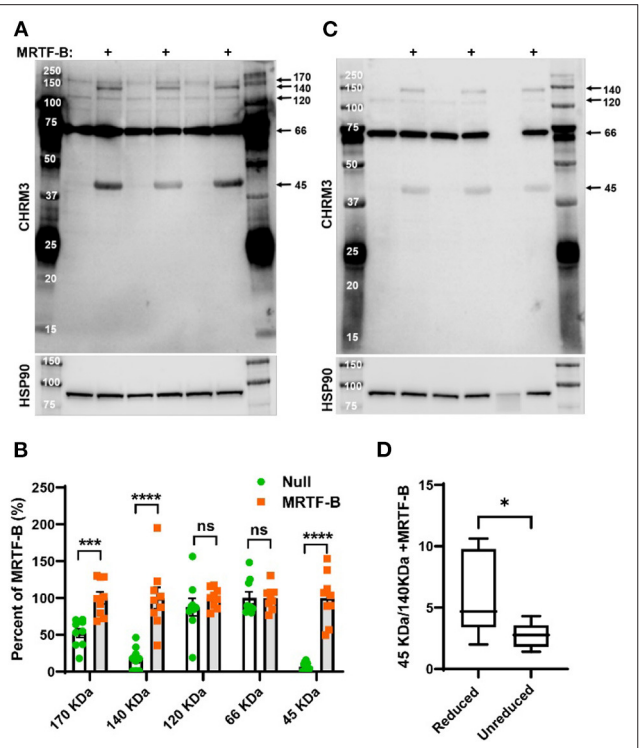

FIGURE 4 | MRTF-B increases CHRM3 immunoreactive bands in human coronary artery smooth muscle cells. Protein lysates from human coronary artery SMCs treated with null virus and with MRTF-B virus for 120 h, respectively, were used for Western blotting using an antibody raised against a human CHRM3 in **(A)**. After developing the blot, it was stripped and incubated with HSP90 antibody (shown below) to assess equal protein loading. At least five bands were detected with the CHRM3 antibody, and three bands at ≈170, ≈140, and ≈45 kDa changed significantly with MRTF-B as shown in the compiled analysis in **(B)**. Quantification in **(B)** was done using the blots in **(A)**. Proteins from the same original lysates were also prepared in non-reducing conditions, to examine if the relationship between bands changed **(C)**. The volume was insufficient for one of the null samples in this experiment (lane 6). Non-reducing conditions favored the 140 kDa band at the expense of the 45 kDa band **(D)**, suggesting multimerization. $^{****}p < 0.0001$, $^{***}p < 0.001$, and $^{*}p < 0.05$.

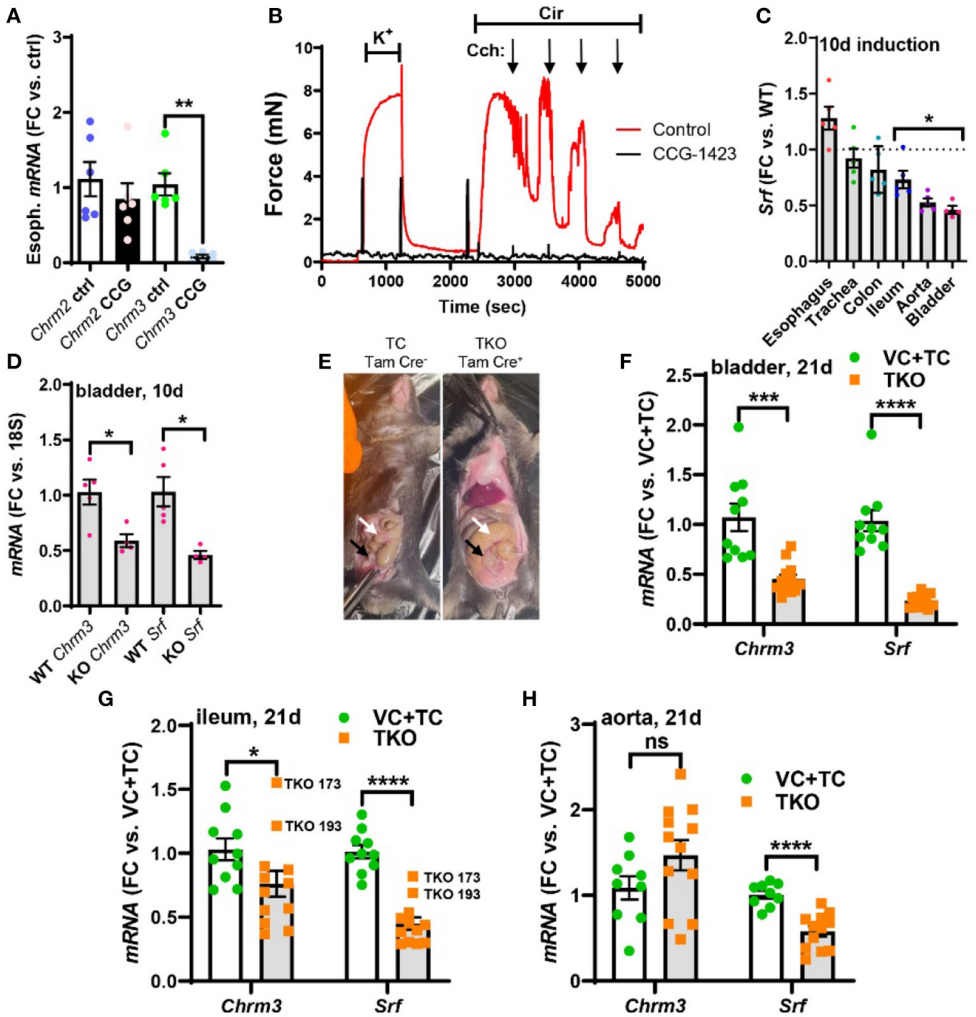

FIGURE 5 | Pharmacological inhibition of MRTF-SRF signaling in organ culture, and knockout of Srf *in vivo*, reduces M3 receptor expression. To examine if MRTF-SRF signaling regulates muscarinic M3 receptor expression *in situ*, we first isolated organs from wild-type C57Bl/6 mice. Organs were split in half and maintained for 96 h in organ culture with vehicle (DMSO) or CCG-1423 (10 μM). A clear reduction of *Chrm3* relative to the house-keeping gene *18 s* was seen in the esophagus **(A)**, but in the remainder of the organs, the house-keeping genes examined declined (not shown). We also found that organ culture of the mouse caudal artery in the presence of CCG-1423 eliminated force development on stimulation with the α1-adrenergic agonist cirazoline **(B)**, suggesting that this experimental paradigm is unsuitable for studying effects on endothelium-dependent dilatation. Mice with SMC-specific knockout of Srf were next obtained by injecting Srffl/fl mice harboring the Myh11-Cre/ERT2 transgene with tamoxifen for 5 consecutive days (knockout: KO). Cre-negative Srffl/fl mice injected with tamoxifen were used as controls (wild-type: WT). Organs were harvested and frozen 10 days after the first injection and transcript levels were determined by RT-qPCR. At this time, body weights were unchanged, but Srf depletion was seen in some organs **(C)**. **(D)** Shows that *Chrm3* was reduced in parallel with *Srf* in the bladder, but this was not seen elsewhere (not shown). We therefore next used mice at 21 days post tamoxifen. Two control groups were included in this second experiment along with the tamoxifen-treated knockouts (TKO): vehicle-treated Cre-positive mice (VC) and tamoxifen-treated Cre-negative mice (TC). At 21 days, mobility on provocation was reduced, the intestines had started to swell [**(E)**, white arrows], and the urinary bladders were often enlarged [**(E)**, black arrows]. Both *Chrm3* and *Srf* were reduced in the bladder **(F)** and ileum **(G)**. For the ileum, the two knockouts with the most modest *Srf* depletion (TKO 173 and TKO 193) are highlighted. No change of *Chrm3* was seen in the aorta **(H)**, despite significant *Srf* depletion. These findings show that MRTF-SRF signaling is critical for *Chrm3* expression in gastrointestinal and urogenital organs *in vivo*. ***$p < 0.001$, **$p < 0.01$, and *$p < 0.05$.

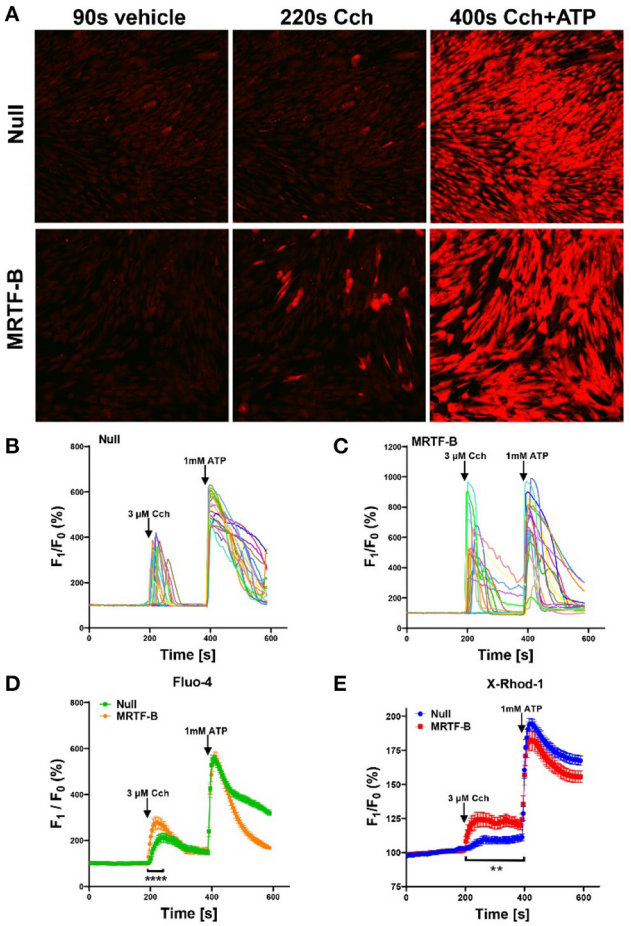

FIGURE 6 | Ca2+ imaging of MRTF-B-transduced human coronary artery SMCs. To examine if MRTF-B transduction increases responsiveness to the muscarinic agonist carbachol, cells were treated as indicated for 5 days in culture. They were subsequently washed and loaded with Fluo-4 and imaged using confocal microscopy. Only a fraction of the cells responded to carbachol [**(A)**, middle], but the responses were larger in MRTF-B-transduced cells. **(B, C)** Show the 20 cells responding best to carbachol in the experiment in **(A)**. **(D)** Shows compiled data from three independent experiments with Fluo-4. The Ca2+ signal between 200 and 250 s was significantly increased by prior MRTF-B transduction. **(E)** Shows intracellular Ca2+ in human coronary artery SMCs after transduction of MRTF-B or null virus, respectively ($N = 6$), but measured Ca2+ using X-Rhod-1. Error bars in **(D,E)** represent 95% confidence intervals. $^{****}p < 0.0001$ and $^{**}p < 0.01$.

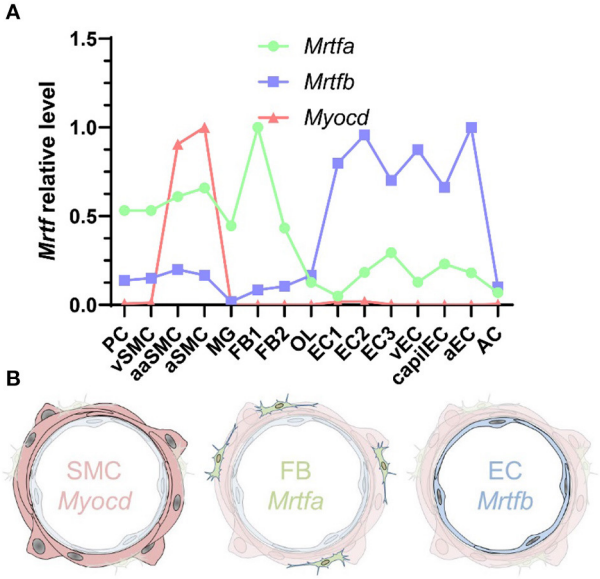

FIGURE 7 | MRTF distribution across the vascular wall. **(A)** Shows cell-averaged mRNA expression data for the indicated transcripts in different cerebrovascular cell types. PC, pericytes; SMC, smooth muscle cells; MG, microglia; OL, oligodendrocytes; FB, fibroblasts; EC, endothelial cells; AC, astrocytes; v, venous; cap, capillary; a, arterial; aa, arteriolar; and 1, 2, and 3, subtype. **(B)** Shows a schematic representation of Myocd in SMCs, Mrtfa in FBs, and Mrtfb in ECs.

frontiers in Physiology

REVIEW
published: 09 September 2021
doi: 10.3389/fphys.2021.734215

The Mechanobiology of Endothelial-to-Mesenchymal Transition in Cardiovascular Disease

*Shahrin Islam[1], Kristina I. Boström[1,2,3], Dino Di Carlo[4,5], Craig A. Simmons[6,7,8], Yin Tintut[1,9,10], Yucheng Yao[1] and Jeffrey J. Hsu[1,3]**

[1]*Division of Cardiology, Department of Medicine, David Geffen School of Medicine at UCLA, Los Angeles, CA, United States,* [2]*UCLA Molecular Biology Institute, Los Angeles, CA, United States,* [3]*Veterans Affairs Greater Los Angeles Healthcare System, Los Angeles, CA, United States,* [4]*Department of Bioengineering, University of California, Los Angeles, Los Angeles, CA, United States,* [5]*Department of Electrical and Computer Engineering, University of California, Los Angeles, Los Angeles, CA, United States,* [6]*Department of Mechanical and Industrial Engineering, University of Toronto, Toronto, ON, Canada,* [7]*Institute of Biomedical Engineering, University of Toronto, Toronto, ON, Canada,* [8]*Translational Biology and Engineering Program, Ted Rogers Centre for Heart Research, Toronto, ON, Canada,* [9]*Department of Physiology, University of California, Los Angeles, Los Angeles, CA, United States,* [10]*Department of Orthopedic Surgery, University of California, Los Angeles, Los Angeles, CA, United States*

Endothelial cells (ECs) lining the cardiovascular system are subjected to a highly dynamic microenvironment resulting from pulsatile pressure and circulating blood flow. Endothelial cells are remarkably sensitive to these forces, which are transduced to activate signaling pathways to maintain endothelial homeostasis and respond to changes in the environment. Aberrations in these biomechanical stresses, however, can trigger changes in endothelial cell phenotype and function. One process involved in this cellular plasticity is endothelial-to-mesenchymal transition (EndMT). As a result of EndMT, ECs lose cell-cell adhesion, alter their cytoskeletal organization, and gain increased migratory and invasive capabilities. EndMT has long been known to occur during cardiovascular development, but there is now a growing body of evidence also implicating it in many cardiovascular diseases (CVD), often associated with alterations in the cellular mechanical environment. In this review, we highlight the emerging role of shear stress, cyclic strain, matrix stiffness, and composition associated with EndMT in CVD. We first provide an overview of EndMT and context for how ECs sense, transduce, and respond to certain mechanical stimuli. We then describe the biomechanical features of EndMT and the role of mechanically driven EndMT in CVD. Finally, we indicate areas of open investigation to further elucidate the complexity of EndMT in the cardiovascular system. Understanding the mechanistic underpinnings of the mechanobiology of EndMT in CVD can provide insight into new opportunities for identification of novel diagnostic markers and therapeutic interventions.

Keywords: endothelial-to-mesenchymal transition, mechanobiology, cardiovascular disease, endothelial, mesenchymal, biomechanical

OPEN ACCESS

Edited by:
Markus Hecker,
Heidelberg University, Germany

Reviewed by:
Guido Krenning,
University Medical Center Groningen, Netherlands
Jingyan Han,
Boston University, United States

****Correspondence:***
Jeffrey J. Hsu
jjhsu@mednet.ucla.edu

Specialty section:
This article was submitted to Vascular Physiology, a section of the journal Frontiers in Physiology

Received: *30 June 2021*
Accepted: *09 August 2021*
Published: *09 September 2021*

Citation:
Islam S, Boström KI, Di Carlo D, Simmons CA, Tintut Y, Yao Y and Hsu JJ (2021) The Mechanobiology of Endothelial-to-Mesenchymal Transition in Cardiovascular Disease. Front. Physiol. 12:734215. doi: 10.3389/fphys.2021.734215

INTRODUCTION

Endothelial cells (ECs) comprise a highly heterogeneous population of cells that line the vasculature and the endocardium in the cardiovascular system (Kalluri et al., 2019; Kalucka et al., 2020). The microenvironment of the ECs is extremely dynamic and subject to multiple mechanical stresses, such as shear stress and cyclic stretch associated with pulsatile blood

flow (Chien, 2007; Charbonier et al., 2019). These stresses exist on a spectrum and can vary depending on the part of the cardiovascular system, as well as in pathologic vs. physiologic conditions. For example, shear stress under physiological conditions ranges from 10 to 70 dynes/cm^2 in the arterial system and 1 to 6 dynes/cm^2 in the venous system. In terms of cyclic strain, the physiologic range is 5 to 10% and strain above 20% is pathological and often observed in hypertension (Peng et al., 2019). In addition to shear stress and cyclic strain, the composition and mechanical properties of the extracellular matrix (ECM) are also crucial to endothelial homeostasis (Iivanainen et al., 2003; Gordon et al., 2020). Perturbations in these biomechanical elements of the microenvironment are sensed by ECs, and these signals are transduced to activate pathways that often result in phenotypic and functional changes (Kovacic et al., 2019). A notable example of this cellular plasticity is when ECs lose their endothelial features and acquire more mesenchymal-like cellular transcripts and functions through a process known as endothelial-to-mesenchymal transition (EndMT). EndMT was originally identified as form of epithelial-to-mesenchymal transition (EMT) playing a key role in the development of the cardiovascular system, but there is burgeoning evidence that it may also contribute to many cardiovascular diseases (CVD; Li et al., 2018; Kovacic et al., 2019). However, it is not yet well quite understood whether EndMT is a consequence of pathological processes involved in CVD or whether it actively contributes to CVD. While this question remains yet to be conclusively answered, the growing evidence linking EndMT to CVD has increased interest in characterizing the molecular and biomechanical changes associated with EndMT. Here, we review the mechanobiology of EndMT in CVD by describing how altered biomechanical factors activate EndMT, detailing the biomechanical hallmarks of EndMT, and summarizing the evidence of mechanically driven EndMT in various pathological contexts (**Figure 1**).

OVERVIEW OF ENDMT

EndMT was first described in the context of heart development as important for valve formation and heart septation, which is described in detail in other reviews (Kovacic et al., 2012, 2019; von Gise and Pu, 2012; Zhang et al., 2018). Many signaling pathways are involved in the activation of EndMT, but the most extensively characterized are part of the transforming growth factor β (TGFβ)/bone morphogenetic protein (BMP) superfamily (Cooley et al., 2014; Krenning et al., 2016; Ma et al., 2020a). Other signaling pathways involved in EndMT include Notch and Wnt signaling (Cheng et al., 2013; Piera-Velazquez and Jimenez, 2019). As EMT can occur in the reverse direction through a process known as mesenchymal-to-epithelial transition (Pei et al., 2019), EndMT also has a reverse counterpart known as mesenchymal-to-endothelial transition that has been shown to contribute to neovascularization after cardiac injury (Ubil et al., 2014).

EndMT pathways can be activated through a variety of biochemical and biomechanical stimuli. Because the TGFβ signaling pathways are the most extensively studied in EndMT, many studies utilize TGFβ isoforms as the main stimulus for EndMT induction (Pérez et al., 2017). TGFβ is a multifunctional protein with highly diverse functions in embryonic development, cell proliferation, fibrosis, and regulation of the inflammatory responses. Cells vary in their responses to TGFβ as a function of their differentiation state and their cytokine milieu (Dobaczewski et al., 2011). TGFβ is often used alone as a stimulus for EndMT or in combination with other pro-inflammatory cytokines, such as tumor necrosis factor-α (TNFα) and interleukin-1β (IL1β), to investigate the impact of inflammation on EndMT in various disease models. Since many forms of CVD, including calcific aortic valve disease (CAVD), atherosclerosis, and vascular calcification, are linked to inflammation, there is increasing interest in understanding how inflammation relates to EndMT (Cho et al., 2018). Furthermore, since the cardiovascular system is dynamic and ECs experience various forms of mechanical stresses as discussed in the previous section, the potential of biomechanical alterations to induce EndMT has been investigated as well (Krenning et al., 2016). In cardiovascular pathological states linked to EndMT, such as endocardial fibroelastosis (EFE) where the role of inflammation is potentially less significant, EndMT pathways may be activated predominantly through these aberrant mechanical stresses or other factors that have yet to be well characterized. Since most forms of CVD involve both biomechanical and biochemical alterations, it is likely that there is a multipronged activation of EndMT pathways.

Heterogeneous Responses to EndMT Stimuli

EC responses to EndMT-promoting stimuli are highly heterogeneous and are dependent on multiple factors (Pinto et al., 2016; Cho et al., 2018). For example, differences in patterns of gene expression were observed when comparing treatment with TNFα of human microvascular ECs (HMECs) vs. macrovascular human umbilical vein endothelial cells (HUVECs; Viemann et al., 2006). With regards to how arterial and venous ECs respond to treatment with EndMT-promoting biochemical stimuli, a recent study demonstrated that co-treatment of HUVECs and human pulmonary artery endothelial cells with TGFβ2 (10 ng/ml) and IL1β (1 ng/ml)

Abbreviations: BMP, Bone morphogenetic protein; CAVD, Calcific aortic valve disease; CHD, Congenital heart disease; CTD, Conotruncal defect; CVD, Cardiovascular diseases; D-flow, disturbed flow; ECM, Extracellular matrix; ECs, Endothelial cells; EFE, Endocardial fibroelastosis; EMT, Epithelial-to-mesenchymal transition; EndMA, Endothelial-to-mesenchymal activation; EndMT, Endothelial-to-mesenchymal transition; GAGs, Glycosaminoglycans; HAECs, Human aortic endothelial cells; HUVECs, Human umbilical vein endothelial cells; IMR, Ischemic mitral regurgitation; MI, Myocardial infarction; MMP, Matrix metalloproteinase; MSC, Mesenchymal stem cell; OFT, Outflow tract; OSS, Oscillatory shear stress; PA, Polyacrylamide; PAH, Pulmonary arterial hypertension; PSS, Pulsatile shear stress; S-flow, Stable flow; SSS, Steady shear stress; TGFβ, Transforming growth factor β; VB, Ventriculobulbar; VE-Cadherin, Vascular endothelial cadherin; VECs, Valvular endothelial cells; VICs, Valvular interstitial cells.

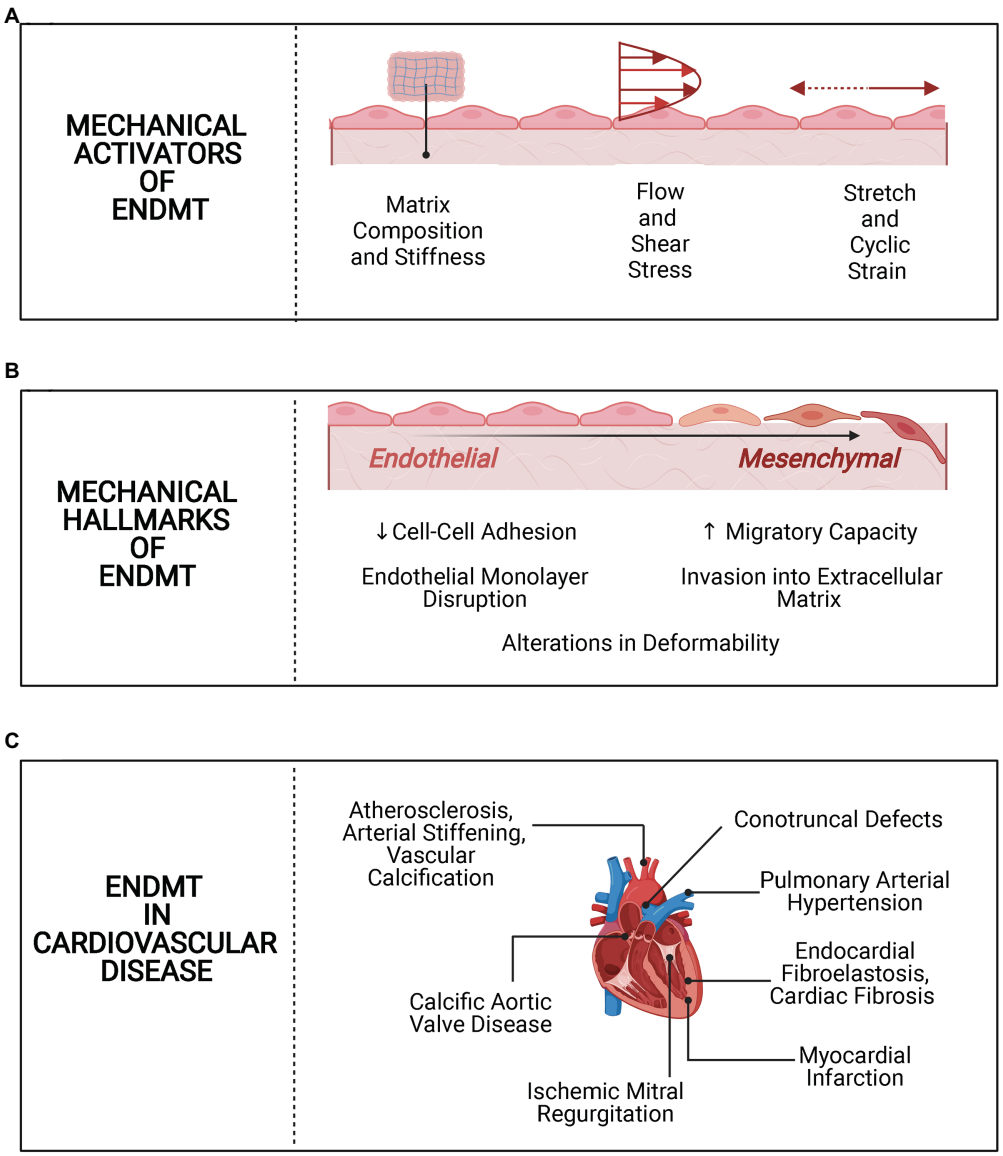

FIGURE 1 | Overview of mechanobiology of endothelial-to-mesenchymal transition (EndMT) in cardiovascular disease (CVD). **(A)** Mechanical activators of EndMT. Alterations in matrix stiffness and composition, shear stress, and cyclic strain activate EndMT in endothelial cells. **(B)** Mechanical hallmarks of EndMT. Following activation of EndMT, there are mechanical changes, such as loss of cell-cell adhesion and increased migration. **(C)** EndMT in CVD. EndMT is implicated in several CVD processes, with a potential role for biomechanical alterations in each.

for 7 days led to EndMT induction but treatment with TGFβ2 (10 ng/ml) or IL1β (1 ng/ml) alone did not (Monteiro et al., 2021). In contrast, another study indicated that treatment of primary human coronary aortic endothelial cells with IL-1β (10 ng/ml) is sufficient to induce EndMT after 24 h (Sánchez-Duffhues et al., 2019). Like these findings, one study recently reported that treatment of HMECs with TNFα led to induction of EndMT in a dose-dependent manner from 20 to 100 ng/ml at 96 h (Adjuto-Saccone et al., 2021) but a previous study indicated that treatment of human intestinal microvascular endothelial cells with TNFα did not induce EndMT even after 6 days (Rieder et al., 2011). These findings highlight the challenge with determining optimal methods of inducing EndMT for *in vitro* experiments due to the heterogeneity in EC responses to these stimuli that depend on multiple factors including EC subtype and dose of stimuli. A deeper characterization of the differential properties of these EC populations is needed.

Like variations in responses to treatment with inflammatory cytokines and growth factors, ECs are also influenced differentially by biomechanical stimuli, such as flow. There are multiple mechanical stresses in the cardiovascular system that are highly variable under physiological and pathological conditions. It has been shown the pattern of expression of adhesion molecules and immune cell adhesion varied not only on which vascular

bed the ECs were derived from but also on whether the ECs were exposed to arterial or venous flow profiles (Methe et al., 2007). The heterogeneity in responses to biomechanical and biochemical stimuli that promote EndMT based on EC subtype is an important consideration for the study of EndMT and further work is required to better characterize the molecular mechanisms that govern these differences.

Mechanical Regulators of EndMT, Mechanosensing, and Mechanotransduction

As discussed in the previous section, EndMT can be induced by various biochemical and biomechanical triggers in the EC microenvironment. Understanding how ECs sense and respond to mechanical forces has been a key focus of vascular biology and is covered extensively in other reviews (Chien, 2007; Krenning et al., 2016; Gordon et al., 2020). Here, we focus on how shear stress, cyclic strain and matrix stiffness, and composition regulate EndMT in CVD, and this section briefly describes how ECs sense and respond to these mechanical stresses that may be more relevant in the context of EndMT.

EC mechanosensors for detecting cyclic strain include stretch-sensitive ion channels and G-protein coupled receptors-like Gαq/11 (Naruse and Sokabe, 1993; Clark et al., 2002). Of note, uniaxial cyclic strain (10%) resulted in conformational change of stretch-sensitive calcium ion channels, such as TRPV4, of capillary ECs through integrin-ECM adhesions. This conformational change resulted in the activation of phosphatidyl inositol-3-kinase (PI3K) and downstream signaling pathways, which led to Rho and Rho-associated kinase (ROCK) mediated focal adhesion and stress fiber remodeling in a direction perpendicular to the applied tension field (Thodeti et al., 2009). This cytoskeletal reorientation is crucial for directional EC migration, which is a feature of EndMT (Lamalice et al., 2007; Clere et al., 2020).

EC responses to cyclic stretch, matrix stiffness, and shear stress are also mediated by integrins and vascular endothelial cadherin (VE-Cadherin; Schwartz and DeSimone, 2008; Tian et al., 2016). VE-Cadherin is the main cell-cell adhesion molecule in the EC monolayer. Mechanical loading of VE-Cadherin triggered cytoskeletal remodeling, which resulted in a force-dependent increase in cellular stiffness, disruption of peripheral junctions, and decrease in focal adhesions through a mechanism that involves ROCK1 and PI3K (Barry et al., 2015). Furthermore, loading of VE-cadherin also increased integrin-dependent cell contractility and disrupted cell-matrix adhesions (Andresen Eguiluz et al., 2017). Because hallmarks of EndMT include cytoskeletal remodeling and disruption of cell-cell junctions, VE-Cadherin likely plays an important role in modulating the responses of ECs to alterations in cyclic stretch, shear stress, and matrix stiffness that can initially activate EndMT pathways.

While the role of these ion channels, receptors, and integrins that are known to be mechanosensors has yet to be fully elucidated in the context of EndMT, a recent study has demonstrated that the receptor Alk5 and downstream Shc were crucial to sensing shear stress and modulating EndMT in atherosclerosis (Mehta et al., 2021). The details of this study are further discussed in Section 5.1. This is the first report of a mechanosensor and mechanotransduction pathway specifically implicated in EndMT. Further work is required to characterize how mechanical signals are detected in EndMT and specifically, which mechanotransduction pathways directly activate or suppress EndMT pathways.

TABLE 1 | Endothelial and mesenchymal markers.

Endothelial markers	Mesenchymal markers
VE-Cadherin	α-smooth muscle actin
CD31	Calponin
von Willebrand factor	Transgelin
Endothelial nitric oxide synthase 3	Versican
CD34	N-Cadherin
Tie2	Tropomyosin 1
Vascular endothelial growth factor receptor 2	Fibulin-5
	Connective tissue growth factor
	Snail
	Vimentin

Markers of EndMT

The general description of EndMT broadly involves the loss of endothelial cellular features and gain of mesenchymal characteristics. The loss of VE-Cadherin is an important marker of EndMT progression. In addition to reduced VE-Cadherin expression, the decrease in expression of CD31, von Willebrand Factor (vWF), and endothelial nitric oxide synthase 3 also indicates the loss of the endothelial cellular phenotype, and the increase in expression of markers, such as α-smooth muscle actin (α-SMA), calponin, transgelin (SM22α), vimentin, and versican, denotes the transition to a mesenchymal state (**Table 1**; Dejana et al., 2017; Sánchez-Duffhues et al., 2018).

However, there is a lack of consensus of an exact molecular and functional definition of EndMT (Kovacic et al., 2019). This is because the expression of these markers is time-dependent and can be variable, which poses a challenge in assessing the presence of EndMT primarily through marker expression. For example, RNA sequencing of HUVECs exposed to low, oscillatory shear stress (OSS; $0.5 \pm 5\,dyne/cm^2$), a potent inducer of EndMT, revealed that endothelial marker genes *NOS3*, *VWF*, and *CD34* were downregulated as early as 6 h after exposure to OSS, whereas mesenchymal marker genes *CDH2*, *TPM1*, and *FBLN5* began to be upregulated around 12 h (Ajami et al., 2017). In contrast, results from another similar RNA sequencing study indicated when HUVECs were subject to OSS ($1 \pm 4\,dyne/cm^2$) for 24 h, there was no significant effect on the expression of endothelial markers vWF, CD31, Tie2, vascular endothelial growth factor receptor 2, and VE-Cadherin, whereas exposure to pulsatile shear stress, which is protective against EndMT, upregulated the expression of these specific markers (Lai et al., 2018). However, this study found that OSS did increase mRNA levels of mesenchymal markers, such as N-Cadherin and

connective tissue growth factor (CTGF). Interestingly, the authors found that quantitative PCR but not RNA sequencing data demonstrated the induction of vimentin by OSS. The variability in findings from these two studies underscore the challenge in utilizing expression of various markers associated with the endothelial and mesenchymal phenotypes as the primary means of assessing EndMT progression.

Endothelial Monolayer Disruption, Invasion, and Migration During EndMT

In addition to the changes in expression of endothelial and mesenchymal markers during EndMT, there are physical changes that occur, such as cytoskeletal remodeling, loss of cell-cell adhesion, and cellular polarity (Gasparics et al., 2016). In the early stages of EndMT, a decrease in intercellular adhesion forces in the endothelial monolayer along with an increase in cellular stiffness has been reported (Sancho et al., 2017). However, parallel processes in EMT suggest that a decrease in cellular stiffness may be important for migration (Osborne et al., 2014), though this has not yet been extensively studied.

Cellular stiffness and the related property of deformability are often used to describe the mechanophenotype of a cell (Kozminsky and Sohn, 2020). For example, induction of EMT in human ovarian cancer cells demonstrated marked differences in the mechanophenotype of epithelial vs. mesenchymal cells, which correlated with EMT-mediated changes in epithelial and mesenchymal markers. The mesenchymal transformed cells were more deformable, and the parallel microfiltration technique used to assess the mechanophenotype of these transformed cells was able to determine whether cells are more mesenchymal or epithelial based on deformability alone (Qi et al., 2015). This technique along with similar microfluidic approaches that allow for monitoring of the dynamic cellular mechanophenotype may be promising label-free methods of overcoming the challenges associated with using cell surface markers as the primary means of assessing EndMT.

Following disruption of the cell-cell adhesions that constrain the ECs in the monolayer, ECs invade and migrate through the ECM, which requires degradation of the ECM and increased cellular motility. While the mechanisms of matrix invasion and migration during EndMT in CVD are not well characterized, there are elements from cancer biology that may be relevant. Tumor cells exhibit two types of cellular motility: (1) a mesenchymal pattern facilitated by matrix metalloproteinases (MMPs), which promotes degradation of the ECM and (2) an amoeboid pattern mediated by Rho/ROCK cytoskeletal contraction (Panková et al., 2010). When TGFβ2 was added to human dermal microvascular ECs, they transitioned to an intermediate mesenchymal state and upregulated the expression of MMP-2 which was proteolytically active (Kryczka et al., 2017). They also showed that this upregulation of MMP-2 was associated with an increase in the motility of the cells undergoing EndMT. Furthermore, inhibition of both MMP-2 and ROCK reduced their motility during EndMT. These results suggest that the increased motility of dermal microvascular ECs during EndMT may be a mixed subtype of the amoeboid and mesenchymal types of migration since it is dependent both on MMP-2 and Rho/ROCK.

Paracrine Role of MMPs in EndMT

Interestingly, MMPs expressed by other cells in the vicinity of ECs may play a regulatory role in EndMT. In an animal model of myocardial infarction (MI), MMP14 expressed in macrophages induced their release of TGFβ1, which subsequently resulted in activation of SMAD2-mediated EndMT pathways in nearby ECs through paracrine signaling. MMP14 silencing *in vivo* corresponded with decreased collagen deposition and cardiac fibrosis after MI (Alonso-Herranz et al., 2020; Lim, 2021). Furthermore, with MMP14 silencing, there was reduced left ventricular dysfunction and dilatation and greater preservation of vascular supply in the cardiac tissue following ischemic injury. When MMP14 was inactivated in these macrophages *in vitro*, there was decreased EndMT. The decreased EndMT following inactivation of MMP14 in these cardiac macrophages may explain the effects of the attenuation of maladaptive sequelae of ischemic injury observed with MMP14 silencing *in vivo*. Thus, MMPs may play an important role in not only facilitating motility of ECs undergoing EndMT, but also in activating EndMT through indirect paracrine signaling.

EndMT Continuum

The phenotypic alterations associated with EndMT appear to exist on a continuum (**Figure 2**). In an intermediate stage of EndMT, or partial EndMT, both endothelial and mesenchymal features may be present, while complete EndMT indicates an essentially entirely mesenchymal state (Dejana and Lampugnani, 2018; Bischoff, 2019). Partial EndMT is thought to play a physiological role in angiogenesis, where ECs lack apical-basal polarity and degrade the ECM but retain some cell-cell adhesion and migrate as a chain of cells instead of as individual cells (Welch-Reardon et al., 2015). Interestingly, a recent study reported a transient mesenchymal activation of ECs along with metabolic adaptions in the first week after MI that was not sustained long term (Tombor et al., 2020, 2021). Furthermore, removal of EndMT-promoting stimuli resulted in a reversal of the mesenchymal phenotype *in vitro*. It is hypothesized that this transient EndMT allows for ECs to migrate and participate in vascularization of ischemic areas. This partial activation has been termed as endothelial-to-mesenchymal activation and opens new avenues of inquiry into how EndMT may not only be a mechanism of maladaptive remodeling following ischemic injury but could also positively influence the healing response through revascularization of ischemic tissue.

The sequence and progression of EndMT are still not yet well understood. In a pathological context of pulmonary arterial hypertension (PAH), cell lineage tracing allowed for the identification of cells in both partial and complete EndMT states with distinct patterns of marker expression and functional properties (Suzuki et al., 2017). The cells classified as partial EndMT cells demonstrated higher expression of endothelial progenitor cell markers, such as CD133/Prom1 and CD34, whereas the cells classified as complete EndMT cells did not

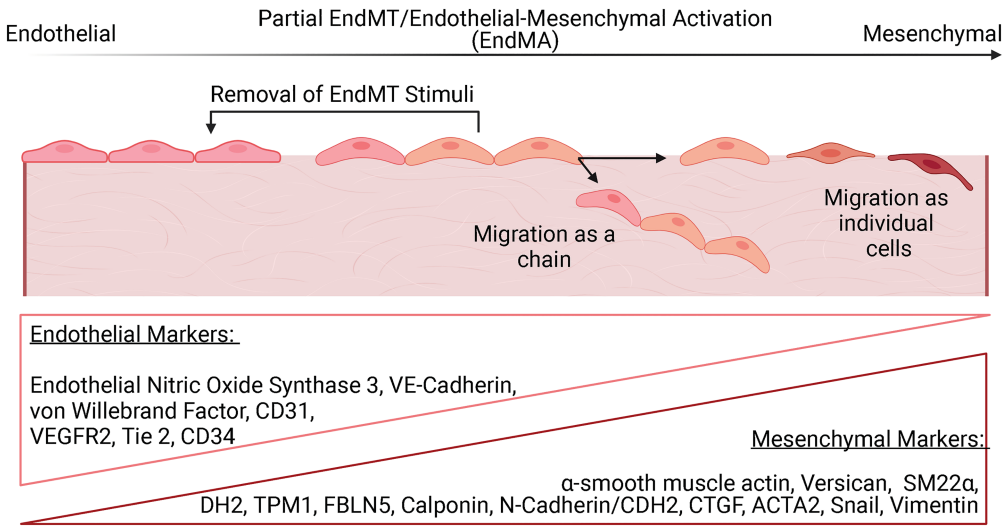

FIGURE 2 | The EndMT continuum. EndMT is thought to exist on a spectrum with evidence for partial activation of EndMT that may be reversed with removal of the EndMT stimuli. Endothelial cells that have undergone partial EndMT can migrate as a chain without loss of cell-cell adhesion. ECs that undergo EndMT can also migrate as individual cells. Complete EndMT is defined as the presence of an entirely mesenchymal state. The progression of EndMT is evaluated by the monitoring the expression of various endothelial and mesenchymal markers, with ECs that have undergone partial EndMT expressing some level of both types of markers.

express these markers but instead expressed Sca-1 and CD105, which are mesenchymal stem cell markers. Furthermore, these complete EndMT cells exhibited higher proliferative and migratory capacity, as well as an additional role in promoting the proliferation of non-endothelium-derived mesenchymal cells through paracrine signaling, suggesting both direct and indirect roles in the pathogenesis of PAH. Though there was coexistence of cells in both partial and complete EndMT states, it was not clear whether cells had to progress through the partial EndMT state to reach the complete EndMT state. EndMT is a complex and multifaceted phenomenon with multiple activators and signaling pathways involved, and the progression of EndMT requires further elucidation.

VALVE DEVELOPMENT AND PATHOLOGY

EndMT is crucial to the formation of the atrioventricular valves and the outflow tract (OFT). Abnormalities in OFT development can result in congenital heart diseases (CHD), such as conotruncal defects (CTD). In patients with CTD, SOX7 mutations have been identified and additional *in vitro* studies demonstrated that SOX7 mutations can lead to impaired EndMT *via* regulation of VE-Cadherin, indicating that the inhibition of EndMT during development may contribute to CTD (Jiang et al., 2021).

There are important mechanical forces that regulate EndMT in normal OFT development (Hove et al., 2003; Bartman et al., 2004; Kalogirou et al., 2014). Aberrations in contractile and hemodynamic forces lead to abnormalities in OFT development that may also contribute to CHD. During the formation of the OFT, increases in wall shear stress resulted in greater Notch1b signaling and EndMT, which then led to ventriculobulbar (VB) valve hyperplasia. In contrast, decreases in contractile forces reduced Notch1b signaling and EndMT, which subsequently resulted in VB valve underdevelopment (Hsu et al., 2019).

In addition to contributing to abnormalities of valve development associated with CHD, EndMT is also involved in other pathological settings of the valves. The following sections describe the role of EndMT in CAVD and ischemic mitral regurgitation (IMR) and how various types of biomechanical alterations can regulate EndMT of valvular ECs.

Calcific Aortic Valve Disease

Calcific aortic valve disease is the third most prevalent cause of CVD (Yutzey et al., 2014). The pathophysiological features of CAVD include aberrant collagen orientation, leaflet thickening, and fibrosis, which can result in hemodynamic abnormalities eventually necessitating valve replacement. Additionally, an active area of investigation is the role of inflammation as one of the underlying mechanisms that drives the initiation and progression of valvular calcification in CAVD (Lim et al., 2016). While initially believed to be a passive, degenerative process, there is now more evidence indicating that valvular calcification is an active and dynamically regulated process with multiple cell types playing a role (Ma et al., 2020b). It is thought that dysregulation of EndMT causes differentiation of resident cells into the osteogenic and fibrotic cell types that result in the calcified, stiff aortic valve leaflets observed in CAVD.

The aortic valve leaflet has a trilaminar structure and is broadly composed of two types of cells: valvular endothelial cells (VECs) and valvular interstitial cells (VICs). Interactions between these cells contribute to the formation of calcific lesions (**Figure 3A**). Indirect coculture of VECs and VICs in hydrogels with equi-biaxial mechanical constraint and

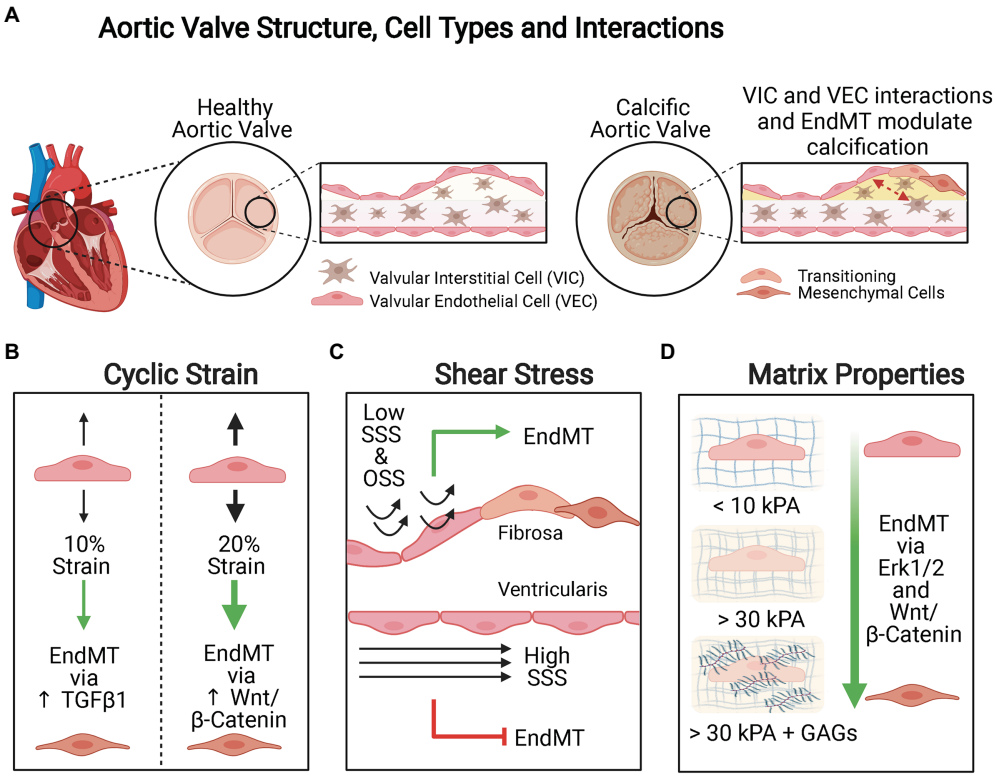

FIGURE 3 | Mechanical modulation of EndMT in valvular endothelial cells (VECs). **(A)** Aortic valve structure, cell types, and interactions. The aortic valve is a trilaminar structure with valvular interstitial cells (VICs) sandwiched in between two layers of VECs. Interactions between the VICs and VECs and EndMT are both important in valvular calcification. **(B)** Cyclic strain. Cyclic strain induces greater extent of EndMT when applied orthogonally to the alignment of the valve endothelium and the pathways activated are magnitude dependent. When VECs are subject to 10% cyclic strain, EndMT is activated *via* TGFβ1 signaling, whereas 20% cyclic strain promotes EndMT *via* Wnt/β-Catenin signaling. **(C)** Shear stress. Low steady shear stress (SSS) and oscillatory shear stress (OSS) promote EndMT, whereas high SSS is protective against EndMT. Calcification is more common on the fibrosa side where VECs are exposed to low SSS or OSS than on the ventricularis side where VECs are subject to high SSS. **(D)** Matrix composition and stiffness. Increasing matrix stiffness and increased glycosaminoglycans (GAGs) content promote EndMT.

supplementation of osteogenic differentiation factors demonstrated that VECs promote enhanced calcification and pathological remodeling of VICs *via* EndMT and osteogenic differentiation when compared to hydrogels seeded with VICs only (Gee et al., 2021). Furthermore, when porcine aortic VECs were treated with TNFα and cultured on a three-dimensional system that allowed transforming and non-transforming cells to be independently isolated and characterized, both non-transformed cells that maintained control levels of endothelial VE-cadherin and eNOS and transformed cells that lost these endothelial characteristics and had increased expression of α-SMA were identified. These results suggest that only a certain subset of VECs may be susceptible to undergoing EndMT under conditions of inflammation and that interactions between non-transformed and transformed cells may also be an important factor in CAVD pathogenesis in addition to interactions between VECs and VICs (Farrar and Butcher, 2014).

While these studies highlight how different cell types interact in the context of EndMT in CAVD, the lineages of the cell types present in calcific lesions in CAVD was not explored. However, a recent single-cell RNA sequencing study detailing a transcriptomic atlas of human aortic valves from both healthy and CAVD patient samples not only demonstrated remarkable cellular heterogeneity in the aortic valve leaflets but also provided more direct evidence of EndMT as the process that leads to the differentiation of resident VICs and VECs into newly identified valve-derived stromal cells that are prominent in only the CAVD samples (Xu et al., 2020). The pseudotime trajectory analysis along with other cellular localization experiments performed in this study suggests that EndMT was actively involved in the thickening of the calcified aortic valve leaflets, rather than a consequence of the CAVD process.

Mechanical Modulation of Valvular EndMT

While single-cell RNA sequencing allowed for the identification of distinct subpopulations of cells and suggested that EndMT contributes to this cellular heterogeneity in human CAVD, it did not provide mechanistic insight into what initiates and promotes EndMT of the resident VECs and differentiation of VICs. This is not yet well understood, but there are studies that have characterized the effect of varying cyclic strain, shear stress, matrix stiffness, cell-cell, and cell-matrix interactions

on VECs, VICs, and EndMT (**Figure 3**). These studies indicated that VECs can undergo EndMT under a variety of conditions, and it is likely that a combination of these factors play a role in promoting EndMT that ultimately drive the initiation and progression of CAVD. It is important to note that many of these studies aim to elucidate the impact of modulating various mechanical parameters on EndMT of VECs in general. Therefore, the findings may be applicable to other valvular pathologies that involve EndMT beyond CAVD.

Cyclic strain induces EndMT of VECs in a magnitude and direction-dependent manner (**Figure 3B**). When VECs were subjected to low strain (10%) representing physiologic conditions, there was increased expression of the mesenchymal marker α-SMA and downregulation of endothelial markers VE-Cadherin and CD31, in addition to increased TGFβ1 signaling. Under conditions of high strain (20%) mimicking pathological conditions, the expression of these markers was modulated *via* increased Wnt/β-catenin signaling (Balachandran et al., 2011). Furthermore, the authors found that cyclic strain applied orthogonally to the alignment of the valve endothelium resulted in more pronounced disruption of cellular microarchitecture, more extensive EndMT, increased contractility in the presence of endothelin-1, and greater basal mechanical tone.

In addition to cyclic strain, VECs also experience different hemodynamic stresses due to pulsatile blood flow (**Figure 3C**). VECs subjected to low steady shear stress (SSS; 2 dyne/cm^2) and OSS demonstrated increased expression of EndMT-related markers Snail and α-SMA, TGFβ1 along with inflammation-related markers ICAM1 and NF-κB1, when compared to cells exposed to high SSS (10 and 20 dyne/cm^2) or static conditions (Mahler et al., 2014). Furthermore, VECs exposed to low SSS condition demonstrated increased matrix invasion. The cells also elongated and aligned perpendicularly to the laminar SSS but not the OSS. These results were consistent with the observation of EndMT on the fibrosa side (facing the aorta) where cells experience low OSS and thought to be the initiating site of inflammation and calcification (Mohler, 2004), whereas EndMT is not observed on ventricularis side (facing the left ventricle) which is exposed to high SSS (Mahler et al., 2013). While these conditions of shear stress utilized may not recapitulate physiological or pathophysiological conditions precisely, these results nonetheless highlight why low SSS or OSS promotes inflammation and EndMT, whereas high SSS is protective against EndMT of VECs.

The components and mechanical properties of the ECM of VECs are also important factors that modulate EndMT (**Figure 3D**). In healthy porcine aortic valve tissue, the fibrosa side has been reported to be stiffer with effective Young's moduli >3 kPa, whereas the ventricularis side is softer with effective Young's moduli <0.5 kPa (Zhao et al., 2011). When healthy porcine aortic VECs were seeded into stiffer gel matrices (~37–50 kPa), they demonstrated greater expression of EndMT-related markers, such as α-SMA, than cells that were seeded into less stiff gel matrices (~2–5 kPa). This suggests that increasing matrix stiffness alone can induce mesenchymal transformation of healthy VECs (Dahal et al., 2017). Furthermore, they found that the presence of glycosaminoglycans (GAGs) in the ECM increased the expression of EndMT-related markers when comparing cells seeded into matrices of similar stiffness. GAGs weakened the cell-ECM adhesion strength, altered ECM binding, and influenced production of collagen I and GAGs by the newly transitioned mesenchymal cells.

The effects of matrix stiffness on EndMT of VECs involve the ERK1/2 and Wnt/β-catenin signaling pathways. When VECs seeded in collagen gels with and without GAGs were treated with the ERK1/2 inhibitor U0126, there was a significant downregulation of EndMT markers and diminished cell invasion into the matrix (Dahal et al., 2017). For VECs seeded into silicone Sylgard 527 substrates, the addition of TGFβ1 preferentially promoted EndMT on VECs seeded into stiffer substrates as demonstrated by enhanced expression mesenchymal α-SMA (Zhong et al., 2018). In these cells, the authors also observed greater β-catenin nuclear translocation. However, treatment of VECs with TGFβ1 and endostatin, which degrades β-catenin, did not reduce disruption of the endothelial monolayer, morphological changes related to EndMT, or loss of VE-cadherin localization to the cell membrane but did significantly reduce the expression of α-SMA. This suggests that β-catenin signaling does not play a role in initiating EndMT in VECs but is required for TGFβ1 mediated transformation of VECs to myofibroblasts.

Ischemic Mitral Regurgitation

Ischemic mitral regurgitation (IMR) is a prevalent cause of valvular disease and is a consequence of leaflet tethering following papillary displacement due to left ventricle dilation after MI (Marwick et al., 2009). Tethering of mitral valve leaflets 8 weeks after MI resulted in notable permanent radial deformation of the leaflets, which led to a complete loss of mechanical anisotropy, significant decrease in radial peak strain, and an increase in the collagen and GAG mass fraction (Howsmon et al., 2020; **Figure 4**). Furthermore, tethered leaflets also stained positively for EndMT-related markers, with more extensive presence of EndMT when there was MI in addition to leaflet tethering (Dal-Bianco et al., 2009, 2016), suggesting that these altered biomechanical stresses may trigger EndMT of mitral VECs.

In a model of leaflet tethering with MI, treatment with losartan reduced the fibrosis and thickening of the mitral valve, suggesting that losartan, which has been associated with inhibition of TGFβ signaling, may partially limit the EndMT-mediated maladaptive response of mitral VECs after MI that eventually leads to IMR (Bartko et al., 2017). Their subsequent studies of how mitral VECs respond in post-infarct conditions revealed an increase in expression of CD45, a protein tyrosine phosphatase, in addition to EndMT-related markers α-SMA and VE-cadherin in mitral valve leaflets. This was also replicated *in vitro* when addition of TGFβ to mitral VECs induced increased expression of CD45 and α-SMA (Bischoff et al., 2016). Inhibiting CD45 reduced expression of α-SMA, indicating that CD45 may regulate EndMT involved in fibrosis and thickening of mitral valve leaflets in IMR. Targeting various aspects of the EndMT pathways at either the level of TGFβ or CD45 can potentially be a promising method of inhibiting the maladaptive response of

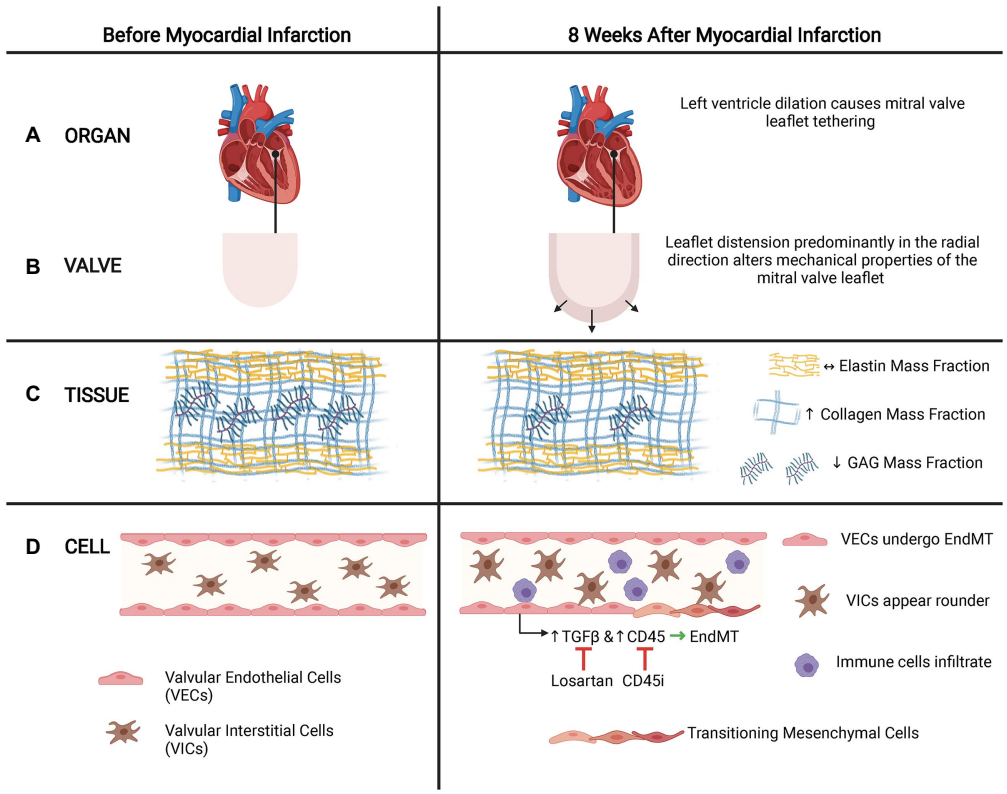

FIGURE 4 | Leaflet tethering and EndMT in ischemic mitral regurgitation (IMR). **(A)**. Organ. After a myocardial infarction, the heart often dilates, which causes tethering of the mitral valves that can lead to IMR. **(B)** Valve. Tethering distends the leaflet predominantly in the radial direction. **(C)** Tissue. Leaflet tethering alters the mitral valve matrix composition by increasing the collagen mass fraction and decreasing the GAG mass fraction. However, the elastic mass fraction does not change. **(D)** Cell. These biomechanical alterations of the valve leaflet may trigger EndMT of the mitral valve endothelial cells *via* mechanisms that involve TGFβ signaling and CD45. Inhibiting TGFβ with losartan or CD45 with a CD45 inhibitor reduces EndMT and associated maladaptive responses observed in IMR. In addition to EndMT of VECs, VICs also appear rounder and immune cells may infiltrate. (Adapted with permission from Howsmon et al., 2020).

mitral VECs to altered mechanical stresses that are associated with the development and progression of IMR. Alternatively, surgical approaches, such as plication of the infarct region that decrease tethering distance and subsequently reduce stretch (Liel-Cohen et al., 2000), may prevent the induction of EndMT pathways that result in the progressive fibrosing and thickening of the mitral valve leaflets.

ENDOCARDIAL FIBROELASTOSIS AND CARDIAC FIBROSIS

Mitral regurgitation and other valvular pathologies, such as mitral stenosis and aortic insufficiency, can lead to the formation of flow jets (Maganti et al., 2010) that alter the hemodynamic stresses experienced by ECs lining the endocardium, which may subsequently promote EndMT of endocardial ECs. In samples from patients with flow disturbances due to stenotic or incompetent valves, there was evidence of EFE in regions where there was exposure to disturbed flow (d-flow) patterns (Weixler et al., 2020). Further staining for EndMT-related markers in those areas demonstrated increased expression of α-SMA, suggesting that EFE may be due to EndMT induced by d-flow patterns and altered shear stress from the valvular defects. In patients with hypoplastic left heart syndrome, EFE progression occurred despite surgical resection if the valvular defect was not addressed. The evidence of EndMT in EFE is consistent with other studies that have correlated increased EndMT in EFE *via* a mechanism that in part involved transcriptional suppression of BMP5 and BMP7 due to abnormal promoter methylation (Xu et al., 2015). While these studies linking EndMT to EFE have increased interest in targeting EndMT as a therapeutic approach, other studies suggest that the fibroblasts present in EFE tissues may arise from embryonic EMT rather than EndMT (Zhang et al., 2017).

EFE is a subtype of cardiac fibrosis. The role of EndMT in cardiac fibrosis more broadly has been debated. Early studies indicated that the majority of fibroblasts that appeared after cardiac injury was derived from EndMT (Zeisberg et al., 2007) and subsequent ones contrarily suggested that fibroblasts did not arise singularly from one specific differentiation program (Ali et al., 2014; Fu et al., 2018). The extent to which EndMT contributes to the cardiac fibrosis and the mechanical regulators of these processes merit further investigation.

VASCULAR DISEASE: ATHEROSCLEROSIS, VASCULAR CALCIFICATION, AND ARTERIAL STIFFENING

Broadly, atherosclerosis and arterial stiffening are distinct but interrelated pathologies in which EndMT may play a role. The following sections highlight emerging evidence indicating the presence of EndMT in these vascular pathologies.

Atherosclerosis and Vascular Calcification

Atherosclerosis is the most prevalent underlying cause of many types of CVD. Broadly, atherosclerosis refers to the progressive accumulation of fat and fibrous content in the intima of the arteries. Over time, the atherosclerotic plaques become more fibrous and undergo calcification (Mohler, 2004; Chen et al., 2020). The plaques often are unstable, and their rupture leads to the formation of thrombi that can occlude the vasculature and lead to acute ischemia. In advanced atherosclerosis, the plaque may cause hemodynamic disturbances by narrowing the arterial lumen. This narrowing impedes blood blow and can also result in ischemia (Libby et al., 2019).

The mechanisms underlying the pathophysiology of atherosclerosis involve multiple cell types, including ECs, fibroblasts, smooth muscle cells, macrophages, and other immune cells. Due to the high prevalence and potential serious consequences of atherosclerosis, there has been immense interest in understanding not only how these various cell types contribute to pathologic progression but also their differentiation trajectories, as well. EndMT is thought to be one key process that leads to the differentiation of resident ECs into pro-atherogenic cells (Chen et al., 2020). Early studies indicated a potential role of EndMT in atherosclerosis by demonstrating the presence of EndMT-related markers in human atherosclerotic lesions and identified hemodynamic alterations as a crucial mediator of EndMT *via* fibroblast growth factor receptor 1 signaling (Chen et al., 2015). Recent single-cell transcriptomic analyses detailing the microanatomy of advanced human atherosclerotic plaques have substantiated the evidence that EndMT may play an active role in the development and progression of atherosclerosis by identifying distinct clusters of ECs in atherosclerotic lesions that demonstrated both smooth muscle and endothelial cellular features (Depuydt et al., 2020).

Atherosclerotic lesions tend to initiate in areas of the vasculature exposed to d-flow, which is a hemodynamic profile characterized by low, OSS (Dai et al., 2004; **Figure 5**). D-flow is linked to EC dysfunction and an atheroprone phenotype. In contrast, stable flow (s-flow) characterized by unidirectional, high laminar shear stress that can either be pulsatile or nonpulsatile is thought to be crucial to EC homeostasis and atheroprotection. Many sensors and pathways involved in transducing hemodynamic signals in ECs have been identified. Of note, Piezo1 is a mechanosensor that modulates responses to s-flow and d-flow differentially (Demos et al., 2020). Piezo1 is a nonselective cation channel that is permeable to calcium. In response to s-flow, Piezo1 activated the PI3K-eNOS pathway involved in atheroprotection. In contrast, d-flow resulted in the activation of the NF-κB pathway associated with a pro-atherogenic phenotype. This pathway involved Piezo 1-dependent activation of annexin A2, which bound integrin α5 and led to subsequent translocation of the complex to lipid rafts (Zhang et al., 2020). There integrin α5 was activated and led to the stimulation of the NF-κB pathway, which resulted in inflammation and formation of atherosclerotic plaques. Because NF-κB is a pathway that is known to be important to inflammation-mediated EndMT (Maleszewska et al., 2013; Pérez et al., 2017), Piezo-1 may play an important mechanosensory role in modulating d-flow induced EndMT in atherosclerosis.

While the role of Piezo1 in EndMT specifically is not yet known, Alk5 is a receptor that has been recently identified as crucial to modulating EndMT induced by d-flow in atherosclerosis (Mehta et al., 2021, 5). Results from this study demonstrated that depletion of Alk5 reduces shear stress-induced EndMT signaling, which involves activation of Smad2 and downstream upregulation of mesenchymal and ECM genes. Alk5 associated with Shc in response to shear stress and modulated EndMT *in vitro* and *in vivo*. Furthermore, deletion of Shc reduced atherosclerotic plaque formation in areas of d-flow *in vivo*. These findings highlight Alk5 and Shc as crucial to mediating the EndMT response in areas of d-flow prone to atherosclerotic plaque formation. Interestingly, tensional force and reconstitution experiments identified Alk5 as mechanosensor unique and sufficient for activation of Smad2 with functions independent of mechanosensors, such as PlxnD1, which plays a role in d-flow induced atherosclerosis (Mehta et al., 2020), and PECAM-1. While these experiments indicated that Alk5 leads to activation of Smad2 which is crucial to a pathway involved in EndMT even in cells that do not express PlxnD1 and PECAM-1, these other mechanosensors may still play a role in activation of other EndMT pathways independent of Smad2. Further work is required to characterize the role of other shear-sensitive mechanosensors in EndMT in atherosclerosis.

In regions exposed to d-flow, the transcription factor TWIST was expressed preferentially and contributed to activating pathways involved in inflammation, EC proliferation, and EndMT (Mahmoud et al., 2016). Downstream of TWIST, EndMT induced by low shear stress associated with d-flow involved the transcription factor Snail (Mahmoud et al., 2017). In contrast, high laminar shear stress associated with s-flow was atheroprotective through the activation of Krüppel-like factor 2 and 5 *via* Erk5 signaling (Moonen et al., 2015). EndMT induced by d-flow was inhibited *via* activation of Erk5.

In addition to promoting atherogenesis, EndMT also contributed to the calcification of atherosclerotic lesions through a mechanism partially mediated by sex-determining region Y-box 2 (SOX2; Boström et al., 2016). The role of inflammation and EndMT in calcification was also investigated by treating human aortic endothelial cells (HAECs) with TNFα and IL-1β to induce EndMT. These transformed cells then underwent osteogenic differentiation in response to BM9. It was found that BMPR2 downregulation and JNK activation were key events in BMP-9

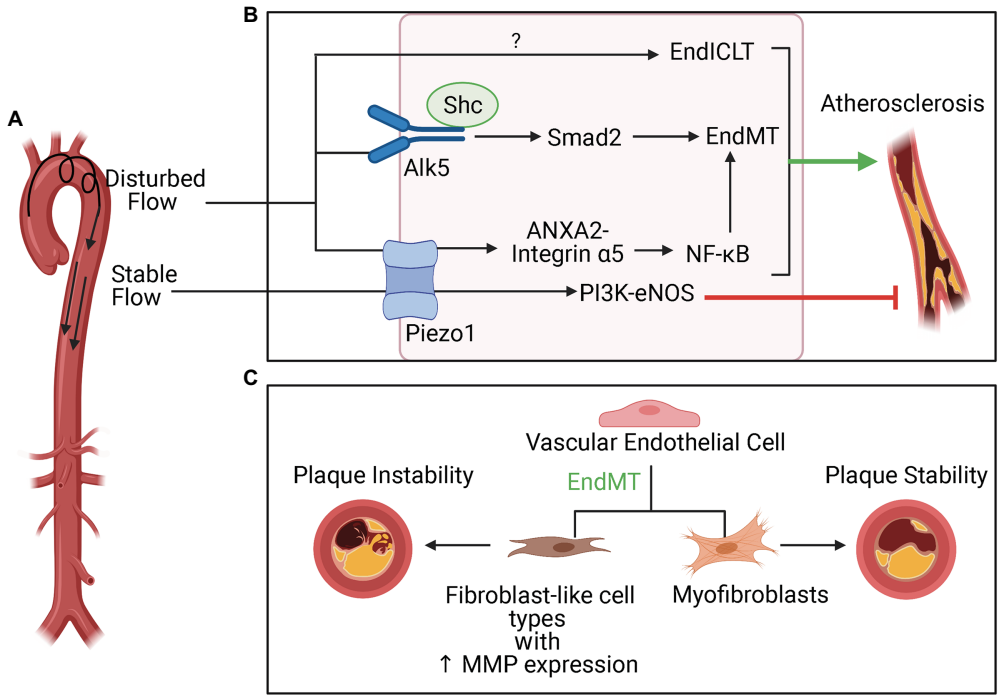

FIGURE 5 | Disturbed flow (d-flow), EndMT, and plaque stability in atherosclerosis. **(A)** d-flow that occurs at the lesser curvature of the aortic arch is atherogenic, whereas stable flow typically presents in the descending aorta is atheroprotective (EndICLT). **(B)** The mechanosensor Piezo1 is crucial to the differential responses to these hemodynamic profiles. In response to d-flow, Piezo1 activates the NF-κB pathway, which is known to be important to inflammation-mediated EndMT. In addition to EndMT, d-flow also activates of endothelial-to-immune-cell-like transition. The mechanosensor Alk5 and associated protein Shc have been directly linked to activation of Smad-2 mediated EndMT pathways in response to d-flow in atherosclerosis. **(C)** EndMT can contribute to both plaque instability and plaque stability depending on whether EndMT results in transition of ECs to fibroblast-like cell types with increased matrix metalloproteinase expression or to myofibroblasts.

induced mineralization (Sánchez-Duffhues et al., 2019). Activation of BMP signaling also induced the expression of serine proteases, such as elastases and kallikreins, which then triggered EndMT of HAECs. Activation of BMP signaling also induced the expression of serine proteases, such as elastases and kallikreins, which then triggered EndMT of HAECs through a pathway that involved mutual regulation of SOX2 and TWIST (Yao et al., 2015). Furthermore, endothelial-specific deletion of SOX2 *in vivo* decreased expression of these serine proteases, EndMT, and aortic calcification, suggesting the crucial role of SOX2 in vascular calcification.

Calcified atherosclerotic plaques can be either unstable or stable, and considerable effort has gone into understanding the mechanisms behind plaque rupture vulnerability (Bentzon et al., 2014). Atherosclerotic plaques that are particularly unstable and more prone to rupture demonstrated greater extent of EndMT (**Figure 5**), which caused ECs to differentiate into fibroblast-like cell types with increased expression of MMPs that contributed to plaque instability (Evrard et al., 2016). On the other hand, EndMT may also contribute to plaque stability. EndMT resulted in the differentiation of ECs into myofibroblast-like cells that populated the thick fibrous cap associated with stable atherosclerotic plaques (Newman et al., 2021).

Along with activation of EndMT pathways, d-flow can also activate pathways that lead ECs to differentiate into other pro-atherogenic cell types. Single-cell RNA sequencing of ECs exposed to d-flow led to the identification of multiple pro-atherogenic cell types, including pro-inflammatory cells, hematopoietic stem cells, endothelial progenitor cells, and immune cell-like phenotypes (Andueza et al., 2020). This remarkable plasticity of ECs in response to d-flow demonstrates how the development and progression of atherosclerotic plaques may involve a complex interplay between multiple pro-inflammatory cell types that arise when the vasculature is exposed to certain hemodynamic stresses. Moreover, the results from this study indicate that certain ECs are more susceptible to undergoing EndMT while others undergo endothelial-to-immune-cell-like transition. Understanding the factors that govern the fate of ECs and determine what type of transition is activated in response to d-flow may be an important consideration to develop targeted therapeutic approaches for atherosclerosis.

Arterial Stiffening

D-flow can also lead to arterial stiffening in the absence of atherosclerosis through a mechanism that partially involved the stimulation of profibrotic genes by thrombospondin-1 (Kim Chan Kim et al., 2017). Certain ECs, such as HUVECs, responded to increased stiffening by upregulating expression of TGF-β2 and enhancing cell-matrix traction stresses (Bastounis et al., 2019).

This increase in TGFβ2 signaling may result in the activation of EndMT pathways, which contribute to EC dysfunction. EndMT as a response to increased stiffness is partially mediated by Glypican 1, a core protein in the glycocalyx layer. HUVECs cultured on polyacrylamide (PA) gels of substrate stiffness 10 kPa, which approximates subendothelial stiffness of aged, unhealthy arteries, demonstrated decreased glycocalyx expression, and increased expression of EndMT markers when compared to cells cultured on softer PA gels (2.5 kPa), which approximates the subendothelial stiffness of young, healthy arteries. The EndMT-related markers that are upregulated are N-cadherin, α-SMA, and Snail, but interestingly, there was no difference in the expression of CD31 on cells cultured on soft vs. stiff gels, indicating that increasing stiffness may only trigger a partial EndMT. When Glypican 1 was silenced in cells are cultured on the 2.5 kPa gels using siRNA, there was an increase in the expression in the EndMT-related markers N-cadherin, α-SMA, and Snail. In a model of age-mediated stiffness, there was reduced expression of Glypican 1 and greater EC dysfunction in older mice compared to young mice. Furthermore, Glypican 1 gene deletion exacerbated EC dysfunction in young mice but not aged mice (Mahmoud et al., 2020). These results suggest that the glycocalyx layer of ECs plays an important protective role against EndMT associated with increasing stiffness of the endothelial microenvironment present in age-mediated arterial stiffening.

CONCLUSION

Since the identification of EndMT as a distinct form of EMT crucial for the physiological development of the cardiovascular system, there has been a growing interest in also understanding its role in various CVD processes. Because ECs in the cardiovascular system are highly sensitive to mechanical stresses that are often distinctly different under physiologic and pathologic conditions, elucidating how variations in biomechanical properties of the EC microenvironment regulate EndMT has been a key focus area. Early studies relied on *in vitro* assessments, animal models, and staining of human pathological specimens to provide evidence linking mechanically driven EndMT to CVD, though it is still quite not yet well understood whether EndMT drives CVD pathogenesis or whether it is a consequence of the pathological progression. The advent of single-cell RNA sequencing analyses has provided more insight into the differentiation trajectory of ECs in samples from patients with CVD. These studies indicate that EndMT may indeed drive the progression of the pathological mechanisms underlying CVD and actively contribute to CVD. In addition to substantiating evidence indicating that EndMT actively contributes to CVD, transcriptomic studies have also increased our understanding of the remarkable plasticity of ECs in response to aberrations in their microenvironment and the time-dependent course of these phenotypic transitions. While some studies indicate that EndMT can exist in a partial and reversible state, the permanence of epigenetic and genetic changes associated with EndMT has yet to be well characterized. Furthermore, there is also now burgeoning evidence that EndMT may have beneficial effects in pathological settings, such as contributing to revascularization after ischemic injury and atherosclerotic plaque stability. This evidence requires careful consideration of how to modulate EndMT in pathological settings as a therapeutic approach. The factors governing the plasticity of ECs and the maladaptive vs. beneficial effects of EndMT in CVD still require further elucidation and may be important for ultimately determining ideal therapeutic targets in CVD.

Nonetheless, it is evident that mechanical factors are important in the activation and regulation of EndMT. In this review, we summarized literature that linked alterations in shear stress, cyclic strain and stretch, and matrix stiffness to EndMT in CAVD, atherosclerosis, IMR, EFE, and arterial stiffening. While the mechanical stresses in the cardiovascular system are highly diverse and are often difficult to recapitulate exactly experimentally, and specific sequential progression of these pathways has yet to be fully detailed, addressing the aberrant mechanical forces that are linked to EndMT may be a promising therapeutic approach. For example, devices or surgical procedures that address the valvular defects that alter hemodynamics in patients with EFE may reduce the extent of EndMT that contributes to EFE. Similarly, reducing leaflet tethering in IMR through plication of the infarct region can reduce the stretch that activates EndMT pathways that contribute to IMR. Furthermore, there have been continued improvements and clinical utilization of computational fluid dynamic modeling to obtain patient-specific wall shear stress measurements in vascular beds, such as the coronary arteries, potentially identifying individuals at increased risk of atherosclerotic disease progression (Gijsen et al., 2019). Integration of such hemodynamic assessments along with a deeper understanding of the signaling pathways that mediate pathological responses to shear (e.g., Alk5) may help to identify therapeutic targets that are particularly effective at preventing or reversing disease progression in these at-risk patient groups.

In contrast to the amount of literature linking alterations in biomechanical stresses to the presence of EndMT in various pathological states, there is a dearth of studies detailing the mechanics associated with the key features of EndMT, such as decreased cell-cell adhesion, increased contractility and motility, and greater migratory and invasive capabilities. These features involve multiscale changes from the subcellular to tissue levels that lead to functional differences of importance in disease pathology, and further investigation of the mechanisms underlying the hallmarks of EndMT will enhance our understanding of EndMT and may help address the fact that there currently is no exact functional and molecular definition of EndMT. Characterization of biomechanical changes that ECs undergo during EndMT may also be a means of finding a mechanical biomarker that can potentially be used for the development of diagnostic tools. Indeed, mechanophenotyping technologies have shown promise by demonstrating the ability to identify cells of varying phenotypes in heterogeneous tumors (Kozminsky and Sohn, 2020). For example, real time deformability cytometry, which utilizes the physical property of cellular deformability to identify cells with increased pathological potential in heterogeneous

tumors, has been proposed as a tool for cytopathology that can enable clinical decision making for screening, staging, and monitoring of treatment efficacy (Di Carlo, 2012). Further, deformability cytometry can help to identify metastatic potential of breast and prostate cancer cells (Ahmmed et al., 2018). Targeting the more metastatic cells may be a more effective means of treatment, and microfluidic technologies not only enable isolation and characterization of more pathogenic cell types from heterogeneous samples but can also allow for screening of therapeutics. While these approaches have not been attempted in the realm of CVD, it is possible that only certain subtypes of ECs are actively contributing to pathological progression in EndMT, and these tools offer a novel way of identifying and isolating these cells by their biomechanical properties.

In addition to lack of this definition of EndMT, there are challenges in tracking EndMT progression due to the variability in marker expression. Furthermore, it is not well understood whether there is differential activation of EndMT dependent on EC subtype and type of EndMT stimuli. More broadly, the role of EndMT in homeostatic conditions beyond development and disease is not well characterized. As the evidence for the role of EndMT in CVD continues to mount, it will become increasingly important to explore these fundamental questions regarding EC plasticity and EndMT mechanobiology. Due to the purported involvement of EndMT in many types of CVD, further investigation into these open avenues of inquiry may lead to the development of novel therapeutics and technologies that could improve CVD diagnosis and treatment.

AUTHOR CONTRIBUTIONS

SI: conceptualization, methodology, investigation, and writing of manuscript. KB, DD, CS, YT, and YY: methodology and investigation. JH: conceptualization, investigation, writing of manuscript, supervision, and project administration. All authors contributed to the article and approved the submitted version.

FUNDING

Funding for this work was provided in part by the NIH/NHLBI [grant numbers 1K08HL151961 (JH), HL81397 (KB), HL151391 (YT), HL137647 (YT), and HL139675 (YY)], NIH/NIA [grant number AG061586 (YT)], NIH/NINDS [grant number NS79353 (YY)], the Presidential Early Career Award for Scientists and Engineers [grant number N00014-16-1-2997 (DD)], and the American Heart Association [Student Scholarship in Cardiovascular Disease (SI) and Howard S. Silverman Scholarship (SI)].

ACKNOWLEDGMENTS

The authors would like to acknowledge Dr. Linda L. Demer (UCLA) for her support and guidance for the project. Additionally, all figures were created with the use of BioRender.com.

REFERENCES

Adjuto-Saccone, M., Soubeyran, P., Garcia, J., Audebert, S., Camoin, L., Rubis, M., et al. (2021). TNF-α induces endothelial–mesenchymal transition promoting stromal development of pancreatic adenocarcinoma. *Cell Death Dis.* 12:649. doi: 10.1038/s41419-021-03920-4

Ahmmed, S. M., Bithi, S. S., Pore, A. A., Mubtasim, N., Schuster, C., Gollahon, L. S., et al. (2018). Multi-sample deformability cytometry of cancer cells. *APL Bioeng.* 2:032002. doi: 10.1063/1.5020992

Ajami, N. E., Gupta, S., Maurya, M. R., Nguyen, P., Li, J. Y.-S., Shyy, J. Y.-J., et al. (2017). Systems biology analysis of longitudinal functional response of endothelial cells to shear stress. *Proc. Natl. Acad. Sci. U. S. A.* 114, 10990–10995. doi: 10.1073/pnas.1707517114

Ali, S. R., Ranjbarvaziri, S., Talkhabi, M., Zhao, P., Subat, A., Hojjat, A., et al. (2014). Developmental heterogeneity of cardiac fibroblasts does not predict pathological proliferation and activation. *Circ. Res.* 115, 625–635. doi: 10.1161/CIRCRESAHA.115.303794

Alonso-Herranz, L., Sahún-Español, Á., Paredes, A., Gonzalo, P., Gkontra, P., Núñez, V., et al. (2020). Macrophages promote endothelial-to-mesenchymal transition via MT1-MMP/TGFβ1 after myocardial infarction. *elife* 9:e57920. doi: 10.7554/eLife.57920

Andresen Eguiluz, R. C., Kaylan, K. B., Underhill, G. H., and Leckband, D. E. (2017). Substrate stiffness and VE-cadherin mechano-transduction coordinate to regulate endothelial monolayer integrity. *Biomaterials* 140, 45–57. doi: 10.1016/j.biomaterials.2017.06.010

Andueza, A., Kumar, S., Kim, J., Kang, D.-W., Mumme, H. L., Perez, J. I., et al. (2020). Endothelial reprogramming by disturbed flow revealed by single-cell RNA and chromatin accessibility study. *Cell Rep.* 33:108491. doi: 10.1016/j.celrep.2020.108491

Balachandran, K., Alford, P. W., Wylie-Sears, J., Goss, J. A., Grosberg, A., Bischoff, J., et al. (2011). Cyclic strain induces dual-mode endothelial-mesenchymal transformation of the cardiac valve. *Proc. Natl. Acad. Sci. U. S. A.* 108, 19943–19948. doi: 10.1073/pnas.1106954108

Barry, A. K., Wang, N., and Leckband, D. E. (2015). Local VE-cadherin mechanotransduction triggers long-ranged remodeling of endothelial monolayers. *J. Cell Sci.* 128, 1341–1351. doi: 10.1242/jcs.159954

Bartko, P. E., Dal-Bianco, J. P., Guerrero, J. L., Beaudoin, J., Szymanski, C., Kim, D.-H., et al. (2017). Effect of losartan on mitral valve changes After myocardial infarction. *J. Am. Coll. Cardiol.* 70, 1232–1244. doi: 10.1016/j.jacc.2017.07.734

Bartman, T., Walsh, E. C., Wen, K.-K., McKane, M., Ren, J., Alexander, J., et al. (2004). Early myocardial function affects endocardial cushion development in zebrafish. *PLoS Biol.* 2:E129. doi: 10.1371/journal.pbio.0020129

Bastounis, E. E., Yeh, Y.-T., and Theriot, J. A. (2019). Subendothelial stiffness alters endothelial cell traction force generation while exerting a minimal effect on the transcriptome. *Sci. Rep.* 9:18209. doi: 10.1038/s41598-019-54336-2

Bentzon, J. F., Otsuka, F., Virmani, R., and Falk, E. (2014). Mechanisms of plaque formation and rupture. *Circ. Res.* 114, 1852–1866. doi: 10.1161/CIRCRESAHA.114.302721

Bischoff, J. (2019). Endothelial-to-mesenchymal transition. *Circ. Res.* 124, 1163–1165. doi: 10.1161/CIRCRESAHA.119.314813

Bischoff, J., Casanovas, G., Wylie-Sears, J., Kim, D.-H., Bartko, P. E., Guerrero, J. L., et al. (2016). CD45 expression in mitral valve endothelial cells After myocardial infarction. *Circ. Res.* 119, 1215–1225. doi: 10.1161/CIRCRESAHA.116.309598

Boström, K. I., Yao, J., Guihard, P. J., Blazquez-Medela, A. M., and Yao, Y. (2016). Endothelial-mesenchymal transition in atherosclerotic lesion calcification. *Atherosclerosis* 253, 124–127. doi: 10.1016/j.atherosclerosis.2016.08.046

Charbonier, F. W., Zamani, M., and Huang, N. F. (2019). Endothelial cell Mechanotransduction in the dynamic vascular environment. *Adv. Biosyst.* 3:e1800252. doi: 10.1002/adbi.201800252

Chen, P.-Y., Qin, L., Baeyens, N., Li, G., Afolabi, T., Budatha, M., et al. (2015). Endothelial-to-mesenchymal transition drives atherosclerosis progression. *J. Clin. Invest.* 125, 4514–4528. doi: 10.1172/JCI82719

Chen, P.-Y., Schwartz, M. A., and Simons, M. (2020). Endothelial-to-mesenchymal transition, vascular inflammation, and atherosclerosis. *Front. Cardiovasc. Med.* 7:53. doi: 10.3389/fcvm.2020.00053

Cheng, S.-L., Shao, J.-S., Behrmann, A., Krchma, K., and Towler, D. A. (2013). Dkk1 and MSX2-Wnt7b signaling reciprocally regulate the endothelial-mesenchymal transition in aortic endothelial cells. *Arterioscler. Thromb. Vasc. Biol.* 33, 1679–1689. doi: 10.1161/ATVBAHA.113.300647

Chien, S. (2007). Mechanotransduction and endothelial cell homeostasis: the wisdom of the cell. *Am. J. Physiol. Heart Circ. Physiol.* 292, H1209–H1224. doi: 10.1152/ajpheart.01047.2006

Cho, J. G., Lee, A., Chang, W., Lee, M.-S., and Kim, J. (2018). Endothelial to mesenchymal transition represents a key link in the interaction between inflammation and endothelial dysfunction. *Front. Immunol.* 9:294. doi: 10.3389/fimmu.2018.00294

Clark, C. B., McKnight, N. L., and Frangos, J. A. (2002). Strain and strain rate activation of G proteins in human endothelial cells. *Biochem. Biophys. Res. Commun.* 299, 258–262. doi: 10.1016/S0006-291X(02)02628-1

Clere, N., Renault, S., and Corre, I. (2020). Endothelial-to-mesenchymal transition in cancer. *Front. Cell Dev. Biol.* 8:747. doi: 10.3389/fcell.2020.00747

Cooley, B. C., Nevado, J., Mellad, J., Yang, D., St Hilaire, C., Negro, A., et al. (2014). TGF-β signaling mediates endothelial-to-mesenchymal transition (EndMT) during vein graft remodeling. *Sci. Transl. Med.* 6:227ra34. doi: 10.1126/scitranslmed.3006927

Dahal, S., Huang, P., Murray, B. T., and Mahler, G. J. (2017). Endothelial to mesenchymal transformation is induced by altered extracellular matrix in aortic valve endothelial cells. *J. Biomed. Mater. Res. A* 105, 2729–2741. doi: 10.1002/jbm.a.36133

Dai, G., Kaazempur-Mofrad, M. R., Natarajan, S., Zhang, Y., Vaughn, S., Blackman, B. R., et al. (2004). Distinct endothelial phenotypes evoked by arterial waveforms derived from atherosclerosis-susceptible and -resistant regions of human vasculature. *Proc. Natl. Acad. Sci. U. S. A.* 101, 14871–14876. doi: 10.1073/pnas.0406073101

Dal-Bianco, J. P., Aikawa, E., Bischoff, J., Guerrero, J. L., Handschumacher, M. D., Sullivan, S., et al. (2009). Active adaptation of the tethered mitral valve: insights into a compensatory mechanism for functional mitral regurgitation. *Circulation* 120, 334–342. doi: 10.1161/CIRCULATIONAHA.108.846782

Dal-Bianco, J. P., Aikawa, E., Bischoff, J., Guerrero, J. L., Hjortnaes, J., Beaudoin, J., et al. (2016). Myocardial infarction alters adaptation of the tethered mitral valve. *J. Am. Coll. Cardiol.* 67, 275–287. doi: 10.1016/j.jacc.2015.10.092

Dejana, E., Hirschi, K. K., and Simons, M. (2017). The molecular basis of endothelial cell plasticity. *Nat. Commun.* 8:14361. doi: 10.1038/ncomms14361

Dejana, E., and Lampugnani, M. G. (2018). Endothelial cell transitions. *Science* 362, 746–747. doi: 10.1126/science.aas9432

Demos, C., Williams, D., and Jo, H. (2020). Disturbed flow induces atherosclerosis by Annexin A2-mediated integrin activation. *Circ. Res.* 127, 1091–1093. doi: 10.1161/CIRCRESAHA.120.317909

Depuydt, M. A. C., Prange, K. H. M., Slenders, L., Örd, T., Elbersen, D., Boltjes, A., et al. (2020). Microanatomy of the human atherosclerotic plaque by single-cell Transcriptomics. *Circ. Res.* 127, 1437–1455. doi: 10.1161/CIRCRESAHA.120.316770

Di Carlo, D. (2012). A mechanical biomarker of cell state in medicine. *J. Lab. Autom.* 17, 32–42. doi: 10.1177/2211068211431630

Dobaczewski, M., Chen, W., and Frangogiannis, N. G. (2011). Transforming growth factor (TGF)-β signaling in cardiac remodeling. *J. Mol. Cell. Cardiol.* 51, 600–606. doi: 10.1016/j.yjmcc.2010.10.033

Evrard, S. M., Lecce, L., Michelis, K. C., Nomura-Kitabayashi, A., Pandey, G., Purushothaman, K.-R., et al. (2016). Endothelial to mesenchymal transition is common in atherosclerotic lesions and is associated with plaque instability. *Nat. Commun.* 7:11853. doi: 10.1038/ncomms11853

Farrar, E. J., and Butcher, J. T. (2014). Heterogeneous susceptibility of valve endothelial cells to mesenchymal transformation in response to TNFα. *Ann. Biomed. Eng.* 42, 149–161. doi: 10.1007/s10439-013-0894-3

Fu, X., Khalil, H., Kanisicak, O., Boyer, J. G., Vagnozzi, R. J., Maliken, B. D., et al. (2018). Specialized fibroblast differentiated states underlie scar formation in the infarcted mouse heart. *J. Clin. Invest.* 128, 2127–2143. doi: 10.1172/JCI98215

Gasparics, Á., Rosivall, L., Krizbai, I. A., and Sebe, A. (2016). When the endothelium scores an own goal: endothelial cells actively augment metastatic extravasation through endothelial-mesenchymal transition. *Am. J. Physiol. Heart Circ. Physiol.* 310, H1055–H1063. doi: 10.1152/ajpheart.00042.2016

Gee, T. W., Richards, J. M., Mahmut, A., and Butcher, J. T. (2021). Valve endothelial-interstitial interactions drive emergent complex calcific lesion formation in vitro. *Biomaterials* 269:120669. doi: 10.1016/j.biomaterials.2021.120669

Gijsen, F., Katagiri, Y., Barlis, P., Bourantas, C., Collet, C., Coskun, U., et al. (2019). Expert recommendations on the assessment of wall shear stress in human coronary arteries: existing methodologies, technical considerations, and clinical applications. *Eur. Heart J.* 40, 3421–3433. doi: 10.1093/eurheartj/ehz551

Gordon, E., Schimmel, L., and Frye, M. (2020). The importance of mechanical forces for in vitro endothelial cell biology. *Front. Physiol.* 11:684. doi: 10.3389/fphys.2020.00684

Hove, J. R., Köster, R. W., Forouhar, A. S., Acevedo-Bolton, G., Fraser, S. E., and Gharib, M. (2003). Intracardiac fluid forces are an essential epigenetic factor for embryonic cardiogenesis. *Nature* 421, 172–177. doi: 10.1038/nature01282

Howsmon, D. P., Rego, B. V., Castillero, E., Ayoub, S., Khalighi, A. H., Gorman, R. C., et al. (2020). Mitral valve leaflet response to ischaemic mitral regurgitation: from gene expression to tissue remodelling. *J. R. Soc. Interface* 17:20200098. doi: 10.1098/rsif.2020.0098

Hsu, J. J., Vedula, V., Baek, K. I., Chen, C., Chen, J., Chou, M. I., et al. (2019). Contractile and hemodynamic forces coordinate Notch1b-mediated outflow tract valve formation. *JCI Insight* 5:e124460. doi: 10.1172/jci.insight.124460

Iivanainen, E., Kähäri, V.-M., Heino, J., and Elenius, K. (2003). Endothelial cell–matrix interactions. *Microsc. Res. Tech.* 60, 13–22. doi: 10.1002/jemt.10238

Jiang, X., Li, T., Li, B., Wei, W., Li, F., Chen, S., et al. (2021). SOX7 suppresses endothelial-to-mesenchymal transitions by enhancing VE-cadherin expression during outflow tract development. *Clin. Sci.* 135, 829–846. doi: 10.1042/CS20201496

Kalluri, A. S., Vellarikkal, S. K., Edelman, E. R., Nguyen, L., Subramanian, A., Ellinor, P. T., et al. (2019). Single-cell analysis of the Normal mouse aorta reveals functionally distinct endothelial cell populations. *Circulation* 140, 147–163. doi: 10.1161/CIRCULATIONAHA.118.038362

Kalogirou, S., Malissovas, N., Moro, E., Argenton, F., Stainier, D. Y. R., and Beis, D. (2014). Intracardiac flow dynamics regulate atrioventricular valve morphogenesis. *Cardiovasc. Res.* 104, 49–60. doi: 10.1093/cvr/cvu186

Kalucka, J., de Rooij, L. P. M. H., Goveia, J., Rohlenova, K., Dumas, S. J., Meta, E., et al. (2020). Single-cell transcriptome atlas of murine endothelial cells. *Cell* 180, 764.e20–779.e20. doi: 10.1016/j.cell.2020.01.015

Kim, C. W., Pokutta-Paskaleva, A., Kumar, S., Timmins, L. H., Morris, A. D., Kang, D. W., et al. (2017). Disturbed flow promotes arterial stiffening Through Thrombospondin-1. *Circulation* 136, 1217–1232. doi: 10.1161/CIRCULATIONAHA.116.026361

Kovacic, J. C., Dimmeler, S., Harvey, R. P., Finkel, T., Aikawa, E., Krenning, G., et al. (2019). Endothelial to mesenchymal transition in cardiovascular disease: JACC state-of-the-art review. *J. Am. Coll. Cardiol.* 73, 190–209. doi: 10.1016/j.jacc.2018.09.089

Kovacic, J. C., Mercader, N., Torres, M., Boehm, M., and Fuster, V. (2012). Epithelial-to-mesenchymal and endothelial-to-mesenchymal transition: from cardiovascular development to disease. *Circulation* 125, 1795–1808. doi: 10.1161/CIRCULATIONAHA.111.040352

Kozminsky, M., and Sohn, L. L. (2020). The promise of single-cell mechanophenotyping for clinical applications. *Biomicrofluidics* 14:031301. doi: 10.1063/5.0010800

Krenning, G., Barauna, V. G., Krieger, J. E., Harmsen, M. C., and Moonen, J.-R. A. J. (2016). Endothelial plasticity: shifting phenotypes through force feedback. *Stem Cells Int.* 2016:9762959. doi: 10.1155/2016/9762959

Kryczka, J., Przygodzka, P., Bogusz, H., and Boncela, J. (2017). HMEC-1 adopt the mixed amoeboid-mesenchymal migration type during EndMT. *Eur. J. Cell Biol.* 96, 289–300. doi: 10.1016/j.ejcb.2017.04.002

Lai, B., Li, Z., He, M., Wang, Y., Chen, L., Zhang, J., et al. (2018). Atheroprone flow enhances the endothelial-to-mesenchymal transition. *Am. J. Physiol. Heart Circ. Physiol.* 315, H1293–H1303. doi: 10.1152/ajpheart.00213.2018

Lamalice, L., Le Boeuf, F., and Huot, J. (2007). Endothelial cell migration During angiogenesis. *Circ. Res.* 100, 782–794. doi: 10.1161/01.RES.0000259593.07661.1e

Li, Y., Lui, K. O., and Zhou, B. (2018). Reassessing endothelial-to-mesenchymal transition in cardiovascular diseases. *Nat. Rev. Cardiol.* 15, 445–456. doi: 10.1038/s41569-018-0023-y

Libby, P., Buring, J. E., Badimon, L., Hansson, G. K., Deanfield, J., Bittencourt, M. S., et al. (2019). Atherosclerosis. *Nat. Rev. Dis. Primer* 5:56. doi: 10.1038/s41572-019-0106-z

Liel-Cohen, N., Guerrero, J. L., Otsuji, Y., Handschumacher, M. D., Rudski, L. G., Hunziker, P. R., et al. (2000). Design of a new Surgical Approach for ventricular Remodeling to relieve ischemic mitral regurgitation. *Circulation* 101, 2756–2763. doi: 10.1161/01.CIR.101.23.2756

Lim, G. B. (2021). Macrophages promote endothelial-to-mesenchymal transition after MI. *Nat. Rev. Cardiol.* 18:5. doi: 10.1038/s41569-020-00475-3

Lim, J., Ehsanipour, A., Hsu, J. J., Lu, J., Pedego, T., Wu, A., et al. (2016). Inflammation drives retraction, stiffening, and nodule formation via cytoskeletal machinery in a three-dimensional culture model of aortic stenosis. *Am. J. Pathol.* 186, 2378–2389. doi: 10.1016/j.ajpath.2016.05.003

Ma, J., Sanchez-Duffhues, G., Goumans, M.-J., and Ten Dijke, P. (2020a). TGF-β-induced endothelial to mesenchymal transition in disease and tissue engineering. *Front. Cell Dev. Biol.* 8:260. doi: 10.3389/fcell.2020.00260

Ma, X., Zhao, D., Yuan, P., Li, J., Yun, Y., Cui, Y., et al. (2020b). Endothelial-to-mesenchymal transition in calcific aortic valve disease. *Acta Cardiol. Sin.* 36, 183–194. doi: 10.6515/ACS.202005_36(3).20200213A

Maganti, K., Rigolin, V. H., Sarano, M. E., and Bonow, R. O. (2010). Valvular heart disease: diagnosis and management. *Mayo Clin. Proc.* 85, 483–500. doi: 10.4065/mcp.2009.0706

Mahler, G. J., Farrar, E. J., and Butcher, J. T. (2013). Inflammatory cytokines promote mesenchymal transformation in embryonic and adult valve endothelial cells. *Arterioscler. Thromb. Vasc. Biol.* 33, 121–130. doi: 10.1161/ATVBAHA.112.300504

Mahler, G. J., Frendl, C. M., Cao, Q., and Butcher, J. T. (2014). Effects of shear stress pattern and magnitude on mesenchymal transformation and invasion of aortic valve endothelial cells. *Biotechnol. Bioeng.* 111, 2326–2337. doi: 10.1002/bit.25291

Mahmoud, M. M., Kim, H. R., Xing, R., Hsiao, S., Mammoto, A., Chen, J., et al. (2016). TWIST1 integrates endothelial responses to flow in vascular dysfunction and atherosclerosis. *Circ. Res.* 119, 450–462. doi: 10.1161/CIRCRESAHA.116.308870

Mahmoud, M., Mayer, M., Cancel, L. M., Bartosch, A. M., Mathews, R., and Tarbell, J. M. (2020). The glycocalyx core protein Glypican 1 protects vessel wall endothelial cells from stiffness-mediated dysfunction and disease. *Cardiovasc. Res.* 117, 1592–1605. doi: 10.1093/cvr/cvaa201

Mahmoud, M. M., Serbanovic-Canic, J., Feng, S., Souilhol, C., Xing, R., Hsiao, S., et al. (2017). Shear stress induces endothelial-to-mesenchymal transition via the transcription factor snail. *Sci. Rep.* 7:3375. doi: 10.1038/s41598-017-03532-z

Maleszewska, M., Moonen, J.-R. A. J., Huijkman, N., van de Sluis, B., Krenning, G., and Harmsen, M. C. (2013). IL-1β and TGFβ2 synergistically induce endothelial to mesenchymal transition in an NFκB-dependent manner. *Immunobiology* 218, 443–454. doi: 10.1016/j.imbio.2012.05.026

Marwick, T. H., Lancellotti, P., and Pierard, L. (2009). Ischaemic mitral regurgitation: mechanisms and diagnosis. *Heart* 95, 1711–1718. doi: 10.1136/hrt.2007.135335

Mehta, V., Pang, K.-L., Givens, C. S., Chen, Z., Huang, J., Sweet, D. T., et al. (2021). Mechanical forces regulate endothelial-to-mesenchymal transition and atherosclerosis via an Alk5-Shc mechanotransduction pathway. *Sci. Adv.* 7:eabg5060. doi: 10.1126/sciadv.abg5060

Mehta, V., Pang, K.-L., Rozbesky, D., Nather, K., Keen, A., Lachowski, D., et al. (2020). The guidance receptor plexin D1 is a mechanosensor in endothelial cells. *Nature* 578, 290–295. doi: 10.1038/s41586-020-1979-4

Methe, H., Balcells, M., del Carmen Alegret, M., Santacana, M., Molins, B., Hamik, A., et al. (2007). Vascular bed origin dictates flow pattern regulation of endothelial adhesion molecule expression. *Am. J. Physiol. Heart Circ. Physiol.* 292, H2167–H2175. doi: 10.1152/ajpheart.00403.2006

Mohler, E. R. (2004). Mechanisms of aortic valve calcification. *Am. J. Cardiol.* 94, 1396–1402. doi: 10.1016/j.amjcard.2004.08.013

Monteiro, J. P., Rodor, J., Caudrillier, A., Scanlon, J. P., Spiroski, A.-M., Dudnakova, T., et al. (2021). MIR503HG loss promotes endothelial-to-mesenchymal transition in vascular disease. *Circ. Res.* 128, 1173–1190. doi: 10.1161/CIRCRESAHA.120.318124

Moonen, J.-R. A. J., Lee, E. S., Schmidt, M., Maleszewska, M., Koerts, J. A., Brouwer, L. A., et al. (2015). Endothelial-to-mesenchymal transition contributes to fibro-proliferative vascular disease and is modulated by fluid shear stress. *Cardiovasc. Res.* 108, 377–386. doi: 10.1093/cvr/cvv175

Naruse, K., and Sokabe, M. (1993). Involvement of stretch-activated ion channels in Ca2+ mobilization to mechanical stretch in endothelial cells. *Am. J. Physiol.-Cell Physiol.* 264, C1037–C1044. doi: 10.1152/ajpcell.1993.264.4.C1037

Newman, A. A. C., Serbulea, V., Baylis, R. A., Shankman, L. S., Bradley, X., Alencar, G. F., et al. (2021). Multiple cell types contribute to the atherosclerotic lesion fibrous cap by PDGFRβ and bioenergetic mechanisms. *Nat. Metab.* 3, 166–181. doi: 10.1038/s42255-020-00338-8

Osborne, L. D., Li, G. Z., How, T., O'Brien, E. T., Blobe, G. C., Superfine, R., et al. (2014). TGF-β regulates LARG and GEF-H1 during EMT to affect stiffening response to force and cell invasion. *Mol. Biol. Cell* 25, 3528–3540. doi: 10.1091/mbc.E14-05-1015

Panková, K., Rösel, D., Novotný, M., and Brábek, J. (2010). The molecular mechanisms of transition between mesenchymal and amoeboid invasiveness in tumor cells. *Cell. Mol. Life Sci.* 67, 63–71. doi: 10.1007/s00018-009-0132-1

Pei, D., Shu, X., Gassama-Diagne, A., and Thiery, J. P. (2019). Mesenchymal–epithelial transition in development and reprogramming. *Nat. Cell Biol.* 21, 44–53. doi: 10.1038/s41556-018-0195-z

Peng, Z., Shu, B., Zhang, Y., and Wang, M. (2019). Endothelial response to pathophysiological stress. *Arterioscler. Thromb. Vasc. Biol.* 39, e233–e243. doi: 10.1161/ATVBAHA.119.312580

Pérez, L., Muñoz-Durango, N., Riedel, C. A., Echeverría, C., Kalergis, A. M., Cabello-Verrugio, C., et al. (2017). Endothelial-to-mesenchymal transition: cytokine-mediated pathways that determine endothelial fibrosis under inflammatory conditions. *Cytokine Growth Factor Rev.* 33, 41–54. doi: 10.1016/j.cytogfr.2016.09.002

Piera-Velazquez, S., and Jimenez, S. A. (2019). Endothelial to mesenchymal transition: role in physiology and in the pathogenesis of human diseases. *Physiol. Rev.* 99, 1281–1324. doi: 10.1152/physrev.00021.2018

Pinto, M. T., Covas, D. T., Kashima, S., and Rodrigues, C. O. (2016). Endothelial mesenchymal transition: comparative analysis of different induction methods. *Biol. Proceed. Online* 18:10. doi: 10.1186/s12575-016-0040-3

Qi, D., Kaur Gill, N., Santiskulvong, C., Sifuentes, J., Dorigo, O., Rao, J., et al. (2015). Screening cell mechanotype by parallel microfiltration. *Sci. Rep.* 5:17595. doi: 10.1038/srep17595

Rieder, F., Kessler, S. P., West, G. A., Bhilocha, S., de la Motte, C., Sadler, T. M., et al. (2011). Inflammation-induced endothelial-to-mesenchymal transition: a novel mechanism of intestinal fibrosis. *Am. J. Pathol.* 179, 2660–2673. doi: 10.1016/j.ajpath.2011.07.042

Sánchez-Duffhues, G., García de Vinuesa, A., and ten Dijke, P. (2018). Endothelial-to-mesenchymal transition in cardiovascular diseases: developmental signaling pathways gone awry. *Dev. Dyn.* 247, 492–508. doi: 10.1002/dvdy.24589

Sánchez-Duffhues, G., García de Vinuesa, A., van de Pol, V., Geerts, M. E., de Vries, M. R., Janson, S. G., et al. (2019). Inflammation induces endothelial-to-mesenchymal transition and promotes vascular calcification through downregulation of BMPR2. *J. Pathol.* 247, 333–346. doi: 10.1002/path.5193

Sancho, A., Vandersmissen, I., Craps, S., Luttun, A., and Groll, J. (2017). A new strategy to measure intercellular adhesion forces in mature cell-cell contacts. *Sci. Rep.* 7:46152. doi: 10.1038/srep46152

Schwartz, M. A., and DeSimone, D. W. (2008). Cell adhesion receptors in mechanotransduction. *Curr. Opin. Cell Biol.* 20, 551–556. doi: 10.1016/j.ceb.2008.05.005

Suzuki, T., Carrier, E. J., Talati, M. H., Rathinasabapathy, A., Chen, X., Nishimura, R., et al. (2017). Isolation and characterization of endothelial-to-mesenchymal transition cells in pulmonary arterial hypertension. *Am. J. Physiol. Lung Cell. Mol. Physiol.* 314, L118–L126. doi: 10.1152/ajplung.00296.2017

Thodeti, C. K., Matthews, B., Ravi, A., Mammoto, A., Ghosh, K., Bracha, A. L., et al. (2009). TRPV4 channels mediate cyclic strain-induced endothelial cell reorientation through integrin-to-integrin signaling. *Circ. Res.* 104, 1123–1130. doi: 10.1161/CIRCRESAHA.108.192930

Tian, Y., Gawlak, G., O'Donnell, J. J. 3rd, Birukova, A. A., and Birukov, K. G. (2016). Activation of vascular endothelial growth factor (VEGF) receptor 2

mediates endothelial permeability caused by cyclic stretch. *J. Biol. Chem.* 291, 10032–10045. doi: 10.1074/jbc.M115.690487

Tombor, L., John, D., Glaser, S. F., Luxan, G., Forte, E., Furtado, M., et al. (2020). Single cell sequencing reveals endothelial plasticity with transient mesenchymal activation after myocardial infarction. *Eur. Heart J.* 41:ehaa946.3736. doi: 10.1093/ehjci/ehaa946.3736

Tombor, L. S., John, D., Glaser, S. F., Luxán, G., Forte, E., Furtado, M., et al. (2021). Single cell sequencing reveals endothelial plasticity with transient mesenchymal activation after myocardial infarction. *Nat. Commun.* 12:681. doi: 10.1038/s41467-021-20905-1

Ubil, E., Duan, J., Pillai, I. C. L., Rosa-Garrido, M., Wu, Y., Bargiacchi, F., et al. (2014). Mesenchymal–endothelial transition contributes to cardiac neovascularization. *Nature* 514, 585–590. doi: 10.1038/nature13839

Viemann, D., Goebeler, M., Schmid, S., Nordhues, U., Klimmek, K., Sorg, C., et al. (2006). TNF induces distinct gene expression programs in microvascular and macrovascular human endothelial cells. *J. Leukoc. Biol.* 80, 174–185. doi: 10.1189/jlb.0905530

von Gise, A., and Pu, W. T. (2012). Endocardial and Epicardial epithelial to mesenchymal transitions in heart development and disease. *Circ. Res.* 110, 1628–1645. doi: 10.1161/CIRCRESAHA.111.259960

Weixler, V., Marx, G. R., Hammer, P. E., Emani, S. M., del Nido, P. J., and Friehs, I. (2020). Flow disturbances and the development of endocardial fibroelastosis. *J. Thorac. Cardiovasc. Surg.* 159, 637–646. doi: 10.1016/j.jtcvs.2019.08.101

Welch-Reardon, K. M., Wu, N., and Hughes, C. C. (2015). A role for partial endothelial–mesenchymal transitions in angiogenesis? *Arterioscler. Thromb. Vasc. Biol.* 35, 303–308. doi: 10.1161/ATVBAHA.114.303220

Xu, X., Friehs, I., Zhong Hu, T., Melnychenko, I., Tampe, B., Alnour, F., et al. (2015). Endocardial Fibroelastosis is caused by aberrant endothelial to mesenchymal transition. *Circ. Res.* 116, 857–866. doi: 10.1161/CIRCRESAHA.116.305629

Xu, K., Xie, S., Huang, Y., Zhou, T., Liu, M., Zhu, P., et al. (2020). Cell-type transcriptome atlas of human aortic valves reveal cell heterogeneity and endothelial to mesenchymal transition involved in calcific aortic valve disease. *Arterioscler. Thromb. Vasc. Biol.* 40, 2910–2921. doi: 10.1161/ATVBAHA.120.314789

Yao, J., Guihard, P. J., Blazquez-Medela, A. M., Guo, Y., Moon, J. H., Jumabay, M., et al. (2015). Serine protease activation essential for endothelial-mesenchymal transition in vascular calcification. *Circ. Res.* 117, 758–769. doi: 10.1161/CIRCRESAHA.115.306751

Yutzey, K. E., Demer, L. L., Body, S. C., Huggins, G. S., Towler, D. A., Giachelli, C. M., et al. (2014). Calcific aortic valve disease. *Arterioscler. Thromb. Vasc. Biol.* 34, 2387–2393. doi: 10.1161/ATVBAHA.114.302523

Zeisberg, E. M., Tarnavski, O., Zeisberg, M., Dorfman, A. L., McMullen, J. R., Gustafsson, E., et al. (2007). Endothelial-to-mesenchymal transition contributes to cardiac fibrosis. *Nat. Med.* 13, 952–961. doi: 10.1038/nm1613

Zhang, H., Huang, X., Liu, K., Tang, J., He, L., Pu, W., et al. (2017). Fibroblasts in an endocardial fibroelastosis disease model mainly originate from mesenchymal derivatives of epicardium. *Cell Res.* 27, 1157–1177. doi: 10.1038/cr.2017.103

Zhang, H., Lui, K. O., and Zhou, B. (2018). Endocardial cell plasticity in cardiac development, diseases and regeneration. *Circ. Res.* 122, 774–789. doi: 10.1161/CIRCRESAHA.117.312136

Zhang, C., Zhou, T., Chen, Z., Yan, M., Li, B., Lv, H., et al. (2020). Coupling of integrin α5 to Annexin A2 by flow drives endothelial activation. *Circ. Res.* 127, 1074–1090. doi: 10.1161/CIRCRESAHA.120.316857

Zhao, R., Sider, K. L., and Simmons, C. A. (2011). Measurement of layer-specific mechanical properties in multilayered biomaterials by micropipette aspiration. *Acta Biomater.* 7, 1220–1227. doi: 10.1016/j.actbio.2010.11.004

Zhong, A., Mirzaei, Z., and Simmons, C. A. (2018). The roles of matrix stiffness and ß-catenin Signaling in endothelial-to-mesenchymal transition of aortic valve endothelial cells. *Cardiovasc. Eng. Technol.* 9, 158–167. doi: 10.1007/s13239-018-0363-0

Conflict of Interest: The authors declare that the research was conducted in the absence of any commercial or financial relationships that could be construed as a potential conflict of interest.

Publisher's Note: All claims expressed in this article are solely those of the authors and do not necessarily represent those of their affiliated organizations, or those of the publisher, the editors and the reviewers. Any product that may be evaluated in this article, or claim that may be made by its manufacturer, is not guaranteed or endorsed by the publisher.

frontiers in Physiology

ORIGINAL RESEARCH
published: 04 October 2021
doi: 10.3389/fphys.2021.732564

Cell Type Dependent Suppression of Inflammatory Mediators by Myocardin Related Transcription Factors

*Li Liu[1,2†], Elisabeth Bankell[1†], Catarina Rippe[1], Björn Morén[1], Karin G. Stenkula[1], Bengt-Olof Nilsson[1] and Karl Swärd[1]**

[1] Department of Experimental Medical Science, Lund, Sweden, [2] Department of Urology, Qingyuan People's Hospital, The Sixth Affiliated Hospital of Guangzhou Medical University, Qingyuan, China

OPEN ACCESS

Edited by:
Markus Hecker,
Heidelberg University, Germany

Reviewed by:
Thomas Korff,
Heidelberg University, Germany
Brenda Lilly,
The Research Institute at Nationwide Children's Hospital, United States

***Correspondence:**
Karl Swärd
karl.sward@med.lu.se

[†] These authors have contributed equally to this work and share first authorship

Specialty section:
This article was submitted to Vascular Physiology, a section of the journal Frontiers in Physiology

Received: 29 June 2021
Accepted: 07 September 2021
Published: 04 October 2021

Citation:
Liu L, Bankell E, Rippe C, Morén B, Stenkula KG, Nilsson B-O and Swärd K (2021) Cell Type Dependent Suppression of Inflammatory Mediators by Myocardin Related Transcription Factors. Front. Physiol. 12:732564. doi: 10.3389/fphys.2021.732564

Myocardin related transcription factors (MRTFs: MYOCD/myocardin, MRTF-A, and MRTF-B) play a key role in smooth muscle cell differentiation by activating contractile genes. In atherosclerosis, MRTF levels change, and most notable is a fall of MYOCD. Previous work described anti-inflammatory properties of MRTF-A and MYOCD, occurring through RelA binding, suggesting that MYOCD reduction could contribute to vascular inflammation. Recent studies have muddled this picture showing that MRTFs may show both anti- and pro-inflammatory properties, but the basis of these discrepancies remain unclear. Moreover, the impact of MRTFs on inflammatory signaling pathways in tissues relevant to human arterial disease is uncertain. The current work aimed to address these issues. RNA-sequencing after forced expression of myocardin in human coronary artery smooth muscle cells (hCASMCs) showed reduction of pro-inflammatory transcripts, including *CCL2*, *CXCL8*, *IL6*, and *IL1B*. Side-by-side comparison of MYOCD, MRTF-A, and MRTF-B in hCASMCs, showed that the anti-inflammatory impact was shared among MRTFs. Correlation analyses using human arterial transcriptomic datasets revealed negative correlations between *MYOCD*, *MRTFA*, and *SRF*, on the one hand, and the inflammatory transcripts, on the other. A pro-inflammatory drive from lipopolysaccharide, did not change the size of the suppressive effect of MRTF-A in hCASMCs on either mRNA or protein levels. To examine cell type-dependence, we compared the anti-inflammatory impact in hCASMCs, with that in human bladder SMCs, in endothelial cells, and in monocytes (THP-1 cells). Surprisingly, little anti-inflammatory activity was seen in endothelial cells and monocytes, and in bladder SMCs, MRTF-A was pro-inflammatory. *CXCL8*, *IL6*, and *IL1B* were increased by the MRTF-SRF inhibitor CCG-1423 and by MRTF-A silencing in hCASMCs, but depolymerization of actin, known to inhibit MRTF activity, had no stimulatory effect, an exception being *IL1B*. Co-immunoprecipitation supported binding of MRTF-A to RelA, supporting sequestration of this important pro-inflammatory mediator as a

mechanism. Dexamethasone treatment and silencing of RelA (by 76 ± 1%) however only eliminated a fraction of the MRTF-A effect (≈25%), suggesting mechanisms beyond RelA binding. Indeed, SRF silencing suggested that MRTF-A suppression of *IL1B* and *CXCL8* depends on SRF. This work thus supports an anti-inflammatory impact of MRTF-SRF signaling in hCASMCs and in intact human arteries, but not in several other cell types.

Keywords: cytokines, inflammation, atherosclerosis, human coronary artery, myocardin related transcription factor, differentiation

INTRODUCTION

There has been an intense focus on inflammation as an important driver of atherosclerosis in recent decades (Libby and Hansson, 2019), and it has been demonstrated that knockout of certain chemokines, including monocyte chemoattractant protein-1 (MCP-1 or *CCL2*), reduces atherosclerosis (Gu et al., 1998). Indeed, support for the involvement of MCP-1 (*CCL2*) in the etiology of human cardiovascular disease is strong (McDermott et al., 2005; Georgakis et al., 2019). Moreover, neutralization of the cytokine interleukin 1β (*IL1B*) was shown to reduce non-fatal myocardial infarction, non-fatal stroke, or cardiovascular death (Ridker et al., 2017), all of which are penultimate manifestations of atherosclerosis. The cellular source of the cytokines that promote atherosclerosis is uncertain, but an emerging concept is that plasticity of the resident cells of the vascular wall, including smooth muscle cells (SMCs), may allow for chemokine and cytokine release along with lipid engorgement to promote atherogenesis (Allahverdian et al., 2018; Grootaert and Bennett, 2021).

Myocardin related transcription factors (MRTFs), including myocardin (*MYOCD*), MRTF-A (*MRTFA*), and MRTF-B (*MRTFB*), act together with serum response factor (*SRF*) to drive muscle cell transcription and differentiation (Miano, 2003, 2015; Owens et al., 2004; Parmacek, 2007; Olson and Nordheim, 2010). MRTF-A and MRTF-B are regulated by actin dynamics (Miralles et al., 2003; Staus et al., 2007; Olson and Nordheim, 2010), and by stretch and matrix stiffness (Cui et al., 2015; Hadden et al., 2017), such that they become activated and translocated to the nucleus when actin is polymerized. This allows cells to adapt to mechanical cues. MYOCD shows constitutive nuclear expression, and is considered a master regulator of smooth muscle cell (SMC) differentiation (Owens et al., 2004). However, its expression level falls when SMCs undergo modulation toward a synthetic phenotype (Minami et al., 2012; Ackers-Johnson et al., 2015), and this was found to represent a causal mechanism in atherosclerosis (Ackers-Johnson et al., 2015).

Several studies have documented anti-inflammatory influences of MRTFs. Wang et al. (2012) demonstrated that bone morphogenetic protein 4 (BMP4) reduces the inflammatory mediators *IL1B*, *CXCL2*, and *CCL8* in human pulmonary artery SMCs via MRTF-A. This involves the C-terminus of MRTF-A, and suppression of a NF-κB-RelA-driven inflammation independently of SRF. Moreover, in subsequent work, it was found that MYOCD shares this anti-inflammatory property. Heterozygous MYOCD deficiency amplified surges of *IL6* and *CCL2* following stimulation of mouse aortic SMCs with interleukin 1β (Ackers-Johnson et al., 2015), and it accelerated atherosclerosis (Ackers-Johnson et al., 2015; Xia et al., 2021). MYOCD's role as a guardian against atherosclerosis may thus depend in part on its anti-inflammatory impact in SMCs (Ackers-Johnson et al., 2015), and this may occur through RelA antagonism (Tang et al., 2008; Wang et al., 2012).

While the studies cited above support an anti-inflammatory impact of MRTFs in the vascular wall, other reports have complicated this picture. One study, using rat vascular SMCs found that MRTF-A activates *Il6*, *Il1b*, and *Ccl2* promoter activity (Yang et al., 2014), while another study found that MRTF-A aggravates lipopolysaccharide- (LPS) induced pro-inflammatory transcription in murine and human macrophages through epigenetic mechanisms (Yu et al., 2014). More recently MRTF-A was shown to enhance the angiotensin II-induced inflammatory response and aortic dissection (Ito et al., 2020; Gao et al., 2021). The basis for these apparently contradictory effects of MRTFs is unclear, but may relate to the MRTF family member studied, the cell type or species, or the pro-inflammatory stimulus. Given that atherosclerosis is such a prevalent and costly disease, it is important to clarify the cell type-dependence of the inflammatory impact of MRTFs, if all MRTFs share the same property in the same cell type, and whether the influence of MRTFs in the human coronary artery is pro- or anti-inflammatory.

RESULTS

Myocardin Related Transcription Factors Share an Anti-inflammatory Impact

In a parallel study (submitted to the same thematic issue of this journal, Liu et al., 2021), we generated an RNA-sequencing (RNA-seq) dataset after viral overexpression of myocardin (MYOCD) in human coronary artery SMCs (hCASMCs) for 8 days. Thousands of transcripts were differentially expressed, and among them, numerous inflammatory mediators stood out as being robustly reduced (**Figure 1A**, adjusted $P < 0.0001$ throughout). Among the 13 transcripts plotted in **Figure 1A**, *CXCL8* and *CSF3* were most prominently reduced (by 97.8 ± 0.3% and by 98.6 ± 0.4%, respectively), but several were repressed by > 50%. In view of divergent findings in the literature regarding the inflammatory impact of MRTFs, we set out to examine whether repression of inflammatory mediators was a shared property among the MRTFs in the same cell type. Indeed, in side-by-side adenoviral

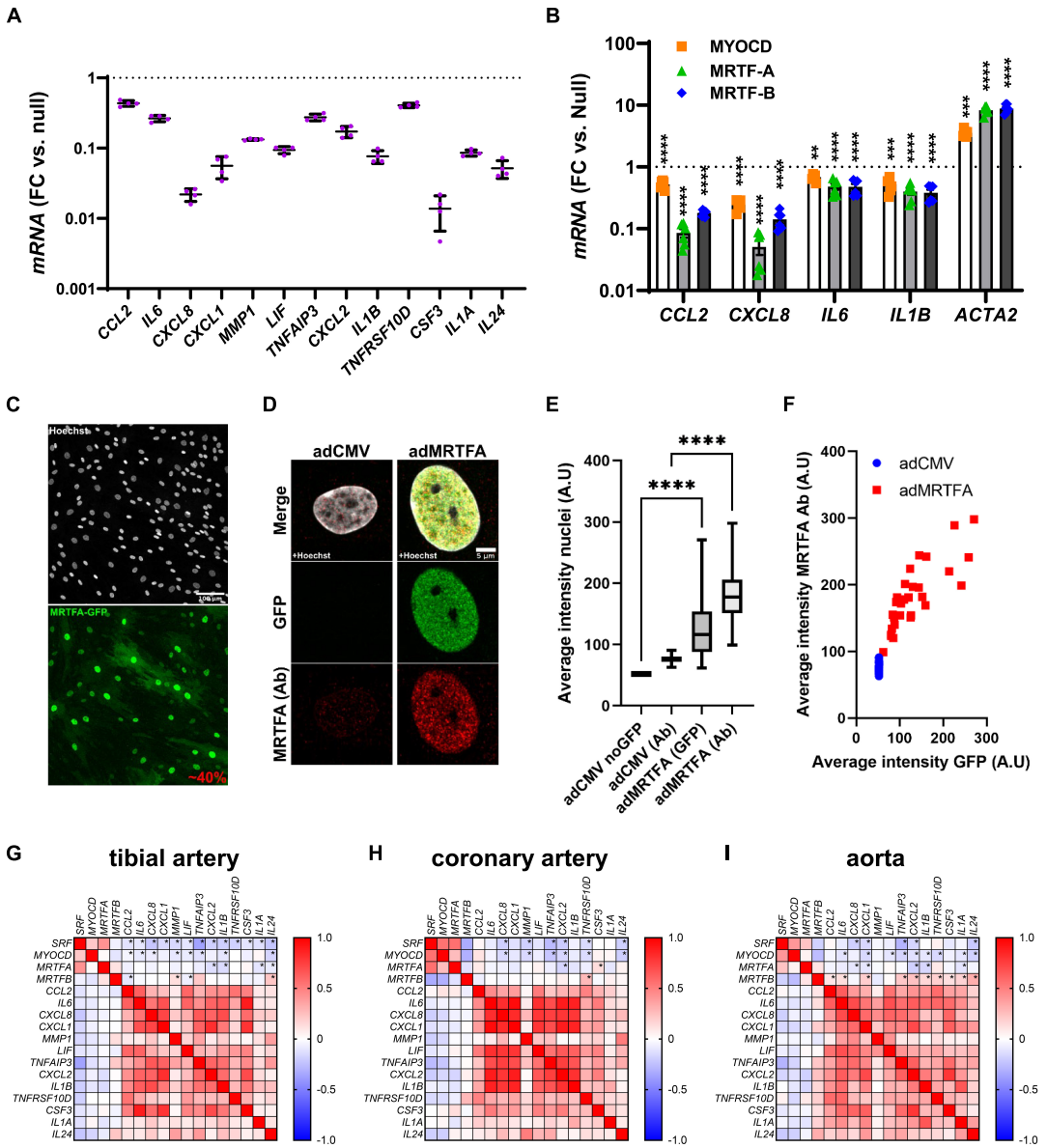

FIGURE 1 | Anti-inflammatory effect of all MRTFs in human coronary artery smooth muscle cells (SMCs). **(A)** Shows mRNA levels for 13 inflammatory mediators in cultured human coronary artery smooth muscle cells (hCASMCs) after myocardin overexpression using an adenovirus (Ad-CMV-MYOCD). FC: fold change; null: Ad-CMV-null virus. Data is from an RNA-sequencing experiments conducted in a parallel study, and the control level is indicated by the dotted line. All changes were significant at an adjusted $P < 0.0001$. Suppression of inflammatory markers by myocardin (MYOCD) confirms previous studies and stimulated us to consider if this property is shared by all MRTFs. Side-by-side adenoviral transductions suggested that MTRF-A and MRTF-B have the same effect in the same cell type (hCASMCs, **(B)**). Confocal imaging showed that 40% of the cells were positive for overexpressed MRTF-A as shown using an eGFP tagged construct **(C)** and a general nuclear stain (Hoechst). In **(D)**, overexpressed and endogenous MRTF-A were labeled separately using the eGFP tag and an antibody, respectively. Quantification showed that nuclear labeling increased after viral transduction **(E)**, as expected, and the nuclear intensity of labeling in the GFP channel increased linearly with MRTF-A antibody staining **(F)**. We also examined correlations at the mRNA level in human arteries **(G–I)**. RNA-seq data was downloaded from the GTExPortal.org and correlation matrices were generated in GraphPad Prism using the Pearson method. Negative correlations (negative *R*-values, blue fills) were seen for *SRF* and *MYOCD* vs. inflammatory mediators in all arteries. Significant correlations are indicated by (*) for the first four rows in each matrix. *MRTFA* performed less well than *MYOCD* and *SRF* with only a handful significant and negative correlations in each artery. *MRTFB* performed poorly, and in this case many correlations were positive. These findings suggested a more pronounced anti-inflammatory impact of *MYOCD*, and *MRTFA* compared to *MRTFB* in the intact human vascular wall, despite similar effects upon overexpression *in vitro*. $^{**}P < 0.01$, $^{***}P < 0.001$, $^{****}P < 0.0001$.

transductions (**Figure 1B**), MYOCD, MRTF-A, and MRTF-B, all reduced *CCL2*, *CXCL8*, *IL6*, and *IL1B* in hCASMCs in comparison to a null construct (Ad-CMV-null or Ad-CMV). Effect sizes varied somewhat (MRTF-A > MRTF-B > MYOCD for *CCL2* and *CXCL8*), but these differences were at least partly reflected in the positive control (*ACTA2*). Taken together, these

findings argue that suppression of inflammation is a shared property among the MRTFs, with only modest differences in effect between individual co-activators in the same family.

The sizeable (>90%) suppression of *CXCL8* and *CSF3* expression by MRTFs was notable because in the past we have seen that only 30–50% of the cells are positive for virally overexpressed MRTFs. We therefore examined transduction efficiency under the current experimental conditions. This was done by labeling of nuclei using Hoechst staining, and by simultaneous labeling of MRTF-A with an antibody and a GFP tag. The GFP tag should report overexpressed MRTF-A, while the antibody should mirror total MRTF-A (overexpressed and endogenous). Low magnification imaging showed that 40% of all nuclei were positive for GFP (**Figure 1C**, two independent experiments). Diffuse cytoplasmic staining was evident in many cells, but nuclear staining was more intense. High magnification imaging focusing on nuclei showed faint endogenous MRTF-A (antibody) staining in nuclei in control conditions (**Figure 1D**, left). After overexpression of MRTF-A, both GFP and antibody staining was more intense (**Figure 1D**, right). Quantification showed that both labels increased in nuclei after transduction (**Figure 1E**), and the association between nuclear GFP intensity and antibody labeling approached a linear relationship (**Figure 1F**). In all, these findings indicate that MRTF-A is exerting its anti-inflammatory action either inside nuclei or in the cytoplasm, and that suppression of some inflammatory mediators is greater than would be predicted from transduction efficiency (≈40%). The latter finding suggests that MRTF-A antagonizes autocrine and paracrine inflammatory feedback loops in cell culture.

Myocardin and MRTF-A Correlate Negatively With Inflammatory Markers in Human Arteries

Our cell culture findings prompted us to examine correlations between MRTFs and inflammatory mediators in human arteries. For this, human RNA-seq data was downloaded from the GTExPortal.org and MRTFs were correlated with the inflammatory mediators identified in **Figure 1A**. We focused initially on the tibial artery because this dataset was the largest (n = 663). As expected, negative (blue fills) associations were seen when *MYOCD* was correlated with the inflammatory mediators (**Figure 1G**, second row in matrix). Similar analyses for *MRTFA* uncovered four negative correlations that reached the level of significance (**Figure 1G**, third row). Somewhat to our surprise, *SRF* performed at least as well as *MYOCD* (**Figure 1G**, top row), and *MRTFB* performed considerably worse than *MYOCD*, despite similar or better repression of inflammatory mediators in SMCs *in vitro* (compare **Figures 1G,B**). Analyses in the remaining two arteries in the database (coronary artery: n = 240, aorta: n = 432), largely echoed findings in the tibial artery (**Figures 1H,I**), but also emphasized that *MRTFB*, in contrast to *MYOCD* and *MRTFA*, often correlates positively with inflammatory transcripts. Taken together, these analyses suggest that MYOCD and MRTF-A, may dampen inflammation in human arteries *in situ*. We focused the remainder of this work on MRTF-A because its activity is amenable to therapy using small molecules, and because it appeared somewhat more effective *in vitro* than the other MRTFs.

Lipopolysaccharide Does Not Affect Suppression of Inflammatory Mediators by MRTF-A

A possible basis for discrepant effects of MRTFs on inflammation in different studies could be the inflammatory status of the cells. To address this possibility, we next compared the effect of MRTF-A in basal conditions, and under pro-inflammatory stimulation with lipopolysaccharide (LPS, 500 ng/ml), a bacterial cell wall component that activates toll-like receptor (TLR4) signaling. Using hCASMCs, all the inflammatory mediators were increased at the mRNA level by LPS. However, inflammatory suppression by MRTF-A was similar in the absence and presence of LPS. *CCL2* for example, was reduced eightfold by MRTF-A under basal conditions and sevenfold in the presence of LPS (**Figure 2A**, leftmost bars). Similar results were seen for the remainder of the inflammatory mediators studied (*CXCL8*, *IL6*, and *IL1B*, **Figure 2A**). This argued against inflammatory status as a critical factor for the direction of the effect.

Next, to ascertain that inflammatory changes at the mRNA level associate with protein level changes, we generated western blots for MCP-1 (*CCL2*), and IL-8 (*CXCL8*). MCP-1 migrated as two bands between 12 and 14 kDa, and both bands were reduced by MRTF-A in the presence and absence of LPS (**Figure 2B**). Similar overall suppression by MRTF-A was obtained for the IL-8 protein in western blots (**Figure 2C**). In keeping with the western blot results, we also found that MRTF-A reduced the levels of MCP-1 and IL-8 in cell lysates when determined using ELISAs (**Figures 2D,E**). MRTF-A-driven changes at the mRNA and protein levels therefore mirror each other.

The Anti-inflammatory Impact of MRTF-A Is Cell Type Dependent

Our findings so far showed that MRTFs share an anti-inflammatory influence, and that this effect is largely independent of inflammatory status, even if the impact of different MRTFs appears to differ considerably in the intact vascular wall. It remained possible that the cell type could matter, and it is indeed known that while MYOCD is enriched in SMCs, MRTF-A and MRTF-B are more widely expressed. We therefore next compared hCASMC with an unrelated human SMC type (bladder, hBSMC), with coronary artery endothelial cells (hCAEC), and with monocytes (THP-1 cells). Strikingly, the effects on *CXCL8*, *IL6*, and *IL1B* differed depending on cell type. Inflammatory suppression was again seen in hCASMCs as expected (**Figure 3A**), but in hBSMC (**Figure 3B**) most of the inflammatory transcripts were increased rather than decreased. In hCAEC, only two inflammatory markers changed, but in opposite directions (**Figure 3C**). Finally, no anti-inflammatory effect was seen in THP-1 cells even if the positive control (*MRTFA*) increased dramatically (**Figure 3D**). Thus, the inflammatory impact of MRTFs seems to be highly cell type dependent.

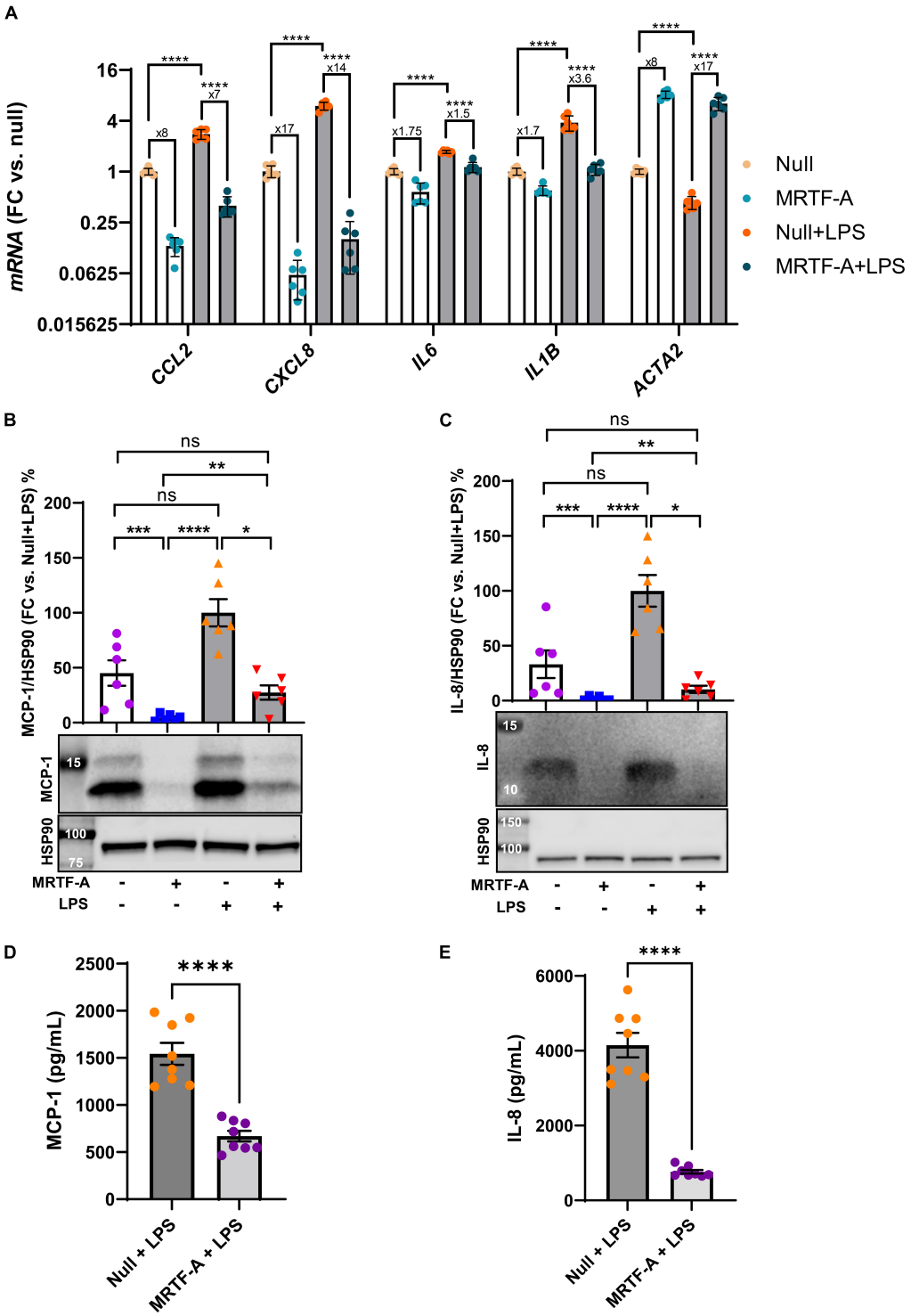

FIGURE 2 | The anti-inflammatory impact of MRTF-A is maintained in pro-inflammatory conditions. **(A)** Human coronary artery smooth muscle cells in culture were transduced with Null and MRTF-A viruses in control conditions (open bars), or with simultaneous treatment with lipopolysaccharide (LPS, 500 ng/ml), to mimic a pro-inflammatory environment (gray bars). After harvesting the cells, RNA was isolated, and inflammatory transcripts were assayed using RT-qPCR. The fold repression by MRTF-A is indicated below the asterisks that indicate significance, showing that MRTF-A was similarly effective in the absence and presence of LPS. *CCL2* for example was reduced eightfold in control conditions and sevenfold in LPS treated cells, and an independent analysis indicated that this difference was not significant. To support MRTF-dependent reductions of inflammatory mediators at the protein level, MCP-1 (*CCL2*, **(B,D)**) and IL-8 (*CXCL8*, **(C,E)**) were examined using western blotting **(B,C)** and ELISAs **(D,E)**. All assays indicted significant MRTF-A-dependent reductions at the protein level, both in the absence and presence of LPS. **P* < 0.05, ***P* < 0.01, ****P* < 0.001, *****P* < 0.0001.

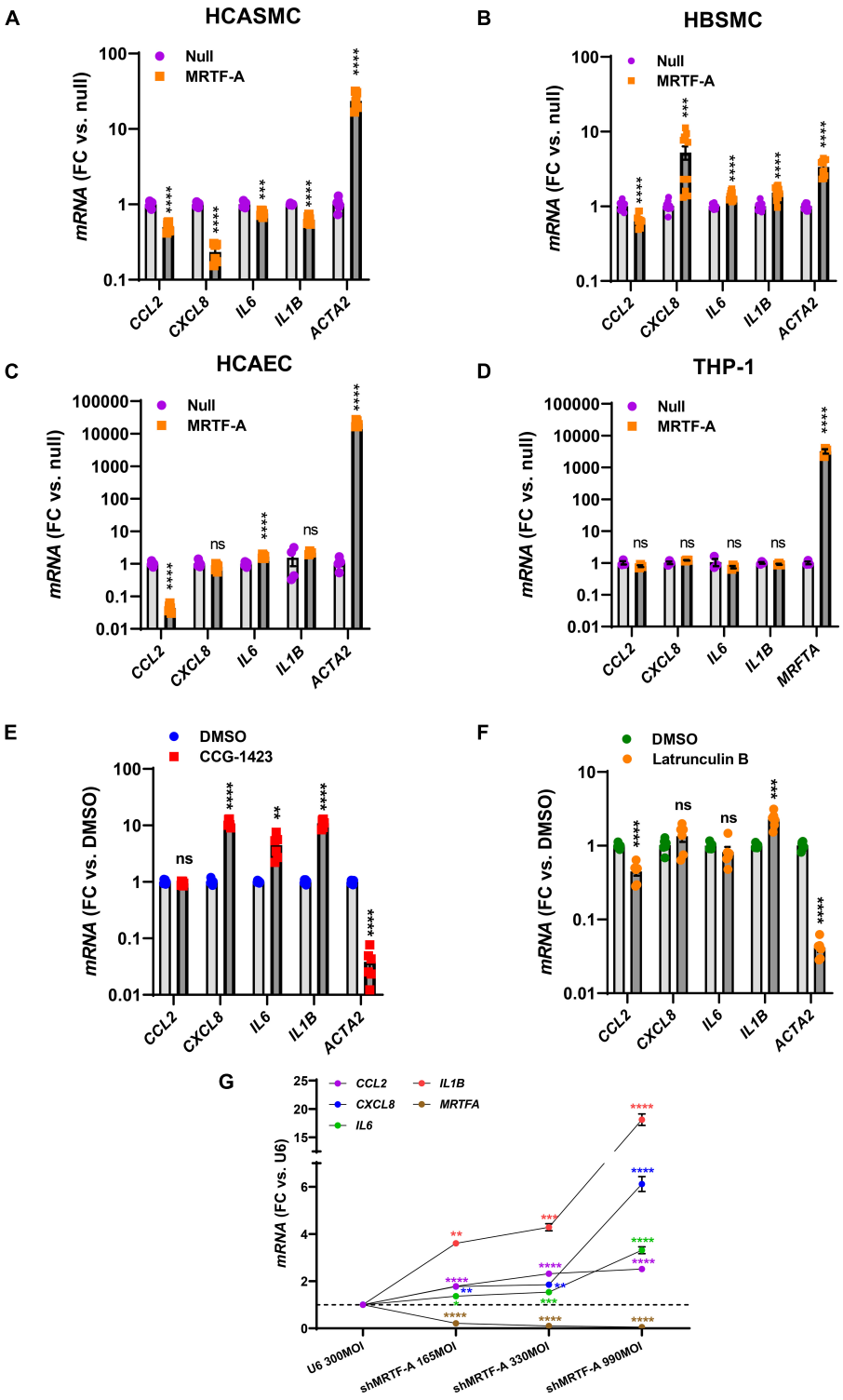

FIGURE 3 | The anti-inflammatory impact of MRTF-A is cell type-dependent. To compare the impact of MRTF-A on inflammation in different cell types, MRTF-A was overexpressed using an adenoviral vector, and using a null vector as control. **(A–D)** Show the effect of MRTF-A on *CCL2*, *CXCL8*, *IL6*, and *IL1B* in human coronary artery SMCs (hCASMC, **(A)**), human bladder SMCs (hBSMC, **(B)**), human coronary artery endothelial cells (hCAEC, **(C)**), and monocytes (THP-1 cells, **(D)**). *ACTA2* was used as positive control in all panels except for THP-1 cells where we instead assayed *MRTFA* itself. **(E)** Shows the effect of the MRTF inhibitor CCG-1423 (10 μM) in hCASMC transduced with MRTF-A. **(F)** Shows the effect of Latrunculin B (100 nM), which depolymerizes actin, on the inflammatory transcripts in hCASMC. **(G)** Shows inflammatory mediators determined by RT-qPCR after silencing MRTF-A using different titers of a short hairpin virus (shMRTF-A). In this experiment U6 represents the control virus. $^{*}P < 0.05$, $^{**}P < 0.01$, $^{***}P < 0.001$, $^{****}P < 0.0001$.

Myocardin Related Transcription Factor Activity Can Be Manipulated to Modulate Inflammation

Small molecule inhibitors of MRTF-SRF signaling have been developed with a view to treat cancer and fibrosis. One of these is CCG-1423, and it inhibits MRTF-SRF driven gene activation with an IC_{50} value in the micromolar range (Evelyn et al., 2007). We predicted that CCG-1423 should increase the inflammatory transcripts in hCASMC if endogenous MRTFs constitutively suppress inflammation. Indeed, with exception for *CCL2*, the inflammatory transcripts were increased by CCG-1423 (10 μM) while the positive control *ACTA2* was reduced as expected (**Figure 3E**).

An important property of MRTF-A and MRTF-B is that they are regulated by the ratio of monomeric to polymeric actin. This depends on binding of MRTF-A and MRTF-B to monomeric actin in the cytoplasm via so called RPEL-motifs. When actin is polymerized, MRTFs move to the nucleus. We therefore treated cells with Latrunculin B (100 nM) which depolymerizes actin, expecting to see increases of the inflammatory transcripts. However, with exception for *IL1B*, none were increased, and *CCL2* was reduced (**Figure 3F**).

To further support an anti-inflammatory action of endogenous MRTF-A we used a short hairpin construct for silencing (shMRTF-A). In keeping with the effect of CCG-1423, silencing of MRTF-A had a significant pro-inflammatory effect with the largest effects seen for *IL1B* and *CXCL8* (**Figure 3G**).

Further Mechanistic Insight

Among the mechanisms that have been proposed to underlie MRTF suppression of inflammation is inhibition of NF-κB signaling through direct interaction with RelA in the nucleus. This subsequently interferes with RelA recruitment to the *IL1B* and *CXCL2* promoters (Wang et al., 2012). Another proposed mechanism is suppression of *CEBPB* and *CEBPD* (Ackers-Johnson et al., 2015), which are important for sustained inflammation. To approach these as possible mechanisms, we first surveyed our initial RNA-seq experiment with MYOCD for plausible targets that were differentially expressed and performed confirmatory RT-qPCR analyses using independent samples. Levels of *RELA*, *RELB*, *NFKB1*, *NFKB2*, *CEBPD*, *SOCS3*, and *TGFB3* are shown for MRTF-A and myocardin overexpression vs. null at two different times of transduction in **Figures 4A,B**, respectively. With exception for *CEBPD* and *TGFB3*, no changes were consistent for both times and both coactivators, despite inflammatory suppression by both MRTFs at both times (not shown).

We also examined some of these mediators at the protein level. No measurable changes of NFκB1, and NFκB2 were detected under basal conditions (not shown). After stimulation with LPS, P105 (NFκB1) and P100 (NFκB2) were reduced in most samples (**Figures 4C,D**), but this was not reflected in group averages (not shown), and the active forms (P50/P52) could not be reliably quantified. The only consistent finding at the protein level was that RelA and RelB were increased as shown in independent time-course studies (**Figure 4E** through **4G**), and this was consistent with small increases at the mRNA level, at least for RelB (compare **Figures 4A,F**). Altogether, this suggested that protein level changes of NFκB1, NFκB2, RelA, or RelB are unlikely to contribute to the anti-inflammatory effect of MRTF-A. We did not further pursue *CEBPB* and *TGFB3* as mechanistic explanations, because they were reported to be important for late phase resolution of inflammation. Taken together, we thus felt that the reported direct interaction between MRTF-A and RelA (Tang et al., 2008; Wang et al., 2012), occurring independently of SRF, appeared as the most attractive mechanism.

To support interaction between MRTF-A and Rel proteins we next performed co-immunoprecipitation (co-IP) experiments. Control and MRTF-A antibody resins were incubated with lysates from cells where MRTF-A had been overexpressed. After washing and elution, dot blotting was performed (**Figure 5A**). RelA, RelB, and MRTF-A were detectable in the flow through (FC: flow through control; FM: flow through MRTF-A), as expected. Importantly, RelA and RelB were also detected in the eluate from the MRTF-A antibody resin (EM: MRTF-A eluate), but not in the eluate from the control resin (EC: control eluate; **Figure 5A**). This was particularly striking for RelB. Similar results were obtained for RelA when assayed in the eluates using western blotting (**Figure 5B**). Altogether, this supported the previously reported model that MRTF-A may bind and sequester Rel proteins, causing inhibition of inflammatory signaling as depicted graphically in **Figure 5C**.

In the inactive state, RelA and p50 are bound by Inhibitor of κB (IκBα) in the cytosol. Upon inflammatory stimulation, such as with LPS, IκBα is degraded, releasing RelA for nuclear translocation. Corticosteroids, including dexamethasone, prevent nuclear translocation of the RelA complex (Clark, 2007). We therefore predicted that inflammatory suppression by MRTF-A should be smaller in the presence of dexamethasone (as depicted graphically in **Figure 5C**). To test this, we overexpressed MRTF-A in control conditions and after treatment with dexamethasone (3 μM). The inflammatory mediators were then assayed by RT-qPCR. We observed that MRTF-A-driven suppression of *CCL2* and *IL1B* was smaller after treatment with dexamethasone compared to vehicle ($P < 0.0003$ for relative suppression, using Null and Null + dexamethasone independently for normalization, note that **Figure 5D** shows data normalized to Null only). This appears consistent with our co-IP experiment and with the work of Wang et al. (2012), showing Rel titration as the key mechanism. Importantly, relative suppression of *CXCL8* was not significantly affected (13- vs. 19-fold, $P > 0.05$), and the effect of MRTF-A on *IL6* was enhanced in the presence of dexamethasone (4.5- vs. 2.9-fold, $P = 0.0043$). This suggested that MRTF-A-RelA interaction could contribute to repression of a subset of the inflammatory mediators (*CCL2*, *IL1B*), but that other mechanisms may be involved for some of them (*CXCL8*, *IL6*).

To sharpen this conclusion, we repeated the same experiment with short hairpin silencing of RelA (by 75.6 ± 1.0%, $P < 0.0001$, $n = 12$, **Figure 5E**). While the trend was that the anti-inflammatory effect of MRTF-A was dampened (*CCL2*: 11.7-fold→10.5-fold, *CXCL8*: 23.1-fold→17.5-fold, *IL6*:

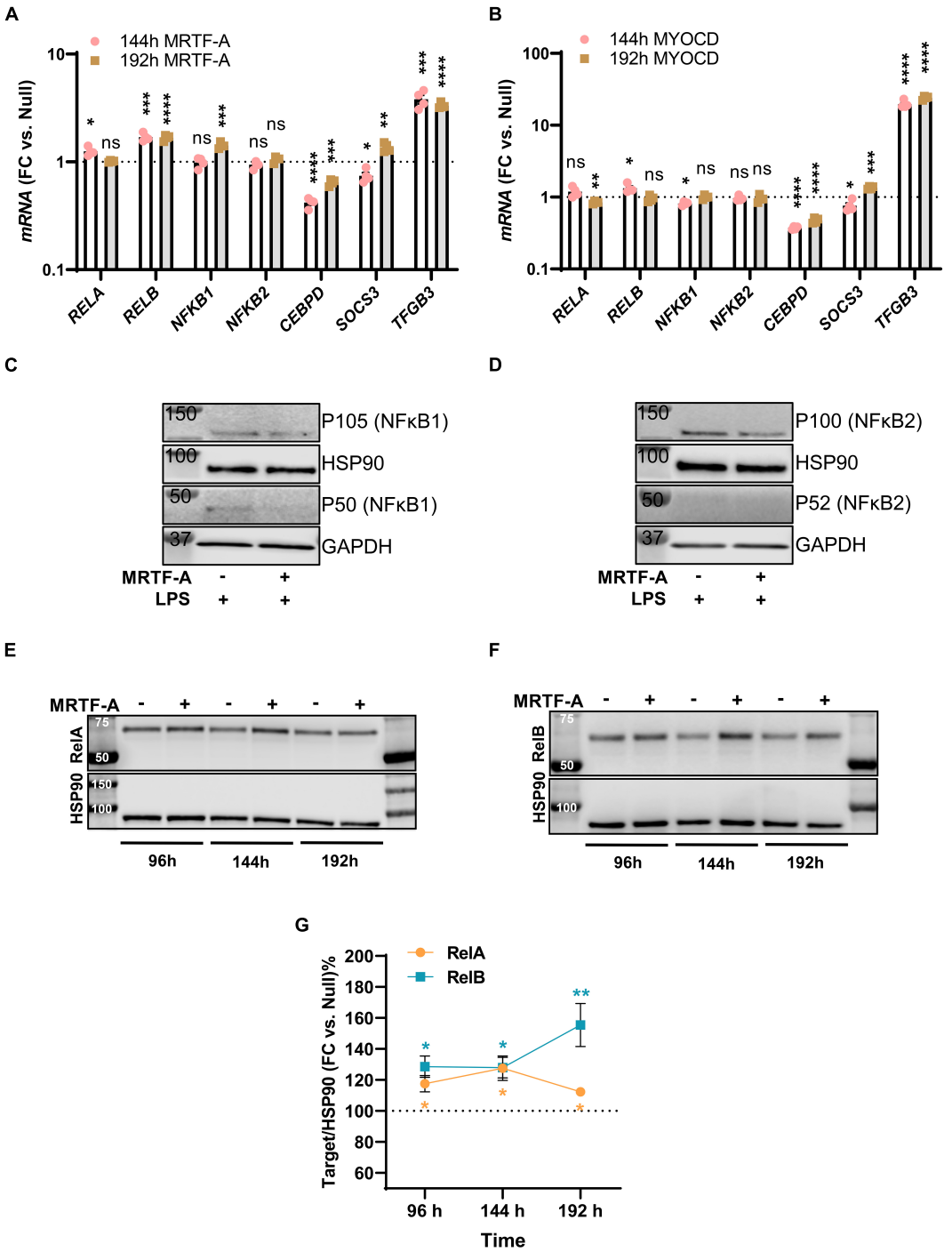

FIGURE 4 | Only modest remodeling of the inflammatory apparatus by MRTF-A. Transcripts of possible relevance for inflammation were identified in an RNA-seq experiment where MYOCD was overexpressed in human coronary artery smooth muscle cells. These transcripts were then examined by RT-qPCR at two different times of overexpression of MRTF-A **(A)** and MYOCD **(B)**, respectively. **(C,D)** Show western blots after treatment with null virus and MRTF-A virus in the presence of LPS. The only consistent differences observed by western blotting were modest increases of RelA **(E,G)** and RelB **(F,G)**. $^{*}P < 0.05$, $^{**}P < 0.01$, $^{***}P < 0.001$, $^{****}P < 0.0001$.

1.8-fold→1.4-fold, *IL1B*: 1.8-fold→1.6-fold), the overall effect was a mere 25% dampening of fold repression (overall *P*-value: 0.0043), and only the effects on *CXCL8* ($P = 0.026$) and *IL6* ($P = 0.0019$) were individually significant. Taken together, these findings argue that mechanisms beyond Rel binding and inhibition are involved in inflammatory suppression by MRTF-A.

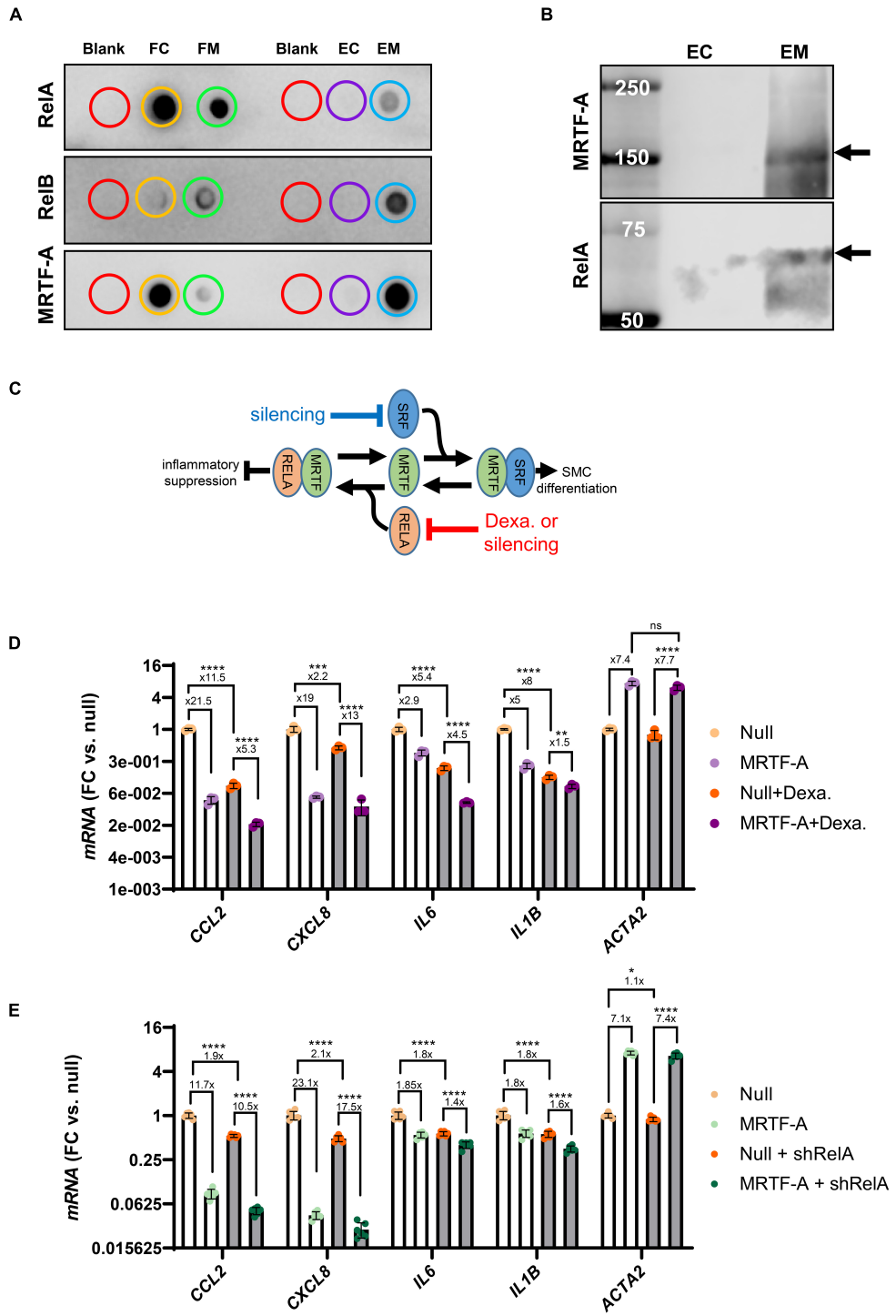

FIGURE 5 | MRTF-A interacts with RelA and RelB. To explore if MRTF-A binds RelA and RelB, we performed co-immunoprecipitations followed by dot blotting **(A)**. Lysates from cells where MRTF-A was overexpressed were incubated with control resin and with MRTF-A-antibody-conjugated resin. Flow through (FC: flow through control; FM: flow through MRTF-A) from both columns contained RelA, RelB, and MRTF-A. RelA, RelB and MRTF-A were moreover detectable in the eluate from the MRTF-A column (EM: eluate MRTF-A) but in the in the eluate from the control column (EC: eluate control). Western blotting **(B)** of the eluates showed the RelA band at the expected molecular weight. These findings support a model where MRTF binding to Rel proteins suppresses inflammation **(C)**. **(C)** Also depicts the hypothesis that RelA suppression, by glucocorticoid receptor stimulation or silencing, should mitigate inflammatory suppression by MRTF-A. **(D,E)** Test this hypothesis using dexamethasone (glucocorticoid receptor agonist, 3 μM) or short hairpin silencing (200 MOI of shRELA). For the experiments in **(D,E)**, the fold repression is given. Independent testing showed that the fold repression of *CCL2* and *IL1B* by MRTF-A was reduced by dexamethasone. In contrast, fold suppression of *CXCL8* and *IL6* was unaffected. For RelA silencing, *CXCL8* and *IL6* suppression by MRTF-A were significantly reduced, but the overall effect, where MRTF-A suppression of inflammation was reduced by ≈25%, was also significant. $^{*}P < 0.05$, $^{**}P < 0.01$, $^{***}P < 0.001$, $^{****}P < 0.0001$.

Serum Response Factor Is Involved in Suppression of *IL1B* and *CXCL8* by MRTF-A

Our findings so far highlighted mechanisms beyond RelA titration by MRTF-A for inflammatory suppression, and our correlation analyses using human arteries suggested a possible role of SRF. We therefore next examined silencing of SRF using a short hairpin construct (Ad-shSRF). We focused initially on *IL1B* in view of its relevance for cardiovascular disease and we used hCASMC where MRTF-A had been overexpressed. In this setting, gradual reduction of *SRF* using four different doses of silencer, increased *IL1B* (**Figure 6A**, negative slope), while the classical MRTF-SRF target gene calponin (*CNN1*) was reduced (**Figure 6B**, positive slope). This was also evident when data was plotted relative to the dose of the virus (multiplicity of infection, MOI) rather than relative to the level of SRF (**Figure 6C**). Suppression of *IL1B* by MRTF-A therefore depends on SRF in the setting of silencing.

To determine the effect of SRF silencing for the remainder of the inflammatory mediators, we used the RNA from cells treated with the highest titer of Ad-shSRF virus in **Figure 6C**. Beyond *IL1B*, *CXCL8* was also increased as shown in **Figure 6D**. *CCL2* and *IL6* on the other hand were reduced. This argues that SRF is involved in suppression of *IL1B* and *CXCL8* by MRTF-A, and that, in the SRF silencing situation, *CCL2* and *IL6* behave as if their regulation depended more on the reported (Wang et al., 2012) RelA sequestration by MRTF-A (that is, silencing of SRF makes more MRTFs available for RelA binding according to the model in **Figure 5C**). To corroborate the SRF dependence of *IL1B* and *CXCL8*, we next repeated SRF silencing without simultaneous overexpression of MRTF-A. Silencing of SRF again increased *IL1B* and *CXCL8* (**Figure 6E**) while *CCL2* and *IL6* were reduced. In all, this suggested MRTF-A-SRF signaling as a mechanism of suppression of *IL1B* and *CXCL8*, and MRTF-A dependent RelA titration as a mechanism of suppression of *CCL2* (and possibly *IL6*).

To explore the possibility that SRF acts directly via DNA elements at the *CXCL8* (IL-8) locus, we examined this sequence in the genome browser. ENCODE ChIP-seq data supported RelA binding ≈4 kb upstream of the gene (**Figure 6F**, blue ellipse). No SRF binding was documented. Putative SRF-binding sequences were however noted within 1450 bases from the transcription start site (red sites in **Figure 6F**). We therefore used this sequence in a promoter reporter assay. This promoter was however not suppressed by MRTF-A (**Figure 6G**), arguing that regulation of *CXCL8* by MRTF-SRF signaling depends on other DNA regions, perhaps regions in the vicinity of the more distant RelA-binding site.

We next sought to examine if Srf is important for *Il1b* expression *in vivo*. For this we used smooth muscle specific and inducible knockouts of Srf. Cre-mediated deletion of Srf was achieved by intraperitoneal injections of tamoxifen for 5 consecutive days in mice carrying floxed *Srf* alleles and a tamoxifen activatable and smooth muscle specific Cre transgene. Mice were euthanized on day 20–21 after the first injection. We used both Cre-positive vehicle injected mice (VC) and Cre-negative mice injected with tamoxifen (TC) as controls and compared these with the tamoxifen inducible knockouts (TKO). After isolation of RNA from the aorta, we measured *Srf* and *Il1b* using RT-qPCR. The two control groups did not differ with respect to Srf expression (**Figure 6H**, left), and *Srf* was depleted in the knockouts (TKO) as expected. However, aortic *Il1b* was reduced by tamoxifen in the control mice, and no increase from this level was apparent in the Srf knockouts (**Figure 6H**). This argued that tamoxifen has an anti-inflammatory effect that is independent of Srf depletion and that may hide Srf-dependent regulation. This makes the model unsuitable for studying inflammation.

We finally overexpressed SRF both alone and together with MRTF-A in hCASMCs. Curiously, repression of *IL1B* was lost on overexpression of SRF (**Figure 6I**). For *CXCL8*, we noted that SRF had a suppressive effect on its own (**Figure 6J**). For *CCL2* and *IL6* MRTF suppression remained unchanged by simultaneous overexpression of SRF (**Figures 6K,L**). Overexpression of SRF therefore further implicates SRF in suppression of *CXCL8*, but this experiment is difficult to interpret for the remainder of the inflammatory mediators.

DISCUSSION

The present work confirms previous studies showing that MRTFs have an anti-inflammatory impact in certain cell types, most notably hCASMC. However, the outcomes of this investigation are intriguing in some important and novel regards. One is that we find all MRTFs to exert an anti-inflammatory effect when overexpressed in the same primary cell type, and yet only MYOCD and MRTF-A leave a suppressive mark on inflammatory transcripts in intact human arteries. The latter finding was made using the largest material yet exploited in support of inflammatory suppression by MRTF-A/MYOCD in the vascular wall of humans. Despite this, knockout of MYOCD or MRTF-A have directionally opposite effects on atherosclerosis in the mouse. That is, while homozygous deletion of MRTF-A reduces atherosclerosis (Minami et al., 2012), hemizygous deletion of MYOCD increases it (Ackers-Johnson et al., 2015). Upon first reflection, this contradiction makes little sense, but it is possible that the different MRTFs are expressed in entirely different cell types with different roles in vascular inflammation. Indeed, in parallel work (Liu et al., 2021) we find that MYOCD is enriched in SMCs as expected, and that MRTF-B is enriched in endothelial cells, while MRTF-A primarily resides in fibroblasts. Additional explanations for the discrepant effects of MRTF-A and MYOCD in atherosclerosis include coactivator-specific effects. One such effect, that appears to differ between different MRTFs, relates to lipid uptake. While MYOCD reduces lipid uptake into hCASMCs (Ackers-Johnson et al., 2015), MRTF-A has the opposite effect as it increases low density lipoprotein (LDL) uptake via LDL receptors (Alajbegovic et al., 2021). Overall, the impact of different MRTFs on atherosclerosis therefore seems most consistent with their reported effects on lipid uptake.

On the mechanistic level, we report an important, and previously overlooked, finding, namely that SRF is somehow

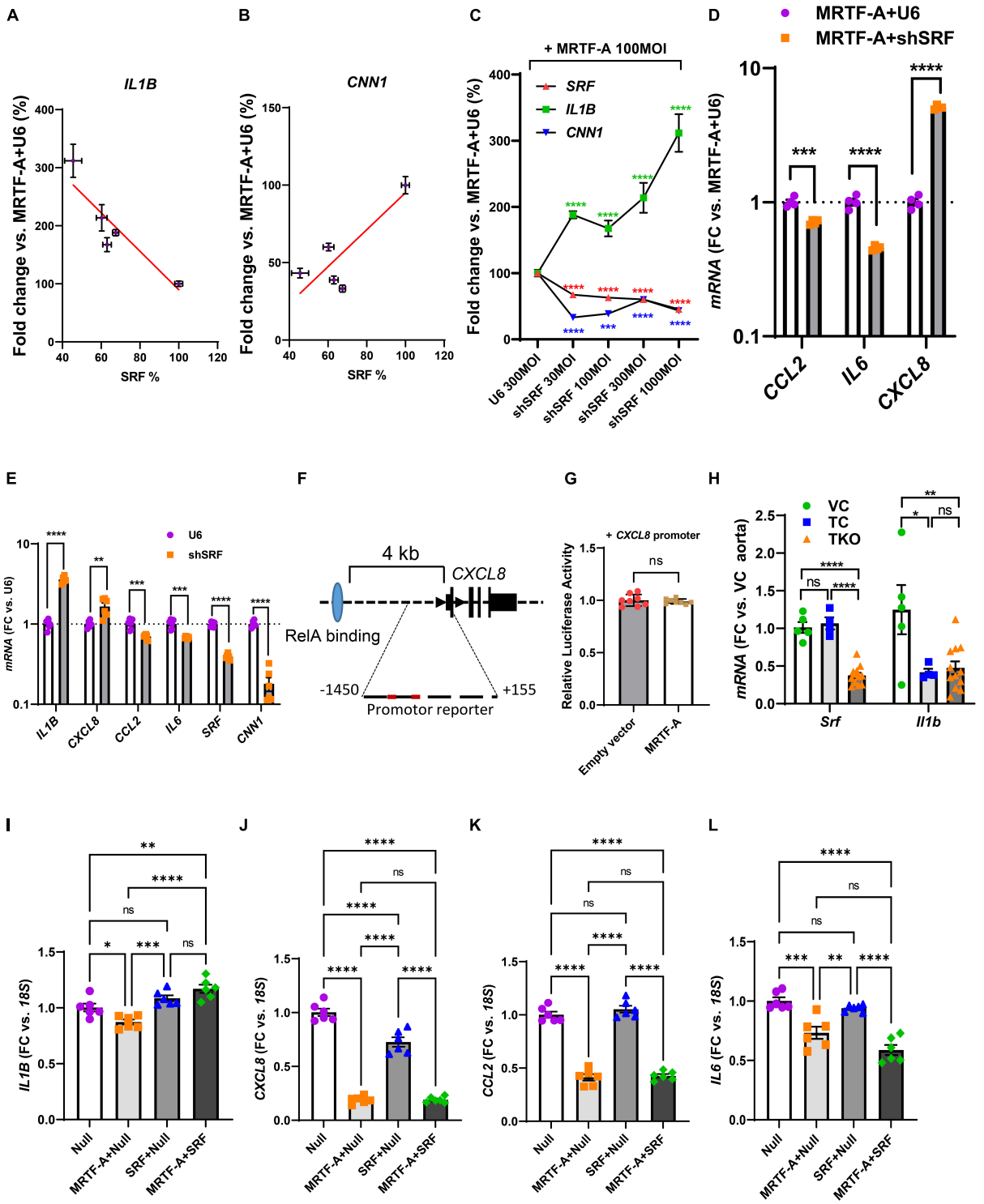

FIGURE 6 | SRF is important for regulation of *IL1B* and *CXCL8*. **(A–C)** Human coronary SMCs were transduced with MRTF-A along with different titers of Ad-h-shSRF for knockdown of SRF. After harvesting the cells and isolation of RNA, *SRF*, *IL1B*, and *CNN1* were assayed using RT-qPCR. In **(A,B)**, *IL1B* and *CNN1* were plotted vs. the relative *SRF* level in the respective samples. In **(C)**, *SRF*, *IL1B*, and *CNN1* were plotted vs. the titer (multiplicity of infection, MOI) of the short hairpin virus. **(D)** Shows the remainder of the inflammatory mediators in control vs. SRF-depleted cells (1000 MOI). **(E)** Is like **(D)**, except that SRF silencing was done without simultaneous overexpression of MRTF-A. **(F)** Shows the gene locus for human *CXCL8* and binding of RelA (light blue oval) 4 kb upstream of the transcription start site. The proximal promoter contained two DNA sequences with two deviations each from the classical SRF-binding sequence. When testing this sequence in a reporter assay, no suppression by MRTF-A was however, seen **(G)**. In **(H)**, *Srf* and *Il1b* were assayed in the aorta from smooth muscle specific and inducible Srf

(Continued)

FIGURE 6 | (Continued)
knockout mice. Because knockout was induced by tamoxifen, two control groups were included in addition to the knockout group. Vehicle controls (VC) are Cre-positive mice injected with sunflower oil, whereas tamoxifen controls (TC) are Cre-negative mice injected with tamoxifen. Knockouts (TKO) are Cre-positive mice injected with tamoxifen. All mice are homozygous for the floxed *Srf* allele. **(I–L)** Show the effect of overexpression of SRF in the absence and presence of MRTF-A. SRF was capable of suppressing *CXCL8* on its own but was without effect on *CCL2* and *IL6*. $^{*}P < 0.05$, $^{**}P < 0.01$, $^{***}P < 0.001$, $^{****}P < 0.0001$.

involved in suppression of some inflammatory transcripts by MRTF-A. This includes *IL1B* whose neutralization in a clinical trial was found to reduce cardiovascular mortality (Ridker et al., 2017), and *CXCL8*. Our findings with *CCL2*, on the other hand, are consistent with the reported RelA titration by MRTF-A (Wang et al., 2012). Therefore, not one mechanism, but many, must be responsible for MRTF-dependent suppression of inflammation. SRF is important, often critical, for binding of MRTFs to DNA, and such binding in the vicinity of the *IL1B* and *CXCL8* loci could impede attachment of another stimulatory factor. Alternatively, the effect could involve a downstream target gene, or e.g., chromatin remodeling. We were not successful in further defining the DNA regions involved using a promoter reporter assay for *CXCL8*, but our efforts were not exhaustive.

When attempting to support involvement of Srf in mice *in vivo*, we observed that tamoxifen, required for Cre-mediated gene excision in our model, had an anti-inflammatory impact 21 days after the first tamoxifen injection. We are uncertain of the basis of this anti-inflammatory effect, which could involve promiscuous binding of steroid-like chemistries to glucocorticoid receptors, or estrogen receptor modulation, but similar effects have been reported previously (Lamas et al., 2015). We are therefore forced to conclude that tamoxifen-dependent gene excision is unsuitable for studying the role of MRTF-SRF signaling in inflammation. Importantly, however, involvement of SRF for *CXCL8* regulation was demonstrated in cultured SMCs using both silencing and overexpression, and it was further supported by correlation analyses in a large human material.

It is currently unclear to us why forced overexpression of MRTF-A has so drastically different effects in different cell types. Inflammatory status is not a key underlying factor as suggested by our LPS experiments. However, some other cell-specific factor must play a role because we see rather different effects of MRTF-A in coronary and bladder SMCs. Identification of this factor could perhaps resolve the puzzling fact that MRTFs may be both pro- and anti-inflammatory. It is interesting to note that the proposed mechanism of the pro-inflammatory impact of MRTF-A in THP-1 cells involves the epigenetic modifiers Ash2, Wdr5, and Set1 (Yu et al., 2014). At least one of these (Ash2/*ASCL2*) is expressed at a very low level in the coronary artery (GTExPortal.org). One possibility therefore is that Ash2 determines the directionality of the effect.

Here, we show that overexpression of MRTFs downregulate several pro-inflammatory transcripts and proteins relevant for vascular pathophysiology and development of vascular disease. However, the RNA-seq experiment providing impetus for the present work (Liu et al., 2021) revealed additional pro-inflammatory genes, such as *SGPP2* (sphingosine 1-phosphate phosphatase 2), *IL32* (interleukin 32), and *TSLP* (thymic stromal lymphopoietin), as being repressed. Notably, downregulation of *SGPP2* gene activity and sphingosine 1-phosphate phosphatase 2 protein levels reduces TNFα-induced *IL1B* and *CXCL8* production in endothelial cells, and moreover, knockdown of NF-κB/RelA shows that SGPP2 is an NF-κB-regulated gene (Mechtcheriakova et al., 2007). Our RNA-seq experiment also revealed that *LACC1* (laccase domain containing 1), which encodes an oxidoreductase that stimulates fatty-acid oxidation, increases (3.3-fold). Loss of function mutations in *LACC1* associate with several inflammatory diseases, such as juvenile idiopathic arthritis and Crohn's disease (Szymanski and Ombrello, 2018), offering the interesting possibility that MRTFs may antagonize inflammation in part via upregulation of *LACC1*. Yet another example is *DUSP1*, which is partly responsible for the anti-inflammatory action of dexamethasone (Abraham et al., 2006), and that was increased 1.5-fold. Thus, MRTFs may regulate many genes associated with inflammation beyond those corroborated here, underscoring a pleiotropic anti-inflammatory action, and making these coactivators possible targets for treatment of inflammatory diseases including atherosclerosis.

MRTFs, particularly MRTF-A, are sensitive to a variety of mechanical inputs, including substrate stiffness (Foster et al., 2017; Hadden et al., 2017), externally applied forces (Zhao et al., 2007; Chan et al., 2010; Cui et al., 2015), and geometric constraints (Jain et al., 2013). Blood pressure as well as arterial stiffness could therefore affect vascular inflammation via MRTFs, and this could be a way to compensate for the increased lipid uptake into SMCs via LDL receptors (Alajbegovic et al., 2021). However, mechanical signals to MRTFs involve the actin cytoskeleton (Zhao et al., 2007; Chan et al., 2010; Sward et al., 2016), and we find here that depolymerization of actin does not consistently increase the inflammatory mediators regulated by MRTF-A; in fact *CCL2* was significantly decreased, while *IL1B* increased. Our findings therefore caution against generalizations and calls for studies of distinct target genes, rather than relying on reporter assays, and comparing the impact of different mechanical modalities and protocols. It would, for example, be of interest to know if there was such a thing as a healthy level of mechanical input on SMCs in the vascular wall, akin to the local optimum of MRTF activity seen on substrates of different stiffness (Hadden et al., 2017). Nonetheless, using reporter assays, others have shown consistent increases of NF-κB activity using Latrunculin (Jain et al., 2013).

In summary, the present work confirms previous reports showing that MRTFs have a broad anti-inflammatory impact by suppressing numerous cytokines in human coronary artery SMCs. This effect is equal to, or greater, than the effect of dexamethasone. We also find that *MYOCD*, *MRTFA*, and *SRF* correlate negatively with many inflammatory transcripts in human arteries, supporting an anti-inflammatory impact *in situ*. Our mechanistic studies suggest that the underlying mechanism

of action cannot solely depend on RelA sequestration, and that SRF appears to be involved in regulation of *IL1B* and *CXCL8*. Taken together, this work supports the concept that phenotypic modulation of SMCs involves toggling between contractile and inflammatory phenotypes, in addition to the classical paradigm where SMCs switch between contractile and synthetic phenotypes (Thyberg et al., 1983; Miano, 2003).

MATERIALS AND METHODS

Primary Cell Culture, Viral Transduction, and Cell Treatments

Human coronary artery smooth muscle cells (hCASMCs, Thermo Scientific/Gibco, C0175C) were cultured in Medium 231 (Thermo Scientific, M231500) with growth supplement (5% SMGS: Life Technologies, S00725) and 50U/50 μg/ml penicillin/streptomycin (PEST, Biochrom, A2212). Human bladder smooth muscle cells (hBSMCs) were isolated from human detrusor strips (Zhu et al., 2017) and cultured in DMEM/Ham's F-12 medium with glutamine (Biochrom, FG4815), 10% fetal bovine serum (FBS: Biochrom, S0115), and 50 U/50 μg/ml PEST. Human coronary artery endothelial cells (hCAECs, Lonza, CC-2585) were cultured in EGM-2 MV, Microvascular Endothelial Cell Growth Medium-2 BulletKit (Lonza, CC-3202), which contains EBM-2 Basal Medium (Lonza, CC-3156) and EGM-2 MV Microvascular Endothelial Cell Growth Medium SingleQuots supplements (Lonza, CC-4147). These primary cells were kept in a standard cell culture incubator at 37℃, in 95% air and 5% CO_2, and used in passages 3–9.

Adenoviral vectors for overexpression and silencing were purchased from Vector Biolabs. Ad-h-MYOCD (ADV-216227), Ad-h-MKL1/eGFP (MRTF-A, ADV-215499), Ad-h-MKL2 (MRTF-B, ADV-215500), Ad-h-SRF (ADV-224323) and Ad-CMV-Null (#1300) were for overexpressing target genes. Ad-h-shSRF (shADV-224323), Ad-h-shRELA (shADV-220994), Ad-U6-h-MKL1-shRNA (shADV-215497) and Ad-GFP-U6-shRNA (#1122) were for silencing target genes. Among them, Ad-CMV-Null (#1300) and Ad-GFP-U6-shRNA (#1122) were used as negative controls. Cells were harvested at 96 h after viral transduction unless specified.

CCG-1423 is a Rho/SRF pathway inhibitor and it was purchased from Tocris Bioscience (#5233). After 24 h in low-serum conditions (2% SMGS), hCASMCs were treated with 10 μM CCG-1423 or the corresponding volume of DMSO (Sigma-Aldrich, #D5879) in 2% SMGS M231 medium for 24 h.

Latrunculin B for depolymerizing actin was purchased from Calbiochem (#428020). After 24 h in low-serum conditions (2% SMGS), cells were treated with 100 nM Latrunculin B or the corresponding volume of DMSO (Sigma-Aldrich, #D5879) in 2% SMGS M231 medium for 24 h. Cells were then harvested for isolating RNA.

LPS (*E. coli* LPS 0111:B4) was purchased from Sigma-Aldrich and was dissolved in PBS. hCASMCs were treated with LPS (500 ng/ml) for 24 h following 72 h of virus transduction or for 48 h following 96 h of virus transduction.

Dexamethasone (Sigma-Aldrich) was dissolved in DMSO, and a final concentration of 3 μM was used in the experiments. hCASMCs were transduced with virus for 72 h and then treated with dexamethasone for additional 24 h before harvesting for RT-PCR. Controls received vehicle as appropriate.

RNA Isolation and RT-qPCR

After viral transduction or treatment with agents, cells were washed in cold phosphate-buffered saline (PBS, Sigma-Aldrich, P4417) and lysed in Qiazol (Qiagen, #79306). RNA was isolated using the Qiagen miRNeasy mini kit (Qiagen, #217004) in a QIAcube workstation. To determine RNA purity and concentration we used the NanoDrop 2000c (Thermo Scientific) instrument. For RT-qPCR we used the Quantifast SYBR Green RT-PCR kit (Qiagen, 204156) and QuantiTect Primer assays from Qiagen [*CCL2* (QT00212730), *IL6* (QT00083720), *IL1B* (QT00021385), *CXCL8* (QT00000322), *SRF* (QT00084063), *ACTA2* (QT000088102), *CNN1* (QT00067718), *RELA* (QT01007370), *RELB* (QT00038640), *NFKB1* (QT00063791), *NFKB2* (QT00012404), *CEBPD* (QT00219373), *SOCS3* (QT00244580), *TGFB3* (QT00001302), *MRTFA* (QT00067921), *18S* (QT00199367), *Il1b* (QT01048355), *Srf* (QT00126378), *18s* (QT02448075)] to amplify target genes in the StepOnePlus qPCR cycler (Applied Biosystems). Qiagen considers the exact primer sequences proprietary. We used *18S* or *18s* as a housekeeping reference gene and the Pfaffl method to calculate the fold changes (vs. Null or U6).

Confocal Imaging

Cells were fixed in 4% PFA in physiological buffer for 30 min, then permeabilized and blocked using physiological buffer with 1% BSA, 1% goat serum and 1% triton for 2 h. Cells were labeled with primary antibody overnight in the same buffer without detergent (1% BSA, 1% goat serum). The next day, cells were washed and labeled with secondary antibody for 4 h. Nuclei were stained using Hoechst at the last step. For imaging, nuclei were localized using low resolution overviews and imaged using a minimal pinhole centered at the nuclei to obtain signal within the nuclei and minimizing out of focus signal. For analysis FIJI was used. Nuclei were segmented using a threshold in the Hoechst channel and all the signal inside the nuclei was measured as mean gray value for both GFP and MRTF-A-antibody stains.

Correlation Analyses Using GTEX Data

RNA-sequencing data from human organs was downloaded in 2020 from the GTExPortal.org (Consortium, 2013; Consortium, 2015) using R-scripts described elsewhere (Krawczyk et al., 2015; Sward et al., 2019). Transcript read counts (in TPM, transcripts per million) for *SRF*, *MYOCD*, *MRTFA*, and *MRTFB* were correlated with 13 inflammatory transcripts identified in an RNA-seq experiment where MYOCD was overexpressed. The study describing this RNA-seq experiment was submitted in parallel to the Frontiers' theme in Cardiovascular mechanobiology (Liu et al., 2021) and has been deposited with the temporary submission ID SUB9688745, and release date 2022-06-01 (or with the release of linked data). Correlation matrices for MRTFs and the inflammatory transcripts were generated using the Pearson

method using GraphPad Prism in all three arteries represented in the GTExPortal.

THP1 Cells and Plasmid Transfection

The human THP-1 monocyte cell line was purchased from ATCC and cultured in RMPI-1640 medium supplemented with GlutaMAX (Thermo Scientific, 61870036), 10% FBS and antibiotics (penicillin 50 U/ml, streptomycin 50 μg/ml). The cells were grown in a water-jacketed cell incubator at 37°C and 5% CO_2 in air. The medium was renewed every 2–3 day and the cells were passaged once the cell density reached 8×10^5 cells/ml.

THP-1 cells were transfected with the p3xFLAG-MKL1 plasmid (Addgene, plasmid #11978) using Lipofectamine LTX Reagent with PLUS Reagent (Invitrogen, 15338030) according to the manufacturer's instructions for 96 h before the cells were harvested and RNA isolated (miRNeasy, Qiagen).

Protein Isolation and Western Blotting

Following virus transduction and LPS-treatment, hCASMCs were washed with cold (4°C) PBS, harvested in SDS sample buffer, and lysed by sonication on ice for 10 s. Total protein concentration was determined using the BioRad DC protein assay (BioRad, #5000112) and adjusted to ensure equal protein concentrations across samples (1 μg/μl). Protein lysates were loaded on SDS-PAGE Criterion TGX 4-15% or Any-kD precast gels (BioRad, #5671084, #5671124) and proteins were transferred to 0.2 μm nitrocellulose membranes (BioRad, #1704159) using the Trans-Blot Turbo Transfer System (BioRad). To be able to detect all the protein targets, the lysates were sometimes loaded as technical replicates. The membrane was blocked for 2 h with 1% casein/TBS (1:1) (BioRad, #1610782) in room temperature and then cut horizontally using the ladder as guidance. The membrane strips were then incubated with monoclonal primary antibodies as follows: MCP-1 (CCL2, 1 μg/ml, Abcam, ab9669), IL8 (CXCL8, 1:500, Cell Signaling, #94407), RelA (NFκB/p65, 1:1000, Cell Signaling, #8242), RelB (1:1000, Cell Signaling, #10544), NFκB1 (p105/p50, 1:1000, Cell Signaling, #13586), NFκB2 (p100/p52, 1:1000, Cell Signaling, #4882), HSP90 (1:1000, BD Biosciences, #610418), and GAPDH (1:3000, Merck Millipore, #MAB374) for 96 h at 4°C. To visualize the protein bands, membranes were incubated with HRP-conjugated secondary antibodies (1:5000, Cell Signaling, #7076 and #7074) for 2 h and the bands were detected using Supersignal West Femto substrate (Thermo Fisher Scientific, #34096) and the LI-COR Odyssey Fc instrument (LI-COR Biosciences). For quantification, all band were normalized to their respective loading controls (HSP90 and/or GAPDH) on the same membrane.

ELISAs

Enzyme-linked immunosorbent assays (ELISAs) were performed to measure IL-8 and MCP-1 protein levels in lysates of hCASMC treated with LPS. To obtain cell lysates, cells were harvested in cold PBS and sonicated 3 × 10 s on ice. The lysate was then centrifuged at 1800 × g for 5 min at 4°C and the supernatant was collected. The assays were performed using the Human IL-8/CXCL8 DuoSet ELISA kit (#DY208) and the Human CCL2/MCP-1 Quantikine ELISA kit (#DCP00), both from R&D Systems. We adhered to protocols provided by the manufacturer.

Co-immunoprecipitation

Co-immunoprecipitation (co-IP) of MRTF-A-binding proteins was performed using the Pierce co-IP kit (Thermo Scientific, #26149) according to the manufacturer's instructions. Briefly, ∼26 μg purified MRTF-A antibody (Bethyl Laboratories, #A302-202A) was immobilized to the AminoLink Plus Coupling Resin in a column for 2 h in room temperature. To rule out non-specific interactions with the resin, a column containing Control Resin provided with the kit was used as a negative control. hCASMCs were washed with PBS and lysed in cold Lysis/Wash Buffer. The lysate was pre-cleared using Control Agarose Resin and 1 mg of the lysate was added to both columns and incubated overnight at 4°C. The resins were washed with IP Lysis/Wash Buffer before the MRTF-A protein complexes were eluted in Elution Buffer. The samples were analyzed by western blotting. For this, the eluted proteins were mixed with Lane Marker Sample Buffer and 100 mM DTT (Sigma-Aldrich), separated on an SDS-PAGE Criterion TGX 4–15% precast gel (Bio-Rad), transferred to a nitrocellulose membrane and blocked for 2h in room temperature. To detect MRTF-A-RelA protein interaction, the membrane was incubated for 3 days with primary RelA antibody (NFκB/p65, 1:1,000, Cell Signaling, #8242), and using MRTF-A primary antibody (MKL1/MRTF-A, 1:1,000, Cell Signaling, #14760) as a positive control. Immunoreactivity for RelA, RelB and MRTF-A was also assessed by Dot Blot. Briefly, 1 μl of the eluate was dotted onto a nitrocellulose membrane. The membrane was blocked with 1% casein/TBS (1:1) for 2 h in room temperature and then incubated for 3 days in primary antibodies for RelA (NFκB/p65, 1:1,000, Cell Signaling, #8242), RelB (1:1,000, Cell Signaling, #10544) and MRTF-A (MKL1/MRTF-A, 1:1,000, Cell Signaling, #14760). To visualize the proteins of interest for both western blot and dot blot, the membranes were incubated with HRP-conjugated secondary antibodies (1:5,000, Cell Signaling, #7076 and #7074) for 2 h and the immunoreactivity was detected using the SuperSignal West Femto substrate. Images were acquired using the LI-COR Odyssey Fc instrument (LI-COR Biosciences).

Promoter Reporter Assay in HEK293 Cells

A plasmid containing the *CXCL8* promoter in a luciferase reporter vector was purchased from Tebu-bio (Gene information, 217HPRM30547-PG04). HEK293 cells were seeded in 24 well plates and the media were changed for antibiotic-free DMEM medium (contain 10% FBS) after 24 h. The CXCL8 promoter reporter plasmid (0.25 μg) and p3xFLAG-MKL1 plasmid (0.25 μg, Addgene, #11978) were co-transfected into HEK293 cells using Lipofectamine 2000 (Thermo Fisher Scientific, #11668030) following the manufacturer's protocol. 96 h after transfection, medium was collected to measure the luciferase activity and the alkaline phosphatase release separately using the Secrete-Pair Dual Luminescence Assay Kit (Tebu-bio, #LFO32).

Knockout of Srf

Inducible and SMC-specific knockout of Srf in mice was accomplished as described (accompanying paper submitted to Frontier's theme on mechanobiology, Liu et al., 2021). Floxed Cre-negative mice treated with tamoxifen (TC) and Floxed Cre-positive mice treated with vehicle (VC) were used as controls. Mice were sacrificed on day 20 and day 21 after the first tamoxifen injection. After sacrifice, the aorta was cleaned in physiological buffer using microdissection instruments. It was then blotted on filter paper to remove excess fluid and frozen on dry ice. Ten control mice (5 VC, and 5 TC) and 12 knockout mice (TKO) were used, but one of the TC mice was excluded due to low RNA yield. RNA was isolated as described above.

DATA AVAILABILITY STATEMENT

The datasets presented in this study can be found in online repositories. The names of the repository/repositories and accession number(s) can be found below: BioSample database and accessions SAMN19277810, SAMN19277811, SAMN19277812, SAMN19277813, SAMN19277814, SAMN19277815, SAMN19277816, and SAMN19277817 (https://www.ncbi.nlm.nih.gov/biosample/19277810; https://www.ncbi.nlm.nih.gov/biosample/19277811; https://www.ncbi.nlm.nih.gov/biosample/19277812; https://www.ncbi.nlm.nih.gov/biosample/19277813; https://www.ncbi.nlm.nih.gov/biosample/19277814; https://www.ncbi.nlm.nih.gov/biosample/19277815; https://www.ncbi.nlm.nih.gov/biosample/19277816; and https://www.ncbi.nlm.nih.gov/biosample/19277817).

ETHICS STATEMENT

The animal study was reviewed and approved by the Malmö—Lunds djurförsöksetiska nämnd, approval number 5-8-18-16388/2020.

AUTHOR CONTRIBUTIONS

LL, EB, CR, B-ON, and KS participated in the study design. LL and EB collected data. BM and KGS were responsible for imaging. KS generated the funding. KS wrote the manuscript, and all authors were involved in manuscript revisions. All authors have read and approved the submitted version.

FUNDING

This work was supported by the grants from the Swedish Research Council (VR, 2020-00908) and the Heart-Lung Foundation (20200222).

ACKNOWLEDGMENTS

We thank Katarzyna Kawka for genotyping and tamoxifen injections, and Samuel Cerps for invaluable assistance with the ELISAs.

REFERENCES

Abraham, S. M., Lawrence, T., Kleiman, A., Warden, P., Medghalchi, M., Tuckermann, J., et al. (2006). Antiinflammatory effects of dexamethasone are partly dependent on induction of dual specificity phosphatase 1. *J. Exp. Med.* 203, 1883–1889. doi: 10.1084/jem.20060336

Ackers-Johnson, M., Talasila, A., Sage, A. P., Long, X., Bot, I., Morrell, N. W., et al. (2015). Myocardin regulates vascular smooth muscle cell inflammatory activation and disease. *Arterioscler. Thromb. Vasc. Biol.* 35, 817–828. doi: 10.1161/ATVBAHA.114.305218

Alajbegovic, A., Holmberg, J., Daoud, F., Rippe, C., Kalliokoski, G., Ekman, M., et al. (2021). MRTFA overexpression promotes conversion of human coronary artery smooth muscle cells into lipid-laden foam cells. *Vascul. Pharmacol.* 138:106837. doi: 10.1016/j.vph.2021.106837

Allahverdian, S., Chaabane, C., Boukais, K., Francis, G. A., and Bochaton-Piallat, M. L. (2018). Smooth muscle cell fate and plasticity in atherosclerosis. *Cardiovasc. Res.* 114, 540–550. doi: 10.1093/cvr/cvy022

Chan, M. W., Chaudary, F., Lee, W., Copeland, J. W., and Mcculloch, C. A. (2010). Force-induced myofibroblast differentiation through collagen receptors is dependent on mammalian diaphanous (mDia). *J. Biol. Chem.* 285, 9273–9281. doi: 10.1074/jbc.M109.075218

Clark, A. R. (2007). Anti-inflammatory functions of glucocorticoid-induced genes. *Mol. Cell. Endocrinol.* 275, 79–97. doi: 10.1016/j.mce.2007.04.013

Consortium, G. T. (2013). The Genotype-Tissue Expression (GTEx) project. *Nat. Genet.* 45, 580–585. doi: 10.1038/ng.2653

Consortium, G. T. (2015). Human genomics. The Genotype-Tissue Expression (GTEx) pilot analysis: multitissue gene regulation in humans. *Science* 348, 648–660. doi: 10.1126/science.1262110

Cui, Y., Hameed, F. M., Yang, B., Lee, K., Pan, C. Q., Park, S., et al. (2015). Cyclic stretching of soft substrates induces spreading and growth. *Nat. Commun.* 6:6333. doi: 10.1038/ncomms7333

Evelyn, C. R., Wade, S. M., Wang, Q., Wu, M., Iniguez-Lluhi, J. A., Merajver, S. D., et al. (2007). CCG-1423: a small-molecule inhibitor of RhoA transcriptional signaling. *Mol. Cancer Ther.* 6, 2249–2260. doi: 10.1158/1535-7163.MCT-06-0782

Foster, C. T., Gualdrini, F., and Treisman, R. (2017). Mutual dependence of the MRTF-SRF and YAP-TEAD pathways in cancer-associated fibroblasts is indirect and mediated by cytoskeletal dynamics. *Genes Dev.* 31, 2361–2375. doi: 10.1101/gad.304501.117

Gao, P., Gao, P., Zhao, J., Shan, S., Luo, W., Slivano, O. J., et al. (2021). MKL1 cooperates with p38MAPK to promote vascular senescence, inflammation, and abdominal aortic aneurysm. *Redox Biol.* 41:101903. doi: 10.1016/j.redox.2021.101903

Georgakis, M. K., Malik, R., Bjorkbacka, H., Pana, T. A., Demissie, S., Ayers, C., et al. (2019). Circulating Monocyte Chemoattractant Protein-1 and Risk of Stroke: meta-Analysis of Population-Based Studies Involving 17 180 Individuals. *Circ. Res.* 125, 773–782. doi: 10.1161/CIRCRESAHA.119.315380

Grootaert, M. O. J., and Bennett, M. R. (2021). Vascular smooth muscle cells in atherosclerosis:Time for a reassessment. *Cardiovasc. Res.* 8:cvab046. doi: 10.1093/cvr/cvab046

Gu, L., Okada, Y., Clinton, S. K., Gerard, C., Sukhova, G. K., Libby, P., et al. (1998). Absence of monocyte chemoattractant protein-1 reduces atherosclerosis in low density lipoprotein receptor-deficient mice. *Mol. Cell.* 2, 275–281. doi: 10.1016/S1097-2765(00)80139-2

Hadden, W. J., Young, J. L., Holle, A. W., Mcfetridge, M. L., Kim, D. Y., Wijesinghe, P., et al. (2017). Stem cell migration and mechanotransduction on linear stiffness gradient hydrogels. *Proc. Natl. Acad. Sci. U. S. A.* 114, 5647–5652. doi: 10.1073/pnas.1618239114

Ito, S., Hashimoto, Y., Majima, R., Nakao, E., Aoki, H., Nishihara, M., et al. (2020). MRTF-A promotes angiotensin II-induced inflammatory response and aortic dissection in mice. *PLoS One* 15:e0229888. doi: 10.1371/journal.pone.0229888

Jain, N., Iyer, K. V., Kumar, A., and Shivashankar, G. V. (2013). Cell geometric constraints induce modular gene-expression patterns via redistribution of HDAC3 regulated by actomyosin contractility. *Proc. Natl. Acad. Sci. U. S. A.* 110, 11349–11354. doi: 10.1073/pnas.1300801110

Krawczyk, K. K., Yao Mattisson, I., Ekman, M., Oskolkov, N., Grantinge, R., Kotowska, D., et al. (2015). Myocardin Family Members Drive Formation of Caveolae. *PLoS One* 10:e0133931. doi: 10.1371/journal.pone.0133931

Lamas, A. Z., Caliman, I. F., Dalpiaz, P. L., De Melo, A. F. Jr., Abreu, G. R., Lemos, E. M., et al. (2015). Comparative effects of estrogen, raloxifene and tamoxifen on endothelial dysfunction, inflammatory markers and oxidative stress in ovariectomized rats. *Life Sci.* 124, 101–109. doi: 10.1016/j.lfs.2015.01.004

Libby, P., and Hansson, G. K. (2019). From Focal Lipid Storage to Systemic Inflammation: jACC Review Topic of the Week. *J. Am. Coll. Cardiol.* 74, 1594–1607. doi: 10.1016/j.jacc.2019.07.061

Liu, L., Rippe, C., Hansson, O., Kryvokhyzha, D., Fisher, S., Ekman, M., et al. (2021). Regulation of the muscarinic m3 receptor by myocardin-related transcription factors. *Front. Physiol.* 12. doi: 10.3389/fphys.2021.710968.

McDermott, D. H., Yang, Q., Kathiresan, S., Cupples, L. A., Massaro, J. M., Keaney, J. F. Jr., et al. (2005). CCL2 polymorphisms are associated with serum monocyte chemoattractant protein-1 levels and myocardial infarction in the Framingham Heart Study. *Circulation* 112, 1113–1120. doi: 10.1161/CIRCULATIONAHA.105.543579

Mechtcheriakova, D., Wlachos, A., Sobanov, J., Kopp, T., Reuschel, R., Bornancin, F., et al. (2007). Sphingosine 1-phosphate phosphatase 2 is induced during inflammatory responses. *Cell. Signal.* 19, 748–760. doi: 10.1016/j.cellsig.2006.09.004

Miano, J. M. (2003). Serum response factor: toggling between disparate programs of gene expression. *J. Mol. Cell. Cardiol.* 35, 577–593. doi: 10.1016/S0022-2828(03)00110-X

Miano, J. M. (2015). Myocardin in biology and disease. *J. Biomed. Res.* 29, 3–19. doi: 10.7555/JBR.29.20140151

Minami, T., Kuwahara, K., Nakagawa, Y., Takaoka, M., Kinoshita, H., Nakao, K., et al. (2012). Reciprocal expression of MRTF-A and myocardin is crucial for pathological vascular remodelling in mice. *EMBO J.* 31, 4428–4440. doi: 10.1038/emboj.2012.296

Miralles, F., Posern, G., Zaromytidou, A. I., and Treisman, R. (2003). Actin dynamics control SRF activity by regulation of its coactivator MAL. *Cell* 113, 329–342. doi: 10.1016/S0092-8674(03)00278-2

Olson, E. N., and Nordheim, A. (2010). Linking actin dynamics and gene transcription to drive cellular motile functions. *Nat. Rev. Mol. Cell. Biol.* 11, 353–365. doi: 10.1038/nrm2890

Owens, G. K., Kumar, M. S., and Wamhoff, B. R. (2004). Molecular regulation of vascular smooth muscle cell differentiation in development and disease. *Physiol. Rev.* 84, 767–801. doi: 10.1152/physrev.00041.2003

Parmacek, M. S. (2007). Myocardin-related transcription factors: critical coactivators regulating cardiovascular development and adaptation. *Circ. Res.* 100, 633–644. doi: 10.1161/01.RES.0000259563.61091.e8

Ridker, P. M., Everett, B. M., Thuren, T., Macfadyen, J. G., Chang, W. H., Ballantyne, C., et al. (2017). Antiinflammatory Therapy with Canakinumab for Atherosclerotic Disease. *N. Engl. J. Med.* 377, 1119–1131. doi: 10.1056/NEJMoa1707914

Staus, D. P., Blaker, A. L., Taylor, J. M., and Mack, C. P. (2007). Diaphanous 1 and 2 regulate smooth muscle cell differentiation by activating the myocardin-related transcription factors. *Arterioscler. Thromb. Vasc. Biol.* 27, 478–486. doi: 10.1161/01.ATV.0000255559.77687.c1

Sward, K., Krawczyk, K. K., Moren, B., Zhu, B., Matic, L., Holmberg, J., et al. (2019). Identification of the intermediate filament protein synemin/SYNM as a target of myocardin family coactivators. *Am. J. Physiol. Cell. Physiol.* 317, C1128–C1142. doi: 10.1152/ajpcell.00047.2019

Sward, K., Stenkula, K. G., Rippe, C., Alajbegovic, A., Gomez, M. F., and Albinsson, S. (2016). Emerging roles of the myocardin family of proteins in lipid and glucose metabolism. *J. Physiol.* 594, 4741–4752. doi: 10.1113/JP271913

Szymanski, A. M., and Ombrello, M. J. (2018). Using genes to triangulate the pathophysiology of granulomatous autoinflammatory disease: nOD2, PLCG2 and LACC1. *Int. Immunol.* 30, 205–213. doi: 10.1093/intimm/dxy021

Tang, R. H., Zheng, X. L., Callis, T. E., Stansfield, W. E., He, J., Baldwin, A. S., et al. (2008). Myocardin inhibits cellular proliferation by inhibiting NF-kappaB(p65)-dependent cell cycle progression. *Proc. Natl. Acad. Sci. U. S. A.* 105, 3362–3367. doi: 10.1073/pnas.0705842105

Thyberg, J., Palmberg, L., Nilsson, J., Ksiazek, T., and Sjolund, M. (1983). Phenotype modulation in primary cultures of arterial smooth muscle cells. On the role of platelet-derived growth factor. *Differentiation* 25, 156–167. doi: 10.1111/j.1432-0436.1984.tb01351.x

Wang, D., Prakash, J., Nguyen, P., Davis-Dusenbery, B. N., Hill, N. S., Layne, M. D., et al. (2012). Bone morphogenetic protein signaling in vascular disease: anti-inflammatory action through myocardin-related transcription factor A. *J. Biol. Chem.* 287, 28067–28077. doi: 10.1074/jbc.M112.379487

Xia, X. D., Yu, X. H., Chen, L. Y., Xie, S. L., Feng, Y. G., Yang, R. Z., et al. (2021). Myocardin suppression increases lipid retention and atherosclerosis via downregulation of ABCA1 in vascular smooth muscle cells. *Biochim. Biophys. Acta Mol. Cell. Biol. Lipids* 1866:158824. doi: 10.1016/j.bbalip.2020.158824

Yang, Y., Cheng, X., Tian, W., Zhou, B., Wu, X., Xu, H., et al. (2014). MRTF-A steers an epigenetic complex to activate endothelin-induced pro-inflammatory transcription in vascular smooth muscle cells. *Nucleic Acids Res.* 42, 10460–10472. doi: 10.1093/nar/gku776

Yu, L., Weng, X., Liang, P., Dai, X., Wu, X., Xu, H., et al. (2014). MRTF-A mediates LPS-induced pro-inflammatory transcription by interacting with the COMPASS complex. *J. Cell. Sci.* 127, 4645–4657. doi: 10.1242/jcs.152314

Zhao, X. H., Laschinger, C., Arora, P., Szaszi, K., Kapus, A., and Mcculloch, C. A. (2007). Force activates smooth muscle alpha-actin promoter activity through the Rho signaling pathway. *J. Cell. Sci.* 120, 1801–1809. doi: 10.1242/jcs.001586

Zhu, B., Rippe, C., Thi Hien, T., Zeng, J., Albinsson, S., Stenkula, K. G., Uvelius, B., and Sward, K. (2017). Similar regulatory mechanisms of caveolins and cavins by myocardin family coactivators in arterial and bladder smooth muscle. *PLoS One* 12:e0176759. doi: 10.1371/journal.pone.0176759

Conflict of Interest: The authors declare that the research was conducted in the absence of any commercial or financial relationships that could be construed as a potential conflict of interest.

Publisher's Note: All claims expressed in this article are solely those of the authors and do not necessarily represent those of their affiliated organizations, or those of the publisher, the editors and the reviewers. Any product that may be evaluated in this article, or claim that may be made by its manufacturer, is not guaranteed or endorsed by the publisher.

frontiers in Physiology

ORIGINAL RESEARCH
published: 06 October 2021
doi: 10.3389/fphys.2021.735915

Classical and Non-classical Fibrosis Phenotypes Are Revealed by Lung and Cardiac Like Microvascular Tissues On-Chip

*Akinola Akinbote[1,2], Violeta Beltran-Sastre[1], Marta Cherubini[1], Roberta Visone[3,4], Cynthia Hajal[4], Defne Cobanoglu[1,2] and Kristina Haase[1]**

[1] European Molecular Biology Laboratory, Barcelona, Spain, [2] Heidelberg University, Faculty of Biosciences, Heidelberg, Germany, [3] Politecnico di Milano, Department of Electronics, Information, and Bioengineering, Milan Italy, [4] Massachusetts Institute of Technology, Department of Mechanical Engineering, Cambridge, MA, United States

Fibrosis, a hallmark of many cardiac and pulmonary diseases, is characterized by excess deposition of extracellular matrix proteins and increased tissue stiffness. This serious pathologic condition is thought to stem majorly from local stromal cell activation. Most studies have focused on the role of fibroblasts; however, the endothelium has been implicated in fibrosis through direct and indirect contributions. Here, we present a 3D vascular model to investigate vessel-stroma crosstalk in normal conditions and following induced fibrosis. Human-induced pluripotent stem cell-derived endothelial cells (hiPSC-ECs) are co-cultured with (and without) primary human cardiac and lung fibroblasts (LFs) in a microfluidic device to generate perfusable microvasculature in cardiac- and pulmonary-like microenvironments. Endothelial barrier function, vascular morphology, and matrix properties (stiffness and diffusivity) are differentially impacted by the presence of stromal cells. These vessels (with and without stromal cells) express inflammatory cytokines, which could induce a wound-healing state. Further treatment with transforming growth factor-β (TGF-β) induced varied fibrotic phenotypes on-chip, with LFs resulting in increased stiffness, lower MMP activity, and increased smooth muscle actin expression. Taken together, our work demonstrates the strong impact of stromal-endothelial interactions on vessel formation and extravascular matrix regulation. The role of TGF-β is shown to affect co-cultured microvessels differentially and has a severe negative impact on the endothelium without stromal cell support. Our human 3D *in vitro* model has the potential to examine anti-fibrotic therapies on patient-specific hiPSCs in the future.

Keywords: fibrosis on-chip, cardiac fibrosis, pulmonary fibrosis, microvasculature, microfluidics, ECM remodeling, TGF-β, matrix metalloproteases

OPEN ACCESS

Edited by:
Markus Hecker,
Heidelberg University, Germany

Reviewed by:
Alexander Widiapradja,
The University of Sydney, Australia
Martin Thunemann,
Boston University, United States
Valeria Orlova,
Leiden University Medical Center, Netherlands

****Correspondence:***
Kristina Haase
kristina.haase@embl.es

Specialty section:
This article was submitted to Vascular Physiology, a section of the journal Frontiers in Physiology

Received: *03 July 2021*
Accepted: *31 August 2021*
Published: *06 October 2021*

Citation:
Akinbote A, Beltran-Sastre V, Cherubini M, Visone R, Hajal C, Cobanoglu D and Haase K (2021) Classical and Non-classical Fibrosis Phenotypes Are Revealed by Lung and Cardiac Like Microvascular Tissues On-Chip. Front. Physiol. 12:735915. doi: 10.3389/fphys.2021.735915

INTRODUCTION

Organ fibrosis is responsible for a third of all fatalities globally and is a clinical hallmark of many cardiac and pulmonary diseases (Zeisberg and Kalluri, 2013). Fibrosis is characterized by excess deposition and remodeling of extracellular matrix (ECM) proteins, immune cell activation, and

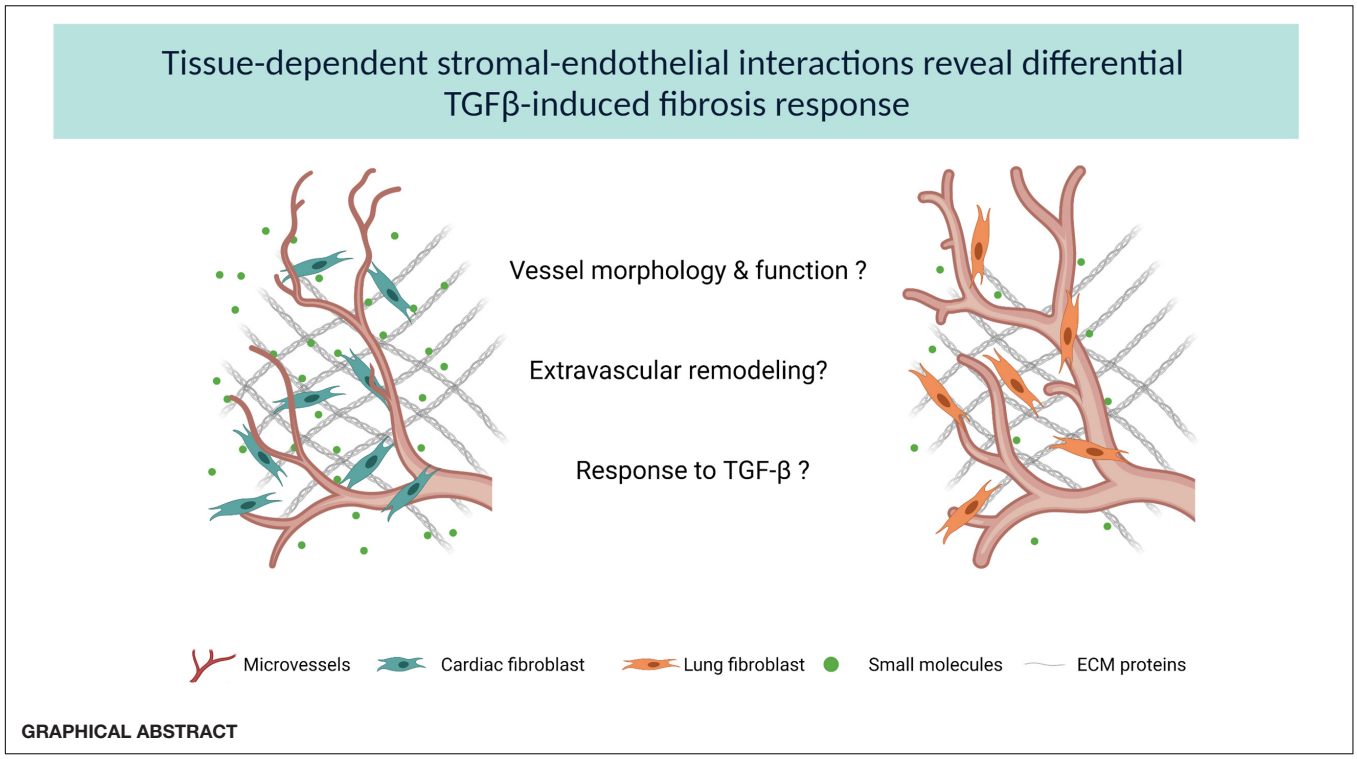

GRAPHICAL ABSTRACT

increased tissue stiffness, wherein a continued activation of fibroblasts results in a myofibroblast phenotype (Hinz et al., 2001; Wynn and Ramalingam, 2012). In both cardiac and pulmonary tissues, fibrosis can be divided up into two stages—characterized by matrix remodeling, inflammation, initial myofibroblast activation during the early stages; and increased matrix accumulation (scarring), presence of macrophages, and continued fibroblast activation during the later stages (Murtha et al., 2017). Myofibroblasts are implicated in excessive deposition of ECM proteins, are hyperproliferative, express alpha-smooth muscle actin (αSMA), and are more contractile than the native stromal cell population. As a result, there is a subsequent build-up of ECM proteins, such as collagen, which in turn increases tissue stiffness and activates more fibroblasts toward a myofibroblast phenotype—resulting in a deleterious positive feedback loop. While ECM deposition is an essential part of the wound healing cascade, if left unchecked, it can lead to pathological fibrosis. This compromises the structure and function of the native tissue, eventually resulting in organ failure (Anversa et al., 1991).

Various etiologies of cardiac and pulmonary diseases, such as idiopathic pulmonary fibrosis and ischemic heart disease, involve fibrotic tissue remodeling prior to the clinical manifestation of end-stage organ failure (Wynn and Ramalingam, 2012). While several factors such as microenvironmental stiffness, reactive oxygen species, growth factors, and cytokines, have been implicated in both cardiac and pulmonary fibrosis, transforming growth factor-β (TGF-β) has been identified as a central actor (Wynn and Ramalingam, 2012; Koliaraki et al., 2020; Wang et al., 2020, 2021). Continued secretion of TGF-β results in increased proliferation and activation of myofibroblasts resulting in dysfunctional ECM remodeling. Despite the many studies on fibrosis using *in vitro* and *in vivo* models, we are still limited in our understanding of disease progression in regards to the fibrotic response. This limitation has been attributed, in part, to inadequate humanized models which often fail to capture complex pathophysiology and predict drug interactions; animal models (*in vivo)* do not account for species-dependent differences while 2D models (*in vitro*) lack the complexity to model human tissue. As such, there has been a move toward more complex *in vitro* 3D models such as microfluidic (on-chip) and organoid systems.

In vitro models of cardiac and pulmonary fibrosis have mainly focused on stromal-parenchyma interactions and have largely excluded the role of the endothelium in modulating the fibrotic response (Alsafadi et al., 2017; Aghajanian et al., 2019; Mastikhina et al., 2020; Mejías et al., 2020; Sacchi et al., 2020; Wang et al., 2020). Endothelial cells (ECs), which line the vessels that pervade all tissues and actively participate in health and disease, have been implicated in pathological fibrosis, from its onset through its progression. It has been proposed that an endothelial mesenchymal transition (endoMT), vascular inflammatory response activation, endothelial senescence, and vessel rarefaction all contribute to fibrosis (Zeisberg et al., 2007a,b; Johnson and DiPietro, 2013; Pardali et al., 2017; Sun et al., 2020). While the role of the vasculature in fibrosis is becoming increasingly recognized, there is a need to characterize vascular phenotypic changes resultant from the onset of fibrosis. The use of functionally vascularized *in vitro* models that replicate hallmarks (adverse ECM remodeling, myofibroblast activation, and increased tissue stiffness) of cardiac and pulmonary fibrosis

is yet to be achieved. Considering that both the heart and lung are highly vascularized, it is of critical importance to examine the role of vessels and stromal-endothelial crosstalk in tissue-specific fibrosis.

To address this unmet need, we employed a 3D perfusable microvascular model to first understand the contributions of stromal cells to microvascular and extravascular matrix remodeling. Next, we use this system to induce fibrosis using TGF-β in cardiac- and pulmonary-like vascular tissues in a controlled manner. By culturing human-induced pluripotent stem cell-derived endothelial cells (hiPSC-ECs) with (or without) human primary cardiac (CFs) or lung fibroblasts (LFs), we demonstrate the impact of these stromal cells on endothelial barrier function, microvascular morphology, and ECM properties. Subsequent antagonization of our system with TGF-β reveals the severe impact of a fibrotic phenotype on vascular stability, and the time and dose-dependent effects on microvascular tissues (μVTs) in lung vs cardiac-like microenvironments. Treatment resulted in differential effects on αSMA expression, matrix remodeling, MMP activity, and changes in vascular stability between the two microvascular tissue types. Using the hiPSC-EC derived microvasculature, we were able to investigate the crosstalk with the local stromal population and minimize tissue-dependent endothelial cell heterogeneity. Our findings suggest that lung and cardiac μVTs respond to TGF-β in a differential manner, with LFs contributing to the development of a classical fibrotic phenotype and cardiac fibroblasts a non-classical phenotype.

MATERIALS AND METHODS

Cell Culture

Commercially available (and characterized) hiPSC-ECs were purchased from Cellular Dynamics (Fujifilm) and were cultured in endothelial media (VascuLife, Lifeline cell systems) with an additional 10 ml L-glutamine and 10% Fetal Bovine Serum on 30 μg/ml human fibronectin (Sigma) coated T-75 flasks. Primary normal human lung fibroblasts (NHLF) and primary normal human ventricular cardiac fibroblasts (NHCF-V) were purchased from Lonza. All cells were used between passages 5 and 7. NHLFs were cultured in Fibrolife media (Lifeline cell systems) on 50 μg/ml rat tail collagen I (Merck) coated T-75 flasks. NHCF-Vs were cultured in FibroLife supplemented with 10% FBS. All cells were cultured at 37°C and 5% CO_2, and a complete media change was conducted every other day. To culture the optimal cell numbers for device seeding, hiPSC-ECs were subdivided into 2 × T-150 flasks after the first passage and grown again to 80–90% confluency.

Device Fabrication

As previously described (Haase et al., 2019), devices were fabricated using PDMS (SYLGARD^{TM} 184 Silicone Elastomer Kit, Dow). The elastomer and cross-linker were mixed in a 10:1 ratio, per manufacturer's recommendations, degassed using a vacuum desiccator, and poured onto a fabricated mold, and degassed a second time. PDMS was then cured at 60°C overnight and individual devices were cut, punched, and air-plasma bonded (Harrick systems) to clean glass slides. While hydrophilic, a 100 μg/ml Poly-D-Lysine (Sigma) coating was applied for >2 h before rinsing with sterile MilliQ water three times. These devices were then incubated at 60°C overnight, reinstating hydrophobicity. Prior to cell seeding, all devices were sterilized under ultraviolet light for at least 30 min.

Device Seeding and Formation of Microvessels

Fibrinogen derived from bovine plasma (Sigma) was reconstituted in phosphate-buffered saline (PBS) to a working concentration of 6 mg/ml before use. Thrombin (Sigma) was diluted to a 4 U/ml working solution in cold VascuLife medium. Endothelial cells and stromal cells were then dissociated and mixed with the appropriate volume of thrombin and fibrinogen solution to make up final concentrations of 6 million cells/ml and 1.2 million cells/ml, respectively, resulting in a 5:1 ratio, as previously described (Haase et al., 2019). To seed one device, an 18 μl cell + thrombin (final concentration of 2U) suspension was mixed with an equal volume of fibrinogen solution (final concentration of 3 mg/mL). Following insertion into the gel channel, the mixture was allowed to polymerize for 20–30 min at 37°C in a humidified chamber. VascuLife media was supplemented with 50 ng/ml vascular endothelial growth factor A (VEGF; PeproTech) and was added to each media channel. The media was refreshed daily (150 μL) and cultured under static conditions.

Transforming Growth Factor-β Treatments

On day 4, microvessels were treated with one of two TGF-β treatment regimens (low concentration/short-term and high-concentration/long-term), with daily media changes. The low concentration/short-term regimen consisted of a 5 ng/ml TGF-β supplemented growth media (replenished daily) until day 7 of culture. The high concentration/long-term regimen consisted of a 25 ng/ml TGF-β supplemented growth media (replenished daily) until day 11 of culture. For 2D experiments, lung and cardiac fibroblasts were seeded in 6-well plates at 100,000 cells per well using FibroLife growth medium (2% FBS). Cells were then treated with 0, 5, or 25 ng/ml TGF-β supplemented growth medium for 48 h, with complete daily media change.

Cytokine Analysis

For 3D cytokine analysis, supernatants were pooled from $n = 4$ devices on day 5. We employed a human angiogenesis array (Abcam, ab134000) according to the manufacturer's instructions. The relative expression of cytokines (measured by fluorescent intensity) was compared between all groups, corrected to the negative controls on each array, and normalized to the positive controls, using the monoculture as the reference array. For 2D cytokine collection, lung and cardiac fibroblasts were seeded in 6-well plates at 100,000 cells per well using FibroLife growth medium (2% FBS). Supernatants were collected after 48 h in

culture. The cytokine profile was analyzed using the same human angiogenesis array (Abcam, ab134000). The relative expression of cytokines (measured by fluorescent intensity) was compared between all groups and normalized to the positive controls and negative controls. The blots were visualized using the Fusion FX Spectra (Vilber, France).

Growth Factors

Exogenous VEGF (PeproTech, 100-20) was made up at a stock concentration of 100 μg/ml in 0.1% Bovine Serum Albumin (BSA) PBS and was supplemented in media at a concentration of 50 ng/ml. TGF-β1 (PeproTech, 100-21) was made up at a stock concentration of 50 μg/ml in 0.2% BSA 4 mM HCl and used at 5, 10, and 25 ng/mL, as indicated.

MMP Expression

Supernatants were collected and pooled from n = 4 TGF-β treated devices on day 7, kept briefly on ice, then stored at −80°C until use. Using two separate DuoSet ELISA KITs (R&D systems, DY901B and DY911), the concentration of MMP-1 and MMP-9 were determined for TGF-β treated conditions per the manufacturer's instructions. Briefly, MMP concentrations were derived using measured absorbance values (with wavelength correction at 590 nm) compared to provided standards, accounting for the sample's dilution factor. For MMP1 detection, samples were prepared in a 1:500 dilution with the reagent diluent. While for MMP9, samples were prepared in a 1:1 ratio. The growth media was used as a control, to account for any exogenous MMPs from the added FBS. Measurements were done in triplicate with lung and cardiac fibroblast only controls.

Permeability Measurements

Microvessels were perfused on day 7 with 70 kDa FITC dextran (Merck) using a pressure gradient. Briefly, both media channels were emptied, then 40 μl of the fluorescent solute (100 μg/ml FITC dextran in vascular growth medium) was added to one media channel. Following perfusion through the microvessels, to halt convection, an additional 40 μl was added to the other media channel. After 1 min, time-lapse (3 × 3-min intervals) confocal z-stack images were acquired at a 5 μm step size and ≈20–25 slices. Analysis was done as previously described (Haase et al., 2019), using the equation below:

$$P(t) = \frac{A_T(I_{T_f} - I_{T_0})}{p_v t(I_{V_0} - I_{T_0})}$$

Where p_v is the vessel perimeter, I is the fluorescent intensity which is linearly related to the concentration of the fluorophore. $P(t)$ is the approximated permeability P (cm/s) and A_T is the extravascular tissue area.

Vessel Morphology Quantification

The maximum projected images of the FITC-dextran channels at t = 0 were used to quantify the morphology of the microvascular networks. Briefly, a custom Fiji macro was generated to process the images as follows: projections of maximum intensity of the FITC channel in the z-direction, Gaussian filter smoothing (with 3 iterations with sigma values of 3, 2, and 2), followed by adaptive local thresholding using the Phansalkar method (k = 0.5, r = 0.75, at a radius of 150 pixels), binarization, and the removal of outliers of radius 3 pixels. The built-in *Analyze particles* and *2D skeletonize* plug-ins were employed (**Supplementary Figure 2**). The morphological quantifications were then normalized to the area of the fully perfused regions, as these measurements were performed on FITC-dextran channels.

Extravascular Diffusivity

Small molecule diffusivity in the extravascular space was determined for each μVT condition using fluorescence recovery after photobleaching (FRAP), as previously described (Haase et al., 2020). After perfusion with a 70 kDa FITC-dextran into the microvessels, μVTs were incubated at 37°C for ≥1 h, to allow for total diffusion throughout the hydrogel (in the intra- and extravascular space). Intra- and extravascular regions are still detectable, as shown by outlines in **Figure 3A**. Bleaching was performed in 30 μm diameter regions, with 30 s total bleach + recovery. Over 10 measurements were taken per device. Time-lapse imaging was performed to capture the bleaching and subsequent recovery of fluorescence in the extravascular regions. These images were then analyzed using a MATLAB FRAP analysis tool (Jönsson et al., 2008) to correlate the changes in fluorescence intensity with time (**Figure 3B**). The diffusion time was estimated using L^2/D, where D is the diffusivity of the fluorescent particle and L is the maximum distance between blood vessels (in our case, the diameter of the bleached area; Dewhirst and Secomb, 2017).

Immunofluorescence Staining

Fixation was performed using 4% paraformaldehyde for 20 min prior to washing with PBS and subsequent solubilization using 0.1% Triton-X (10 mins). Samples were then incubated in applicable blocking buffer, PBS + BSA + serum of the secondary antibody, for more than 1 h. Primary antibodies were diluted in wash buffer (0.5% BSA in PBS) and were added to the samples and incubated overnight at 4°C. After overnight incubation, samples were washed with wash buffer and incubated with the appropriate secondary antibodies and counterstains (>2 h). Samples were rinsed with PBS and either imaged immediately or mounted on coverslips (for 2D samples) using Fluoromount-G (Invitrogen) and stored at 4°C before imaging. To stain microvessels within a device, a pressure gradient was applied across the gel for all staining and wash steps.

Nanoindenter Measurements

The effective Young's Modulus of fibrin hydrogels was measured using the Chiaro Nanoindenter (Optics 11, Amsterdam, Netherlands). Nanoindentation measurements were done at room temperature using spherical probe tips with a mean radius of 28.5 ± 3.12 μm and an average stiffness of 0.026 ± 0.002 N/M, respectively. To access the gel/tissue

in a device, a scalpel was gently used to cut away the top layer of PDMS with minimal gel agitation (**Figure 3D**). Prior to the probe insertion, the gel chamber was topped up with growth medium to ensure the gel remained fully hydrated during measurements. The probe was calibrated in media and then gently submerged into the liquid of the device containing the hydrogel. Measurements were performed with an indentation depth of 12 μm (∼2.4% of ∼500 μm thick hydrogel), using the manufacturer's indentation control function in the adhesion mode. An approach speed of 50 μm/s was employed. The effective Young's modulus was derived from load-indentation curves by fitting to the standard Hertz model and assuming a Poisson's ratio of 0.5, using the manufacturer's data analysis plug-in. On average, ∼16 measurements were analyzed per sample with an $n \geq 3$.

Statistics

Unless noted otherwise, one-way ANOVA was used to assess statistical significance across conditions at $P < 0.05$, and a *post-hoc* Tukey test was performed as a means comparison using OriginPro8. Data shown here are from $n \geq 3$ devices with at least 2 measurements per device, except for the nanoindentation measurements (∼16 measurements per device) and unless otherwise specified.

Western Blot

Gels were extracted using a scalpel to cut away the top layer of PDMS with minimal gel agitation. Each extract was directly transferred to 100 μl RIPA buffer on ice for tissue lysis. Samples were immediately frozen at −80°C for at least 30 min prior to sonication. Extracts were homogenized on ice using a Bioruptor® Sonication System with at least three freeze-sonicate-freeze cycles until the gel was fragmented. All samples were vortexed for 30 s and then centrifuged for 5 min at 4°C at maximum speed. Protein concentrations were determined from the supernatant using the Pierce™ BCA Protein Assay Kit according to the manufacturer's protocols. 10 μg of measured protein in lysates were then added to 4x sample buffer (Laemmli buffer + DDT) and RIPA buffer to make a 50 μl solution. Samples were then heated at 95°C for 5 min before gel loading in Mini-PROTEAN TGX Gels (BIO-RAD). Membranes were then blocked for 1 h on a rocker at RT in 5% nonfat dried milk powder in tris-buffered saline, 0.1% Tween-20 (TBST) after gel transfer. After blocking, antibodies for collagen-1 (Abcam, ab260043, 1:2000), α-SMA (Abcam, ab5694, 1:1000), and β-actin (Merck, A1978, 1:2000) were incubated at 4°C overnight on a rocker plate. Antibody binding was quantified using horseradish peroxidase-conjugated secondary anti-mouse (Abcam, ab205719, 1: 10,000) or anti-rabbit (Abcam, ab205718, 1: 10,000) after 1-h incubation. The blots were visualized using the Fusion FX Spectra (Vilber, France). Protein expression was normalized to β-actin expression using ImageJ. 2D cultures were extracted using a cell scraper and lysed on ice with RIPA buffer, then immediately homogenized for 10 min prior to vortexing.

RESULTS

Stromal Cells Impact Morphology of Human-Induced Pluripotent Stem Cell-Derived Microvasculature

Using our previous microfluidic design (Haase et al., 2019; Offeddu et al., 2019), hiPSC-ECs were cultured with (or without) human primary cardiac (CFs) or LFs to generate microvessels in tissue-like microenvironments (**Figure 1A**). Adapting our previously published protocol (Haase et al., 2019), cells were encapsulated in a fibrin gel, with an endothelial to stromal cell ratio of 5:1, in the middle chamber of a macro-scaled fluidic device. After several days in culture, hiPSC-ECs coalesce to form a well-connected vascular network with open lumens, as seen in confocal images for mono- and co-cultures (**Figure 1B**). Actin staining demonstrates stromal cell association with the endothelium in both co-cultures (**Figure 1B** and **Supplementary Figure 1**). Vascular morphology measurements were quantified in perfused regions of mono- and co-cultured vessels on day 7 of culture, revealing the strong influence of stromal cells in these networks (**Figures 1C–H**). Parameters including vessel (effective) diameter, area coverage, junction and branch densities, connectivity, and average branch length were all compared. Both lung and cardiac fibroblasts result in increased branching of the networks and reduced vessel diameters. Moreover, the average branch length is significantly reduced. Notably, in the case of the cardiac fibroblast co-cultures, the vessel area was also significantly reduced, and vessels appeared quite narrow (**Figures 1C**, **2** and **Supplementary Figures 1**, **2**). Perfusion was demonstrated using fluorescently labeled dextran coursing through the microvessel lumen (**Figure 2**). Perfusion of cardiac co-cultures was difficult and did not always result in fully perfused networks across the vascular bed.

Stromal Cells Affect Endothelial Barrier Properties

Perfusion with FITC-labeled 70 kDa dextran into the microvessels at day 7 allowed for measurements of vascular permeability, as previously described (Haase et al., 2019). By tracing the flux of the fluorescent solute from intra- to extra-vascular regions (see perfused vessels in **Figure 2A**) we determined that LFs did not affect barrier function; however, cardiac fibroblasts resulted in significantly reduced barrier function (increased permeability) compared to hiPSC-EC monoculture vessels (**Figure 2B**). The values reported for both mono-cultured and lung co-cultured microvessels are similar to those reported previously for hiPSC-EC vessels (Hajal et al., 2021) and similar to *in vivo* (non-human) measurements [summarized in Offeddu et al. (2019)]. We hypothesized that co-culture with stromal cells could contribute to an altered angiogenic profile. Therefore, we collected supernatants from microvessels (and fibroblasts seeded in fibrin gels alone) on day 5 post-seeding and performed a cytokine array. A semi-quantitative analysis demonstrated many similarities between the mono- and co-culture vessels

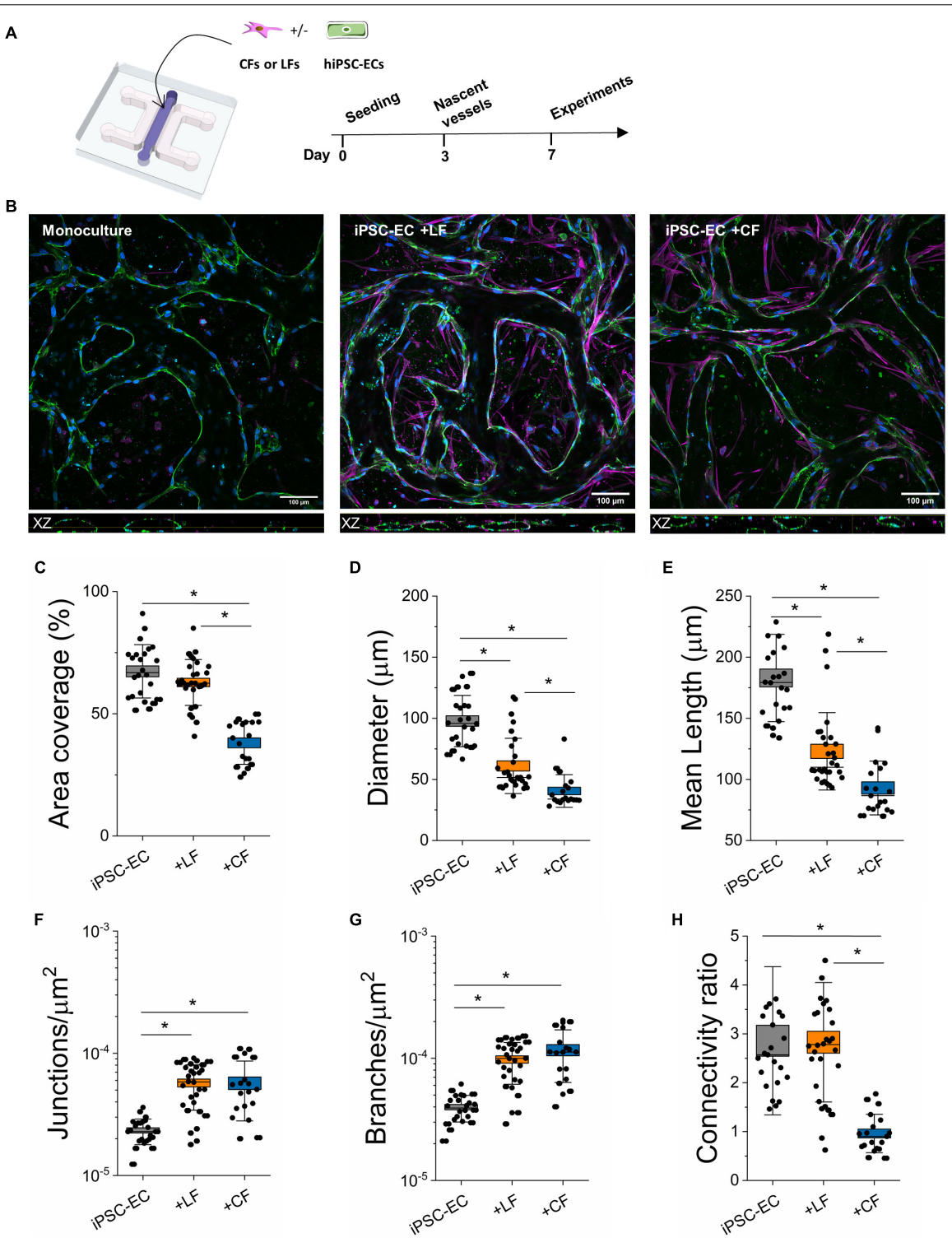

FIGURE 1 | Stromal cells alter the morphology of hiPSC-EC derived microvessels. **(A)** Schematic of the on-chip PDMS device used to generate hiPSC-derived microvessels. Cells are encapsulated within a fibrin hydrogel in the central channel and form microvascular networks as early as day 3. **(B)** Representative confocal images of microvascular networks taken at 20x. L-R: Microvessels derived from hiPSC-EC monoculture, hiPSC-EC and lung fibroblast co-culture, and hiPSC-EC and cardiac fibroblast co-culture. Microvessels were stained for a known endothelial marker, CD31 (green), and were counterstained by phalloidin (magenta) and Dapi (blue). Top: XY plane of formed microvascular networks. Bottom: orthogonal (XZ-plane) images of microvessels showing open lumens. **(C–H)** Comparison of morphological parameters between mono- and co-cultures. Shown are data from 3 separate experiments with ≥10 devices per condition. Box plots demonstrate SD (outer whiskers) and SE (box edge). Significance is shown by $^*P < 0.05$, using one-way ANOVA and a subsequent Tukey means comparison test.

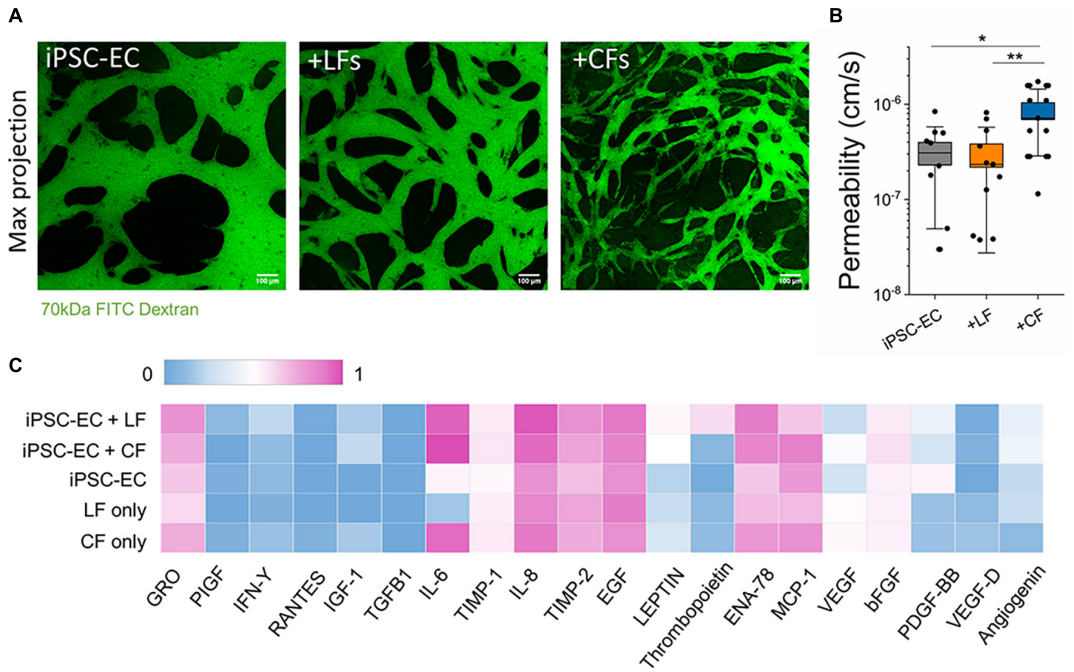

FIGURE 2 | Endothelial barrier function is affected by stromal cells. **(A)** Confocal maximum projection images demonstrating microvessels perfused with 70 kDa FITC dextran (green). The scale bar is 100 μm. **(B)** Endothelial permeability to 70 kDa FITC dextran, measured at day 7. CF co-culture significantly decreases endothelial barrier function. Shown are data from 3 separate experiments. Box plots demonstrate SD (outer whiskers) and SE (box edge). Significance is shown by $^{*}P < 0.05$, $^{**}P < 0.01$ using a *t*-test to compare with mono-cultured and co-cultured vessels. **(C)** Cytokine profiling using an antibody array from supernatant collected from microvessels at day 5. The measured intensity of the expressed cytokines was normalized intensity to the positive and negative controls on the array.

(**Figure 2C**). There were pronounced differences in ENA-78 and PDGF-BB between mono- and co-cultures, and overall high levels of IL-6, IL-8, TIMP-1, and TIMP-2 in all microvessels; most of these cytokines are negligibly expressed in the culture medium alone (**Supplementary Figure 6**). Notedly, IL-6 is increased in both 3D cultured CFs alone and when co-cultured with hiPSC-ECs. A separate cytokine profile of 2D cultured CFs again showed an increased expression of inflammatory factors CFs in comparison to LFs, despite both being cultured in a low-serum (2% FBS) medium (**Supplementary Figure 3A**).

Lung and Cardiac Fibroblasts Differentially Alter Extravascular Tissue

Fibroblasts are known to continually remodel the ECM *in vivo* and are implicated in tissue homeostasis and pathophysiology (Di Carlo and Peduto, 2018; Koliaraki et al., 2020; Buechler et al., 2021). However, less is known regarding their contribution to this process in the microvascular niche. Here, two approaches were employed to examine the impact of stromal cells on extravascular matrix remodeling. First, FRAP techniques, as previously described (Haase et al., 2020), were performed in the extravascular space to determine diffusivity. A 70 kDa FITC-dextran was perfused into the vessels, followed by incubation for several hours, to allow for total diffusion throughout the hydrogel (in the intra- and extravascular space). Vessel regions are still detectable in the device, as shown by outlines in **Figure 3A**. Time-lapse imaging was performed to capture the bleaching and subsequent recovery of fluorescence in the extravascular regions. These images were then analyzed using a MATLAB FRAP analysis tool (Jönsson et al., 2008) to correlate the changes in fluorescence intensity with time (**Figure 3B**). The diffusion time can be estimated using L^2/D, where D is the diffusivity of the fluorescent particle and L is the maximum distance between blood vessels (Dewhirst and Secomb, 2017). With an L of 30 μm, mean diffusion times for 70 kDa size molecules for the cardiac-like, lung-like, and monoculture μVTs were 24.2 ± 0.32, 25.79 ± 0.59, and 23.76 ± 0.26 s, respectively. Microvessels in the LF co-cultures resulted in extravascular regions with significantly reduced diffusivity in comparison to mono-cultured hiPSC-EC vessels (**Figure 3C**). Surprisingly, the cardiac co-cultured microvessels did not result in any significant change in diffusivity compared with monocultured vessels. Second, we aimed to correlate our findings from FRAP measurements with the mechanical properties of the microvessel tissues. Nanoindentation experiments were performed on the microvessel tissues following 7 days in culture. By carefully cutting away the PDMS using a surgical blade, the nanoindenter was used to probe the tissue stiffness of the various microvessels (**Figures 3D–F**). As expected, hydrogels containing vessels are significantly stiffer than fibrin (cultured in devices until day 7) alone. However, more importantly, LF co-cultured vessels

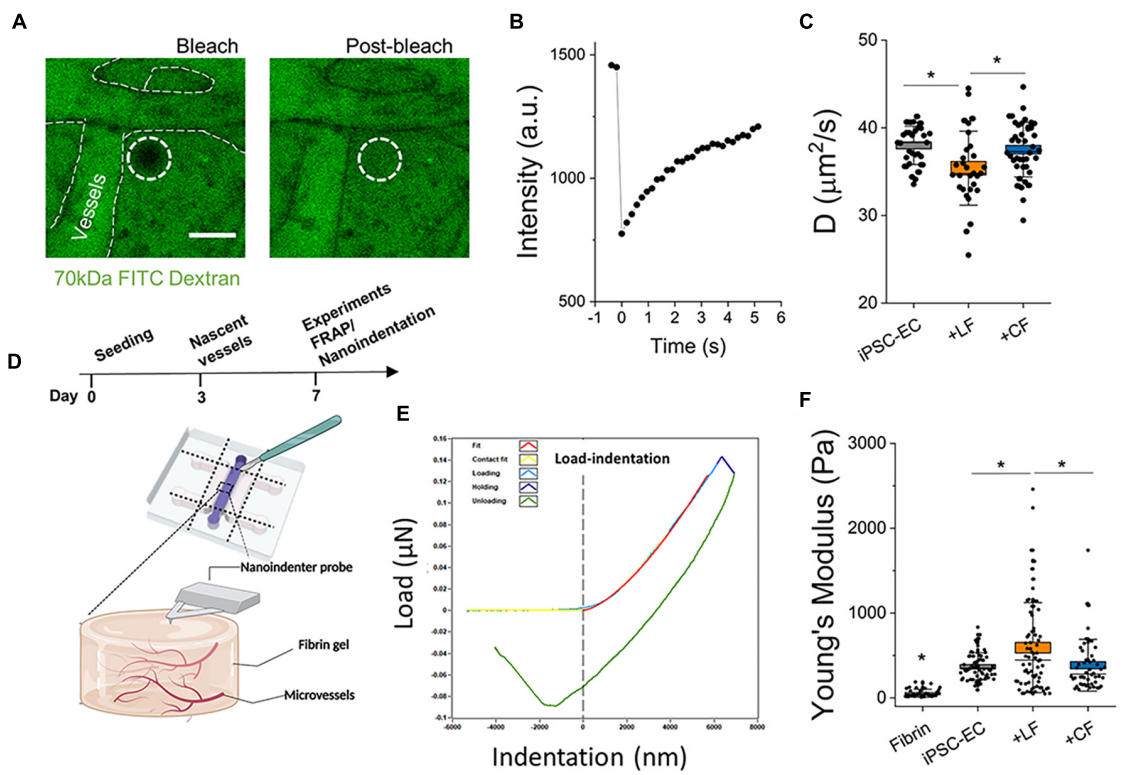

FIGURE 3 | Stromal cells impact extravascular matrix properties. **(A)** Representative images of FRAP measurements in the extravascular regions performed on day 7. Images show bleached and post-bleached regions—as indicated by the dotted white circle. **(B)** Example of post-bleach recovery, as measured by fluorescent intensity over time. **(C)** Diffusivity measurements of the extravascular regions from the different microvessels. **(D)** Experiment timeline for FRAP and schematic of nanoindentation measurements. **(E)** A representative load-indentation graph of the gel-microvessel substrate. The vertical dotted line indicates the intersection of the contact point. **(F)** Measured effective Young's modulus for Microvessels at day 7. Box plots demonstrate SD (outer whiskers) and SE (box edge). Significance is shown by $^*P < 0.05$, using one-way ANOVA and a subsequent Tukey means comparison test.

result in increased tissue stiffness, compared to both cardiac and mono-cultured hiPSC-EC vessels (**Figure 3F**) following 7 days of culture.

Transforming Growth Factor-β Treatment Induces Fibroblast-Specific Matrix Remodeling

Transforming growth factor-β has been widely utilized in replicating fibrotic hallmarks, such as the activation of myofibroblasts and increased ECM protein deposition (Wynn and Ramalingam, 2012; Pardali et al., 2017; Lemos and Duffield, 2018; Sun et al., 2020). Here, microvascular tissues were treated on day 4 (after the formation of nascent microvessels) with either one of two different TGF-β treatment regimens: low concentration/short-term and high-concentration/long-term (**Figure 4A**). These regimens served as lower and upper TGF-β thresholds examined previously in alternative *in vitro* fibrotic models (Thannickal et al., 2003; Jeon et al., 2014; Walker et al., 2019; Mastikhina et al., 2020; Mejías et al., 2020). Following treatment in the μVTs, we measured changes in stiffness using nanoindentation (**Figure 4B**) and corresponding αSMA (**Figure 4C**) and collagen levels (**Supplementary Figure 5**) by western blotting. In both regimens, there were no changes in the measured stiffness, αSMA expression, or collagen I expression between the treated and untreated hiPSC-EC microvessels. On the other hand, TGF-β treated LF co-cultures significantly increased in stiffness and correspondingly increased in αSMA expression. Surprisingly, TGF-β treated cardiac-like μVTs resulted in a decrease in the measured stiffness and αSMA expression; however, the microenvironment stiffness was only significantly affected under high-concentration/long-term treatments. No measurable differences in collagen expression were observed between the control and treated groups.

In an attempt to correlate the observed changes in stiffness with changes in ECM protein degradation, we next measured MMP activity in response to TGF-β treatment in the various μVTs (**Figure 4D**). Supernatants were collected from μVTs treated by the short-term/low concentration regimens and were analyzed by ELISA. Fibroblast-only controls (in fibrin) showed comparable expression to growth media for MMP-9, where FBS contains MMPs, as previously observed (Hu and Beeton, 2010). There was a marked increase in the endogenous expression of MMP 1 and -9 in vascularized μVTs. MMP-1 was highly expressed in the cardiac co-culture, in contrast with the low

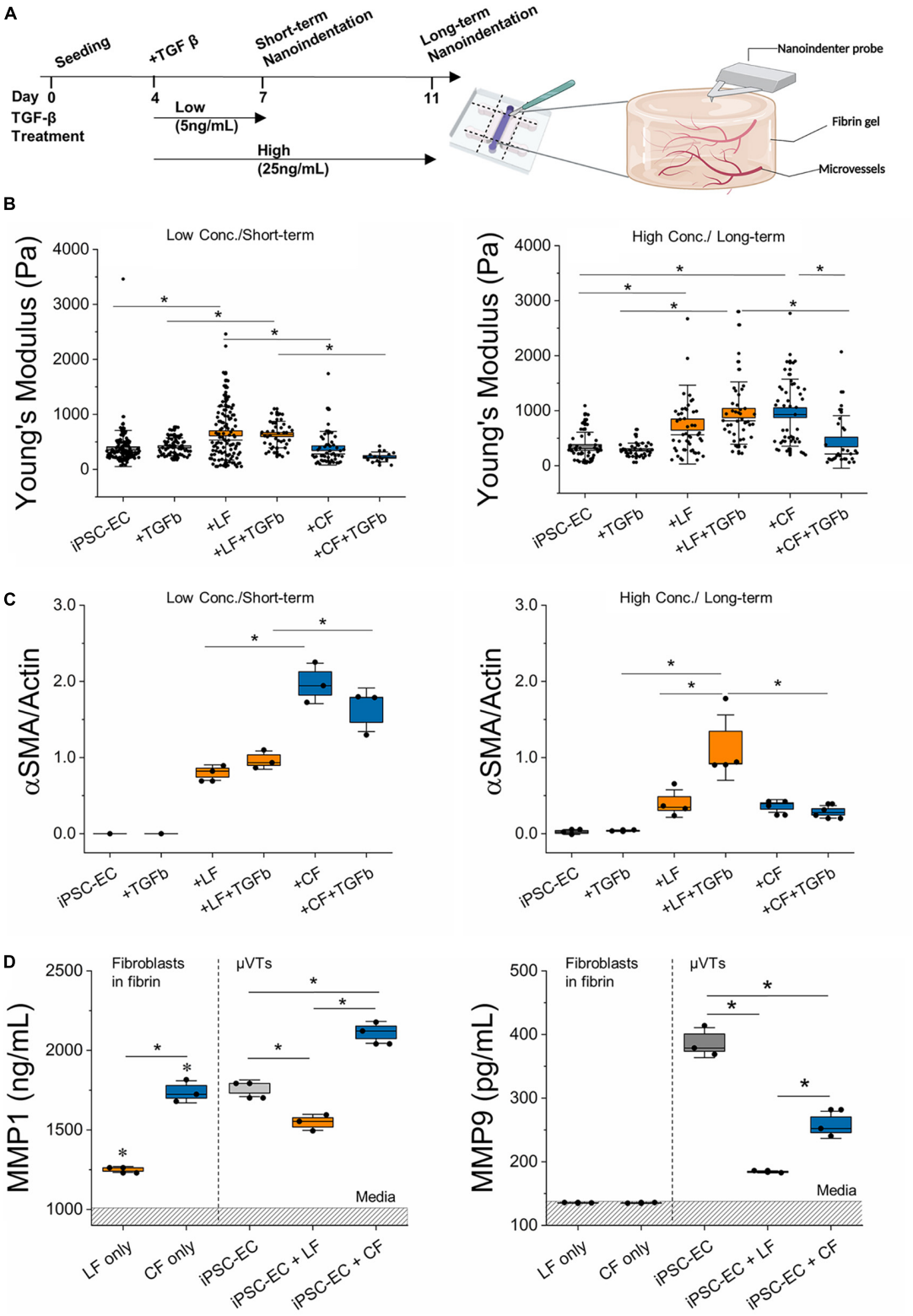

FIGURE 4 | TGF-β treatment induces differential stromal-cell matrix remodeling. **(A)** Schematic diagram of TGF-β treatment regimens and subsequent nanoindentation experiments. **(B)** Measured effective Young's modulus of the microvessels for the low concentration/short-term and high concentration/long-term conditions. **(C)** Relative αSMA expression in the different treatment regimens determined by Western Blot (for iPSC-EC low conc./short-term $n = 3$ samples were pooled). **(D)** MMP 1 and MMP 9 expressed in TGF-β treated microvascular tissues measured by ELISA. Dashed region is the mean value for media. Significance is shown by $^*P < 0.05$, using a one-way ANOVA and a subsequent Tukey means comparison test. Box plots demonstrate SD (outer whiskers) and SE (box edge).

expression in the lung co-culture. Fibroblast only cultures are significantly different from their respective μVTs. MMP-9 was expressed in higher amounts in the treated hiPSC-EC μVTs than in both co-cultures, corresponding with their relatively soft microenvironment, particularly in comparison to lung μVTs.

Phase-contrast images taken on days 7 and 10 also showed significant morphological changes resultant from the high-concentration/long-term regimen (**Supplementary Figure 4**). In general, TGF-β treated microvessels appear thinner than the untreated controls; vascular density decreased as the lumens narrowed and were more occluded. Overall, fibroblast co-cultured microvessels were more resilient to the treatment compared to the monoculture hiPSC-EC vessels.

DISCUSSION

Leveraging our experience in generating perfusable microvascular networks (Haase et al., 2019, 2020), we established perfusable lung- and cardiac-like microvascular tissues on-chip. To the best of our knowledge, we are the first to report microvascular morphometric changes in hiPSC-EC derived microvessels and alterations in extravascular matrix properties, due to the presence of tissue-specific fibroblasts. We employed hiPSC-ECs to understand how tissue-dependent stromal-endothelial interactions influence the fibrotic response in a controlled manner. This approach allowed us to isolate the influences of the local stromal population and minimize tissue-dependent endothelial cell heterogeneity, which has been shown to influence health and disease (Aird, 2007; Augustin and Koh, 2017; Pasut et al., 2021). Our results demonstrate a clear impact of lung and cardiac fibroblasts on the formation of hiPSC-EC derived microvessels. In both co-cultures, fibroblasts clearly associated with vasculature and strongly impacted their morphology, largely resulting in smaller diameter vessels and increased branching (**Figure 1B** and **Supplementary Figure 2**). Other *in vitro* models have demonstrated the importance of stromal-endothelial cell crosstalk in promoting vessel stability (Whisler et al., 2014; Zeinali et al., 2018; Mejías et al., 2020). Despite the same initial seeding ratio, cardiac fibroblasts, unlike those from the lung, led to narrower vessels and reduced endothelial barrier function. Moreover, LFs, as opposed to cardiac, significantly reduce extravascular diffusivity and increased the overall stiffness of μVTs in comparison to hiPSC-EC μVTs. Endothelial-stromal cell crosstalk results in varied effects for lung and cardiac μVTs and their extravascular microenvironments, which is summarized in **Figure 5**.

Considering its strong association with fibrosis, TGF-β was used to induce an increased fibrotic-like state in our μVTs. Treatment with TGF-β had a severe impact on vascular stability, resulting in loss of viable networks in the absence of stromal cells (**Supplementary Figure 4**). Interestingly, this effect was abrogated by the presence of lung and cardiac fibroblasts. In all TGF-β treated microvessels, network density appeared reduced, similar to previous observations *in vitro* in HUVEC-derived microvessels and bone marrow-derived human mesenchymal stem cells (Jeon et al., 2014). Reduction in microvessel density has been implicated in fibrosis *in vivo*, but whether rarefaction is an initiator, contributor, or a consequence of fibrosis is still unknown (Sun et al., 2020). A lower vascular density can advance fibrosis via hypoxia-induced fibroblast activation (Ballermann and Obeidat, 2014) and the upregulation of LOXL2 production (a prominent actor in collagen crosslinking) in exosomes secreted from hypoxic endothelial cells (de Jong et al., 2016). Future studies on vascular rarefaction in the context of TGF-β induced fibrosis on-chip could help elucidate its role in fibrosis.

Fibrotic mechanisms in cardiac and lung fibrosis have been hypothesized to differ in terms of apoptotic cell sources, outcome, timeline, collagen degradation, and anatomic location (Johnson and DiPietro, 2013; Murtha et al., 2017). A possible contributor to these observed differences could be attributed to the differential fibroblast response in vascular-matrix remodeling marked by differences in expressed αSMA levels, inflammatory profiles, MMP activity, and associated microvascular tissue stiffness, as observed herein. TGF-β treatment resulted in concentration-and-time-dependent changes in extravascular matrix remodeling for the lung- and cardiac-like μVTs (**Figure 4B**). For the lung-like μVTs, an increase in tissue stiffness and a corresponding significant increase in αSMA was observed due to long-term treatments at high concentrations (**Figures 4B,C** and **Supplementary Figure 5**). Various groups have reported different concentrations (1–50 ng/ml) of TGF-β and treatment durations (24 h to 3 weeks) to induce fibrosis *in vitro*; longer treatment periods have been observed to induce distinct classical fibrotic phenotypes with human donor cells (Thannickal et al., 2003; Jeon et al., 2014; Walker et al., 2019; Mastikhina et al., 2020; Mejías et al., 2020). However, the opposite trend was observed here in the cardiac vessels – reduced stiffness and a corresponding lower expression of αSMA (**Figure 4**). Notably, untreated cardiac-like μVTs resulted in a significant increase in stiffness over the long-term culture period, yet the addition of TGF-β led to a softening effect. Tissue stiffness has been reported previously to play a role in fibroblast activation and tissue remodeling (Shi et al., 2013; El-Mohri et al., 2017; Yeh et al., 2017; Notari et al., 2018; Wang et al., 2020, 2021). Softer microenvironments reduce fibroblast activation *in vivo* and in cardiac explant models (Notari et al., 2018; Wang et al., 2021). This decreased stiffness from TGF-β treatment could contribute to the reduced αSMA expression – taken here as an indicator of a reduced activated fibroblast population.

It has been suggested that the abundance of inflammatory factors in the early stages of cardiac fibrosis reduces TGF-β responsiveness, delaying myofibroblast activation and ECM protein deposition (Dobaczewski et al., 2011; Frangogiannis, 2014; Murtha et al., 2017). Our hiPSC-EC derived vessels (with and without stromal cells) express inflammatory cytokines (**Figure 3C**). Given that our vessels are cultured in a fibrin hydrogel, it is also possible that the normal (untreated) microvessel environment on-chip promotes a wound-healing state. Increased ENA-78 and IL-6 expression in these vessels suggest an inflammatory-like environment, and both factors have been previously implicated in fibrosis (Walz et al., 1997; Arenberg et al., 1998; Wynn and Ramalingam, 2012; Tanaka et al., 2014).

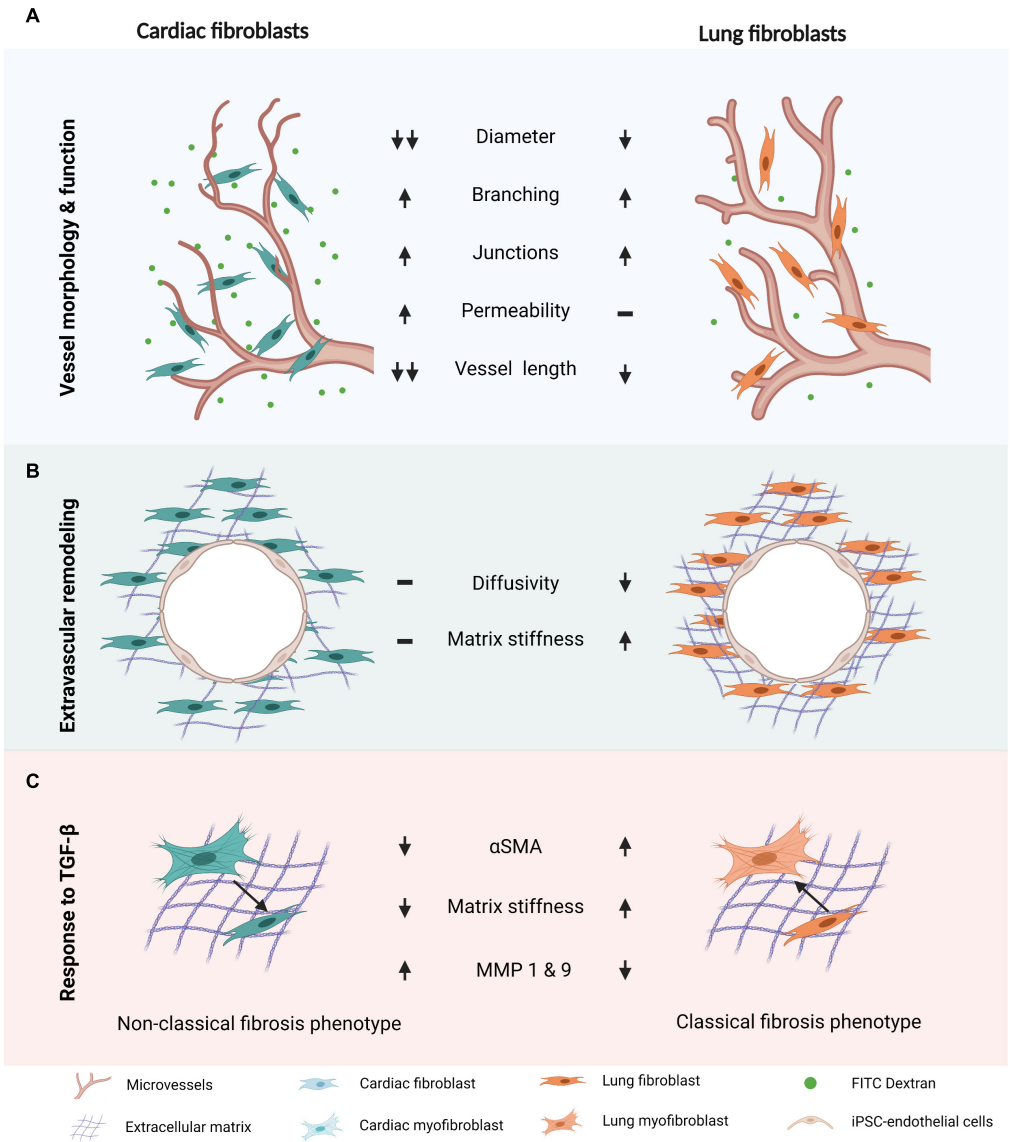

FIGURE 5 | Differential response of cardiac and pulmonary-like microvascular tissues in induced fibrosis. **(A)** Vessel morphology and endothelial barrier function are impacted by stromal cell type. **(B)** Extravascular matrix is differentially remodeled in cardiac and lung microvascular tissues. **(C)** There is a differential response to TGF-β stimulation in the cardiac and lung microvascular tissues. In **(A,B)**, trends are in comparison to the monoculture microvascular tissue properties.

Moreover, proinflammatory cytokines have been implicated in endothelial junction disruption, influencing endothelial barrier function (Wallez and Huber, 2008; Dejana et al., 2009; Alimperti et al., 2017). μVTs showed increased expression of inflammatory factors in both the cardiac fibroblast-only and cardiac-microvessel co-culture (**Figure 3C**). Additionally, a 2D array showed increased expression of inflammatory factors from cardiac, in comparison to LFs despite both being cultured in low-serum (2% FBS) medium (**Supplementary Figure 3A**). From our results, we expect that the differences in inflammatory signaling (increased IL-6) contribute to the observed differences in endothelial barrier function in the cardiac co-culture system (**Figures 2B,C** and **Supplementary Figure 3A**), but this needs to be confirmed in future studies. This increased inflammatory phenotype of the cardiac fibroblasts is consistent with reports of a prolonged inflammatory stage in cardiac fibrosis (Murtha et al., 2017). These differences in pro-inflammatory cytokines could delay the response to TGF-β in the cardiac-like μVTs, contributing to the different timelines observed in cardiac and pulmonary fibrosis.

The complex interplay between tissue inhibitors of metalloproteases (TIMPs) and MMPs also regulate the fate of ECM remodeling; however, there is limited information on the role of TIMPs in lung fibrosis (Murtha et al., 2017). Moreover, lung and cardiac fibrosis both lead to increased collagen synthesis; yet, cardiac fibrosis has been shown to result

in increased collagen degradation during early stages of the disease. Increased remodeling activity results in the breakdown of the collagen network in the case of cardiac fibrosis, while in the lung, it leads to collagen processing and maturation (Fan et al., 2012; Johnson and DiPietro, 2013; Murtha et al., 2017). Additionally, the upregulation of protease inhibitors, such as TIMPs, occurs after the inflammatory stage in cardiac fibrosis further contributing to the reported characteristics of early-stage fibrosis. These differences could explain the contrasting trends between cardiac- and lung-specific μVTs, which quite clearly follow unique timelines in ECM remodeling and production. Additionally, the differential effects of TGF-β on matrix regulation via MMP regulation could contribute to these differences (Uría et al., 1998; Padua and Massagué, 2009; Lian et al., 2021). TGF-β has been reported to up-regulate MMPs and down-regulate TIMPs in cancer cells, human fibroblasts, and endothelial cells (Uría et al., 1998; Padua and Massagué, 2009; Hsieh et al., 2010; Moore-Smith et al., 2017); conversely, it has also been implicated in downregulation of MMPs and the upregulation of TIMPs (Leivonen et al., 2013), suggesting a tissue and context-dependent role in matrix remodeling (Padua and Massagué, 2009; Krstic and Santibanez, 2014).

Our results demonstrate MMP-1 and MMP-9 (which act on collagen I and collagen IV, respectively) activity in all TGF-β stimulated μVTs (**Figure 4D**). Although FBS in the culture medium contains MMPs (Hu and Beeton, 2010), there was a marked increase in endogenous expression of MMP- 1 and -9 in treated microtissues. MMP-1 is an interstitial collagenase and acts on collagen I-III, VII, VIII, and gelatin. MMP-1 was highly expressed in the cardiac co-culture and lowest in the lung co-culture. Collagen I is the most abundant structural protein in fibrotic remodeling, and increased degradation activity could partially explain the decreased tissue mechanical properties observed in the TGF-β treated cardiac μVTs (**Figure 4**). MMP-9, which acts on collagen IV (a basement membrane protein), was also differentially expressed in the two tissues. It is naturally lower in fibroblasts and is mostly expressed by endothelial cells, to modulate their basement membrane (Lindner et al., 2012; Florence et al., 2017; Quintero-Fabián et al., 2019). MMP-9 was expressed highly in hiPSC-EC μVTs, suggesting that endothelial cells are largely responsible for MMP-9 induced remodeling. Lower MMP-1 activity in the lung co-cultures could explain a reduced ECM degradation and increased apparent stiffness of these tissues.

The differential expression of MMPs in tissue-specific fibroblasts has been explored by other groups (Collins et al., 2001; Lindner et al., 2012). Lindner et al. explored the mRNA expression of a range of MMPs in response to inflammatory cues using tissue necrotic factor-alpha (TNF-α) treatment on 2D cultured human fibroblasts. Cardiac fibroblasts, compared to LFs, showed a higher expression of MMP1. Conversely, they report that LFs showed a higher expression of MMP-9 than cardiac fibroblasts. While our data indicate that stromal cells alone in 3D fibrin gels do not express MMP-9 (above values seen in culture media), the mechanical cues from our 3D microenvironment and TGF-β treatment (as opposed to TNF-α) could contribute to these differences. Exploring the role of TIMPs, MMPs, the extent of collagen crosslinking (Tzortzaki et al., 2006; Barry-Hamilton et al., 2010), and cellular proliferation, in these tissue-specific microenvironments could also provide a better understanding of the different modes of vascular and extravascular remodeling.

Our data suggests the capacity of our model to recapitulate certain hallmarks of early-stage fibrosis (<2 weeks). Longer-term culture (21 days or more) might allow for the role of the endothelium in end-stage fibrosis to be revealed, where collagen accumulation is more evident. It has been suggested that the genetic modification of the ETV2 gene (to generate endothelial cells from fibroblasts) or the immortalization of endothelial lines using human telomerase reverse transcriptase can help extend the longevity of endothelial cells *in vitro* (Pham et al., 2018; Wan et al., 2021; Zhang et al., 2021)—which is a current limitation of our model and a major goal of our future studies. Beyond expected differences between various tissue sources, there is also expected variability between donor sources. Here, using primary cell lines we observed baseline differences in inflammatory cytokine expression and αSMA expression in stromal populations before TGF-β treatments (**Supplementary Figure 3**). This baseline αSMA expression in stromal cells could be, in part, attributed to the non-physiologic stiffness of the culture substrate. e.g., 3GPa for standard culture plastic vs 21 kPa for a healthy adult heart. Approaches toward "deactivating" or reducing the myofibroblast state *in vitro* are currently under investigation (Tatullo et al., 2016; Herum et al., 2017; Gilles et al., 2020; Mastikhina et al., 2020; Wang et al., 2021). However, our findings suggest that both the cardiac and LFs conserved their respective phenotypes, correlating with existing literature on differential fibrosis timelines, inflammatory profiles, and MMP activity. Future studies aim to derive all cell types from the same hiPSC donor which will provide valuable insight into patient-specific responses (from healthy and diseased sources). The pathogenesis of fibrosis in these two distinct organs will undoubtedly lead to differences in response times and remodeling behaviors, the exact mechanisms of which remain an open question and the focus of our future investigations.

In conclusion, functionally perfusable microvessels in cardiac- and lung-like microenvironments were developed on-chip to elucidate key stromal-endothelial interactions in vascular and extravascular tissue remodeling. Endothelial barrier function, vascular morphology, and matrix properties (tissue stiffness and diffusivity) are differentially impacted by the presence of lung and cardiac stromal cells. Classical hallmarks of fibrotic phenotypes were demonstrated in lung-like microenvironments, resulting in increased stiffness and αSMA expression in response to TGF-β treatment. Cardiac microvessels resulted in tissue softening upon TGF-β treatment and a correlated decrease in αSMA expression, suggesting tissue-specific differential matrix remodeling in comparison to lung μVTs. Differences in baseline pro-inflammatory cytokines, as well as MMP-1 and MMP-9 activity, between the two tissue type fibroblasts, correlate with the observed tissue-specific mechanisms seen *in vivo*. Our results lay the groundwork for future long-term studies into the mechanisms behind these varied fibrotic phenotypes

observed and provide insight into tissue-dependent fibrotic pathogenesis. Given the sensitivity of the system, hiPSCs from patients suffering from fibrosis could be used in a similar approach in the future to examine potential therapeutics.

DATA AVAILABILITY STATEMENT

The raw data supporting the conclusions of this article will be made available by the authors at request, without undue reservation.

AUTHOR CONTRIBUTIONS

AA performed and analyzed experiments and wrote the manuscript. VB-S performed and analyzed western blot experiments and contributed to experimental planning. MC performed some ELISA experiments and contributed to experimental planning. RV, DC, and CH performed preliminary experiments. KH directed and performed some of the experiments and contributed to editing the manuscript. All authors contributed to the article and approved the submitted version.

FUNDING

AA, VB-S, MC, DC, and KH were supported by funds from the European Molecular Biology Laboratory. DC was partly supported by the Erasmus plus program. RV was supported by a Progetto Rocca doctoral fellowship. CH was supported by the Ludwig Center for Molecular Oncology Graduate Fellowship.

ACKNOWLEDGMENTS

Graphics in **Figures 3–5** were created using BioRender.com. We thank our colleague, Jorge Lazaro Farre, EMBL Barcelona, for his assistance in the early stages of developing the image segmentation pipeline.

SUPPLEMENTARY MATERIAL

The Supplementary Material for this article can be found online at: https://www.frontiersin.org/articles/10.3389/fphys.2021.735915/full#supplementary-material

REFERENCES

Aghajanian, H., Kimura, T., Rurik, J. G., Hancock, A. S., Leibowitz, M. S., Li, L., et al. (2019). Targeting cardiac fibrosis with engineered T cells. *Nature* 573, 430–433. doi: 10.1038/s41586-019-1546-z

Aird, W. C. (2007). Phenotypic heterogeneity of the endothelium. *Circ. Res.* 100, 158–173. doi: 10.1161/01.RES.0000255691.76142.4a

Alimperti, S., Mirabella, T., Bajaj, V., Polacheck, W., Pirone, D. M., Duffield, J., et al. (2017). Three-dimensional biomimetic vascular model reveals a RhoA, Rac1, and N-cadherin balance in mural cell–endothelial cell-regulated barrier function. *Proc. Natl. Acad. Sci. U.S.A.* 114, 8758–8763. doi: 10.1073/pnas.1618333114

Alsafadi, H. N., Staab-Weijnitz, C. A., Lehmann, M., Lindner, M., Peschel, B., Königshoff, M., et al. (2017). An ex vivo model to induce early fibrosis-like changes in human precision-cut lung slices. *Am. J. Physiol. Lung Cell. Mol. Physiol.* 312, L896–L902. doi: 10.1152/ajplung.00084.2017

Anversa, P., Olivetti, G., and Capasso, J. M. (1991). Cellular basis of ventricular remodeling after myocardial infarction. *Am. J. Cardiol.* 68, 7–16. doi: 10.1016/0002-9149(91)90256-K

Arenberg, D. A., Keane, M. P., DiGiovine, B., Kunkel, S. L., Morris, S. B., Xue, Y. Y., et al. (1998). Epithelial-neutrophil activating peptide (ENA-78) is an important angiogenic factor in non-small cell lung cancer. *J. Clin. Invest.* 102, 465–472. doi: 10.1172/JCI3145

Augustin, H. G., and Koh, G. Y. (2017). Organotypic vasculature: from descriptive heterogeneity to functional pathophysiology. *Science* 357:eaal2379. doi: 10.1126/science.aal2379

Ballermann, B. J., and Obeidat, M. (2014). Tipping the balance from angiogenesis to fibrosis in CKD. *Kidney Int. Suppl.* 4, 45–52. doi: 10.1038/kisup.2014.9

Barry-Hamilton, V., Spangler, R., Marshall, D., McCauley, S., Rodriguez, H. M., Oyasu, M., et al. (2010). Allosteric inhibition of lysyl oxidase–like-2 impedes the development of a pathologic microenvironment. *Nat. Med.* 16, 1009–1017. doi: 10.1038/nm.2208

Buechler, M. B., Pradhan, R. N., Krishnamurty, A. T., Cox, C., Calviello, A. K., Wang, A. W., et al. (2021). Cross-tissue organization of the fibroblast lineage. *Nature* 593, 575–579. doi: 10.1038/s41586-021-03549-5

Collins, H. M., Morris, T. M., and Watson, S. A. (2001). Spectrum of matrix metalloproteinase expression in primary and metastatic colon cancer: relationship to the tissue inhibitors of metalloproteinases and membrane type-1-matrix metalloproteinase. *Br. J. Cancer* 84, 1664–1670. doi: 10.1054/bjoc.2001.1831

de Jong, O. G., van Balkom, B. W. M., Gremmels, H., and Verhaar, M. C. (2016). Exosomes from hypoxic endothelial cells have increased collagen crosslinking activity through up-regulation of lysyl oxidase-like 2. *J. Cell. Mol. Med.* 20, 342–350. doi: 10.1111/jcmm.12730

Dejana, E., Tournier-Lasserve, E., and Weinstein, B. M. (2009). The control of vascular integrity by endothelial cell junctions: molecular basis and pathological implications. *Dev. Cell* 16, 209–221. doi: 10.1016/j.devcel.2009.01.004

Dewhirst, M. W., and Secomb, T. W. (2017). Transport of drugs from blood vessels to tumour tissue. *Nat. Rev. Cancer* 17, 738–750. doi: 10.1038/nrc.2017.93

Di Carlo, S. E., and Peduto, L. (2018). The perivascular origin of pathological fibroblasts. *J. Clin. Invest.* 128, 54–63. doi: 10.1172/JCI93558

Dobaczewski, M., Chen, W., and Frangogiannis, N. G. (2011). Transforming growth factor (TGF)-β signaling in cardiac remodeling. *J. Mol. Cell. Cardiol.* 51, 600–606. doi: 10.1016/j.yjmcc.2010.10.033

El-Mohri, H., Wu, Y., Mohanty, S., and Ghosh, G. (2017). Impact of matrix stiffness on fibroblast function. *Mater. Sci. Eng. C* 74, 146–151. doi: 10.1016/j.msec.2017.02.001

Fan, D., Takawale, A., Lee, J., and Kassiri, Z. (2012). Cardiac fibroblasts, fibrosis and extracellular matrix remodeling in heart disease. *Fibrogenesis Tissue Repair* 5, 15. doi: 10.1186/1755-1536-5-15

Florence, J. M., Krupa, A., Booshehri, L. M., Allen, T. C., and Kurdowska, A. K. (2017). Metalloproteinase-9 contributes to endothelial dysfunction in atherosclerosis via protease activated receptor-1. *PLoS One* 12:e0171427. doi: 10.1371/journal.pone.0171427

Frangogiannis, N. G. (2014). The inflammatory response in myocardial injury, repair, and remodelling. *Nat. Rev. Cardiol.* 11, 255–265. doi: 10.1038/nrcardio.2014.28

Gilles, G., McCulloch, A. D., Brakebusch, C. H., and Herum, K. M. (2020). Maintaining resting cardiac fibroblasts in vitro by disrupting mechano-transduction. *PLoS OnE* 15:e0241390. doi: 10.1371/journal.pone.0241390

Haase, K., Gillrie, M. R., Hajal, C., and Kamm, R. D. (2019). Pericytes contribute to dysfunction in a human 3D model of placental microvasculature through VEGF—Ang—Tie2 signaling. *Adv. Sci.* 6:1900878. doi: 10.1002/advs.201900878

Haase, K., Offeddu, G. S., Gillrie, M. R., and Kamm, R. D. (2020). Endothelial regulation of drug transport in a 3D vascularized tumor model. *Adv. Funct. Mater.* 30:2002444. doi: 10.1002/adfm.202002444

Hajal, C., Shin, Y., Li, L., Serrano, J. C., Jacks, T., and Kamm, R. D. (2021). The CCL2-CCR2 astrocyte-cancer cell axis in tumor extravasation at the brain. *Sci. Adv.* 7:eabg8139. doi: 10.1126/sciadv.abg8139

Herum, K. M., Choppe, J., Kumar, A., Engler, A. J., and McCulloch, A. D. (2017). Mechanical regulation of cardiac fibroblast profibrotic phenotypes. *Mol. Biol. Cell* 28, 1871–1882. doi: 10.1091/mbc.E17-01-0014

Hinz, B., Celetta, G., Tomasek, J. J., Gabbiani, G., and Chaponnier, C. (2001). Alpha-smooth muscle actin expression upregulates fibroblast contractile activity. *Mol. Biol. Cell* 12, 2730–2741.

Hsieh, H.-L., Wang, H.-H., Wu, W.-B., Chu, P.-J., and Yang, C.-M. (2010). Transforming growth factor-β1 induces matrix metalloproteinase-9 and cell migration in astrocytes: roles of ROS-dependent ERK- and JNK-NF-κB pathways. *J. Neuroinflammation* 7:88. doi: 10.1186/1742-2094-7-88

Hu, X., and Beeton, C. (2010). Detection of functional matrix metalloproteinases by zymography. *J. Vis. Exp.* 45:2445. doi: 10.3791/2445

Jeon, J. S., Bersini, S., Whisler, J. A., Chen, M. B., Dubini, G., Charest, J. L., et al. (2014). Generation of 3D functional microvascular networks with mural cell-differentiated human mesenchymal stem cells in microfluidic vasculogenesis systems. *Integr. Biol. Quant. Biosci. Nano Macro* 6, 555–563. doi: 10.1039/c3ib40267c

Johnson, A., and DiPietro, L. A. (2013). Apoptosis and angiogenesis: an evolving mechanism for fibrosis. *FASEB J.* 27, 3893–3901. doi: 10.1096/fj.12-214189

Jönsson, P., Jonsson, M. P., Tegenfeldt, J. O., and Höök, F. (2008). A method improving the accuracy of fluorescence recovery after photobleaching analysis. *Biophys. J.* 95, 5334–5348. doi: 10.1529/biophysj.108.134874

Koliaraki, V., Prados, A., Armaka, M., and Kollias, G. (2020). The mesenchymal context in inflammation, immunity and cancer. *Nat. Immunol.* 21, 974–982. doi: 10.1038/s41590-020-0741-2

Krstic, J., and Santibanez, J. F. (2014). Transforming growth factor-beta and matrix metalloproteinases: functional interactions in tumor stroma-infiltrating myeloid cells. *Sci. World J.* 2014, e521754. doi: 10.1155/2014/521754

Leivonen, S.-K., Lazaridis, K., Decock, J., Chantry, A., Edwards, D. R., and Kähäri, V.-M. (2013). TGF-β-elicited induction of tissue inhibitor of metalloproteinases (TIMP)-3 expression in fibroblasts involves complex interplay between smad3, p38α, and ERK1/2. *PLoS One* 8:e57474. doi: 10.1371/journal.pone.0057474

Lemos, D. R., and Duffield, J. S. (2018). Tissue-resident mesenchymal stromal cells: implications for tissue-specific antifibrotic therapies. *Sci. Transl. Med.* 10:eaan5174.

Lian, G.-Y., Wang, Q.-M., Mak, T. S.-K., Huang, X.-R., Yu, X.-Q., and Lan, H.-Y. (2021). Inhibition of tumor invasion and metastasis by targeting TGF-β-Smad-MMP2 pathway with Asiatic Acid and Naringenin. *Mol. Ther. Oncol.* 20, 277–289. doi: 10.1016/j.omto.2021.01.006

Lindner, D., Zietsch, C., Becher, P. M., Schulze, K., Schultheiss, H.-P., Tschöpe, C., et al. (2012). Differential expression of matrix metalloproteases in human fibroblasts with different origins. *Biochem. Res. Int.* 2012:e875742. doi: 10.1155/2012/875742

Mastikhina, O., Moon, B.-U., Williams, K., Hatkar, R., Gustafson, D., Mourad, O., et al. (2020). Human cardiac fibrosis-on-a-chip model recapitulates disease hallmarks and can serve as a platform for drug testing. *Biomaterials* 233:119741. doi: 10.1016/j.biomaterials.2019.119741

Mejías, J. C., Nelson, M. R., Liseth, O., and Roy, K. (2020). A 96-well format microvascularized human lung-on-a-chip platform for microphysiological modeling of fibrotic diseases. *Lab. Chip* 20, 3601–3611. doi: 10.1039/D0LC00644K

Moore-Smith, L. D., Isayeva, T., Lee, J. H., Frost, A., and Ponnazhagan, S. (2017). Silencing of TGF-β1 in tumor cells impacts MMP-9 in tumor microenvironment. *Sci. Rep.* 7:8678. doi: 10.1038/s41598-017-09062-y

Murtha, L. A., Schuliga, M. J., Mabotuwana, N. S., Hardy, S. A., Waters, D. W., Burgess, J. K., et al. (2017). The processes and mechanisms of cardiac and pulmonary fibrosis. *Front. Physiol.* 8:777. doi: 10.3389/fphys.2017.00777

Notari, M., Ventura-Rubio, A., Bedford-Guaus, S. J., Jorba, I., Mulero, L., Navajas, D., et al. (2018). The local microenvironment limits the regenerative potential of the mouse neonatal heart. *Sci. Adv.* 4:eaao5553. doi: 10.1126/sciadv.aao5553

Offeddu, G. S., Haase, K., Gillrie, M. R., Li, R., Morozova, O., Hickman, D., et al. (2019). An on-chip model of protein paracellular and transcellular permeability in the microcirculation. *Biomaterials* 212, 115–125. doi: 10.1016/j.biomaterials.2019.05.022

Padua, D., and Massagué, J. (2009). Roles of TGFβ in metastasis. *Cell Res.* 19, 89–102. doi: 10.1038/cr.2008.316

Pardali, E., Sanchez-Duffhues, G., Gomez-Puerto, M. C., and Ten Dijke, P. (2017). TGF-β-induced endothelial-mesenchymal transition in fibrotic diseases. *Int. J. Mol. Sci.* 18:2157. doi: 10.3390/ijms18102157

Pasut, A., Becker, L. M., Cuypers, A., and Carmeliet, P. (2021). Endothelial cell plasticity at the single-cell level. *Angiogenesis* 24, 311–326. doi: 10.1007/s10456-021-09797-3

Pham, M. T., Pollock, K. M., Rose, M. D., Cary, W. A., Stewart, H. R., Zhou, P., et al. (2018). Generation of human vascularized brain organoids. *Neuroreport* 29, 588–593. doi: 10.1097/WNR.0000000000001014

Quintero-Fabián, S., Arreola, R., Becerril-Villanueva, E., Torres-Romero, J. C., Arana-Argáez, V., Lara-Riegos, J., et al. (2019). Role of matrix metalloproteinases in angiogenesis and cancer. *Front. Oncol.* 9:1370. doi: 10.3389/fonc.2019.01370

Sacchi, M., Bansal, R., and Rouwkema, J. (2020). Bioengineered 3D models to recapitulate tissue fibrosis. *Trends Biotechnol.* 38, 623–636. doi: 10.1016/j.tibtech.2019.12.010

Shi, Y., Dong, Y., Duan, Y., Jiang, X., Chen, C., and Deng, L. (2013). Substrate stiffness influences TGF-β1-induced differentiation of bronchial fibroblasts into myofibroblasts in airway remodeling. *Mol. Med. Rep.* 7, 419–424. doi: 10.3892/mmr.2012.1213

Sun, X., Nkennor, B., Mastikhina, O., Soon, K., and Nunes, S. S. (2020). Endothelium-mediated contributions to fibrosis. *Semin. Cell Dev. Biol.* 101, 78–86. doi: 10.1016/j.semcdb.2019.10.015

Tanaka, T., Narazaki, M., and Kishimoto, T. (2014). IL-6 in inflammation, immunity, and disease. *Cold Spring Harb. Perspect. Biol.* 6:a016295. doi: 10.1101/cshperspect.a016295

Tatullo, M., Marrelli, M., Falisi, G., Rastelli, C., Palmieri, F., Gargari, M., et al. (2016). Mechanical influence of tissue culture plates and extracellular matrix on mesenchymal stem cell behavior: a topical review. *Int. J. Immunopathol. Pharmacol.* 29, 3–8. doi: 10.1177/0394632015617951

Thannickal, V. J., Lee, D. Y., White, E. S., Cui, Z., Larios, J. M., Chacon, R., et al. (2003). Myofibroblast differentiation by transforming growth factor-β1 Is dependent on cell adhesion and integrin signaling via focal adhesion kinase*. *J. Biol. Chem.* 278, 12384–12389. doi: 10.1074/jbc.M208544200

Tzortzaki, E. G., Koutsopoulos, A. V., Dambaki, K. I., Lambiri, I., Plataki, M., Gordon, M. K., et al. (2006). Active remodeling in idiopathic interstitial pneumonias: evaluation of collagen types XII and XIV. *J. Histochem. Cytochem.* 54, 693–700. doi: 10.1369/jhc.5A6835.2006

Uría, J. A., Jiménez, M. G., Balbín, M., Freije, J. M. P., and López-Otín, C. (1998). Differential effects of transforming growth factor-β on the expression of collagenase-1 and collagenase-3 in human fibroblasts *. *J. Biol. Chem.* 273, 9769–9777. doi: 10.1074/jbc.273.16.9769

Walker, E. J., Heydet, D., Veldre, T., and Ghildyal, R. (2019). Transcriptomic changes during TGF-β-mediated differentiation of airway fibroblasts to myofibroblasts. *Sci. Rep.* 9:20377. doi: 10.1038/s41598-019-56955-1

Wallez, Y., and Huber, P. (2008). Endothelial adherens and tight junctions in vascular homeostasis, inflammation and angiogenesis. *Biochim. Biophys. Acta BBA Biomembr.* 1778, 794–809. doi: 10.1016/j.bbamem.2007.09.003

Walz, A., Schmutz, P., Mueller, C., and Schnyder-Candrian, S. (1997). Regulation and function of the CXC chemokine ENA-78 in monocytes and its role in disease. *J. Leukoc. Biol.* 62, 604–611. doi: 10.1002/jlb.62.5.604

Wan, Z., Zhang, S., Zhong, A. X., Shelton, S. E., Campisi, M., Sundararaman, S. K., et al. (2021). A robust vasculogenic microfluidic model using human immortalized endothelial cells and Thy1 positive fibroblasts. *Biomaterials* 276:121032. doi: 10.1016/j.biomaterials.2021.121032

Wang, X., Pierre, V., Liu, C., Senapati, S., Park, P. S.-H., and Senyo, S. E. (2021). Exogenous extracellular matrix proteins decrease cardiac fibroblast activation in stiffening microenvironment through CAPG. *J. Mol. Cell. Cardiol.* 159, 105–119. doi: 10.1016/j.yjmcc.2021.06.001

Wang, X., Senapati, S., Akinbote, A., Gnanasambandam, B., Park, P. S.-H., and Senyo, S. E. (2020). Microenvironment stiffness requires decellularized cardiac extracellular matrix to promote heart regeneration in the neonatal mouse heart. *Acta Biomater.* 113, 380–392. doi: 10.1016/j.actbio.2020.06.032

Whisler, J. A., Chen, M. B., and Kamm, R. D. (2014). Control of perfusable microvascular network morphology using a multiculture microfluidic system. *Tissue Eng. Part C Methods* 20, 543–552. doi: 10.1089/ten.tec.2013.0370

Wynn, T. A., and Ramalingam, T. R. (2012). Mechanisms of fibrosis: therapeutic translation for fibrotic disease. *Nat. Med.* 18, 1028–1040. doi: 10.1038/nm.2807

Yeh, Y.-C., Corbin, E. A., Caliari, S. R., Ouyang, L., Vega, S. L., Truitt, R., et al. (2017). Mechanically dynamic PDMS substrates to investigate changing cell environments. *Biomaterials* 145, 23–32. doi: 10.1016/j.biomaterials.2017.08.033

Zeinali, S., Bichsel, C. A., Hobi, N., Funke, M., Marti, T. M., Schmid, R. A., et al. (2018). Human microvasculature-on-a chip: anti-neovasculogenic effect of nintedanib in vitro. *Angiogenesis* 21, 861–871. doi: 10.1007/s10456-018-9631-8

Zeisberg, E. M., Potenta, S., Xie, L., Zeisberg, M., and Kalluri, R. (2007a). Discovery of endothelial to mesenchymal transition as a source for carcinoma-associated fibroblasts. *Cancer Res.* 67, 10123–10128.

Zeisberg, E. M., Tarnavski, O., Zeisberg, M., Dorfman, A. L., McMullen, J. R., Gustafsson, E., et al. (2007b). Endothelial-to-mesenchymal transition contributes to cardiac fibrosis. *Nat. Med.* 13, 952–961. doi: 10.1038/nm1613

Zeisberg, M., and Kalluri, R. (2013). Cellular Mechanisms of Tissue Fibrosis. 1. Common and organ-specific mechanisms associated with tissue fibrosis. *Am. J. Physiol. Cell Physiol.* 304, C216–C225. doi: 10.1152/ajpcell.00328.2012

Zhang, S., Wan, Z., and Kamm, D. R. (2021). Vascularized organoids on a chip: strategies for engineering organoids with functional vasculature. *Lab. Chip* 21, 473–488. doi: 10.1039/D0LC01186J

Conflict of Interest: The authors declare that the research was conducted in the absence of any commercial or financial relationships that could be construed as a potential conflict of interest.

The handling editor MH shares the secondary affiliation of the authors AA and DC. All parties confirm the absence of any collaboration during review.

frontiers in Physiology

ORIGINAL RESEARCH
published: 14 October 2021
doi: 10.3389/fphys.2021.727338

Effects of Low and High Aneurysmal Wall Shear Stress on Endothelial Cell Behavior: Differences and Similarities

Sandrine Morel[1,2], Sabine Schilling[3,4], Mannekomba R. Diagbouga[1], Matteo Delucchi[3], Marie-Luce Bochaton-Piallat[1], Sylvain Lemeille[1], Sven Hirsch[3†] and Brenda R. Kwak[1†]*

[1] Department of Pathology and Immunology, Faculty of Medicine, University of Geneva, Geneva, Switzerland, [2] Neurosurgery Division, Department of Clinical Neurosciences, Faculty of Medicine, Geneva University Hospitals, Geneva, Switzerland, [3] Institute of Applied Simulation, Zurich University of Applied Sciences, Wädenswil, Switzerland, [4] Institute of Tourism and Mobility, Lucerne School of Business, Lucerne University of Applied Sciences and Arts, Lucerne, Switzerland

OPEN ACCESS

Edited by:
Markus Hecker,
Heidelberg University, Germany

Reviewed by:
Jaap Diederik Van Buul,
University of Amsterdam, Netherlands
Andreas H. Wagner,
Heidelberg University, Germany

***Correspondence:**
Brenda R. Kwak
brenda.kwakchanson@unige.ch

† These authors have contributed equally to this work and share senior authorship

Specialty section:
This article was submitted to Vascular Physiology, a section of the journal Frontiers in Physiology

Received: 18 June 2021
Accepted: 21 September 2021
Published: 14 October 2021

Citation:
Morel S, Schilling S, Diagbouga MR, Delucchi M, Bochaton-Piallat M-L, Lemeille S, Hirsch S and Kwak BR (2021) Effects of Low and High Aneurysmal Wall Shear Stress on Endothelial Cell Behavior: Differences and Similarities. Front. Physiol. 12:727338. doi: 10.3389/fphys.2021.727338

Background: Intracranial aneurysms (IAs) result from abnormal enlargement of the arterial lumen. IAs are mostly quiescent and asymptomatic, but their rupture leads to severe brain damage or death. As the evolution of IAs is hard to predict and intricates medical decision, it is essential to improve our understanding of their pathophysiology. Wall shear stress (WSS) is proposed to influence IA growth and rupture. In this study, we investigated the effects of low and supra-high aneurysmal WSS on endothelial cells (ECs).

Methods: Porcine arterial ECs were exposed for 48 h to defined levels of shear stress (2, 30, or 80 dyne/cm^2) using an Ibidi flow apparatus. Immunostaining for CD31 or γ-cytoplasmic actin was performed to outline cell borders or to determine cell architecture. Geometry measurements (cell orientation, area, circularity and aspect ratio) were performed on confocal microscopy images. mRNA was extracted for RNAseq analysis.

Results: ECs exposed to low or supra-high aneurysmal WSS were more circular and had a lower aspect ratio than cells exposed to physiological flow. Furthermore, they lost the alignment in the direction of flow observed under physiological conditions. The effects of low WSS on differential gene expression were stronger than those of supra-high WSS. Gene set enrichment analysis highlighted that extracellular matrix proteins, cytoskeletal proteins and more particularly the actin protein family were among the protein classes the most affected by shear stress. Interestingly, most genes showed an opposite regulation under both types of aneurysmal WSS. Immunostainings for γ-cytoplasmic actin suggested a different organization of this cytoskeletal protein between ECs exposed to physiological and both types of aneurysmal WSS.

Conclusion: Under both aneurysmal low and supra-high WSS the typical arterial EC morphology molds to a more spherical shape. Whereas low WSS down-regulates the expression of cytoskeletal-related proteins and up-regulates extracellular matrix

proteins, supra-high WSS induces opposite changes in gene expression of these protein classes. The differential regulation in EC gene expression observed under various WSS translate into a different organization of the ECs' architecture. This adaptation of ECs to different aneurysmal WSS conditions may affect vascular remodeling in IAs.

Keywords: intracranial aneurysm, endothelial cell, wall shear stress, cell shape, differential gene expression, cytoskeleton

INTRODUCTION

Intracranial aneurysms (IAs) resulting from the deformation and enlargement of the lumen in arteries of the circle of Willis affect three to five percent of the population (Lawton and Vates, 2017). Most of the IAs are quiescent and asymptomatic, but their rupture leads to severe brain damage or death. Decision to treat an unruptured IA has to be taken considering (1) the annual rupture rate of the IA which is depending of patient and aneurysm characteristics, and (2) the mortality and morbidity rates associated with the treatment of the IA (Greving et al., 2014; Etminan et al., 2015). Despite intense research it is today still impossible to precisely predict the rupture probability of an individual IA. To better forecast the evolution of an unruptured IA, a broad understanding of the IA pathophysiology is needed.

Biomechanical forces are considered as important actors in IA initiation, growth and rupture (Munarriz et al., 2016; Diagbouga et al., 2018). Wall shear stress (WSS) defined as the tangential force per unit area imposed by the blood flow on the arterial wall per unit area is sensed by endothelial cells (ECs). In cerebral arteries, optimal function of ECs is associated with a physiological WSS of 20–30 dyne/cm^2 (Zhao et al., 2015). Under laminar shear stress, cells are aligned in the direction of the flow and are in a quiescent and cytoprotective state (Kwak et al., 2014). Whereas the role of high WSS gradients on the initiation of IA formation is well established, the impact of WSS on IA growth and rupture is less understood (Meng et al., 2014; Staarmann et al., 2019). Flow patterns change in evolving IAs depending on their location, geometry (especially IA neck dimension) and their parental artery's geometry. In human IAs, low WSS close to 2 dyne/cm^2 is typically observed in wide-neck aneurysms with a slow recirculating flow whereas supra-high WSS (> 70 dyne/cm^2) is found in aneurysms with impinging jet flow (Meng et al., 2014; Munarriz et al., 2016; Staarmann et al., 2019). These aneurysmal flow patterns affect IA pathophysiology: while low WSS seems to promote atherosclerotic, inflammatory and thrombotic processes, supra-high WSS has been associated with smooth muscle cell phenotypic changes and apoptosis (Meng et al., 2014; Munarriz et al., 2016; Cebral et al., 2019; Frosen et al., 2019; Staarmann et al., 2019).

Both low and supra-high WSS can alter normal endothelium toward a dysfunctional state, a process called "endothelial injury." In the past two decades, many studies revealed that ECs are able to detect and to respond in a specific manner to defined changes in shear stress magnitude, frequency or direction, this way dictating vascular pathophysiology (Kwak et al., 2014; Jiang et al., 2015). For instance, vulnerable or stable atherosclerotic lesions could be induced in mouse carotid arteries *in vivo* in response to low laminar or oscillatory WSS, respectively, using a shear stress-modifying cuff (Cheng et al., 2006). ECs are equipped with a multitude of potential shear stress sensors including membrane-associated molecules (e.g., ion channels, receptors, adhesion molecules), the glycocalyx and specific membrane microdomains such as caveolae and primary cilia (Ando and Yamamoto, 2013; Kwak et al., 2014). We recently reported that the EC response to aneurysmal low WSS was dampened in ECs without primary cilium, leading to disorganized intercellular junctions and increased endothelial permeability (Diagbouga et al., 2021). Altered endothelial function is supposed to be an important factor for the increased severity of IA disease observed in polycystic kidney disease (PKD) patients, a genetic disorder affecting primary cilia (Cho et al., 2021). Little is known, however, on the potential differences in endothelial dysfunction/injury induced by the diverse flow magnitudes in IAs. In the present study, we investigated the changes in EC gene expression and cellular morphology following exposure to low or supra-high WSS.

MATERIALS AND METHODS

Cell Culture and Flow Experiments

Coronary arteries of 8-month-old pigs were obtained from a nearby slaughterhouse. Primary arterial ECs were isolated as previously described (Hao et al., 2002) and cultured in Dulbecco's Modified Eagle Medium (DMEM) supplemented with 10% fetal calf serum and 100 g/mL heparin. Cells were grown in dishes coated with 1% gelatin (Sigma-Aldrich) at 37°C in a humidified atmosphere containing 5% CO_2. For flow experiments, cells were seeded on 1% gelatin coated Ibidi μ-Slides VI$^{0.4}$ at 30.000 cells per channel and grown until confluence. Laminar shear stress of 2, 30, or 80 dyne/cm^2 was applied for 48 h using an Ibidi flow system as previously described (Pfenniger et al., 2012; Denis et al., 2019; Diagbouga et al., 2021).

Immunofluorescence

Cultured cells were fixed in ice-cold 100% methanol for 5 min and stained using primary antibodies recognizing CD31 (endothelial cell membrane receptor, Santa Cruz sc-1506, 1/50) or γ-cytoplasmic actin (mAb 2A3, 1/100) (Dugina et al., 2009) for 2 h at room temperature. Next, Alexa Fluor 568-conjugated anti-goat and 488-conjugated

anti-mouse antibodies (Thermo Fisher Scientific, 1/2000) were used for signal detection. Nuclei were counterstained with 4′,6-diamidino-2-phenylindol (DAPI). Fluorescence was preserved using Ibidi mounting medium. Images were obtained by confocal laser scanning microscopy (Leica SP5 or Zeiss LSM800 Airyscan). Images were analyzed using the NIH Image software (NIH AutoExtractor 1.51; National Institutes of Health).

Quantifying Cell Shape Changes and Cell Orientation

The angle γ between the blood flow direction, which is for the remainder of the paper to be assumed to be in the positive x-axis direction, and each cell's major axis characterized the cell's orientation. Measured angles were between 0° and 180°. As the cell's major axis orientation should be independent of an angle measurement in clockwise or anti-clockwise direction, we projected all angles γ' from the second quadrant to the first quadrant *via* $\gamma = 180° - \gamma$'. We introduced the circularity measure $C = 4\pi A/L^2$, with A for the area of the cell and L its perimeter. Whereas this measure is 1 for a perfectly circular cell, it is smaller than 1 for all other cell shapes. Cell elongation was quantified by the aspect ratio of the cell's fitted ellipse. That is, the ratio of major axis to minor axis. All geometry measurements based on confocal microscopy of porcine arterial ECs were performed with the imaging processing package Fiji (Schindelin et al., 2012).

We assumed the null hypothesis that the samples in the three different flow conditions for each cell shape measure originate from the same distribution. Assuming an error probability of $\alpha = 0.01$ we rejected the null hypothesis for all three quantifications performing Kruskal-Wallis-tests resulting in significant p-values ($p < 10^{-6}$). Subsequently, we performed for each shape measure pairwise two-sided Wilcoxon rank-sum-tests between the flow conditions with the Holm-Bonferoni correction for multiple testing (Holm, 1979). If the difference between two flow conditions was significant ($p < 0.01$), the small characters below the box plots in **Figure 1** differ. All statistical tests were performed with the package visStatistics (Schilling, 2021) using the statistical software R (R Core Team, 2020).

Library Preparation, Sequencing, Read Mapping to the Reference Genome

Total RNA was isolated from porcine arterial ECs using the nucleospin RNA II kit (Machery-Nagel) according to the manufacturers' instructions. Three independent experiments were performed for each WSS condition, systematically comparing the WSS 2 dyne/cm^2 vs. 30 dyne/cm^2 or 80 dyne/cm^2 vs. 30 dyne/cm^2 from the same donor and cell passage. The quality of all samples was verified using the Agilent 2100 Bioanalyzer with the Agilent RNA 6000 Nano Kit (Agilent Technologies). cDNA libraries were constructed by the genomic platform of the University of Geneva using the Illumina TruSeq RNA sample preparation kit according to the manufacturers' protocol. Libraries were sequenced using single-end (100 nt-long) on Illumina HiSeq2000. FastQ reads were mapped to the ENSEMBL reference genome (Sscrofa11.1.96) using STAR version 2.4.0j (Dobin et al., 2013) with standard settings, except that any reads mapping to more than one location of the genome (ambiguous reads) were discarded ($m = 1$). Sequence data have been submitted to GEO database under accession number GSE173928. A unique gene model was used to quantify reads per gene. Briefly, the model considers all annotated exons of all annotated protein coding isoforms of a gene to create a unique gene where the genomic region of all exons was considered as coming from the same RNA molecule and merged together.

RNAseq Data Analysis

All reads overlapping the exons of each unique gene model were reported using featureCounts version 1.4.6-p1 (Liao et al., 2014). Gene expression was reported as raw counts and in parallel normalized in reads per kilobase million (RPKM) in order to filter out genes with low expression value (1 RPKM) before calling for differentially expressed genes. Library size normalizations and differential gene expression calculations were performed using the package edgeR (Robinson et al., 2010) designed for the R software (R Core Team, 2020). Only genes having a significant fold-change ≥ 2 and the Benjamini-Hochberg corrected p-value < 0.05 were considered for the differentially expressed genes analysis.

Gene Set Enrichment Analysis

Families and sub-families of proteins were downloaded from PANTHER database for *Sus scrofa* and used to generate gene sets. Genes were ranked by their calculated fold-changes (decreasing ranking). A gene set analysis using the gene set enrichment analysis (GSEA) package Version 2.2 (Mootha et al., 2003; Subramanian et al., 2005) from the Broad Institute (MIT, Cambridge, MA) was used to analyze the pattern of differential gene expression between the two groups. Gene set permutations were performed 1,000 times for each analysis. The Normalized Enrichment Score (NES) was calculated for each gene set. GSEA results with a nominal False Discovery Rate (FDR) < 0.05 and abs(NES) > 1 were considered significant.

PANTHER Gene Ontology

Differentially expressed genes (either in 2 dyne/cm^2 or 80 dyne/cm^2 vs. 30 dyne/cm^2) were annotated with the PANTHER tool gene ontology: protein class and represented in pie charts. 1: Calcium-binding proteins (PC00060); 2: Cell adhesion molecules (PC00069); 3: Cell junction proteins (PC00070); 4: Chaperones (PC00072); 5: Chromatin/chromatin-binding, or -regulatory proteins (PC00077); 6: Cytoskeletal proteins (PC00085); 7: Defense/immunity proteins (PC00090); 8: Extracellular matrix proteins (PC00102); 9: Gene-specific transcriptional regulators (PC00264); 10: Intercellular signal molecules (PC00207); 11: Membrane traffic proteins (PC00150); 12: Metabolite interconversion enzymes (PC00262); 13: Nucleic acid binding proteins (PC00171); 14: Protein modifying enzymes (PC00260); 15: Protein-binding activity modulators (PC00095); 16: Scaffold/adaptor proteins (PC00226); 17: Structural proteins

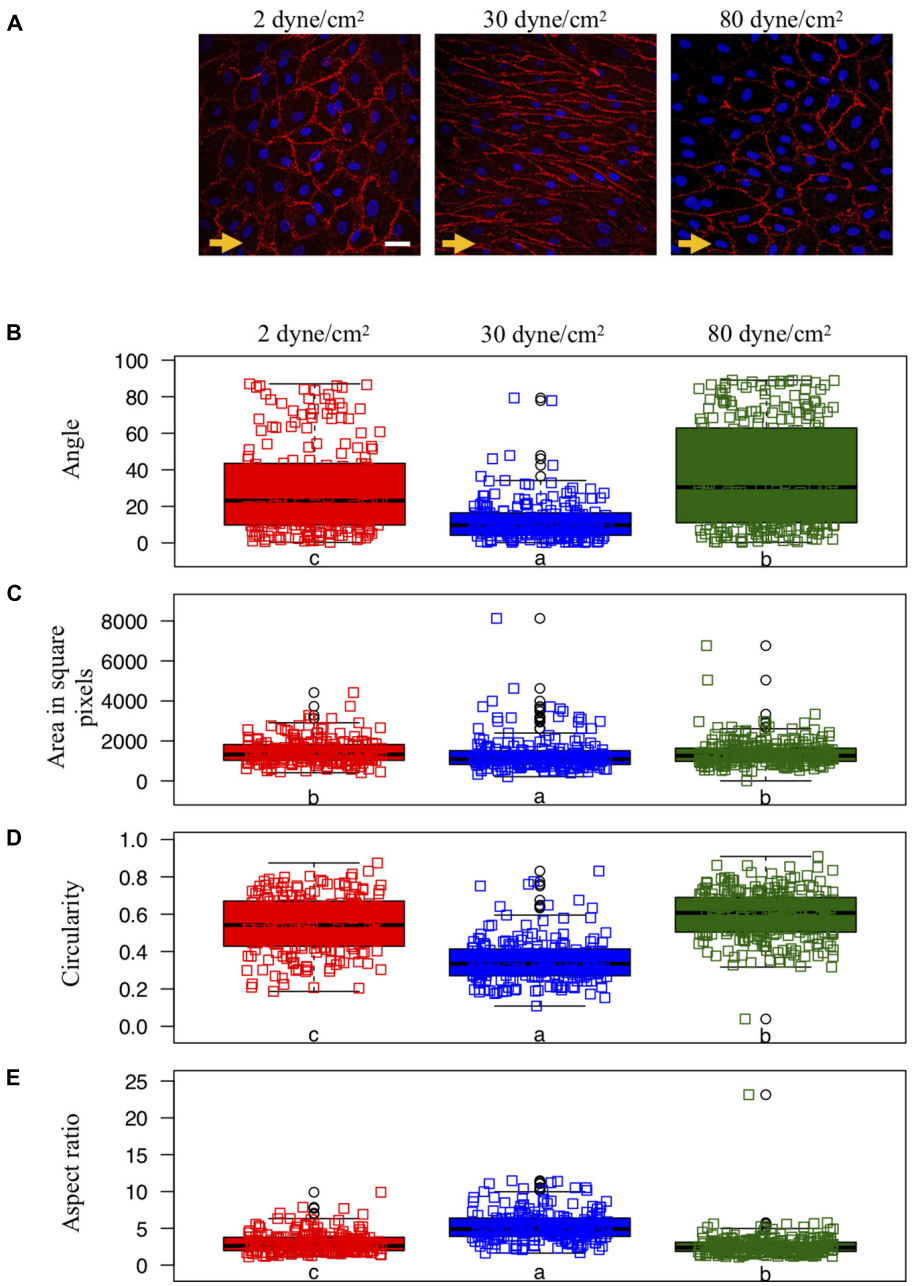

FIGURE 1 | Endothelial cell shape and organization under various shear stress conditions. **(A)** Representative examples of ECs exposed to different *in vitro* conditions of shear stress: aneurysmal low shear stress = 2 dyne/cm^2 (left panel), physiological shear stress = 30 dyne/cm^2 (middle panel) or aneurysmal supra-high shear stress = 80 dyne/cm^2 (right panel). The direction of the flow is indicated by orange arrows. CD31 immunostaining (in red) denotes the cell borders. Nuclei were stained with DAPI (in blue). Scale bar represents 20 μm. **(B–E)** Quantification of EC shapes parametrized by the angle between each cell's major axis and flow **(B)**, the area **(C)**, the circularity **(D)** and the aspect ratio **(E)**. ECs were exposed to low (N = 208), physiological (N = 195) or supra-high (N = 271) conditions of shear stress. Results are shown as individual values and as boxed plots ± interquartile range. Two box plots sharing the same letter show no statistically significant difference ($p < 0.01$). Data points located above or below the box plot's whiskers are considered outliers, defined as 1.5 times above or below the interquartile range, and marked by black circles.

(PC00211); 18: Transfer/carrier proteins (PC00219); 19: Translational proteins (PC00263); 20: Transmembrane signal receptors (PC00197); 21: Transporters (PC00227); 22: Viral or transposable element proteins (PC00237). Heatmaps were generated in R using the package pheatmap (Kolde, 2019). **Figure 2C** represents logFC (vs. respective control) for 2 dyne/cm^2 and 80 dyne/cm^2 conditions. **Supplementary Figure 1** represents scaled RPKM values of genes of interest in replicates.

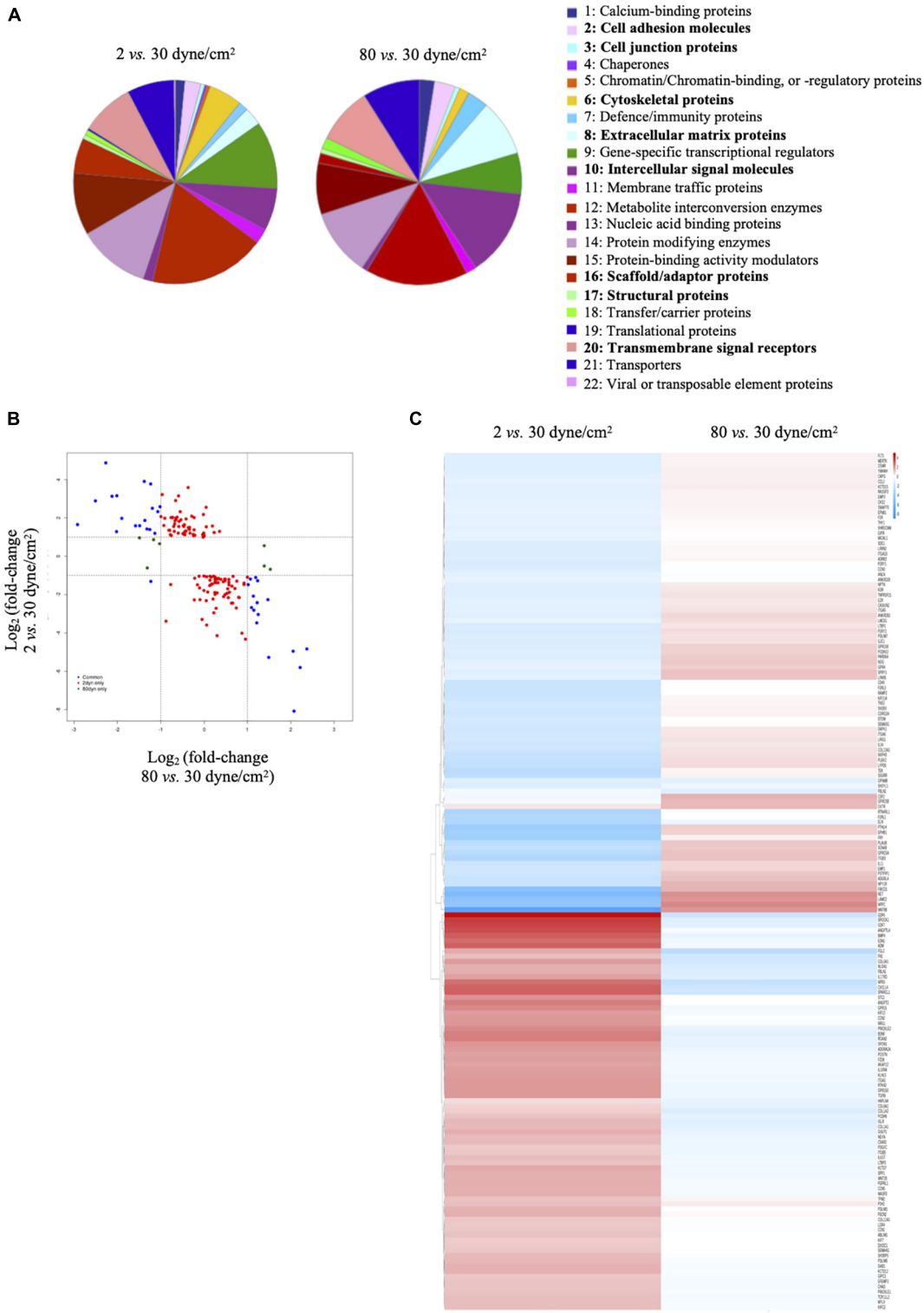

FIGURE 2 | Low and supra-high shear stress affect protein classes distribution. **(A)** Pie charts of differentially expressed genes in ECs exposed to 2 dyne/cm^2 vs. 30 dyne/cm^2 (left panel) or 80 dyne/cm^2 vs. 30 dyne/cm^2 (right panel) based on Gene Ontology functional protein class. **(B)** Fold change expression level comparison of differentially expressed genes from the 8 protein classes written in bold in panel **(A)**. Red dots show genes modified in 2 vs. 30 dyne/cm^2 only, green dots show genes modified in 80 vs. 30 dyne/cm^2 only, and blue dots show genes modified in 2 vs. 30 dyne/cm^2 and in 80 vs. 30 dyne/cm^2. **(C)** Heat maps showing up- and down-regulation of common genes under 2 vs. 30 dyne/cm^2 and 80 vs. 30 dyne/cm^2.

For both heatmaps, genes were organized by hierarchical clustering using the function hclust in R.

RESULTS

Endothelial Cell Shape and Orientation Are Altered Under Aneurysmal Wall Shear Stress Conditions

Porcine arterial ECs typically show a cobblestone morphology under static culture conditions [(Hao et al., 2002); not shown] and present an elongated shape and orientation in the direction of the flow after exposure for 48 h to a physiological WSS of 30 dyne/cm^2 (**Figure 1A**—middle). However, ECs exposed to either type of aneurysmal WSS (2 or 80 dyne/cm^2) failed to elongate (**Figure 1A**—left and right).

We quantified cell orientation and cell shape changes of the ECs under physiological WSS as well as under low and supra-high aneurysmal WSS by keeping track of each cell's orientation, area, circularity and aspect ratio (**Figures 1B–E**). Whereas under physiological flow conditions, the ECs' major axes were aligned toward the direction of flow (corresponding to an angle of 0°), this cell orientation was lost under both types of aneurysmal WSS (**Figure 1B**). Note that a completely random orientation of the cells would be reflected in an angle distribution centered around 45° and spread over the whole angle range between 0° and 90°. The cells' surface area was smallest under physiological flow conditions and increased to a similar extend under both types of aneurysmal WSS (**Figure 1C**). Likewise, circularity was small under physiological flow conditions and increased under both types of aneurysmal WSS with highest value found at 80 dyne/cm^2 (**Figure 1D**). Accordingly, the aspect ratio followed an inverted pattern with the highest value, denoting a high level of elongation, at the physiological WSS of 30 dyne/cm^2 (**Figure 1E**). Thus, ECs lost their elongation and alignment in the direction of the flow, became roundish and increased their surface area under both types of aneurysmal flow conditions.

Low and Supra-High Wall Shear Stress Differentially Affect Endothelial Cell Gene Expression

To obtain insight in the molecules involved in the endothelial shape changes observed in response to the different aneurysmal flow conditions, we performed unbiased transcriptomics (RNAseq) to compare gene expression levels in ECs exposed to physiological (30 dyne/cm^2), low aneurysmal (2 dyne/cm^2) or supra-high aneurysmal (80 dyne/cm^2) WSS.

Visualizing the data in Volcano plots illustrates the divergence in magnitude of response when comparing low aneurysmal or supra-high aneurysmal WSS vs. physiological WSS. Indeed, when exposed to low aneurysmal shear stress, ECs showed approximately 5-fold more genes affected than when exposed to supra-high aneurysmal shear stress. The comparison of 2 dyne/cm^2 to 30 dyne/cm^2 identified 604 and 543 up- and down-regulated genes (**Figure 3A** and **Supplementary Table 1**). The same comparison between 80 dyne/cm^2 and 30 dyne/cm^2 yielded only 134 and 114 up- and down-regulated genes (**Figure 3B** and **Supplementary Table 2**). As illustrated in the Venn diagram of **Figure 3C**, 170 differentially expressed genes in low aneurysmal flow overlapped with differentially expressed genes in supra-high aneurysmal flow, indicating that they are regulated under pathological conditions independently of the magnitude of WSS. Moreover, 977 genes were uniquely affected under WSS of 2 dyne/cm^2 and 77 genes were uniquely affected by WSS of 80 dyne/cm^2. As an internal control, we compared the respective 30 dyne/cm^2 physiological conditions with each other and revealed only 30 differentially expressed genes among the 10,446 tested genes (data not shown).

Next, we performed GSEA to identify essential pathways regulated by each aneurysmal WSS condition. Remarkably, GSEA performed in all up- and down-regulated genes showed that NES were inverted between 2 vs. 30 dyne/cm^2 and 80 vs. 30 dyne/cm^2 (**Figure 3D**). Whereas cytoskeletal proteins and more particularly actin or actin-binding proteins were among the classes the most up-regulated by supra-high WSS, these protein classes were down-regulated by low aneurysmal WSS. Conversely, various classes of extracellular matrix proteins were the most up-regulated by low WSS and these protein classes were down-regulated by pathological supra-high WSS.

To obtain further insight into biological functions of the differentially expressed genes, we performed a protein class functional annotation. Important differences were observed in protein classes known to determine cell shape and interactions, such as cell adhesion molecules, cell junction proteins, cytoskeletal proteins, extracellular matrix proteins, intercellular signal molecules, scaffold/adaptor proteins, structural proteins and transmembrane signal receptors (**Figure 2A**). A total of 208 genes in these 8 protein classes were differentially expressed between physiological and aneurysmal WSS (**Supplementary Table 3**), of which 159 and 14 were modified after the exposure to 2 dyne/cm^2 or 80 dyne/cm^2, respectively. The expression levels of 35 genes were affected by both types of aneurysmal WSS. Interestingly, the expression of these genes was regulated in an opposite direction by the pathological shear stresses (**Figure 2B**, blue dots). A heatmap representation comparing the alteration of gene expression in response to either aneurysmal WSS revealed an inverted regulation of nearly all differentially expressed genes (**Figure 2C**). The opposite gene expression patterns were observed in each of the three independent experiments with primary arterial ECs of different donors (**Supplementary Figure 1**), further emphasizing a consistent, robust and precise adaptation to different pathological conditions. Altogether, our results show that low and supra-high aneurysmal WSS induce important and opposite regulation of gene expression in ECs involving, among others, cytoskeletal and extracellular matrix proteins.

Low and Supra-High Wall Shear Stress Differentially Affect Endothelial Cell γ-Cytoplasmic Actin Organization

Members of the actin protein family play critical roles in many aspects of eukaryotic cell biology, including cell shape

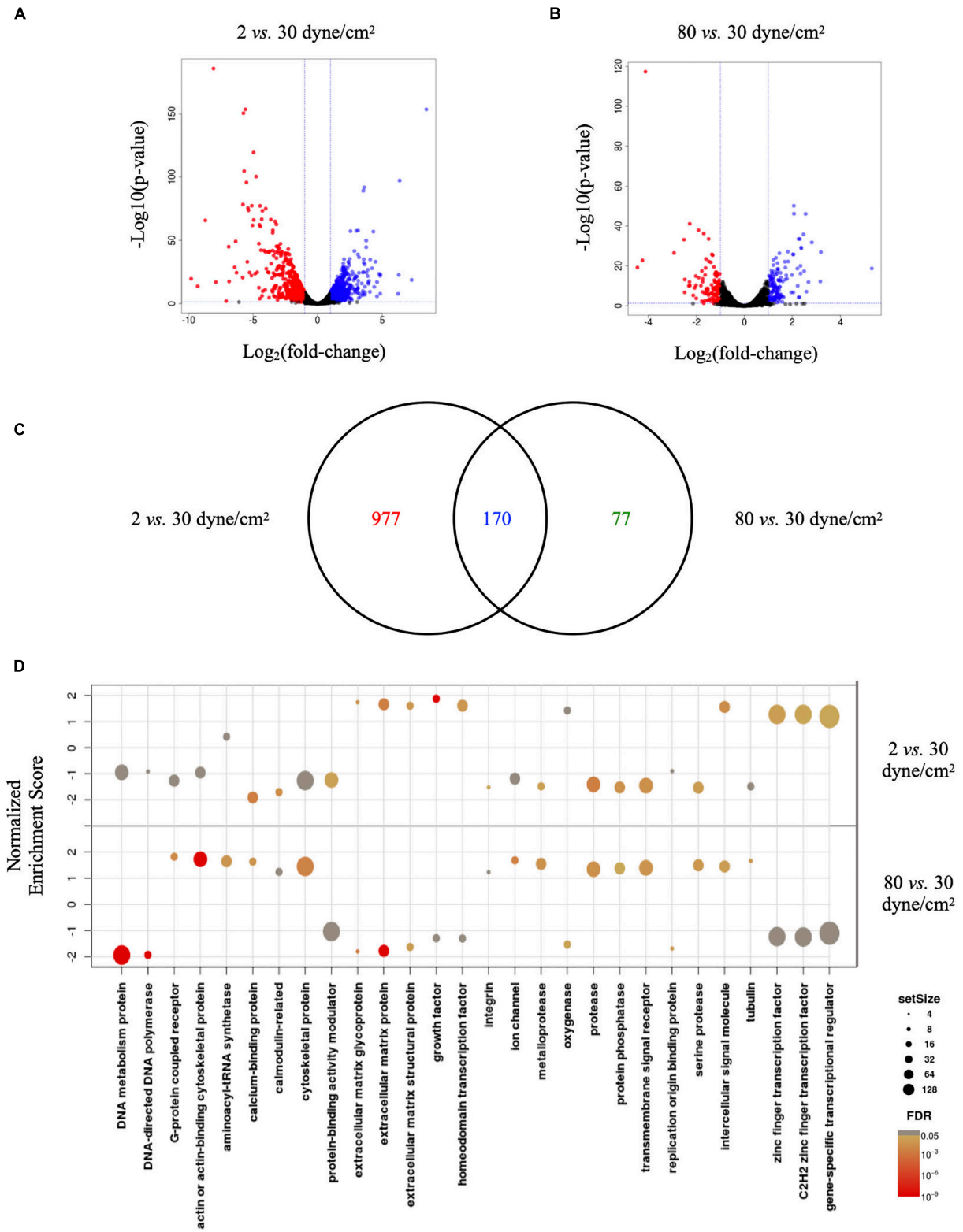

FIGURE 3 | Low and supra-high shear stress affect endothelial cell genes expression. **(A,B)** Volcano plots displaying differential expressed genes in ECs under 2 vs. 30 dyne/cm^2 **(A)** and 80 vs. 30 dyne/cm^2 **(B)**. Blue and red dots represent the up- and down-regulated genes, respectively. **(C)** Venn diagram showing the number of shear stress-induced differentially expressed genes in ECs exposed to 2 vs. 30 dyne/cm^2 or to 80 vs. 30 dyne/cm^2. Colors represent differentially expressed genes in 2 dyne/cm^2 (red), differentially expressed genes in 80 dyne/cm^2 (green) or genes common between the two conditions (blue). **(D)** GSEA identifying essential pathways regulated by each aneurysmal WSS condition.

maintenance, cell motility and cell contraction (Blanchoin et al., 2014). In vertebrates, six actin isoforms have been identified, each encoded by a different gene: two are typical of striated muscle (α-skeletal and α-cardiac actin), two are mainly found in smooth muscle (α- and γ-smooth muscle actin), and two are ubiquitous (β- and γ-cytoplasmic actin) (Dugina et al., 2009; Chaponnier and Gabbiani, 2016; Belvitch et al., 2018). To monitor the cells' architecture in response to low and supra-high aneurysmal WSS, immunostainings were performed for γ-cytoplasmic actin in arterial ECs exposed to 2, 30 or 80 dyne/cm^2 (**Figure 4**). In ECs exposed to the physiological flow of 30 dyne/cm^2, γ-cytoplasmic actin formed an organized filamentous network, which was aligned in the direction of the flow (**Figure 4**—middle). Some features of the filamentous γ-cytoplasmic actin network were still observed in ECs exposed to low aneurysmal WSS, however, an increased density of γ-cytoplasmic actin filaments was observed in the peri-nuclear region of the ECs (**Figure 4**—left). In ECs exposed to supra-high WSS, γ-cytoplasmic actin filaments were preferentially found along the cell borders and in peri-nuclear regions (**Figure 4**—right). Together, these results indicate that the differential regulation in EC gene expression observed under various WSS translate into a different organization of the ECs' architecture.

DISCUSSION

Initiation of IAs resulting in the deformation and enlargement of the arterial lumen is favored by high WSS and a high WSS gradient (WSSG) (Meng et al., 2014). Once IAs are formed, the aneurysm wall can be exposed to low, normal or supra-high values of WSS depending on the location and the geometry of the IA. Growing IAs change their geometry and as a result experience changing biomechanical forces over their life-time. The consequences of different and varying WSS for the evolution of IA disease are still poorly defined. In the present study, we show *in vitro* that ECs exposed to low or supra-high aneurysmal WSS were more circular than ECs exposed to physiological flow, and that they lost their alignment in the direction of the flow. We established that the effects of low WSS on differential gene expression were stronger than those of supra-high WSS. Moreover, low and supra-high aneurysmal WSS showed opposite regulation of gene expression in ECs involving cytoskeletal and extracellular matrix proteins. Finally, the differential regulation in EC gene expression observed under various pathological WSS translated into a different organization of the ECs' architecture.

Hemodynamic forces play a key role in vascular physiology and pathophysiology. The mechanisms of how flow disturbances lead to endothelial dysfunction have been extensively studied in the context of atherosclerosis (Cheng et al., 2006; Kwak et al., 2014; Jiang et al., 2015). Little is known for other arterial diseases such as IAs, although a combination of computational fluid dynamics and *en face* immunofluorescence on human IAs has recently demonstrated increased activation of the pro-inflammatory transcription factor Nuclear Factor Kappa B in regions of oscillatory shear stress (OSS), similar to earlier studies involving atherosclerosis (Baeriswyl et al., 2019). Atherosclerotic lesions typically develop at arterial branch points or bifurcations, regions of the vascular tree exposed to OSS. The ECs in those regions are known to have a polygonal shape and a non-systematic positioning. Actin filaments in ECs of disturbed flow regions in general are shorter, irregular oriented and tend to cluster to the cells border (Kim et al., 1989). Cytoskeletal displacement or deformation in ECs has been proposed to be involved in the gene regulation toward a pro-inflammatory phenotype induced by OSS (Vartanian et al., 2010; Macek Jilkova et al., 2014; Speight et al., 2016). Similar to the architectural changes in arterial ECs exposed to OSS, we observed in our study a rearrangement of γ-cytoplasmic actin in ECs exposed to low or supra-high aneurysmal shear stress. The ECs rearranged from a highly organized filamentous network oriented in the direction of physiological blood flow to a disordered network clustered around their nuclei or alongside the cell edges with subtle but consistent differences between the two types of aneurysmal flow. Integrity of cell architecture is influenced by cytoskeletal proteins in which actin family play an important role (Pasquier et al., 2015; Dugina et al., 2019). Reorganization of cytoplasmic actins alters cell morphology. In fibroblasts and epithelial cells (Dugina et al., 2009), and more recently in endothelial cells (Pasquier et al., 2015), reduced expression of β- or γ-cytoplasmic actin have been shown to influence not only cell morphology, but also affect cell polarity, mobility or adhesion. In addition, the actin cytoskeleton has been proposed to provide a scaffold to stabilize the glycocalyx (Li and Wang, 2018). In our study, the differences in cytoskeletal rearrangement may stand at the basis for the differences in gene expression observed under low or supra-high aneurysmal shear stress.

Chronically elevated flow conditions, as observed in severely stenotic regions associated with atherosclerotic disease, are a well-known trigger for arterial remodeling (Gijsen et al., 2013; Munarriz et al., 2016). In an earlier study, DNA microarrays were used to profile EC gene expression in response to very high WSS (10 Pa; 100 dyne/cm^2; 24 h) (Dolan et al., 2012). Compared to regular WSS (2 Pa; 20 dyne/cm^2) or no-flow, very high WSS modulated gene expression in ways that promoted an anti-coagulant, anti-inflammatory, proliferative, and promatrix remodeling phenotypes, comprising genes essential for an adaptive expansive remodeling like *plasminogen activator, urokinase, tissue plasminogen activator, metalloproteinase ADAMTS1/6,* and *tissue inhibitor of metalloproteinase 3 (TIMP3)* (Dolan et al., 2012). In our study, *urokinase-type plasminogen activator*, *urokinase plasminogen activator surface receptor* and *ADAMTS* genes were down- and up-regulated under low and supra-high aneurysmal WSS, respectively. The expression of *TIMP3* was down-regulated under low aneurysmal WSS. These findings illustrate a tendency for more expansive remodeling in IAs exposed to supra-high aneurysmal WSS. In another study, Dolan et al. (2011) exposed ECs to IA initiating conditions using a flow chamber with constant-height channels to create regions of uniform (elevated) WSS and converging and diverging channels to create positive and negative WSSG, respectively. Similar to our study, highly elevated WSS (28.4 Pa; 284 dyne/cm^2) inhibited EC alignment to flow (Dolan et al., 2011). In addition, increased EC proliferation and apoptosis was observed under

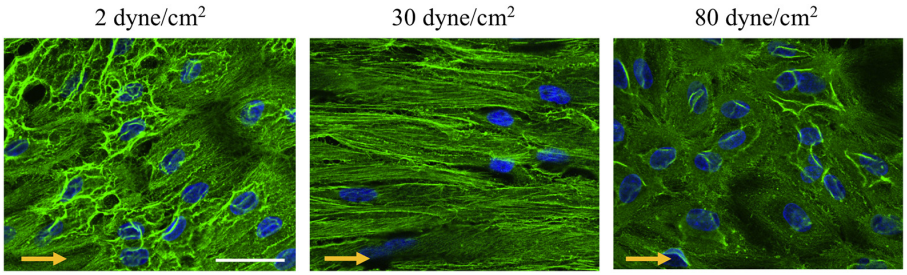

FIGURE 4 | γ-cytoplasmic actin organization in endothelial cells exposed to different levels of shear stress. Representative examples of γ-cytoplasmic actin immunostainings (in green) performed on ECs exposed to 2 (left panel), 30 (middle panel) or 80 (right panel) dyne/cm^2 for 48 h. Nuclei were stained with DAPI (in blue). Scale bar represents 20 μm. The direction of the flow is indicated by orange arrows.

elevated WSS, which was accentuated by a positive WSSG (+ 980 Pa/m) and suppressed by negative WSSG (–1120 Pa/m). The authors concluded that EC responses to positive WSSG may contribute to pathogenic remodeling that occurs at bifurcations preceding IA formation.

Although genetic predisposition has an important role in IA disease, little is known about the genetic architecture of IAs. Among the initial candidate genes discovered in gene expression and genome-wide linkage analyses are type III collagen (*COL3A1*), endoglin (*ENG*), fibrillin (*FBN1*), α1-antitrypsin (*SERPINA1*) and polycystin (*PKD1*, *PKD2*) (Nahed et al., 2007; Zhou et al., 2018), supporting observations of increased risk for IA formation in individuals with connective tissue disorders or PKD. A recent cross-ethnic genome-wide association study performed on 10,754 IA cases and 306,882 controls of European and East Asian ancestry has discovered a total of 17 risk loci of which 11 were new (Bakker et al., 2020). Many of these genes have known or putative roles in blood vessel physiology and blood pressure regulation, and an important role of ECs in IA development and rupture was proposed (Bakker et al., 2020). For some of these genes we found changes in the expression profiles. Locus 10q23.33 (rs11187838) and 15q25.1 (rs8034191) described in Bakker et al. (2020) and coding for the genes *PLCE1* (phospholipase C epsilon 1) and *HYKK* (hydroxylysine kinase) were up-regulated in ECs exposed to low vs. physiological WSS, whereas *STARD13* (StAR-related lipid transfer domain protein 13, locus 13q13.1, rs3742321) was down-regulated. STARD13 is a Rho GTPase-activating protein involved in regulation of cytoskeletal reorganization, cell proliferation, and cell motility. This is in line with our findings and supports the importance of these processes in the remodeling of IAs.

We have chosen to use primary porcine arterial ECs for this study, as this species is known to be very similar to humans with respect to cardiovascular anatomy, physiology, metabolism and disease (Crisostomo et al., 2016; Tsang et al., 2016). Moreover, porcine coronary EC isolation does not require the use of laboratory animals (3Rs principles). Even though in human the diameter of arteries in the circle of Willis resembles the one of coronary arteries (Dodge et al., 1992; Rai et al., 2013), the use of primary ECs isolated from porcine coronary arteries remains a limitation of our study as their properties may not completely recapitulate the ones of ECs in cerebral arteries. Moreover, both types of ECs are *in situ* exposed to different flow patterns and pressures. In this respect, it should also be noted that in our *in vitro* flow system ECs are exposed to a defined constant flow rather than to pulsatile flow as they experience *in vivo*. Finally, the porcine arterial ECs were cultured on 1% gelatin, a commonly used substrate for ECs in culture. A change in substrate may affect the basic properties of ECs and possibly induce subtle changes in their response to shear stress (Dessalles et al., 2021). Although we expect that the strong and opposite regulation in gene expression of cytoskeletal and extracellular matrix proteins observed in ECs exposed to low and supra-high aneurysmal WSS would be largely maintained on different substrates, this remains to be proven.

In addition of being exposed to shear stress caused by blood flow, ECs are subjected to cyclic strain caused by intravascular pressure, the level of which varies along the vascular tree. Under physiological conditions, the (elastic) human aorta undergoes about 10% increase in diameter, whereas (muscular) peripheral arteries undergo only 5% cyclic circumferential stretch (CCS) (Anwar et al., 2012). Physiological CCS is known to participate in vascular maintenance by regulating processes such as cell proliferation, morphology and extracellular matrix formation (Wang et al., 2003; Yoshigi et al., 2003; Li and Sumpio, 2005; Nishimura et al., 2006). The precise level of cyclic stretch in saccular IAs is unknown, but it is in general considered to be very low due to a combination of altered pulse waves and the low compliance of the IA wall. As the IA enlarges and its vessel wall becomes stiffer, ECs will thus gradually loose the cyclic stimulation required for their normal functioning. To this date, most studies on the response of ECs to CCS have focused on ECs exposed to high level of cyclic stretch as observed in hypertensive patients (Munarriz et al., 2016; Ando and Yamamoto, 2021) or at the prospective site of IA formation (Koseki et al., 2020) and very little is known onto the effects of reduced CCS on EC physiology. Such studies, and mostly studies in which various hemodynamic stresses are combined, remain one of the main challenges in the field of EC mechanobiology (Dessalles et al., 2021) but are expected to contribute greatly to our understanding of the pathogenesis of IAs and the prediction of IA rupture.

DATA AVAILABILITY STATEMENT

The code and dataset analyzed for the cell shape and orientation analysis are available on Github.com/hirshlab/aneurysmalWSSonEC, version 1.0 (https://github.com/hirsch-lab/aneurysmalWSSonEC). RNA sequencing data have been submitted to the GEO database under accession number GSE173928 (https://www.ncbi.nlm.nih.gov/geo/query/acc.cgi?acc=GSE173928).

AUTHOR CONTRIBUTIONS

SM: acquisition of data, analysis of data, interpretation of analysis, and drafting of manuscript. SS: acquisition of data, analysis of data, interpretation of analysis, and revision of manuscript. MRD: acquisition of data and revision of manuscript. MD and SL: analysis of data and revision of manuscript. M-LB-P: materials provider and revision of manuscript. SH and BK: design and conceptualization of the study, interpretation of analysis, drafting of manuscript. All authors contributed to the article and approved the submitted version.

FUNDING

This study was supported by grants from the Swiss SystemsX.ch initiative, evaluated by the Swiss National Science Foundation (to BK and SH), the Swiss Heart Foundation (to BK), the Gottfried und Julia Bangerter-Rhyner-Stiftung (to BK), the Novartis Foundation for medical-biological research (to BK), and the Fondation Privée des HUG (to BK).

ACKNOWLEDGMENTS

We thank Christine Chaponnier for kindly providing us with the antibody against the γ-cytoplasmic actin.

SUPPLEMENTARY MATERIAL

The Supplementary Material for this article can be found online at: https://www.frontiersin.org/articles/10.3389/fphys.2021.727338/full#supplementary-material

Supplementary Figure 1 | Heatmap showing reproducibility of expression (in RPKM) of the differentially expressed genes. Results are shown for primary arterial ECs of 3 different donors submitted to 2 dyne/cm^2 and 80 dyne/cm^2.

Supplementary Table 1 | Differentially expressed genes in ECs exposed to 2 dyne/cm^2 vs. ECs exposed to 30 dyne/cm^2.

Supplementary Table 2 | Differentially expressed genes in ECs exposed to 80 dyne/cm^2 vs. ECs exposed to 30 dyne/cm^2.

Supplementary Table 3 | Genes with an up- or down- regulated expression in the 8 following protein classes: Cell adhesion molecules, Cell junction proteins, Cytoskeletal proteins, Extracellular matrix proteins, Intercellular signal molecules, Scaffold/adaptor proteins, Structural proteins and Transmembrane signal receptors.

REFERENCES

Ando, J., and Yamamoto, K. (2013). Flow detection and calcium signalling in vascular endothelial cells. *Cardiovasc. Res.* 99, 260–268. doi: 10.1093/cvr/cvt084

Ando, J., and Yamamoto, K. (2021). Hemodynamic Forces, Endothelial Mechanotransduction, and Vascular Diseases. *Magn. Reson. Med. Sci.* doi: 10.2463/mrms.rev.2021-0018 [Epub Online ahead of print].

Anwar, M. A., Shalhoub, J., Lim, C. S., Gohel, M. S., and Davies, A. H. (2012). The effect of pressure-induced mechanical stretch on vascular wall differential gene expression. *J. Vasc. Res.* 49, 463–478. doi: 10.1159/000339151

Baeriswyl, D. C., Prionisti, I., Peach, T., Tsolkas, G., Chooi, K. Y., Vardakis, J., et al. (2019). Disturbed flow induces a sustained, stochastic NF-kappaB activation which may support intracranial aneurysm growth in vivo. *Sci. Rep.* 9:4738. doi: 10.1038/s41598-019-40959-y

Bakker, M. K., van der Spek, R. A. A., van Rheenen, W., Morel, S., Bourcier, R., Hostettler, I. C., et al. (2020). Genome-wide association study of intracranial aneurysms identifies 17 risk loci and genetic overlap with clinical risk factors. *Nat. Genet.* 52, 1303–1313. doi: 10.1038/s41588-020-00725-7

Belvitch, P., Htwe, Y. M., Brown, M. E., and Dudek, S. (2018). Cortical Actin Dynamics in Endothelial Permeability. *Curr. Top. Membr.* 82, 141–195. doi: 10.1016/bs.ctm.2018.09.003

Blanchoin, L., Boujemaa-Paterski, R., Sykes, C., and Plastino, J. (2014). Actin dynamics, architecture, and mechanics in cell motility. *Physiol. Rev.* 94, 235–263. doi: 10.1152/physrev.00018.2013

Cebral, J. R., Detmer, F., Chung, B. J., Choque-Velasquez, J., Rezai, B., Lehto, H., et al. (2019). Local Hemodynamic Conditions Associated with Focal Changes in the Intracranial Aneurysm Wall. *AJNR Am. J. Neuroradiol.* 40, 510–516.

Chaponnier, C., and Gabbiani, G. (2016). Monoclonal antibodies against muscle actin isoforms: epitope identification and analysis of isoform expression by immunoblot and immunostaining in normal and regenerating skeletal muscle. *F1000Res.* 5:416. doi: 10.12688/f1000research.8154.1

Cheng, C., Tempel, D., van Haperen, R., van der Baan, A., Grosveld, F., Daemen, M. J., et al. (2006). Atherosclerotic lesion size and vulnerability are determined by patterns of fluid shear stress. *Circulation* 113, 2744–2753. doi: 10.1161/CIRCULATIONAHA.105.590018

Cho, Y., Tong, A., Craig, J. C., Mustafa, R. A., Chapman, A., Perrone, R. D., et al. (2021). Establishing a Core Outcome Set for Autosomal Dominant Polycystic Kidney Disease: report of the Standardized Outcomes in Nephrology-Polycystic Kidney Disease (SONG-PKD) Consensus Workshop. *Am. J. Kidney Dis.* 77, 255–263. doi: 10.1053/j.ajkd.2020.05.024

Crisostomo, V., Sun, F., Maynar, M., Baez-Diaz, C., Blanco, V., Garcia-Lindo, M., et al. (2016). Common swine models of cardiovascular disease for research and training. *Lab. Anim.* 45, 67–74. doi: 10.1038/laban.935

Denis, J. F., Diagbouga, M. R., Molica, F., Hautefort, A., Linnerz, T., Watanabe, M., et al. (2019). KLF4-Induced Connexin40 Expression Contributes to Arterial Endothelial Quiescence. *Front. Physiol.* 10:80. doi: 10.3389/fphys.2019.00080

Dessalles, C. A., Leclech, C., Castagnino, A., and Barakat, A. I. (2021). Integration of substrate- and flow-derived stresses in endothelial cell mechanobiology. *Commun. Biol.* 4:764. doi: 10.1038/s42003-021-02285-w

Diagbouga, M. R., Morel, S., Bijlenga, P., and Kwak, B. R. (2018). Role of hemodynamics in initiation/growth of intracranial aneurysms. *Eur. J. Clin. Invest.* 48:e12992. doi: 10.1111/eci.12992

Diagbouga, M. R., Morel, S., Cayron, A. F., Haemmerli, J., Georges, M., Hierck, B. P., et al. (2021). Primary cilia control endothelial permeability by regulating expression and location of junction proteins.

Cardiovasc. Res. [Epub Online ahead of print]. doi: 10.1093/cvr/cvab165

Dobin, A., Davis, C. A., Schlesinger, F., Drenkow, J., Zaleski, C., Jha, S., et al. (2013). STAR: ultrafast universal RNA-seq aligner. *Bioinformatics* 29, 15–21. doi: 10.1093/bioinformatics/bts635

Dodge, J. T. Jr., Brown, B. G., Bolson, E. L., and Dodge, H. T. (1992). Lumen diameter of normal human coronary arteries. Influence of age, sex, anatomic variation, and left ventricular hypertrophy or dilation. *Circulation* 86, 232–246. doi: 10.1161/01.CIR.86.1.232

Dolan, J. M., Meng, H., Singh, S., Paluch, R., and Kolega, J. (2011). High fluid shear stress and spatial shear stress gradients affect endothelial proliferation, survival, and alignment. *Ann. Biomed. Eng.* 39, 1620–1631. doi: 10.1007/s10439-011-0267-8

Dolan, J. M., Sim, F. J., Meng, H., and Kolega, J. (2012). Endothelial cells express a unique transcriptional profile under very high wall shear stress known to induce expansive arterial remodeling. *Am. J. Physiol. Cell Physiol.* 302, C1109–C1118. doi: 10.1152/ajpcell.00369.2011

Dugina, V., Zwaenepoel, I., Gabbiani, G., Clement, S., and Chaponnier, C. (2009). Beta and gamma-cytoplasmic actins display distinct distribution and functional diversity. *J. Cell Sci.* 122, 2980–2988. doi: 10.1242/jcs.041970

Dugina, V. B., Shagieva, G. S., and Kopnin, P. B. (2019). Biological Role of Actin Isoforms in Mammalian Cells. *Biochemistry* 84, 583–592. doi: 10.1134/S0006297919060014

Etminan, N., Brown, R. D. Jr., Beseoglu, K., Juvela, S., Raymond, J., Morita, A., et al. (2015). The unruptured intracranial aneurysm treatment score: a multidisciplinary consensus. *Neurology* 85, 881–889. doi: 10.1212/WNL.0000000000001891

Frosen, J., Cebral, J., Robertson, A. M., and Aoki, T. (2019). Flow-induced, inflammation-mediated arterial wall remodeling in the formation and progression of intracranial aneurysms. *Neurosurg. Focus.* 47:E21. doi: 10.3171/2019.5.FOCUS19234

Gijsen, F., van der Giessen, A., van der Steen, A., and Wentzel, J. (2013). Shear stress and advanced atherosclerosis in human coronary arteries. *J. Biomech.* 46, 240–247. doi: 10.1016/j.jbiomech.2012.11.006

Greving, J. P., Wermer, M. J., Brown, R. D. Jr., Morita, A., Juvela, S., Yonekura, M., et al. (2014). Development of the PHASES score for prediction of risk of rupture of intracranial aneurysms: a pooled analysis of six prospective cohort studies. *Lancet Neurol.* 13, 59–66. doi: 10.1016/S1474-4422(13)70263-1

Hao, H., Ropraz, P., Verin, V., Camenzind, E., Geinoz, A., Pepper, M. S., et al. (2002). Heterogeneity of smooth muscle cell populations cultured from pig coronary artery. *Arterioscler. Thromb. Vasc. Biol.* 22, 1093–1099. doi: 10.1161/01.ATV.0000022407.91111.E4

Holm, S. A. (1979). Simple Sequentially Rejective Multiple Test Procedure. *Scand. J. Stat.* 6, 65–70.

Jiang, Y. Z., Manduchi, E., Jimenez, J. M., and Davies, P. F. (2015). Endothelial epigenetics in biomechanical stress: disturbed flow-mediated epigenomic plasticity *in vivo and in vitro*. *Arterioscler. Thromb. Vasc. Biol.* 35, 1317–1326. doi: 10.1161/ATVBAHA.115.303427

Kim, D. W., Gotlieb, A. I., and Langille, B. L. (1989). *In vivo* modulation of endothelial F-actin microfilaments by experimental alterations in shear stress. *Arteriosclerosis* 9, 439–445. doi: 10.1161/01.ATV.9.4.439

Kolde, R. (2019). *pheatmap: Pretty Heatmaps Version:1.0.12*. Available Online at: https://cran.r-project.org/web/packages/pheatmap/index.html (accessed June 17, 2021).

Koseki, H., Miyata, H., Shimo, S., Ohno, N., Mifune, K., Shimano, K., et al. (2020). Two Diverse Hemodynamic Forces, a Mechanical Stretch and a High Wall Shear Stress, Determine Intracranial Aneurysm Formation. *Transl. Stroke Res.* 11, 80–92. doi: 10.1007/s12975-019-0690-y

Kwak, B. R., Back, M., Bochaton-Piallat, M. L., Caligiuri, G., Daemen, M. J., Davies, P. F., et al. (2014). Biomechanical factors in atherosclerosis: mechanisms and clinical implications. *Eur. Heart J.* 35, 3013–3020. doi: 10.1093/eurheartj/ehu353

Lawton, M. T., and Vates, G. E. (2017). Subarachnoid Hemorrhage. *N. Engl. J. Med.* 377, 257–266. doi: 10.1056/NEJMcp1605827

Li, W., and Sumpio, B. E. (2005). Strain-induced vascular endothelial cell proliferation requires PI3K-dependent mTOR-4E-BP1 signal pathway. *Am. J. Physiol. Heart Circ. Physiol.* 288, H1591–H1597. doi: 10.1152/ajpheart.00382.2004

Li, W., and Wang, W. (2018). Structural alteration of the endothelial glycocalyx: contribution of the actin cytoskeleton. *Biomech. Model Mechanobiol.* 17, 147–158. doi: 10.1007/s10237-017-0950-2

Liao, Y., Smyth, G. K., and Shi, W. (2014). featureCounts: an efficient general purpose program for assigning sequence reads to genomic features. *Bioinformatics* 30, 923–930. doi: 10.1093/bioinformatics/btt656

Macek Jilkova, Z., Lisowska, J., Manet, S., Verdier, C., Deplano, V., Geindreau, C., et al. (2014). CCM proteins control endothelial beta1 integrin dependent response to shear stress. *Biol. Open* 3, 1228–1235. doi: 10.1242/bio.20140132

Meng, H., Tutino, V. M., Xiang, J., and Siddiqui, A. (2014). High WSS or low WSS? Complex interactions of hemodynamics with intracranial aneurysm initiation, growth, and rupture: toward a unifying hypothesis. *AJNR Am. J. Neuroradiol.* 35, 1254–1262. doi: 10.3174/ajnr.A3558

Mootha, V. K., Lindgren, C. M., Eriksson, K. F., Subramanian, A., Sihag, S., Lehar, J., et al. (2003). PGC-1alpha-responsive genes involved in oxidative phosphorylation are coordinately downregulated in human diabetes. *Nat. Genet.* 34, 267–273. doi: 10.1038/ng1180

Munarriz, P. M., Gomez, P. A., Paredes, I., Castano-Leon, A. M., Cepeda, S., and Lagares, A. (2016). Basic Principles of Hemodynamics and Cerebral Aneurysms. *World Neurosurg.* 88, 311–319. doi: 10.1016/j.wneu.2016.01.031

Nahed, B. V., Bydon, M., Ozturk, A. K., Bilguvar, K., Bayrakli, F., and Gunel, M. (2007). Genetics of intracranial aneurysms. *Neurosurgery* 60, 213–225. doi: 10.1227/01.NEU.0000249270.18698.BB

Nishimura, K., Li, W., Hoshino, Y., Kadohama, T., Asada, H., Ohgi, S., et al. (2006). Role of AKT in cyclic strain-induced endothelial cell proliferation and survival. *Am. J. Physiol. Cell Physiol.* 290, C812–C821. doi: 10.1152/ajpcell.00347.2005

Pasquier, E., Tuset, M. P., Sinnappan, S., Carnell, M., Macmillan, A., and Kavallaris, M. (2015). gamma-Actin plays a key role in endothelial cell motility and neovessel maintenance. *Vasc. Cell* 7, 2. doi: 10.1186/s13221-014-0027-2

Pfenniger, A., Wong, C., Sutter, E., Cuhlmann, S., Dunoyer-Geindre, S., Mach, F., et al. (2012). Shear stress modulates the expression of the atheroprotective protein Cx37 in endothelial cells. *J. Mol. Cell. Cardiol.* 53, 299–309. doi: 10.1016/j.yjmcc.2012.05.011

R Core Team (2020). *R: a language and environment for statistical computing*. Vienna, Austria: R Foundation for Statistical Computing.

Rai, A. T., Hogg, J. P., Cline, B., and Hobbs, G. (2013). Cerebrovascular geometry in the anterior circulation: an analysis of diameter, length and the vessel taper. *J. Neurointerv. Surg.* 5, 371–375. doi: 10.1136/neurintsurg-2012-010314

Robinson, M. D., McCarthy, D. J., and Smyth, G. K. (2010). edgeR: a Bioconductor package for differential expression analysis of digital gene expression data. *Bioinformatics* 26, 139–140. doi: 10.1093/bioinformatics/btp616

Schilling, S. (2021). *visStatistics: Automated Visualization of Statistical Tests Version:0.1.1*. Available Online at: https://CRAN.R-project.org/package=visStatistics (accessed June 17, 2021).

Schindelin, J., Arganda-Carreras, I., Frise, E., Kaynig, V., Longair, M., Pietzsch, T., et al. (2012). Fiji: an open-source platform for biological-image analysis. *Nat. Methods* 9, 676–682. doi: 10.1038/nmeth.2019

Speight, P., Kofler, M., Szaszi, K., and Kapus, A. (2016). Context-dependent switch in chemo/mechanotransduction *via* multilevel crosstalk among cytoskeleton-regulated MRTF and TAZ and TGFbeta-regulated Smad3. *Nat. Commun.* 7:11642. doi: 10.1038/ncomms11642

Staarmann, B., Smith, M., and Prestigiacomo, C. J. (2019). Shear stress and aneurysms: a review. *Neurosurg. Focus* 47:E2. doi: 10.3171/2019.4.FOCUS19225

Subramanian, A., Tamayo, P., Mootha, V. K., Mukherjee, S., Ebert, B. L., Gillette, M. A., et al. (2005). Gene set enrichment analysis: a knowledge-based approach for interpreting genome-wide expression profiles. *Proc. Natl. Acad. Sci. U. S. A.* 102, 15545–15550. doi: 10.1073/pnas.0506580102

Tsang, H. G., Rashdan, N. A., Whitelaw, C. B., Corcoran, B. M., Summers, K. M., and MacRae, V. E. (2016). Large animal models of cardiovascular disease. *Cell Biochem. Funct.* 34, 113–132. doi: 10.1002/cbf.3173

Vartanian, K. B., Berny, M. A., McCarty, O. J., Hanson, S. R., and Hinds, M. T. (2010). Cytoskeletal structure regulates endothelial cell immunogenicity independent of fluid shear stress. *Am. J. Physiol. Cell Physiol.* 298, C333–C341. doi: 10.1152/ajpcell.00340.2009

Wang, B. W., Chang, H., Lin, S., Kuan, P., and Shyu, K. G. (2003). Induction of matrix metalloproteinases-14 and -2 by cyclical mechanical stretch is mediated by tumor necrosis factor-alpha in cultured human umbilical vein endothelial cells. *Cardiovasc. Res.* 59, 460–469. doi: 10.1016/S0008-6363(03)00428-0

Yoshigi, M., Clark, E. B., and Yost, H. J. (2003). Quantification of stretch-induced cytoskeletal remodeling in vascular endothelial cells by image processing. *Cytometry A* 55, 109–118. doi: 10.1002/cyto.a.10076

Zhao, X., Zhao, M., Amin-Hanjani, S., Du, X., Ruland, S., and Charbel, F. T. (2015). Wall shear stress in major cerebral arteries as a function of age and gender–a study of 301 healthy volunteers. *J. Neuroimaging* 25, 403–407. doi: 10.1111/jon.12133

Zhou, S., Dion, P. A., and Rouleau, G. A. (2018). Genetics of Intracranial Aneurysms. *Stroke* 49, 780–787. doi: 10.1161/STROKEAHA.117.018152

Conflict of Interest: The authors declare that the research was conducted in the absence of any commercial or financial relationships that could be construed as a potential conflict of interest.

Publisher's Note: All claims expressed in this article are solely those of the authors and do not necessarily represent those of their affiliated organizations, or those of the publisher, the editors and the reviewers. Any product that may be evaluated in this article, or claim that may be made by its manufacturer, is not guaranteed or endorsed by the publisher.

frontiers in Physiology

REVIEW
published: 19 November 2021
doi: 10.3389/fphys.2021.769321

Lin11-Isl1-Mec3 Domain Proteins as Mechanotransducers in Endothelial and Vascular Smooth Muscle Cells

*Alexandra Sporkova[1], Subhajit Ghosh[1], Jaafar Al-Hasani[1,2] and Markus Hecker[1,2]**

[1]*Department of Cardiovascular Physiology, Heidelberg University, Heidelberg, Germany,* [2]*DZHK (German Centre for Cardiovascular Research) Partner Site, Heidelberg/Mannheim, Germany*

OPEN ACCESS

Edited by:
Steffen-Sebastian Bolz, University of Toronto, Canada

Reviewed by:
Erik Nicolaas Theodorus Petrus Bakker, University of Amsterdam, Netherlands
William F. Jackson, Michigan State University, United States
Luis A. Martinez-Lemus, University of Missouri, United States
Kim Dora, University of Oxford, United Kingdom

***Correspondence:**
Markus Hecker
hecker@physiologie.uni-heidelberg.de

Specialty section:
This article was submitted to Vascular Physiology, a section of the journal Frontiers in Physiology

Received: *01 September 2021*
Accepted: *26 October 2021*
Published: *19 November 2021*

Citation:
Sporkova A, Ghosh S, Al-Hasani J and Hecker M (2021) Lin11-Isl1-Mec3 Domain Proteins as Mechanotransducers in Endothelial and Vascular Smooth Muscle Cells. Front. Physiol. 12:769321. doi: 10.3389/fphys.2021.769321

Arterial hypertension is the leading risk factor for cardiovascular morbidity and mortality worldwide. However, little is known about the cellular mechanisms underlying it. In small arteries and arterioles, a chronic increase in blood pressure raises wall tension and hence stretches, namely, the medial vascular smooth muscle cells (VSMC) but also endothelial cell (EC) to cell contacts. Initially compensated by an increase in vascular tone, the continuous biomechanical strain causes a prominent change in gene expression in both cell types, frequently driving an arterial inward remodeling process that ultimately results in a reduction in lumen diameter, stiffening of the vessel wall, and fixation of blood pressure, namely, diastolic blood pressure, at the elevated level. Sensing and propagation of this supraphysiological stretch into the nucleus of VSMC and EC therefore seems to be a crucial step in the initiation and advancement of hypertension-induced arterial remodeling. Focal adhesions (FA) represent an important interface between the extracellular matrix and Lin11-Isl1-Mec3 (LIM) domain-containing proteins, which can translocate from the FA into the nucleus where they affect gene expression. The varying biomechanical cues to which vascular cells are exposed can thus be rapidly and specifically propagated to the nucleus. Zyxin was the first protein described with such mechanotransducing properties. It comprises 3 C-terminal LIM domains, a leucine-rich nuclear export signal, and N-terminal features that support its association with the actin cytoskeleton. In the cytoplasm, zyxin promotes actin assembly and organization as well as cell motility. In EC, zyxin acts as a transcription factor, whereas in VSMC, it has a less direct effect on mechanosensitive gene expression. In terms of homology and structural features, lipoma preferred partner is the nearest relative of zyxin among the LIM domain proteins. It is almost exclusively expressed by smooth muscle cells in the adult, resides like zyxin at FA but seems to affect mechanosensitive gene expression indirectly, possibly *via* altering cortical actin dynamics. Here, we highlight what is currently known about the role of these LIM domain proteins in mechanosensing and transduction in vascular cells.

Keywords: lipoma preferred partner, zyxin, mechanosensing, mechanotransduction, LIM domain proteins, vascular cells, arterial remodeling

INTRODUCTION

Blood vessels are constantly exposed to mechanical forces. The physical properties of the flowing blood are sensed by the endothelial cells (EC), which, under conditions of laminar flow, adapt both functionally and structurally to alterations in unidirectional shear stress. Mechanical forces propagated along the extracellular matrix (ECM) of the blood vessel wall are also perceived by the smooth muscle cells (SMC) of the medial layer of arteries and veins. This mechanosensing ability is pivotal for normal physiology and function and allows blood vessels to dynamically adjust their structure and function to biomechanical forces generated by altered hemodynamics. When arteries are chronically exposed to elevated circumferential wall tension, such as during hypertension, the quiescent contractile phenotype of the vascular SMC changes to secretory and growth promoting (Rensen et al., 2007; Saleh et al., 2016). This chronic increase in blood pressure frequently drives an initially adaptive inward remodeling process in small arteries and arterioles that eventually becomes maladaptive due to narrowing of the lumen and stiffening of the ECM. Both processes spur an increase in peripheral resistance that ultimately contributes to a fixation of diastolic blood pressure at a supraphysiological level. In addition to vascular SMC, the increased circumferential wall tension strains the lateral EC to EC contacts thus causing a change in the phenotype of these cells that seems to support the eventually maladaptive remodeling process(es) in the wall of these blood vessels.

Focal adhesions (FA) are integrin-containing, dynamic multiprotein structures that physically link the intracellular cytoskeleton, particularly cortical actin bundles, to the extracellular matrix (Geiger et al., 2009). They are thus ideally positioned to transduce extracellular biomechanical signals to the cell interior by altering the interaction of multiple signal transduction proteins with the cytoskeleton. More than 50 proteins associate with FA, and their composition varies greatly and is highly dynamic depending on the cell type and its interaction with the environment. A large and diverse group of mechanotransducing proteins that associate with FA are LIM domain (Lin-11, lsl-1 and Mec-3)-containing proteins (Sang et al., 2014; Kadrmas and Beckerle, 2004). LIM domains are double zinc finger structures that serve as interaction sites for specific signal transduction proteins. They facilitate the assembly of multiprotein complexes, for example, at the FA, that affect the cellular phenotype by controlling cellular motility, proliferation, or apoptosis through the regulation of gene expression. This plasticity is particularly important in vascular SMC, which exhibit a contractile non-migratory phenotype in the quiescent state but are highly promigratory during vasculogenesis. In response to vascular injury or in hypertension, vascular SMC become highly migratory and growth promoting, too, but under these conditions, they may contribute to – depending on the size of the arterial blood vessel – inward (small arteries and arterioles) or outward (conduit arteries) remodeling. Raised intraluminal pressure or mitogens, such as angiotensin II, stimulate vascular SMC to increase their mass of contractile proteins. Therefore, both mechanosensing and transduction by the medial SMC in arterial blood vessels are crucial to the dynamic regulation of the cellular phenotype in the face of changing hemodynamic forces.

Recent studies indicate that the mechanism(s) by which LIM domain proteins mediate mechanotransduction is highly conserved from yeast to mammalian cells. LIM domain-containing regions of 18 diverse LIM domain proteins have been shown to exclusively bind the stretched conformation of actin in mouse embryonal fibroblasts (Sun et al., 2020; Winkelman et al., 2020). Thus, when the actin conformation is changed by a biomechanical stimulus, specific binding sites for LIM domain proteins are unmasked. Vice versa, when actomyosin contractility is suppressed, the association of LIM domain proteins with actin and FA is also diminished (Kuo et al., 2011; Schiller et al., 2011). These findings indicate that LIM domain-mediated mechanosensing in cells is linked to the conformational state of the subset of cortical actin fibers that activate specific mechanotransduction pathways. Two structurally closely related LIM domain proteins, zyxin and lipoma preferred partner (LPP), seem to play an important functional role in the cardiovascular system. The broad spectrum of cellular pathways these proteins take part in comprises migration, proliferation, hypertrophy, and apoptosis and is a result of a large diversity of protein partners with which LPP and zyxin interact. Whereas the function of zyxin in vascular cells, especially in EC and vascular SMC, has already been well characterized (Cataruzza et al., 2004; Wójtowicz et al., 2010), the mechanotransducer role of LPP, the expression of which is restricted to SMC, in particular vascular SMC (Gorenne et al., 2003; Nelander et al., 2003), requires further investigation (*cf.* **Figure 1**). Interestingly, both LIM domain proteins only respond to a particular deforming stimulus, that is, increased stretch due to a rise in circumferential wall tension. Shear stress, that is, the unidirectional dragging force of the flowing blood, to which only EC are subjected, is probably too weak to elicit a translocation of zyxin from FA to the nucleus in EC, while osmotic stress does neither affect the redistribution of LPP nor that of zyxin in vascular SMC.

STRUCTURE OF LPP AND ZYXIN

Even though LPP, on the protein level, shares only 41% sequence identity with zyxin, which in part is due to differences in length, that is, LPP is about 5% longer than zyxin both in humans and in the mouse, the organizational structure of both proteins is quite similar (**Figure 2**). Both zyxin and LPP contain three LIM domains at the C-terminal region and a proline-rich region (PRR) within their N-terminal sequence, which contains several phosphorylation sites and favors the formation of complexes with other proteins such as α-actinin (Petit et al., 1996). It is believed that both the LIM domain region and the PRR serve as docking sites for either rather different or the same cellular proteins (Feuerstein et al., 1994; Schmeichel and Beckerle, 1994). Moreover, zyxin contains four ActA repeats that serve as vasodilator-stimulated phosphoprotein (VASP) binding sites and one nuclear export signal (NES) between this VASP-binding region and the LIM domains (**Figure 2**). The nuclear export signal seems to be conserved among all zyxin family members (Siddiqui et al., 2021). There is a minor difference in the structure of the LPP protein compared to

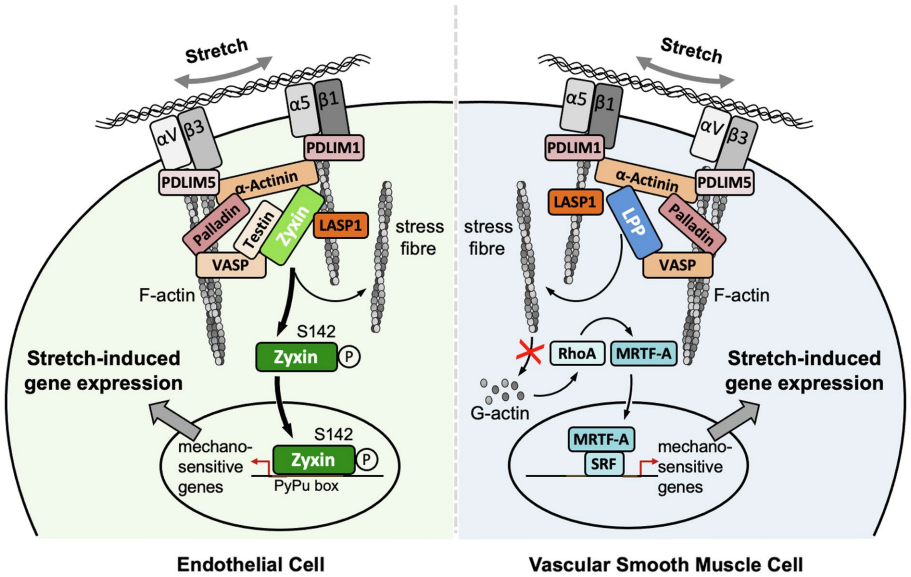

FIGURE 1 | Localization and putative mechanisms of action of zyxin in EC and LPP in vascular SMC. Note that the putative mechanism of action of LPP is derived from our findings on the mechanism of action of zyxin in vascular SMC. Both LIM domain proteins seem to serve the same function in vascular SMC, that is, to maintain their quiescent contractile phenotype. Note that there is no LPP expression in adult EC of mouse or human origin. αVβ3 and α5β1, corresponding integrins; LASP1, LIM and SH3 domain protein 1; MRTF-A, myocardin-related transcription factor A; PDLIM1, PDZ and LIM domain protein 1; PDLIM5, PDZ and LIM domain protein 5; SRF, serum response factor.

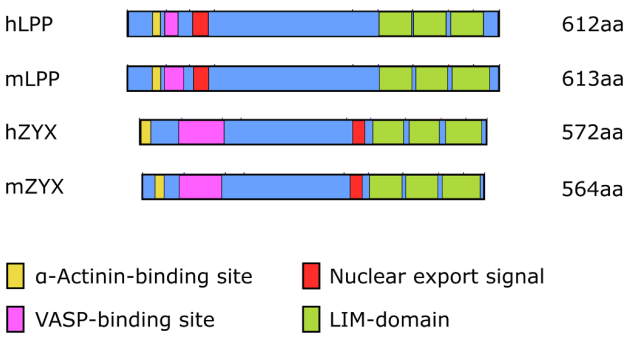

FIGURE 2 | Organizational structure of human (h) and mouse (m) LPP and zyxin proteins depicting the α-actinin and VASP-binding sites close to the N-terminus as well as the three LIM domains close to the C-terminus. The length [number of amino acids (aa)] of the individual proteins is indicated on the right. Note the different localization of the nuclear export signal and the overall difference in length between LPP and zyxin in both species.

zyxin in this region in that LPP harbors only two ActA repeats, that is, VASP interaction domains, and that the single NES is located just distal to the ActA repeats rather than proximal to the first LIM domain, as in zyxin. Moreover, the PRR, which enables interaction of LPP with cytoskeletal components, including actin stress fibers and α-actinin (Li et al., 2003), lies farther from the N-terminus as in zyxin and competes for the same binding partners as zyxin but with much lower affinity.

In the cell, zyxin is mainly found at FA and along stress fibers (Nix and Beckerle, 1997). Its retention at the stress fibers is also sensitive to mechanical signals so that conditions interfering with cellular contractility result in a reduced concentration of zyxin at the stress fibers (Lele et al., 2006). In mechanically stimulated cells, zyxin directly binds to α-actinin and the cytoskeletal regulatory proteins Ena(bled)/VASP and thus contributes to the maintenance of stress fiber formation. By controlling actin assembly and function, zyxin further contributes to the structural integrity of the actin cytoskeleton (Hoffman et al., 2012). Zyxin also accumulates at sites of stress fiber damage induced by excessive strain, resulting in its rapid repair (Smith et al., 2010).

Similar to zyxin, LPP is localized to FA and cell–cell junctions, but unlike zyxin, it is only modestly expressed along stress fibers (Petit et al., 2000). At the FA, LPP binds to the ends of the actin filaments and supports cell attachment. It also interacts with VASP family members and is involved in the spatial organization of actin. In addition, the cellular distribution of LPP is affected by the biomechanical properties of the microenvironment of the cell. While LPP localizes to broad adhesion sites located toward the cell membrane when vascular SMC are grown on rigid surfaces, more elastic surfaces result in a more punctuate cellular localization of LPP (Jin et al., 2009).

LPP and zyxin share structural characteristics (**Figure 2**) and binding partners (*cf.* **Figure 1**). They are co-expressed in vascular SMC *in vivo*, as observed in the medial SMC of larger and smaller diameter arteries in mice and humans, but not in EC (see below). Similarly, many fibroblast-like cells and epithelial cells *in vitro* co-express LPP and zyxin (Li et al., 2003). In cultured vascular SMC, LPP and zyxin are both found at the FA (Ghosh et al., 2015), more precisely at the

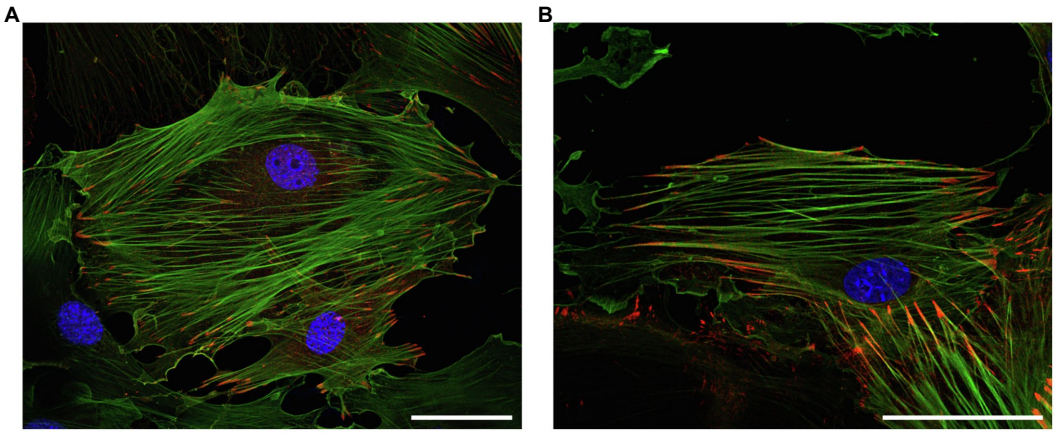

FIGURE 3 | Representative immunofluorescence analysis of the intracellular localization of (top) LPP and (bottom) zyxin in cultured vascular SMC isolated from the aorta of 3-month old C57BL/6 wildtype mice. The vascular SMC (passage 3) were seeded directly on microscopic slides, fixed with *p*-formaldehyde, and stained for LPP or zyxin with a corresponding anti-LPP (HPA017342) or anti-zyxin (HPA004835) primary antibody at a dilution of 1:75 together with a primary anti-α-smooth muscle actin (α-SMA, F3777, all Sigma-Aldrich) at a dilution of 1:200. Images were recorded using a Leica TCS SP8 laser scanning confocal microscope. Both proteins (red fluorescence) mainly localize to the interface between FA and the (tips of the) cortical actin cytoskeleton, which is chiefly organized in stress fibers indicative of a mainly quiescent contractile phenotype of the cultured vascular SMC. The nuclei were counterstained with DAPI (blue fluorescence). The size marker corresponds to 50 μm.

tips of the cortical actin fibers (**Figure 3**), where they interact with other FA-associated proteins, such as α-actinin and VASP (*cf.* **Figure 1**). While this localization has been confirmed for zyxin in native murine vascular SMC (Suresh et al., 2012), this is very likely true for LPP, too, but requires experimental verification. The similar localization of both LIM domain proteins at FA in vascular SMC may have functional implications. While loss of zyxin in cultured SMC produces a shift toward the synthetic phenotype with enhanced migration of cells in a two- and three-dimensional environment as well as decreased contractility associated with improper actin assembly, overexpression of LPP in zyxin-deficient (cultured) vascular SMC fully reverts their phenotype to the quiescent contractile state (Ghosh et al., 2015). On the other hand, cultured LPP-deficient vascular SMC, which also display a synthetic phenotype, fully return to normal upon overexpression of zyxin. Due to this apparent physiological compensation, it is rather difficult to pinpoint the specific role(s) that both LIM domain proteins play in vascular SMC *in vivo*. A large network of interacting proteins could perhaps explain why zyxin cannot displace LPP from its α-actinin binding sites at FA (Li et al., 2003). This may contribute to their differential targeting to subcellular compartments and, together with the restriction of expression of LPP to (vascular) SMC in adult mice (see below), may result in significantly differing functional role(s) in the cardiovascular system.

EXPRESSION OF ZYXIN AND LPP IN THE CARDIOVASCULAR SYSTEM

Besides subtle differences in their intracellular distribution, there are specific differences in the expression of LPP and zyxin that likely impact their functional role in the cardiovascular system. Studies indicate that LPP is a smooth muscle cell-specific protein in the adult tissues of several species, including mouse, rabbit, and guinea pig (Gorenne et al., 2003; Nelander et al., 2003). In the mouse, expression of the *Lpp* gene is driven by an alternative promoter in intron 2 harboring a CArG box that is an serum response factor (SRF)/myocardin-responsive element targeting *Lpp* expression to tissues with large proportions of SMC (Petit et al., 2008). As a result, translation of the protein starts rather late in exon 5 and finishes rather late near the 5′ end of exon 13 (**Figure 4**). The primary transcript of the human *LPP* gene looks somewhat different from the mouse hnRNA (**Figure 5**), there is no alternative promoter in any of the preceding introns, and translation starts in exon 4 and ends at the 3′ end of exon 11. On the other hand, translation results in a remarkably similar protein, also in terms of length.

Data from gene expression profiling studies indicate that LPP is also predominantly expressed by SMC in human tissues [these data have been deposited in the European nucleotide archive (ENA) at EMBL-EBI]. Although LPP has been detected in SMC of the urinary bladder, lung, ovaries, and gastrointestinal tract, among other tissues, a high level of LPP expression was consistently found in vascular SMC. Aorta, vena cava, saphenous vein, tibial artery, and coronary artery all show abundant expression of LPP (Bgee Database, 2021). Proteomics data show that LPP is also expressed in the atrium and the ventricles of the heart but significantly lower than in the aorta or vena cava (PRIDE database available at: https://www.ebi.ac.uk/pride/). Single-cell expression profiling data also show strong enrichment of LPP in vascular SMC as compared to, for example, cardiomyocytes (Human Protein Atlas, 2021). LPP is also expressed in several human cell types, including cardiomyocytes,

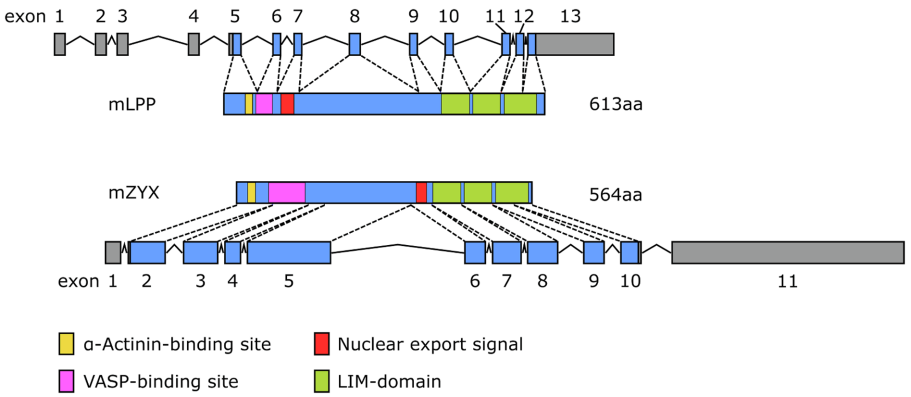

FIGURE 4 | Comparison of the exon-intron structure of the primary transcripts (hnRNA) of the murine (top) *Lpp* and (bottom) *Zyx* gene and their corresponding protein products (mLPP, mZYX). The color coding for the functional elements in both proteins corresponds to that of **Figure 2**.

EC, and fibroblasts *in vitro*, but these data have to be interpreted with caution. Cultured cells are plastic and undergo a phenotypic change associated with changes in the expression profiles of marker genes. For example, in the adult mouse, LPP is not expressed by EC (see below), whereas it is readily detected both in human and mouse EC in culture. Similarly, although LPP has been detected in cardiomyocytes *in vitro* (Hooper et al., 2012), it is not expressed by cardiomyocytes in the heart of adult mice *ex vivo* but clearly detectable in their epicardial arteries and veins (Gorenne et al., 2003). In summary, these data suggest that LPP is consistently enriched in the vasculature, in particular in medial vascular SMC in the mouse and in humans.

While zyxin appears to be expressed across different human tissues, including aorta, heart, endometrium, lung, stomach, and urinary bladder (Bgee Database, 2021), single-cell expression data consistently show enhanced expression of zyxin by the EC. This has been shown for EC of the lung, heart, eye, and liver. Similarly, zyxin is consistently expressed at high levels across several human EC types and lines. While enrichment in EC seems to be specific for zyxin but not LPP, similarly to LPP, zyxin is also expressed by vascular SMC (*cf.* Human Protein Atlas, 2021). Translation of zyxin mRNA in the mouse starts near the 5′ end of exon 2 and results in a protein that is 8% shorter than its LPP counterpart (**Figure 4**). Moreover, there is no alternative promoter in the preceding intron, which may explain the lack of restriction to vascular SMC in the adult mouse. The human primary transcript of the *ZYX* gene looks quite similar to its mouse equivalent and results in a protein that is slightly longer than the murine protein with the α-actinin-binding region moved right next to the N-terminus (**Figure 5**). It is unlikely that these subtle differences have a major impact on the tissue distribution of zyxin in mice and humans, let alone the relative enrichment in EC.

Data from our group reveal that LPP expression in the adult mouse is highly enriched in the medial layer of conduit as well as resistance-sized arteries (**Figures 6A,C**). On the other hand, we could not detect any LPP protein in the endothelial monolayer of these different caliber arterial blood vessels (**Figure 6**). This contrasts with the abundance of zyxin,

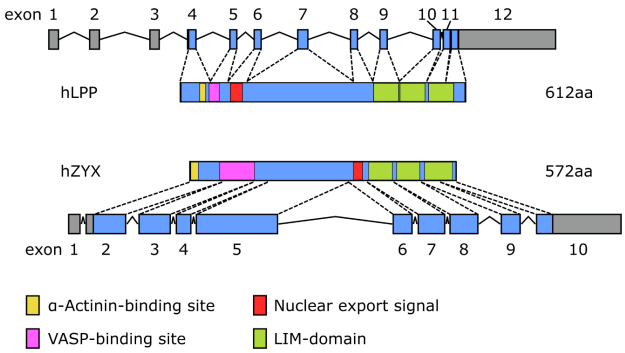

FIGURE 5 | Comparison of the exon-intron structure of the primary transcripts (hnRNA) of the human (top) *LPP* and (bottom) *ZYX* gene and their corresponding protein products (hLPP, hZYX). The color coding for the functional elements in both proteins corresponds to that of **Figure 2**.

which we consistently detected in the EC of both small and larger caliber arterial blood vessels (**Figures 6B,D**). Like LPP, zyxin is detected in the medial SMC layer of these arteries but at a (much) lower level than LPP (**Figure 6**).

While both zyxin and LPP play an important role in regulation of the cytoskeletal organization, bioinformatic analyses of structural data suggest that all members of the zyxin family share similarities with transcriptional regulators (Siddiqui et al., 2021), indicating that these cytoskeletal regulators may perceive the mechanical stimulation at FA and relay this information to the nucleus, presumably by different means, to accordingly affect gene expression and cellular phenotype.

ZYXIN CONTROLS MECHANOSENSITIVE GENE EXPRESSION BOTH DIRECTLY AND INDIRECTLY

Zyxin was the first LIM domain protein described to shuttle between FA and the nucleus (Nix and Beckerle, 1997). It can

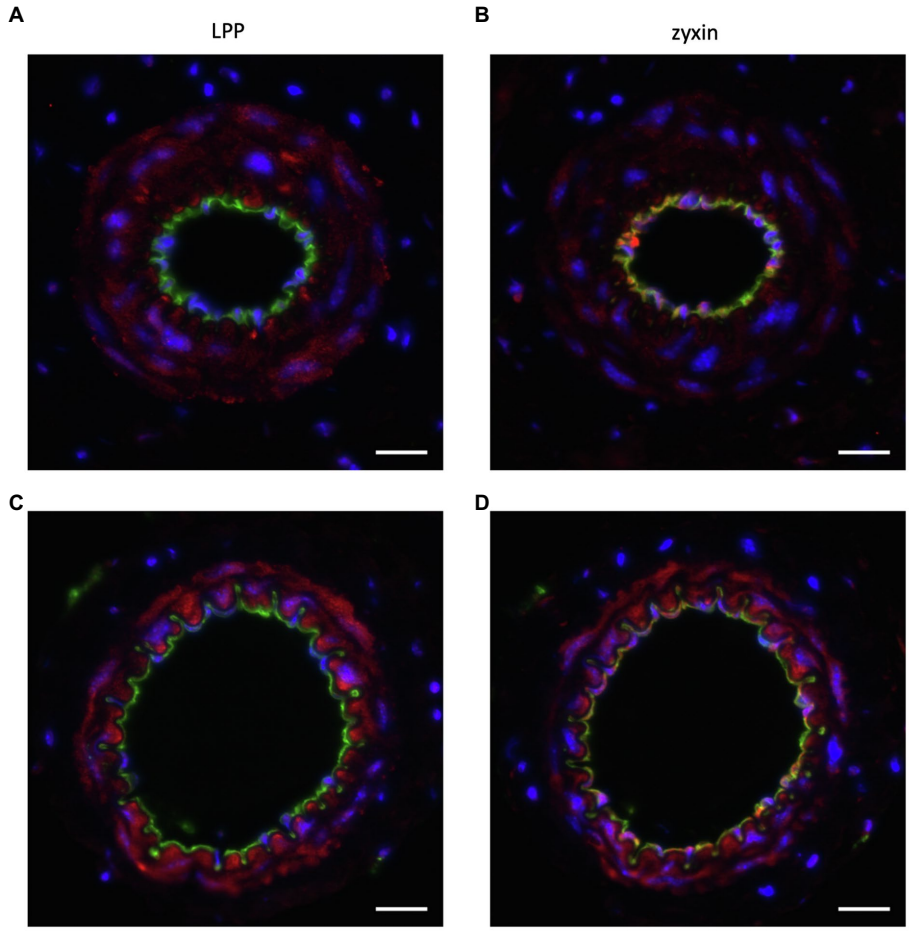

FIGURE 6 | Representative immunofluorescence analysis of the cellular distribution of **(A**,**C)** LPP and **(B**,**D)** zyxin in cross sections of the **(A**,**B)** mouse femoral and **(C**,**D)** mouse mesenteric artery. The isolated blood vessels were fixed with *p*-formaldehyde overnight, embedded in paraffin, and 3 µm-thin sections were stained with primary antibodies directed against LPP (HPA017342, Sigma-Aldrich, 1:75) or zyxin (HPA004835, Sigma-Aldrich, 1:75) together with primary antibodies directed against α-SMA (F3777, Sigma-Aldrich, 1–200) or CD31 (AF3628, R&D Systems, 1:200). Nuclei were counterstained with DAPI (blue fluorescence). Images were recorded using an Olympus IX3 epifluorescence microscope. The size marker corresponds to 20 µm. LPP (red fluorescence) selectively localizes to the medial SMC layer of both arteries (α-SMA-positive area, not shown), whereas zyxin (red fluorescence) is detected both in the intimal layer, that is, in the EC, and in the medial layer of both arteries. In particular in the femoral artery, there is a clear co-detection of zyxin and CD31 (green fluorescence) as indicated by the yellow fluorescence. Since CD31 is present in the EC membrane, while zyxin localizes to the cytoplasm and/or the nucleus, the remainder of the EC reveal positive CD31 immunoreactivity right next to that of zyxin. This also holds true for the mesenteric artery with some yellow fluorescence detectable, too. When compared to LPP, zyxin immunofluorescence in the medial SMC layer of both arteries is clearly weaker.

form complexes with transcription factors and inhibit the activity of genes responsible for embryonic stem cell status implying a role in the phenotype control of cells in general (Parshina et al., 2020). In cardiomyocytes *in vitro*, zyxin translocates to the nucleus upon exposure to atrial natriuretic peptide (ANP) and subsequently activates anti-apoptotic signaling cascades (Kato et al., 2005). Furthermore, multiple studies indicate that zyxin plays an important role in transducing biomechanical cues to the nucleus in vascular SMC and EC but also in fibroblasts.

In biomechanically stimulated vascular SMC, zyxin indirectly controls the expression of mechanosensitive genes including the B-type receptor for endothelin-1 (ET_B-receptor), tenascin-C, and plasminogen activator inhibitor-1 (PA-1; Cattaruzza et al., 2004; Ghosh et al., 2015). In fact, zyxin regulates the majority of genes (about 90%) that are affected by cyclic deformation (stretch) in vascular SMC derived from the mouse aorta (Ghosh et al., 2015). Silencing of zyxin compromises the contractility of vascular SMC (Sun et al., 2012), and on a similar note, vascular SMC derived from the aorta of zyxin knockout mice exhibit a shift from the quiescent, contractile to the activated synthetic phenotype (see above). The absence of zyxin in vascular SMC results in a more growth promoting, promigratory, and less contractile phenotype and exposure to cyclic stretch further accentuates the synthetic phenotype of these cells (Ghosh et al., 2015). This switch from the quiescent contractile to the activated synthetic phenotype is associated with major changes in the control of mechanosensitive gene expression. Enhanced

RhoA activity with subsequent translocation of myocardin-related transcription factor A (MRTF-A) to the nucleus, where it associates with SRF, appears to drive adaptations in mechanosensitive gene expression that are associated with the aforementioned shift in phenotype in human or mouse cultured vascular SMC devoid of zyxin (Ghosh et al., 2015). Knockdown of MRTF-A reversed the changes in mechanosensitive gene expression in zyxin-deficient vascular SMC. While MRTF-A also accumulates in the nucleus of wild-type cultured vascular SMC upon stretch, it does so to a much smaller extent than in zyxin-deficient vascular SMC.

Zyxin also controls mechanosensitive gene expression in EC where it utilizes a quite distinct molecular mechanism and very different kinetics of activation (Wójtowicz et al., 2010; Suresh et al., 2012). Although the threshold for translocation of zyxin to the nucleus is higher in EC in culture as compared to cultured vascular SMC (Ghosh et al., 2015), both in human and mouse EC zyxin rapidly (within minutes) translocates from the FA to the nucleus upon exposure to cyclic stretch. In contrast, shear stress, irrespective of its intensity, has no effect on the nuclear translocation of zyxin in both types of EC. In the nucleus, zyxin binds to a specific *cis*-regulatory element, termed PyPu (for pyrimidine-purine) box, in the promoter of most mechanosensitive EC genes, thereby affecting their expression and apparently stabilizing their phenotype (Wójtowicz et al., 2010; *cf.* **Figure 1**). In essence, this effect of zyxin is very similar to its activity in vascular SMC where it stabilizes their differentiated phenotype, albeit indirectly, during supraphysiological biomechanical stress by preventing actin dynamics-driven MRTF-A-mediated mechanosensitive gene expression (Ghosh et al., 2015). Conversely, lack of zyxin in both human and mouse cultured EC gives rise to a pro-inflammatory and ECM-remodeling phenotype that may even result in endothelial-to-mesenchymal transition.

The signal transduction cascade that enables zyxin to dissociate from FA and subsequently translocate to the nucleus in EC upon stretch is a rather complex multistep process. It comprises a presumably G_q-protein-coupled receptor/diacylglycerol-mediated activation (Storch et al., 2012) of canonical transient receptor potential channel type 3 (TRPC3) triggering a small influx of extracellular calcium that leads to the release of preformed endothelin-1 from intracellular stores. Binding of endothelin-1 to the G_q-protein-coupled ET_B-receptor on the surface of the EC reinforces the rise in intracellular calcium, which in turn causes the release of ANP from the endothelial cells. Binding of ANP to the A-type guanylyl cyclase receptor (GC-A or NPR-A) causes activation of protein kinase G, which in turn phosphorylates zyxin at serine 142 thereby enabling it to dissociate from the FA and translocate to the nucleus of the EC (Wójtowicz et al., 2010, Suresh et al., 2012; *cf.* **Figure 7**).

The way by which TRPC3 gets activated in human stretched cultured EC seems to comprise a G_q-protein-coupled receptor – which is not the angiotensin II type-1 receptor due to lack of effect of losartan – that in turn causes activation of phospholipase $C\beta_1$ (*cf.* **Figure 8C**) resulting in the formation of diacylglycerol and inositol-1,4,5-trisphosphate. TRPC3, 6, and 7 are DAG-sensitive (Dietrich et al., 2005), and among those, TRPC3 has been identified by us (Suresh et al., 2012) to be the TRP channel in cultured human and native mouse EC responsible for initiating the stretch-dependent translocation of zyxin to the nucleus. TRPC3 activation by stretch can be mimicked by using the DAG analogue 1-oleoyl-2-acetyl-sn-glycerol (OAG), and exposure of EC to OAG results in rapid translocation of zyxin to the nucleus, which is virtually abolished by the selective TRPC3 inhibitor Pyr3 (**Figure 8A**). Likewise, OAG-induced expression of a prototypic target gene of zyxin in EC, *CXCL8* encoding the CXC chemokine interleukin-8 (IL-8), is strongly inhibited following TRPC3 blockade with Pyr3 (**Figure 8B**). In addition, Pyr3 strongly inhibits nuclear translocation of zyxin as well as stimulation of *CXCL8* expression in human EC in response to cyclic stretch (**Figures 8D,E**), reinforcing the notion that a G_q-protein-coupled receptor in EC acts as a mechanosensor, which *via* DAG-dependent activation of TRPC3 triggers the phosphorylation and nuclear translocation of zyxin. In the nucleus, zyxin seems to act as a transcription factor responsible for the direct transactivation (or repression) of a multitude of mechanosensitive genes that results in a stabilization of the EC phenotype when blood pressure is chronically increased (*cf.* **Figure 7**).

Altogether, these data indicate that zyxin is an important mechanotransducer strategically localized to the interface between the ECM and the cytoskeleton that directly influences the phenotypic properties of EC and indirectly those of vascular SMC in response to changes in their biomechanical environment, notably exposure to supraphysiological tensile stress.

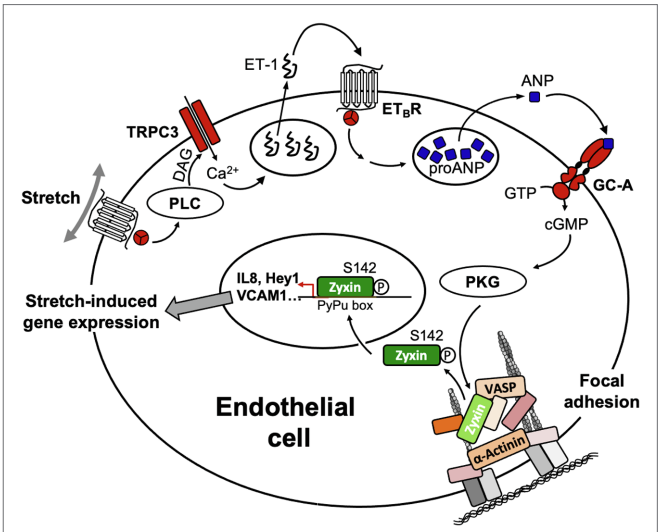

FIGURE 7 | Scheme of the signal transduction cascade in EC ultimately leading to translocation of zyxin from FA to the nucleus. ANP, atrial natriuretic peptide; DAG, diacylglycerol; ET-1, endothelin-1; ET_BR, B-type endothelin-1 receptor; GC-A, A-type guanylyl cyclase receptor; PLC, phospholipase C; PKG, protein kinase G; TRPC3, transient receptor potential cation channel subfamily C member 3; VASP, vasodilator-stimulated phosphoprotein.

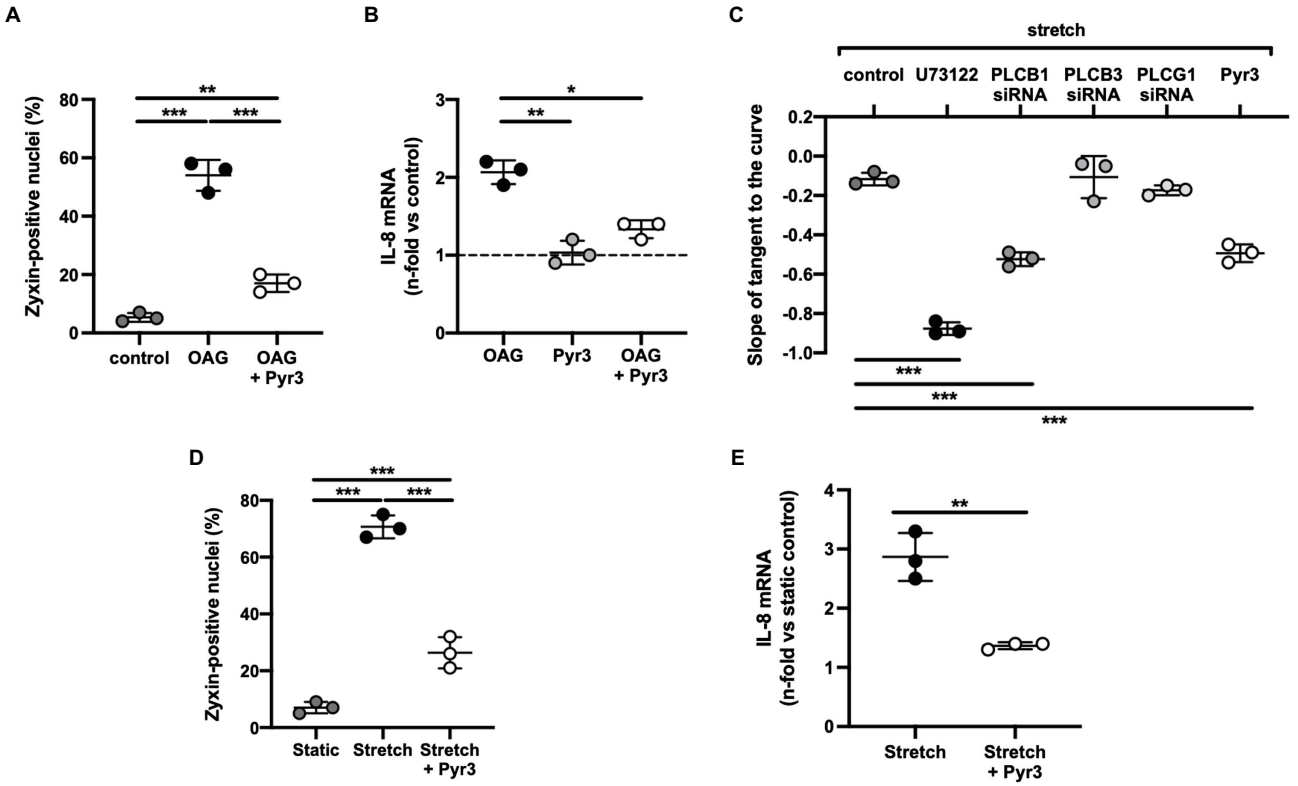

FIGURE 8 | (A) 1-Oleoyl-2-acetyl-sn-glycerol (OAG)-induced activation of zyxin in human umbilical vein endothelial cells (HUVEC). Summary of the quantitative (immunofluorescence) analysis of zyxin-positive nuclei in control cells (passage 1) and after treatment with the diacylglycerol analogue OAG (100 μm) alone for 24 h or following a 6 h pre-incubation with the TRPC3-selective inhibitor Pyr3 [ethyl-1-(4-(2,3,3-trichloroacrylamide)phenyl)-5-(trifluoromethyl)-1H-pyrazole-4-carboxylate; 10 μm]. A primary rabbit polyclonal anti-zyxin antibody (Suresh et al., 2012) was used at a dilution of 1:250. Images were obtained using an Olympus IX81 confocal microscope equipped with an IXDSU disk unit and analyzed by using the cell^R software package. Two-way ANOVA with Sidak post-test for multiple comparisons, $^{**}p<0.01$, $^{***}p<0.001$ as indicated, $n=3$ for each group. **(B)** Analysis of IL-8 gene expression by real-time RT-PCR analysis (Ghosh et al., 2015) in passage 1 HUVEC following the same treatment, $^{*}p<0.05$, $^{**}p<0.01$ as indicated, $n=3$ for each group. The dashed line represents the IL-8 mRNA level in control cells under static conditions. **(C)** Cyclic stretch-induced calcium transients in Fura-2-loaded HUVEC (passage 0) stretched for 50 cycles using elastic membranes. Five μM each of U73122 (pan-phospholipase C inhibitor) and Pyr3 was used. In addition, cells were transfected with siRNA against phospholipase $C\beta_1$, β_3 and γ_1 (resulting in a 42, 35 and 38% knockdown, respectively) followed by the same stretch protocol. Quantitative analysis of the rate of decay (phase II) of the stretch-induced calcium transient by ratiometric imaging, $^{***}p<0.01$ as indicated, $n=3$ for each group. **(D)** TRPC3 channel inhibition by Pyr3 strongly reduces stretch-induced zyxin activation in HUVEC. Quantitative summary of the percentage of zyxin-positive nuclei in control HUVEC (passage 1) under static conditions or following 6 h of cyclic stretch without or with prior treatment by Pyr3 (10 μM). HUVEC were seeded onto collagen I-coated BioFlex elastomers (Flexercell) and stretched or not with a sinusoidal profile at 0.5 Hz and 10% cyclic elongation. $^{***}p<0.01$ as indicated, $n=3$ for each group. **(E)** Analysis of IL-8 mRNA abundance in HUVEC (performed as described under B) following the same treatment. Two-tailed student's *t*-test, $^{**}p<0.01$, $n=3$ for each group.

ROLE OF LPP AS A MECHANOTRANSDUCER

The role of LPP in mechanotransduction in vascular cells has not yet been described in such detail as that of zyxin. This is mainly due to the lack of the corresponding knockout mice, which ideally should be raised on the same genetic background as the zyxin knockout mice (C57BL/6), and an in-depth characterization of their respective phenotypes *in vivo*. Essentially, all knowledge about LPP to date originates from *in vitro* work with cultured cells or cell lines. However, when considering that LPP, in contrast to zyxin, is highly enriched in SMC, and in particular in vascular SMC (Gorenne et al., 2003; Nelander et al., 2003; Petit et al., 2008), in both mice and humans (see above), and its established role in the proliferation and migration of tumor cells, its role in the vasculature as a modulator of the SMC phenotype under tensile stress surely deserves proper attention.

CONTROL OF LPP EXPRESSION

In vascular SMC, myocardin is a potent co-activator of SRF. SRF in turn activates expression of a subset of SMC-specific marker genes and also enhances LPP expression (Gorenne et al., 2003, 2006). This activation depends on the RhoA/ROCK pathway, and accordingly, inhibitors of this pathway decrease myocardin expression and, among other SMC-specific genes, expression of the *Lpp* gene, too, suggesting that the *Lpp* gene shares transcriptional regulatory mechanisms common to SMC-specific genes. Increased activity of focal adhesion kinase (FAK) also

positively regulates expression of the *Lpp* gene (Gorenne et al., 2003; Jin et al., 2007). Accordingly, FAK-deficient vascular SMC express lower levels of LPP protein and exhibit impaired migration. However, when the transcription factors Prx1a and 1b are overexpressed in these cells, abundance of LPP is increased, suggesting that *Lpp* expression is also regulated by Prx1 homebox transcription factors (Jin et al., 2007). Both Prx1a and 1b are highly expressed in the developing cardiovascular system, especially in larger arteries and veins. It is interesting to note that *Prx1* knockout mice display abnormal morphologies of the greater blood vessels (Bergwerff et al., 2000). One can only speculate at this point whether products of genes under the control of Prx1, possibly including *Lpp*, regulate proper migration of vascular SMC during vasculogenesis and that their absence thus leads to structural abnormalities of the developing blood vessels.

Although expression of LPP is very low in the adult heart as compared to that in vascular SMC (Petit et al., 1996; Human Protein Atlas, 2021), and according to our own data essentially confined to the conduit and resistance-sized arteries and veins in the adult mouse heart, pressure overload of the left ventricle caused by aortic constriction in the rat seems to increase LPP expression in the whole myocardium (Hooper et al., 2012). It should be noted, however, that in this study, LPP protein abundance in neonatal ventricles was severalfold higher than in the adult ventricles and that there was not much of a difference in LPP protein between the (unaffected) right and the (presumably hypertrophic) left ventricle in the adult rats. Since all other data were obtained with cardiac cells *in vitro*, it remains to be determined whether and in which cell type LPP provides a link between cytoskeletal remodeling and mechanical overload in the heart. In another study by the same group, knockdown of LPP by small interfering RNA impaired the adaptive response of neonatal rat cardiomyocytes to mechanical overload by compromising myofibrillogenesis (Hooper et al., 2013). Whether LPP plays a similar protective role in adult cardiomyocytes or *in vivo* is not known.

LPP REGULATES GENE EXPRESSION AND CELL MIGRATION

One plausible mechanism how LPP may mediate cytoskeletal remodeling in response to mechanical stimuli is by activation of specific response genes that mediate these structural adaptations. LPP can shuttle to the nucleus and exhibit gene transcription activation capacity *in vitro* as measured by using a GAL-4 transactivation assay in HeLa cells. This is mediated by the two LIM domains and the proline-rich region (Petit et al., 2000). Upon exposure of cells to biomechanical deformation, LPP only transiently translocates to the nucleus where it may exhibit some transactivation capacity or function as a transcriptional co-activator to mediate the adaptive changes in gene expression in response to mechanical stress (Siddiqui et al., 2021). When the nuclear export sequence is removed or the nuclear export signal CRM1 is inhibited, LPP accumulates in the nucleus (Petit et al., 2000), emphasizing the nuclear-cytoplasmic shuttling role of LPP.

LPP is also capable of enhancing expression of PEA3-dependent genes *in vitro* (Guo et al., 2006) that are involved in neuronal development or mediation of fibroblast growth factor signaling (Roehl and Nüsslein, 2001; Firnberg and Neubüser, 2002; Livet et al., 2002). In addition, PEA3 controls genes encoding certain matrix metalloproteinases (MMP) involved in degradation of the ECM (Grunewald et al., 2009). ETV5 is a member of a PEA3 subfamily and a partner of LPP in controlling transcription. Together with LPP, it induces re-organization of cell–cell and cell-substrate contacts and promotes cell migration. In the context of cancer progression, where uncontrolled migration of and invasion by tumor cells is a pivotal feature, this effect of LPP on ETV5-dependent gene expression may reinforce epithelial-to-mesenchymal transition and expansion of the tumor into neighboring tissues (Colas et al., 2012). However, inadequate migratory behavior is associated with other pathologies as well, including atherogenesis and maladaptive hypertension-induced arterial remodeling.

Originally, LPP was discovered in a subset of lipomas as a fusion protein with high mobility group A2 (HMGA2). This fusion protein, in which the carboxy-terminal LIM domains of LPP are fused to the amino-terminal end of HMGA2, has been shown to facilitate the migration of tumor cells (Grunewald et al., 2009). In the cardiovascular system, modulating the phenotype of vascular SMC and degradation of the ECM are important steps for these cells to migrate from the media to form a sub-endothelial neointima following vascular injury (Owens, 1995). In fact, several studies have suggested a role for LPP in the migration of vascular SMC. These cells are capable of perceiving changes in stiffness and composition of the ECM. When grown on denatured collagen type 1 that simulates the microenvironment in an injured conduit artery (or vein), they upregulate expression of the *LPP* gene (Jin et al., 2009). A similar situation occurs in arterial blood vessels where both LPP and one of its preferred binding partners, paladin, are highly abundant not only in the media but also in the neointima of injured conduit arteries, again implying a functional role of LPP in the migratory behavior of vascular SMC (Gorenne et al., 2006; Jin et al., 2007). In medial SMC invading the neointima, LPP together with palladin is recruited to podosomes, that is, motile and highly dynamic actin structures found in vascular SMC in atherosclerosis (Jin et al., 2009).

In the context of tumor progression and spreading, LPP may in fact facilitate the abnormal migratory behavior of cancer cells by playing a regulatory role in the formation and function of invadopodia that promote metastasis (Ngan et al., 2017). When overexpressed in HIVS-125 cells (human SMC line), LPP enhances migration and cell spreading (Jin et al., 2007), and when LPP expression is attenuated, the invasiveness of tumor cells is also decreased (Grunewald et al., 2009). These findings suggest that the mechanosensory and perhaps mechanoregulatory function of LPP can also be employed by such cells in a pathological setting. It should be emphasized, however, that none of these findings have been obtained with cells or tissues derived from, for example, mice deficient for LPP. Moreover, *in vivo* or *ex vivo* studies of *Lpp* knockout mice are necessary to shed more light on the physiological role of LPP in blood

vessels because studies with cultured cells may not adequately reflect the physiological conditions. This is especially noteworthy with regard to *Lpp* gene expression in adult mice being restricted to SMC, in particular to vascular SMC (see above). In addition, studies with cells that overexpress LPP do not accurately reflect the physiological role of LPP as overexpression of LPP disrupts normal LPP signaling and leads to a concentration-dependent upregulation of PEA3-dependent gene products including, for example, various MMP. Overexpression of these proteases would favor ECM destabilization and cell migration as frequently observed in different cancer cell lines (Guo et al., 2006; Grunewald et al., 2009). Another aspect to consider when interpreting *in vitro* findings is that vascular SMC attain a fibroblast-like phenotype in culture and that expression of characteristic marker genes and transduction pathways is modified in cultured cells (Jackson et al., 1997). This may be particularly true for LPP, which also belongs to the core of SMC-specific genes.

In contrast to its promigratory effect in LPP-overexpressing cultured cells or cancer cell lines, LPP may act as a fine-tuning protein regulating the migratory behavior of vascular SMC in response to biomechanical stimulation. While facilitating migration during vascular injury or vasculogenesis when SMC transit to a promigratory and growth-promoting state, in the absence of a specific biomechanical stimulus, LPP may support gene expression and signaling pathways associated with the quiescent contractile state. In fact, LPP was shown to act as a suppressor of cell migration associated with malignant cancer phenotypes. In lung cancer cells, MMP15 is a direct transcriptional target of LPP and ETV5. MMP15 degrades N-cadherin and weakens cell–cell contacts and thus can attenuate migration (Kuriyama et al., 2016). Similarly, recent studies suggest that a dual role of LIM proteins is plausible (promigratory vs. anti-migratory). As an example, four and a half LIM domains protein 1 (FHL-1) can act both as a tumor suppressor and a growth-promoting signaling molecule, depending on its association with diverse cellular signals (Wei and Zhang, 2020).

In fact, zyxin has also been shown to exhibit opposing actions on the migratory behavior of cells depending on the cellular context. Overexpression of zyxin in human hepatocellular cancer cells was associated with increased invasiveness and migratory abilities of these cells (Sy et al., 2006). In contrast, zyxin attenuated tumor growth, reconstituted FA organization with the actin cytoskeleton and decreased cell motility in a Ewing sarcoma model (Amsellem et al., 2005). This second action of zyxin would correspond with our results from zyxin-deficient vascular SMC that display increased migration and proliferation and poor contractile capacity, but upon re-expression of zyxin or LPP switch their phenotype back to the quiescent contractile state (Ghosh et al., 2015).

CONCLUSION

In summary, LIM domain proteins, such as zyxin and LPP act, depending on the type of vascular cell, as mechanotransducers directly (zyxin) or indirectly (LPP) propagating the biomechanical stress signal into the nucleus and a change in gene expression that aims at maintaining the cells in a quiescent state. While expression of LPP seems to be restricted to vascular SMC in the adult, zyxin is highly abundant in EC. LPP presumably indirectly, *via* activation of MRTF-A relays changes in biomechanical load on the actin cytoskeleton and ECM-cell contacts (FA) to the nucleus. By acting as a sensor of the state of the cortical actin cytoskeleton, it modulates its structure and function under the complex and variable conditions of biomechanical stimulation. Markers of the differentiated state of vascular SMC are highly dependent on cytoskeletal dynamics so that, depending on the (patho) physiological context, corresponding changes in gene expression support the cells to remain in a quiescent contractile state. Zyxin, on the other hand, plays a dominant role as a mechanotransducer in EC that translocates from the FA to the nucleus where it can directly transactivate mechanosensitive genes, but has also some functional overlap with LPP in vascular SMC. Considering the presumably complex role these two mechanotransducers play in the cardiovascular system, more mechanistic studies but also animal experimental *in vivo* models are required to delineate the mechanisms through which these LIM domain proteins stabilize the quiescent phenotype of these cells in the face of a supraphysiological prolonged tensile stress as it occurs, for example, in arterial hypertension. This may eventually pave the way toward therapeutic strategies aiming at maintaining expression of these LIM domain proteins in vascular cells.

AUTHOR CONTRIBUTIONS

AS and MH conceived and wrote the manuscript. SG and JA-H performed experiments and contributed the data. JA-H contributed part of the figures. All authors provided critical feedback and contributed to the final manuscript.

FUNDING

This work was supported by an individual research grant from the Deutsche Forschungsgemeinschaft to MH (HE 1587/12–1).

REFERENCES

Amsellem, V., Kryszke, M. H., Hervy, M., Subra, F., Athman, R., Leh, H., et al. (2005). The actin cytoskeleton-associated protein zyxin acts as a tumor suppressor in Ewing tumor cells. *Exp. Cell Res.* 304, 443–456. doi: 10.1016/j.yexcr.2004.10.035

Bergwerff, M., Gittenberger-de Groot, A. C., Wisse, L. J., DeRuiter, M. C., Wessels, A., Martin, J. F., et al. (2000). Loss of function of the Prx1 and Prx2 homeobox genes alters architecture of the great elastic arteries and ductus arteriosus. *Virchows Arch.* 436, 12–19. doi: 10.1007/PL00008193

Bgee Database (2021). LPP expression. Available at: https://bgee.org/?page=gene&gene_id=ENSG00000145012, and zyxin expression: https://bgee.org/?page=gene&gene_id=ENSG00000159840 (Accessed April 15, 2021).

Cattaruzza, M., Lattrich, C., and Hecker, M. (2004). Focal adhesion protein zyxin is a mechanosensitive modulator of gene expression in vascular smooth muscle cells. *Hypertension* 43, 726–730. doi: 10.1161/01.HYP.0000119189.82659.52

Colas, E., Muinelo-Romay, L., Alconada, A., Llaurado, M., Monge, M., Barbazan, J., et al. (2012). ETV5 cooperates with LPP as a sensor of extracellular signals and promotes EMT in endometrial carcinomas. *Oncogene* 31, 4778–4788. doi: 10.1038/onc.2011.632

Dietrich, A., Kalwa, H., Rost, B. R., and Gudermann, T. (2005). The diacylglycerol-sensitive TRPC3/6/7 subfamily of cation channels: functional characterization and physiological relevance. *Pflugers Arch.* 451, 72–80. doi: 10.1007/s00424-005-1460-0

Feuerstein, R., Wang, X., Song, D., Cooke, N. E., and Liebhaber, S. A. (1994). The LIM/double zinc-finger motif functions as a protein dimerization domain. *Proc. Natl. Acad. Sci.* 91, 10655–10659. doi: 10.1073/pnas.91.22.10655

Firnberg, N., and Neubüser, A. (2002). FGF signaling regulates expression of Tbx2, Erm, Pea3, and Pax3 in the early nasal region. *Dev. Biol.* 247, 237–250. doi: 10.1006/dbio.2002.0696

Geiger, B., Spatz, J. P., and Bershadsky, A. D. (2009). Environmental sensing through focal adhesions. *Nat. Rev. Mol. Cell Biol.* 10, 21–33. doi: 10.1038/nrm2593

Ghosh, S., Kollar, B., Nahar, T., Suresh, B. S., Wojtowicz, A., Sticht, C., et al. (2015). Loss of the mechanotransducer zyxin promotes a synthetic phenotype of vascular smooth muscle cells. *J. Am. Heart Assoc.* 4:e001712. doi: 10.1161/JAHA.114.001712

Gorenne, I., Jin, L., Yoshida, T., Sanders, J. M., Sarembock, I. J., Owens, G. K., et al. (2006). LPP expression during in vitro smooth muscle differentiation and stent-induced vascular injury. *Circ. Res.* 98, 378–385. doi: 10.1161/01.RES.0000202802.34727.fd

Gorenne, I., Nakamoto, R. K., Phelps, C. P., Beckerle, M. C., Somlyo, A. V., and Somlyo, A. P. (2003). LPP, a LIM protein highly expressed in smooth muscle. *Am. J. Physiol. Cell Physiol.* 285, C674–C685. doi: 10.1152/ajpcell.00608.2002

Grunewald, T. G. P., Paesdag, S. M., and Butt, E. (2009). Cell adhesion and transcriptional activity – defining the role of the novel protooncogene LPP. *Transl. Oncol.* 2, 107–116. doi: 10.1593/tlo.09112

Guo, B., Sallis, R. E., Greenall, A., Petit, M. M., Jansen, E., Young, L., et al. (2006). The LIM domain protein LPP is a coactivator for the ETS domain transcription factor PEA3. *Mol. Cell. Biol.* 26, 4529–4538. doi: 10.1128/MCB.01667-05

Hoffman, L. M., Jensen, C. C., Chaturvedi, A., Yoshigi, M., and Beckerle, M. C. (2012). Stretch-induced actin remodeling requires targeting of zyxin to stress fibers and recruitment of actin regulators. *Mol. Biol. Cell* 23, 1846–1859. doi: 10.1091/mbc.E11-12-1057

Hooper, C. L., Dash, P. R., and Boateng, S. Y. (2012). Lipoma preferred partner is a mechanosensitive protein regulated by nitric oxide in the heart. *FEBS Open Bio.* 2, 135–144. doi: 10.1016/j.fob.2012.05.005

Hooper, C. L., Paudyal, A., Dash, P. R., and Boateng, S. Y. (2013). Modulation of stretch-induced myocyte remodeling and gene expression by nitric oxide: a novel role for lipoma preferred partner in myofibrillogenesis. *Am. J. Physiol. Heart Circ. Physiol.* 304, H1302–H1313. doi: 10.1152/ajpheart.00004.2013

Human Protein Atlas (2021) Zyxin expression. Available at: https://www.proteinatlas.org/ENSG00000159840-ZYX/celltype, and LPP expression: https://www.proteinatlas.org/ENSG00000145012-LPP/celltype (Accessed April 15, 2021).

Jackson, W. J., Huebner, J. M., and Rusch, N. J. (1997). Enzymatic isolation and characterization of single vascular smooth muscle cells from cremasteric arterioles. *Microcirculation* 4, 35–50. doi: 10.3109/10739689709148316

Jin, L., Hastings, N. E., Blackman, B. R., and Somlyo, A. V. (2009). Mechanical properties of the extracellular matrix alter expression of smooth muscle protein LPP and its partner palladin; relationship to early atherosclerosis and vascular injury. *J. Muscle Res. Cell Motil.* 30, 41–55. doi: 10.1007/s10974-009-9173-1

Jin, L., Kern, M. J., Otey, C. A., Wamhoff, B. R., and Somlyo, A. V. (2007). Angiotensin II, focal adhesion kinase, and PRX1 enhance smooth muscle expression of lipoma preferred partner and its newly identified binding partner palladin to promote cell migration. *Circ. Res.* 100, 817–825. doi: 10.1161/01.RES.0000261351.54147.de

Kadrmas, J. L., and Beckerle, M. C. (2004). The LIM domain: from the cytoskeleton to the nucleus. *Nat. Rev. Mol. Cell Biol.* 5, 920–931. doi: 10.1038/nrm1499

Kato, T., Muraski, J., Chen, Y., Tsujita, Y., Wall, J., Glembotski, C. C., et al. (2005). Atrial natriuretic peptide promotes cardiomyocyte survival by cGMP-dependent nuclear accumulation of zyxin and Akt. *J. Clin. Invest.* 115, 2716–2730. doi: 10.1172/JCI24280

Kuo, J. C., Han, X., Hsiao, C. T., Yates, J. R. 3rd, and Waterman, C. M. (2011). Analysis of the myosin-II-responsive focal adhesion proteome reveals a role for β-Pix in negative regulation of focal adhesion maturation. *Nat. Cell Biol.* 13, 383–393. doi: 10.1038/ncb2216

Kuriyama, S., Yoshida, M., Yano, S., Aiba, N., Kohno, T., Minamiya, Y., et al. (2016). LPP inhibits collective cell migration during lung cancer dissemination. *Oncogene* 35, 952–964. doi: 10.1038/onc.2015.155

Lele, T. P., Pendse, J., Kumar, S., Salanga, M., Karavitis, J., and Ingber, D. E. (2006). Mechanical forces alter zyxin unbinding kinetics within focal adhesions of living cells. *J. Cell. Physiol.* 207, 187–194. doi: 10.1002/jcp.20550

Li, B., Zhuang, L., Reinhard, M., and Trueb, B. (2003). The lipoma preferred partner LPP interacts with alpha-actinin. *J. Cell Sci.* 116, 1359–1366. doi: 10.1242/jcs.00309

Livet, J., Sigrist, M., Stroebel, S., De Paola, V., Price, S. R., Henderson, C. E., et al. (2002). ETS gene Pea3 controls the central position and terminal arborization of specific motor neuron pools. *Neuron* 35, 877–892. doi: 10.1016/S0896-6273(02)00863-2

Nelander, S., Mostad, P., and Lindahl, P. (2003). Prediction of cell type-specific gene modules: identification and initial characterization of a core set of smooth muscle-specific genes. *Genome Res.* 13, 1838–1854. doi: 10.1101/gr.1197303

Ngan, E., Stoletov, K., Smith, H. W., Common, J., Muller, J. W., Lewis, J. D., et al. (2017). LPP is a Src substrate required for invadopodia formation and efficient breast cancer lung metastasis. *Nat. Commun.* 8, 1–5. doi: 10.1038/ncomms15059

Nix, D. A., and Beckerle, M. C. (1997). Nuclear-cytoplasmic shuttling of the focal contact protein, zyxin: a potential mechanism for communication between sites of cell adhesion and the nucleus. *J. Cell Biol.* 138, 1139–1147. doi: 10.1083/jcb.138.5.1139

Owens, G. K. (1995). Regulation of differentiation of vascular smooth muscle cells. *Physiol. Rev.* 75, 487–517. doi: 10.1152/physrev.1995.75.3.487

Parshina, E. A., Eroshkin, F. M., Orlov, E. E., Gyoeva, F. K., Shokhina, A. G., Staroverov, D. B., et al. (2020). Cytoskeletal protein Zyxin inhibits the activity of genes responsible for embryonic stem cell status. *Cell Rep.* 33:108396. doi: 10.1016/j.celrep.2020.108396

Petit, M. M., Fradelizi, J., Golsteyn, R. M., Ayoubi, T. A., Menichi, B., Louvard, D., et al. (2000). LPP, an actin cytoskeleton protein related to zyxin, harbors a nuclear export signal and transcriptional activation capacity. *Mol. Biol. Cell* 11, 117–129. doi: 10.1091/mbc.11.1.117

Petit, M. M., Lindskog, H., Larsson, E., Wasteson, P., Athley, E., Breuer, S., et al. (2008). Smooth muscle expression of lipoma preferred partner is mediated by an alternative intronic promoter that is regulated by serum response factor/myocardin. *Circ. Res.* 103, 61–69. doi: 10.1161/CIRCRESAHA.108.177436

Petit, M. M., Mols, R., Shoenmakers, E. F., Mandahl, N., and Van de Ven, W. J. (1996). LPP, the preferred fusion partner gene of HMGIC in lipomas, is a novel member of the LIM protein gene family. *Genomics* 36, 118–129. doi: 10.1006/geno.1996.0432

Rensen, S., Doevendans, P., and Van Eys, G. (2007). Regulation and characteristics of vascular smooth muscle cell phenotypic diversity. *Neth. Heart J.* 15, 100–108. doi: 10.1007/BF03085963

Roehl, H., and Nüsslein, V. C. (2001). Zebrafish pea3 and erm are general targets of FGF8 signalling. *Curr. Biol.* 11, 503–507. doi: 10.1016/S0960-9822(01)00143-9

Saleh, A.-S. T., Iratni, R., and Eid, A. H. (2016). Anti-atherosclerotic plants which modulate the phenotype of vascular smooth muscle cells. *Phytomed. Int. J. Phytother. Phytopharm.* 23, 1068–1081. doi: 10.1016/j.phymed.2015.10.016

Sang, M., Ma, L., Sang, M., Zhou, X., Gao, W., and Geng, C. (2014). LIM-domain-only proteins: multifunctional nuclear transcription coregulators that interacts with diverse proteins. *Mol. Biol. Rep.* 41, 1067–1073. doi: 10.1007/s11033-013-2952-1

Schiller, H. B., Friedel, C. C., Boulegue, C., and Fässler, R. (2011). Quantitative proteomics of the integrin adhesome show a myosin II-dependent recruitment of LIM domain proteins. *EMBO Rep.* 12, 259–266. doi: 10.1038/embor.2011.5

Schmeichel, K. L., and Beckerle, M. C. (1994). The LIM domain is a modular protein-binding interface. *Cell* 79, 211–219. doi: 10.1016/0092-8674(94)90191-0

Siddiqui, M. Q., Badmalia, M. D., and Patel, T. R. (2021). Bioinformatic analysis of structure and function of LIM domains of human Zyxin family proteins. *Int. J. Mol. Sci.* 22:2647. doi: 10.3390/ijms22052647

Smith, M. A., Blankman, E., Gardel, M. L., Luettjohann, L., Waterman, C. M., and Beckerle, M. C. (2010). A zyxin-mediated mechanism for actin stress fiber maintenance and repair. *Dev. Cell* 19, 365–376. doi: 10.1016/j.devcel.2010.08.008

Storch, U., Forst, A., Philipp, M., Gudermann, T., and Schnitzel, M. M. (2012). Transient receptor potential channel 1 (TRPC1) reduces calcium permeability in heteromeric channel complexes. *J. Biol. Chem.* 287, 3530–3540. doi: 10.1074/jbc.M111.283218

Sun, Z., Huang, S., Li, Z., and Meininger, G. A. (2012). Zyxin is involved in regulation of mechanotransduction in arteriole smooth muscle cells. *Front. Physiol.* 3:472. doi: 10.3389/fphys.2012.00472

Sun, X., Phua, D. Y. Z., Axiotakis, L. Jr., Smith, M. A., Blankman, E., Gong, R., et al. (2020). Mechanosensing through direct binding of tensed F-actin by LIM domains. *Dev. Cell* 55, 468–482. doi: 10.1016/j.devcel.2020.09.022

Suresh, B. S., Wojtowicz, A., Freichel, M., Birnbaumer, L., Hecker, M., and Cattaruzza, M. (2012). Mechanism of stretch-induced activation of the mechanotransducer zyxin in vascular cells. *Sci. Signal.* 5:ra91. doi: 10.1126/scisignal.2003173

Sy, S. H., Lai, P. B., Pang, E., Wong, N. L., To, K. F., Johnson, P. J., et al. (2006). Novel identification of zyxin upregulations in the motile phenotype of hepatocellular carcinoma. *Mod. Pathol.* 19, 1108–1116. doi: 10.1038/modpathol.3800626

Wei, X., and Zhang, H. (2020). Four and a half LIM domains protein 1 can be as a double-edged sword in cancer progression. *Cancer Biol. Med.* 17, 270–281. doi: 10.20892/j.issn.2095-3941.2019.0420

Winkelman, J. D., Anderson, C. A., Suarez, C., Kovar, D. R., and Gardel, M. L. (2020). Evolutionarily diverse LIM domain-containing proteins bind stressed actin filaments through a conserved mechanism. *Proc. Natl. Acad. Sci.* 117, 25532–25542. doi: 10.1073/pnas.2004656117

Wójtowicz, A., Babu, S. S., Li, L., Gretz, N., Hecker, M., and Cattaruzza, M. (2010). Zyxin mediation of stretch-induced gene expression in human endothelial cells. *Circ. Res.* 107, 898–902. doi: 10.1161/CIRCRESAHA.110.227850

Conflict of Interest: The authors declare that the research was conducted in the absence of any commercial or financial relationships that could be construed as a potential conflict of interest.

Publisher's Note: All claims expressed in this article are solely those of the authors and do not necessarily represent those of their affiliated organizations, or those of the publisher, the editors and the reviewers. Any product that may be evaluated in this article, or claim that may be made by its manufacturer, is not guaranteed or endorsed by the publisher.

frontiers in Physiology

REVIEW
published: 23 December 2021
doi: 10.3389/fphys.2021.771960

Mechanobiology of Microvascular Function and Structure in Health and Disease: Focus on the Coronary Circulation

*Maarten M. Brandt[1], Caroline Cheng[1,2], Daphne Merkus[1,3,4], Dirk J. Duncker[1] and Oana Sorop[1]**

[1]Division of Experimental Cardiology, Department of Cardiology, Erasmus MC, University Medical Center Rotterdam, Rotterdam, Netherlands, [2]Division of Internal Medicine and Dermatology, Department of Nephrology and Hypertension, University Medical Center Utrecht, Utrecht, Netherlands, [3]Walter Brendel Center of Experimental Medicine (WBex), LMU Munich, Munich, Germany, [4]German Center for Cardiovascular Research (DZHK), Partner Site Munich, Munich Heart Alliance (MHA), Munich, Germany

OPEN ACCESS

Edited by:
Luciana Venturini Rossoni, University of São Paulo, Brazil

Reviewed by:
Camilla Ferreira Wenceslau, University of South Carolina, United States
Raquel Hernanz, Rey Juan Carlos University, Spain
Roger Lyrio Santos, Federal University of Espirito Santo, Brazil

***Correspondence:**
Oana Sorop
o.sorop@erasmusmc.nl

Specialty section:
This article was submitted to Vascular Physiology, a section of the journal Frontiers in Physiology

Received: *07 September 2021*
Accepted: *11 November 2021*
Published: *23 December 2021*

Citation:
Brandt MM, Cheng C, Merkus D, Duncker DJ and Sorop O (2021) Mechanobiology of Microvascular Function and Structure in Health and Disease: Focus on the Coronary Circulation. Front. Physiol. 12:771960. doi: 10.3389/fphys.2021.771960

The coronary microvasculature plays a key role in regulating the tight coupling between myocardial perfusion and myocardial oxygen demand across a wide range of cardiac activity. Short-term regulation of coronary blood flow in response to metabolic stimuli is achieved via adjustment of vascular diameter in different segments of the microvasculature in conjunction with mechanical forces eliciting myogenic and flow-mediated vasodilation. In contrast, chronic adjustments in flow regulation also involve microvascular structural modifications, termed remodeling. Vascular remodeling encompasses changes in microvascular diameter and/or density being largely modulated by mechanical forces acting on the endothelium and vascular smooth muscle cells. Whereas in recent years, substantial knowledge has been gathered regarding the molecular mechanisms controlling microvascular tone and how these are altered in various diseases, the structural adaptations in response to pathologic situations are less well understood. In this article, we review the factors involved in coronary microvascular functional and structural alterations in obstructive and non-obstructive coronary artery disease and the molecular mechanisms involved therein with a focus on mechanobiology. Cardiovascular risk factors including metabolic dysregulation, hypercholesterolemia, hypertension and aging have been shown to induce microvascular (endothelial) dysfunction and vascular remodeling. Additionally, alterations in biomechanical forces produced by a coronary artery stenosis are associated with microvascular functional and structural alterations. Future studies should be directed at further unraveling the mechanisms underlying the coronary microvascular functional and structural alterations in disease; a deeper understanding of these mechanisms is critical for the identification of potential new targets for the treatment of ischemic heart disease.

Keywords: microvascular remodeling, microvascular density, microvascular dysfunction, coronary blood flow, endothelial dysfunction, ischemic heart disease, microvascular disease

INTRODUCTION

The coronary microvasculature plays a key role in the tight coupling between myocardial perfusion and myocardial oxygen demand across a wide range of cardiac activity. Short-term regulation of coronary blood flow (CBF) in response to metabolic stimuli is achieved via adjustment of vascular diameter in different segments of the microvasculature in conjunction with mechanical forces eliciting myogenic and flow-mediated responses (Duncker and Bache, 2008). In contrast, chronic adjustments in flow regulation also involve structural modifications of the microvasculature, termed remodeling. Vascular remodeling encompasses changes in microvascular diameter and/or density and is largely modulated by mechanical forces acting on the endothelium and vascular smooth muscle cells (VSMCs). Moreover, metabolic and endothelial factors controlling vascular tone also play an important role in maintaining the integrity of the microvascular network. Such factors have been shown to be altered in pathological situations.

Especially in the setting of ischemic heart disease (IHD), distal to a proximal epicardial artery stenosis, mechanical determinants of vascular tone, such as perfusion pressure, extravascular compression and flow, are altered, possibly contributing to microvascular remodeling. Moreover, even in the absence of a coronary obstruction, risk factors commonly seen in patients with IHD, such as diabetes, hypercholesterolemia, hypertension and aging, result in microvascular dysfunction and remodeling, impairing myocardial perfusion (Padro et al., 2020; Sorop et al., 2020). Such risk factors could also exacerbate microvascular structural and functional alterations in the myocardium distal to a flow-limiting coronary stenosis possibly contributing to the residual ischemia still present in many patients long after recanalization of the obstructed artery.

Although in recent years more data have been gathered regarding coronary microvascular function in patients at different stages of cardiovascular disease, the microvascular structural alterations, including vascular (arteriolar and capillary) density and collateralization, as well as remodeling of the vascular wall, still remain incompletely understood (Padro et al., 2020; Sorop et al., 2020). A deeper understanding of the mechanisms responsible for these changes is critical for the identification of potential new targets for the treatment of IHD. In this review, we present an overview of available data in humans and animal models, regarding the alterations in microvascular structure from an early stage, with the mere presence of cardiovascular risk factors, to a later stage, with overt IHD, with considerable hemodynamic consequences. Vascular function and its contribution to remodeling has been reviewed elsewhere (Pant et al., 2014; Fang et al., 2019). Here, we will mainly focus on the effects of biomechanical forces on vascular tone and structure in health and disease.

CORONARY MICROVASCULAR FUNCTION AND STRUCTURE IN THE HEALTHY HEART

The primary function of the coronary circulation is to transport oxygen and nutrients to the myocardium. During increased metabolic demand, myocardial perfusion must increase commensurately with the increase in myocardial oxygen consumption, which is mainly achieved via regulation of coronary microvascular resistance (Hastings et al., 1982; Duncker and Bache, 2008; Goodwill et al., 2017). Several decades of intense scientific effort has improved our understanding of the physiological processes involved in these adaptive responses and the mechanisms involved. We will briefly discuss the different regulators of vascular tone and structure, focusing primarily on mechanical factors.

Control of Vascular Tone in the Healthy Heart

The increase in myocardial oxygen consumption of the left ventricle, as required during exercise or stress, is principally met by an increase in oxygen delivery and thus in CBF, as the myocardium already has a high oxygen extraction at rest (>70%). The increase in CBF can amount up to 4–5 times the resting flow in the healthy heart (Duncker and Bache, 2008), and is mainly achieved by a reduction in vascular resistance. Under normal circumstances, proximal epicardial arteries (>400 μm in diameter) serve as conduit vessels as they contribute minimally (<5%) to overall coronary vascular resistance (Goodwill et al., 2017). The major loci of coronary vascular resistance are the coronary small arteries and arterioles (20–400 μm in diameter), responding to changes in physical forces (wall stress and shear stress), as well as metabolic needs of the tissue, while less than 20% of the resistance resides in the capillaries and venules (Chilian et al., 1986; Goodwill et al., 2017). The acute and/or chronic modulation of coronary vascular resistance in response to changes in myocardial oxygen demand, involves both active (vascular tone) and passive (extravascular compressive and intravascular distending mechanical forces) changes in vessel diameter.

An optimal level of vascular diameter is thus achieved by a tightly regulated balance between a variety of vasoactive mechanisms, including metabolic, endothelial, neurohumoral and mechanical factors. The latter includes passive vascular responses to changes in the mechanical environment produced by myocardial compression and intravascular distending pressure, but also active responses contributing to vascular tone, such as myogenic response and flow-mediated response induced by changes in the perfusion pressure and shear stress. These mechanisms exert specific influences on different segments of the microvasculature (Jones et al., 1993a; Muller et al., 1996; Laughlin et al., 2012; Duncker et al., 2015) with the distal, smallest arterioles (<100 μm diameter) being most sensitive to myocyte-derived metabolic stimuli, whereas wall stress-induced myogenic mechanisms are dominant in the intermediate larger arterioles and small arteries (100–200 μm) and flow-mediated dilation dominates the vasomotor tone of small arteries (200–400 μm). The most important vasoactive mechanisms regulating vascular tone are individually described below and summarized in **Figure 1**.

Neurohumoral Factors

Neural stimulation also affects tone, as sympathetic and parasympathetic (vagal) nerves innervate different segments of the coronary vasculature, although their influence on coronary vascular tone differs between rest and exercise. Thus, while cardiac sympathetic activity is limited at rest, increased sympathetic activity contributes to exercise-induced hyperemia (Duncker and Bache, 2008; Goodwill et al., 2017). Neural stimulation exerts its effects on vascular tone via an interaction between the direct effects on vascular smooth muscle cells and stimulation of nitric oxide (NO) release from the endothelium.

During sympathetic activation, coronary tone is modulated by norepinephrine release from sympathetic nerves, and by circulating epinephrine and norepinephrine (Goodwill et al., 2017). In conduit arteries, sympathetic stimulation leads to a net vasodilator response mediated by an interaction between $alpha_1$-mediated vasoconstriction and beta-mediated vasodilation (Goodwill et al., 2017). In the coronary resistance vessels, the effect of sympathetic activation on vascular tone depends on the net actions of $beta_1$-mediated increases in myocardial oxygen consumption, $beta_1$- and $beta_2$-mediated coronary vasodilation, and $alpha_1$-mediated vasoconstriction (Laughlin et al., 2012). In the healthy heart, exercise-induced beta-adrenergic "feed-forward" dilation predominates over alpha adrenergic constriction (Duncker and Bache, 2008), with contributions of both $beta_2$- and $beta_1$-receptors (Gao et al., 2010), resulting in an increase in CBF that matches the increase in myocardial oxygen consumption. Alpha-adrenergic blockade can induce vasodilation by blocking the vasoconstrictor influence of $alpha_1$- and $alpha_2$-adrenoceptors, with $alpha_1$-adrenoceptors being more predominant in small coronary arteries (>100 μm) and both $alpha_1$- and $alpha_2$-adrenoceptors present in arterioles (<100 μm) (Duncker and Bache, 2008). Data show little evidence for alpha-adrenergic coronary vasoconstrictor influences at rest, but alpha-adrenergic constriction is augmented both at rest and during exercise in the presence of coronary endothelial dysfunction involving both $alpha_1$- and $alpha_2$-adrenoceptors (Heusch et al., 2000; Laughlin et al., 2012).

The role of vagal activity in the control of CBF at rest and during exercise has been shown to be negligible, as vagal tone to the myocardium is progressively withdrawn during increased levels of exercise (Duncker and Bache, 2008) although this appears to be species-dependent. Human and canine coronary resistance arteries have shown endothelium-dependent dilation to acetylcholine resulting in increases in CBF (Laughlin et al., 2012). Besides its role as a cholinergic neurotransmitter, non-neuronal acetylcholine was also shown to play a role in endothelial mechanotransduction, by being released by the endothelial cells (ECs) in response to flow, resulting in vasodilation (Wilson et al., 2016). Additionally, in swine, in which acetylcholine produces vasoconstriction, an interaction was observed of sympathetic and parasympathetic influences on coronary vascular tone during exercise. Thus, beta-adrenergic vasodilation was enhanced by withdrawal of the muscarinic receptor-mediated inhibition (Duncker et al., 1998). However, in dogs, where acetylcholine results in net vasodilation, parasympathetic effects are weak at rest and negligible during exercise (Duncker and Bache, 2008).

In conclusion, the autonomic nervous system is able to modulate the coupling between coronary flow and myocardial

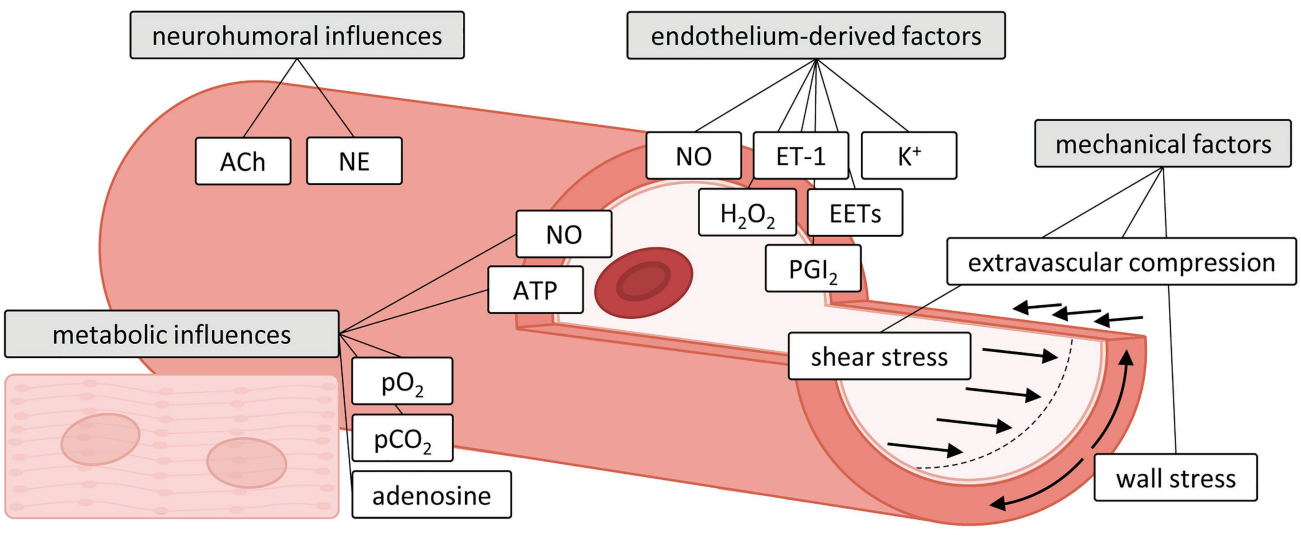

FIGURE 1 | Influences of metabolic, neurohumoral, endothelium-derived and mechanical factors on the microvasculature. Adapted with permission from Duncker and Bache (2008). ACh, acetylcholine; ATP, adenosine triphosphate; EETs, epoxyeicosatrienoic acids; ET-1, endothelin-1; H_2O_2, hydrogen peroxide; NE, norepinephrine; NO, nitric oxide; pCO_2, dissolved carbon dioxide; PGI_2, prostacyclin; pO_2, oxygen tension.

metabolism, with minimal activity at rest, and net beta-adrenergic feed-forward vasodilation during exercise.

Endothelial Factors

Vascular endothelium is one of the major determinants of vascular tone, by releasing various vasoactive substances in response to different stimuli. These factors include powerful vasodilators, such as NO, prostaglandins, and epoxyeicosatrienoic acids (EETs), K^+ and H_2O_2, which induce endothelium-derived hyperpolarization (EDH; Laughlin et al., 2012). Studies have shown that NO-dependent responses occur primarily in small arteries and large arterioles (100–300 μm) and involve cyclic guanosine monophosphate (cGMP)-dependent hyperpolarization of VSMCs via the opening of specific K^+ channels (Dick and Tune, 2010). Prostaglandin release has been shown to contribute to coronary reactive hyperemia but only in the presence of inhibition of NO synthesis, suggesting interaction of the two mechanisms (Puybasset et al., 1996). Additionally, although the exact nature of the factors involved in EDH (acting primarily on arterioles <100 μm) remains incompletely understood, several potential candidates (EETs, K^+, H_2O_2) have been shown to be regulators of vascular tone in response to different stimuli such as shear stress, bradykinin or adenosine stimulation (Gutterman et al., 2016). Conversely, ET-1 has been identified as potent vasoconstrictor. Although its role appears to be rather modest under physiologic conditions, it becomes more important in disease states such as coronary artery disease (Sorop et al., 2008). Moreover, prostaglandin F2α, thromboxane and serotonin have been shown to be potent vasoconstrictors, also in pathological situations such as endothelial injury and coronary artery disease (Goodwill et al., 2017).

Metabolic Factors

Metabolic activity of the heart is one of the major factors regulating coronary vascular resistance. In order to maintain function and accommodate the high metabolic demand, the heart relies on aerobic metabolism to convert metabolic substrates into energy molecules, ATP. The exact nature of the factors and mechanisms responsible for local microvascular metabolic tone control is still not completely understood (Deussen et al., 2012), but several tissue-derived metabolites have traditionally been proposed to play a role in the regulation of coronary microvascular resistance during increased metabolic demand. These include dissolved O_2 and CO_2, as well as adenosine, involving activation of various K^+ channels (Gerlach and Deuticke, 1966; Tune, 2007; Goodwill et al., 2017), although the specific contribution of each type of K^+ channel remains a matter of debate. An increase in myocardial adenosine was originally proposed to link the flow regulation during changes in metabolism (Feigl, 2004). Thus, during increased myocardial oxygen consumption, a fall in myocardial oxygen tension could produce myocardial adenosine release and subsequent coronary vasodilation (Berne, 1963). However, in both human and animal studies, adenosine blockade did not affect vasodilation during physiological increases in myocardial oxygen consumption (Bache et al., 1988; Edlund et al., 1989; Duncker and Bache, 2008) in the healthy heart. In contrast, adenosine was shown to play an important role in coronary vasodilation during ischemia (Laxson et al., 1993). More recently, other factors, such as adenine nucleotides (ATP) or NO released from erythrocytes during hypoxia, have been proposed to mediate metabolic vasodilation (Gorman et al., 2010), although proof for their involvement is still lacking (Laughlin et al., 2012; Goodwill et al., 2017). K_{ATP} channel blockade impaired CBF in hypoxia; however, this response was only transient and K_{ATP} channel blockade did not impair exercise hyperemia (Duncker et al., 1993). Importantly, the mechanisms described above do not work independently, as studies in animal models have suggested that K_{ATP} channels, adenosine and NO interact in different manners to control coronary flow control during exercise. Thus, in dogs these three interacting mechanisms fully control coronary perfusion during exercise (Ishibashi et al., 1998). This may at least in part be species dependent, as in swine a residual exercise-induced vasodilation upon inhibition of these mechanisms was still present (Merkus et al., 2003). Finally, mitochondria-derived hydrogen peroxide (H_2O_2) has also been suggested as possible mediator coupling CBF to metabolism in the heart, through modulating the opening probability of voltage-gated K^+ channels. Consistent with this proposal, blockade of voltage-gated K^+ channels was shown to impair the balance between CBF and myocardial metabolism (Berwick et al., 2012; Deussen et al., 2012; Goodwill et al., 2017; Ohanyan et al., 2017). Nevertheless, despite intense research efforts, the mechanisms controlling CBF during high metabolic demand still remain incompletely understood.

Mechanical Factors

In addition to the above described mechanisms, the vascular wall also contributes to modulation of vascular tone in response to biophysical forces exerted by both the flowing blood as well as the surrounding tissue. Flowing blood not only exerts a frictional force on the endothelial lining termed fluid shear stress, but the vessel wall also has to withstand blood pressure, which results in tension in the vessel wall. Wall stress and shear stress exert important physiological effects on the vascular cells through the process of mechanotransduction, resulting in both acute and chronic adaptations of the vascular caliber. For example, the ECs continuously sense the magnitude, direction and the pulsatility of shear stress, and are able to generate vasoactive substances, such as NO, prostacyclin and H_2O_2 producing an acute increase in vascular diameter. The vasodilation in response to an increase in flow is termed "flow-mediated dilation," and is well conserved across species and vascular beds, although the magnitude of endothelium-dependent dilation and the underlying mechanism depends strongly on the species, vascular bed, vessel size, and age (Beyer et al., 2017). Arterial shear stresses range from 10 dyn/cm^2 in the aorta to 50 dyn/cm^2 in smaller arterioles, while the venous system has lower shears from 1 dyn/cm^2 in the vena cava to approximately 20 dyn/cm^2 in the venules (Papaioannou and Stefanadis, 2005; Givens and Tzima, 2016). Additionally, *in vivo*, depending on the vessel geometry (size, curvature,

presence of a bifurcation or a coronary obstruction), the blood flow exhibits different patterns, falling into two major categories; laminar and disturbed flow. Laminar flow, characterized by mainly unidirectional uniform flow, occurs mostly in straight vascular segments, inducing EC alignment in the direction of flow with low cellular turnover. Pulsatile or steady laminar flow was shown to stimulate the production of factors supporting endothelial survival, quiescence and barrier function and increases the expression of anti-inflammatory genes with atheroprotective properties (Chatzizisis et al., 2007; Reinhart-King et al., 2008). Disturbed flow, also termed atheroprone flow, is characterized by oscillatory, turbulent and low flow patterns, present in vascular areas with bifurcations and curvatures (Cheng et al., 2006). ECs subjected to disturbed flow do not align in the flow direction and show increased proliferation and proinflammatory gene profiles (Chatzizisis et al., 2007) resulting in increased endothelial permeability and enhanced monocyte adhesion (Zhou et al., 2014). The mechanisms involved in flow-mediated dilation are also dependent on size; conduit vessels rely primarily on NO while the microcirculation utilizes a variety of mediators, including NO, prostacyclin and EDH. Additionally, the complex arterial architecture, with branching points and curved regions, induces different flow and shear patterns on the endothelium, greatly influencing EC function (Davies, 2009).

Additionally, the effects of cyclic stretch and pressure gradient across the endothelial layer (transmural pressure) also induce endothelial deformation, formation of endothelial ridges and alterations in endothelial function, as well as reorientation of VSMC contractile filaments from the circumferential to radial direction (Greensmith and Duling, 1984). These architectural changes may influence the pressure-induced myogenic activation and VSMC constriction leading to acute or chronic alterations in vascular responses (Lockette et al., 1986; Luscher et al., 1987). The myogenic response is the main mechanism allowing the coronary circulation to maintain constant blood flow in the face of changes in perfusion pressure, i.e., coronary autoregulation. This is achieved by constriction of coronary resistance vessels in response to an increase in intravascular distending pressure and dilation in response to a decrease in pressure. Arterioles of ~100 µm in diameter are particularly sensitive to developing myogenic tone. This response is endothelium-independent and involves VSMC activation by changes in the intracellular Ca^{2+} concentration (Kuo et al., 1988; Sorop et al., 2003), mainly via L-type Ca^{2+} channels (Jensen et al., 2017). Additionally, regional differences in myogenic tone have been found across the ventricular wall. Thus, due to the lower perfusion pressure (as a result of the resistance of the transmurally penetrating vessels and the increased extravascular compression), the sub-endocardial resistance arterioles show reduced myogenic responses as compared to subepicardial arterioles (Kuo et al., 1988). Mechanosensing of both flow and pressure is thought to result from multiple cellular components as will be discussed later.

Regulation of Vascular Structure and Architecture

Vasodilator reserve of the microvasculature is computed as the ratio between maximal hyperemic flow and basal flow. The maximal flow is strongly dependent on the vascular architecture, the biomechanical characteristics of the vascular segments and their number (arterial and capillary density). Biomechanical properties of the vasculature play an important role in determining the minimal and maximal vascular resistance by limiting the vasoconstrictor and vasodilator reserve of the coronary vasculature. The vasoactive responses are limited by the thickness and structure of the vascular layers, in particular the organization of the VSMC layers and the extracellular matrix. The vascular structure is controlled by local forces and it is thought that shear stress, induced by the local flow profile and the wall stress related to the blood pressure, play a major role (Jones et al., 1993a,b). Additionally, chronic alterations in vascular tone induced by vasoactive substances can also result in changes in the vascular wall structure.

Alterations in the vascular structure are termed "remodeling" of the vessel wall and have been classified (Mulvany et al., 1996) in either eutrophic, hypotrophic or hypertrophic remodeling, depending on the changes in the wall cross-sectional area (**Figure 2**). Eutrophic remodeling describes vascular remodeling with preserved wall cross-sectional area around a smaller or larger lumen, hypotrophic remodeling involves loss of vascular wall components, while in hypertrophic remodeling the cross-sectional area of the vascular wall increases. Furthermore, depending on the changes in lumen diameter, vascular remodeling can be categorized as inward or outward remodeling, where a decrease in vascular lumen denotes inward remodeling while the opposite is called outward remodeling

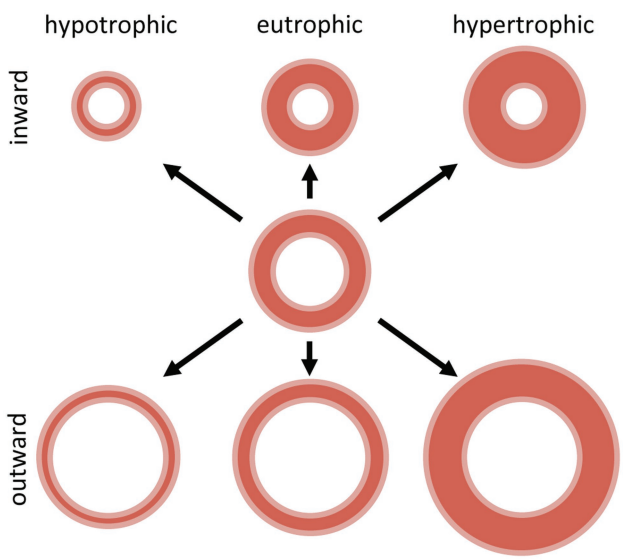

FIGURE 2 | Schematic representation of inward and outward hypotrophic, eutrophic and hypertrophic vascular remodeling. Adapted with permission from Mulvany et al. (1996).

(**Figure 2**). Vascular remodeling is thus related to the amount of tissue in the vascular wall, and its organization around the luminal diameter, affecting the biomechanical properties and limiting the distensibility and thus the luminal diameter of that specific vascular segment. However, there is evidence that even under normal circumstances, the vessel wall is not quiescent, as vessels undergo continuous turnover of wall components, thereby contributing to homeostasis (Van Den Akker et al., 2010).

Most studies assessing small artery remodeling have been performed *in vitro* in isolated vessels or based on histological examination (measurement of cross-sectional areas) of vascular segments fixated under pressure (Bakker et al., 2004, 2005; Van Den Akker et al., 2010; Tuna et al., 2013). While the latter approach might seem more physiologically relevant, since the vessels are not removed from their surrounding tissue, a direct comparison with the "pre-diseased" state is difficult and one-to-one comparison to similar healthy vessels from the exact same location is impossible. The *in vitro* approach (based on diameter lumen measurements in conjunction with optical/histological assessment of the wall/lumen ratio) has been used by many research groups, and enables the study of the vascular segment prior to and following exposure to the mechanical stimulus needed to induce the remodeling response. Passive pressure-diameter curves performed at different points in time allow for the observation of the process dynamics and a more complete characterization of the remodeling type. Additionally, the *in vitro* set-up is ideal to study the mechanisms underlying vascular remodeling. Conversely, removal of the vessel from the myocardium completely abolishes the natural contribution of any metabolic stimuli to this process.

Using *in vitro* culture of isolated small arteries, it has been shown that chronic vasoconstriction was sufficient to induce vascular inward remodeling, while vasodilation did not affect the vascular diameter or even resulted in outward remodeling (Bakker et al., 2002, 2003; Pistea et al., 2005, 2008; Sorop et al., 2006). Additionally, even in the absence of active constriction, vessels cultured at low pressures maintaining a small lumen diameter remodeled in the course of a couple of days, whereas pharmacological vasodilation significantly attenuated the inward remodeling (Sorop et al., 2006). Importantly, vessels cultured under flow remained more dilated than vessels cultured without flow, and flow inhibited the inward remodeling (Pistea et al., 2005). Bakker et al. studied the mechanisms involved in wall stress-induced vascular remodeling in more detail (Bakker et al., 2005), demonstrating tissue transglutaminase (TG2) as one of the crucial mediators of crosslinking between the extracellular matrix proteins, limiting vascular distensibility. Several factors have subsequently been shown to be involved in modulating TG2 activity, including NO, Ca^{2+} and GTP/GDP concentrations, but also the redox state in the micro-environment (Van Den Akker et al., 2010; Del Campo et al., 2013; Huelsz-Prince et al., 2013). Bakker et al., (2005) postulated that the mechanical force exerted by VSMCs during contraction, directly activates TG2, which further results in crosslinking of extracellular matrix components, explaining the link between smooth muscle activation and inward remodeling (Bakker et al., 2005). Additionally, *in vitro* studies also indicate that matrix metalloproteinases (MMPs) are activated in VSMCs subjected to either stationary stretch (Meng et al., 1999; Asanuma et al., 2003; Lehoux et al., 2004) or cyclic stretch (Grote et al., 2003), or in arteries exposed to longitudinal tension (Jackson et al., 2002), possibly contributing to a continuous turnover of matrix elements and counterbalancing the activation of TG2. Distal to small arteries and arterioles, and strongly dependent on the activation and remodeling status of these proximal vessels, the capillary network is involved in the oxygen delivery to the cardiomyocytes. Although its contribution to the total vascular resistance is below 10%, (Chilian et al., 1986), alterations in capillary density, especially in the subendocardium, have important consequences for local myocardial function. In order to compensate for a higher oxygen demand and lower perfusion pressures, the subendocardial capillary to fiber ratio is higher (~1) than in the subepicardial layer, (~0.8); however, these ratios have been shown to be strongly affected by different pathologies (Duncker and Bache, 2008). Loss of microvascular density, i.e., vascular rarefaction, is a key component of various pathologies. Factors contributing to capillary rarefaction include removal of angiogenic stimuli or generation of anti-angiogenic substances, flow discontinuation, disruption of endothelial-pericyte association and endothelial dysfunction (Goligorsky, 2010). It is important to realize that different disease entities, particularly metabolic syndrome, hypertension and aging, as well as the presence of a proximal obstruction, resulting in metabolic and/or hemodynamic alterations, can have a large impact on both function and structure of the coronary microvasculature, and hence on vascular resistance and myocardial perfusion. The impact of these diseases on the microvascular structure and architecture will be discussed below.

Biomechanical Signaling in Microvascular Function and Remodeling

Chronic increases or decreases in shear stress and wall tension have been shown to induce vessel remodeling to maintain proper tissue perfusion. Changes in shear stress lead to proportional changes in vascular diameter to the extent that the original levels of shear stress are restored (Langille, 1996; Tuttle et al., 2001; Baeyens and Schwartz, 2016), suggesting shear stress to be a set variable controlled by endothelial-mediated dilation and remodeling. Given the important influence of mechanical forces on vascular function and structure, the understanding of mechanosensing mechanisms by which ECs and VSMCs convert physical stimuli to biological responses has been an active field of research, although data exclusively for the coronary circulation are limited and to date these mechanisms have been studied mainly *in vitro*. Below, we will discuss data obtained in different vascular beds, on the main molecular contributors to mechanosensing. The pathways discussed are summarized in **Figure 3**.

Ion Channels

Ion channels are pore-forming proteins regulating the distribution of ions across the cell membrane, thereby enabling the establishment of a resting membrane potential.

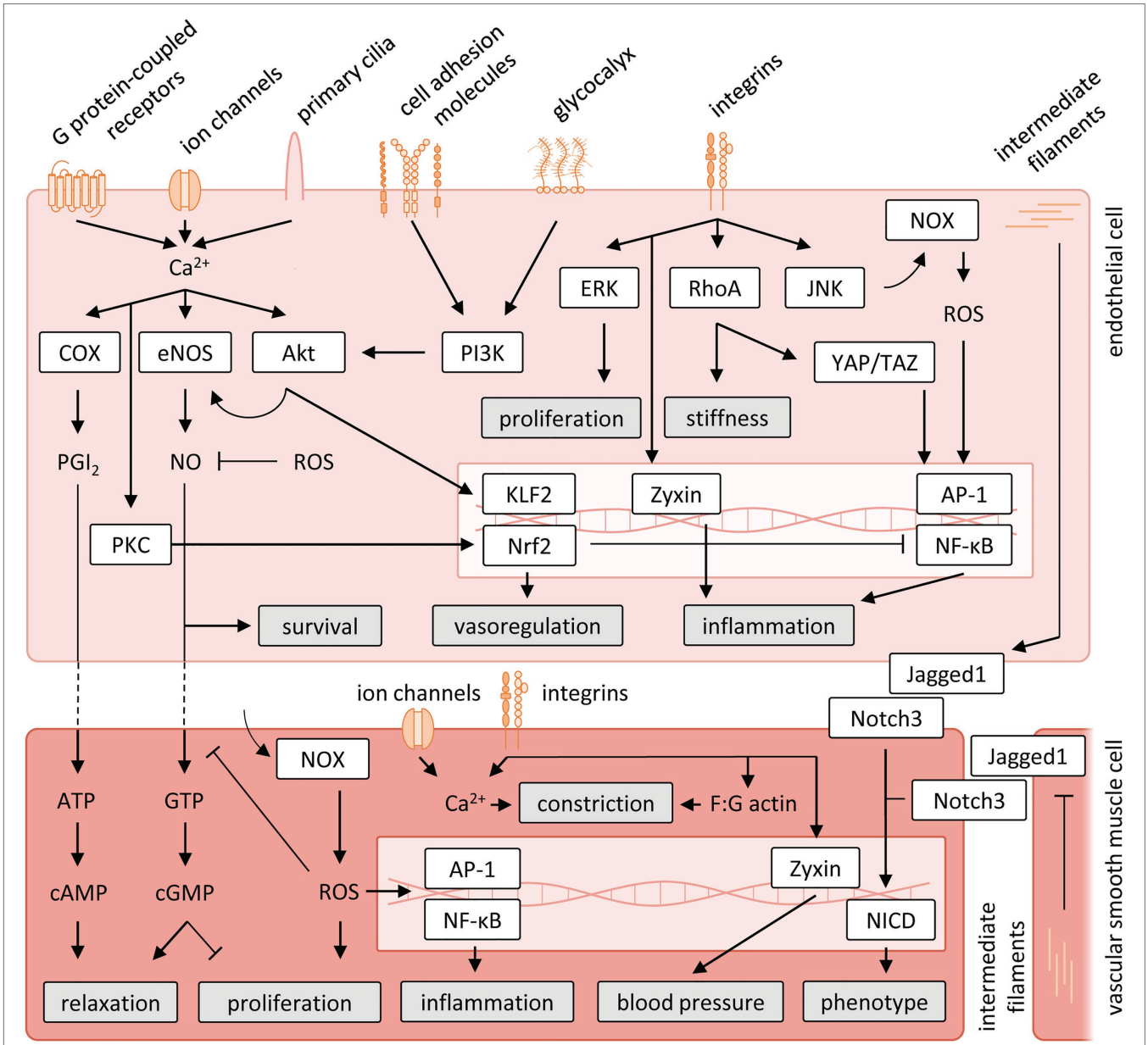

FIGURE 3 | Schematic representation of vascular mechanosensing and signal transduction cascades. Akt, protein kinase B; AP-1, activator protein 1; ATP, adenosine triphosphate; cAMP, cyclic adenosine monophosphate; cGMP, cyclic guanosine monophosphate; COX, cyclooxygenase; eNOS, endothelial nitric oxide; ERK, extracellular signal-regulated kinases; GTP, guanosine triphosphate; JNK, jun N-terminal kinase; KLF2, krüppel-like Factor 2; NF-κB, nuclear factor-κB; NOX, nicotinamide adenine dinucleotide phosphate oxidase; NO, nitric oxide; Nrf2, nuclear factor erythroid 2-like 2; PGI_2, prostacyclin; PI3K, phosphatidylinositol 3-kinase; PKC, protein kinase C; RhoA, Ras homolog family member A; ROS, reactive oxygen species; YAP/TAZ, yes-associated protein/transcriptional coactivator with PDZ-binding motif.

A large variety of ion channels is expressed by coronary microvascular ECs (Kefaloyianni and Coetzee, 2011) and VSMCs (Tykocki et al., 2017). For many of these ion channels, it has been shown that both shear stress and cyclic stretch can trigger their reversible deformation, directly affecting the opening of these channels and thereby the translation of mechanical stimuli into biomechanical signaling (Folgering et al., 2008). Well described ion channels sensing vascular mechanical stimuli include transient receptor potential (TRP) channels, Piezo channels and the epithelial sodium channel (ENaC).

The TRP family consists of conserved membrane proteins that mostly function as non-selective cation channels. Many of these TRP channels, including TRPC1, TRPC6, TRPV4, TRPM7 and TRPP2, are involved in mechanical stress-induced signaling by raising intracellular Ca^{2+} levels in ECs (Inoue et al., 2009), resulting in activation of calmodulin and subsequent production of prostacyclin (PGI_2) and NO. In VSMCs, PGI_2 induces relaxation

via protein kinase A (PKA) after conversion of adenosine triphosphate (ATP) into cyclic adenosine monophosphate (cAMP). Similarly, NO stimulates the conversion of guanosine triphosphate (GTP) in VSMCs into cyclic guanosine monophosphate (cGMP), leading to protein kinase G (PKG) activation and VSMC relaxation (Kohler and Hoyer, 2007). In addition, in some—but not all—vascular beds there is also evidence for spreading of the endothelial hyperpolarization into neighboring VSMCs via myoendothelial gap junctions, closing L-type voltage-gated Ca^{2+} channels leading to vasorelaxation (Sandow et al., 2002; Conejo et al., 2007). Conversely, wall stress-induced Ca^{2+} influx via TRP channels in VSMCs results in membrane depolarization, stimulating vasoconstriction (Hill-Eubanks et al., 2014).

In addition to TRP channels, Piezo channels have also frequently been linked to mechanosensing and subsequent signaling. Using short interference RNA-mediated knockdown studies in a neuroblastoma cell line, Piezo1 and Piezo2 were shown to act as mechanically activated cation channels (Coste et al., 2010). In later studies, overexpression of Piezo1 in non-mechanically responsive human embryonic kidney (HEK) 293T cells was demonstrated to result in elevated Ca^{2+} influx upon exposure to shear stress (Dubin et al., 2017). Conversely, knockdown of Piezo1 in ECs largely prevented shear-induced endothelial alignment, indicating that Piezo1 plays a prominent role in the structural remodeling of the vasculature in response to mechanical stimuli (Ranade et al., 2014). Piezo1 was shown to initiate a rapid influx of Ca^{2+} in ECs when exposed to shear, similar to TRP channels inducing vasodilation via NO (Wang et al., 2016a; Jin et al., 2021). Besides stimulation of endothelial nitric oxide synthase (eNOS) activity, Piezo1 and TRP channels are also involved in shear-induced transcriptional regulation. Loss of TRPV4 or Piezo1 results in reduced activation of krüppel-like factor 2 (KLF2; Gerhold and Schwartz, 2016). KLF2, in concert with nuclear factor erythroid 2-like (Nrf2), regulates shear-induced transcription of many genes involved in vasoregulation (enhanced transcription of eNOS and C-natriuretic peptide, reduced ET-1 and angiotensin-converting enzyme transcription), inflammation [reduced transcription of inflammatory genes by blocking the activity of nuclear factor-κB (NF-κB) and activator protein 1 (AP-1)] and oxidative stress (enhanced transcription of antioxidant genes such as NAD(P)H dehydrogenase quinone 1 and catalase), and as such, acts as an important determinant of vascular remodeling (Novodvorsky and Chico, 2014).

Epithelial sodium channel is a sodium selective ion channel that has primarily been studied in cells of the distal nephrons in the kidney (Bhalla and Hallows, 2008). More recently, endothelial influx of sodium ions via ENaC was shown to regulate cellular actin dynamics. Enhanced activation, which occurs in response to acute changes in shear stress, results in stabilization of cortical actin, a thin actin mesh directly underneath the plasma membrane, into its filamentous form (F-actin), producing a stiffer cell-cortex (Warnock et al., 2014).

Cytoskeleton and Intermediate Filaments

Intermediate filaments, together with actin filaments and microtubules, comprise the cytoskeleton. Critical to a multitude of cell functions, including the maintenance of cell shape and organization, as well as facilitation of cell migration and protein and vesicle trafficking, the cytoskeleton is also recognized as an important mechanosensing and mechanotransduction structure.

As part of the cytoskeleton, the intermediate filament Vimentin has unique strain stiffening behavior, with Vimentin filaments being flexible at low stretch, but become more rigid at high stretch levels (Antfolk et al., 2017). This contributes to stabilization of the intracellular environment when cells are exposed to high mechanical forces, thereby stimulating cell survival and function. Additionally, in mesenteric resistance arteries, Vimentin was shown to be required for flow-mediated vasodilation (Henrion et al., 1997). In isolated ECs, Vimentin responded to shear stress by increased phosphorylation at serine 38, resulting in stabilization of Jagged1 on the endothelial membrane and subsequent Notch3 binding and signaling in VMSCs. In VSMCs, exposure to cyclic stretch promotes Vimentin polymerization, reduced Jagged1 expression and subsequent reduced Notch3 signaling in neighboring VSMCs (Van Engeland et al., 2019). Binding of Jagged1 to Notch3 receptor triggers cleavage and release of the Notch intracellular domain (NICD), which translocates into the nucleus to act as a transcription factor for target genes, including Hes1 and Hey1, that regulate vascular cell behavior. During development, Notch activation by ECs guides mural cell recruitment to sprouting vessels and VSMC differentiation (Stassen et al., 2020). Vimentin was shown to regulate Notch signaling during angiogenesis by consolidating the Jagged1/Notch signaling response at the expense of Delta-like ligand 4 (DLL4)/ Notch signaling (Antfolk et al., 2017). In mature arteries, Notch signaling between ECs and VSMCs, as well as between different layers of VSMCs, plays a central role in guiding the adaptation of the media in response to mechanical stimuli, regulating VSMC contractile versus synthetic phenotype, as well as proliferation and survival (Loerakker et al., 2018; Morris et al., 2019; Stassen et al., 2020).

Cell Adhesion Molecules

Cell adhesion molecules (CAMs) play an important role in maintaining tissue structure by providing physical cell-to-cell and cell-to-matrix adherence. Several prominent endothelial CAMs, including platelet endothelial cell adhesion molecule-1 (PECAM-1) and vascular endothelial cadherin (VE-cadherin), both constitutively expressed in virtually all ECs, were shown to be key players in mechanotransduction. PECAM-1 is a transmembrane receptor belonging to the immunoglobulin superfamily which provides endothelial cell-to-cell adhesion via homophilic interaction with surrounding ECs (Paddock et al., 2016). Application of both shear and stretch has been shown to produce tension on PECAM-1 resulting in rapid PECAM-1 phosphorylation (Fleming et al., 2005), which was independent of shear- and stretch-induced Ca^{2+} influx but rather involves tyrosine-protein kinase Fyn resulting in recruitment of both growth factor receptor-bound protein 2 (GRB2)-associated binding protein 1 and Src homology region 2 domain-containing phosphatase-2 (SHP-2). Upon phosphorylation of PECAM-1, the recruited SHP-2 initiates rapid but temporal extracellular signal regulated kinase (ERK)

1/2 activation, regulating cell proliferation (Xu et al., 2016). Similar to PECAM-1, VE-cadherin is also a transmembrane glycoprotein providing cell-to-cell adherence via homophilic interactions (Brasch et al., 2011). Using antibody-coated magnetic beads, force application on VE-cadherin resulted in cellular stiffening and cytoskeletal reorganization, illustrating the mechanical stress sensing abilities of VE-cadherin (Barry et al., 2015). However, exposing a mixture of wildtype and VE-cadherin knockout ECs to flow, prompted alignment (in the direction of flow) of VE-cadherin expressing cells, even in the absence of homophilic adhesion, which suggests that VE-cadherin acts as an adaptor, rather than as receptor, in this response (Tzima et al., 2005). This was confirmed in non-vascular COS-7 cells, which only aligned to flow when co-transfected with plasmids encoding PECAM-1, VE-cadherin and vascular endothelial growth factor receptor 2 (VEGFR2; Tzima et al., 2005). Other studies indicated that, in response to flow, VE-cadherin links PECAM-1 to VEGFR2 leading to ligand-independent activation of VEGFR2 and subsequent activation of phosphatidylinositol-3-OH kinase (PI3K; Jin et al., 2003). PI3K further activates serine/threonine kinase protein kinase B (Akt) which stimulates eNOS-induced production of vasodilatory NO, as well as ERK5-mediated dissociation of histone deacetylase 5 (HDAC5) from myocyte enhancer-binding factor 2 (MEF2), leading to enhanced shear-induced transcription of KLF2 (Chistiakov et al., 2017). Additionally, PI3K inhibits binding and subsequent degradation of Nrf2 by kelch-like ECH-associated protein 1 (KEAP-1; Dai et al., 2007).

Integrins, another class of CAMs, are transmembrane receptors that facilitate the connection between the extracellular matrix and the cytoskeleton, like intermediate filaments, putting them in a unique position to transmit physical stimuli. They are heterogenous in structure, being composed of various combinations of α and β subunits. Direct assessment of endothelial integrin conformational changes, as well as antibody-mediated blockade of the shear-induced response, has provided evidence for the involvement of integrins in mechanical signal transduction. Shear stress-induced changes in integrin conformation increase their affinity for extracellular matrix proteins, such as fibronectin, laminin and collagen (Shyy and Chien, 2002), binding to these substrates leading to the formation of focal adhesion complexes, which link the actin cytoskeleton to the extracellular environment and simultaneously stimulate the activation of focal adhesion kinase (FAK; Fang et al., 2019). Via activation of Rap1 guanine exchange factor C3G, FAK stimulates the activation of ERK, thereby enhancing cellular proliferation and migration (Shyy and Chien, 2002). Furthermore, in isolated ECs and VSMCs it has been demonstrated that in response to cyclic stretch, focal adhesion protein Zyxin dissociates from the focal adhesion complex and accumulates in the nucleus (Cattaruzza et al., 2004; Wojtowicz et al., 2010), enhancing transcription of inflammatory genes in ECs and upregulating the ET-1 B receptor (ET_B-R) in VSMCs. Elevation of intravascular pressure also results in enhanced filamentous:globular (F:G) actin ratios in VSMCs. This polymerization of actin aids in the development of myogenic tone, as evidenced by impaired constriction of VSMCs exposed to actin polymerization inhibitors cytochalasins and latrunculin. The exact mechanism by which strain induces actin polymerization in VSMCs is not completely understood, but it most likely occurs via integrin-mediated activation of protein kinase C (PKC) and RhoA (Cipolla et al., 2002).

Additionally, activation of endothelial integrins also occurs indirectly upon exposure to shear. PI3K activation by the tri-molecular complex composed of PECAM-1, VEGFR2 and VE-cadherin leads to an integrin-mediated, substrate-dependent mechanotransduction response. Thus, PI3K-mediated activation of integrins bound to collagen initiate a protein kinase A-dependent repression of RhoA, leading to reduced synthesis of cellular stress fibers and endothelial stiffness. Conversely, activation of integrins bound to fibronectin stimulates RhoA-mediated stiffness and enhances activation of inflammatory signaling via NF-κB (Collins et al., 2014). Moreover, integrin-mediated activation of RhoA also stimulates yes-associated protein (YAP) and transcriptional coactivator with PDZ-binding motif (TAZ), initiating the transcription of a variety of inflammatory genes by activating AP-1 via jun n-terminal kinase (JNK; Wang et al., 2016b).

G Proteins and G Protein-Coupled Receptors

G proteins are membrane-bound guanine nucleotide-binding proteins acting as molecular switches to enable the transmission of external stimuli into the cell. They can be subdivided in monomeric small GTPases and heterotrimeric G protein complexes consisting of an α, β and γ subunit, both of which are regulated in their activity by their ability to bind and hydrolyze guanosine triphosphate (GTP) to guanosine diphosphate (GDP). Heterotrimeric G proteins have previously been shown to operate as mechanosensitive initiators of signaling. Onset of flow rapidly induced GTP binding in human umbilical vein ECs (HUVECs; Gudi et al., 1996). Using G protein-loaded phospholipid bilayer vesicles, it was later demonstrated that shear-induced activation of G proteins ($G_{\alpha q}$ and $G_{\alpha i3}$) was independent of an intact cytoskeleton or receptor-mediated signaling (Gudi et al., 1998). Short interference RNA-mediated knockdown of $G_{\alpha q}$ illustrated its requirement in shear-induced activation of endothelial Ras, implicating a direct role for G protein signaling in mitogen-activated protein kinase (MAPK) activity (Gudi et al., 2003).

There are, however, also studies showing evidence for biomechanical G protein-coupled receptor signaling (GPCR). It has, for instance, been observed that application of shear, stretch or a membrane-fluidizing agent to bovine aortic ECs, resulted in a rapid and ligand-independent conformation change of the bradykinin B_2 GPCR (Chachisvilis et al., 2006), known to activate MAPKs and to initiate phospholipase-mediated increase in intracellular Ca^{2+}, leading to eNOS activation. Similarly, activation of GPCR sphingosine-1 phosphate (S1P) receptor-1, which like bradykinin B_2 GPCR is expressed by coronary ECs (Figueroa et al., 2001; Liu et al., 2016), was shown to induce flow-dependent activation of ERK, Akt and eNOS. In line with activation of bradykinin B_2 GPCR, activation of S1P receptor-1 is ligand-independent as ligand binding-deficient mutants of S1P receptor-1 were able to functionally restore the shear-mediated actions of S1P receptor-1 knockout in HUVECs (Jung et al., 2012).

More recently, G Protein-Coupled Receptor 68 (GPR68), which is primarily expressed in ECs of small diameter arteries (murine third-order mesenteric), has also been suggested to be a flow responsive GPCR, as indicated by the shear-induced Ca^{2+} influx in HEK293T cells overexpressing GPR68. *Ex vivo* cannulation experiments comparing the shear response of third-order mesenteric arteries from wildtype and GPR68 knockout mice, demonstrated an impaired flow-mediated dilation in absence of GPR68. Moreover, eNOS inhibition could almost completely block flow-mediated dilation in arteries of both wildtype and knockout mice, indicating that GPR68 presumably functions upstream of the NO pathway (Xu et al., 2018).

Interestingly, GPCR-mediated signaling upon mechanical stress has also been described in VSMCs. Exposure of VSMCs to hypo-osmotic shock to increase membrane tension, resembling mechanical stretch, was shown to result in increased intracellular Ca^{2+} levels causing VSMC contraction. Remarkably, this influx of Ca^{2+} could be blocked by losartan, an inhibitor of the GPCR angiotensin II receptor type 1 (AT1-R; Schleifenbaum et al., 2014).

Glycocalyx

The glycocalyx is a thin (up to 500 nm), negatively charged, gel-like structure on the luminal side of the membrane of healthy endothelium, and as such, it has also been observed in the coronary circulation (Becker et al., 2010). It is composed of proteoglycans and glycoproteins, such as heparan sulfate and hyaluronic acid. It regulates endothelial barrier function, leukocyte adhesion and coagulation, but has also been linked directly to mechanotransduction. Thus, Syndecan-1 and -4, heparin sulfate and proteoglycans, which attach the glycocalyx to the cytoskeleton, were shown to be indispensable for proper shear-induced activation of Akt. Moreover, loss of endothelial syndecan expression impaired endothelial alignment to the direction of flow, lowered the transcription of flow-induced transcription factors KLF2 and KLF4, and stimulated the transcription of a variety of pro-inflammatory cytokines (Voyvodic et al., 2014). The glycocalyx also plays a role in flow-mediated dilation, as demonstrated by heparin challenge-induced displacement of proteins bound to heparan sulfate proteoglycans in mice, which led to impaired arteriolar vasodilation during reactive hyperemia (Vanteeffelen et al., 2007). Similarly, *ex vivo* analysis of rat mesenteric arteries loaded with a fluorescent NO indicator illustrated that enzymatic removal of heparan sulfate abolished flow-induced NO synthesis (Yen et al., 2015). Moreover, application of mechanical stretch to microvascular ECs was shown to induce Ca^{2+}-dependent NO production, but only in the presence of heparan sulfate and hyaluronic acid (Dragovich et al., 2016).

There is also evidence linking the actions of individual components of the glycocalyx to PECAM-1-mediated mechanosignaling. It has been shown that PECAM-1 associates with G protein $G_{aq/11}$ in ECs exposed to laminar shear and that pharmacological inhibition, as well as enzymatic removal of heparan sulfate abrogated this association (Dela Paz et al., 2014). Although the exact consequence of the association between these proteins is not completely understood, it illustrates how mechanosensors apparently act in parallel, perhaps even interact, rather than operate individually.

Primary Cilia

Primary (non-motile) cilia are hair-like protrusions of the apical cell membrane, structurally composed of 9 microtubule doublets that are directly linked to the intracellular cytoskeleton. Most mammalian cell types, including coronary ECs (Singh et al., 2020), possess these non-motile cilia. However, the length of these cilia is variable, with ECs exposed to high shear stress tending to have shorter cilia than ECs exposed to relatively low shear stress (Mohieldin et al., 2016). Evidence for the involvement of cilia in mechanosignaling came initially from a study subjecting ECs isolated from *Tg737* mutant mice, an orthologous gene of intraflagellar transport 88 (IFT88, involved in cilium biogenesis), to flow (Nauli et al., 2008). Thus, *Tg737* mutant ECs, lacking functional cilia, were unable to initiate shear-induced NO synthesis. Further studies indicated that a complex of polycystin-1 (PC1), a transmembrane glycoprotein regulating the function of the Ca^{2+} permeable cation channel polycystin-2 (PC2), is responsible for the intracellular conversion of the flow-mediated activation of cilia. Both PC1 and PC2 are particularly enriched in the ciliary membrane and knockout of either PC1 or PC2 is sufficient to block shear-mediated Ca^{2+} influx and subsequent NO production by eNOS (Aboualaiwi et al., 2009). The polycystin-mediated influx of Ca^{2+}, in addition to shear-induced intracellular Ca^{2+} release via other mechanotransduction routes, also activates PKC (Saternos and AbouAlaiwi, 2015). PKC, in turn, phosphorylates Nrf2 at Ser-40, which—in concert with the PI3K-mediated dissociation of Nrf2 from KEAP-1—stimulates shear-induced transcriptional activation of Nrf2 (Huang et al., 2002; Hsieh et al., 2009).

CORONARY MICROVASCULAR FUNCTION AND STRUCTURE IN DISEASE

In more than 50% of patients with coronary artery disease, percutaneous coronary intervention re-establishes coronary artery patency, however without completely restoring myocardial perfusion (Uren et al., 1993a,b; Niccoli et al., 2009, 2010) indicating that microvascular dysfunction is a critical contributor to ischemia distal to an epicardial stenosis. Risk factors, such as metabolic dysregulation and diabetes, age, and hypertension present in a large proportion of the patients with coronary artery disease and have been shown to impact both the macro- and microvasculature (Padro et al., 2020; Sorop et al., 2020). Among the factors involved, endothelial dysfunction—significantly impacted by these risk factors—appears to be an important contributor to the development of micro- and macrovascular disease (Sorop et al., 2020; Van De Wouw et al., 2020, 2021). In addition, changes in hemodynamic factors inducing vascular remodeling (Sorop et al., 2008; Weil et al., 2020), as well as microvascular rarefaction (Sorop et al., 2018; Van De Wouw et al., 2020) may also play a role in the

co-existence of macro- and microvascular disease. While microvascular endothelial dysfunction has been studied more extensively in this context, the mechanical determinants of the microvascular architecture and their interaction are less well understood.

Indeed, the presence of a proximal coronary obstruction, resulting in alterations in distal pressure and flow (Hoogendoorn et al., 2020; De Nisco et al., 2021), has also been shown to impact the distal microvasculature both at the functional and structural level, and the presence of risk factors may exacerbate these effects. On the other hand, episodes of myocardial ischemia may trigger angiogenesis from adjacent regions with still intact perfusion as well as outward remodeling of pre-existing connecting vessels (arteriogenesis) in a process of collateralization. This allows for a, at least partial, restoration of myocardial blood flow to the area distal to the stenosis. We will discuss below how different pathologies, such as the presence of cardiovascular risk factors and a chronic coronary artery stenosis contribute to development and/or aggravation of microvascular dysfunction and microvascular remodeling including diameter and density alterations (**Figure 4**). Furthermore, our current understanding of the mechanisms involved in these processes initiated by, or interfering with, biomechanical signaling will be addressed.

Metabolic Dysregulation

Metabolic dysregulation includes conditions such as metabolic syndrome, obesity, insulin resistance, diabetes mellitus, hypercholesterolemia and hypertriglyceridemia, that either alone or in combination contribute to coronary artery disease and stroke (Cho et al., 2018).

Clinical and experimental studies have shown that metabolic dysregulation is associated with perturbations in CBF control during increased metabolic demand (Berwick et al., 2012; Paneni et al., 2013; Crea et al., 2014; Duncker et al., 2015; Badimon et al., 2017; Van De Wouw et al., 2020). Indeed, metabolic syndrome and obesity are associated with impaired coronary flow reserve (CFR; Di Carli et al., 2003; Pirat et al., 2008; Zorach et al., 2018), which also worsens with the onset of type 2 diabetes (Kondo et al., 2001; Schindler et al., 2006). These studies are supported by observations in dogs (Setty et al., 2003) and swine with co-morbidities (Bender et al., 2016; Van De Wouw et al., 2020), demonstrating progressive impairment of myocardial oxygen delivery during graded treadmill exercise, suggesting that the mechanisms responsible include both microvascular dysfunction and remodeling. Indeed, acute hyperglycemia in young subjects impaired adenosine-mediated increase in CBF (Di Carli et al., 2003). Additionally, swine subjected to 2.5 months of hyperglycemia and hypercholesterolemia showed impaired endothelial function of isolated coronary small arteries, mediated via loss of NO, despite preserved VSMC function (Van Den Heuvel et al., 2012). Indeed, hyperglycemia and hypercholesterolemia can induce a state of oxidative stress, which is a state in which the formation of reactive oxygen species (ROS), including superoxide anion, hydroxyl anion or H_2O_2 exceeds the antioxidant defense mechanisms. Superoxide anions can directly interact with NO, thereby limiting NO bioavailability and resulting in the formation of the pro-inflammatory peroxynitrite. In the same animal model studied 15 months after induction of hyperglycemia and hypercholesterolemia (Sorop et al., 2016), increased vasoconstrictor response to ET-1 was observed, which was ET_B-mediated. Surprisingly, the endothelium-dependent vasodilation to bradykinin was no longer reduced as compared to control, although the contribution of EDH to the bradykinin-induced dilation was reduced (Sorop et al., 2016). Interestingly, at this stage, these microvascular alterations were also observed in non-diabetic, hypercholesterolemic swine. Similarly, obesity has also been shown to increase coronary microvascular sensitivity to vasoconstrictors (ET-1, prostaglandin H2 or thromboxane A_2) in animal models (Berwick et al., 2012) and humans (Barton et al., 2012; Campia et al., 2012). In addition to endothelial dysfunction, VSMC function is also affected by metabolic dysregulation, as in obese Ossabaw swine with metabolic syndrome, 16 weeks of high fat diet resulted in increased coronary vasoconstriction mediated by altered electromechanical coupling between K_V and $Ca_{V1.2}$ channels in VSMCs (Berwick et al., 2013).

A metabolic dysregulation-associated increase in sympathetic activity has also been documented both in patients and animal models, resulting in exaggerated alpha-adrenergic coronary vasoconstriction (Huggett et al., 2004; Dincer et al., 2006). Additionally, substantial evidence indicates that activation of the renin angiotensin aldosterone system (RAAS) associated with adipose tissue-derived angiotensinogen, as well as adipocyte-derived free fatty acids (FFAs) and leptin, results in microvascular dysfunction and impaired CFR, possibly due to increased angiotensin II-mediated vasoconstriction (Kachur et al., 2018). Indeed, perivascular adipose tissue-derived adipokines such as leptin, resistin, IL-6 and TNF-α are potent pro-inflammatory molecules promoting oxidative stress in the endothelium and altering endothelial function and NO bioavailability, either directly or via increased ET-1 production.

Furthermore, leptin derived from perivascular fat also promotes coronary arterial vasoconstriction and VSMC proliferation via Rho kinase signaling (Bagi et al., 2011; Noblet et al., 2016). Additionally, adipocyte-derived circulating FFA and hyperglycemia-induced advanced glycation end products (AGE) lead to increased oxidative stress, thereby limiting NO bioavailability, as well as increased production of vasoconstrictor factors such as thromboxane A2 and ET-1 (Creager et al., 2003).

The sustained vasoconstriction induced by the various mechanisms described above may contribute to structural vascular alterations. Indeed, not only changes in microvascular function have been documented in metabolic dysregulation, but microvascular structure is also affected. In Ossabaw swine, 16 weeks of metabolic syndrome induced by a high fat/high fructose diet resulted in impaired myocardial perfusion and blunted response to adenosine, associated with reduced microvascular density (Li et al., 2012). In the same animal model, 6 months of metabolic syndrome and high-fat diet resulted in impaired hyperemic flow associated with augmented coronary myogenic tone, hypertrophic inward remodeling of the coronary resistance arteries and capillary rarefaction (Trask et al., 2012).

Such alterations can be due to the deleterious effects of the metabolic dysregulation on the molecular mechanisms involved

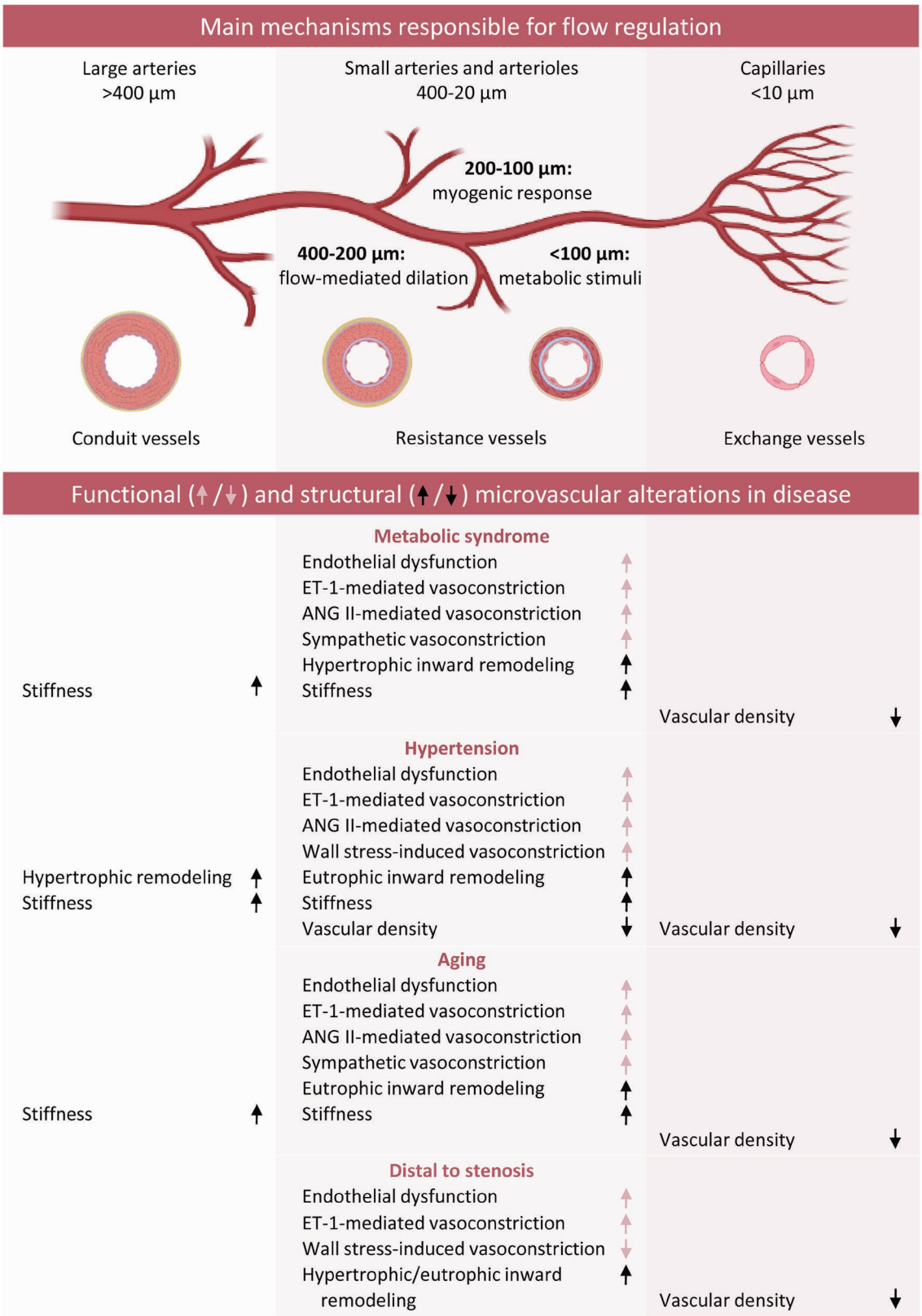

FIGURE 4 | Schematic overview of functional and structural coronary microvascular alterations in the presence of classic risk factors. Red arrows refer to changes in vascular function, whereas black arrows refer to vascular remodeling. ANG II, Angiotensin II; ET-1, endothelin-1.

in mechanosensing. Thus, metabolic syndrome has previously been demonstrated to be detrimental to the endothelial glycocalyx, as evidenced by shedding-induced increase of glycocalyx components in the bloodstream of type 1 and type 2 diabetic patients, thereby reducing shear-induced eNOS activity and NO production (Nieuwdorp et al., 2006; Broekhuizen et al., 2010). Recent data in obese mice also indicate that breakdown of the glycocalyx induced by metabolic derangements impairs the function of the inward rectifying K^+ channel $K_{ir}2.1$, thereby limiting the endothelial response to flow (Fancher et al., 2020). Additionally, metabolic syndrome-associated inflammation, FFAs and hyperglycemia have all been linked to activation of endothelial NADPH oxidase (NOX; Devallance et al., 2019), stimulating the production of ROS and uncoupling of eNOS. The consequent reduction in NO bioavailability not only affects vascular tone, but, over time, may also results in impaired cGMP-mediated inhibition of VSMC proliferation and hypertrophic remodeling (Tanner et al., 2000). Moreover, adipose tissue-derived pro-inflammatory adipokines potentiate VSMC proliferation, either directly via leptin (Oda et al., 2001), or indirectly via paracrine signaling through NF-κB-induced infiltration of macrophages (Zampetaki et al., 2005; Spescha et al., 2014). Leptin enhances the expression of collagen, fibronectin, transforming growth factor (TGF)-β and connective tissue growth factor (CTGF; Martinez-Martinez et al., 2014). In combination with decreased NO-mediated S-nitrosylation of TG2 (Jung et al., 2013), enhancing its ECM crosslinking activity, this elevated ECM transcription could contribute to the observed stiffening of small arteries in swine after 15 months of high fat diet in absence of vascular wall hypertrophy (Sorop et al., 2016).

Together with microvascular dysfunction and structural abnormalities of the vascular wall, alterations in vascular density may also contribute to the perturbations in CBF and oxygen delivery and even regional ischemia during exercise observed in humans (Camici and Crea, 2007; Bairey Merz et al., 2017) and animals with co-morbidities (Setty et al., 2003; Bender et al., 2016, van de Wouw et al., 2020). Indeed, in freshly explanted hearts of diabetic patients, lower capillary density and pericyte loss as compared to non-diabetic subjects were reported, accompanied by a lower angiopoietin 1/angiopoietin 2 ratio (Hinkel et al., 2017). Similarly, in the left ventricle of obese subjects, lower capillary densities were observed as compared to lean subjects (Campbell et al., 2013). These data were confirmed in different animal models, including obese Zucker rats (Toblli et al., 2004), obese Wistar–Kyoto rats with metabolic syndrome (Machado et al., 2017) and obese diabetic *db*/*db* mice (Gonzalez-Quesada et al., 2013). The pathways contributing to this capillary rarefaction were mostly associated with VEGF signaling, but inflammatory factors, certain miRNAs and even changes in ECM composition have also been shown to take part in metabolic derangement-induced capillary rarefaction (Paavonsalo et al., 2020).

Hypertension

Arterial hypertension, defined as a systolic blood pressure ≥ 140 mmHg and/or a diastolic blood pressure ≥ 90 mmHg (Unger et al., 2020), continues to increase in prevalence worldwide, especially in developing countries, mainly as a result of an unhealthy lifestyle. Arterial hypertension is an independent risk factor for coronary artery disease and stroke (Chobanian et al., 2003; Benjamin et al., 2019) and frequently co-exists with other aggravating pathologies, such as diabetes and chronic kidney disease, underlying their onset and progression. An important contributor to myocardial ischemia in patients with arterial hypertension is coronary microvascular dysfunction, (Modolo et al., 2015). Indeed, antihypertensive treatment has been able to improve both basal and hyperemic flow in patients (Neglia et al., 2011). In hypertensive rats, this effect was shown to be attributable to improved microvascular function and the reverse remodeling of intramural coronary arterioles (Neglia et al., 2011).

In the microvasculature, an increased blood pressure results in elevated circumferential stress (σ), which, according to the law of Laplace ($\sigma = P \times R/h$, where P is transmural pressure, R is vessel radius, and h is wall thickness), can be normalized by lowering the luminal diameter or by increasing the wall thickness. These responses, aimed to normalize wall stress, are thought to be protective in the short term. However, the increase in vascular resistance and subsequent impairment in maximal dilation (reduced flow reserve) are detrimental over time. The molecular mechanisms responsible for these adaptations have been mostly studied in cell culture or *in vitro* experiments using isolated peripheral small arteries, while less data in the coronary vessels are available.

To orchestrate the acute reduction of the luminal diameter, VSMCs exposed to circumferential stretch undergo depolarization, leading to activation of L-type Ca^{2+} channel $Ca_v1.2$ and subsequent myogenic vasoconstriction. Several mechanosensitive ion channels, including TRPC6, TRPM4 and KCNQ (Welsh et al., 2002; Earley et al., 2007; Zhong et al., 2010) as well as ciliary PC1 and PC2 (Sharif-Naeini et al., 2009) contribute to this stretch-induced depolarization. Moreover, ligand-independent activation of the mechanosensitive GPCR $AT_{1a}R$ has also been shown to induce myogenic vasoconstriction in response to elevated blood pressure in resistance vessels (Schleifenbaum et al., 2014). Additionally, hypertension-induced elevation of circumferential stretch results in activation of endothelial NOX and subsequent scavenging of NO by ROS (Spescha et al., 2014). In isolated ECs, it was demonstrated that this ROS production is initiated by stretch-induced activation of integrin α5β1, causing phosphorylation of JNK and $p66^{shc}$, eventually activating NOX (Spescha et al., 2014). The impairment in NO bioavailability is aggravated by hypertensive agents such as salt, ET-1, angiotensin II, renin and vasopressin (Neglia et al., 2011), which further contributes to enhanced vasoconstriction and adds to the increased vascular resistance (Lassegue and Griendling, 2004; Neglia et al., 2011).

In hypertensive animal models, medial hypertrophic remodeling, associated with VSMC proliferation, has been shown to occur in small arteries whereas eutrophic remodeling, marked by VSMC reorientation and ECM deposition, was the most common form of remodeling in the more distal arterioles (Owens et al., 1988; Stacy and Prewitt, 1989). An explanation

for the different types of inward remodeling in vascular segments of different sizes is not readily found, but may be due to a difference in sensitivity to mechanical stimuli along the vasculature with flow-induced responses affecting the vascular tone mainly in proximal vessels and myogenic influences in more distal vessels. The variations in sensitivity to mechanical stimuli are accompanied by vessel size-related variations in lumen/wall (R/h) ratio, and therefore wall stress (σ). In arterioles these variables are both much smaller than in, for instance, the aorta leading to a different optimal response for a given increase in blood pressure (P) (Feihl et al., 2006). However, the responses in the proximal and distal vasculature may also be related, in that an increase in peripheral vascular resistance in patients with hypertension can result in reduced shear stress in large arteries by inducing low peak systolic blood flow velocity and a low shear rate (Khder et al., 1998), thereby resulting in impaired shear-induced NO synthesis and progression of endothelial dysfunction.

Intriguingly, the exact nature of remodeling is also related to the pathologies underlying hypertension. Studies in small subcutaneous or omental vessels isolated from non-diabetic patients with essential hypertension indicated that these vessels undergo eutrophic remodeling (Schiffrin and Deng, 1996; Intengan et al., 1999; Schiffrin et al., 2000; Park and Schiffrin, 2001), whereas hypertension associated with diabetes or renovascular disease was shown to promote media hypertrophy in small arteries (Rizzoni et al., 1996; Schofield et al., 2002; Endemann et al., 2004). It could be speculated that the presence of co-morbidities such as diabetes and renovascular disease induces systemic low-grade inflammation and enhances oxidative stress, which in turn could directly interact with the outcome of mechanosignaling pathways. Lack of NO bioavailability, due to ROS scavenging in ECs, not only impairs NO-mediated NF-κB inactivation via S-nitrosylation (Kelleher et al., 2007), but also limits cGMP-mediated inhibition of VSMC proliferation. Wall stress-induced activation of NOX in ECs may subsequently result in ROS-mediated stimulation of AP-1 (Brandes et al., 2014). A similar activation of NF-κB and AP-1 has been observed in isolated coronary VSMCs in response to stretch (Hishikawa et al., 1997). Activation of these factors in both ECs and VSMCs, potentially coinciding with stretch-mediated nuclear accumulation of the focal adhesion protein Zyxin (Cattaruzza et al., 2004; Wojtowicz et al., 2010), results in transcription of inflammatory factors, including interleukin 6 (IL-6) and monocyte chemoattractant protein 1 (MCP-1), thereby stimulating monocyte extravasation (Zampetaki et al., 2005; Spescha et al., 2014). By secreting a variety of MMPs, these monocytes facilitate extracellular matrix reorganization and VSMC reorientation, thereby potentiating structural arterial remodeling (Intengan and Schiffrin, 2001; Wenzel, 2019). IL-6 also enhances VSMC motility (Wang and Newman, 2003), and like MCP-1, directly stimulates VSMC proliferation (Ikeda et al., 1991; Viedt et al., 2002). In addition, the stretch-activated Ca^{2+} channel Piezo1 also appears to be prominently involved in hypertension-dependent arterial remodeling. Piezo1 is highly expressed in VSMCs of murine small-diameter arteries (e.g., cutaneous caudal artery and cerebral arteries) and, while it is not involved in the myogenic response, VSMC-specific knockout attenuates hypertension-induced inward remodeling and VSMC hypertrophy in the cutaneous caudal resistance artery. The exact mechanism by which Piezo1 orchestrates arterial remodeling upon activation by wall stress is not completely understood, but Ca^{2+}-dependent activation of TG2 may be involved (Retailleau et al., 2015).

A consistent finding in both clinical and experimental hypertension is capillary rarefaction, either structural (anatomic absence) or functional (non-perfusion), indicating that hypertension-induced vascular remodeling is not restricted to resistance arteries (Feihl et al., 2006). Experimental data in rat models of hypertension show reduced structural myocardial capillary density in adult hypertensive animals, but interestingly, this was age-dependent, as young animals showed normal capillary densities despite significantly hypertrophied ventricles (Tomanek et al., 1982). These animal findings are in agreement with data in young and adult patients with aortic stenosis-induced cardiac hypertrophy, also showing capillary rarefaction only at adult age (Rakusan et al., 1992). Interestingly, structural capillary rarefaction may be preceded by functional capillary rarefaction, as data in non-diabetic hypertensive patients show that functional capillary rarefaction parameters (percent capillary recruitment in nailfold skin) were lower in patients with modest hypertension and correlated with endothelial dysfunction, despite normal structural capillary density (Cheng et al., 2008). Functional capillary rarefaction may thus be the result of upstream arteriolar dysfunction resulting in perturbations in capillary perfusion.

Although the pathophysiology underlying the hypertension-induced rarefaction is still not fully understood, several mechanisms have been proposed, either related to loss of existing vasculature or insufficient growth of new vasculature (angiogenesis). In mesenteric and skeletal muscle microvasculature of spontaneously hypertensive rats, for instance, it has been shown that rarefaction induced by endothelial apoptosis was attenuated by systemic application of cell permeable superoxide scavengers Tempol and Tiron, indicating the involvement of excessive ROS formation (Kobayashi et al., 2005). Moreover, it has been demonstrated that low or absent mechanical shear, downstream of inward remodeled resistance arteries, could hamper KLF2-mediated inhibition of Smad2 phosphorylation, thereby enhancing endothelial to mesenchymal transition and subsequent vascular loss (Boon et al., 2007; Lee et al., 2017). Furthermore, altered shear could also lead to rarefaction via impaired NO synthesis, causing reduced NO-dependent production of vascular endothelial growth factor (VEGF) by VSMCs, which stimulates endothelial survival (Dulak et al., 2000). Besides its role in vasodilation and endothelial survival, NO stimulates endothelial proliferation and migration, important mediators of angiogenesis. This has been clearly illustrated in eNOS-deficient mice, in which impaired angiogenesis and arteriogenesis induced by hindlimb ischemia could be restored by adenoviral expression of constitutively active eNOS (Yu et al., 2005). Similarly, coronary occlusion in mongrel dogs triggered a myocardial ischemia-induced increase in capillary density, which could be blocked by L-NAME (Matsunaga et al., 2002). This study showed that, in the absence of NO, enhanced activity of MMP-2 and -9 results in degradation

of plasminogen into the antiangiogenic factor angiostatin. With respect to hypertension-induced impairment of angiogenesis, there is also evidence that reduced numbers of circulating endothelial progenitor cells (EPCs) are involved (Hill et al., 2003; Imanishi et al., 2005). Although the cause of the reduced number of EPCs in hypertension is still unclear, the finding that lowering blood pressure by angiotensin receptor blockers (Bahlmann et al., 2005) or ACE inhibitors (Pirro et al., 2007) could restore their circulating numbers, in combination with their role in vascular repair, maintenance and angiogenesis, is consistent with the concept that shortage of these cells contributes to hypertension-induced rarefaction.

Aging

Advanced age is another independent risk factor for development and progression of coronary artery disease, IHD and heart failure, contributing to morbidity and mortality worldwide (Dhingra and Vasan, 2012). Data from both patient and animal studies indicate that aging induces changes in the functional and structural properties of the vascular system (Paneni et al., 2017). Vascular ageing comprises different aspects of arterial wall injury accumulated over a long period of time due to factors such as oxidative stress, low-grade inflammation, and activation of the sympathetic nervous system, all resulting in increased vascular stiffness (Laurent and Boutouyrie, 2021). In large arteries, augmented arterial stiffness results in an increase in the velocity of the pressure wave, which together with a stiffer peripheral vasculature results in augmentation of the systolic blood pressure and increased cardiac afterload.

Arterial stiffening involves changes in extracellular components of the arterial wall due to proteolytic degradation of elastin fibers shifting the load towards stiffer collagen fibres (Duca et al., 2016). VSMCs also undergo age-dependent changes such as alterations in the activity of the contractile filaments as well as in the molecular signaling pathways regulating actin polymerization, both directly contributing to the vascular stiffening (Kajuluri et al., 2021). Furthermore, adhesion to the extracellular matrix is increased (Zhu et al., 2012).

Further data point towards aging-associated endothelial dysfunction, showing that aging induces flattening and enlargement of ECs as well as cytoskeleton alterations affecting mobility and proliferation (Yeh et al., 2000; Shi et al., 2004). In the endothelium of aging rats, changes in gap-junction distribution and connexin expression were seen, which resulted in dysfunctional and leaky vessels (Yeh et al., 2000). Moreover, reduced NO bioavailability was documented in aging animals (Csiszar et al., 2002; Leblanc et al., 2008, 2009; Kang et al., 2009, 2011), related to endothelial inflammation (Csiszar et al., 2004), similarly to data obtained in aging healthy subjects, which indicate impairments in both NO and prostanoid pathways (Singh et al., 2002). This was confirmed in the human coronary circulation, where arteriolar flow-mediated dilation was shown to evolve from prostacyclin in the young, to NO in adulthood and to H_2O_2 later in life and/or with onset of coronary artery disease (Beyer et al., 2017). Furthermore, blunted flow-mediated dilation occurs with age, as shown in both humans (Drexler et al., 1989; Zeiher et al., 1993) and animal models (Csiszar et al., 2002; Kang et al., 2009) and could be improved by antioxidant therapy (Kang et al., 2009).

Moreover, increased expression and elevated plasma levels of pro-inflammatory ET-1, as observed in ECs isolated from old vs young healthy subjects (Donato et al., 2009), were also associated with endothelial dysfunction, possibly via ROS-induced reduction in eNOS expression and activity (Wedgwood and Black, 2005). In 23 months old Fisher 344 rats, ROS production was shown to originate from NOX (Adler et al., 2003), presumably in response to age-related low-grade systemic inflammation. In addition, vascular oxidative stress can result from endothelial and VSMC mitochondrial dysfunction, the efficiency of the mitochondrial respiratory chain diminishing with age, causing electron leakage and subsequent release of ROS (Ungvari et al., 2007). Accumulating evidence furthermore suggests that Nrf2 is involved in the age-related high vascular ROS levels. Besides its role in flow-mediated signaling, Nrf2 is a redox sensitive transcription factor stimulating the transcription of a variety of genes involved in the antioxidant response. In the aged vasculature, however, there is a markedly lower expression and activation of Nrf2 (Ungvari et al., 2011a,b), possibly due to an age-related impairment of mechanosensitive activation of Nrf2 (Ungvari et al., 2019). However, this proposed aging-induced impairment of shear-mediated Nrf2 activation cannot explain why reporter studies in statically cultured VSMCs isolated from aged macaques demonstrate lower H_2O_2-induced transcriptional activity of Nrf2 when compared with the activity in cells isolated from young animals (Ungvari et al., 2011a). Regardless of what causes Nrf2 dysfunction in the aging vasculature, it limits oxidative stress resilience and stimulates NF-κB-mediated inflammation.

In addition to scavenging of NO by ROS, impaired eNOS activation has also been linked to ageing, as different studies have illustrated that shear-induced eNOS activation is blunted in the endothelium of aged animals (Sun et al., 2004; Yang et al., 2009). This could be mediated by lower availability of the eNOS substrate L-arginine and eNOS dimerizing co-factor tetrahydrobiopterin (BH4; Yang et al., 2009), but also by age-related ECM remodeling and subsequent stiffness. Aging is, as mentioned above, associated with increased ECM crosslinking, which, in combination with impaired elastin synthesis and enhanced elastin fragmentation and calcification, results in arterial stiffness. In cultured ECs, exposure to pulsatile flow leads to PI3K-mediated activation of Akt and subsequent eNOS activation in distensible, but not in stiff tubules (Peng et al., 2003). Similarly, exposure of ECs to laminar flow when cultured on hydrogels with mechanical properties resembling those of young blood vessels has been shown to induce higher NO production when compared to ECs cultured on stiff hydrogels (Kohn et al., 2015). Recent studies in human skeletal muscle biopsies have also demonstrated that a lower eNOS phosphorylation in aged tissue in response to acute passive leg movement-induced flow was accompanied by lower phosphorylation of PECAM-1, suggesting this endothelial mechanosensor may be involved in reduced shear-stress responsiveness (Gliemann et al., 2018).

Besides functional alterations, aging also promotes structural vascular changes in coronary resistance vessels (Hanna et al., 2014; Mccallinhart et al., 2018). Data from the Framingham heart study indicate that, with ageing, systolic blood pressure

slowly increases due to increased peripheral vascular resistance and arterial stiffness (Franklin et al., 1997). Additionally, aging-induced blunting of beta adrenergic-mediated vasodilation, as well as activation of the RAAS system in the aged arterial wall may also contribute to the rise in systolic blood pressure in the ageing population (Jiang et al., 2008). Animal studies showed that aging results in increase in angiotensin II and aortic MMP-2 activity, inducing arterial remodeling (Wang et al., 2003, 2005). Moreover, as discussed earlier, the increase in blood pressure resulting from the increased vascular resistance induces arterial inward remodeling, promoting a further increase in blood pressure, forming a vicious circle.

Aging induces vascular alterations not only at the arterial level, but studies in dogs indicate that capillary density and length was also lower in the endocardium of old animals (Tomanek et al., 1991). This might be explained by the decreased angiogenic capacity of the aging heart as pathways central to vessel formation, such as hypoxia-inducible factor-1α (HIF-1α), PGC-1α, and eNOS, are affected by aging (Lahteenvuo and Rosenzweig, 2012), contributing to the mismatch between angiogenesis and cardiac hypertrophy in the aged heart. This impaired angiogenic response, besides the overall downregulation of angiogenic growth factors in aged tissue, seems to result from endothelial dysfunction and the associated low bioavailability of NO, which as described before, is an important mediator of angiogenesis (Matsunaga et al., 2002; Yu et al., 2005).

Intriguingly, vascular aging appears to progress differently in men and women (Dupont et al., 2019). The onset of menopause, which marks the end of a woman's menstrual cycles, is associated with accelerated vascular aging, different from the gradual alterations in vascular function and structure as occur with chronological aging (Lakatta and Levy, 2003). The main mechanisms responsible relate to the hormonal changes inducing endothelial dysfunction, as it has been shown that reduced estrogen-mediated generation of NO likely underlies the progressive decline in endothelial function (Green et al., 2014). The reduced NO bioavailability is multifactorial, however, impaired availability of BH4 (Moreau et al., 2012), increased oxidative stress (Novella et al., 2012) and inflammation (Moreau et al., 2013) are likely contributors. Additionally, postmenopause has been associated with elevations in the vasoconstrictors ET-1 and norepinephrine (Green et al., 2014). Such imbalance between NO, ET-1 and norepinephrine contributes to the impaired vasodilation and sustained vasoconstriction observed in postmenopausal animal models (Knowlton and Lee, 2012), as well as to the increased arterial stiffness (Zaydun et al., 2006). Additionally, estrogen may not only enhance vascular relaxation via increased NO production, but may also promote angiogenesis. Estrogen receptor alpha gene knockout was associated with a decrease in VEGF levels and capillary rarefaction in the heart (Jesmin et al., 2010). In accordance with these findings, estrogen can inhibit TNFα-induced apoptosis by binding to its estrogen β-receptor, which induces Akt phosphorylation and Notch1 expression, thereby promoting vascular EC survival (Fortini et al., 2017). Altogether, these functional and structural alterations may explain, at least in part, the ischemic symptoms observed in postmenopausal women with chest pain, but no evidence of obstructive coronary artery disease.

Chronic Coronary Artery Stenosis

Presence of a stenosis in an epicardial coronary artery has hemodynamic consequences for the distal vasculature. With severe stenosis, pressure and flow distal to the stenosis are compromised, resulting in impaired perfusion of the distal myocardium. An important clinical parameter used to define a stenosis as flow-limiting is the coronary pressure derived fractional flow reserve (FFR). This is the ratio between pressure distal and proximal to the stenosis during maximal coronary vasodilation, which is considered flow-limiting if below 0.8. Another parameter used for diagnostic and interventional purposes is CFR, which is defined as the maximum CBF, divided by the resting CBF and has a cut-off value of 2 (Stegehuis et al., 2018).

Due to the pressure drop across a flow-limiting stenosis, the perfusion pressure for the distal vasculature gradually decreases, lowering wall stress and thus the myogenic response due to blunted stimulation of stretch-activated mechanosensors (TRPs, KCNQ, etc.; Welsh et al., 2002; Earley et al., 2007; Zhong et al., 2010). The stenosis-induced impairment of perfusion and the resulting hypoxia may furthermore trigger red blood cell-dependent vasodilation via ATP release and subsequent activation of eNOS, S-nitrosohemoglobin-dependent bioactivity and NO synthesis via reduction of nitrite by deoxyhemoglobin (Kulandavelu et al., 2015). These autoregulatory mechanisms aim to lower vascular resistance in order to maintain flow and tissue oxygenation (Duncker et al., 2015). However, these mechanisms will be exhausted below perfusion pressures of about 40 mmHg, especially in the subendocardium, where the driving pressure is even lower due to the extra resistance of the transmural vessels and the increased extravascular compression, resulting in subendocardial ischemia.

Although microvascular dysfunction may be present already in the absence of a proximal coronary obstruction due to the presence of various comorbidities, hemodynamic changes induced by the stenosis in the distal vasculature can also directly cause alterations in both function and structure of the microvasculature, contributing to the reduced CFR in the myocardial area supplied by the stenotic artery. In a coronary stenosis model in dogs, a progressive increase in distal vascular resistance was documented in the first hours after the placement of the occluder, which was suggested to be mediated by withdrawal of the adenosine-induced vasodilation (Gorman et al., 1985). In a porcine model, 3 months after placing of an external occluder around the proximal LAD, increased vasoconstrictor response to ET-1 was present in subendocardial arterioles distal to the stenosis (Sorop et al., 2008). Vascular functional studies in chronically occluded hearts showed that endothelium-dependent relaxation in response to either bradykinin, substance P or adenosine diphosphate (ADP), was significantly impaired in arterioles isolated from the collateral-dependent region as compared with arterioles from the remote area in the same heart or compared with vessels from control, nonoccluded hearts (Sellke et al., 1992, 1996a,b; Park et al., 1996; Sodha et al., 2008). In contrast, reactivity to the endothelium-independent NO donor nitroprusside was not affected (Park et al., 1996; Griffin et al., 2001; Sodha et al., 2008). In Yucatan miniswine, 22 weeks after the placement of an ameroid occluder around the LCX, the

bradykinin-mediated dilation in collateral-dependent arterioles was impaired, and could be improved by exercise-induced BK_{Ca}-channel activation, suggesting a possible role for H_2O_2 (Xie et al., 2013). The vasoconstrictor response to ET-1 also appeared to be significantly increased in collateral-dependent arterioles or arterioles from the stenotic area, as compared to remote arterioles, a response that was due to a loss of ET_B receptor-mediated vasodilation (Park et al., 1996; Sorop et al., 2008). Combined, these data suggest that, even in absence of comorbidities, hemodynamic changes in the microvasculature distal to a coronary stenosis or occlusion impair NO bioavailability. Paradoxically, both total levels of eNOS, as well as phosphorylation of eNOS were shown to be increased in Yucatan miniswine arterioles distal to a coronary occluder (Xie et al., 2012). It is in that light, however, important to note that uncoupling of the eNOS dimer, due to oxidation of co-factor BH4, results in eNOS-mediated production of superoxide rather than NO (Channon, 2004).

The functional alterations distal to a coronary stenosis or occlusion were associated with structural changes in vessels of different sizes. Thus, in both swine and rats, the presence of a gradual proximal occlusion resulted in inward remodeling of the resistance arteries, either hypertrophic or eutrophic (Mills et al., 1994; Sorop et al., 2008; Canty and Suzuki, 2012). Additionally, microvascular (200–500 μm diameter) and capillary rarefaction was documented both in the subepicardium and the subendocardium (Urbieta Caceres et al., 2011), all these changes contributing to a reduced CFR and an increased minimal microvascular resistance in the myocardium distal to the stenosis. These data contrast with observations in patients with a coronary artery stenosis (Verhoeff et al., 2005) in which, upon revascularization, a maintained or even slightly reduced minimal microvascular resistance was observed. Such discrepancy may have several explanations. On the one side, vascular remodeling may have been influenced by the medication of the patients. Indeed, inward remodeling of isolated arterioles at low traluminal pressure, as present distal to a significant proximal stenosis was prevented by incubation with Ca^{2+} antagonist amlodipine (Sorop et al., 2006). On the other side, such changes in vascular diameter and density (arterial or capillary) may vary in time during the progression but also after the removal of the stenosis. A recent study by Weil et al., in swine, has shown that distal to a critical stenosis subendocardial arterioles show inward remodeling with increased arteriolar wall thickness and a reduction in lumen area. Interestingly, this was compensated by an increase in arteriolar as well as capillary density. However, 1 month after revascularization, such compensatory adaptation was lost, as subendocardial arteriolar and capillary density normalized, but the arterial inward remodeling persisted (Weil et al., 2020). These findings can explain the reduced subendocardial flow reserve late after revascularization despite a near normal vasodilator reserve immediately after PCI as seen in the study by Verhoeff et al. (2005). Furthermore, the persistent coronary microvascular inward remodeling could explain the blunted vasodilator response to dobutamine observed one month following revascularization, in swine, during increased myocardial oxygen demand (Kelly et al., 2011).

Vascular remodeling at the arteriolar level may be related to alterations in the microvascular (endothelial) function, such as the increased vasoconstrictor response to ET-1 as shown in the arterioles distal to a chronic LAD stenosis (Sorop et al., 2008), but altered mechanical factors may also contribute to this response. As such, altered extravascular compression by the dysfunctional hibernating or stunned myocardium (Canty and Fallavollita, 2005; Sorop et al., 2008; Canty and Suzuki, 2012) may result in abnormal mechanosensing. In addition, the blunted myogenic response as shown in sub-endocardial arterioles distal to the stenosis (Sorop et al., 2008) in conjunction with the reduced perfusion pressure and flow may promote inward remodeling, as seen in resistance arteries cultured at 40 mmHg (Sorop et al., 2006). Similarly, reduction of blood flow in mesenteric arteries by means of artery ligation resulted in eutrophic inward remodeling four weeks after surgery (Pourageaud and De Mey, 1997). This inward remodeling could partially be explained by observations in isolated ECs, demonstrating that low wall stress results in transcriptional activation of NF-κB (Pedrigi et al., 2017), which promotes vascular remodeling via monocyte recruitment and VSMC proliferation. Activation of NF-κB, in combination with poor perfusion-associated hypoxia and subsequent activation of HIF1α, furthermore stimulates transcription of ET-1 (Yamashita et al., 2001; Bourque et al., 2011; Stow et al., 2011). Experiments in a murine endothelium-specific ET-1 overexpression model illustrate that, besides its vasoconstrictor effects, ET-1 enhances the media to lumen ratio in mesenteric resistance vessels (Amiri et al., 2004). In cultured coronary artery VSMCs (Wu et al., 2007) and mesenteric arteries (Amiri et al., 2004), ET-1 was also shown to stimulate ROS production, which is prominently involved in remodeling of resistance arteries (Pires et al., 2010; Martinez-Lemus et al., 2011). The intermediate filament Vimentin, on the other hand, seems to prevent low flow-induced medial hypertrophy, as illustrated by a substantially increased wall thickness and VSMCs displaying a proliferative synthetic phenotype in ligated carotid arteries of Vimentin knock-out mice when compared with ligated carotids of wildtype mice (Schiffers et al., 2000; Van Engeland et al., 2019).

CONCLUSIONS AND FUTURE DIRECTIONS

The coronary microvasculature depends critically on acute as well as chronic adaptations of vascular diameter, density, and structural dimension to couple myocardial perfusion to myocardial oxygen demand. The effectiveness of these adaptations, however, is impeded by classic cardiovascular risk factors, including metabolic dysregulation, hypertension, aging and atherosclerosis. Accumulating evidence indicates that these risk factors modulate the interaction between the myriad of mechanisms regulating vascular function and structure and the many biomechanical cues, including shear stress, wall stress and stretch, and extravascular compressive forces, and the signal transduction pathways they induce.

Here, we discussed the involvement and consequences of biomechanical signal transduction cascades on functional and

structural modifications of the coronary microvasculature and how they are influenced by the different risk factors (**Figure 4**). Although IHD patients often present with different combinations of these risk factors, and therefore most likely benefit from a tailored therapeutic approach focussed at normalization of hemodynamics (e.g., blood pressure) or restoration of mechanotransduction (e.g., glycocalyx in diabetes), it has become apparent that certain mechanistic and phenotypic aspects of coronary microvascular dysfunction overlap. Dysfunctional NO synthesis, as well as excessive ROS production, both linked to altered mechanosignaling (**Figure 4**), are consistently implicated in the pathophysiology of IHD and therefore, eNOS and NOX represent interesting therapeutic targets. **Figure 4** furthermore illustrates that a reduction in microvascular density is a common feature of IHD in the presence of metabolic disorders and hypertension, as well as upon aging. Attenuating vascular rarefaction could therefore be a promising approach, in which novel insights in the behavior of pericytes, detachment of which from the microvasculature often precedes functional and structural vascular rarefaction (Kramann et al., 2017), may provide novel therapeutic leads. From studies in the field of oncology it has come forward, however, that especially for therapies aimed at modulating the microvasculature, perhaps even the angiogenic capacity, a tissue-specific approach is highly desirable, a challenge for which recent findings regarding the use of adeno-associated viruses in cardiac disease may provide a useful solution (Hinkel et al., 2017).

In order to fully understand the mechanisms underlying the alterations in coronary perfusion with the aim to improve the perspective of patients with IHD, it is essential that future studies acknowledge and deepen our understanding of the central role played by biomechanical signaling in the coronary microvasculature. In this regard, an integrative approach, taking both functional and structural modifications in consideration, will be essential.

AUTHOR CONTRIBUTIONS

MB and OS drafted the manuscript. DD, CC, and DM reviewed and approved the final version of the manuscript. All authors contributed to the article and approved the submitted version.

FUNDING

We acknowledge the support from the Dutch CardioVascular Alliance: An initiative with support of the Dutch Heart Foundation (Grants 2017B018 ARENA-PRIME and 2020B008 RECONNEXT).

REFERENCES

Aboualaiwi, W. A., Takahashi, M., Mell, B. R., Jones, T. J., Ratnam, S., Kolb, R. J., et al. (2009). Ciliary polycystin-2 is a mechanosensitive calcium channel involved in nitric oxide signaling cascades. *Circ. Res.* 104, 860–869. doi: 10.1161/CIRCRESAHA.108.192765

Adler, A., Messina, E., Sherman, B., Wang, Z., Huang, H., Linke, A., et al. (2003). NAD(P)H oxidase-generated superoxide anion accounts for reduced control of myocardial O2 consumption by NO in old Fischer 344 rats. *Am. J. Physiol. Heart Circ. Physiol.* 285, H1015–H1022. doi: 10.1152/ajpheart.01047.2002

Amiri, F., Virdis, A., Neves, M. F., Iglarz, M., Seidah, N. G., Touyz, R. M., et al. (2004). Endothelium-restricted overexpression of human endothelin-1 causes vascular remodeling and endothelial dysfunction. *Circulation* 110, 2233–2240. doi: 10.1161/01.CIR.0000144462.08345.B9

Antfolk, D., Sjoqvist, M., Cheng, F., Isoniemi, K., Duran, C. L., Rivero-Muller, A., et al. (2017). Selective regulation of Notch ligands during angiogenesis is mediated by vimentin. *Proc. Natl. Acad. Sci. U. S. A.* 114, E4574–E4581. doi: 10.1073/pnas.1703057114

Asanuma, K., Magid, R., Johnson, C., Nerem, R. M., and Galis, Z. S. (2003). Uniaxial strain upregulates matrix-degrading enzymes produced by human vascular smooth muscle cells. *Am. J. Physiol. Heart Circ. Physiol.* 284, H1778–H1784. doi: 10.1152/ajpheart.00494.2002

Bache, R. J., Dai, X. Z., Schwartz, J. S., and Homans, D. C. (1988). Role of adenosine in coronary vasodilation during exercise. *Circ. Res.* 62, 846–853. doi: 10.1161/01.RES.62.4.846

Badimon, L., Bugiardini, R., Cenko, E., Cubedo, J., Dorobantu, M., Duncker, D. J., et al. (2017). Position paper of the European Society of Cardiology-working group of coronary pathophysiology and microcirculation: obesity and heart disease. *Eur. Heart J.* 38, 1951–1958. doi: 10.1093/eurheartj/ehx181

Baeyens, N., and Schwartz, M. A. (2016). Biomechanics of vascular mechanosensation and remodeling. *Mol. Biol. Cell* 27, 7–11. doi: 10.1091/mbc.E14-11-1522

Bagi, Z., Feher, A., Cassuto, J., Akula, K., Labinskyy, N., Kaley, G., et al. (2011). Increased availability of angiotensin AT 1 receptors leads to sustained arterial constriction to angiotensin II in diabetes - role for Rho-kinase activation. *Br. J. Pharmacol.* 163, 1059–1068. doi: 10.1111/j.1476-5381.2011.01307.x

Bahlmann, F. H., De Groot, K., Mueller, O., Hertel, B., Haller, H., and Fliser, D. (2005). Stimulation of endothelial progenitor cells: a new putative therapeutic effect of angiotensin II receptor antagonists. *Hypertension* 45, 526–529. doi: 10.1161/01.HYP.0000159191.98140.89

Bairey Merz, C. N., Pepine, C. J., Walsh, M. N., and Fleg, J. L. (2017). Ischemia and No Obstructive Coronary Artery Disease (INOCA): developing evidence-based therapies and research agenda for the next decade. *Circulation* 135, 1075–1092. doi: 10.1161/CIRCULATIONAHA.116.024534

Bakker, E. N., Buus, C. L., Spaan, J. A., Perree, J., Ganga, A., Rolf, T. M., et al. (2005). Small artery remodeling depends on tissue-type transglutaminase. *Circ. Res.* 96, 119–126. doi: 10.1161/01.RES.0000151333.56089.66

Bakker, E. N., Sorop, O., Spaan, J. A., and Vanbavel, E. (2004). Remodeling of resistance arteries in organoid culture is modulated by pressure and pressure pulsation and depends on vasomotion. *Am. J. Physiol. Heart Circ. Physiol.* 286, H2052–H2056. doi: 10.1152/ajpheart.00978.2003

Bakker, E. N., Van Der Meulen, E. T., Van Den Berg, B. M., Everts, V., Spaan, J. A., and Vanbavel, E. (2002). Inward remodeling follows chronic vasoconstriction in isolated resistance arteries. *J. Vasc. Res.* 39, 12–20. doi: 10.1159/000048989

Bakker, E. N., Versluis, J. P., Sipkema, P., Vanteeffelen, J. W., Rolf, T. M., Spaan, J. A., et al. (2003). Differential structural adaptation to haemodynamics along single rat cremaster arterioles. *J. Physiol.* 548, 549–555. doi: 10.1113/jphysiol.2002.035907

Barry, A. K., Wang, N., and Leckband, D. E. (2015). Local VE-cadherin mechanotransduction triggers long-ranged remodeling of endothelial monolayers. *J. Cell Sci.* 128, 1341–1351. doi: 10.1242/jcs.159954

Barton, M., Baretella, O., and Meyer, M. R. (2012). Obesity and risk of vascular disease: importance of endothelium-dependent vasoconstriction. *Br. J. Pharmacol.* 165, 591–602. doi: 10.1111/j.1476-5381.2011.01472.x

Becker, B. F., Chappell, D., and Jacob, M. (2010). Endothelial glycocalyx and coronary vascular permeability: the fringe benefit. *Basic Res. Cardiol.* 105, 687–701. doi: 10.1007/s00395-010-0118-z

Bender, S. B., De Beer, V. J., Tharp, D. L., Bowles, D. K., Laughlin, M. H., Merkus, D., et al. (2016). Severe familial hypercholesterolemia impairs the

regulation of coronary blood flow and oxygen supply during exercise. *Basic Res. Cardiol.* 111:61. doi: 10.1007/s00395-016-0579-9

Benjamin, E. J., Muntner, P., Alonso, A., Bittencourt, M. S., Callaway, C. W., Carson, A. P., et al. (2019). Heart Disease and Stroke Statistics-2019 update: a report from the American Heart Association. *Circulation* 139, e56–e528. doi: 10.1161/CIR.0000000000000659

Berne, R. M. (1963). Cardiac nucleotides in hypoxia: possible role in regulation of coronary blood flow. *Am. J. Phys.* 204, 317–322. doi: 10.1152/ajplegacy.1963.204.2.317

Berwick, Z. C., Dick, G. M., O'leary, H. A., Bender, S. B., Goodwill, A. G., Moberly, S. P., et al. (2013). Contribution of electromechanical coupling between Kv and Ca v1.2 channels to coronary dysfunction in obesity. *Basic Res. Cardiol.* 108:370. doi: 10.1007/s00395-013-0370-0

Berwick, Z. C., Dick, G. M., and Tune, J. D. (2012). Heart of the matter: coronary dysfunction in metabolic syndrome. *J. Mol. Cell. Cardiol.* 52, 848–856. doi: 10.1016/j.yjmcc.2011.06.025

Beyer, A. M., Zinkevich, N., Miller, B., Liu, Y., Wittenburg, A. L., Mitchell, M., et al. (2017). Transition in the mechanism of flow-mediated dilation with aging and development of coronary artery disease. *Basic Res. Cardiol.* 112:5. doi: 10.1007/s00395-016-0594-x

Bhalla, V., and Hallows, K. R. (2008). Mechanisms of ENaC regulation and clinical implications. *J. Am. Soc. Nephrol.* 19, 1845–1854. doi: 10.1681/ASN.2008020225

Boon, R. A., Fledderus, J. O., Volger, O. L., Van Wanrooij, E. J., Pardali, E., Weesie, F., et al. (2007). KLF2 suppresses TGF-beta signaling in endothelium through induction of Smad7 and inhibition of AP-1. *Arterioscler. Thromb. Vasc. Biol.* 27, 532–539. doi: 10.1161/01.ATV.0000256466.65450.ce

Bourque, S. L., Davidge, S. T., and Adams, M. A. (2011). The interaction between endothelin-1 and nitric oxide in the vasculature: new perspectives. *Am. J. Phys. Regul. Integr. Comp. Phys.* 300, R1288–R1295. doi: 10.1152/ajpregu.00397.2010

Brandes, R. P., Weissmann, N., and Schroder, K. (2014). Nox family NADPH oxidases in mechano-transduction: mechanisms and consequences. *Antioxid. Redox Signal.* 20, 887–898. doi: 10.1089/ars.2013.5414

Brasch, J., Harrison, O. J., Ahlsen, G., Carnally, S. M., Henderson, R. M., Honig, B., et al. (2011). Structure and binding mechanism of vascular endothelial cadherin: a divergent classical cadherin. *J. Mol. Biol.* 408, 57–73. doi: 10.1016/j.jmb.2011.01.031

Broekhuizen, L. N., Lemkes, B. A., Mooij, H. L., Meuwese, M. C., Verberne, H., Holleman, F., et al. (2010). Effect of sulodexide on endothelial glycocalyx and vascular permeability in patients with type 2 diabetes mellitus. *Diabetologia* 53, 2646–2655. doi: 10.1007/s00125-010-1910-x

Camici, P. G., and Crea, F. (2007). Coronary microvascular dysfunction. *N. Engl. J. Med.* 356, 830–840. doi: 10.1056/NEJMra061889

Campbell, D. J., Somaratne, J. B., Prior, D. L., Yii, M., Kenny, J. F., Newcomb, A. E., et al. (2013). Obesity is associated with lower coronary microvascular density. *PLoS One* 8:e81798. doi: 10.1371/journal.pone.0081798

Campia, U., Tesauro, M., and Cardillo, C. (2012). Human obesity and endothelium-dependent responsiveness. *Br. J. Pharmacol.* 165, 561–573. doi: 10.1111/j.1476-5381.2011.01661.x

Canty, J. M. Jr., and Fallavollita, J. A. (2005). Hibernating myocardium. *J. Nucl. Cardiol.* 12, 104–119. doi: 10.1016/j.nuclcard.2004.11.003

Canty, J. M. Jr., and Suzuki, G. (2012). Myocardial perfusion and contraction in acute ischemia and chronic ischemic heart disease. *J. Mol. Cell. Cardiol.* 52, 822–831. doi: 10.1016/j.yjmcc.2011.08.019

Cattaruzza, M., Lattrich, C., and Hecker, M. (2004). Focal adhesion protein zyxin is a mechanosensitive modulator of gene expression in vascular smooth muscle cells. *Hypertension* 43, 726–730. doi: 10.1161/01.HYP.0000119189.82659.52

Chachisvilis, M., Zhang, Y. L., and Frangos, J. A. (2006). G protein-coupled receptors sense fluid shear stress in endothelial cells. *Proc. Natl. Acad. Sci. U. S. A.* 103, 15463–15468. doi: 10.1073/pnas.0607224103

Channon, K. M. (2004). Tetrahydrobiopterin: regulator of endothelial nitric oxide synthase in vascular disease. *Trends Cardiovasc. Med.* 14, 323–327. doi: 10.1016/j.tcm.2004.10.003

Chatzizisis, Y. S., Coskun, A. U., Jonas, M., Edelman, E. R., Feldman, C. L., and Stone, P. H. (2007). Role of endothelial shear stress in the natural history of coronary atherosclerosis and vascular remodeling: molecular, cellular, and vascular behavior. *J. Am. Coll. Cardiol.* 49, 2379–2393. doi: 10.1016/j.jacc.2007.02.059

Cheng, C., Daskalakis, C., and Falkner, B. (2008). Capillary rarefaction in treated and untreated hypertensive subjects. *Ther. Adv. Cardiovasc. Dis.* 2, 79–88. doi: 10.1177/1753944708089696

Cheng, C., Tempel, D., Van Haperen, R., Van Der Baan, A., Grosveld, F., Daemen, M. J., et al. (2006). Atherosclerotic lesion size and vulnerability are determined by patterns of fluid shear stress. *Circulation* 113, 2744–2753. doi: 10.1161/CIRCULATIONAHA.105.590018

Chilian, W. M., Eastham, C. L., and Marcus, M. L. (1986). Microvascular distribution of coronary vascular resistance in beating left ventricle. *Am. J. Phys.* 251, H779–H788. doi: 10.1152/ajpheart.1986.251.4.H779

Chistiakov, D. A., Orekhov, A. N., and Bobryshev, Y. V. (2017). Effects of shear stress on endothelial cells: go with the flow. *Acta Physiol.* 219, 382–408. doi: 10.1111/apha.12725

Cho, N. H., Shaw, J. E., Karuranga, S., Huang, Y., Da Rocha Fernandes, J. D., Ohlrogge, A. W., et al. (2018). IDF Diabetes Atlas: global estimates of diabetes prevalence for 2017 and projections for 2045. *Diabetes Res. Clin. Pract.* 138, 271–281. doi: 10.1016/j.diabres.2018.02.023

Chobanian, A. V., Bakris, G. L., Black, H. R., Cushman, W. C., Green, L. A., Izzo, J. L. Jr., et al. (2003). Seventh report of the Joint National Committee on prevention, detection, evaluation, and treatment of high blood pressure. *Hypertension* 42, 1206–1252. doi: 10.1161/01.HYP.0000107251.49515.c2

Cipolla, M. J., Gokina, N. I., and Osol, G. (2002). Pressure-induced actin polymerization in vascular smooth muscle as a mechanism underlying myogenic behavior. *FASEB J.* 16, 72–76. doi: 10.1096/cj.01-0104hyp

Collins, C., Osborne, L. D., Guilluy, C., Chen, Z., O'brien, E. T. 3rd, Reader, J. S., et al. (2014). Haemodynamic and extracellular matrix cues regulate the mechanical phenotype and stiffness of aortic endothelial cells. *Nat. Commun.* 5:3984. doi: 10.1038/ncomms4984

Conejo, V. A., De Haro, R., Sosa-Melgarejo, J., and Mendez, J. D. (2007). New insights in endothelial and smooth muscle cell communication. *Biomed. Pharmacother.* 61, 173–179. doi: 10.1016/j.biopha.2006.10.009

Coste, B., Mathur, J., Schmidt, M., Earley, T. J., Ranade, S., Petrus, M. J., et al. (2010). Piezo1 and Piezo2 are essential components of distinct mechanically activated cation channels. *Science* 330, 55–60. doi: 10.1126/science.1193270

Crea, F., Camici, P. G., and Bairey Merz, C. N. (2014). Coronary microvascular dysfunction: an update. *Eur. Heart J.* 35, 1101–1111. doi: 10.1093/eurheartj/eht513

Creager, M. A., Luscher, T. F., Cosentino, F., and Beckman, J. A. (2003). Diabetes and vascular disease: pathophysiology, clinical consequences, and medical therapy: part I. *Circulation* 108, 1527–1532. doi: 10.1161/01.CIR.0000091257.27563.32

Csiszar, A., Ungvari, Z., Edwards, J. G., Kaminski, P., Wolin, M. S., Koller, A., et al. (2002). Aging-induced phenotypic changes and oxidative stress impair coronary arteriolar function. *Circ. Res.* 90, 1159–1166. doi: 10.1161/01.RES.0000020401.61826.EA

Csiszar, A., Ungvari, Z., Koller, A., Edwards, J. G., and Kaley, G. (2004). Proinflammatory phenotype of coronary arteries promotes endothelial apoptosis in aging. *Physiol. Genomics* 17, 21–30. doi: 10.1152/physiolgenomics.00136.2003

Dai, G., Vaughn, S., Zhang, Y., Wang, E. T., Garcia-Cardena, G., and Gimbrone, M. A. Jr. (2007). Biomechanical forces in atherosclerosis-resistant vascular regions regulate endothelial redox balance via phosphoinositol 3-kinase/Akt-dependent activation of Nrf2. *Circ. Res.* 101, 723–733. doi: 10.1161/CIRCRESAHA.107.152942

Davies, P. F. (2009). Hemodynamic shear stress and the endothelium in cardiovascular pathophysiology. *Nat. Clin. Pract. Cardiovasc. Med.* 6, 16–26. doi: 10.1038/ncpcardio1397

De Nisco, G., Chiastra, C., Hartman, E. M. J., Hoogendoorn, A., Daemen, J., Calo, K., et al. (2021). Comparison of swine and human computational hemodynamics models for the study of coronary atherosclerosis. *Front. Bioeng. Biotechnol.* 9:731924. doi: 10.3389/fbioe.2021.731924

Del Campo, L., Guvenc Tuna, B., Ferrer, M., Van Bavel, E., and Bakker, E. N. (2013). Testosterone and beta-oestradiol prevent inward remodelling of rat small mesenteric arteries: role of NO and transglutaminase. *Clin. Sci.* 124, 719–728. doi: 10.1042/CS20120700

Dela Paz, N. G., Melchior, B., Shayo, F. Y., and Frangos, J. A. (2014). Heparan sulfates mediate the interaction between platelet endothelial cell adhesion molecule-1 (PECAM-1) and the Galphaq/11 subunits of heterotrimeric G proteins. *J. Biol. Chem.* 289, 7413–7424. doi: 10.1074/jbc.M113.542514

Deussen, A., Ohanyan, V., Jannasch, A., Yin, L., and Chilian, W. (2012). Mechanisms of metabolic coronary flow regulation. *J. Mol. Cell. Cardiol.* 52, 794–801. doi: 10.1016/j.yjmcc.2011.10.001

Devallance, E., Li, Y., Jurczak, M. J., Cifuentes-Pagano, E., and Pagano, P. J. (2019). The role of NADPH oxidases in the etiology of obesity and metabolic syndrome: contribution of individual isoforms and cell biology. *Antioxid. Redox Signal.* 31, 687–709. doi: 10.1089/ars.2018.7674

Dhingra, R., and Vasan, R. S. (2012). Age as a risk factor. *Med. Clin. North Am.* 96, 87–91. doi: 10.1016/j.mcna.2011.11.003

Di Carli, M. F., Janisse, J., Grunberger, G., and Ager, J. (2003). Role of chronic hyperglycemia in the pathogenesis of coronary microvascular dysfunction in diabetes. *J. Am. Coll. Cardiol.* 41, 1387–1393. doi: 10.1016/S0735-1097(03)00166-9

Dick, G. M., and Tune, J. D. (2010). Role of potassium channels in coronary vasodilation. *Exp. Biol. Med.* 235, 10–22. doi: 10.1258/ebm.2009.009201

Dincer, U. D., Araiza, A. G., Knudson, J. D., Molina, P. E., and Tune, J. D. (2006). Sensitization of coronary alpha-adrenoceptor vasoconstriction in the prediabetic metabolic syndrome. *Microcirculation* 13, 587–595. doi: 10.1080/10739680600885228

Donato, A. J., Gano, L. B., Eskurza, I., Silver, A. E., Gates, P. E., Jablonski, K., et al. (2009). Vascular endothelial dysfunction with aging: endothelin-1 and endothelial nitric oxide synthase. *Am. J. Physiol. Heart Circ. Physiol.* 297, H425–H432. doi: 10.1152/ajpheart.00689.2008

Dragovich, M. A., Chester, D., Fu, B. M., Wu, C., Xu, Y., Goligorsky, M. S., et al. (2016). Mechanotransduction of the endothelial glycocalyx mediates nitric oxide production through activation of TRP channels. *Am. J. Phys. Cell Physiol.* 311, C846–C853. doi: 10.1152/ajpcell.00288.2015

Drexler, H., Zeiher, A. M., Wollschlager, H., Meinertz, T., Just, H., and Bonzel, T. (1989). Flow-dependent coronary artery dilatation in humans. *Circulation* 80, 466–474. doi: 10.1161/01.CIR.80.3.466

Dubin, A. E., Murthy, S., Lewis, A. H., Brosse, L., Cahalan, S. M., Grandl, J., et al. (2017). Endogenous piezo1 can confound mechanically activated channel identification and characterization. *Neuron* 94:e263. doi: 10.1016/j.neuron.2017.03.039

Duca, L., Blaise, S., Romier, B., Laffargue, M., Gayral, S., El Btaouri, H., et al. (2016). Matrix ageing and vascular impacts: focus on elastin fragmentation. *Cardiovasc. Res.* 110, 298–308. doi: 10.1093/cvr/cvw061

Dulak, J., Jozkowicz, A., Dembinska-Kiec, A., Guevara, I., Zdzienicka, A., Zmudzinska-Grochot, D., et al. (2000). Nitric oxide induces the synthesis of vascular endothelial growth factor by rat vascular smooth muscle cells. *Arterioscler. Thromb. Vasc. Biol.* 20, 659–666. doi: 10.1161/01.ATV.20.3.659

Duncker, D. J., and Bache, R. J. (2008). Regulation of coronary blood flow during exercise. *Physiol. Rev.* 88, 1009–1086. doi: 10.1152/physrev.00045.2006

Duncker, D. J., Koller, A., Merkus, D., and Canty, J. M. Jr. (2015). Regulation of coronary blood flow in health and ischemic heart disease. *Prog. Cardiovasc. Dis.* 57, 409–422. doi: 10.1016/j.pcad.2014.12.002

Duncker, D. J., Stubenitsky, R., and Verdouw, P. D. (1998). Autonomic control of vasomotion in the porcine coronary circulation during treadmill exercise: evidence for feed-forward beta-adrenergic control. *Circ. Res.* 82, 1312–1322. doi: 10.1161/01.RES.82.12.1312

Duncker, D. J., Van Zon, N. S., Altman, J. D., Pavek, T. J., and Bache, R. J. (1993). Role of K+ATP channels in coronary vasodilation during exercise. *Circulation* 88, 1245–1253. doi: 10.1161/01.CIR.88.3.1245

Dupont, J. J., Kenney, R. M., Patel, A. R., and Jaffe, I. Z. (2019). Sex differences in mechanisms of arterial stiffness. *Br. J. Pharmacol.* 176, 4208–4225. doi: 10.1111/bph.14624

Earley, S., Straub, S. V., and Brayden, J. E. (2007). Protein kinase C regulates vascular myogenic tone through activation of TRPM4. *Am. J. Physiol. Heart Circ. Physiol.* 292, H2613–H2622. doi: 10.1152/ajpheart.01286.2006

Edlund, A., Sollevi, A., and Wennmalm, A. (1989). The role of adenosine and prostacyclin in coronary flow regulation in healthy man. *Acta Physiol. Scand.* 135, 39–46. doi: 10.1111/j.1748-1716.1989.tb08548.x

Endemann, D. H., Pu, Q., De Ciuceis, C., Savoia, C., Virdis, A., Neves, M. F., et al. (2004). Persistent remodeling of resistance arteries in type 2 diabetic patients on antihypertensive treatment. *Hypertension* 43, 399–404. doi: 10.1161/01.HYP.0000112029.03691.e7

Fancher, I. S., Le Master, E., Ahn, S. J., Adamos, C., Lee, J. C., Berdyshev, E., et al. (2020). Impairment of flow-sensitive inwardly rectifying K(+) channels via disruption of glycocalyx mediates obesity-induced endothelial dysfunction. *Arterioscler. Thromb. Vasc. Biol.* 40, e240–e255. doi: 10.1161/ATVBAHA.120.314935

Fang, Y., Wu, D., and Birukov, K. G. (2019). Mechanosensing and mechanoregulation of endothelial cell functions. *Compr. Physiol.* 9, 873–904. doi: 10.1002/cphy.c180020

Feigl, E. O. (2004). Berne's adenosine hypothesis of coronary blood flow control. *Am. J. Physiol. Heart Circ. Physiol.* 287, H1891–H1894. doi: 10.1152/classicessays.00003.2004

Feihl, F., Liaudet, L., Waeber, B., and Levy, B. I. (2006). Hypertension: a disease of the microcirculation? *Hypertension* 48, 1012–1017. doi: 10.1161/01.HYP.0000249510.20326.72

Figueroa, C. D., Marchant, A., Novoa, U., Forstermann, U., Jarnagin, K., Scholkens, B., et al. (2001). Differential distribution of bradykinin B(2) receptors in the rat and human cardiovascular system. *Hypertension* 37, 110–120. doi: 10.1161/01.HYP.37.1.110

Fleming, I., Fisslthaler, B., Dixit, M., and Busse, R. (2005). Role of PECAM-1 in the shear-stress-induced activation of Akt and the endothelial nitric oxide synthase (eNOS) in endothelial cells. *J. Cell Sci.* 118, 4103–4111. doi: 10.1242/jcs.02541

Folgering, J. H., Sharif-Naeini, R., Dedman, A., Patel, A., Delmas, P., and Honore, E. (2008). Molecular basis of the mammalian pressure-sensitive ion channels: focus on vascular mechanotransduction. *Prog. Biophys. Mol. Biol.* 97, 180–195. doi: 10.1016/j.pbiomolbio.2008.02.006

Fortini, F., Vieceli Dalla Sega, F., Caliceti, C., Aquila, G., Pannella, M., Pannuti, A., et al. (2017). Estrogen receptor beta-dependent Notch1 activation protects vascular endothelium against tumor necrosis factor alpha (TNFalpha)-induced apoptosis. *J. Biol. Chem.* 292, 18178–18191. doi: 10.1074/jbc.M117.790121

Franklin, S. S., Gustin, W. T., Wong, N. D., Larson, M. G., Weber, M. A., Kannel, W. B., et al. (1997). Hemodynamic patterns of age-related changes in blood pressure. The Framingham Heart Study. *Circulation* 96, 308–315. doi: 10.1161/01.CIR.96.1.308

Gao, F., De Beer, V. J., Hoekstra, M., Xiao, C., Duncker, D. J., and Merkus, D. (2010). Both beta1- and beta2-adrenoceptors contribute to feedforward coronary resistance vessel dilation during exercise. *Am. J. Physiol. Heart Circ. Physiol.* 298, H921–H929. doi: 10.1152/ajpheart.00135.2009

Gerhold, K. A., and Schwartz, M. A. (2016). Ion channels in endothelial responses to fluid shear stress. *Physiology* 31, 359–369. doi: 10.1152/physiol.00007.2016

Gerlach, E., and Deuticke, B. (1966). Comparative studies on the formation of adenosine in the myocardium of different animal species in oxygen deficiency. *Klin. Wochenschr.* 44, 1307–1310. doi: 10.1007/BF01716603

Givens, C., and Tzima, E. (2016). Endothelial mechanosignaling: does one sensor fit all? *Antioxid. Redox Signal.* 25, 373–388. doi: 10.1089/ars.2015.6493

Gliemann, L., Rytter, N., Piil, P., Nilton, J., Lind, T., Nyberg, M., et al. (2018). The endothelial mechanotransduction protein platelet endothelial cell adhesion molecule-1 is influenced by aging and exercise training in human skeletal muscle. *Front. Physiol.* 9:1807. doi: 10.3389/fphys.2018.01807

Goligorsky, M. S. (2010). Microvascular rarefaction: the decline and fall of blood vessels. *Organogenesis* 6, 1–10. doi: 10.4161/org.6.1.10427

Gonzalez-Quesada, C., Cavalera, M., Biernacka, A., Kong, P., Lee, D. W., Saxena, A., et al. (2013). Thrombospondin-1 induction in the diabetic myocardium stabilizes the cardiac matrix in addition to promoting vascular rarefaction through angiopoietin-2 upregulation. *Circ. Res.* 113, 1331–1344. doi: 10.1161/CIRCRESAHA.113.302593

Goodwill, A. G., Dick, G. M., Kiel, A. M., and Tune, J. D. (2017). Regulation of coronary blood flow. *Compr. Physiol.* 7, 321–382. doi: 10.1002/cphy.c160016

Gorman, M. W., Rooke, G. A., Savage, M. V., Jayasekara, M. P., Jacobson, K. A., and Feigl, E. O. (2010). Adenine nucleotide control of coronary blood flow during exercise. *Am. J. Physiol. Heart Circ. Physiol.* 299, H1981–H1989. doi: 10.1152/ajpheart.00611.2010

Gorman, M. W., Wangler, R. D., Dewitt, D. F., and Sparks, H. V. Jr. (1985). Progressive vasomotor changes in ischaemic myocardium. *Acta Medica Scand. Suppl.* 694, 38–44. doi: 10.1111/j.0954-6820.1985.tb08798.x

Green, D. J., Dawson, E. A., Groenewoud, H. M., Jones, H., and Thijssen, D. H. (2014). Is flow-mediated dilation nitric oxide mediated?: a meta-analysis. *Hypertension* 63, 376–382. doi: 10.1161/HYPERTENSIONAHA.113.02044

Greensmith, J. E., and Duling, B. R. (1984). Morphology of the constricted arteriolar wall: physiological implications. *Am. J. Phys.* 247, H687–H698. doi: 10.1152/ajpheart.1984.247.5.H687

Griffin, K. L., Woodman, C. R., Price, E. M., Laughlin, M. H., and Parker, J. L. (2001). Endothelium-mediated relaxation of porcine collateral-dependent arterioles is improved by exercise training. *Circulation* 104, 1393–1398. doi: 10.1161/hc3601.094274

Grote, K., Flach, I., Luchtefeld, M., Akin, E., Holland, S. M., Drexler, H., et al. (2003). Mechanical stretch enhances mRNA expression and proenzyme release of matrix metalloproteinase-2 (MMP-2) via NAD(P)H oxidase-derived reactive oxygen species. *Circ. Res.* 92, e80–e86. doi: 10.1161/01.RES.0000077044.60138.7C

Gudi, S. R., Clark, C. B., and Frangos, J. A. (1996). Fluid flow rapidly activates G proteins in human endothelial cells. Involvement of G proteins in mechanochemical signal transduction. *Circ. Res.* 79, 834–839. doi: 10.1161/01.RES.79.4.834

Gudi, S., Huvar, I., White, C. R., Mcknight, N. L., Dusserre, N., Boss, G. R., et al. (2003). Rapid activation of Ras by fluid flow is mediated by Galpha(q) and Gbetagamma subunits of heterotrimeric G proteins in human endothelial cells. *Arterioscler. Thromb. Vasc. Biol.* 23, 994–1000. doi: 10.1161/01.ATV.0000073314.51987.84

Gudi, S., Nolan, J. P., and Frangos, J. A. (1998). Modulation of GTPase activity of G proteins by fluid shear stress and phospholipid composition. *Proc. Natl. Acad. Sci. U. S. A.* 95, 2515–2519. doi: 10.1073/pnas.95.5.2515

Gutterman, D. D., Chabowski, D. S., Kadlec, A. O., Durand, M. J., Freed, J. K., Ait-Aissa, K., et al. (2016). The human microcirculation: regulation of flow and beyond. *Circ. Res.* 118, 157–172. doi: 10.1161/CIRCRESAHA.115.305364

Hanna, M. A., Taylor, C. R., Chen, B., La, H. S., Maraj, J. J., Kilar, C. R., et al. (2014). Structural remodeling of coronary resistance arteries: effects of age and exercise training. *J. Appl. Physiol.* 117, 616–623. doi: 10.1152/japplphysiol.01296.2013

Hastings, A. B., White, F. C., Sanders, T. M., and Bloor, C. M. (1982). Comparative physiological responses to exercise stress. *J. Appl. Physiol. Respir. Environ. Exerc. Physiol.* 52, 1077–1083. doi: 10.1152/jappl.1982.52.4.1077

Henrion, D., Terzi, F., Matrougui, K., Duriez, M., Boulanger, C. M., Colucci-Guyon, E., et al. (1997). Impaired flow-induced dilation in mesenteric resistance arteries from mice lacking vimentin. *J. Clin. Invest.* 100, 2909–2914. doi: 10.1172/JCI119840

Heusch, G., Baumgart, D., Camici, P., Chilian, W., Gregorini, L., Hess, O., et al. (2000). Alpha-adrenergic coronary vasoconstriction and myocardial ischemia in humans. *Circulation* 101, 689–694. doi: 10.1161/01.CIR.101.6.689

Hill, J. M., Zalos, G., Halcox, J. P., Schenke, W. H., Waclawiw, M. A., Quyyumi, A. A., et al. (2003). Circulating endothelial progenitor cells, vascular function, and cardiovascular risk. *N. Engl. J. Med.* 348, 593–600. doi: 10.1056/NEJMoa022287

Hill-Eubanks, D. C., Gonzales, A. L., Sonkusare, S. K., and Nelson, M. T. (2014). Vascular TRP channels: performing under pressure and going with the flow. *Physiology* 29, 343–360. doi: 10.1152/physiol.00009.2014

Hinkel, R., Howe, A., Renner, S., Ng, J., Lee, S., Klett, K., et al. (2017). Diabetes mellitus-induced microvascular destabilization in the myocardium. *J. Am. Coll. Cardiol.* 69, 131–143. doi: 10.1016/j.jacc.2016.10.058

Hishikawa, K., Oemar, B. S., Yang, Z., and Luscher, T. F. (1997). Pulsatile stretch stimulates superoxide production and activates nuclear factor-kappa B in human coronary smooth muscle. *Circ. Res.* 81, 797–803. doi: 10.1161/01.RES.81.5.797

Hoogendoorn, A., Kok, A. M., Hartman, E. M. J., De Nisco, G., Casadonte, L., Chiastra, C., et al. (2020). Multidirectional wall shear stress promotes advanced coronary plaque development: comparing five shear stress metrics. *Cardiovasc. Res.* 116, 1136–1146. doi: 10.1093/cvr/cvz212

Hsieh, C. Y., Hsiao, H. Y., Wu, W. Y., Liu, C. A., Tsai, Y. C., Chao, Y. J., et al. (2009). Regulation of shear-induced nuclear translocation of the Nrf2 transcription factor in endothelial cells. *J. Biomed. Sci.* 16:12. doi: 10.1186/1423-0127-16-12

Huang, H. C., Nguyen, T., and Pickett, C. B. (2002). Phosphorylation of Nrf2 at Ser-40 by protein kinase C regulates antioxidant response element-mediated transcription. *J. Biol. Chem.* 277, 42769–42774. doi: 10.1074/jbc.M206911200

Huelsz-Prince, G., Belkin, A. M., Vanbavel, E., and Bakker, E. N. (2013). Activation of extracellular transglutaminase 2 by mechanical force in the arterial wall. *J. Vasc. Res.* 50, 383–395. doi: 10.1159/000354222

Huggett, R. J., Burns, J., Mackintosh, A. F., and Mary, D. A. (2004). Sympathetic neural activation in nondiabetic metabolic syndrome and its further augmentation by hypertension. *Hypertension* 44, 847–852. doi: 10.1161/01.HYP.0000147893.08533.d8

Ikeda, U., Ikeda, M., Oohara, T., Oguchi, A., Kamitani, T., Tsuruya, Y., et al. (1991). Interleukin 6 stimulates growth of vascular smooth muscle cells in a PDGF-dependent manner. *Am. J. Phys.* 260, H1713–H1717. doi: 10.1152/ajpheart.1991.260.5.H1713

Imanishi, T., Moriwaki, C., Hano, T., and Nishio, I. (2005). Endothelial progenitor cell senescence is accelerated in both experimental hypertensive rats and patients with essential hypertension. *J. Hypertens.* 23, 1831–1837. doi: 10.1097/01.hjh.0000183524.73746.1b

Inoue, R., Jian, Z., and Kawarabayashi, Y. (2009). Mechanosensitive TRP channels in cardiovascular pathophysiology. *Pharmacol. Ther.* 123, 371–385. doi: 10.1016/j.pharmthera.2009.05.009

Intengan, H. D., Deng, L. Y., Li, J. S., and Schiffrin, E. L. (1999). Mechanics and composition of human subcutaneous resistance arteries in essential hypertension. *Hypertension* 33, 569–574. doi: 10.1161/01.HYP.33.1.569

Intengan, H. D., and Schiffrin, E. L. (2001). Vascular remodeling in hypertension: roles of apoptosis, inflammation, and fibrosis. *Hypertension* 38, 581–587. doi: 10.1161/hy09t1.096249

Ishibashi, Y., Duncker, D. J., Zhang, J., and Bache, R. J. (1998). ATP-sensitive K+ channels, adenosine, and nitric oxide-mediated mechanisms account for coronary vasodilation during exercise. *Circ. Res.* 82, 346–359. doi: 10.1161/01.RES.82.3.346

Jackson, Z. S., Gotlieb, A. I., and Langille, B. L. (2002). Wall tissue remodeling regulates longitudinal tension in arteries. *Circ. Res.* 90, 918–925. doi: 10.1161/01.RES.0000016481.87703.CC

Jensen, L. J., Nielsen, M. S., Salomonsson, M., and Sorensen, C. M. (2017). T-type Ca(2+) channels and autoregulation of local blood flow. *Channels* 11, 183–195. doi: 10.1080/19336950.2016.1273997

Jesmin, S., Mowa, C. N., Sultana, S. N., Shimojo, N., Togashi, H., Iwashima, Y., et al. (2010). VEGF signaling is disrupted in the hearts of mice lacking estrogen receptor alpha. *Eur. J. Pharmacol.* 641, 168–178. doi: 10.1016/j.ejphar.2010.05.020

Jiang, L., Wang, M., Zhang, J., Monticone, R. E., Telljohann, R., Spinetti, G., et al. (2008). Increased aortic calpain-1 activity mediates age-associated angiotensin II signaling of vascular smooth muscle cells. *PLoS One* 3:e2231. doi: 10.1371/journal.pone.0002231

Jin, Y. J., Chennupati, R., Li, R., Liang, G., Wang, S., Iring, A., et al. (2021). Protein kinase N2 mediates flow-induced eNOS activation and vascular tone regulation. *J. Clin. Invest.* 131:e145734. doi: 10.1172/JCI145734

Jin, Z. G., Ueba, H., Tanimoto, T., Lungu, A. O., Frame, M. D., and Berk, B. C. (2003). Ligand-independent activation of vascular endothelial growth factor receptor 2 by fluid shear stress regulates activation of endothelial nitric oxide synthase. *Circ. Res.* 93, 354–363. doi: 10.1161/01.RES.0000089257.94002.96

Jones, C. J., Kuo, L., Davis, M. J., and Chilian, W. M. (1993a). Distribution and control of coronary microvascular resistance. *Adv. Exp. Med. Biol.* 346, 181–188. doi: 10.1007/978-1-4615-2946-0_17

Jones, C. J., Kuo, L., Davis, M. J., and Chilian, W. M. (1993b). Myogenic and flow-dependent control mechanisms in the coronary microcirculation. *Basic Res. Cardiol.* 88, 2–10. doi: 10.1007/BF00788525

Jung, S. M., Jandu, S., Steppan, J., Belkin, A., An, S. S., Pak, A., et al. (2013). Increased tissue transglutaminase activity contributes to central vascular stiffness in eNOS knockout mice. *Am. J. Physiol. Heart Circ. Physiol.* 305, H803–H810. doi: 10.1152/ajpheart.00103.2013

Jung, B., Obinata, H., Galvani, S., Mendelson, K., Ding, B. S., Skoura, A., et al. (2012). Flow-regulated endothelial S1P receptor-1 signaling sustains vascular development. *Dev. Cell* 23, 600–610. doi: 10.1016/j.devcel.2012.07.015

Kachur, S., Morera, R., De Schutter, A., and Lavie, C. J. (2018). Cardiovascular risk in patients with prehypertension and the metabolic syndrome. *Curr. Hypertens. Rep.* 20:15. doi: 10.1007/s11906-018-0801-2

Kajuluri, L. P., Singh, K., and Morgan, K. G. (2021). Vascular aging, the vascular cytoskeleton and aortic stiffness. *Explor. Med.* 2, 186–197. doi: 10.37349/emed.2021.00041

Kang, L. S., Chen, B., Reyes, R. A., Leblanc, A. J., Teng, B., Mustafa, S. J., et al. (2011). Aging and estrogen alter endothelial reactivity to reactive oxygen species in coronary arterioles. *Am. J. Physiol. Heart Circ. Physiol.* 300, H2105–H2115. doi: 10.1152/ajpheart.00349.2010

Kang, L. S., Reyes, R. A., and Muller-Delp, J. M. (2009). Aging impairs flow-induced dilation in coronary arterioles: role of NO and H(2)O(2). *Am. J.*

Physiol. Heart Circ. Physiol. 297, H1087–H1095. doi: 10.1152/ajpheart.00356.2009

Kefaloyianni, E., and Coetzee, W. A. (2011). Transcriptional remodeling of ion channel subunits by flow adaptation in human coronary artery endothelial cells. *J. Vasc. Res.* 48, 357–367. doi: 10.1159/000323475

Kelleher, Z. T., Matsumoto, A., Stamler, J. S., and Marshall, H. E. (2007). NOS2 regulation of NF-kappaB by S-nitrosylation of p65. *J. Biol. Chem.* 282, 30667–30672. doi: 10.1074/jbc.M705929200

Kelly, R. F., Cabrera, J. A., Ziemba, E. A., Crampton, M., Anderson, L. B., Mcfalls, E. O., et al. (2011). Continued depression of maximal oxygen consumption and mitochondrial proteomic expression despite successful coronary artery bypass grafting in a swine model of hibernation. *J. Thorac. Cardiovasc. Surg.* 141, 261–268. doi: 10.1016/j.jtcvs.2010.08.061

Khder, Y., Briancon, S., Petermann, R., Quilliot, D., Stoltz, J. F., Drouin, P., et al. (1998). Shear stress abnormalities contribute to endothelial dysfunction in hypertension but not in type II diabetes. *J. Hypertens.* 16, 1619–1625. doi: 10.1097/00004872-199816110-00008

Knowlton, A. A., and Lee, A. R. (2012). Estrogen and the cardiovascular system. *Pharmacol. Ther.* 135, 54–70. doi: 10.1016/j.pharmthera.2012.03.007

Kobayashi, N., Delano, F. A., and Schmid-Schonbein, G. W. (2005). Oxidative stress promotes endothelial cell apoptosis and loss of microvessels in the spontaneously hypertensive rats. *Arterioscler. Thromb. Vasc. Biol.* 25, 2114–2121. doi: 10.1161/01.ATV.0000178993.13222.f2

Kohler, R., and Hoyer, J. (2007). "Role of TRPV4 in the mechanotransduction of shear stress in endothelial cells," in *TRP Ion Channel Function in Sensory Transduction and Cellular Signaling Cascades*. eds. W. B. Liedtke and S. Heller (Boca Raton, FL: CRC Press/Taylor & Francis).

Kohn, J. C., Zhou, D. W., Bordeleau, F., Zhou, A. L., Mason, B. N., Mitchell, M. J., et al. (2015). Cooperative effects of matrix stiffness and fluid shear stress on endothelial cell behavior. *Biophys. J.* 108, 471–478. doi: 10.1016/j.bpj.2014.12.023

Kondo, I., Mizushige, K., Hirao, K., Nozaki, S., Tsuji, T., Masugata, H., et al. (2001). Ultrasonographic assessment of coronary flow reserve and abdominal fat in obesity. *Ultrasound Med. Biol.* 27, 1199–1205. doi: 10.1016/S0301-5629(01)00427-6

Kramann, R., Wongboonsin, J., Chang-Panesso, M., Machado, F. G., and Humphreys, B. D. (2017). Gli1(+) pericyte loss induces capillary rarefaction and proximal tubular injury. *J. Am. Soc. Nephrol.* 28, 776–784. doi: 10.1681/ASN.2016030297

Kulandavelu, S., Balkan, W., and Hare, J. M. (2015). Regulation of oxygen delivery to the body via hypoxic vasodilation. *Proc. Natl. Acad. Sci. U. S. A.* 112, 6254–6255. doi: 10.1073/pnas.1506523112

Kuo, L., Davis, M. J., and Chilian, W. M. (1988). Myogenic activity in isolated subepicardial and subendocardial coronary arterioles. *Am. J. Phys.* 255, H1558–H1562. doi: 10.1152/ajpheart.1988.255.6.H1558

Lahteenvuo, J., and Rosenzweig, A. (2012). Effects of aging on angiogenesis. *Circ. Res.* 110, 1252–1264. doi: 10.1161/CIRCRESAHA.111.246116

Lakatta, E. G., and Levy, D. (2003). Arterial and cardiac aging: major shareholders in cardiovascular disease enterprises: part I: aging arteries: a "set up" for vascular disease. *Circulation* 107, 139–146. doi: 10.1161/01.CIR.0000048892.83521.58

Langille, B. L. (1996). Arterial remodeling: relation to hemodynamics. *Can. J. Physiol. Pharmacol.* 74, 834–841. doi: 10.1139/y96-082

Lassegue, B., and Griendling, K. K. (2004). Reactive oxygen species in hypertension; an update. *Am. J. Hypertens.* 17, 852–860. doi: 10.1016/j.amjhyper.2004.02.004

Laughlin, M. H., Davis, M. J., Secher, N. H., Van Lieshout, J. J., Arce-Esquivel, A. A., Simmons, G. H., et al. (2012). Peripheral circulation. *Compr. Physiol.* 2, 321–447. doi: 10.1002/cphy.c100048

Laurent, S., and Boutouyrie, P. (2021). Vascular ageing - state of play, gaps and key issues. *Heart Lung Circ.* 30, 1591–1594. doi: 10.1016/j.hlc.2021.06.528

Laxson, D. D., Homans, D. C., and Bache, R. J. (1993). Inhibition of adenosine-mediated coronary vasodilation exacerbates myocardial ischemia during exercise. *Am. J. Phys.* 265, H1471–H1477. doi: 10.1152/ajpheart.1993.265.5.H1471

Leblanc, A. J., Reyes, R., Kang, L. S., Dailey, R. A., Stallone, J. N., Moningka, N. C., et al. (2009). Estrogen replacement restores flow-induced vasodilation in coronary arterioles of aged and ovariectomized rats. *Am. J. Phys. Regul. Integr. Comp. Phys.* 297, R1713–R1723. doi: 10.1152/ajpregu.00178.2009

Leblanc, A. J., Shipley, R. D., Kang, L. S., and Muller-Delp, J. M. (2008). Age impairs Flk-1 signaling and NO-mediated vasodilation in coronary arterioles. *Am. J. Physiol. Heart Circ. Physiol.* 295, H2280–H2288. doi: 10.1152/ajpheart.00541.2008

Lee, E. S., Boldo, L. S., Fernandez, B. O., Feelisch, M., and Harmsen, M. C. (2017). Suppression of TAK1 pathway by shear stress counteracts the inflammatory endothelial cell phenotype induced by oxidative stress and TGF-beta1. *Sci. Rep.* 7:42487. doi: 10.1038/s41598-017-18420-9

Lehoux, S., Lemarie, C. A., Esposito, B., Lijnen, H. R., and Tedgui, A. (2004). Pressure-induced matrix metalloproteinase-9 contributes to early hypertensive remodeling. *Circulation* 109, 1041–1047. doi: 10.1161/01.CIR.0000115521.95662.7A

Li, Z. L., Woollard, J. R., Ebrahimi, B., Crane, J. A., Jordan, K. L., Lerman, A., et al. (2012). Transition from obesity to metabolic syndrome is associated with altered myocardial autophagy and apoptosis. *Arterioscler. Thromb. Vasc. Biol.* 32, 1132–1141. doi: 10.1161/ATVBAHA.111.244061

Liu, W., Liu, B., Liu, S., Zhang, J., and Lin, S. (2016). Sphingosine-1-phosphate receptor 2 mediates endothelial cells dysfunction by PI3K-Akt pathway under high glucose condition. *Eur. J. Pharmacol.* 776, 19–25. doi: 10.1016/j.ejphar.2016.02.056

Lockette, W., Otsuka, Y., and Carretero, O. (1986). The loss of endothelium-dependent vascular relaxation in hypertension. *Hypertension* 8, II61–II66. doi: 10.1161/01.hyp.8.6_pt_2.ii61

Loerakker, S., Stassen, O., Ter Huurne, F. M., Boareto, M., Bouten, C. V. C., and Sahlgren, C. M. (2018). Mechanosensitivity of jagged-notch signaling can induce a switch-type behavior in vascular homeostasis. *Proc. Natl. Acad. Sci. U. S. A.* 115, E3682–E3691. doi: 10.1073/pnas.1715277115

Luscher, T. F., Raij, L., and Vanhoutte, P. M. (1987). Endothelium-dependent vascular responses in normotensive and hypertensive Dahl rats. *Hypertension* 9, 157–163. doi: 10.1161/01.HYP.9.2.157

Machado, M. V., Vieira, A. B., Da Conceicao, F. G., Nascimento, A. R., Da Nobrega, A. C. L., and Tibirica, E. (2017). Exercise training dose differentially alters muscle and heart capillary density and metabolic functions in an obese rat with metabolic syndrome. *Exp. Physiol.* 102, 1716–1728. doi: 10.1113/EP086416

Martinez-Lemus, L. A., Zhao, G., Galinanes, E. L., and Boone, M. (2011). Inward remodeling of resistance arteries requires reactive oxygen species-dependent activation of matrix metalloproteinases. *Am. J. Physiol. Heart Circ. Physiol.* 300, H2005–H2015. doi: 10.1152/ajpheart.01066.2010

Martinez-Martinez, E., Miana, M., Jurado-Lopez, R., Bartolome, M. V., Souza Neto, F. V., Salaices, M., et al. (2014). The potential role of leptin in the vascular remodeling associated with obesity. *Int. J. Obes.* 38, 1565–1572. doi: 10.1038/ijo.2014.37

Matsunaga, T., Weihrauch, D. W., Moniz, M. C., Tessmer, J., Warltier, D. C., and Chilian, W. M. (2002). Angiostatin inhibits coronary angiogenesis during impaired production of nitric oxide. *Circulation* 105, 2185–2191. doi: 10.1161/01.CIR.0000015856.84385.E9

Mccallinhart, P. E., Sunyecz, I. L., and Trask, A. J. (2018). Coronary microvascular remodeling in type 2 diabetes: synonymous with early aging? *Front. Physiol.* 9:1463. doi: 10.3389/fphys.2018.01463

Meng, X., Mavromatis, K., and Galis, Z. S. (1999). Mechanical stretching of human saphenous vein grafts induces expression and activation of matrix-degrading enzymes associated with vascular tissue injury and repair. *Exp. Mol. Pathol.* 66, 227–237. doi: 10.1006/exmp.1999.2260

Merkus, D., Haitsma, D. B., Fung, T. Y., Assen, Y. J., Verdouw, P. D., and Duncker, D. J. (2003). Coronary blood flow regulation in exercising swine involves parallel rather than redundant vasodilator pathways. *Am. J. Physiol. Heart Circ. Physiol.* 285, H424–H433. doi: 10.1152/ajpheart.00916.2002

Mills, I., Fallon, J. T., Wrenn, D., Sasken, H., Gray, W., Bier, J., et al. (1994). Adaptive responses of coronary circulation and myocardium to chronic reduction in perfusion pressure and flow. *Am. J. Phys.* 266, H447–H457. doi: 10.1152/ajpheart.1994.266.2.H447

Modolo, R., De Faria, A. P., Paganelli, M. O., Sabbatini, A. R., Barbaro, N. R., Nascimento, B. B., et al. (2015). Predictors of silent myocardial ischemia in resistant hypertensive patients. *Am. J. Hypertens.* 28, 200–207. doi: 10.1093/ajh/hpu140

Mohieldin, A. M., Zubayer, H. S., Al Omran, A. J., Saternos, H. C., Zarban, A. A., Nauli, S. M., et al. (2016). Vascular endothelial primary cilia: mechanosensation

and hypertension. *Curr. Hypertens. Rev.* 12, 57–67. doi: 10.2174/1573402111666150630140615

Moreau, K. L., Deane, K. D., Meditz, A. L., and Kohrt, W. M. (2013). Tumor necrosis factor-alpha inhibition improves endothelial function and decreases arterial stiffness in estrogen-deficient postmenopausal women. *Atherosclerosis* 230, 390–396. doi: 10.1016/j.atherosclerosis.2013.07.057

Moreau, K. L., Meditz, A., Deane, K. D., and Kohrt, W. M. (2012). Tetrahydrobiopterin improves endothelial function and decreases arterial stiffness in estrogen-deficient postmenopausal women. *Am. J. Physiol. Heart Circ. Physiol.* 302, H1211–H1218. doi: 10.1152/ajpheart.01065.2011

Morris, H. E., Neves, K. B., Montezano, A. C., Maclean, M. R., and Touyz, R. M. (2019). Notch3 signalling and vascular remodelling in pulmonary arterial hypertension. *Clin. Sci.* 133, 2481–2498. doi: 10.1042/CS20190835

Muller, J. M., Davis, M. J., and Chilian, W. M. (1996). Integrated regulation of pressure and flow in the coronary microcirculation. *Cardiovasc. Res.* 32, 668–678. doi: 10.1016/S0008-6363(96)00111-3

Mulvany, M. J., Baumbach, G. L., Aalkjaer, C., Heagerty, A. M., Korsgaard, N., Schiffrin, E. L., et al. (1996). Vascular remodeling. *Hypertension* 28, 505–506

Nauli, S. M., Kawanabe, Y., Kaminski, J. J., Pearce, W. J., Ingber, D. E., and Zhou, J. (2008). Endothelial cilia are fluid shear sensors that regulate calcium signaling and nitric oxide production through polycystin-1. *Circulation* 117, 1161–1171. doi: 10.1161/CIRCULATIONAHA.107.710111

Neglia, D., Fommei, E., Varela-Carver, A., Mancini, M., Ghione, S., Lombardi, M., et al. (2011). Perindopril and indapamide reverse coronary microvascular remodelling and improve flow in arterial hypertension. *J. Hypertens.* 29, 364–372. doi: 10.1097/HJH.0b013e328340a08e

Niccoli, G., Burzotta, F., Galiuto, L., and Crea, F. (2009). Myocardial no-reflow in humans. *J. Am. Coll. Cardiol.* 54, 281–292. doi: 10.1016/j.jacc.2009.03.054

Niccoli, G., Kharbanda, R. K., Crea, F., and Banning, A. P. (2010). No-reflow: again prevention is better than treatment. *Eur. Heart J.* 31, 2449–2455. doi: 10.1093/eurheartj/ehq299

Nieuwdorp, M., Van Haeften, T. W., Gouverneur, M. C., Mooij, H. L., Van Lieshout, M. H., Levi, M., et al. (2006). Loss of endothelial glycocalyx during acute hyperglycemia coincides with endothelial dysfunction and coagulation activation in vivo. *Diabetes* 55, 480–486. doi: 10.2337/diabetes.55.02.06.db05-1103

Noblet, J. N., Goodwill, A. G., Sassoon, D. J., Kiel, A. M., and Tune, J. D. (2016). Leptin augments coronary vasoconstriction and smooth muscle proliferation via a Rho-kinase-dependent pathway. *Basic Res. Cardiol.* 111:25. doi: 10.1007/s00395-016-0545-6

Novella, S., Dantas, A. P., Segarra, G., Medina, P., and Hermenegildo, C. (2012). Vascular aging in women: is estrogen the fountain of youth? *Front. Physiol.* 3:165. doi: 10.3389/fphys.2012.00165

Novodvorsky, P., and Chico, T. J. (2014). The role of the transcription factor KLF2 in vascular development and disease. *Prog. Mol. Biol. Transl. Sci.* 124, 155–188. doi: 10.1016/B978-0-12-386930-2.00007-0

Oda, A., Taniguchi, T., and Yokoyama, M. (2001). Leptin stimulates rat aortic smooth muscle cell proliferation and migration. *Kobe J. Med. Sci.* 47, 141–150.

Ohanyan, V., Yin, L., Bardakjian, R., Kolz, C., Enrick, M., Hakobyan, T., et al. (2017). Kv1.3 channels facilitate the connection between metabolism and blood flow in the heart. *Microcirculation* 24:e12334. doi: 10.1111/micc.12334

Owens, G. K., Schwartz, S. M., and Mccanna, M. (1988). Evaluation of medial hypertrophy in resistance vessels of spontaneously hypertensive rats. *Hypertension* 11, 198–207. doi: 10.1161/01.HYP.11.2.198

Paavonsalo, S., Hariharan, S., Lackman, M. H., and Karaman, S. (2020). Capillary rarefaction in obesity and metabolic diseases-organ-specificity and possible mechanisms. *Cells* 9:2683. doi: 10.3390/cells9122683

Paddock, C., Zhou, D., Lertkiatmongkol, P., Newman, P. J., and Zhu, J. (2016). Structural basis for PECAM-1 homophilic binding. *Blood* 127, 1052–1061. doi: 10.1182/blood-2015-07-660092

Padro, T., Manfrini, O., Bugiardini, R., Canty, J., Cenko, E., De Luca, G., et al. (2020). ESC working group on coronary pathophysiology and microcirculation position paper on 'coronary microvascular dysfunction in cardiovascular disease'. *Cardiovasc. Res.* 116, 741–755. doi: 10.1093/cvr/cvaa003

Paneni, F., Beckman, J. A., Creager, M. A., and Cosentino, F. (2013). Diabetes and vascular disease: pathophysiology, clinical consequences, and medical therapy: part I. *Eur. Heart J.* 34, 2436–2443. doi: 10.1093/eurheartj/eht149

Paneni, F., Diaz Canestro, C., Libby, P., Luscher, T. F., and Camici, G. G. (2017). The aging cardiovascular system: understanding it at the cellular and clinical levels. *J. Am. Coll. Cardiol.* 69, 1952–1967. doi: 10.1016/j.jacc.2017.01.064

Pant, R., Marok, R., and Klein, L. W. (2014). Pathophysiology of coronary vascular remodeling: relationship with traditional risk factors for coronary artery disease. *Cardiol. Rev.* 22, 13–16. doi: 10.1097/CRD.0b013e31829dea90

Papaioannou, T. G., and Stefanadis, C. (2005). Vascular wall shear stress: basic principles and methods. *Hell. J. Cardiol.* 46, 9–15.

Park, K. W., Lowenstein, E., Dai, H. B., Lopez, J. J., Stamler, A., Simons, M., et al. (1996). Direct vasomotor effects of isoflurane in subepicardial resistance vessels from collateral-dependent and normal coronary circulation of pigs. *Anesthesiology* 85, 584–591. doi: 10.1097/00000542-199609000-00018

Park, J. B., and Schiffrin, E. L. (2001). Small artery remodeling is the most prevalent (earliest?) form of target organ damage in mild essential hypertension. *J. Hypertens.* 19, 921–930. doi: 10.1097/00004872-200105000-00013

Pedrigi, R. M., Papadimitriou, K. I., Kondiboyina, A., Sidhu, S., Chau, J., Patel, M. B., et al. (2017). Disturbed cyclical stretch of endothelial cells promotes nuclear expression of the pro-atherogenic transcription factor NF-kappaB. *Ann. Biomed. Eng.* 45, 898–909. doi: 10.1007/s10439-016-1750-z

Peng, X., Haldar, S., Deshpande, S., Irani, K., and Kass, D. A. (2003). Wall stiffness suppresses Akt/eNOS and cytoprotection in pulse-perfused endothelium. *Hypertension* 41, 378–381. doi: 10.1161/01.HYP.0000049624.99844.3D

Pirat, B., Bozbas, H., Simsek, V., Yildirir, A., Sade, L. E., Gursoy, Y., et al. (2008). Impaired coronary flow reserve in patients with metabolic syndrome. *Atherosclerosis* 201, 112–116. doi: 10.1016/j.atherosclerosis.2008.02.016

Pires, P. W., Deutsch, C., Mcclain, J. L., Rogers, C. T., and Dorrance, A. M. (2010). Tempol, a superoxide dismutase mimetic, prevents cerebral vessel remodeling in hypertensive rats. *Microvasc. Res.* 80, 445–452. doi: 10.1016/j.mvr.2010.06.004

Pirro, M., Schillaci, G., Menecali, C., Bagaglia, F., Paltriccia, R., Vaudo, G., et al. (2007). Reduced number of circulating endothelial progenitors and HOXA9 expression in CD34+ cells of hypertensive patients. *J. Hypertens.* 25, 2093–2099. doi: 10.1097/HJH.0b013e32828e506d

Pistea, A., Bakker, E. N., Spaan, J. A., Hardeman, M. R., Van Rooijen, N., and Vanbavel, E. (2008). Small artery remodeling and erythrocyte deformability in L-NAME-induced hypertension: role of transglutaminases. *J. Vasc. Res.* 45, 10–18. doi: 10.1159/000109073

Pistea, A., Bakker, E. N., Spaan, J. A., and Vanbavel, E. (2005). Flow inhibits inward remodeling in cannulated porcine small coronary arteries. *Am. J. Physiol. Heart Circ. Physiol.* 289, H2632–H2640. doi: 10.1152/ajpheart.00205.2005

Pourageaud, F., and De Mey, J. G. (1997). Structural properties of rat mesenteric small arteries after 4-wk exposure to elevated or reduced blood flow. *Am. J. Phys.* 273, H1699–H1706. doi: 10.1152/ajpheart.1997.273.4.H1699

Puybasset, L., Bea, M. L., Ghaleb, B., Giudicelli, J. F., and Berdeaux, A. (1996). Coronary and systemic hemodynamic effects of sustained inhibition of nitric oxide synthesis in conscious dogs. Evidence for cross talk between nitric oxide and cyclooxygenase in coronary vessels. *Circ. Res.* 79, 343–357. doi: 10.1161/01.RES.79.2.343

Rakusan, K., Flanagan, M. F., Geva, T., Southern, J., and Van Praagh, R. (1992). Morphometry of human coronary capillaries during normal growth and the effect of age in left ventricular pressure-overload hypertrophy. *Circulation* 86, 38–46. doi: 10.1161/01.CIR.86.1.38

Ranade, S. S., Qiu, Z., Woo, S. H., Hur, S. S., Murthy, S. E., Cahalan, S. M., et al. (2014). Piezo1, a mechanically activated ion channel, is required for vascular development in mice. *Proc. Natl. Acad. Sci. U. S. A.* 111, 10347–10352. doi: 10.1073/pnas.1409233111

Reinhart-King, C. A., Fujiwara, K., and Berk, B. C. (2008). Physiologic stress-mediated signaling in the endothelium. *Methods Enzymol.* 443, 25–44. doi: 10.1016/S0076-6879(08)02002-8

Retailleau, K., Duprat, F., Arhatte, M., Ranade, S. S., Peyronnet, R., Martins, J. R., et al. (2015). Piezo1 in smooth muscle cells is involved in hypertension-dependent arterial remodeling. *Cell Rep.* 13, 1161–1171. doi: 10.1016/j.celrep.2015.09.072

Rizzoni, D., Porteri, E., Castellano, M., Bettoni, G., Muiesan, M. L., Muiesan, P., et al. (1996). Vascular hypertrophy and remodeling in secondary hypertension. *Hypertension* 28, 785–790. doi: 10.1161/01.HYP.28.5.785

Sandow, S. L., Tare, M., Coleman, H. A., Hill, C. E., and Parkington, H. C. (2002). Involvement of myoendothelial gap junctions in the actions of

endothelium-derived hyperpolarizing factor. *Circ. Res.* 90, 1108–1113. doi: 10.1161/01.RES.0000019756.88731.83

Saternos, H. C., and Aboualaiwi, W. A. (2015). "Implications of dysfunction of mechanosensory cilia in polycystic kidney disease," in *Polycystic Kidney Disease*. ed. X. Li (Brisbane, AU: Codon Publications).

Schiffers, P. M., Henrion, D., Boulanger, C. M., Colucci-Guyon, E., Langa-Vuves, F., Van Essen, H., et al. (2000). Altered flow-induced arterial remodeling in vimentin-deficient mice. *Arterioscler. Thromb. Vasc. Biol.* 20, 611–616. doi: 10.1161/01.ATV.20.3.611

Schiffrin, E. L., and Deng, L. Y. (1996). Structure and function of resistance arteries of hypertensive patients treated with a beta-blocker or a calcium channel antagonist. *J. Hypertens.* 14, 1247–1255. doi: 10.1097/00004872-199610000-00014

Schiffrin, E. L., Park, J. B., Intengan, H. D., and Touyz, R. M. (2000). Correction of arterial structure and endothelial dysfunction in human essential hypertension by the angiotensin receptor antagonist losartan. *Circulation* 101, 1653–1659. doi: 10.1161/01.CIR.101.14.1653

Schindler, T. H., Cardenas, J., Prior, J. O., Facta, A. D., Kreissl, M. C., Zhang, X. L., et al. (2006). Relationship between increasing body weight, insulin resistance, inflammation, adipocytokine leptin, and coronary circulatory function. *J. Am. Coll. Cardiol.* 47, 1188–1195. doi: 10.1016/j.jacc.2005.10.062

Schleifenbaum, J., Kassmann, M., Szijarto, I. A., Hercule, H. C., Tano, J. Y., Weinert, S., et al. (2014). Stretch-activation of angiotensin II type 1a receptors contributes to the myogenic response of mouse mesenteric and renal arteries. *Circ. Res.* 115, 263–272. doi: 10.1161/CIRCRESAHA.115.302882

Schofield, I., Malik, R., Izzard, A., Austin, C., and Heagerty, A. (2002). Vascular structural and functional changes in type 2 diabetes mellitus: evidence for the roles of abnormal myogenic responsiveness and dyslipidemia. *Circulation* 106, 3037–3043. doi: 10.1161/01.CIR.0000041432.80615.A5

Sellke, F. W., Kagaya, Y., Johnson, R. G., Shafique, T., Schoen, F. J., Grossman, W., et al. (1992). Endothelial modulation of porcine coronary microcirculation perfused via immature collaterals. *Am. J. Phys.* 262, H1669–H1675. doi: 10.1152/ajpheart.1992.262.6.H1669

Sellke, F. W., Li, J., Stamler, A., Lopez, J. J., Thomas, K. A., and Simons, M. (1996a). Angiogenesis induced by acidic fibroblast growth factor as an alternative method of revascularization for chronic myocardial ischemia. *Surgery* 120, 182–188. doi: 10.1016/S0039-6060(96)80286-8

Sellke, F. W., Wang, S. Y., Stamler, A., Lopez, J. J., Li, J., Li, J., et al. (1996b). Enhanced microvascular relaxations to VEGF and bFGF in chronically ischemic porcine myocardium. *Am. J. Phys.* 271, H713–H720. doi: 10.1152/ajpheart.1996.271.2.H713

Setty, S., Sun, W., and Tune, J. D. (2003). Coronary blood flow regulation in the prediabetic metabolic syndrome. *Basic Res. Cardiol.* 98, 416–423. doi: 10.1007/s00395-003-0418-7

Sharif-Naeini, R., Folgering, J. H., Bichet, D., Duprat, F., Lauritzen, I., Arhatte, M., et al. (2009). Polycystin-1 and -2 dosage regulates pressure sensing. *Cell* 139, 587–596. doi: 10.1016/j.cell.2009.08.045

Shi, Q., Aida, K., Vandeberg, J. L., and Wang, X. L. (2004). Passage-dependent changes in baboon endothelial cells–relevance to in vitro aging. *DNA Cell Biol.* 23, 502–509. doi: 10.1089/1044549041562294

Shyy, J. Y., and Chien, S. (2002). Role of integrins in endothelial mechanosensing of shear stress. *Circ. Res.* 91, 769–775. doi: 10.1161/01.RES.0000038487.19924.18

Singh, S., Adam, M., Matkar, P. N., Bugyei-Twum, A., Desjardins, J. F., Chen, H. H., et al. (2020). Endothelial-specific Loss of IFT88 Promotes Endothelial-to-Mesenchymal Transition and Exacerbates Bleomycin-induced Pulmonary Fibrosis. *Sci. Rep.* 10:4466. doi: 10.1038/s41598-020-78906-x

Singh, N., Prasad, S., Singer, D. R., and Macallister, R. J. (2002). Ageing is associated with impairment of nitric oxide and prostanoid dilator pathways in the human forearm. *Clin. Sci.* 102, 595–600. doi: 10.1042/CS20010262

Sodha, N. R., Boodhwani, M., Clements, R. T., Feng, J., Xu, S. H., and Sellke, F. W. (2008). Coronary microvascular dysfunction in the setting of chronic ischemia is independent of arginase activity. *Microvasc. Res.* 75, 238–246. doi: 10.1016/j.mvr.2007.06.008

Sorop, O., Bakker, E. N., Pistea, A., Spaan, J. A., and Vanbavel, E. (2006). Calcium channel blockade prevents pressure-dependent inward remodeling in isolated subendocardial resistance vessels. *Am. J. Physiol. Heart Circ. Physiol.* 291, H1236–H1245. doi: 10.1152/ajpheart.00838.2005

Sorop, O., Heinonen, I., Van Kranenburg, M., Van De Wouw, J., De Beer, V. J., Nguyen, I. T. N., et al. (2018). Multiple common comorbidities produce left ventricular diastolic dysfunction associated with coronary microvascular dysfunction, oxidative stress, and myocardial stiffening. *Cardiovasc. Res.* 114, 954–964. doi: 10.1093/cvr/cvy038

Sorop, O., Merkus, D., De Beer, V. J., Houweling, B., Pistea, A., Mcfalls, E. O., et al. (2008). Functional and structural adaptations of coronary microvessels distal to a chronic coronary artery stenosis. *Circ. Res.* 102, 795–803. doi: 10.1161/CIRCRESAHA.108.172528

Sorop, O., Spaan, J. A., Sweeney, T. E., and Vanbavel, E. (2003). Effect of steady versus oscillating flow on porcine coronary arterioles: involvement of NO and superoxide anion. *Circ. Res.* 92, 1344–1351. doi: 10.1161/01.RES.0000078604.47063.2B

Sorop, O., Van De Wouw, J., Chandler, S., Ohanyan, V., Tune, J. D., Chilian, W. M., et al. (2020). Experimental animal models of coronary microvascular dysfunction. *Cardiovasc. Res.* 116, 756–770. doi: 10.1093/cvr/cvaa002

Sorop, O., Van Den Heuvel, M., Van Ditzhuijzen, N. S., De Beer, V. J., Heinonen, I., Van Duin, R. W., et al. (2016). Coronary microvascular dysfunction after long-term diabetes and hypercholesterolemia. *Am. J. Physiol. Heart Circ. Physiol.* 311, H1339–H1351. doi: 10.1152/ajpheart.00458.2015

Spescha, R. D., Glanzmann, M., Simic, B., Witassek, F., Keller, S., Akhmedov, A., et al. (2014). Adaptor protein p66(Shc) mediates hypertension-associated, cyclic stretch-dependent, endothelial damage. *Hypertension* 64, 347–353. doi: 10.1161/HYPERTENSIONAHA.113.02129

Stacy, D. L., and Prewitt, R. L. (1989). Effects of chronic hypertension and its reversal on arteries and arterioles. *Circ. Res.* 65, 869–879. doi: 10.1161/01.RES.65.4.869

Stassen, O., Ristori, T., and Sahlgren, C. M. (2020). Notch in mechanotransduction - from molecular mechanosensitivity to tissue mechanostasis. *J. Cell Sci.* 133:jcs250738. doi: 10.1242/jcs.250738

Stegehuis, V. E., Wijntjens, G. W., Piek, J. J., and Van De Hoef, T. P. (2018). Fractional flow reserve or coronary flow reserve for the assessment of myocardial perfusion: implications of FFR as an imperfect reference standard for myocardial ischemia. *Curr. Cardiol. Rep.* 20:77. doi: 10.1007/s11886-018-1017-4

Stow, L. R., Jacobs, M. E., Wingo, C. S., and Cain, B. D. (2011). Endothelin-1 gene regulation. *FASEB J.* 25, 16–28. doi: 10.1096/fj.10-161612

Sun, D., Huang, A., Yan, E. H., Wu, Z., Yan, C., Kaminski, P. M., et al. (2004). Reduced release of nitric oxide to shear stress in mesenteric arteries of aged rats. *Am. J. Physiol. Heart Circ. Physiol.* 286, H2249–H2256. doi: 10.1152/ajpheart.00854.2003

Tanner, F. C., Meier, P., Greutert, H., Champion, C., Nabel, E. G., and Luscher, T. F. (2000). Nitric oxide modulates expression of cell cycle regulatory proteins: a cytostatic strategy for inhibition of human vascular smooth muscle cell proliferation. *Circulation* 101, 1982–1989. doi: 10.1161/01.CIR.101.16.1982

Toblli, J. E., Cao, G., Derosa, G., Di Gennaro, F., and Forcada, P. (2004). Angiotensin-converting enzyme inhibition and angiogenesis in myocardium of obese Zucker rats. *Am. J. Hypertens.* 17, 172–180. doi: 10.1016/j.amjhyper.2003.10.006

Tomanek, R. J., Aydelotte, M. R., and Torry, R. J. (1991). Remodeling of coronary vessels during aging in purebred beagles. *Circ. Res.* 69, 1068–1074. doi: 10.1161/01.RES.69.4.1068

Tomanek, R. J., Searls, J. C., and Lachenbruch, P. A. (1982). Quantitative changes in the capillary bed during developing, peak, and stabilized cardiac hypertrophy in the spontaneously hypertensive rat. *Circ. Res.* 51, 295–304. doi: 10.1161/01.RES.51.3.295

Trask, A. J., Katz, P. S., Kelly, A. P., Galantowicz, M. L., Cismowski, M. J., West, T. A., et al. (2012). Dynamic micro- and macrovascular remodeling in coronary circulation of obese Ossabaw pigs with metabolic syndrome. *J. Appl. Physiol.* 113, 1128–1140. doi: 10.1152/japplphysiol.00604.2012

Tuna, B. G., Bakker, E. N., and Vanbavel, E. (2013). Relation between active and passive biomechanics of small mesenteric arteries during remodeling. *J. Biomech.* 46, 1420–1426. doi: 10.1016/j.jbiomech.2013.03.010

Tune, J. D. (2007). Control of coronary blood flow during hypoxemia. *Adv. Exp. Med. Biol.* 618, 25–39. doi: 10.1007/978-0-387-75434-5_3

Tuttle, J. L., Nachreiner, R. D., Bhuller, A. S., Condict, K. W., Connors, B. A., Herring, B. P., et al. (2001). Shear level influences resistance artery remodeling: wall dimensions, cell density, and eNOS expression. *Am. J. Physiol. Heart Circ. Physiol.* 281, H1380–H1389. doi: 10.1152/ajpheart.2001.281.3.H1380

Tykocki, N. R., Boerman, E. M., and Jackson, W. F. (2017). Smooth muscle ion channels and regulation of vascular tone in resistance arteries and arterioles. *Compr. Physiol.* 7, 485–581. doi: 10.1002/cphy.c160011

Tzima, E., Irani-Tehrani, M., Kiosses, W. B., Dejana, E., Schultz, D. A., Engelhardt, B., et al. (2005). A mechanosensory complex that mediates the endothelial cell response to fluid shear stress. *Nature* 437, 426–431. doi: 10.1038/nature03952

Unger, T., Borghi, C., Charchar, F., Khan, N. A., Poulter, N. R., Prabhakaran, D., et al. (2020). 2020 International Society of Hypertension global hypertension practice guidelines. *Hypertension* 75, 1334–1357. doi: 10.1161/HYPERTENSIONAHA.120.15026

Ungvari, Z., Bailey-Downs, L., Gautam, T., Sosnowska, D., Wang, M., Monticone, R. E., et al. (2011a). Age-associated vascular oxidative stress, Nrf2 dysfunction, and NF-{kappa}B activation in the nonhuman primate *Macaca mulatta*. *J. Gerontol. A Biol. Sci. Med. Sci.* 66A, 866–875. doi: 10.1093/gerona/glr092

Ungvari, Z., Bailey-Downs, L., Sosnowska, D., Gautam, T., Koncz, P., Losonczy, G., et al. (2011b). Vascular oxidative stress in aging: a homeostatic failure due to dysregulation of NRF2-mediated antioxidant response. *Am. J. Physiol. Heart Circ. Physiol.* 301, H363–H372. doi: 10.1152/ajpheart.01134.2010

Ungvari, Z., Orosz, Z., Labinskyy, N., Rivera, A., Xiangmin, Z., Smith, K., et al. (2007). Increased mitochondrial H2O2 production promotes endothelial NF-kappaB activation in aged rat arteries. *Am. J. Physiol. Heart Circ. Physiol.* 293, H37–H47. doi: 10.1152/ajpheart.01346.2006

Ungvari, Z., Tarantini, S., Nyul-Toth, A., Kiss, T., Yabluchanskiy, A., Csipo, T., et al. (2019). Nrf2 dysfunction and impaired cellular resilience to oxidative stressors in the aged vasculature: from increased cellular senescence to the pathogenesis of age-related vascular diseases. *Geroscience* 41, 727–738. doi: 10.1007/s11357-019-00107-w

Urbieta Caceres, V. H., Lin, J., Zhu, X. Y., Favreau, F. D., Gibson, M. E., Crane, J. A., et al. (2011). Early experimental hypertension preserves the myocardial microvasculature but aggravates cardiac injury distal to chronic coronary artery obstruction. *Am. J. Physiol. Heart Circ. Physiol.* 300, H693–H701. doi: 10.1152/ajpheart.00516.2010

Uren, N. G., Crake, T., Lefroy, D. C., De Silva, R., Davies, G. J., and Maseri, A. (1993a). Delayed recovery of coronary resistive vessel function after coronary angioplasty. *J. Am. Coll. Cardiol.* 21, 612–621. doi: 10.1016/0735-1097(93)90092-F

Uren, N. G., Marraccini, P., Gistri, R., De Silva, R., and Camici, P. G. (1993b). Altered coronary vasodilator reserve and metabolism in myocardium subtended by normal arteries in patients with coronary artery disease. *J. Am. Coll. Cardiol.* 22, 650–658. doi: 10.1016/0735-1097(93)90172-W

Van De Wouw, J., Sorop, O., Van Drie, R. W. A., Joles, J. A., Danser, A. H. J., Verhaar, M. C., et al. (2021). Reduced nitric oxide bioavailability impairs myocardial oxygen balance during exercise in swine with multiple risk factors. *Basic Res. Cardiol.* 116:50. doi: 10.1007/s00395-021-00891-7

Van De Wouw, J., Sorop, O., Van Drie, R. W. A., Van Duin, R. W. B., Nguyen, I. T. N., Joles, J. A., et al. (2020). Perturbations in myocardial perfusion and oxygen balance in swine with multiple risk factors: a novel model of ischemia and no obstructive coronary artery disease. *Basic Res. Cardiol.* 115:21. doi: 10.1007/s00395-020-0778-2

Van Den Akker, J., Schoorl, M. J., Bakker, E. N., and Vanbavel, E. (2010). Small artery remodeling: current concepts and questions. *J. Vasc. Res.* 47, 183–202. doi: 10.1159/000255962

Van Den Heuvel, M., Sorop, O., Koopmans, S. J., Dekker, R., De Vries, R., Van Beusekom, H. M., et al. (2012). Coronary microvascular dysfunction in a porcine model of early atherosclerosis and diabetes. *Am. J. Physiol. Heart Circ. Physiol.* 302, H85–H94. doi: 10.1152/ajpheart.00311.2011

Van Engeland, N. C. A., Suarez Rodriguez, F., Rivero-Muller, A., Ristori, T., Duran, C. L., Stassen, O., et al. (2019). Vimentin regulates Notch signaling strength and arterial remodeling in response to hemodynamic stress. *Sci. Rep.* 9:12415. doi: 10.1038/s41598-019-48218-w

Vanteeffelen, J. W., Brands, J., Jansen, C., Spaan, J. A., and Vink, H. (2007). Heparin impairs glycocalyx barrier properties and attenuates shear dependent vasodilation in mice. *Hypertension* 50, 261–267. doi: 10.1161/HYPERTENSIONAHA.107.089250

Verhoeff, B. J., Siebes, M., Meuwissen, M., Atasever, B., Voskuil, M., De Winter, R. J., et al. (2005). Influence of percutaneous coronary intervention on coronary microvascular resistance index. *Circulation* 111, 76–82. doi: 10.1161/01.CIR.0000151610.98409.2F

Viedt, C., Vogel, J., Athanasiou, T., Shen, W., Orth, S. R., Kubler, W., et al. (2002). Monocyte chemoattractant protein-1 induces proliferation and interleukin-6 production in human smooth muscle cells by differential activation of nuclear factor-kappaB and activator protein-1. *Arterioscler. Thromb. Vasc. Biol.* 22, 914–920. doi: 10.1161/01.ATV.0000019009.73586.7F

Voyvodic, P. L., Min, D., Liu, R., Williams, E., Chitalia, V., Dunn, A. K., et al. (2014). Loss of syndecan-1 induces a pro-inflammatory phenotype in endothelial cells with a dysregulated response to atheroprotective flow. *J. Biol. Chem.* 289, 9547–9559. doi: 10.1074/jbc.M113.541573

Wang, S., Chennupati, R., Kaur, H., Iring, A., Wettschureck, N., and Offermanns, S. (2016a). Endothelial cation channel PIEZO1 controls blood pressure by mediating flow-induced ATP release. *J. Clin. Invest.* 126, 4527–4536. doi: 10.1172/JCI87343

Wang, L., Luo, J. Y., Li, B., Tian, X. Y., Chen, L. J., Huang, Y., et al. (2016b). Integrin-YAP/TAZ-JNK cascade mediates atheroprotective effect of unidirectional shear flow. *Nature* 540, 579–582. doi: 10.1038/nature20602

Wang, Z., and Newman, W. H. (2003). Smooth muscle cell migration stimulated by interleukin 6 is associated with cytoskeletal reorganization. *J. Surg. Res.* 111, 261–266. doi: 10.1016/S0022-4804(03)00087-8

Wang, M., Takagi, G., Asai, K., Resuello, R. G., Natividad, F. F., Vatner, D. E., et al. (2003). Aging increases aortic MMP-2 activity and angiotensin II in nonhuman primates. *Hypertension* 41, 1308–1316. doi: 10.1161/01.HYP.0000073843.56046.45

Wang, M., Zhang, J., Spinetti, G., Jiang, L. Q., Monticone, R., Zhao, D., et al. (2005). Angiotensin II activates matrix metalloproteinase type II and mimics age-associated carotid arterial remodeling in young rats. *Am. J. Pathol.* 167, 1429–1442. doi: 10.1016/S0002-9440(10)61229-1

Warnock, D. G., Kusche-Vihrog, K., Tarjus, A., Sheng, S., Oberleithner, H., Kleyman, T. R., et al. (2014). Blood pressure and amiloride-sensitive sodium channels in vascular and renal cells. *Nat. Rev. Nephrol.* 10, 146–157. doi: 10.1038/nrneph.2013.275

Wedgwood, S., and Black, S. M. (2005). Endothelin-1 decreases endothelial NOS expression and activity through ETA receptor-mediated generation of hydrogen peroxide. *Am. J. Phys. Lung Cell. Mol. Phys.* 288, L480–L487. doi: 10.1152/ajplung.00283.2004

Weil, B. R., Suzuki, G., and Canty, J. M. Jr. (2020). Transmural variation in microvascular remodeling following percutaneous revascularization of a chronic coronary stenosis in swine. *Am. J. Physiol. Heart Circ. Physiol.* 318, H696–H705. doi: 10.1152/ajpheart.00502.2019

Welsh, D. G., Morielli, A. D., Nelson, M. T., and Brayden, J. E. (2002). Transient receptor potential channels regulate myogenic tone of resistance arteries. *Circ. Res.* 90, 248–250. doi: 10.1161/hh0302.105662

Wenzel, P. (2019). Monocytes as immune targets in arterial hypertension. *Br. J. Pharmacol.* 176, 1966–1977. doi: 10.1111/bph.14389

Wilson, C., Lee, M. D., and Mccarron, J. G. (2016). Acetylcholine released by endothelial cells facilitates flow-mediated dilatation. *J. Physiol.* 594, 7267–7307. doi: 10.1113/JP272927

Wojtowicz, A., Babu, S. S., Li, L., Gretz, N., Hecker, M., and Cattaruzza, M. (2010). Zyxin mediation of stretch-induced gene expression in human endothelial cells. *Circ. Res.* 107, 898–902. doi: 10.1161/CIRCRESAHA.110.227850

Wu, W., Platoshyn, O., Firth, A. L., and Yuan, J. X. (2007). Hypoxia divergently regulates production of reactive oxygen species in human pulmonary and coronary artery smooth muscle cells. *Am. J. Phys. Lung Cell. Mol. Phys.* 293, L952–L959. doi: 10.1152/ajplung.00203.2007

Xie, W., Parker, J. L., and Heaps, C. L. (2012). Effect of exercise training on nitric oxide and superoxide/H(2)O(2) signaling pathways in collateral-dependent porcine coronary arterioles. *J. Appl. Physiol.* 112, 1546–1555. doi: 10.1152/japplphysiol.01248.2011

Xie, W., Parker, J. L., and Heaps, C. L. (2013). Exercise training-enhanced, endothelium-dependent dilation mediated by altered regulation of BK(Ca) channels in collateral-dependent porcine coronary arterioles. *Microcirculation* 20, 170–182. doi: 10.1111/micc.12016

Xu, S., Ha, C. H., Wang, W., Xu, X., Yin, M., Jin, F. Q., et al. (2016). PECAM1 regulates flow-mediated Gab1 tyrosine phosphorylation and signaling. *Cell. Signal.* 28, 117–124. doi: 10.1016/j.cellsig.2015.12.007

Xu, J., Mathur, J., Vessieres, E., Hammack, S., Nonomura, K., Favre, J., et al. (2018). GPR68 senses flow and is essential for vascular physiology. *Cell* 173:e716. doi: 10.1016/j.cell.2018.03.076

Yamashita, K., Discher, D. J., Hu, J., Bishopric, N. H., and Webster, K. A. (2001). Molecular regulation of the endothelin-1 gene by hypoxia. Contributions of hypoxia-inducible factor-1, activator protein-1, GATA-2, AND p300/CBP. *J. Biol. Chem.* 276, 12645–12653. doi: 10.1074/jbc.M011344200

Yang, Y. M., Huang, A., Kaley, G., and Sun, D. (2009). eNOS uncoupling and endothelial dysfunction in aged vessels. *Am. J. Physiol. Heart Circ. Physiol.* 297, H1829–H1836. doi: 10.1152/ajpheart.00230.2009

Yeh, H. I., Chang, H. M., Lu, W. W., Lee, Y. N., Ko, Y. S., Severs, N. J., et al. (2000). Age-related alteration of gap junction distribution and connexin expression in rat aortic endothelium. *J. Histochem. Cytochem.* 48, 1377–1389. doi: 10.1177/002215540004801008

Yen, W., Cai, B., Yang, J., Zhang, L., Zeng, M., Tarbell, J. M., et al. (2015). Endothelial surface glycocalyx can regulate flow-induced nitric oxide production in microvessels in vivo. *PLoS One* 10:e0117133. doi: 10.1371/journal.pone.0117133

Yu, J., Demuinck, E. D., Zhuang, Z., Drinane, M., Kauser, K., Rubanyi, G. M., et al. (2005). Endothelial nitric oxide synthase is critical for ischemic remodeling, mural cell recruitment, and blood flow reserve. *Proc. Natl. Acad. Sci. U. S. A.* 102, 10999–11004. doi: 10.1073/pnas.0501444102

Zampetaki, A., Zhang, Z., Hu, Y., and Xu, Q. (2005). Biomechanical stress induces IL-6 expression in smooth muscle cells via Ras/Rac1-p38 MAPK-NF-kappaB signaling pathways. *Am. J. Physiol. Heart Circ. Physiol.* 288, H2946–H2954. doi: 10.1152/ajpheart.00919.2004

Zaydun, G., Tomiyama, H., Hashimoto, H., Arai, T., Koji, Y., Yambe, M., et al. (2006). Menopause is an independent factor augmenting the age-related increase in arterial stiffness in the early postmenopausal phase. *Atherosclerosis* 184, 137–142. doi: 10.1016/j.atherosclerosis.2005.03.043

Zeiher, A. M., Drexler, H., Saurbier, B., and Just, H. (1993). Endothelium-mediated coronary blood flow modulation in humans. Effects of age, atherosclerosis, hypercholesterolemia, and hypertension. *J. Clin. Invest.* 92, 652–662. doi: 10.1172/JCI116634

Zhong, X. Z., Harhun, M. I., Olesen, S. P., Ohya, S., Moffatt, J. D., Cole, W. C., et al. (2010). Participation of KCNQ (Kv7) potassium channels in myogenic control of cerebral arterial diameter. *J. Physiol.* 588, 3277–3293. doi: 10.1113/jphysiol.2010.192823

Zhou, J., Li, Y. S., and Chien, S. (2014). Shear stress-initiated signaling and its regulation of endothelial function. *Arterioscler. Thromb. Vasc. Biol.* 34, 2191–2198. doi: 10.1161/ATVBAHA.114.303422

Zhu, Y., Qiu, H., Trzeciakowski, J. P., Sun, Z., Li, Z., Hong, Z., et al. (2012). Temporal analysis of vascular smooth muscle cell elasticity and adhesion reveals oscillation waveforms that differ with aging. *Aging Cell* 11, 741–750. doi: 10.1111/j.1474-9726.2012.00840.x

Zorach, B., Shaw, P. W., Bourque, J., Kuruvilla, S., Balfour, P. C. Jr., Yang, Y., et al. (2018). Quantitative cardiovascular magnetic resonance perfusion imaging identifies reduced flow reserve in microvascular coronary artery disease. *J. Cardiovasc. Magn. Reson.* 20:14. doi: 10.1186/s12968-018-0435-1

Conflict of Interest: The authors declare that the research was conducted in the absence of any commercial or financial relationships that could be construed as a potential conflict of interest.

Publisher's Note: All claims expressed in this article are solely those of the authors and do not necessarily represent those of their affiliated organizations, or those of the publisher, the editors and the reviewers. Any product that may be evaluated in this article, or claim that may be made by its manufacturer, is not guaranteed or endorsed by the publisher.

Advantages of publishing in Frontiers

OPEN ACCESS
Articles are free to read for greatest visibility and readership

FAST PUBLICATION
Around 90 days from submission to decision

HIGH QUALITY PEER-REVIEW
Rigorous, collaborative, and constructive peer-review

TRANSPARENT PEER-REVIEW
Editors and reviewers acknowledged by name on published articles

Frontiers
Avenue du Tribunal-Fédéral 34
1005 Lausanne | Switzerland

Visit us: www.frontiersin.org
Contact us: frontiersin.org/about/contact

REPRODUCIBILITY OF RESEARCH
Support open data and methods to enhance research reproducibility

DIGITAL PUBLISHING
Articles designed for optimal readership across devices

FOLLOW US
@frontiersin

IMPACT METRICS
Advanced article metrics track visibility across digital media

EXTENSIVE PROMOTION
Marketing and promotion of impactful research

LOOP RESEARCH NETWORK
Our network increases your article's readership